Springer Theses
Recognizing Outstanding Ph.D. Research

Terrance John Hadlington

On the Catalytic Efficacy of Low-Oxidation State Group 14 Complexes

Springer

Springer Theses

Recognizing Outstanding Ph.D. Research

Aims and Scope

The series "Springer Theses" brings together a selection of the very best Ph.D. theses from around the world and across the physical sciences. Nominated and endorsed by two recognized specialists, each published volume has been selected for its scientific excellence and the high impact of its contents for the pertinent field of research. For greater accessibility to non-specialists, the published versions include an extended introduction, as well as a foreword by the student's supervisor explaining the special relevance of the work for the field. As a whole, the series will provide a valuable resource both for newcomers to the research fields described, and for other scientists seeking detailed background information on special questions. Finally, it provides an accredited documentation of the valuable contributions made by today's younger generation of scientists.

Theses are accepted into the series by invited nomination only and must fulfill all of the following criteria

- They must be written in good English.
- The topic should fall within the confines of Chemistry, Physics, Earth Sciences, Engineering and related interdisciplinary fields such as Materials, Nanoscience, Chemical Engineering, Complex Systems and Biophysics.
- The work reported in the thesis must represent a significant scientific advance.
- If the thesis includes previously published material, permission to reproduce this must be gained from the respective copyright holder.
- They must have been examined and passed during the 12 months prior to nomination.
- Each thesis should include a foreword by the supervisor outlining the significance of its content.
- The theses should have a clearly defined structure including an introduction accessible to scientists not expert in that particular field.

More information about this series at http://www.springer.com/series/8790

Terrance John Hadlington

On the Catalytic Efficacy of Low-Oxidation State Group 14 Complexes

Doctoral Thesis accepted by
Monash University, Australia

Springer

Author
Dr. Terrance John Hadlington
Institut für Chemie
Technische Universität Berlin
Berlin
Germany

Supervisor
Prof. Cameron Jones
Monash University
Clayton
Australia

ISSN 2190-5053 ISSN 2190-5061 (electronic)
Springer Theses
ISBN 978-3-319-51806-0 ISBN 978-3-319-51807-7 (eBook)
DOI 10.1007/978-3-319-51807-7

Library of Congress Control Number: 2016961344

Printed on acid-free paper

This Springer imprint is published by Springer Nature
The registered company is Springer International Publishing AG
The registered company address is: Gewerbestrasse 11, 6330 Cham, Switzerland

Supervisor's Foreword

The Ph.D. thesis of Dr. Terrance John Hadlington is a groundbreaking collection of results, and is truly deserving of a place in the Springer Theses series. Over his time at Monash University he succeeded in the synthesis of numerous landmark compounds, and developed novel complexes leading to highly efficient catalysts with group 14 elements at their reactive centres. This has effectively borne a new sub-discipline in low-oxidation state group 14 chemistry. Further, it has given us a deeper understanding of the subtle differences of bonding within these species, shown how this can be affected through innovative ligand design, and utilised this in order to modify the reactivity of group 14 element complexes. Terrance's persistence, hard work, curiosity and creativity have led to a remarkable body of work which has already seen a strong reception in the literature.

Terrance's work is rooted in a thorough review of the known literature involving the synthesis and reactivity of low-oxidation state group 14 species, and of main-group catalysis. Understanding the importance of coordination environment in regard to the reactivity of a low-oxidation state group 14 element centre has allowed for the development of ligands which are capable of stabilising previously unknown chemical moieties, such as 2-coordinate hydrido tetrylenes, whilst dramatically enhancing their reactivity relative to higher coordinate examples. Ultimately, this has led to the first examples of hydrido tetrylenes being applied in catalytic transformations, with remarkably high activities which are in fact comparable with those for transition metal counterparts. Through stoichiometric studies, Terrance was able to define reaction mechanisms beyond the vast majority of previous reports for related reactions. A highlight of this side of this thesis is the in-depth probing of the reduction of CO_2 with boranes, for which Terrance isolated numerous intermediates, and defined their synthesis and further reactivity in the context of a catalytic cycle. This has given invaluable insight into the transformation of what is likely to become a commodity feedstock, and will undoubtedly aid chemists in designing more efficient catalysts for this process in the future. Terrance's synthetic methodologies for the several landmark complexes he was successful in isolating will surely have a lasting impact in this field, and I have no

doubt that he will move forward to follow a career as a prolific inorganic chemist. It was a delight to have Terrance as a Ph.D. student and as a colleague, and I very much look forward to seeing where his research takes him in the future.

Melbourne
August 2016

Prof. Cameron Jones

Preface

Chapter 1 gives a brief overview of the concepts key to low-oxidation state main-group chemistry. This covers oxidation state and electronic configuration, bonding in the heavier alkenes and alkynes, kinetic stabilisation, and reductive routes to low-oxidation state element complexes.

Chapter 2 summarises bulky ligands commonly used in the kinetic stabilisation of low-oxidation state element species, and the synthesis of group 14 element(II) halide complexes, which act as precursors to further low-oxidation state chemistry. Following from this, the synthesis of novel bulky monodentate amide ligands is discussed, as is their utilisation in the synthesis of group 14 element(II) halide precursors.

Chapter 3 investigates the use of the aforementioned group 14 element(II) halide precursors in the synthesis of amido-substituted heavier alkyne analogues (i.e. LEEL, E = Ge and Sn), and the reactivity thereof. These reactivity studies cover H_2 activation, CO_2 reduction, and cycloaddition/insertion reactions, involving reversible processes and CH-activation. The activation of H_2 led to the isolation of group 14 element(II) hydride species, which have been shown to be in equilibrium with monomeric hydride species in solution (i.e. hydrido tetrelenes). Further increasing the ligand's bulk led to the solid-state characterisation of two examples of monomeric amido Ge(II) hydride species.

Chapter 4 presents the further reactivity of the aforementioned group 14 element (II) hydride species. This culminated in the synthesis of numerous amido alkyl and amido alkoxy germylenes and stannylenes through hydroelementation of aldehydes, ketones, and alkenes. The addition to alkenes was found, in some cases, to be reversible, and led to examples of alkene isomerisation at a Ge(II) centre.

Chapter 5 addresses the use of group 14 element(II) species in catalysis, initially through stoichiometric studies involving germylenes and stannylenes discussed in Chap. 4. The efficient hydroboration of aldehydes and ketones is described, catalysed by Ge(II) and Sn(II) hydride complexes (i.e. those described in Chap. 3), with the mechanism of reaction studied through in depth kinetic experiments and DFT analyses. The efficient hydroboration of CO_2 was also achieved, with rates comparable to those achieved for transition-metal systems. The mechanism of this

reaction has been elucidated to some degree through stoichiometric reactivity studies.

Chapter 6 describes the synthesis of a novel boryl amide ligand, and its use in the stabilisation of low-oxidation state group 14 compounds. This largely acts as a comparison between the electronics and sterics of this ligand and those seen in Chaps. 2–5, and as such highlights the importance in understanding how reactivities involved in this thesis can be affected through ligand modification.

Berlin, Germany Dr. Terrance John Hadlington

Parts of this thesis have been published in the following journal articles

1. Efficient Reduction of Carbon Dioxide to Methanol Equivalents Catalyzed by Two-Coordinate Amido-Germanium(II) and Tin(II) Hydride Complexes; Hadlington, T. J., Hermann, M., Frenking, G., and Jones, C., *accepted to ACS Catalysis*.
2. Stabilization of a Two-Coordinate, Acyclic Diaminosilylene (ADASi): Completion of the Series of Isolable Diaminotetrylenes, :E(NR_2)$_2$ (E = Group 14 Element); Hadlington, T. J., Abdalla, J. A. B., Tirfoin, R., Aldridge, S., and Jones., C., *Chem. Commun.*, **2016**, *52*, 1717–1720.
3. Two-Coordinate Group 14 Element(II) Hydrides as Reagents for the Facile, and Sometimes Reversible, Hydrogermylation/Hydrostannylation of Unactivated Alkenes and Alkynes; Hadlington, T. J., Hermann, M., Frenking, G., and Jones, C., *Chem. Sci.*, **2015**, *6*, 7249–7257.
4. Reactivity of Amido-Digermynes, LGeGeL (L = Bulky Amide), toward Olefins and Related Molecules: Facile Reduction, C−H Activation, and Reversible Cycloaddition of Unsaturated Substrates; Hadlington, T. J., Li, J., Hermann, M., Davey, A., Frenking, G., and Jones C., *Organometallics*, **2015**, *34*, 3175–3185.
5. Two-coordinate Hydrido-Germylenes; Hadlington, T. J., Schwarze, B., Izgorodina, E. I., and Jones, C., *Chem. Commun.*, **2015**, *51*, 6854–6857.
6. Low Coordinate Germanium(II) and Tin(II) Hydride Complexes: Efficient Catalysts for the Hydroboration of Carbonyl Compounds; Hadlington, T. J., Hermann, M., Frenking, G., and Jones, C., *J. Am. Chem. Soc.*, **2014**, *136*, 3028–3031.
7. A Singly Bonded Amido-Distannyne: H_2 Activation and Isocyanide Coordination; T. J. Hadlington and C. Jones, *Chem. Commun.*, **2014**, *50*, 2321–2323.
8. Synthesis and Characterization of Extremely Bulky Amido-Germanium(II) Halide Complexes; T. J. Hadlington, J. Li, C. Jones, *Can. J. Chem.*, **2014**, *92*, 427–433.
9. Activation of H_2 by a Multiply Bonded Amido–Digermyne: Evidence for the Formation of a Hydrido–Germylene; T. J. Hadlington, M. Hermann, J. Li, G. Frenking, and C. Jones, *Angew. Chem.*, **2013**, *52*, 10199–10203; *selected as a* ***Hot Paper***.
10. Synthesis and Crystal Structures of Two Bulky bis(Amido)Germylenes; E. W. Y. Wong, T. J. Hadlington and C. Jones, *Main Group Met. Chem.*, **2013**, *36*, 133–136.

11. Extremely Bulky Amido and Amidinato Complexes of Boron and Aluminium Halides: Synthesis and Reduction Studies; E. W. Y. Wong, D. Dange, L. Fohlmeister, T. J. Hadlington, and C. Jones, *Aust. J. Chem.*, **2013**, *66*, 1144–1154.
12. Utilizing Steric Bulk to Stabilize Molybdenum Aminogermylyne and Aminogermylene Complexes; J. Hicks, T. J. Hadlington, C. Schenk, J. Li, and C. Jones, *Organometallics*, **2013**, *32*, 323–329.

Acknowledgements

First and foremost, I'd like to thank Cameron for his support and guidance throughout the past three and a half years, for giving me the opportunity to learn everything I have over the this time, and helping me in doing so. I'll never forget the importance of following through with every avenue, and the importance of being thorough!! These are lessons I will take with me throughout both my career and life.

To Prof. Simon Aldridge I also extend warm thanks, for allowing me to work alongside him and his research group in Oxford University, and to the members of that group who made me feel welcome (particularly Rémi for beer times). It's always nice to be reminded what real architecture looks like.

To Prof. Gernot Frenking and Markus Hermann, for their continued interest in theoretical studies of our chemistry, which have given valuable insights into numerous individual studies contained herein.

To my family, whom, although several thousand miles away, have supported me when times got tough. Thank you.

And finally, to all of the friends that I've made along the way, at university and otherwise, you have ultimately made my life in Melbourne much more than just studying towards a Ph.D., you're all great.

Contents

Abbreviations

Å	Ångström, 1×10^{-10} m
Ar	A general aryl substituent
Ar*	2,6-$(Ph_2CH)_2$-4-MePh
$Ar^{\dagger}$	2,6-$(Ph_2CH)_2$-4-Pr^iPh
$Ar^{\#}$	2,6-$(Ph_2CH)_2$-4-Bu^tPh
Ar^{∂}	2,6-$(Xyl_2CH)_2$-4-MePh
Ar"	2,6-{(4-$Bu^tPh)_2CH$}-4-MePh
^{Ar}L*	(Ar)(Ar*)N^-, Ar = Ph, Xyl, F6Xyl, Mes, or Tripp
^{Ar}Terph	A tephenyl ligand, with an aryl group (i.e. Mes, Dipp, Tripp) at the 2,6-poistions
Bbt	2,6-{$(TMS)_2CH\}_2$-4-{$(TMS)_3C$}Ph
Bbp	2,6-{$(TMS)_2CH\}_2$Ph
Bu^n	Primary butyl
Bu^t	Tertiary butyl
br	Broad
cal	Calorie (1 kcal = 4.184 J)
COD	Cyclooctadiene
Cy	Cyclohexyl
d	Doublet
decomp.	Decomposition
δ	Chemical shift in NMR spectroscopy (ppm)
ΔE_{hybrid}	The energy of hybridisation in forming *sp*-character bonds
ΔE_{sp}	The energy separating the valence *s* and *p* orbitals
DFT	Density Functional Theory
Dipp	2,6-diisopropylphenyl
^{Dipp}DAB	$[\{N(Dipp)C(H)\}_2]^{2-}$
^{Dipp}nacnac	$[\{(Dipp)NC(CH_3)\}_2CH]^-$
E	An element
e^-	Electron
Et	Ethyl

η^n	Designates coordination to the metal centre in a "side-on" fashion through n atoms
F6Xyl	3,5-$(CF_3)_2$Ph
HMDS	Hexamethyldisilazane
HOMO	Highest Occupied Molecular Orbital
Hz	Hertz, s^{-1}
Pr^i	*Iso*-propyl
^{iPr}L*	$(Pr^i{}_3Si)(Ar^*)N^-$
^{iPr}L†	$(Pr^i{}_3Si)(Ar^\dagger)N^-$
^{iPr}L$^\partial$	$(Pr^i{}_3Si)(Ar^\partial)N^-$
^{iPr}L"	$(Pr^i{}_3Si)(Ar^\#)N^-$
IR	Infra Red
J	Joule
$^nJ_{E,E'}$	Coupling constant between nuclei E and E' separated by n bonds (Hz)
K	Kelvin
κ	Designates a chelate ring that includes one or more dative bonds
L	A ligand
LUMO	Lowest Unoccupied Molecular Orbital
M	A metal
m	Molar (mol L^{-1})
M^+	A molecular ion
m	Multiplet (NMR); Medium (IR)
Me	Methyl
Mes	2,4,6-trimethylphenyl
Mes*	2,4,6-tri-*tert*-butylphenyl
^{Mes}nacnac	$[\{N(Mes)C(CH_3)\}_2CH]^-$
^{Mes}nacnac^{tBu}	$[\{N(Mes)C(Bu^t)\}_2CH]^-$
MG	Main-Group
mol	Mole
M.P.	Melting Point
MS	Mass Spectrometry
μ	Designates a bridging atom, or subunit, in a molecular structure
nacnac	A general β-diketiminate ligand
NBO	Natural Bond Order
NHC	N-heterocyclic carbene
NMR	Nuclear Magnetic Resonance
OA	Oxidative Addition
Ph	Phenyl
^{PhMe}L*	$(Ph_2MeSi)(Ar^*)N^-$
^{PhSi}L*	$(Ph_3Si)(Ar^*)N^-$
ppm	Parts per million
q	Quartet
R	General organic substituent
RE	Reductive Elimination

s	Singlet (NMR); Strong (IR)
sept	Septet
t	Triplet
Tbt	2,6-{$(TMS)_2CH$}$_2$-4-{$(TMS)_2CH$}Ph
^{tBuO}L*	{$(Bu^tO)_3Si$}(Ar*)N^-
^{tBuO}L†	{$(Bu^tO)_3Si$}($Ar^\dagger$)N^-
^{tBuO}L$^\partial$	{$(Bu^tO)_3Si$}(Ar^∂)N^-
TM	Transition Metal
TMS	Trimethylsilyl
^{TMS}L*	(TMS)(Ar*)N^-
^{TMS}BoN$^-$	(TMS){(^{Dipp}DAB)B}N^-
^{tBu}nacnac	[{(Dipp)NC(t Bu)}$_2$CH]$^-$
Trip	2,4,6-triisopropylphenyl
UV	Ultra Violet
v	Very
VT	Variable Temperature
w	Weak
ν/cm^{-1}	Wavenumber
X	A halide
Xyl	3,5-dimethylphenyl

Chapter 1
General Introduction

Contrary to the wide ranging nature of *d*- and *f*-block chemistry, that of the *s*- and *p*-block elements has classically been accepted as limited to one or two stable oxidation states outside of the elemental species, thus curtailing the broader reactivity of compounds involving these elements. However, the past two decades have seen tremendous growth in the area of low-oxidation state and low-coordinate main-group (MG) chemistry, resulting in an expansion of readily available oxidation states for MG elements. This has often led to reactivity that has drawn comparisons to that of transition-metals (TM) [1]. There are a number of concepts key to the understanding of this relatively new area of chemistry, which this introduction shall attempt to succinctly address.

1.1 Low-Oxidation State Main-Group Chemistry

In knowing the reluctance of MG elements to deviate from their classical oxidation states, chemists have tried for many years to stabilise complexes containing MG elements in non-classical oxidation states; such is the area of low-oxidation state MG chemistry. As the name states, this is chemistry involved in stabilising complexes containing MG elements in oxidation-states between their common oxidation state and the zero oxidation state. Theoretically this is difficult to achieve due to the propensity of such compounds to disproportionate to the element and compounds containing the element in its classically stable oxidation state. In addition, they can undergo oligomeristaion reactions. In contemporary chemistry, bulky ligands are utilised in order to kinetically stabilise such compounds, and to allow analysis of their electronic structures and their reactivity.

T.J. Hadlington, *On the Catalytic Efficacy of Low-Oxidation State Group 14 Complexes*, Springer Theses, DOI 10.1007/978-3-319-51807-7_1

1.2 Oxidation States and the Inert-Pair Effect

Central to any inorganic chemical transformation is the oxidation state of the elements involved. This relates to the number of electrons associated to an element, or perhaps more clearly, the charge remaining on an element when all bonds to different atoms have been removed [2]. Note that bonds to the same element don't affect the oxidation state due to the two element centres having the same electronegativities, and hence the electrons in said bond are evenly distributed between these two element centres.

As stated, the elements of the MG differ greatly from the TMs, largely due to the latter having access to a variety of oxidation states [3]. Generally, these have little energy barrier between them, allowing for facile oxidative addition (OA) and reductive elimination (RE) type reactivity, and related small-molecule activation processes. Elements of the *s*-block classically can only access +1 (group 1) and +2 (group 2) oxidation states, with the lighter *p*-block elements following a similar trend related to their valence electron count. The only real deviation from the common single oxidation-state trend in the MG occurs upon descending the p-block, leading to what is known as the Inert Pair effect [4].

As an example, group 14 elements hold four valence electrons, and have the general electronic configuration ns^2p^2, leading to tetravalent compounds being common for the lighter group 14 elements (C, Si, Ge, Sn). However, the heaviest element, lead, favourably maintains a +2 oxidation state in its compounds, with the remaining two electrons forming a lone-pair [4]. This arises from the increase in the energy of hybridisation, E_{hybrid}, as the group is descended; the n*s* and n*p* energy gap (ΔE_{sp}) increases as the *s*-orbitals contract with the increased nuclear charge [5]. Due to the proximity of the 1*s* orbital to the nucleus, its electrons accelerate to near the speed of light for the heavier elements (i.e. Pb in group 14), and hence gain mass, with concomitant contraction of the valence *s*-orbital. Due to the angular momentum related to the *p*-orbitals, this does not have such a great effect on the core *p*-orbital. This 'relativistic effect' directly causes an increase in E_{hybrid} due to the resulting large energy gap between the valence *s*- and *p*-orbitals, and hence the energy of forming bonds using *s*-electrons is large for the heavier elements. This is also the case for remaining 6th period *p*-block elements. Whilst lead rarely utilises *s*-block electrons in bonding, the remaining heavier group 14 elements (Si, Ge, Sn) also have large ΔE_{sp} values relative to carbon, and hence the degree of *sp*-mixing in bonding in complexes of Si, Ge, and Sn is greatly reduced, relative to C (vide infra). It is worthy of note that, in the context of low-oxidation state group 14 chemistry, that if the energy barrier between the +2 and +4 oxidation states could be made narrow for a given element, then TM-type reactivity could theoretically be achieved (i.e. OA and RE).

1.2.1 Bonding in the Heavier Ditetrelenes

The understanding of bonding in low oxidation state MG complexes has developed greatly over the previous 40 years. Early calculations suggested that multiple bonding was not possible between heavier MG elements. This hypothesis was coined the "Double Bond rule", whereby inner-shell repulsion between two *p*-block elements with quantum numbers greater than or equal to 3 prevents sufficient *p*-orbital overlap to form a sufficiently strong π-bond [6, 7]. Related studies suggested that this phenomenon was due to the relatively greater strength of *s*- or *p*-based σ-bonds over *s*- or *p*-based π-bonds in such compounds [8].

This rule, of course, has since been disproved. In 1974, the structural characterisation of the divalent tin species, $\{(TMS)_2CH\}_2Sn$ (TMS = $[Me_3Si]^-$) revealed it to in fact be the Sn=Sn bonded dimer [9], $[\{(TMS)_2CH\}_2Sn]_2$ (Scheme 1.1), with the Sn–Sn distance (2.764(2) Å) being considerably shorter than the average Sn–Sn single bond (mean of published Sn–Sn bonds = 2.993 Å). Importantly, the two C–Sn–C fragments are *trans*-pyramidalised out of the plane of the double bond, much unlike the planar configuration of alkenes, thus giving the first experimental evidence for the differing hybridisation in the bonding in alkenes and the heavier congeners thereof. In 1981, both the groups of West and Yoshifuji reported on further dimeric *p*-block compounds in non-classical oxidation states. These featured element-element multiple bonds, involving silicon(II) ($\{(Mes)_2Si\}_2$, Mes = 2,4,6-Me_3Ph) and phosphorus(I) $\left(\{(Mes*)P\}_2, Mes* = 2,4,6-Bu^t_3Ph\right)$, respectively (Scheme 1.1) [10, 11]. As a side note, whilst the synthesis of the P(I) dimer involved an alkaline-earth metal reduction (vide infra), the disilene was generated through irradiation of a formally Si(II) species ($Mes_2Si(TMS)_2$), which, at low-temperatures formed a monomeric acyclic silylene, Mes_2Si:, through elimination of dimeric Me_6Si_2. Monomeric acyclic silylenes are extremely rare even today, and are highly reactive. Hence, the reactivity of this intermediate will be discussed in more depth where relevant (Chap. 6).

As is the case with $[\{(TMS)_2CH\}_2Sn]_2$, both $(\{(Mes)_2Si\}_2$ and $\{(Mes*)P\}_2$ feature *trans*–pyramidalised structures. This can be explained through the ΔE_{sp} for the heavier *p*-block elements: as this energy gap increases down a group, so does the potential energy of mixing of these orbitals (viz. *sp*-hybridisation in alkanes, alkenes, and alkynes). For parent EH_2 species (E = C, Si, Ge, Sn and Pb), this relates to the singlet-triplet gap at the element centre: for carbon, this gap was in fact found to be negative, at −14 kcal mol^{-1}, resulting in a triplet carbene, which dimerises to form what we call an sp^2 hybridised C=C bond (Fig. 1.1) [12]. The heavier elements have a greater singlet-triplet gap, directly related to their ΔE_{sp} values (Si, Ge, Sn, and Pb = 16.7, 21.8, 24.8, and 34.8 kcal mol^{-1}, respectively), and hence are more stable in the singlet state (i.e. ns^2p^0) [12]. The E=E bond for these species, then, involves donation of an sp^2-character lone-pair of electrons on one E to an empty *p*-orbital on another (Fig. 1.1). Thus, the *trans*-pyramidalisation of, say, $[\{(TMS)_2CH\}_2Sn]_2$ is borne out of the need for such a geometry to allow for adequate overlap of a filled sp^2-character orbital on one element centre with an

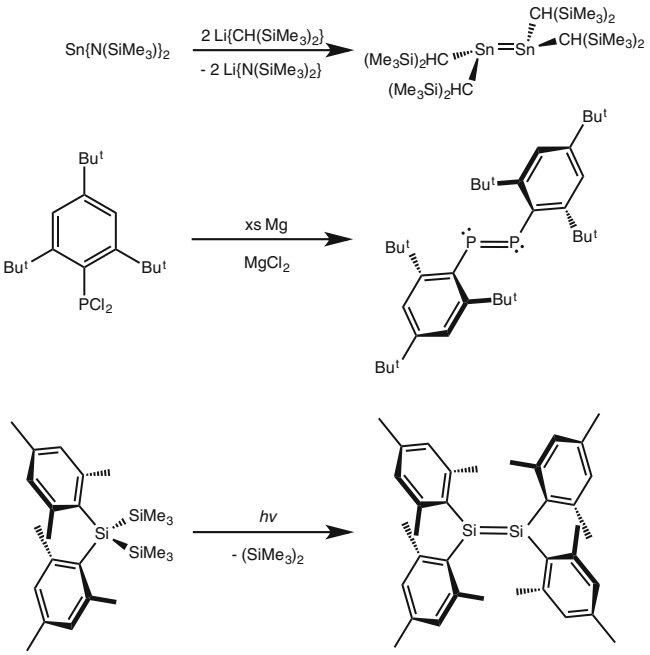

Scheme 1.1 Synthesis of the first examples of element-element multiply bonded main-group species

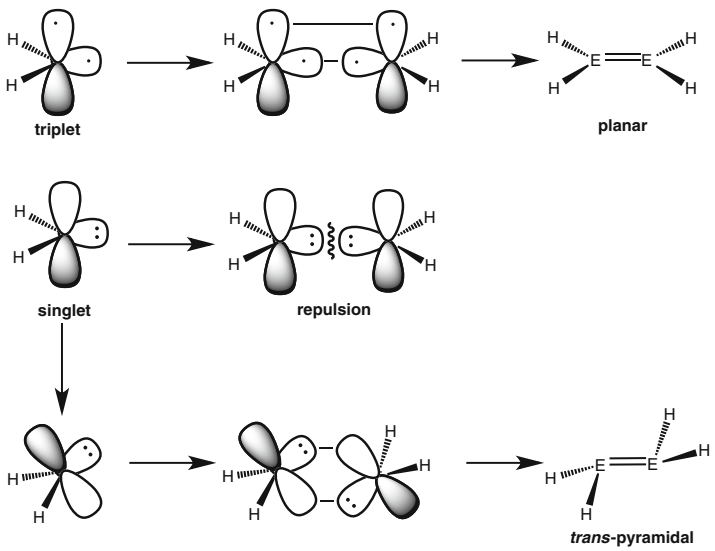

Fig. 1.1 Dimerisation of singlet and triplet EH_2 fragments (E = C-Pb)

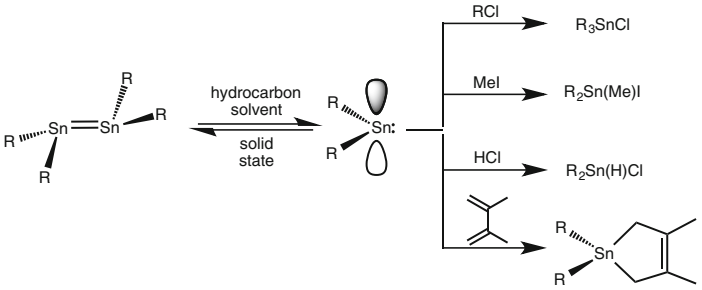

Scheme 1.2 Reactivity of the *pseudo*-monomeric stannylene, R_2Sn (R=CH(SiMe$_3$)$_2$)

empty *p*-orbital on its neighbour (Fig. 1.1). Due to the increased stability of the singlet state as group 14 is descended, so the *trans*-pyramidalisation effect is amplified for the heavier congeners of doubly E–E bonded group 14 species, with many planar disilene species now known [13–16].

It is worthy of note that, given the dative nature of the bonding in the heavier ditetrelenes, they may exist as monomeric species (viz. carbenes). Indeed, the seminal work of Lappert exemplified this, whereby small ligand modifications led to either monomeric or dimeric tetrelenes in the solid state [17, 18]. Further, the dimeric Sn(II) species, $[\{(TMS)_2CH\}_2Sn]_2$, is monomeric in hydrocarbon solvents, as is its germanium counterpart, $\{(TMS)_2CH\}_2Ge$ [17, 18]. Due to their relatively narrow HOMO-LUMO gaps, bond activations can occur at such group 14 element (II) centres (e.g. oxidative addition, [4+1] cycloaddition) [19, 20]. This concept is central to the potential application of group 14 elements in catalysis, and will be discussed in more depth in Chap. 5. Examples of such reactivity reported by Lappert and co-workers are outlined in Scheme 1.2 [20].

1.2.2 Bonding in the Heavier Ditetrylynes

In line with the observations described in Sect. 1.2.1, the bonding situation in the heavier alkyne analogues, LEEL (L = a ligand, E = Si–Pb), also sees significant variation with changing degrees of valence *sp*-mixing, which decreases down group 14 with increased effective nuclear charge. Computational work by Nagase and co-workers predicted the lowest energy geometries for the parent heavier alkyne analogues, HEEH, which in fact revealed the dibridged/butterfly structures, E(μ-H)$_2$E, to be the energy minima for all heavier elements of group 14 (Si–Pb) [21–23]. Where H was replaced by bulkier substituents, however, these minima disappeared from the calculated potential energy surface [22, 24, 25]. Importantly, for the HEEH species, a linear structure, comparable to that of acetylene (HCCH), was relatively unstable in all cases, collapsing to a *trans*-bent structure [21]. The energy gain on isomerisation was also seen to increase as the group was descended (i.e. 36.3 kcal mol^{-1} gain from Si $\rightarrow$ Pb). Both observations relate to the increase in

ΔE_{sp} as the group is descended. In a similar fashion to the hypothetical fragment CH_2, CH has a low lying quartet ground state due to its ΔE_{sp} being extremely narrow (16.7 kcal mol^{-1}) [26], thus allowing for hybridisation. This leads to direct triple bond formation with no geometry change at the CH fragment (Fig. 1.2). The quartet ground state is unstable for the remaining members of group 14, with the doublet state being the lowest energy form of EH (E = Si–Pb) [21]. Hence, the one *p*-orbital radical can form a single π-bond, whilst the *sp*-character lone-pair of electrons effectively forms a dative bond with an empty *p*-orbital of the neighbouring E (Fig. 1.2) (viz. dimerisation of EH_2 fragments).

Further to this, as the *sp*-character lone-pair becomes higher in *s*-character as the group is descended, it becomes less involved in bonding interactions. That is, the propensity for the formation of a dative double bond between the two element centres decreases, and the bond order tends towards 1. This has been experimentally observed by Power and co-workers [27], and will be discussed in Chap. 3. By this trend, the heavier alkyne analogues can exist in bonding modes between the extremes, **i** and **ii** (Scheme 1.3), having resonance forms **iii** and **iv**. The diradicaloid

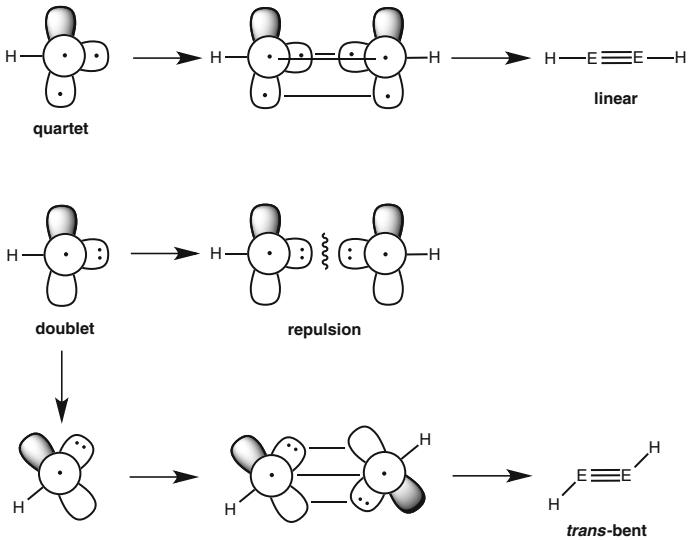

Fig. 1.2 The dimerisation of doublet and quartet EH fragments (E = C-Pb)

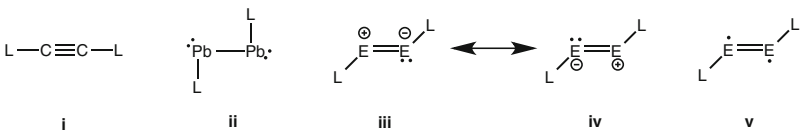

Scheme 1.3 Canonical forms of the ditetrylynes

canonical form, **v**, is perhaps the most interesting of these possible bonding modes, potentially being highly reactive. Indeed, for silicon and germanium alkyne analogues this diradicaloid character has been calculated to be significant, and is a potential reason behind their greater reactivity relative to the tin and lead congeners (see Chap. 3) [28]. This radical character is thought to arise from the effective "slipping" of the $\pi_{\text{in-plane}}$ bonding of heavier alkyne analogues upon forming *trans*-bent structures, allowing for mixing of this bonding orbital with the σ*-orbital, thus forming an essentially non-bonding orbital with lobes on each Ge centre, i.e. a diradicaloid. This is in keeping with bond orders observed in structurally characterised aryl-digermynes, which are generally close to 2 [1, 28].

1.2.3 Kinetic Stabilisation

The thermodynamic instability of low-oxidation state main-group species played a key role in the belated development of their chemistry. The attempted isolation of such species prior to the last two to three decades has been thwarted by their tendency to either oligomerise, due to the relative weakness of their multiple bonds, or disproportionate due to the thermodynamic instability of their non-classical oxidation states [29–32]. In order to overcome these issues, kinetic stabilisation is employed. As such, the use of bulky and/or chelating ligands increases the energy barrier to oligomerisation and disproportionation, thus stabilising these otherwise inaccessible compounds. Since such a realisation, a huge number of species have be synthesised using this kinetic stabilisation method [14]. The ligands used in such chemistry are broadly discussed in Chap. 2.

1.2.4 Accessing Low-Oxidation State Main-Group Complexes

The synthesis of low-oxidation state main-group complexes is a constantly expanding field, largely due to the great level of interest in the further reactivity of these species. The routes taken to access such complexes have therefore also seen major developments over the past two decades. Whilst some more niche routes have been taken (e.g. West's irradiation of a tetravalent Si species in the synthesis of the Si(II) compound, $\{(Mes)_2Si\}_2$), there are two more common routes to such complexes: utilising readily available low-oxidation state precursors (e.g. in the synthesis of $[\{CH(SiMe_3)_2\}Sn]_2$), and the reduction of higher oxidation state precursors (e.g. in the synthesis of $\{(Mes^*)P\}_2$).

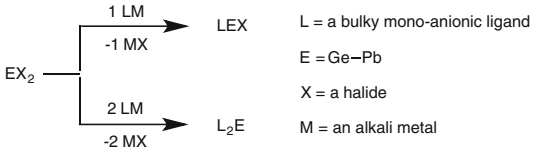

Scheme 1.4 Salt metathesis reactions involving group 14 element(II) dihalides

1.2.4.1 Salt-Metathesis with Low-Oxidation State Halide Sources

Whilst compounds of the group 14 elements in the +2 oxidation state are not hard to come by, they are still classed as low-oxidation state. They can be relatively easily accessed through utilisation of the element(II) dihalide species, which are readily available for purchase, aside from Si(II) derivatives (vide infra). Thus, salt metathesis reactions involving alkali metal salts of ligands (e.g. amides, alkyls, silyls) have been successfully employed in the synthesis of a plethora of tetrylene analogues, such as $\{(SiMe_3)_2N\}_2E$ (E = Ge–Pb) and $[\{CH(SiMe_3)_2\}E]_2$ (E = Sn, Pb, Scheme 1.4) [17–19]. More recently, examples of mono-metathesis, yielding species of the general formula LEX (L = a bulky ligand, E = Ge–Pb, X = a halide) have been reported (Scheme 1.4) [33, 34], and these products used for further low-oxidation state chemistry (e.g. reduction to E(I) complexes). More specific examples of the synthesis of such kinetically stabilised halides will be discussed in Chap. 2.

1.2.4.2 Reduction of Element Halide Precursors

Group 14 element(II) halide complexes, precursors to lower oxidation state species, can generally be accessed from element dihalides, as described above. For silicon, however, there are no readily available Si(II) dihalide species, and hence it is not uncommon to access low oxidation state Si compounds by reduction of Si(IV) trihalide precursor compounds. There are numerous reducing agents available, in that one only requires a species whose reduction potential is greater than that of the species being reduced. Common reducing agents are the elemental alkali metals and alkaline earth metals, both of which form halide species with high lattice enthalpies, which aids in driving the reaction. For example, the diphosphene, $\{(Mes^*)P\}_2$, was synthesised by the reduction of the aryl P(III) dichloride, $(Mes^*)PCl_2$, with elemental Mg, with the formation of $MgCl_2$. However, one major downside of these highly reducing metals is that their stoichiometric use is not straightforward, often leading to over reduction or decomposition [35, 36].

More recently, carbenes have seen wide use in the reduction of Si(IV) species. It was found that the addition of two equivalents of the NHC (NHC = N-heterocyclic carbene), $IPr\left(IPr =: C[N(Dipp)C(H)]_2, Dipp = 2,6 - Pr^i_2Ph\right)$, to $SiCl_3H$ resulted

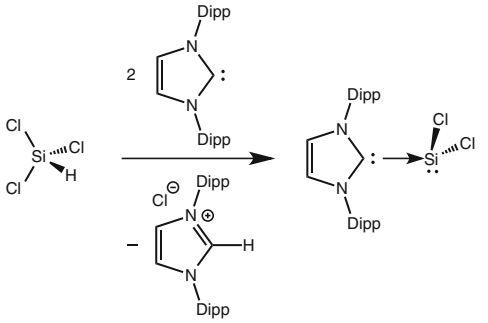

Scheme 1.5 The reduction of $SiCl_3H$ to IPr.$SiCl_2$ with IPr

in the reductive formation of IPr.$SiCl_2$, with concomitant formation of IPr.HCl as an insoluble by-product (Scheme 1.5) [37]. This is particularly useful in that the NHC is hydrocarbon-soluble, and so can be accurately used in stoichiometric quantities. The Si(II) product, IPr.$SiCl_2$, has seen further use as a silicon(II) dihalide precursor [38], but is as yet not widely available. This route has been employed in related silicon and tin chemistry, for example using alternative NHCs and Si(IV) precursors (e.g. the reduction of $\left(Bu^t_3Si\right)Si(H)_2Cl$); and in the reduction of Sn(IV) starting materials (e.g. $(Tripp)SnH_3, Tripp = 2,4,6{-}Pr^i_3Ph$; see Chap. 4) [39, 40].

One highly important reducing agent, which has been widely applied during studies reported herein, is the Mg(I) dimer synthesised in our group, $\{(^{Mes}nacnac)Mg\}_2$ ($^{Mes}nacnac = [HC\{N(Mes)C(Me)\}]^-$). In itself the compound is fundamentally important, being one of the first examples of a species containing a Mg–Mg bond [41, 42]. Further to this, however, as the compound holds two Mg(I) centres, it acts as a two-centre two-electron reducing agent [42, 43]. This species overcomes problems encountered with commonly used alkali metal reducing agents, in that it is a relatively mild reductant, and so is not seen to over reduce complexes. In addition, it is a hydrocarbon soluble crystalline solid, aiding in its stoichiometric use and controlled addition. By-products of halide reductions using $\{(^{Mes}nacnac)Mg\}_2$ are $\{(^{Mes}nacnac)MgX\}_2$ complexes (X = a halide), which are generally insoluble in common hydrocarbon solvents. This acts as an entropic driving force, in addition to aiding reaction work-up. Such Mg(I) dimers have seen wide successful in the reduction of numerous complexes of MG elements and TMs, as well is in the reductive transformation of small-molecules such as CO_2 and azides (e.g. see Scheme 1.6) [44–46].

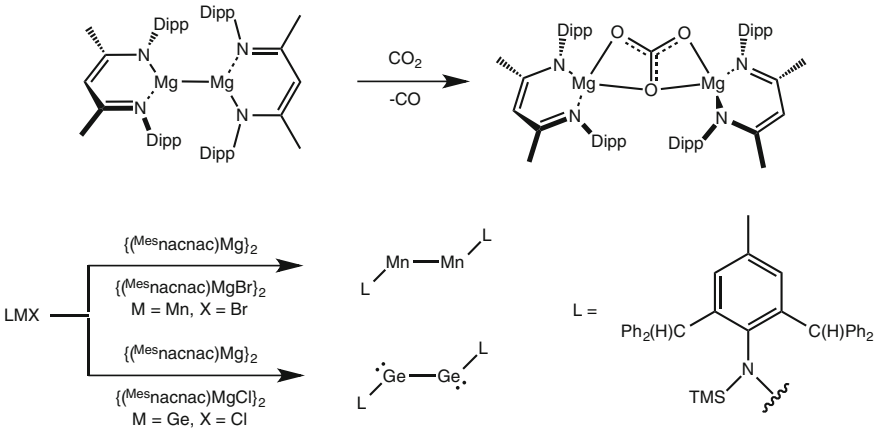

Scheme 1.6 The utilisation of Mg(I) dimers as facile two-centre two-electron reducing agents in both organic and inorganic transformations

References

1. Power PP (2010) Main-group elements as transition metals. Nature 463:171
2. Parkin G (2006) Valence, oxidation number, and formal charge: Three related but fundamentally different concepts. J Chem Educ 83:791
3. Cotton FA, Wilkinson G, Murillo CA, Bochmann M (1933) Advanced inorganic chemistry, 6th ed. Wiley, Chichester, United Kingdom
4. Sidgwick NV (1933) Ann Rep 20:120
5. Pyykkö P (1988) Relativistic effects in structural chemistry. Chem Rev 88:563
6. Goubeau J (1957) Mehrfachbindungen in der anorganischen chemie. Angew Chem 69:77
7. Jutzi P (1975) New element-carbon (p-p)π bonds. Angew Chem Int Ed 14:232
8. Mulliken RS (1950) Overlap integrals and chemical binding. J Am Chem Soc 72:4493
9. Goldberg DE, Harris DH, Lappert MF, Thom KM (1976) A new synthesis of divalent group 4B alkyls M[CH($SiMe_3$)$_2$]$_2$(M = Ge or Sn), and the crystal and molecular strcuture of the tin compound. JCS Chem Comm 120:261
10. West R, Fink MJ, Michl J (1981) Tetramesityldisilene, a stable compound containing a silicon-silicon double bond. Science 214:1343
11. Yoshifuji M, Shima I, Inamoto N (1981) Synthesis and structure of bis (2,4,6-tri-tert-butylphenyl)diphosphene: isolation of a true phosphobenzene. J Am Chem Soc 103:4587
12. Trinquier G (1990) Double bonds and bridged structures in the heavier analogs of ethylene. J Am Chem Soc 112:2130
13. Shepherd BD, Powell DR, West R (1989) Synthesis, geometrical isomerism, and crystal structure of a highly hindered disilene. Organometallics 8:2664
14. Kira M, Maruyama D, Kabuto C, Ebata K, Sakurai H (1994) Stable tetrakis(trialkylsilyl)-disilenes; synthesis, X-ray structures, and UV/VIS spectra. Angew Chem Int Ed 33:1489
15. Kobayashi M, Hayakawa N, Nakabayashi K, Matsuo T, Hashizume D, Fueno H, Tanaka K, Tamao K (2014) Highly coplanar (E)-1,2-Di(1-naphthyl)disilene Involving a distinct CH–π interaction with the perpendicularly oriented protecting eind group. Chem Lett 4:432
16. Fischer RC, Power PP (2010) π-bonding and the lone pair effect in multiple bonds involving heavier main group elements: Developments in the new millennium. Chem Rev 110:3877

17. Davidson PJ, Harris DH, Lappert MF (1976) Subvalent Group 4B metal alkyls and amides. Part I. The synthesis and physical properties of kinetically stable bis[bis(trimethysilyl) methyl]-germanium(II), -tin(II), and -lead(II). JCS Dalton 6:2268
18. Fjeldberg T, Schilling BER, Thorne AJ, Haaland A, Lappert MF (1986) Subvalent Group 4B metal alkyls and amides. Part 8. Germanium and tin carbene analogues MR_2[M = Ge or Sn, R = $CH(SiMe_3)_2$]: syntheses and structures in the gas phase (electron diffraction); molecular-orbital calculations for MH_2 and $GeMe_2$. J Chem Soc Dalton Trans 5:1551
19. Hitchcock PB, Jasim HA, Lappert MF, Leung W, Rai AW, Taylor RE (1991) Subvalent group 14 metal compounds-XIII. Oxidative addition reactions of germanium and tin amides $M(NR_2)_2$ (R = $SiMe_3$, M = Ge OR Sn) with sulphur, selenium, tellurium or MeOOCC=CCOOMe; X-ray structures of $[Ge(NR_2)_2(\mu\text{-Te})]_2$ and Polyhedron 10:1203
20. Cotton JD, Davidson PJ, Lappert MF (1976) Subvalent Group 4B metal alkyls and amides. Part II. The chemistry and properties of bis[bis(trimethylsilyl)methyl]tin(II) and its lead analogue. J Chem Soc Dalton Trans 6:2275
21. Nagase S, Kobayashi K, Takagi N (2000) Triple bonds between heavier Group 14 elements. A theoretical approach. J Organometall Chem 611:264
22. Colegrove BT, Schaefer HF III (1990) Disilyne (Si_2H_2) revisited. J Phys Chem 94:5593
23. Höhn MM, Amos RD, Kobayashi R, Handy NC (1993) Structure and properties of disilyne. J Chem Phys 98:7107
24. Takagi N, Nagase S (2001) Substituent effects on germanium−germanium and tin−tin triple bonds. Organometallics 20:5498
25. Chen Y, Hartmann M, Diedenhofen M, Frenking G (2001) Turning a transition state into a minimum—the nature of the bonding in diplumbylene compounds RPbPbR (R=H, Ar). Angew Chem Int Ed 40:2052
26. Huber KP, Herzberg G (1979) Molecular spectra and molecular structure, vol. IV, Van Nostrand–Rheinhold, New York
27. Pu L, Twamley B, Power PP (2000) Synthesis and characterization of 2,6-$Trip_2H_3C_6PbPbC_6H_3$-2,6-$Trip_2$ (Trip = C_6H_2-2,4,6-*i*-Pr_3): A Stable heavier group 14 element analogue of an alkyne. J Am Chem Soc 122:3524
28. Jung Y, Brynda M, Power PP, Head-Gordon M (2006) Ab initio quantum chemistry calculations on the electronic structure of heavier alkyne congeners: Diradical character and reactivity. J Am Chem Soc 128:7185
29. Kipping FS, Sands JE (1921) XCIII.—Organic derivatives of silicon. Part XXV. Saturated and unsaturated silicohydrocarbons, Si_4Ph_8. J Chem Soc Trans, 830
30. Erlich P (1907) Lancet 173:351
31. Kohler H, Michaelis A (1877) Ueber phenylphosphin und phosphobenzol (diphosphenyl). Ber Dtsch Chem Ges 10:807
32. Cowley AH (1984) Double bonding between the heavier main-group elements: From reactive intermediates to isolable molecules. Polyhedron 3:389
33. Li J, Stasch A, Schenk C, Jones C (2011) Extremely bulky amido-group 14 elementchloride complexes: Potential synthons for low oxidation state main group chemistry. Dalton Trans 40:10448
34. Pu L, Olmstead MM, Power PP (1998) Synthesis and characterization of the monomeric terphenyl−metal halides Ge(Cl){C_6H_3-2,6-$Trip_2$} (Trip = C_6H_2-2,4,6-*i*-Pr_3) and Sn(I){C_6H_3-2,6-$Trip_2$} and the terphenyl−metal amide Sn{$N(SiMe_3)_2$}{C_6H_3-2,6-$Trip_2$}. Organometallics 17:5602
35. Su J, Li XW, Crittendon RC, Robinson GH (1997) How short is a -Ga:Ga- triple bond? synthesis and molecular structure of Na_2[Mes*$_2C_6H_3$-Ga:Ga-C_6H_3Mes*$_2$] (Mes* = 2,4,6-*i*-$Pr_3C_6H_2$): The first gallyne. J Am Chem Soc 119:5471
36. Pu L, Senge MO, Olmstead MM, Power PP (1998) Synthesis and characterization of Na_2{Ge(C_6H_3-2,6-$Trip_2$)}$_2$ and K_2{Sn(C_6H_3-2,6-$Trip_2$)}$_2$(Trip = -C_6H_2-2,4,6-*i*-Pr_3): A new class of multiply bonded main group compounds. J Am Chem Soc 120:12682
37. Ghadwal RS, Roesky HW, Merkel S, Henn J, Stalke D (2009) Lewis base stabilized dichlorosilylene. Angew Chem 121:5793

38. Ghadwal RS, Azhakar R, Roesky HW (2013) Dichlorosilylene: A high temperature transient species to an indispensable building block. Acc Chem Res 46:444
39. Inoue S, Eisenhut C (2013) A dihydrodisilene transition metal complex from an N-heterocyclic carbene-stabilized silylene monohydride. J Am Chem Soc 135:18315
40. Sindlinger CP, Wesemann L (2014) Hydrogen abstraction from organotin di- and trihydrides by N-heterocyclic carbenes: a new method for the preparation of NHC adducts to tin(II) species and observation of an isomer of a hexastannabenzene derivative [R_6Sn_6]. Chem Sci 5:2739
41. Green SP, Jones C, Stasch A (2007) Stable magnesium(I) compounds with Mg-Mg bonds. Science 318:1754
42. Bonyhady SJ, Jones C, Nembenna S, Stasch A, Edwards AJ, McIntyre GJ (2010) β-diketiminate-stabilized Magnesium(I) dimers and Magnesium(II) hydride complexes: Synthesis, characterization, adduct formation, and reactivity studies. Chem Eur J 16:938
43. Stasch A, Jones C (2011) Stable dimeric magnesium(I) compounds: from chemical landmarks to versatile reagents. Dalton Trans 40:5659
44. Lalrempuia R, Stasch A, Jones C (2013) The reductive disproportionation of CO2 using a magnesium(I) complex: analogies with low valent f-block chemistry. Chem Sci 4:4383
45. Fohlmeister L, Liu S, Schulten C, Moubaraki B, Stasch A, Cashion JD, Murray KS, Gagliardi L, Jones C (2012) Low-coordinate Iron(I) and Manganese(I) dimers: Kinetic stabilization of an exceptionally short Fe-Fe multiple bond. Angew Chem Int Ed 51:8294
46. Li J, Schenk C, Goedecke C, Frenking G, Jones C (2011) A digermyne with a Ge–Ge single bond that activates dihydrogen in the solid state. J Am Chem Soc 133:18622

Chapter 2
The Development of Extremely Bulky Amide Ligands and Their Application to the Synthesis of Group 14 Element(II) Halide Complexes

2.1 Introduction

As described in Chap. 1, the isolation of some of the first examples of low-oxidation state main-group (MG) complexes has involved the use of sterically demanding and poly-dentate ligand systems, which kinetically stabilise reactive element centres. Two main classes of mono-anionic ligand have been successfully applied in such MG chemistry: chelating ligands and mono-dentate ligands. Here, some of the more important examples of such ligands will be discussed, as will their use in the synthesis of group 14 element halide complexes.

2.1.1 The Use of Sterically Demanding Chelating Ligands in Group 14 Element(II) Chemistry

The large majority of examples of low-oxidation state MG complexes have involved the use of chelating ligands for the stabilisation of the reactive element centre [1–4]. Logically, the higher coordination environment at the element is beneficial on the grounds that potentially reactive frontier orbitals are occupied, and a lesser propensity of the species towards aggregation is achieved in solution and the solid state. For the sake of this discussion, only three classes of such ligands will be considered here (Fig. 2.1).

These ligand classes have seen extremely wide use. Their complexes have been successfully utilised in numerous applications, such as in lanthanide catalysed transformations [5–7], as chemical vapour deposition (CVD) precursors [1, 5–8], and in the synthesis of a plethora of low-oxidation state transition metal (TM) and MG element species [9–11]. Further, they are relatively straightforward to synthesise, and, importantly, are easily diversified in their electronics and steric encumbrance. Here, their general syntheses will be briefly discussed, along side

T.J. Hadlington, *On the Catalytic Efficacy of Low-Oxidation State Group 14 Complexes*, Springer Theses, DOI 10.1007/978-3-319-51807-7_2

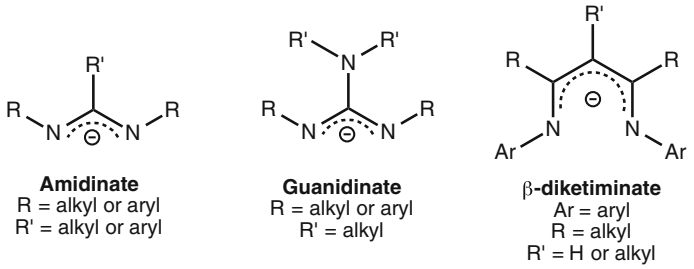

Fig. 2.1 Examples of widely utilised nitrogen-donor anionic chelating ligands

their use in the synthesis of MG, and specifically group 14 element halide complexes.

Of relevance to the chemistry in this thesis are the N,N′-bis(aryl) amidinates, which are readily accessible by two routes. The simplest of such ligands (R = Ar, R′ = H, Fig. 2.1) can be synthesised by the condensation of two equivalents of an aniline with ortho-formate, with the loss of three equivalents of ethanol (Scheme 2.1), generating the amidine which can then be deprotonated to give the amidinate. For modified ligand backbones (R′ = aryl or alkyl, Fig. 2.1), the parent bis(aryl) or bis(alkyl) carbodiimide can be reacted with one equivalent of a lithium alkyl or aryl, affording the lithium amidinate [12]. The protonated ligand is formed upon hydrolysis. Related guanidine ligands are largely derived from carbodimide precursors, in a similar route to functionalised amidines. The reaction of an alkali metal salt of a secondary amine with a bis(aryl) carbodiimide forms the alkali metal guanidinate, which can be hydrolysed to give the protonated guanidine (Scheme 2.1) [13]. These methods have been used to generate a diverse array of such pro-ligands, generally with low cost and good availability of the precursors involved.

Scheme 2.1 Common routes to amidine and gunaidine pro-ligands

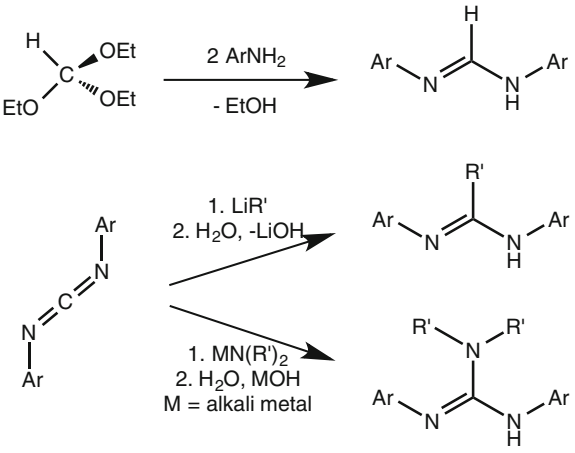

The third class of chelating ligand to be discussed here, the so-called β-diketiminate ligands, are related to the acetyl-acetonate (acac) ligand, which is extremely common in coordination chemistry. Indeed, the simplest route to protonated β-diketimine pro-ligands involves double condensation of an aniline to the acac unit, with trapping of released water (e.g. using Dean-Stark apparatus) aiding reaction completion [14]. Using this method the backbone 'pentyl' unit remains (Fig. 2.1, R = Me, R′ = H), and the aryl substituents can easily be varied. Post-synthetic modification of these systems has been used to introduce a methyl group at the R′ position (Fig. 2.1), by first deprotonation of the backbone, followed by quenching with MeI [15]. Modification of R in these ligands involves an entirely different approach, whereby the ligand is effectively made in two halves, with one being lithiated and recombined with its own precursor in a salt elimination reaction (Scheme 2.2) [16]. Although seemingly negligible, these minor modifications of the ligand backbone have led to surprising differences in reactivity of subsequent complexes [15].

These three classes of pro-ligands are largely utilised in subsequent syntheses via similar routes. That is, deprotonation with an alkali-metal base followed by salt metathesis [17], or ligand exchange/protolysis [17]. Generation of ligated MG compounds has also been achieved by the direct reaction of carbodiimides with *s*- or *p*-block amide or aryl complexes, although this route has been far more prominent in the synthesis of guanidinate complexes [18].

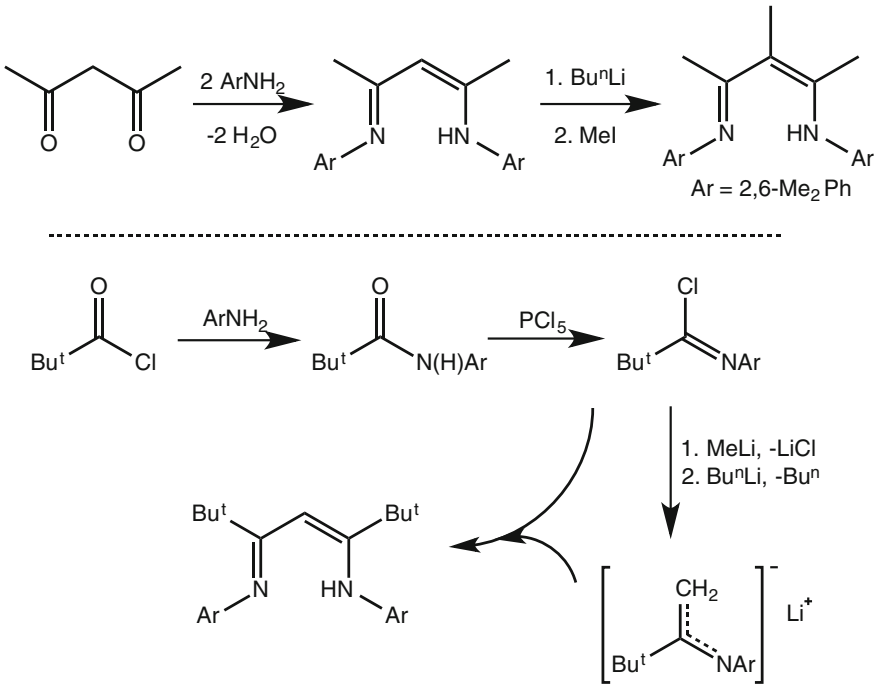

Scheme 2.2 Synthetic routes to general and modified prtonated β-diketimine pro-ligands

The formation of group 14 element(II) species bearing amidinate or guanidinate ligands has almost exclusively involved salt metathesis reactions of alkali metal salts of the ligands with element(II) dihalides. All structurally characterised Ge(II) derivatives are monomeric in the solid state, likely due to both the chelating nature of the ligands and their bulk [19–23]. All bar one example of the Sn(II) derivatives are monomeric, with the one dimeric example having relatively small R groups (R = Bu^t, Fig. 2.1). These are all synthesised via the salt elimination reactions of the Li-salts of the ligands with $SnCl_2$, and are isolated in moderate yields (≥50%) [24–26]. Conversely, all structurally characterised amidinato and guanidinato Pb(II) halides are dimeric in the solid state, with the halide ligands bridging the two metal centres, a testament to the greater ionic radius of lead(II) [27]. The isolated yields of these Pb(II) compounds are much lower than those of the lighter congeners (*ca.* 30%), again likely due to the greater ionic radius of Pb(II), which can lead to subsequent disproportionation and redistribution of the product. Worthy of note is Si(II) amidinate chemistry, due to the rarity of stable Si(II) species. Where ^{tBu}Am was employed (Fig. 2.1, R = Bu^t and R′ = Ph), the Si(IV) trichloride complex, (^{tBu}Am)$SiCl_3$, could be synthesised via salt metathesis. Subsequently reducing this with potassium metal led to the isolation of a rare example of a Si(II) monochloride, (^{tBu}Am)SiCl, albeit in a low yield (10%, Scheme 2.3) [28]. Subsequently, a higher yielding route (90%, Scheme 2.3) to (^{tBu}Am)SiCl was developed, whereby the lithium salt of ^{tBu}Am is reacted with $SiCl_3H$, followed by $Li\{N(TMS)_2\}$ (TMS = $SiMe_3$) (Scheme 2.3) [29]. In all cases the N–C–N–E (E = Si, Ge, Sn, or Pb) central ring is planar, with E–X bonds bent out of the plane due to the presence of a lone-pair of electrons at the group 14 element(II) centres. Generally, the two N–E bonds are of similar length, as are the two C-N backbone bonds, suggesting a delocalised charge across the ligand.

Numerous group 14 element(II) halide complexes have been synthesised using nacnac ligands, with all structurally characterised examples being monomeric in the

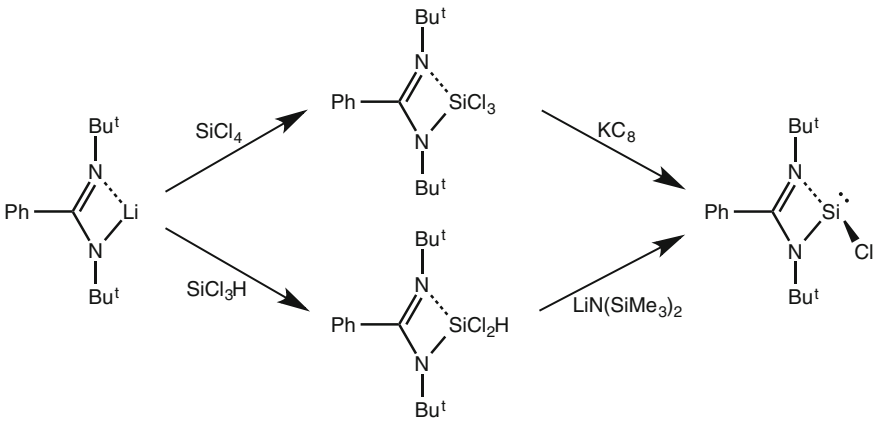

Scheme 2.3 Synthesis of amidinato Si(II) chloride, (^{tBu}Am)SiCl, via two routes

solid state, including those bearing the smaller β-diketiminate ligand, ^{Ph}nacnac (^{Ph}nacnac = $[CH(PhNCMe)_2]^-$). Further, all β-diketiminato Pb(II) halide complexes are monomeric, conversely to amidinato and guanidinato analogues (vide supra). It is likely that this is due to the increased bite angle of the six-membered ring, relative to the four-membered ring formed by complexed amidinates and guanidinates. The increased bite angle leads to a greater effective steric bulk around the element centre, reducing the likelihood of dimerisation. Although no three-coordinate nacnac Si(II) halide species are known, there are three examples stabilised through coordination to a TM fragment, synthesised through addition of HCl to a silylene in the presence of a TM precursor (vide infra.) [30, 31]. Examples of a β-diketiminato germanium(II) fluoride [32], several chlorides [33–35], bromides [36], and one iodide [33] are known, as are related tin(II) [36–38] and lead(II) systems [39, 40].

With the exception of the Bu^t-backbone β-diketiminate complexes, (^{Dipp}nacnac^{tBu})EX (E = Ge or Sn, X = halide; ^{Dipp}nacnac^{tBu} = $[(DippNCBu^t)_2CH]^-$, Dipp = 2,6-Pr^i_2Ph), the central 6-membered rings of β-diketiminato group 14 element(II) complexes are largely planar, with a delocalised ligand charge similar to the amidinate and guanidinate systems, where the two C–N distances are similar, as are the two backbone C–C distances. Again, the E–X bonds in these systems are all bent out of this plane, as one would expect, due to the presence of a stereo-active lone-pair of electrons at the group 14 element (II) centres. All group 14 element(II) species incorporating common β-diketiminate ligands (e.g. ^{Dipp}nacnac = $[(DippNCMe)CH]^-$) are made via salt metathesis routes, with a large number being prepared from in situ generated Li-salts of the β-diketiminate ligands.

2.1.2 *The Use of Sterically Demanding Monodentate Ligands in Group 14 Element(II) Chemistry*

The expansion in the number of monodentate bulky ligands seeing use in low-oxidation state MG chemistry has largely occurred within the past 20 years, stemming from the isolation of the first P–P multiple bond, which relied upon stabilisation by the Mes* ligand (Mes* = 2,4,6-$(Bu^t)_3$Ph) [41]. Since then, extensive work has been carried out on the expansion of such chemistry, leading to the development of novel super-bulky ligands: for example, two classes of aryl-based ligand sets, and one class of super-bulky monodentate amide ligands have been developed, which will be discussed here. The latter has been pioneered by our group, and the former by the groups of Power and Tokitoh, independently. Accounts of alternative bulky ligands have also been seen (e.g. Sekiguchi's anionic silyl ligand, $[Si(TMS)_2(Pr^i)]^-$) [42], which shall not be considered here. They will, however, be discussed in later chapters where relevant.

The ligand class developed by Power's group involves a terphenyl unit; that is, a central phenyl ring, with flanking phenyl rings at the *ortho*-positions, with *meta*-

and *para*-substitution in some cases. Although examples of these were initially synthesised by other groups [43], Power's group pioneered their development into far more bulky and electronically diverse ligands, in addition to their use in a diverse range of chemistries. Some examples of these ligands are given in Scheme 2.4. Generally, these are synthesised by the reaction of, first, in situ generated 2,6-dichlorophenyl magnesiumbromide, via reaction of 2,6-dichloro-1-iodobenzene with ethyl magnesiumbromide. This is then reacted with an excess of an aryl Grignard reagent resulting in the 2,6-bis(aryl)phenyl magnesium halide, which is converted to the 1-iodobenzene derivative through quenching with I_2, and loss of a magnesium dihalide (Scheme 2.4). The Li-salts of these ligands can be formed through reaction with $LiBu^n$, which can be isolated as pure solids before subsequent use in salt-metathesis reactions [44].

These ligands have been extremely successful in stabilising a number of novel and highly interesting species incorporating a range of transition and MG elements, with a particular highlight being the isolation of the first heavier alkyne analogues, LEEL (L = terphenyl ligand, E = Si–Pb) [45]. More specific accounts of such examples will be discussed where necessary in later chapters. In regards to group 14 element halides, a small number of Si(IV) halide species incorporating terphenyl ligands are known, and are generally unremarkable [46, 47]. Two examples of 3-coordinate carbene-stabilised aryl silicon(II) chlorides have been reported (e.g. {(^{Mes}Terph)SiCl.TMC}; TMC =:C{N(Me)C(Me)}$_2$), and were synthesised by the reduction of the $ArSiCl_2H$ precursors (Ar = ^{Mes}Terph or ^{Tripp}Terph) with two equivalents of TMC [48]. Related Ge(II) analogues (e.g. {(^{Mes}Terph)GeCl.TMC}) were synthesised, however, uncoordinated terphenyl germanium(II) halides are also known (e.g. (^{Tripp}Terph)GeCl, ^{Tripp}Terph = 2,6-(2,4,6-Pr^i_3Ph)Ph). Interestingly, structurally characterised examples of terphenyl Ge(II) halides exhibit both monomeric and dimeric structures, even where the same ligand is employed, but when crystallised from different solvents [49–51]. This is likely due to differing crystal packing factors where solvent is present in the lattice. The dimeric structures

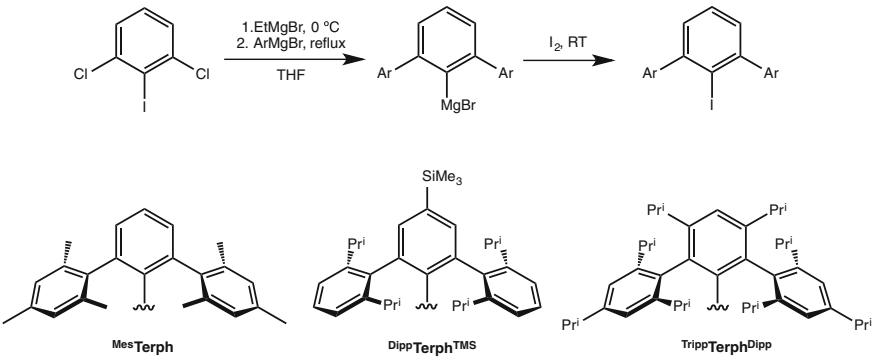

Scheme 2.4 A general synthesis of terphenyl ligands (*above*), and some examples of terphenyl ligands utilised in the literature (*below*)

involve Ge = Ge double bonding, i.e. a digermene, due to the lone-pair on each Ge centre donating to the empty *p*-orbital on the neighbouring Ge centre, a common observation for Ge(II) dimers [52]. However, no fluctionality between such dimers and monomers in solution has been described for these systems. The case is similar for terphenyl Sn(II) halide complexes, which are mostly dimeric in the solid state, but which exhibit monomeric structures with small changes in ligand electronics or crystallisation solvent (e.g. (^{Tripp}Terph)SnCl.C_6H_{14}) [50, 51, 53–55]. There are relatively few terphenyl Pb(II) halides reported, however those that have been synthesised were isolated in surprisingly high yields (55–70%) [56–58]. All bar one of the Pb(II) species are dimeric in the solid state, with bridging halides, with no remarkable structural characteristics. Further discussions of the importance of these element(II) halide 'presursors' will be addressed in subsequent chapters.

The bulky aryl ligands developed by Tokitoh and co-workers again involve a 2,6-disubstitution of a central aryl unit (Scheme 2.5). The substitution in this case is with $(Me_3Si)_2CH$- groups, resulting in very different electronics to the described terphenyl ligand set. There are a handful of ligands utilised by Tokitoh, differing only in the *para*-substitution of the central ring: a proton at this position gives Bbp, a third $(Me_3Si)_2CH$- unit gives Tbt, and a $(Me_3Si)_3C$- unit gives Bbt (Scheme 2.5). As an example, Bbp is synthesised by reacting 1-bromo-2,6-bis(dibromomethyl) benzene with a 20-fold excess of Me_3SiCl and five equivalents of elemental Mg. Following reflux, the bromide of the ligand is isolated in a moderate yield [59]. The related pro-ligands are synthesised in a similar manner. The arylbromides can be treated with $LiBu^t$ to generate Li-salts in situ for further reactivity.

This class of silylated ligand has seen most promising results with the synthesis of Si(II) and Ge(II) species. Having said that, there are in fact only one of each of these species containing a halide ligand structurally characterised, i.e. {(Bbt)SiBr}$_2$ and {(Bbt)GeBr}$_2$ [60, 61]. Both are dimeric in the solid state, featuring element-element double bonds, and have a seen a broad range of further chemistry,

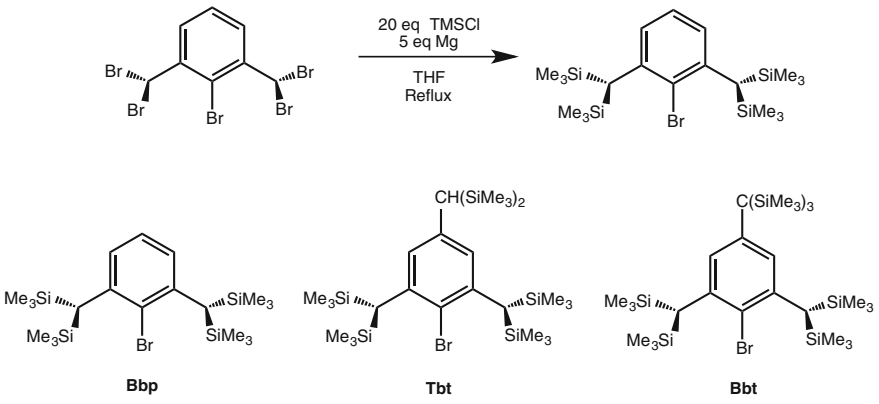

Scheme 2.5 The synthesis of the super-bulky aryl ligand, Bbp (*above*), and some examples of super-bulky silyl-substituted aryl ligands utilised in the literature (*below*)

which will be discussed in later chapters. The 1,2-dibromodisilene,{(Bbt)SiBr}$_2$, was shown to undergo mono-metathesis reactions with metal alkyl or aryl species (i.e. Grignard and lithium reagents) to yield unprecedented mixed 1-alkyl- or 1-aryl-2-bromodisilenes (e.g. {(Bbt)(Br)Si = Si(Me)(Bbt)}). Interestingly, the same Si(II) dibromo species undergoes ligand activation upon being heated in C_6D_6 (100 °C, 10 h), a process which was hypothesised to occur via initial migration of one Br^- ligand to the neighbouring silicon centre, giving the mixed valence [{(Bbt)Br_2Si}-Si(Bbt)], which is effectively an aryl-silyl silylene (Scheme 2.6). However, this was not strictly observed or isolated, with only the product involving activation of one flanking TMS group being characterised. In contrast, the bonding situation in the {(Bbt)GeBr}$_2$ species, which has the longest reported Ge = Ge bond to date, is considerably different. This species was shown to dissociate to two of the respective monomeric (Bbt)(Br)Ge: species in solution, with this equilibrium being temperature dependant (Scheme 2.6). This was the first demonstration of such a phenomenon, and is indicative of the weak donor-acceptor type bonding involved in these systems.

As mentioned, no Sn(II) or Pb(II) monohalides have been synthesised using Tokitoh's ligand systems. Only two Sn(IV) bromides have been characterised, e.g. (Bbt)(Br)Sn{$(C_2H_2)_2CH_2$}, and were isolated as precursors to stannabenzene derivatives [62]. Similarly, only one Pb(IV) compound has been characterised using this ligand system, $(Bbt)_2PbBr_2$, and this was the first structurally characterised four-coordinate diorgano-dihaloplumbane [63].

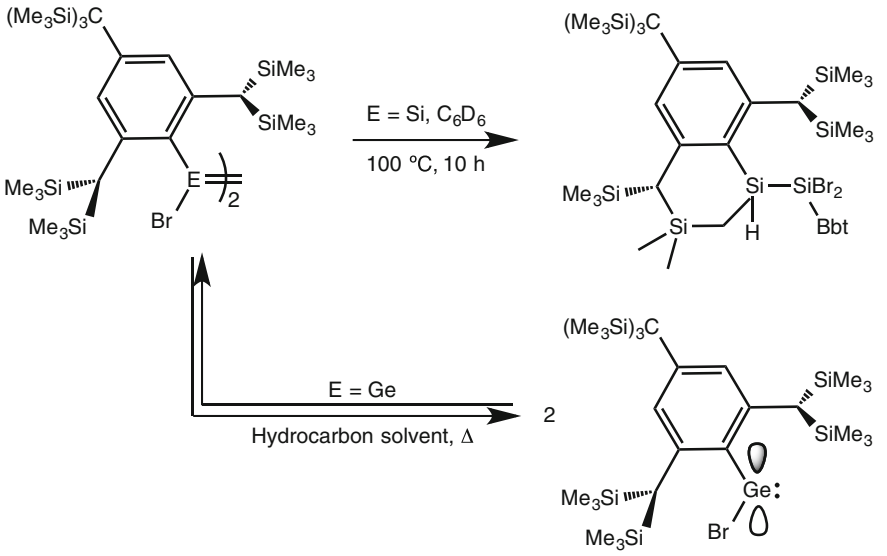

Scheme 2.6 Intramolecular CH-activation by a disilene (*above*), and temperature-dependant dissociation of a digermene to two monomeric germylenes in solution (*below*)

The third and final class of ligand to be discussed here are the bulky aryl-silyl amide ligands, developed by our group. These have seen considerable success stabilising complexes involving elements from across the periodic table, notable examples of which will be discussed in subsequent chapters. These ligands can be seen as a bulkier extension of the widely utilised hexamethyldisilazide ligand (HMDS, $^{-}N(TMS)_2$) [17]. This is however generally not bulky enough for modern low-oxidation state chemistry, and has since seen derivatisation to the bulkier $^{-}N(Dipp)(TMS)$ [17] which has also seen extensive use. The aryl-silyl amides discussed here can be seen as direct extensions of this class of ligand.

These aryl-silyl amides are particularly straightforward in their syntheses, being complete in two steps from low-cost starting materials. First, a condensation between a *para*-substituted aniline and two equivalents of benzhydrol yields the bulky 2,4,6-trisubstituted aniline group (R = Me, Ar^*NH_2, **1**; R = Pr^i, $Ar^{\dagger}NH_2$, **2**; R = Bu^t, $Ar^{\#}NH_2$, **3**; Scheme 2.7) [64]. Deprotonation with $LiBu^n$ followed by quenching with a tri-substituted chlorosilane yields the pro-ligands in high yields. Prior to this thesis, there were three reported examples of monodentate amides utilising the Ar* unit, and one ligand for each of the $Ar^{\dagger}$ and $Ar^{\#}$ units (see Scheme 2.7 for secondary amines) [65]. For the synthesis of group 14 element(II) halide complexes, the Li-salt of the ligands was generated in situ through reaction with $LiBu^n$, and subsequent reaction with ECl_2 (E = Ge-Pb).

These ligands have been utilised in the synthesis of a range of group 14 element (II) chlorides, and a handful of Si(IV) halide compounds. The latter consist of amido-trichlorosilanes, amido-tribromosilanes, and one amido-dichlorosilane. All species were isolated in moderate to high yields, and represent surprisingly rare examples of structurally characterised amido silicon(IV) halides. However, they are unremarkable in their structures, and warrant no in-depth discussion. All ligands were successfully employed in stabilising amido Ge(II) chloride complexes, with all being isolated in good yield. All such complexes are monomeric in the solid state,

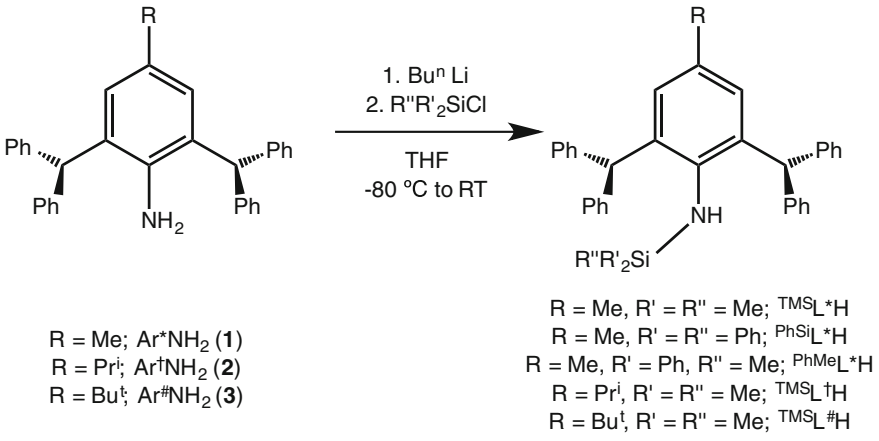

Scheme 2.7 Synthetic routes to a variety of super-bulky aryl-silyl secondary amines

and have bent N–Ge–Cl moieties, due to the presence of a stereoactive lone pair of electrons at Ge(II). Similarly, all ligands aside from $^{TMS}L^{\#}$ were utilised in synthesising amido Sn(II) chlorides, in good yield. Aside from these species being monomeric in the solid state, they have no remarkable structural features. However, their monomeric character is indicative of the extreme steric bulk of the class of monodentate ligand used in their formation. It is worthy of note that this monomeric character may, in part, be due to the lone-pair residing on the nitrogen donor atom of the ligand. As this nitrogen sits in a trigonal-planar environment, there is likely some overlap between its *p*-lone pair and the empty *p*-orbital at the element(II) centres, hence reducing the likelihood of E = E donor-acceptor type bonding in these compounds, and therefore lessening their propensity to dimerise.

It was only possible to isolate two Pb(II) chloride complexes using this ligand set, namely (^{TMS}L*)PbCl and (^{PhMe}L*)PbCl. Further, it was mentioned that addition of the lithium salts of these ligands to the $PbCl_2$ starting material resulted in formation of elemental lead, with subsequent low yields of the amido Pb(II) chlorides (41 and 8%, respectively). The sensitivity of these species suggests their use in further chemistry is likely limited. Both species are dimeric in the solid state, having bridging halides, and are otherwise unremarkable.

2.2 Research Proposal

Although there has been great success involving the employment of monodentate amide ligands in low-oxidation state MG chemistry over recent decades [17], the range of available ligands of extreme steric bulk is relatively lacking, as is their electronic diversity. In the past, slight modifications to existing ligand parameters have lead to surprisingly diverse differences in electronic structures of resultant low-oxidation state compounds. As such, we sought novel, extremely bulky mono-dentate amide ligands that are accessible in few steps and at low cost, preferably using the bulky Ar* group, or closely related aromatic systems. Further, we wished to investigate their use in the synthesis of low-coordinate amido group 14 element(II) halides for use in subsequent chemistry.

2.3 Results and Discussion

2.3.1 Synthesis of Extremely Bulky Secondary Amines

Given the knowledge our group possesses regarding the synthesis and reactivity of super-bulky monodentate aryl-silyl amides in low-oxidation state chemistry, we sought to expand upon the current range of available ligands in this class, and to

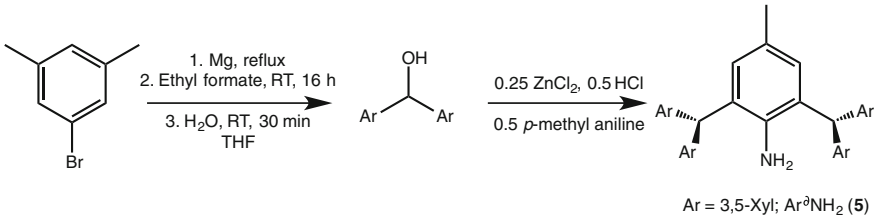

Scheme 2.8 The synthesis of the novel bulky aniline, $Ar^{Ə}NH_2$, **5** ($Ar^{Ə}$ = 2,6-bis{bis(3,5-dimethylphenyl)methyl}-4-methylaniline)

apply them to low-oxidation state and low-coordination number group 14 element chemistry.

2.3.1.1 Extremely Bulky Anilines

In the development of aryl-silyl amine pro-ligands, there are two obvious points of modification: the silyl group and the flanking aryl groups. Recently, Straub and co-workers published the synthesis of a modified aniline, whereby four flanking *p*-Bu^tPh groups were employed, replacing the flanking Ph groups of Ar^*NH_2 (**1**) ($Ar''NH_2$, **4**) [64]. We sought to utilise this novel aniline, and synthesise derivatives thereof. This synthetic procedure, outlined in Scheme 2.8, involves forming an aryl Grignard reagent, quenching this with ethyl formate and water to form a bis(aryl) methanol derivative, followed by condensing two equivalents of this with a *para*-substituted aniline. We have now extended this to the synthesis of 2,6-bis{bis(3,5-dimethylphenyl)methyl}-4-methylaniline ($Ar^{Ə}NH_2$, **5**, Scheme 2.8), which, with **4**, has potential for the synthesis of novel aryl-silyl amide ligands. The synthesis of 2,6-bis{bis(2,4,6-trimethylphenyl)methyl}-4-methylaniline was also attempted via the same route. However, although mass spectrometry showed the presence of a product with the desired mass, ^1H NMR spectroscopy showed a mixture of several products which could not be purified.

2.3.1.2 Extremely Bulky Aryl-Silyl Amines

With several tetraphenyl-substituted anilines in hand, novel secondary amines were targeted. Two bulky chloro-silanes were selected that have seen use in both organic and inorganic chemistry previously, namely tri-*iso*-propylchloro silane, and tri-*tert*-butoxychloro silane. The former is readily available for purchase, with the latter being easily synthesised from $SiCl_4$ and $KOBu^t$ [66]. Initially, both of these silyl chlorides were reacted with $Ar^†N(H)Li$ (**2.Li**), which was generated in situ from the reaction of **2** with $LiBu^n$ in THF. Unlike previously synthesised aryl-silyl amides from our group, which form in such reactions carried out between −80 °C and

ambient temperature, **2.Li** did not react with either Pr^i_3 SiCl or $(Bu^tO)_3$SiCl until being heated to near reflux in THF. Thus, $^{iPr}L^{\dagger}H$ ($^{iPr}L^{\dagger}H = (Pr^i_3Si)N(H)Ar^{\dagger}$, **6**) quantitatively formed after heating **2.Li** with Pr^i_3SiCl at 55 °C for 24 h. The bulkier $^{tBuO}L^{\dagger}H$ ($^{tBuO}L^{\dagger}H = \{(Bu^tO)_3Si\}N(H)Ar^{\dagger}$, **7**) took somewhat longer, with the reaction being complete after 48 h. The reaction with $(Bu^tO)_3$SiCl was also extended to **1**, yielding $^{tBuO}L^*H$ ($^{tBuO}L^*H = \{(Bu^tO)_3Si\}N(H)Ar^*$, **8**). This synthetic method is outlined in Scheme 2.9. The formation of the secondary amines was clear by a ^{1}H NMR spectroscopic analysis, with no **2** or **1** being present, and new resonances for the silyl and NH moieties appearing. These amines are air and moisture stable colourless crystalline solids, following recrystallisation from warm hexane.

Following the synthesis of these two amines, we sought to expand the range to examples prepared from the bulkier anilines, **4** and **5**. The reaction of Pr^i_3SiCl with Ar″N(H)Li (**4.Li**) was complete after heating at 55 °C for 32 h, forming $^{iPr}L''H$ ($^{iPr}L''H = (Pr^i_3$ Si)N(H)Ar″, **9**) in good yield. Although $(Bu^tO)_3$SiCl was not reacted with **4.Li**, the extremely bulky amine, $^{tBuO}L^{\partial}H$ ($^{tBuO}L^{\partial}H = \{(Bu^tO)_3Si\}N(H)Ar^{\partial}$, **10**), was formed in moderate yield from the reaction of $(Bu^tO)_3$SiCl with Ar^{∂}N(H)Li (**5.Li**) at 55 °C for 72 h. The related amine, $^{iPr}L^{\partial}NH$ ($^{iPr}L^{\partial}NH = (Pr^i_3Si)N(H)Ar^{\partial}$, **11**), was similarly formed from Pr^i_3SiCl and **5.Li**. As with **7** and **8**, a ^{1}H NMR spectroscopic analysis showed consumption of starting materials, and little to no free aniline in the reaction mixture. Again, this synthetic method is outlined in Scheme 2.9. In each case, crystallisation from minimal hexane or pentane yielded the pure amines in moderate to good yields. All are air and moisture stable under ambient conditions. All amines synthesised show a characteristic NH stretch at ~3200 cm^{-1} in their IR spectra, and exhibited molecular ion peaks in their accurate mass spectra. Molecular structures of **9–11** are

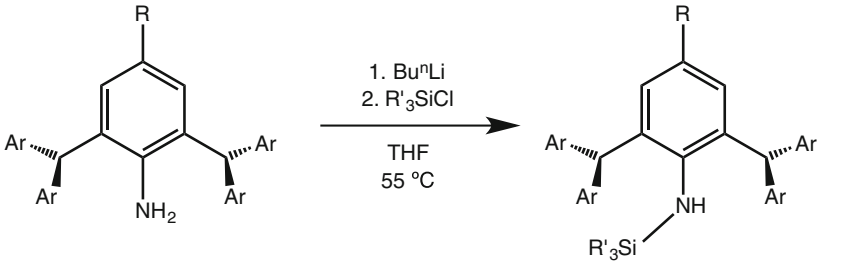

R = Me, Ar = Ph; Ar^*NH_2 (**1**)
R = Pr^i, Ar = Ph; $Ar^{\dagger}NH_2$ (**2**)
R = Bu^t, Ph; $Ar^{\#}NH_2$ (**3**)
R = Me, Ar = *p*-Bu^tPh; $Ar^{''}NH_2$ (**4**)
R = Me, Ar = 3,5-Xyl; $Ar^{\partial}NH_2$ (**5**)

R = R' = Pr^i, Ar = Ph (**6**)
R = Pr^i, R' = Bu^tO, Ar = Ph (**7**)
R = Me, R' = Bu^tO, Ar = Ph (**8**)
R = Me, R' = Pr^i, Ar = *p*-Bu^tPh (**9**)
R = Me, R' = Bu^tO, Ar = 3,5-Xyl (**10**)
R = Me, R' = Pr^i, Ar = 3,5-Xyl (**11**)

Scheme 2.9 The synthesis of novel bulky secondary aryl-silyl amines

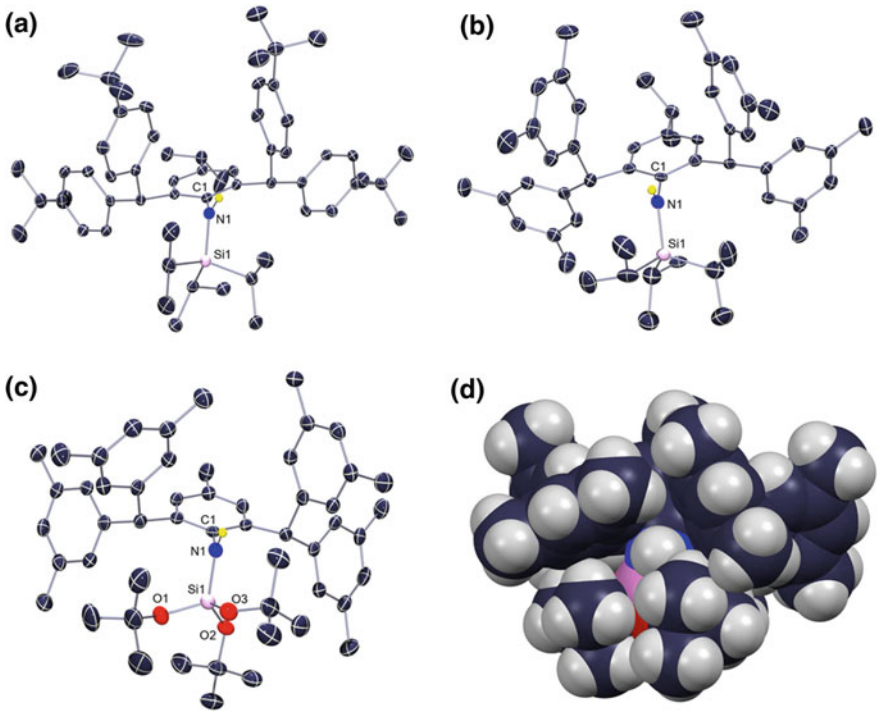

Fig. 2.2 ORTEP representations of **a** ^{iPr}L″H (**9**), **b** ^{iPr}L$^{\partial}$H (**10**), and **c** ^{tBuO}L$^{\partial}$H (**11**), with thermal ellipsoids at 50% probability. All hydrogens, except amine protons, are removed for clarity. **d** The space filling diagram of ^{tBuO}L$^{\partial}$H

depicted in Fig. 2.2. Although these are generally unremarkable, the space-filling diagram of **11** does give a good idea of the extent of the steric bulk of these ligands. That is, there is very little space about the NH moiety which results from the pocket formed by the aryl and silyl substituents.

2.3.1.3 Extremely Bulky Bis(aryl) Amines

Despite the success that previously employed aryl-silyl amides have enjoyed in low-oxidation MG chemistry (e.g. DippN(H)TMS), very little work has been undertaken on the synthesis of super-bulky bis(alkyl) or bis(aryl) amides. Within our group, the lability of the N–Si bond in DippN(H)TMS has been a problem in the presence of strong reducing agents (e.g. KC_8) [67]. Therefore, we sought the facile synthesis of bulky bis(aryl) amines, generally not a straightforward proposition. However, the advent of Pd-catalysed transformations, and more importantly, the Buchwald-Hartwig amination, gives a synthetic route to such secondary amines (i.e. anilines cross-coupled with aryl halides) [68]. Prior to this thesis, the most

bulky reported examples of bis(aryl) amines synthesised through this protocol were DippN(H)Tripp (Tripp = 2,4,6-$^{i}Pr_3Ph$), and an isolated example of secondary a terphenyl amine ({2,6-$(Ph)_2Ph$}N(H)Tripp) [69]. The former had been generated by Shao and co-workers, using an NHC-coordinated $PdCl_2$ catalyst, Im($PdCl_2$)IPr (**12**) (Im = 1-methylimidazole; IPr =:C{N(Dipp)C(H)}$_2$). They achieved this with remarkably low catalyst loadings (1.0 mol%), and with an extremely wide scope of substituents [70, 71]. As such, this catalyst system seemed a good candidate for the coupling of Ar*NH_2 with aryl halides.

We initially attempted the coupling of **1** with the relatively small PhBr. The aryl bromide, as opposed to the chloride, was chosen as these are generally easier to couple [68], which would likely be beneficial given the large bulk of the Ar* moiety in **1**. A reaction mixture containing **12**, **1**, PhBr and KOBu^{t} (in a 0.05:1:1.2:1.2 ratio) gave 80% conversion to what appeared to be the target PhN(H)Ar* (^{Ph}L*H, **13**) after 2 h in refluxing toluene, based on a ^{1}H NMR spectroscopic analysis of the crude reaction mixture (Scheme 2.10). This was signified by consumption of 80% of **1**, and the appearance of a new set of signals corresponding to the target compound. A NH resonance was also observed at $\delta \sim 4.5$ ppm, shifted down field relative to that of Ar*NH_2 due to electron delocalisation about the two aromatic substituents, deshielding the NH proton (N.B. the NH_2 resonance of Ar*NH_2 is observed at ~3.2 ppm). It also appeared as though all PhBr had been consumed, possibly through homo-coupling side reactions. However, the addition of a further 2 mol% of catalyst, **12**, and 0.4 equivalents of PhBr resulted in complete conversion to the desired secondary amine. The procedure was also successful with 3,5-Me_2PhBr (yielding ^{Xyl}L*H, **14**), 3,5-$(CF_3)_2$PhBr (yielding ^{F6Xyl}L*H, **15**), 2,4,6-Me_3PhBr (yielding ^{Mes}L*H, **16**), and 2,4,6-Pr^{i}_3PhBr (yielding ^{Tripp}L*H, **19**). It was found that a stepwise addition of catalyst and aryl bromide was optimal for the complete conversion to the secondary amines, with a fair excess of both the aryl bromide and KOBu^{t} being beneficial (Scheme 2.10). Hence, the reaction of 1 equivalent of **1**, 1.4 equivalents of KOBu^{t}, and just 2.5 mol% of **12** and 0.65 equivalents of aryl bromide, was heated at reflux in toluene for 2 h (Scheme 2.10).

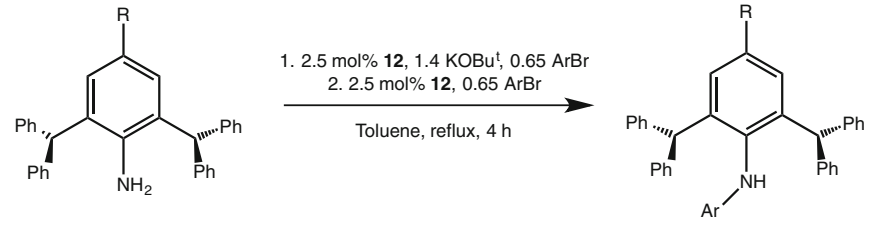

R = Me, Ar = Ph; Ar*NH_2 (**1**)
R = Pr^{i}, Ar = Ph; Ar$^{\dagger}NH_2$ (**2**)
R = Bu^{t}, Ph; Ar$^{\#}NH_2$ (**3**)

R = Me, Ar = Ph (**13**)
R = Me, Ar = 3,5-Xyl (**14**)
R = Me, Ar = 3,5-$(CF_3)_2$Ph (**15**)
R = Me, Ar = Mes (**16**)
R = Pr^{i}, Ar = Mes (**17**)
R = Bu^{t}, Ar = Mes (**18**)
R = Me, Ar = Tripp (**19**)

Scheme 2.10 Synthesis of the super-bulky bis(aryl) secondary amines, **13–19**, using a Pd-catalysed coupling reaction

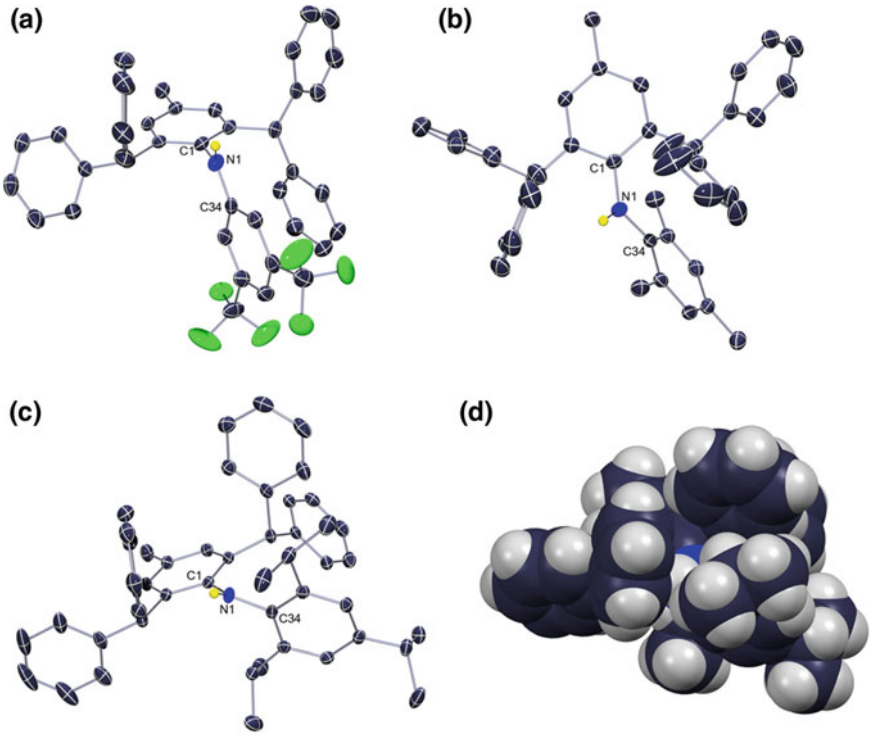

Fig. 2.3 ORTEP representations of **a** ^{F6Xyl}L*H (**15**), **b** ^{Mes}L*H (**16**), and **c** ^{Tripp}L*H (**19**), with thermal ellipsoids at 50% probability. All protons, aside from the amine protons, are removed for clarity. **d** The space filling diagram of ^{Tripp}L*H

Subsequently, a further 2.5 mol% of **12** and 0.65 equivalents of aryl bromide were added. Heating under reflux for a further two hours led to complete conversion to the secondary amines. Following studies with **1** as the aniline, we attempted coupling **2** and **3** with MesBr, both of which gave the desired amines in high yield (^{Mes}L†H = MesN(H)Ar†, **17**; ^{Mes}L$^{\#}$ = MesN(H)Ar$^{\#}$, **18**). Note that these are some of the bulkiest products from such couplings reported to date.

All of these species have highly downfield shifted NH resonances in their ^{1}H NMR spectra, likely for reasons already discussed. Crystals of **15**, **16**, and **19** suitable for X-ray crystallography were grown, and their solid state structures elucidated. All are relatively unremarkable, and are shown in Fig. 2.3. The space filling diagram of **19** is shown so as to indicate the pocket formed around the NH moiety. It is clear, however, that these ligands are not of equivalent bulk to the previously discussed aryl-silyl amines, particularly **9**. Nevertheless, their utility in amido group 14 element(II) halide synthesis has been explored.

2.3.2 Synthesis of Group 14 Element(II) Halide Complexes

2.3.2.1 Aryl-Silyl Amido Group 14 Element(II) Halide Complexes

We sought to use prepared ligands in the generation of group 14 element(II) halide complexes. For the aryl-silyl amides, in situ deprotonation of the amine with $LiBu^n$ in THF was attempted, in order to generate the lithium amides. This was successful for **6**, **9**, and **11**. However, the ligands containing the $(Bu^tO)_3Si$- group (**7**, **8**, and **10**), were only successfully deprotonated with KH and a catalytic amount of HMDS (5 mol%), giving good isolated yields of the potassium amides (**7.K**, **8.K**, and **10.K**). Addition of THF solutions of these lithium or potassium amides to solutions of $GeCl_2$.dioxane in THF generally led to promising results. All ligands aside from **10.K** gave clean reactions mixtures, with one new species, presumably the LGeCl complex, and small amounts (typically <15%) of protonated ligand, LH. In the case of **10.K**, around 50% of the protonated ligand, **10**, was observed in the reaction mixture. Due to the high solubility of both **10** and the presumed ($^{tBuO}L^{\partial}$)GeCl product in hydrocarbon solvents, these two species were inseparable, and therefore this system was not pursued. However, all other germanium(II) species were isolated, their syntheses being summarised in Scheme 2.11. All display signals

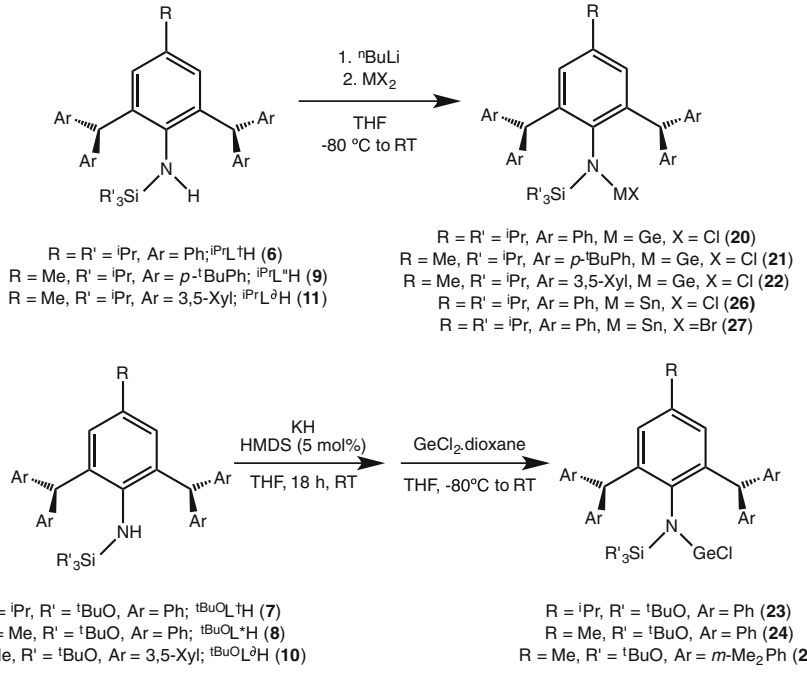

Scheme 2.11 Synthesis of aryl-silyl amido germanium(II) and tin(II) halide complexes, **20**–**27**

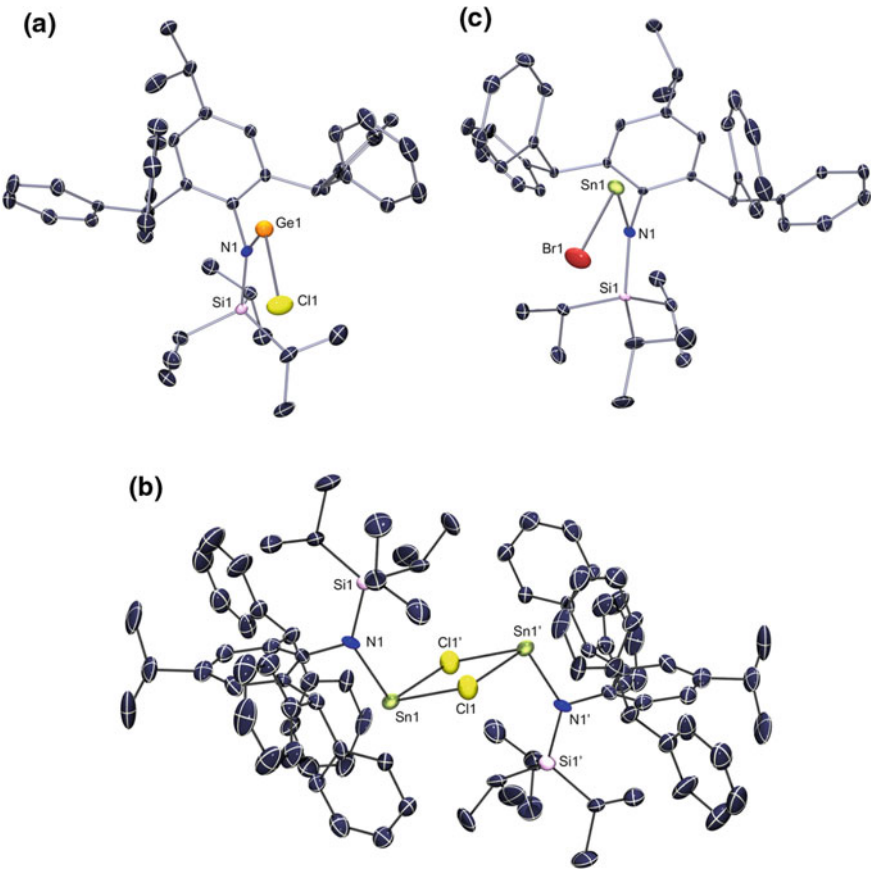

Fig. 2.4 ORTEP representations of **a** ($^{iPr}L^{\dagger}$)GeCl (**20**), **b** ($^{iPr}L^{\dagger}$)SnCl (**26**), and **c** ($^{iPr}L^{\dagger}$)SnBr (**27**), with thermal ellipsoids at 50% probability. All protons are omitted for clarity. Selected distances (Å) and angles (°) for **20**: Ge1–Cl1 2.248(1), N1–Ge1 1.898(3), Si1–N1 1.799(3), N1–Ge1–Cl1 105.76(9), Si1–N1–Ge1 138.00(2); **26**: Sn1–Cl1 2.545(3), Sn1–Cl1' 2.898(3), Sn1–Sn1 4.278(1), N1–Sn1 2.125(6), Si1–N1 1.763(8), N1–Sn1–Cl1 99.37(2), N1–Sn1–Cl1′ 108.50(2), Sn1–Cl1–Sn1' 103.44(9), Si1–N1–Sn1 133.16(4); **27**: Sn1–Br1 2.5782(4), N1–Sn1 2.114(2), Si1–N1 1.774 (2), N1–Sn1–Br1 104.89(6), Si1–N1–Sn1 138.50(1)

suggesting a single ligand environment in their ^{1}H NMR spectra, which is in keeping with their proposed formulations.

Only one of these amido-germanium(II) chloride complexes was structurally characterised, ($^{iPr}L^{\dagger}$)GeCl (**20**), and its structure is displayed in Fig. 2.4. As one may expect, **20** is monomeric in the solid state, as were the previously reported examples utilising related Ar*-based amide ligands (vide supra) [65]. This is likely due to the bulk of the ligand, but also because of *p*-orbital lone-pair donation from the N-donor atom of the ligand to the Ge(II) centre. The N–Ge–Cl angle of 105.76 (9)° is indicative of a stereo-active lone pair at the Ge(II) centre.

Only one ligand was utilised in the synthesis and isolation of amido Sn(II) halides, i.e. in (^{iPr}L†)SnCl (**26**) and (^{iPr}L†)SnBr (**27**) (Scheme 2.11). However, **8.K** was utilised in the in situ synthesis of (^{tBuO}L*)SnCl, which was used for the subsequent synthesis and isolation of (^{tBuO}L*)SnOBu^{t} (see Chap. 3). Interestingly, **26** is dimeric in the solid state, in contrast to previously reported examples of amido tin(II) chlorides utilising the bulky Ar* group. Conversely, **27** is monomeric in the solid state, despite the larger bromide ligand, suggesting the dimerisation energy of **26** is low and of the order of crystal packing forces. Compound **27** represents the first structurally characterised example of a monomeric 2-coordinate amido tin(II) bromide. Both **26** and **27** show strongly bent N–Sn–X (X = Cl or Br) angles, again due to the presence of a stereo-active lone-pair of electrons at the Sn(II) centres.

We were not successful in isolating any amido lead halide species using these novel aryl-silyl amide ligands. Generally, instantaneous deposition of elemental lead was seen upon addition of alkali-metal salts of the amide ligands to lead(II) halides, with ^{1}H NMR analyses showing the protonated amine ligand to be the major constituent of the reaction mixtures.

2.3.2.2 Bis(aryl) Amido Group 14 Element(II) Halide Complexes

All bar one of the bis(aryl) amide ligands were successfully used in the synthesis of germanium(II) chloride complexes (Scheme 2.12), with deprotonated **14** yielding a mixture of hydrocarbon-insoluble species and protonated ligand, ^{Xyl}L*H. All other amido germanium(II) chloride complexes were isolated in moderate to good yields. Although none of these species were crystallographically characterised, they were characterised by ^{1}H and ^{13}C NMR spectroscopy, IR spectroscopy and mass spectrometry. All species displayed one ligand environment as judged by NMR spectroscopic studies, although resonances observed in the NMR spectra of **33** were

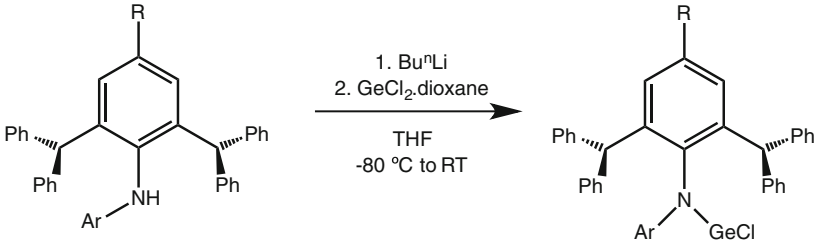

R = Me, Ar = Ph; ^{Ph}L*H (**13**)
R = Me, Ar = 3,5-(CF$_3$)$_2$Ph; ^{F6Xyl}L*H (**15**)
R = Me, Ar = Mes; ^{Mes}L*H (**16**)
R = Pr^{i}, Ar = Mes; ^{Mes}L†H (**17**)
R = Bu^{t}, Ar = Mes; ^{Mes}L$^{\#}$H (**18**)
R = Me, Ar = Tripp, ^{Tripp}L*H (**19**)

R = Me, Ar = Ph (**28**)
R = Me, Ar = 3,5-(CF$_3$)$_2$Ph (**29**)
R = Me, Ar = Mes (**30**)
R = ^{i}Pr, Ar = Mes (**31**)
R = ^{t}Bu, Ar = Mes (**32**)
R = Me, Ar = Tripp (**33**)

Scheme 2.12 Synthesis of bis(aryl) germanium(II) chloride species

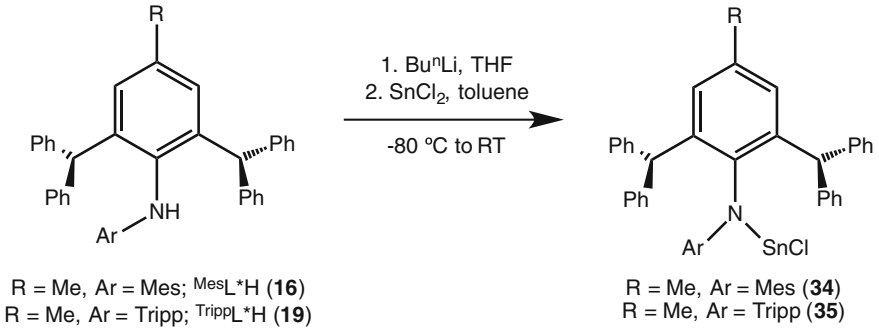

R = Me, Ar = Mes; ^{Mes}L*H (**16**)
R = Me, Ar = Tripp; ^{Tripp}L*H (**19**)

R = Me, Ar = Mes (**34**)
R = Me, Ar = Tripp (**35**)

Scheme 2.13 Synthesis of bis(aryl) amido tin(II) chloride species

highly broadened, presumably due to the bulk of the Tripp group, hindering both its own free rotation and that of the Ar* substituent.

All attempted syntheses of amido tin(II) halide complexes using these bis(aryl) amides in THF yielded only protonated ligand and elemental tin. However, conducting the same reactions in toluene, using deprotonated **16** and **19**, yielded the corresponding amido tin(II) chlorides, (^{Mes}L*)SnCl (**34**) and (^{Tripp}L*)SnCl (**35**), in moderate isolated yields (Scheme 2.13). As with the corresponding Ge(II) species, these two Sn(II) halide complexes were not structurally characterised, but were characterised by ^{1}H and ^{13}C NMR spectroscopy, IR spectroscopy and mass spectrometry. As for **33**, the NMR spectra of **35** display broadened resonances likely due to hindered substituent rotation brought about by the steric bulk of the Tripp group.

Again, no lead(II) halide complexes were synthesised using this ligand class, with only elemental lead and protonated ligand being observed in reaction mixtures.

2.4 Conclusion

In conclusion, several new silyl-aryl and bis(aryl) amine pro-ligands and anionic amide ligands have been synthesised. The steric bulk of these rival that of any other reported monodentate anionic ligands reported to date. A number of these ligands were successfully employed in the stabilisation of low-coordinate amido tin(II) and germanium(II) halide complexes. However, these ligands were unsuccessful in stabilising the related lead(II) halide systems. The use of these novel group 14 element halide species as precursors for the synthesis of low-oxidation state group 14 element complexes will be discussed in subsequent chapters.

2.5 Experimental

^{tBuO}L†H (7). This compound was prepared following a method similar to that for ^{tBuO}L*H, using Ar†NH$_2$ (5.0 g, 10.70 mmol), LiBu^n (7.03 mL, 1.6 M solution, 11.24 mmol), and (Bu^{t}O)$_3$SiCl (3.17 g, 11.24 mmol) (4.5 g, 59%). M.p.: 165–170 °C; ^{1}H NMR (C_6D_6, 400 MHz, 298 K), δ = 0.92 (d, $^3J_{HH}$ = 7.2 Hz, 6H, Ar†-*p*-CH(C*H*$_3$)$_2$), 1.32 (s, 27H, OC(C*H*$_3$)$_3$), 2.24 (s, 1H, N*H*), 2.48 (sept, 1H, C*H*(CH$_3$)$_2$), 6.74 (s, 2H, Ph$_2$C*H*), 6.92 (s, 2H, Ar†-*m*-C*H*), 7.03–7.32 (m, 20H, Ar-*H*); ^{13}C{^{1}H} NMR (C_6D_6, 75.5 MHz, 298 K), δ = 24.1 (Ar†-*p*-CH(*C*H$_3$)$_2$), 32.0 (OC(*C*H$_3$)$_3$), 33.9 (Ar†-*p*-*C*H(CH$_3$)$_2$), 52.1 (Ph$_2$*C*H), 73.6 (O*C*(CH$_3$)$_3$), 126.4, 126.8, 127.8, 128.2, 128.4, 128.8, 130.1, 130.5, 139.8, 142.1, 144.3, 145.3 (Ar-*C*); ^{29}Si{^{1}H} NMR (C_6D_6, 80 MHz, 298 K), δ = −92.3; IR, ν/cm^{-1} (ATR): 3378 (w, NH str.), 3058 (w), 3025 (w), 1803 (w), 1752 (w), 1598 (m), 1491 (m), 1446 (m), 1363 (s), 1182 (s), 1046 (s), 902 (m), 761 (m), 673 (s); MS/EI *m/z* (%): 715 (M$^+$, 45); acc. mass calcd for $C_{47}H_{60}NO_3Si$ (MH$^+$): 714.4342; found: 714.4332.

^{tBuO}L*H (8). To a solution of Ar*NH$_2$ (10.0 g, 22.8 mmol) in THF (100 mL) at −80 °C was added Bu^{n}Li (14.93 mL, 1.6 M solution, 23.9 mmol). The reaction mixture was warmed to ambient temperature and stirred for 2 h, yielding a pink/red suspension. Subsequently, (Bu^{t}O)$_3$SiCl (6.76 g, 23.94 mmol) was added at ambient temperature, and the mixture then heated at 55 °C, with stirring, for 2 days, resulting in a colourless solution. All volatiles were removed in vacuo, and the residue extracted into boiling hexane, and filtered. Removal of volatiles from the filtrate in vacuo and washing of the residue with *ca.* 15 mL of cold hexane yielded ^{tBuO}L*H as an off-white powder (13.4 g, 86%). X-ray quality crystals were grown by slow evaporation of a diethyl ether solution of the compound. M.p.: 182–190 °C; ^{1}H NMR (C_6D_6, 400 MHz, 298 K), δ = 1.33 (s, 27H, OC(C*H*$_3$)$_3$), 1.85 (s, 3H, Ar*-*p*-*Me*), 2.20 (s, 1H, N*H*), 6.73 (s, 2H, Ph$_2$C*H*), 6.88 (s, 2H, *m*-Ar*-*m*-C*H*), 7.00–7.32 (m, 20H, Ar-*H*); ^{13}C{^{1}H} NMR (C_6D_6, 75.5 MHz, 298 K), δ = 21.3 (Ar*-*p*-*C*H$_3$), 32.0 (OC(*C*H$_3$)$_3$), 51.9 (Ph$_2$*C*H), 73.6 (O*C*(CH$_3$)$_3$), 126.4, 126.9, 128.4, 128.8, 129.6, 130.0, 130.5, 133.4, 139.5, 142.3, 143.5, 145.2 (Ar-*C*); ^{29}Si{^{1}H} NMR (C_6D_6, 80 MHz, 298 K), δ = −89.0; IR, ν/cm^{-1} (ATR): 3379 (w, NH str.), 1880 (w), 1750 (w), 1366 (m), 1183 (s), 1045 (s), 900 (m), 670 (s); MS/EI *m/z* (%): 687 (M$^+$, 35); acc. mass calcd for $C_{45}H_{56}NO_3Si$ (MH$^+$): 686.4029; found: 686.4019.

^{iPr}L″H (9). To a solution of Ar″N(H)Li (2.0 g, 2.87 mmol), in THF (20 mL) was added neat Pr$^i_3$SiCl (0.67 mL, 3.16 mmol). The reaction mixture was warmed to 55 °C and stirred for 32 h to give a pale yellow solution. Volatiles were subsequently removed in vacuo, the solid residue extracted into pentane and filtered. Volatiles were removed from the filtrate in vacuo to yield ^{iPr}L″H as a cream micro-crystalline powder. X-ray quality crystals were grown by slow evaporation of a pentane solution (1.8 g, 75%). M.p.: 241–244 °C; ^{1}H NMR (C_6D_6, 500 MHz, 298 K): δ = 0.97 (d, $^3J_{HH}$ = 6.8 Hz, 6H, Ar$^{\#}$-*p*-CH(C*H*$_3$)$_2$), 1.13 (d, $^3J_{HH}$ = 7.6 Hz, 18H, SiPr$^i_3$-CH(C*H*$_3$)$_2$), 1.23 (s, 36H, Ar-C(C*H*$_3$)$_3$), 1.39 (sept, $^3J_{HH}$ = 7.6 Hz, 3H, SiPr$^i_3$-C*H*(CH$_3$)$_2$), 2.22 (s, 1H, N*H*), 2.48 (sept,

$^{3}J_{HH}$ = 6.8 Hz, 1H, Ar$^{\#}$-*p*-C*H*(CH$_3$)$_2$), 6.36 (s, 2H, C*H*(4-Bu^{t}Ph)$_2$), 7.08 (s, 2H, Ar$^{\#}$-*m*-Ar-*H*), 7.27 (br. s, 16H, Ar-*H*); ^{13}C{^{1}H} NMR (C$_6$D$_6$, 75.5 MHz, 298 K): δ = 14.9 (SiPr$^i_3$-*C*H(CH$_3$)$_2$), 19.2 (SiPr$^i_3$-CH(*C*H$_3$)$_2$), 24.1 (Ar$^{\#}$-*p*-CH(*C*H$_3$)$_2$), 31.5 (Ar-C(*C*H$_3$)$_3$), 33.7 (Ar$^{\#}$-*p*-*C*H(CH$_3$)$_2$), 34.4 (Ar-*C*(CH$_3$)$_3$), 51.8 (*C*H(4-Bu^{t}Ph)$_2$), 125.5, 127.5, 129.9, 141.1, 141.3, 142.4, 143.2, 149.0 (Ar-*C*); ^{29}Si{^{1}H} NMR (C$_6$D$_6$, 298 K): δ = 3.2; IR, ν/cm^{-1} (ATR): 3350(br., N-H), 2957(s), 2866(s), 1509 (m), 1363(s), 1268(s), 881(s), 828(s); MS/ES+ *m/z* (%): 692.7 (M$^+$-SiPr$^i_3$, 95); acc. mass (ES+) calc. for C$_{60}$H$_{85}$NSi (MH$^+$): 848.6518, found: 848.6537.

^{tBuO}L$^{∂}$H (10). This compound was prepared following a method similar to that for ^{tBuO}L*H, using Ar$^{∂}$NH$_2$ (2.5 g, 4.53 mmol), LiBu^n (2.97 mL of a 1.6 M solution, 4.76 mmol), and (Bu^{t}O)$_3$SiCl (1.35 g, 4.76 mmol), with the reaction being heated at 55 °C for 3 days. The product was isolated as an off-white crystalline solid (2.2 g, 61%). X-ray quality crystals of ^{tBuO}L$^{∂}$H were grown by slow evaporation of a hexane solution. M.p.: 168–180 °C; ^{1}H NMR (C$_6$D$_6$, 400 MHz, 298 K), ∂ = 1.42 (s, 27 H, OC(C*H*$_3$)$_3$), 1.85 (s, 3 H, Ar$^{∂}$-*p*-*Me*), 2.14 (s, 24 H, Xyl-*m*-Me), 2.39 (s, 1 H, N*H*), 6.74 (s, 4 H, Xyl-*p*-C*H*), 6.75 (s, 2 H, Xyl$_2$C*H*), 7.05 (s, 2 H, Ar$^{∂}$-C*H*), 7.12 (s, 8 H, Xyl-*o*-C*H*); ^{13}C {^{1}H}NMR (C$_6$D$_6$, 75.5 MHz, 298 K), ∂ = 21.3 (Ar$^{∂}$-*p*-*Me*), 21.5 (Xyl-*m*-*Me*), 32.0 (OC(*C*H$_3$)$_3$), 51.7 (Xyl$_2$*C*H), 73.7 O*C*(CH$_3$)$_3$), 128.1, 128.5, 129.9, 132.9, 137.5, 139.4, 142.1, 145.6 (Ar-*C*); ^{29}Si {^{1}H} NMR (C$_6$D$_6$, 80 MHz, 298 K), ∂ = −89.0; IR, ν/cm^{-1} (ATR): 3071 (w), 1599 (m), 1392 (s), 1383 (m), 1110 (s), 1022 (s), 1003 (s), 967 (s), 811 (m), 755 (m), 699 (s), 652 (s); MS/EI *m/z* (%): 799.3 (M$^+$, 35%); acc. mass calcd for C$_{47}$H$_{60}$NO$_3$Si (MH$^+$): 798.5281; found: 798.5271.

^{Ph}L*H (13). To a flame dried Schlenk was added Ar*NH$_2$ (2.0 g, 4.56 mmol), KOBu^t (665 mg, 5.93 mmol, 1.3 equiv), Im(PdCl$_2$)IPr (74 mg, 2.5 mol%), and bromobenzene (0.31 mL, 465 mg, 2.96 mmol). Toluene (50 mL) was added and the reaction was heated to reflux and stirred for 2 h. Following this, a further 2.5 mol% of Pd catalyst was added, as well as a further 0.31 mL bromobenzene. The reaction was again heated under reflux for 2 h, the reaction cooled to ambient temperature, and the solvent removed in vacuo. Extraction with DCM (3 × 25 mL), filtration, and solvent removal from the filtrate in vacuo, followed by hexane washing (2 × 10 mL) afforded a pale brown powder that was analytically pure (1.60 g, 68%). X-ray quality crystals were grown by slow evaporation of hexanes from a solution of the compound. M.p. 142–145 °C; ^{1}H NMR (C$_6$D$_6$, 500 MHz, 298 K): δ = 1.87 (s, 3H, Ar*-*p*-*Me*), 4.39 (s, 1H, N*H*), 5.84 (s, 2H, Ar*-PhC*H*), 6.34 (m, 2H, Ph-*o*-C*H*), 6.73 (m, 2H, Ph-*m*-C*H*), 7.02–7.30 (m, 21H, Ar-*H*). ^{13}C{^{1}H} NMR (C$_6$D$_6$, 75.5 MHz, 298 K): δ = 21.4 (Ar*-*p*-*Me*), 52.4 (Ph$_2$*C*H), 113.1 (Ph-*C*), 118.5 (Ph-*C*), 126.6 (Ph-*C*), 128.63, 129.81, 130.39, 135.91, 136.84, 143.47, 144.17, 144.84, 147.71 (Ar-*C*); IR, ν/cm^{-1} (ATR): 3415 (NH, w), 3001 (br w), 1493 (m), 1452 (m) 1314 (w), 1249 (w), 1176 (w), 1077 (w), 1030 (w), 914 (w), 872 (w), 802 (w), 750 (m), 698 (s); MS/ES *m/z* (%): 516 (M$^+$, 52%), 440 (Ar*NH$^+$, 28%), 169 (Ph$_2$CH$^+$, 100%); acc. mass calcd for C$_{39}$H$_{34}$N (MH$^+$): 516.2686. Found: 516.2679.

^{Xyl}L*H (14). The method for the synthesis of ^{Ph}L*H was followed, but using Ar*NH_2 (5.0 g, 11.4 mmol), KOBu^t (1.78 g, 15.9 mmol), Im($PdCl_2$)IPr catalyst (184 mg, 2.5 mol%), and 3,5-dimethylbromobenzene (1.11 mL, 8.20 mmol) in the initial stage of the reaction; and Im($PdCl_2$)IPr catalyst (184 mg, 2.5 mol%), and 3,5-dimethyl bromobenzene (0.74 mL, 5.47 mmol) in the latter stage of the reaction. The product was isolated as a pale brown powder (4.33 g, 70%). M.p.: 116–118 °C; ^{1}H NMR (C_6D_6, 500 MHz, 298 K): δ = 1.54 (s, 6H, Xyl-*m-Me*), 1.87 (s, 3H, Ar*-*p-Me*), 4.46 (s, 1H, N*H*), 5.93 (s, 2H, Xyl-*o*-C*H*), 6.07 (s, 2H, Ph_2C*H*), 6.41 (s, 1H, Xyl-*p*-C*H*), 6.99–7.09 (m, 22H, Ar-*H*); ^{13}C{^{1}H} NMR (C_6D_6, 75.5 MHz, 298 K): δ = 21.6 (Xyl-*m-Me*), 30.2 (Ar*-*p-Me*), 52.3 (Ar*-Ph_2*C*H), 111.3, 120.7, 126.6, 128.6, 129.9, 130.4, 136.1, 136.7, 139.9, 144.3, 144.6, 147.7 (Ar-*C*), 203.8 (Xyl-*m-C*); IR, ν/cm^{-1} (ATR): 3288 (br w, NH), 3024 (w), 2920 (w), 1703 (m), 1604 (m), 1527 (w), 1492 (w), 1345 (w), 1225 (w), 1077 (w), 1030 (w), 818 (m), 766 (m), 700 (s); MS/ES+ *m/z* (%): 544 (M^+, 97%); acc. mass ESI-MS calcd. for $C_{41}H_{37}N$ (MH^+): 543.2926; found: 543.2895.

^{F6Xyl}L*H (15). The method for the synthesis of ^{Ph}L*H was followed, Ar*NH_2 (5.0 g, 11.4 mmol), KOBu^t (1.78 mg, 15.9 mmol), Im($PdCl_2$)IPr catalyst (184 mg, 2.5 mol%), and 3,5-bis(trifluoromethyl)bromobenzene (1.41 mL, 8.20 mmol) in the initial stage of the reaction; and Im($PdCl_2$)IPr (184 mg, 2.5 mol%) and 3,5-bis (trifluoromethyl)bromobenzene (0.94 mL, 5.47 mmol) in the latter stage of the reaction. The product was isolated as an analytically pure pale-brown solid (2.38 g, 32%). M.p.: 102–108 °C; ^{1}H NMR (C_6D_6, 400 MHz, 298 K): δ = 1.78 (s, 3H, Ar*-*p-Me*), 4.53 (s, 1H, N*H*), 5.54 (s, 2H, Ph_2C*H*), 6.41 (br s, 2H, Ar*-*m*-C*H*), 6.90–7.16 (m, 20H, Ar-*H*); ^{13}C NMR (C_6D_6, 75.5 MHz, 298 K): δ = 21.4 (Ar*-*p-Me*), 52.5 (*C*HPh_2), 112.0 (*C*F_3), 126.8, 127.9, 128.7, 129.6, 130.6, 132.4, 132.8, 133.3, 138.2, 143.2, 144.8, 148.4 (Ar-*C*); ^{19}F NMR (C_6D_6, 282 MHz, 298 K), −62.74 (br s); IR, ν/cm^{-1} (ATR): 3387 (br w, NH), 3026 (w), 1617 (bm), 1494 (m), 1469 (m), 1380 (m), 1274 (s), 1169 (s), 1126 (s), 1031 (w), 997 (w), 956 (w), 866 (w), 698 (s); MS/ES+, *m/z* (%): 652 (M^+, 24%); acc. mass (ESI-MS) calcd. for $C_{41}H_{30}F_6N$ (MH^+): 650.2282; found: 650.2278.

^{Mes}L*H (16). The method for the synthesis of ^{Ph}L*H was followed, but using Ar*NH_2 (5.00 g, 11.37 mmol), KOBu^t (1.66 g, 14.79 mmol), bromomesitylene (1.47 g, 7.39 mmol) and Im($PdCl_2$)IPr catalyst (0.185 g, 2.5 mol%) in the initial stage of the reaction; and Im($PdCl_2$)IPr (0.185 g, 2.5 mol%) and bromomesitylene (1.47 g, 7.39 mmol) in the latter stage of the reaction. The product was isolated as an off-white powder (4.95 g, 78%). X-ray quality crystals were grown by slow evaporation of a diethyl ether solution. M.p.: 254 °C; ^{1}H NMR (C_6D_6, 500 MHz): δ = 1.61 (s, 6H, Mes-*o-Me*), 1.88 (s, 3H, Ar*-*p-Me*), 2.18 (s, 3H, Mes-*p-Me*), 4.32 (s, 1H, N*H*), 5.73 (s, 2H, Ph_2C*H*), 6.73 (s, 2H, Mes-*m*-C*H*), 6.82 (s, 2H, Ar*-*m*-C*H*), 6.99–7.05 (m, 20H, Ar-*H*). ^{13}C{^{1}H} NMR (C_6D_6, 75.5 MHz, 298 K): δ = 18.89 (Mes-*o-Me*), 20.77 (Mes-*p-Me*), 21.24 (Ar*-*p-Me*), 52.93 (Ph_2*C*H), 126.3, 126.1, 128.6, 129.3, 129.7, 130.0, 130.1, 132.3, 138.3, 139.1, 139.3, 144.2 (Ar-*C*); IR, ν/cm^{-1} (ATR): 3402 (br w, NH), 2952 (br w), 1492 (m), 1445 (m), 1328 (m), 1276 (w), 1236 (w), 1160 (w), 1074 (w), 1029 (w), 909 (w), 889 (w), 859

(w), 761 (w), 745 (w), 696 (s); MS/ES *m/z* (%): 558 (M^+, 20%), 169 (Ph_2CH^+, 26%); acc. mass calcd for $C_{42}H_{40}N$ (MH^+): 558.3155; found: 558.3151.

^{Tripp}L*H (19). The method for the synthesis of ^{Ph}L*H was followed, but using Ar*NH_2 (5.0 g, 11.4 mmol), KOBu^t (1.78 mg, 15.9 mmol), Im($PdCl_2$)IPr catalyst (184 mg, 2.5 mol%), and 2,4,6-triisopropylbromobenzene (2.08 mL, 8.20 mmol) in the initial stage of the reaction; and Im($PdCl_2$)IPr (184 mg, 2.5 mol%) and 2,4,6-triisopropylbromobenzene (1.39 mL, 5.47 mmol) in the latter stage of the reaction. The product was isolated by extraction of the crude reaction mixture with hexane, and cooling the extract to −20 °C in order to precipitate unreacted Ar*NH_2. Decanting of the supernatant solution, followed by removal of volatiles in-vacuo and washing with methanol afforded the product as an off-white powder (2.92 g, 41%). M.p. 188–194 °C; ^{1}H NMR (C_6D_6, 500 MHz, 298 K): δ = 0.96 (d, 12H, Tripp-*o*-CH(CH_3)$_2$), 1.29 (d, 6H, Tripp-*p*-C*H*(CH_3)$_2$), 1.88 (s, Ar*-*p-Me*), 2.86 (sept, 1H, Tripp-*p*-C*H*(CH_3)$_2$), 2.87 (sept, 2H, Tripp-*o*-C*H*(CH_3)$_2$), 4.66 (s, 1H, N*H*), 5.93 (s, 2H, Ph_2C*H*), 6.94 (s, 2H, Ar*-*o*-C*H*), 7.01–7.11 (m, 22H, Ar-*H*); ^{13}C NMR (C_6D_6, 75.5 MHz, 298 K); δ = 21.7 (Tripp-*p*-CH(*C*H_3)), 24.4 (Tripp-*o*-CH(*C*H_3)$_2$), 25.3 (Tripp-*o*-*C*H(CH_3)$_2$), 29.1 (Tripp-*p*-*C*H(CH_3)$_2$), 35.2 (Ar*-*p-Me*), 53.0 (Ph_2*C*H), 122.3, 127.2, 129.2, 130.5, 131.5, 132.0, 137.8, 138.1, 140.9, 141.7, 144.2, 145.2 (Ar-*C*); IR, v/cm^{-1} (ATR): 3411 (br m, NH), 2958 (br m), 2362 (s), 1599 (s), 1491 (m), 1444 (s), 1321 (m), 1076 (s), 1030 (s), 872 (s), 748 (m), 898 (s); acc. mass calcd. for $C_{48}H_{52}N$ (MH^+): 642.4099; found: 642.4095.

(^{tBuO}L†)K (7.K). This compound was prepared following a method similar to that for (^{tBuO}L*)K, using ^{tBuO}L†H (4.0 g, 5.61 mmol), KH (292 mg, 7.30 mmol), and hexamethyldisilazane (∼60 μL, 5 mol%). The product was isolated as a free flowing off-white powder which was used without further purification (3.8 g, 90%). ^{1}H NMR (C_6D_6, 400 MHz, 298 K), δ = 1.11 (d, $^3J_{HH}$ = 7.2 Hz, 6H, Ar†-*p*-CH(CH_3)$_2$), 1.47 (s, 27H, OC(CH_3)$_3$), 2.67 (sept, $^3J_{HH}$ = 7.2 Hz, 1H, Ar†-*p*-C*H*(CH$_3$)$_2$), 6.65 (br s, 2H, Ph_2C*H*), 6.86 (br s, 2H, Ar†-*m*-C*H*), 6.90–7.42 (m, 20H, Ar-*H*); ^{13}C {^{1}H}NMR (C_6D_6, 75.5 MHz, 298 K), δ = 24.9 (Ar†-*p*-CH(*C*H$_3$)$_2$), 32.5 (OC(*C*H$_3$)$_3$), 33.7 (Ar†-*p*-*C*H(CH$_3$)$_2$), 52.4 (Ph_2*C*H), 71.0 (O*C*(CH$_3$)$_3$), 125.0, 125.7, 126.1, 127.3, 130.86, 131.1, 136.9, 142.1, 145.3, 147.2, 151.4, 152.9 (Ar-*C*); ^{29}Si{^{1}H} NMR (C_6D_6, 80 MHz, 298 K), δ = −95.4; IR, *v*/cm^{-1} (ATR): 3055 (w), 1593 (m), 1377 (s), 1361 (s), 1234 (m), 1192 (s), 1046 (s), 1031 (s), 811 (m), 767 (m), 696 (s).

(^{tBuO}L*)K (8.K). To a mixture of ^{tBuO}L*H (5.0 g, 7.29 mmol) and KH (350 mg, 8.75 mmol) was added THF (50 mL) and a catalytic amount of hexamethyldisilazane (80 μL, ∼5 mol%). The reaction mixture was then stirred overnight at ambient temperature under a flow of N_2. The resultant suspension was subsequently filtered, volatiles removed from the filtrate in vacuo, and the residue washed with 2 × 10 mL hexane. The residue was then dried under vacuum for 1 h, affording a free-flowing off-white powder which was used without further purification (4.4 g, 76%). ^{1}H NMR (C_6D_6, 400 MHz, 298 K), δ = 1.47 (s, 27H, OC(CH_3)$_3$), 2.20 (s, 3H, Ar*-*p-Me*), 6.64 (br s, 2H, Ph_2C*H*), 6.77 (br s, 2H, Ar*-*m*-C*H*), 6.85–7.41 (m, 20H, Ar-*H*); ^{13}C{^{1}H} NMR (C_6D_6, 75.5 MHz, 298 K), δ = 21.2 (Ar*-*p-Me*), 32.2 (OC(*C*H$_3$)$_3$), 51.9 (Ph_2*C*H), 70.8 (O*C*(CH$_3$)$_3$), 118.2,

125.2, 127.6, 128.5, 128.8, 129.3, 129.8, 130.3, 130.8, 136.8, 148.8, 152.6 (Ar-*C*); ^{29}Si{^{1}H} NMR (C_6D_6, 80 MHz, 298 K), δ = −96.6; IR, *ν*/cm^{-1} (ATR): 3059 (w), 1598 (m), 1372 (s), 1233 (m), 1190 (s), 1048 (s), 1013 (s), 986 (s), 810 (m), 767 (m), 705 (s), 687 (s).

(^{iPr}L†)GeCl (20). This compound was prepared in an analogous fashion to (^{Ph}L*)GeCl, using Bu^{n}Li (2.20 mL of a 1.6 M solution in hexanes), L†H (2.0 g, 3.21 mmol), and $GeCl_2$.dioxane (817 mg, 3.3 mmol). The crude toluene extract was filtered and concentrated to incipient crystallization, then placed at −20 °C overnight to give the title compound as pale yellow crystals (2.21 g, 89%); M. p. 208–212 °C; ^{1}H NMR (C_6D_6, 500 MHz, 298 K): δ = 0.93 (d, $^{3}J_{HH}$ = 6.8 Hz, 6H, Ar†-*p*-CH(C*H*$_3$)$_2$), 1.37 (d, $^{3}J_{HH}$ = 7.6 Hz, 18H, SiPr$^{i}_3$-CH(C*H*$_3$)$_2$), 2.17 (sept, $^{3}J_{HH}$ = 7.6 Hz, 3H, SiPr$^{i}_3$-C*H*(CH$_3$)$_2$), 2.47 (sept, $^{3}J_{HH}$ = 6.8 Hz, 1H, Ar†-*p*-C*H*(CH$_3$)$_2$), 6.27 (s, 2H, C*H*Ph$_2$), 6.82–7.34 (m, 22H, Ar-*H*); ^{13}C{^{1}H} NMR (C_6D_6, 75.5 MHz, 298 K): δ = 15.6 (SiPr$^{i}_3$-*C*H(CH$_3$)$_2$), 20.0 (SiPr$^{i}_3$-CH(*C*H$_3$)$_2$), 23.9 (Ar†-*p*-CH(*C*H$_3$)$_2$), 33.8 (Ar†-*p*-*C*H(CH$_3$)$_2$), 52.4 (*C*HPh$_2$), 125.7, 126.8, 128.8, 129.3, 129.7, 130.1, 131.3, 141.0, 144.0, 144.2, 145.0, 145.8 (Ar-*C*); ^{29}Si{^{1}H} NMR (C_6D_6, 80 MHz, 298 K): δ = 11.5; IR (ATR) ν/cm^{-1}: 2954(s), 2865(s), 1599 (m), 1493(s), 1112(m), 1076(w), 1033(w), 875(s), 698(s); MS/EI *m/z* (%): 467.2 (Ar†NH$_2^+$, 100), 452.2 (^{iPr}L†-Ph$_2$C$^+$, 48), 167.0 (CHPh$_2^+$, 35).

(^{iPr}L″)GeCl (21). This compound was prepared in an analogous fashion to (^{Ph}L*)GeCl, using Bu^{n}Li (0.41 mL, 1.6 M solution in hexane), ^{iPr}L″H (500 mg, 0.59 mmol). The crude residue was washed with hexane (5 mL) to give (^{iPr}L″)GeCl as a pale yellow solid (323 mg, 57%). M.p.: 260–264 °C (dec.); ^{1}H NMR (C_6D_6, 500 MHz, 298 K): δ = 0.98 (d, $^{3}J_{HH}$ = 6.8 Hz, 6H, Ar″-*p*-CH(C*H*$_3$)$_2$), 1.18 (s, 36H, Ar-*p*-C(C*H*$_3$)$_3$), 1.47 (d, $^{3}J_{HH}$ = 7.6 Hz, 18H, SiPr$^{i}_3$-CH(C*H*$_3$)$_2$), 2.28 (br sept, $^{3}J_{HH}$ = 7.6 Hz, 3H, SiPr$^{i}_3$-C*H*(CH$_3$)$_2$), 2.50 (sept, $^{3}J_{HH}$ = 6.8 Hz, 1H, Ar″-*p*-C*H*(CH$_3$)$_2$), 6.30 (s, 2H, (4-Bu^{t}Ph)$_2$C*H*), 7.14–7.38 (m, 18H, Ar-*H*); ^{13}C{^{1}H} NMR (C_6D_6, 75.5 MHz, 298 K): δ = 14.9 (SiPr$^{i}_3$-*C*H(CH$_3$)$_2$), 19.2 (SiPr$^{i}_3$-CH(*C*H$_3$)$_2$), 24.1 (Ar″-*p*-CH(*C*H$_3$)$_2$), 31.5 (Ar-C(*C*H$_3$)$_3$), 33.7 (Ar″-*p*-*C*H(CH$_3$)$_2$), 34.4 (Ar-*C*(CH$_3$)$_3$), 51.8 ((4-Bu^{t}Ph)$_2$*C*H), 125.5, 127.5, 129.9, 130.6, 131.9, 141.1, 141.3, 142.4, 143.2, 149.0 (Ar-*C*); ^{29}Si{^{1}H} NMR (C_6D_6, 298 K): δ = 10.9; IR, ν/cm^{-1} (ATR): 1509(m), 1406(w), 1362(m), 1202(w), 1110(m), 882(s), 826(s), 736(m), 690(m); MS/EI *m/z* (%): 956.5 (M$^+$, 12), 912.5 (M$^+$-Pr^{i}, 100), 847.7 (^{iPr}L″$^+$, 95).

(^{iPr}L†)SnCl (26). Bu^{n}Li (1.10 mL of a 1.6 M solution in hexanes) was added to solution of ^{iPr}L†H (1.0 g, 1.60 mmol) in THF (30 mL) at −80 °C. The resultant solution was warmed to 20 °C and stirred for 4 h. This was then added to a solution of $SnCl_2$ (332 mg, 1.85 mmol) in THF (10 mL) at −80 °C and the reaction mixture slowly warmed to 20 °C overnight. Volatiles were then removed in vacuo and the residue extracted with hot toluene (50 mL). The extract was filtered and volatiles removed from the filtrate in vacuo to yield a yellow-brown solid. This was recrystallized from a concentrated diethyl ether solution placed at −20 °C overnight, yielding the title compound as pale yellow crystals (1.01 g, 73%). M.p. 232–238 °C (dec.); ^{1}H NMR (C_6D_6, 500 MHz, 298 K): δ = 0.95 (d, $^{3}J_{HH}$ = 6.8 Hz, 6H, Ar†-*p*-CH(C*H*$_3$)$_2$), 1.43 (d, $^{3}J_{HH}$ = 7.6 Hz, 18H, SiPr$^{i}_3$-CH(C*H*$_3$)$_2$), 2.18 (sept,

$^{3}J_{HH}$ = 7.6 Hz, 3H, SiPr$^{i}_{3}$-C*H*(CH$_3$)$_2$), 2.47 (sept, $^{3}J_{HH}$ = 6.8 Hz, 1H, Ar†-*p*-C*H*(CH$_3$)$_2$), 6.44 (s, 2H, C*H*Ph$_2$), 6.74–7.32 (m, 20H, Ar-*H*); ^{13}C{^{1}H} NMR (C$_6$D$_6$, 75.5 MHz, 298 K): δ = 16.0 (SiPr$^{i}_{3}$-*C*H(CH$_3$)$_2$), 20.1 (SiPr$^{i}_{3}$-CH(*C*H$_3$)$_2$), 24.1 (Ar†-*p*-CH(*C*H$_3$)$_2$), 33.7 (Ar†-*p*-*C*H(CH$_3$)$_2$), 52.3 (*C*HPh$_2$), 126.6, 126.8, 127.3, 128.8, 129.8, 130.1, 130.4, 131.5, 143.9, 144.0, 145.5, 145.6 (Ar-*C*); ^{29}Si{^{1}H} NMR (C$_6$D$_6$, 80 MHz, 298 K): δ = 9.2; ^{119}Sn{^{1}H} NMR (C$_6$D$_6$, 149 MHz, 298 K): δ = 194.5; IR, ν/cm^{-1} (ATR): 3059(w), 3026(w), 1599(w), 1449(m), 1196 (w), 1075(m), 1032(w), 879(s), 832(s), 761(m); MS/EI *m/z* (%): 778.2 (M^{+}, 1), 734.2 (M^{+}-Pr^{i}, 17), 623.3 (^{iPr}L$^{\dagger+}$, 46), 167.2 (Ph$_2$C^{+}, 33).

(^{iPr}L†)SnBr (27). This compound was prepared in an analogous fashion to (^{iPr}L†)SnCl, but using ^{iPr}L†H (3.00 g, 4.81 mmol), Bu^{n}Li (3.16 mL, 1.6 M solution in hexane), and SnBr$_2$ (1.47 g, 5.29 mmol). The work-up involved solvent removal, extraction into hot toluene, the extract filtered, and volatiles removed again in vacuo. Washing of the residue with hexane afforded (^{iPr}L†)SnBr as an off-white powder, which was of high enough purity for further synthesis (3.28 g, 83%). Crystals of the compound suitable for X-ray diffraction were grown from a concentrated toluene solution at −30 °C. M.p.: 220–225 °C (decomp.); ^{1}H NMR (C$_6$D$_6$, 400 MHz, 298 K), δ = 0.95 (d, $^{3}J_{HH}$ = 6.8 Hz, 6H, Ar†-*p*-CH(C*H*$_3$)$_2$), 1.43 (d, $^{3}J_{HH}$ = 6.8 Hz, 18H, SiPr$^{i}_{3}$- CH(C*H*$_3$)$_2$), 2.23 (sept, $^{3}J_{HH}$ = 6.8 Hz, 3H, SiPr$^{i}_{3}$-C*H*(CH$_3$)$_2$), 2.48 (sept, $^{3}J_{HH}$ = 6.8 Hz, 1H, Ar†-*p*-C*H*(CH$_3$)$_2$), 6.43 (s, 2H, Ph$_2$C*H*), 6.76 (m, 2H, Ar†-*m*-C*H*), 6.90–7.31 (m, 20H, Ar-*H*); ^{13}C{^{1}H} NMR (C$_6$D$_6$, 75.5 MHz, 298 K), δ = 16.1 (SiPr$^{i}_{3}$-*C*H(CH$_3$)$_2$), 20.0 (SiPr$^{i}_{3}$-CH(*C*H$_3$)$_2$), 24.1 (Ar†-*p*-CH(*C*H$_3$)$_2$), 33.7 (Ar†-*p*-*C*H(CH$_3$)$_2$), 52.3 (Ph$_2$*C*H), 126.8, 127.4, 128.5, 128.8, 129.8, 130.5, 131.3, 140.7, 143.8, 144.2, 145.3, 145.7 (Ar-*C*); ^{29}Si{^{1}H} NMR (C$_6$D$_6$, 80 MHz, 298 K), δ = 9.3; ^{119}Sn{^{1}H} NMR (C$_6$D$_6$, 149.2 MHz, 298 K): δ = 290.6; IR, ν/cm^{-1} (ATR): 3058 (w), 3025 (w), 1945 (w), 1873 (w), 1804 (w), 1598 (w), 1378 (m), 1325 (w), 1222 (m), 1195 (m), 1115 (m), 1074 (m), 1031 (m), 878 (s), 831 (s), 760 (m); MS/EI *m/z* (%): 778 (M-Pr^{i+}, 4%), 623 (^{iPr}L$^{\dagger+}$, 52%), 580 (^{iPr}L†-Pr^{i+}, 100%).

(^{Ph}L*)GeCl (28). LiBu^{n} (1.33 mL, 1.6 M solution in hexane) was added to a solution of ^{Ph}L*H (1.00 g, 1.94 mmol) in THF (50 mL) at −80 °C over 5 min. The reaction mixture was warmed to room temperature and stirred for 4 h. The resultant solution was then added to a solution of GeCl$_2$.dioxane (0.494 g, 2.13 mmol) in THF (10 mL) at −80 °C. The resultant solution was warmed to room temperature and stirred for 12 h, whereupon volatiles were removed in vacuo. The residue was extracted with toluene (35 mL), the extract filtered and volatiles removed in vacuo to give (^{Ph}L*)GeCl as a pale yellow solid (0.78 g, 65%). Mp: 94–96 °C; ^{1}H NMR (500 MHz, C$_6$D$_6$, 298 K): *δ* = 1.89 (s, 3H, Ar*-*p*-*Me*), 5.69 (s, 2H, Ph$_2$C*H*), 6.89–7.45 (m, 27H, Ar-*H*); ^{13}C{^{1}H} NMR (75.5 MHz, C$_6$D$_6$): *δ* = 21.4 (Ar*-*p*-*Me*), 52.7 (Ph$_2$*C*H), 119.5, 122.6, 128.6, 129.5, 129.8, 130.5, 130.6, 137.2, 139.7, 143.9, 142.3, 149.1 (Ar-*C*); IR ν/cm^{-1} (ATR): 1492(m), 1445(m), 1308(w), 1256(w), 1231(w), 1177(w), 1122(w), 907(w), 884(w), 750(m), 696(s); MS/EI *m/z* (%): 515.2 (^{Ph}L*H^{+}, 100), 439.1 (Ar*NH^{+}, 6), 167.0 (Ph$_2$CH^{+}, 9).

(^{F6Xyl}L*)GeCl (29). This compound was prepared in an analogous fashion to (^{Ph}L*)GeCl, but using Bu^{n}Li (0.53 mL, 1.6 M in hexane), ^{F6Xyl}L*H (0.50 g, 0.77 mmol), and $GeCl_2$.dioxane (0.20 g, 0.85 mmol). The crude residue was washed with hexane (5 mL) and dried in vacuo to give (^{F6Xyl}L*)GeCl as a pale brown powder (321 mg, 55%). M.p.: 142–145 °C; ^{1}H NMR (C_6D_6, 400 MHz, 298 K): δ 1.78 (s, 3H, Ar*-*p-Me*), 5.48 (s, 2H, Ph_2CH), 6.41–7.68 (m, 25H, Ar-*H*); ^{13}C{^{1}H} NMR (C_6D_6, 75.5 MHz, 298 K): δ 25.2 (Ar*-*p-Me*), 52.7 (Ph_2CH), 69.0 (^{F6}Xyl-*m*-CF_3), 114.2, 117.7, 129.8, 130.4, 132.3, 132.7, 137.9, 138.0, 142.1, 143.8, 144.4, 150.6 (Ar-*C*); ^{19}F NMR (C_6D_6, 282 MHz, 298 K): δ −62.8; IR ν/cm^{-1} (ATR): 3062 (w), 3026 (w), 1610 (m), 1032 (m), 995 (m), 956 (s), 864 (m), 748 (m); MS/EI *m/z* (%): 759.0 (M^+, <1, correct isotopic distribution), 651.1 (^{F6Xyl}L*$^+$, 100).

(^{Mes}L*)GeCl (30). This compound was prepared in an analogous fashion to (^{Ph}L*)GeCl but using Bu^{n}Li (1.85 mL, 1.6 M solution in hexane), ^{Mes}L*H (1.50 g, 2.69 mmol) and $GeCl_2$.dioxane (0.686 g, 2.96 mmol). (^{Mes}L*)GeCl was obtained as a pale yellow solid (1.29 g, 72%). Mp: 155–157 °C; ^{1}H NMR (500 MHz, C_6D_6, 298 K): *δ* = 1.81 (s, 3H, Ar*-*p-Me*), 2.06 (s, 3H, Mes-*p-Me*), 2.27 (br s, 6H, Mes-*o-Me*), 6.14 (br s, 2H, Ph_2CH), 6.65–7.08 (m, 24H, Ar-*H*); ^{13}C{^{1}H} (75.5 MHz, C_6D_6): *δ* = 20.6 (Mes-*p-Me*), 21.0 (Ar*-*p-Me*), 26.7 (br, Mes-*o-Me*), 51.8 (br, Ph_2CH), 127.2 (br), 129.0 (br), 130.8 (br), 131.1 (br), 132.3 (br), 133.0, 133.2, 134.6, 142.5, 143.0, 145.2 (br), 147.2 (Ar-*C*); IR ν/cm^{-1} (ATR): 1433(m), 1369(w), 1235(w), 1216(m), 881(m), 863(bw), 881(m), 756(w), 697(s); MS/EI *m/z* (%): 665.1 (M^+, 2), 557.2 (^{Mes}L*$^+$, 100), 167.0 (Ph_2CH^+, 22); acc. mass. calc for $C_{42}H_{38}ClGeN$: 661.1930, found: 661.1934.

(^{Tripp}L*)GeCl (33). This compound was prepared in an analogous fashion to (^{Ph}L*)GeCl, using Bu^{n}Li (1.07 mL, 1.6 M in hexane), ^{Tripp}L*H (1.00 g, 1.56 mmol), and $GeCl_2$.dioxane (0.397 g, 1.72 mmol). The crude residue was washed with hexane (5 mL) and dried in vacuo to give (^{Tripp}L*)GeCl as a bright yellow powder (970 mg, 82%). M.p.: 96–108 °C (melt), 242–248 °C (decomp.); ^{1}H NMR (C_6D_6, 400 MHz, 298 K): δ 0.51–1.35 (v br, 12H, Tripp-*o*-CH(CH_3)$_2$), 1.23 (d, $^3J_{HH}$ = 6.9 Hz, 6H, Tripp-*p*-CH(CH_3)$_2$), 1.83 (s, 3H, Ar*-*p-Me*), 2.76 (sept, $^3J_{HH}$ = 6.9 Hz, 1H, Tripp-*p*-C*H*(CH_3)$_2$), 3.82 (v br, 2H, Tripp-*o*-C*H*(CH_3)$_2$), 5.89 (br, 2H, C*H*Ph_2), 6.60-7.50 (br m, 24H, Ar-*H*); ^{13}C{^{1}H} NMR (C_6D_6, 75.5 MHz, 298 K): the broadness of the majority of the signals in this spectrum made them difficult to confidently assign; IR ν/cm^{-1} (ATR): 1598 (w), 1164 (w), 1032 (w), 881 (w), 744 (m); MS/EI *m/z* (%): 749.3 (M^+, 5, correct isotopic distribution), 641.4 (^{Tripp}L*$^+$, 100).

References

1. Asay M, Jones C, Driess M (2011) N-heterocyclic carbene analogues with low-valent group 13 and group 14 elements: syntheses, structures, and reactivities of a new generation of multitalented ligands. Chem Rev 111:354

2. Nagendran S, Roesky HW (2008) The chemistry of aluminum(I), silicon(II), and germanium(II). Organometallics 27:457
3. Stasch A, Jones C (2011) Stable dimeric magnesium(I) compounds: from chemical landmarks to versatile reagents. Dalton Trans 40:5659
4. Barrett AGM, Crimmin MR, Hill MS, Procopiou PA (2010) Heterofunctionalization catalysis with organometallic complexes of calcium, strontium and barium. Proc R Soc A 466:927
5. Edelmann FT (2009) Lanthanide amidinates and guanidinates: from laboratory curiosities to efficient homogeneous catalysts and precursors for rare-earth oxide thin films. Chem Soc Rev 38:2253
6. Edelmann FT (2012) Lanthanide amidinates and guanidinates in catalysis and materials science: a continuing success story. Chem Soc Rev 41:7657
7. Edelmann FT (2008) Advances in the coordination chemistry of amidinate and guanidinate ligands. Adv Organomet Chem 57:183
8. Kurek A, Gordon PG, Karle S, Devi A, Barry ST (2014) The Chemistry of guanidine, guanidinium, and guanidinate compounds. Aust J Chem 67:989
9. Barker J, Kilner M (1994) The coordination chemistry of the amidine ligand. Coord Chem Rev 133:219
10. Edelmann FT (1994) N-silylated benzamidines: versatile building blocks in main group and coordination chemistry. Coord Chem Rev 137:403
11. Coles MP (2006) Application of neutral amidines and guanidines in coordination chemistry. Dalton Trans 8:985
12. Hong J, Zhang L, Wang K, Chen Z, Wu L, Zhou X (2013) Synthesis, structural characterization, and reactivity of mono(amidinate) rare-earth-metal bis(aminobenzyl) complexes. Organometallics 32:7312
13. Jin G, Jones C, Junk PC, Lippert KA, Rose RP, Stasch A (2009) Synthesis and characterisation of bulky guanidines and phosphaguanidines: precursors for low oxidation state metallacycles. New J Chem 33:64
14. Rauchfuss TB (2010) Inorganic syntheses, vol 35. Wiley, New Jersey
15. Rodriguez MM, Bill E, Brennessel WW, Holland PL (2011) N_2 reduction and hydrogenation to ammonia by a molecular iron-potassium complex. Science 334:780
16. Budzelaar PHM, van Oorta AB, Orpenb AG (1998) β-Diiminato complexes of V^{III} and Ti^{III} – formation and structure of stable paramagnetic dialkylmetal compounds. Eur J Inorg Chem 10:1485
17. Lappert MF, Protchenko AV, Power PP, Seeber AL (eds) (2008) Metal amide chemistry. Wiley, New Jersey
18. Edelmann FT (2008) Advances in organometallic chemistry. Chapter 3: advances in the coordination chemistry of amidinate and guanidinate ligands, vol 57. Elsevier, Amsterdam, pp 183
19. Green SP, Jones C, Junk PC, Lippert KA, Stasch A (2006) Synthetic, structural and theoretical studies of amidinate and guanidinate stabilised germanium(I) dimers. Chem Commun 38:3978
20. Jones C, Rose RP, Stasch A (2008) Synthesis, characterisation and reactivity of germanium (II) amidinate and guanidinate complexes. Dalton Trans 21:2871
21. Nagendran S, Sen SS, Roesky HW, Koley D, Grubmüller H, Pal A, Herbst-Irmer R (2008) RGe(I)Ge(I)R compound (R = $PhC(NtBu)_2$) with a Ge−Ge single bond and a comparison with the gauche conformation of hydrazine. Organometallics 27:5459
22. Matioszek D, Katir N, Saffon N, Castel A (2010) Halogermanium(II) complexes having phenylamidinate as supporting ligands: syntheses, characterizations, and reactivities. Organometallics 29:3039
23. Chlupatý T, Padělková Z, Lyčka A, Brus J, Růžička A (2012) Reactivity of lithium n-butyl amidinates towards group 14 metal(II) chlorides providing series of hetero- and homoleptic tetrylenes. Dalton Trans 41:5010

24. Nimitsiriwat N, Gibson VC, Marshall EL, White AJP, Dale SH, Elsegood MRJ (2007) Tert-butylamidinate tin(II) complexes: high activity, single-site initiators for the controlled production of polylactide. Dalton Trans 39:4464
25. Sen SS, Kritzler-Kosch MP, Nagendran S, Roesky HW, Beck T, Pal A, Herbst-Irmer R (2010) Synthesis of monomeric divalent tin(II) compounds with terminal chloride, amide, and triflate substituents. Eur J Inorg Chem 33:5304
26. Brym M, Francis MD, Jin G, Jones C, Mills DP, Stasch A (2006) Facile transformations of a 1,3,5-triphosphacyclohexadienyl anion within the coordination sphere of group 13 and 14 elements: synthesis of 1,3-diphosphacyclopentadienyl complexes and phosphaorganometallic cage compounds. Organometallics 25:4799
27. Stasch A, Forsyth CM, Jones C, Junk PC (2008) Thermally stable lead(II) amidinates and guanidinates. New J Chem 32:829
28. So CW, Roesky HW, Magull J, Oswald RB (2006) A Stable silylenoid and a donor-stabilized chlorosilylene: low-coordinate silicon compounds—a never-ending story? Angew Chem Int Ed 45:3948
29. Sen SS, Roesky HW, Stern D, Henn J, Stalke D (2010) High yield access to silylene RSiCl (R = $PhC(NtBu)_2$) and its reactivity toward alkyne: synthesis of stable disilacyclobutene. J Am Chem Soc 132:1123
30. Stoelzel M, Präsang C, Blom B, Driess M (2013) N-heterocyclic silylene (NHSi) rhodium and iridium complexes: synthesis, structure, reactivity, and catalytic ability. Aust J Chem 66:1163
31. Stoelzel M, Präsang C, Inoue S, Enthaler S, Driess M (2012) Hydrosilylation of alkynes by Ni$(CO)_3$-stabilized silicon(II) hydride. Angew Chem Int Ed 51:399
32. Ding Y, Hao H, Roesky HW, Noltemeyer M, Schmidt HG (2001) Synthesis and structures of germanium(II) fluorides and hydrides. Organometallics 20:4806
33. Saur I, Miqueu K, Rima G, Barrau J, Lemierre V, Chrostowska A, Sotiropoulos JM, Pfister-Guillouzo G (2003) New insight into the three-coordinate divalent germanium compounds $L^2GeΣ$ (L^2 = PhNC(Me)CHC(Me)NPh, Σ = Cl, I, Me, OMe). structural, photoelectron spectroscopic, and theoretical analysis. Organometallics 22:3143
34. Woodul WD, Richards AF, Stasch A, Driess M, Jones C (2010) N-heterocyclic germylidenide and stannylidenide anions: Group 14 Metal(II) Cyclopentadienide Analogues. Organometallics 29:3655
35. Xiong Y, Yao S, Driess M (2012) Synthesis and tunable reactivity of N-heterocyclic germylene. Chem Asian J 7:2145
36. Jana A, Schwab G, Roesky HW, Stalke D (2010) Synthesis and characterization of β-diketiminate germanium(II) and tin(II) bromides. Inorg Chim Acta 363:4408
37. Ding Y, Roesky HW, Noltemeyer M, Schmidt HG (2001) Synthesis and structures of monomeric divalent germanium and tin compounds containing a bulky diketiminato ligand. Organometallics 20:1190
38. Jana A, Roesky HW, Schulzke C, Döring A, Beck T, Pal A, Herbst-Irmer R (2009) Facile access of stable divalent tin compounds with terminal methyl, amide, fluoride, and iodide substituents. Inorg Chem 48:193
39. Jana A, Sarish SP, Roesky HW, Leusser D, Objartel I, Stalke D (2011) Pentafluoropyridine as a fluorinating reagent for preparing a hydrocarbon soluble β-diketiminatolead(II) monofluoride. Chem Commun 47:5434
40. Chen M, Fulton JR, Hitchcock PB, Johnstone NC, Lappert MF, Protchenko AV (2007) Synthesis and theoretical studies on rare three-coordinate lead complexes. Dalton Trans 26:2770
41. Yoshifuji M, Shima I, Inamoto N (1981) Synthesis and structure of bis (2,4,6-tri-tert-butylphenyl)diphosphene: isolation of a true phosphobenzene. J Am Chem Soc 103:4587
42. Sekiguchi A, Kinjo R, Ichinohe M (2004) A stable compound containing a silicon-silicon triple bond. Science 305:1755
43. Du CJF, Hart H, Ng KKD (1986) A one-pot synthesis of m-terphenyls, via a two-aryne sequence. J Org Chem 51:3162

44. Schiemenz B, Power PP (1996) Synthesis of sterically encumbered terphenyls and characterization of their metal derivatives $Et_2OLiC_6H_3$-2,6-$Trip_2$ and $Me_2SCuC_6H_3$-2,6-$Trip_2$ (Trip = 2,4,6-*i*-$Pr^3C_6H_2$-). Organometallics 15:958
45. Rivard E, Power PP (2007) Multiple bonding in heavier element compounds stabilized by bulky terphenyl ligands. Inorg Chem 46:10047
46. Simons RS, Haubrich ST, Mork BV (1998) The syntheses and characterization of the bulky terphenyl silanes and chlorosilanes 2,6-$Mes_2C_6H_3SiCl_3$, 2,6-$Trip_2C_6H_3SiCl_3$, 2,6-$Mes_2C_6H_3SiHCl_2$, 2,6-$Trip_2C_6H_3SiHCl_2$, 2,6-$Mes_2C_6H_3SiH_3$, 2,6-$Trip_2C_6H_3SiH_3$ and 2,6-$Mes_2C_6H_3SiCl_2SiCl_3$. Main Grp Chem 2:275
47. Pietschnig R, West R, Powell DR (2000) Reduction of terphenyltrifluorosilanes: C−C insertion products and possible formation of a disilyne. Organometallics 19:2724
48. Filippou AC, Chernov O, Blom B, Stumpf KW, Schnakenburg G (2010) Stable n-heterocyclic carbene adducts of arylchlorosilylenes and their germanium homologues. Chem Eur J 16:2866
49. Stender M, Pu L, Power PP (2001) Stabilized terphenyl-substituted digermene derivatives of simple organic groups and their halide precursors: preference for symmetrically bonded structures. Organometallics 20:1820
50. Pu L, Olmstead MM, Schiemenz B, Power PP (1998) Synthesis and characterization of the monomeric terphenyl−metal halides Ge(Cl){C_6H_3-2,6-$Trip_2$} (Trip = C_6H_2-2,4,6-*i*-Pr_3) and Sn(I){C_6H_3-2,6-$Trip_2$} and the terphenyl−metal amide Sn{$N(SiMe_3)_2$}{C_6H_3-2,6-$Trip_2$}. Organometallics 17:5602
51. Peng Y, Fischer RC, Merrill WA, Fischer J, Pu L, Ellis BD, Fettinger JC, Herberb RH, Power PP (2010) Substituent effects in ditetrel alkyne analogues: multiple vs. single bonded isomers. Chem Sci 1:461
52. Fischer RC, Power PP (2010) π-Bonding and the lone pair effect in multiple bonds involving heavier main group elements: developments in the new millennium. Chem Rev 110:3877
53. Simons RS, Pu L, Olmstead MM, Power PP (1997) Synthesis and characterization of the monomeric diaryls M{C_6H_3-2,6-Mes_2}$_2$ (M = Ge, Sn, or Pb; Mes = 2,4,6-$Me_3C_6H_2$−) and dimeric aryl−metal chlorides [M(Cl){C_6H_3-2,6-Mes_2}]$_2$ (M = Ge or Sn). Organometallics 16:1920
54. Eichler BE, Pu L, Stender M, Power PP (2001) The synthesis and structure of sterically encumbered terphenyl tin(II) halide derivatives: simultaneous existence of monomers and dimers in the crystalline phase. Polyhedron 20:551
55. Pu L, Phillips AD, Richards AF, Stender M, Simons RS, Olmstead MM, Power PP (2003) Germanium and tin analogues of alkynes and their reduction products. J Am Chem Soc 125:11626
56. Hino S, Olmstead MM, Phillips AD, Wright RJ, Power PP (2004) Terphenyl ligand stabilized lead(II) derivatives: steric effects and lead−lead bonding in diplumbenes. Inorg Chem 43:7346
57. Filippou AC, Weidemann N, Schnakenburg G, Rohde H, Philippopoulos AI (2004) Tungsten–lead triple bonds: syntheses, structures, and coordination chemistry of the plumbylidyne complexes trans-[$X(PMe_3)_4W{\equiv}Pb$(2,6-$Trip_2C_6H_3$)]. Angew Chem Int Ed 43:6512
58. Pu L, Twamley B, Power PP (2000) Terphenyl ligand stabilized lead(II) derivatives of simple organic groups: characterization of Pb(R)C_6H_3-2,6-$Trip_2$ (R = Me, t-Bu, or Ph; Trip = C_6H_2-2,4,6-*i*-Pr_3), {Pb(μ-Br)C_6H_3-2,6-$Trip_2$}$_2$, py·Pb(Br)C_6H_3-2,6-$Trip_2$ (py = pyridine), and the bridged plumbylyne complex [{$W(CO)_4$}$_2$(μ-Br)(μ-PbC_6H_3-2,6-$Trip_2$)]. Organometallics 19:2874
59. Agou T, Sugiyama Y, Sasamori T, Sakai H, Furukawa Y, Takagi N, Guo JD, Nagase S, Hashizume D, Tokitoh N (2012) Synthesis of kinetically stabilized 1,2-dihydrodisilenes. J Am Chem Soc 134:4120
60. Sasamori T, Hironaka K, Sugiyama Y, Takagi N, Nagase S, Hosoi Y, Furukawa Y, Tokitoh N (2008) Synthesis and reactions of a stable 1,2-diaryl-1,2-dibromodisilene: a precursor for substituted disilenes and a 1,2-diaryldisilyne. J Am Chem Soc 130:13856

61. Sasamori T, Sugiyama Y, Takeda N, Tokitoh N (2005) Structure and properties of an overcrowded 1,2-dibromodigermene. Organometallics 24:3309
62. Mizuhata Y, Noda N, Tokitoh N (2010) Generation of stannabenzenes and their properties. Organometallics 29:4781
63. Kano N, Tokitoh N, Okazaki R (1997) Synthesis and X-ray crystal structure of Bis{2,4,6- tris [bis(trimethylsilyl)methyl]phenyl}dibromoplumbane: the first monomeric diorganodihaloplumbane in the crystalline state. Organometallics 16:2748
64. Weber SG, Loos C, Rominger F, Straub BF (2012) Synthesis of an extremely sterically shielding N-heterocyclic carbene ligand. ARKIVOC (iii):226
65. Li J, Stasch A, Schenk C, Jones C (2011) Extremely bulky amido-group 14 element chloride complexes: potential synthons for low oxidation state main group chemistry. Dalton Trans 40:10448
66. Beckmann J, Dakternieks D, Duthie A, Larchin ML, Tiekink ERT (2003) tert-Butoxysilanols as model compounds for labile key intermediates of the sol–gel process: crystal and molecular structures of $(t\text{-}BuO)_3SiOH$ and $HO[(t\text{-}BuO)_2SiO]_2H$. Appl Organometal Chem 17:52
67. Li J, Jones C. Unpublished Results
68. Surry DS, Buchwald SL (2011) Dialkylbiaryl phosphines in Pd-catalyzed amination: a user's guide. Chem Sci 2:27
69. Sakakura A, Koshikari Y, Akakura M, Ishihara K (2012) Hydrophobic N,N-diarylammonium pyrosulfates as dehydrative condensation catalysts under aqueous conditions. Org Lett 14:30
70. Zhu L, Ye YM, Shao LX (2012) Well-defined NHC–Pd(II)–Im (NHC=N-heterocyclic carbene; Im=1-methylimidazole) complex catalyzed C–N coupling of primary amines with aryl chlorides. Tetrahedron 68:2414
71. Zhu L, Gaou TT, Shao LX (2011) Well-defined NHC–Pd(II)–Im (NHC=N-heterocyclic carbene; Im=1-methylimidazole) complexes catalyzed amination of aryl chlorides. Tetrahedron 67:5150

Chapter 3
Synthesis and Reactivity of Heavier Alkyne Analogues Stabilised by Extremely Bulky Amide Ligands

3.1 Introduction

Over recent decades, numerous landmark discoveries in the area of main-group chemistry have been realised. Of most relevance to this thesis are the advances that have been made in regards to complexes incorporating the heavier group 14 elements in unusual co-ordination environments and oxidation states. This work has led us to a far greater understanding of discrepancies between the chemistries of these heavier elements and carbon [1–5]. Amongst the most significant of the discoveries in this area are the syntheses and further studies of the heavier alkyne analogues, LEEL (L = a bulky monodentate anionic ligand, E = Si–Pb), which can incorporate a number of the bulky ligands as discussed in Chap. 2. Contrary to the relatively benign alkynes, the heavier analogues thereof (i.e. ditetrelynes) have been shown to be highly reducing, and to have some singlet-biradicaloid character [2], making them effective for the activation of small molecules such as CO_2 and H_2 (vide infra). The first example of a heavier ditetrelyne was a lead derivative isolated by Power in 2000 [6]. Since that time, examples involving the remaining elements of group 14 have been successfully isolated [7]. Here, the generation of these highly reactive species will be discussed, as will some of their further chemistry, so as to highlight their importance in our understanding of contemporary main-group chemistry.

3.1.1 Silicon Analogues of Alkynes

3.1.1.1 Synthesis and Reactivity of 2-Coordinate Disilynes

The first synthesised and fully characterised disilyne, LSiSiL, was reported by the group of Sekiguchi in 2004 [8]. This came after years of suggestions that E–E triple

T.J. Hadlington, *On the Catalytic Efficacy of Low-Oxidation State Group 14 Complexes*, Springer Theses, DOI 10.1007/978-3-319-51807-7_3

bonding was not possible for the heavier elements of the *p*-block [9, 10]. Nevertheless, the isolated disilyne features a triply bonded Si–Si core, kinetically stabilised by two anionic silicon-based ligands (^{Si}L = [Si{CH(TMS)$_2$}$_2$Pr^i]$^-$), each of which bears two bis(TMS)methyl (TMS = trimethylsilyl) groups and one *iso*-propyl group bound to a central 4-coordinate silicon atom. This disilyne, {(^{Si}L)Si}$_2$, is accessed via reduction of the dimeric tetra(bromo) Si(III) precursor, {(^{Si}L)SiBr$_2$}$_2$ with four equivalents of KC_8, and was isolated in a good yield (Scheme 3.1). The Si–Si bond distance of 2.0622(9) Å is considerably shorter than the average Si–Si double bond (2.186 Å [11]) and Si–Si single bond (2.364 Å [11]). As had been computationally predicted [12–14], the disilyne has a *trans*-bent structure, unlike linear alkyne counterparts, suggesting lessened hybridisation between the *s*- and *p*-orbitals at the two Si(0) centres. The *trans*-bending angle (^{Si}L–Si–Si), θ = 137.44 (4)°, is in keeping with those predicted by Shaefer for parent disilyne, HSiSiH (124.5–127.4°), as is the length of the Si–Si triple bond (2.077–2.103 Å) [13]. This discovery further disproved the "double-bond rule", which stated that multiple bonding between elements with a principal quantum number equal to or greater than 3 cannot form multiple element-element bonds, due to Pauli repulsion between the inner shells for these elements [15, 16].

Since this initial publication, three related triply-bonded dimeric Si(I) species have been synthesised, one asymmetric example which relies upon stabilisation from both ^{Si}L and a modified version of ^{Si}L, ^{Si}L′ (^{Si}L′ = [Si{CH(TMS)$_2$}$_2$CH$_2$Bu^t]$^-$) [17], one utilising a novel bulky alkyl ligand, Rs (Rs = 1,1-bis(TMS)-3,3-dimethylbutyl) [18], and an example using the Bbt ligand, discussed in Chap. 2 (Bbt = 2,4,6-{(TMS)$_2$CH}$_3$Ph) [19]. The former two examples of disilynes were synthesised in a similar manner to {(^{Si}L)Si}$_2$, i.e. via reduction of dimeric tetrahalo-Si(III) species, {(^{Si}L′)SiCl$_2$}$_2$ and {(Rs)SiBr$_2$}$_2$, respectively. The

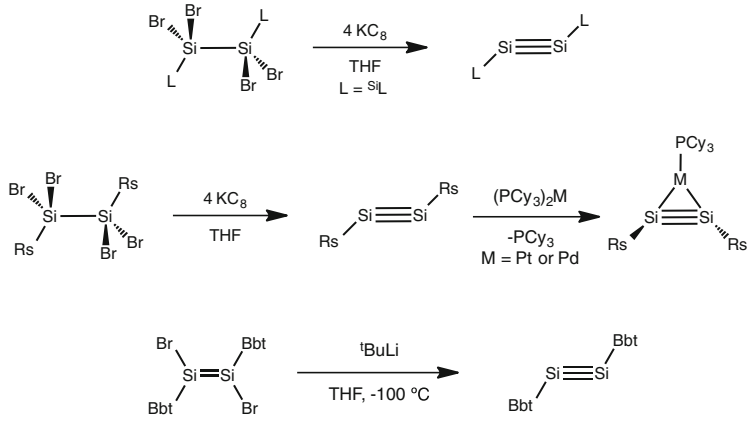

Scheme 3.1 Synthesis of reported disilynes, {(^{Si}L)Si}$_2$, {(Rs)Si}$_2$, and {(Bbt)Si}$_2$

aryl-disilyne, $\{(Bbt)Si\}_2$, was synthesised via reaction of the disilene, $\{(Bbt)SiBr\}_2$, with one equivalent of Bu^tLi, with loss of LiBr and Bu^tBr. All reported disilynes feature a Si–Si triple bond and *trans*-bent structures. All Si–Si distances (2.0569 (12)–2.108(5) Å) and *trans*-bending angles (132.05(7)–138.78(5)°) are within a narrow range, and are in keeping with Shaefer's computational predictions [13].

These species have been shown effective in the reductive coupling of, and cycloaddition with, unsaturated bonds, and the facile activation of B–H bonds and C–H bonds. Although by no means exhaustive, some notable examples of reported disilyne reactivity are outlined in Scheme 3.2 ($\{(^{Si}L)Si\}_2$ [20–23]) and Scheme 3.3 ($\{(Bbt)Si\}_2$ [24, 25]). These examples highlight the reductive capacity of the Si–Si triple bond, relative to C–C triple bonds, as all involve the oxidative cleavage of at least one Si–Si bond component. Indeed, examples of such C–C bond couplings are rare, and certainly not a main-stay of *p*-block chemistry, making these examples quite remarkable.

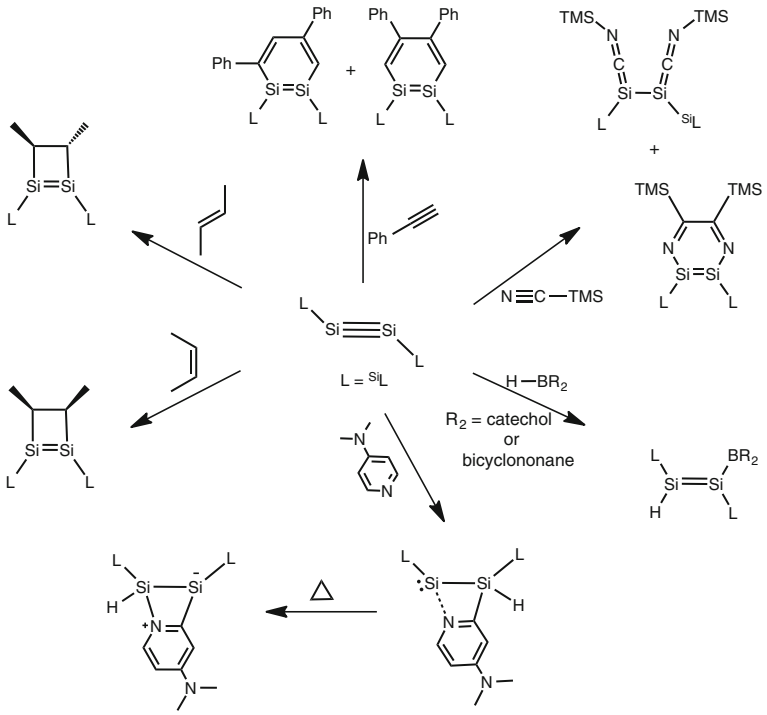

Scheme 3.2 Examples of reactivity of $\{(^{Si}L)Si\}_2$

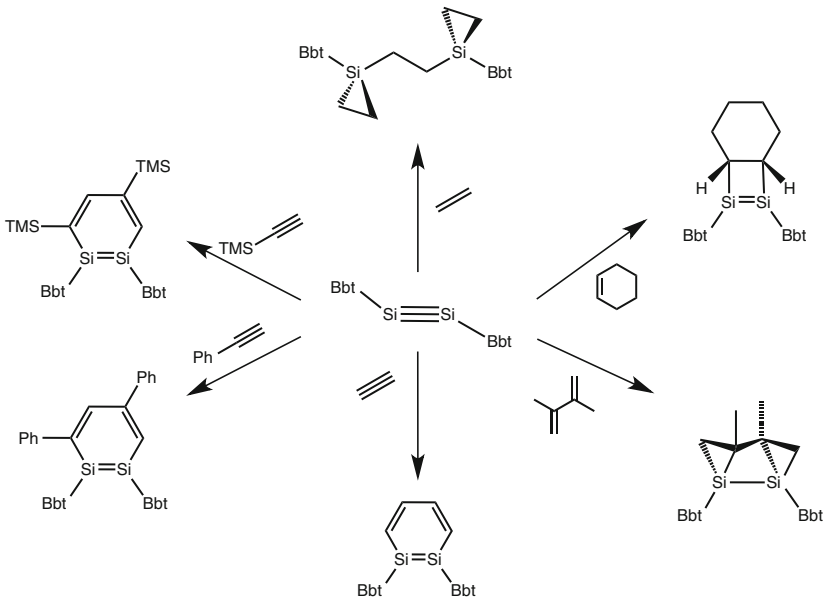

Scheme 3.3 Examples of reactivity of $\{(Bbt)Si\}_2$

3.1.2 Germanium Analogues of Alkynes

3.1.2.1 Synthesis of 2-Coordinate Digermynes

The first example of a Ge(I) dimer, LGeGeL, was reported by Power and co-workers in 2004, and utilised the bulky ^{Dipp}Terph ligand (^{Dipp}Terph = 2,6-(Dipp)$_2$Ph, Dipp = 2, 6-Pr$^i{}_2$Ph) [26]. It was synthesised by the reduction of (^{Dipp}Terph)GeCl with finely divided potassium and was isolated in a moderate yield (Scheme 3.4a). Notable is the Ge–Ge bond length (2.2850(6) Å), which is within the known range for Ge–Ge double bonds (mean Ge–Ge double bond = 2.332 Å) [11], suggesting the presence of non-bonding electron density at the Ge centres, giving the dimer singlet-biradicaloid character [2, 5]. The digermyne also has a *trans*-bent structure (θ = 128.67(8)°) not dissimilar to that observed for the disilynes (vide supra). The increased deviation from linearity can be attributed to an increase in ΔE between the *s*- and *p*- frontier orbitals of the monomemeric germylyne fragments which make up the digermyne, relative to the silylyne fragments which make up a disilyne. This further reduces the *s*-character in the Ge–Ge bond, relative to the Si–Si bond, with an expected reduction in bond order. These observations are in keeping with computational studies on a modified model of $\{(^{Dipp}Terph)Ge\}_2$, viz. $\{(^{Tripp}Terph)Ge\}_2$ (^{Tripp}Terph = 2,6-Tripp$_2$Ph, Tripp = 2, 4, 6-Pr$^i{}_3$Ph) [27]. Despite the lack of a formal triple bond, such species will be referred to as digermynes throughout this thesis. Since Power's initial publication,

several aryl-digermynes and one amido-digermyne have been reported (Scheme 3.4), with great variations in the Ge–Ge bond lengths and bond orders [28–30]. The aryl-substituted examples all display similar Ge–Ge bond lengths (2.2059(8) Å–2.306(3) Å), and likely contain largely double-bond character [28, 29]. Interestingly, the bulkier ligands (e.g. ^{Tripp}Terph^{Dipp}, Bbt) induce some of the shorter Ge–Ge bonds, which is seemingly counterintuitive, and may be due to either dispersion forces or ligand electronics. Conversely to the aryl-stabilised digermynes, the amido-stabilised example, $\{(^{TMS}L^*)Ge\}_2$ ($^{TMS}L^* = \{(SiMe_3)NAr^*\}^-$, Ar* = 2,6-$(Ph_2CH)_2$-4-MePh) displays a much longer Ge–Ge distance, at 2.7093(6) Å, indicative of a Ge–Ge *single* bond. This is verified by theoretical calculations, which show the Ge–Ge bond to be of high *p* character, which gives a basis for the length of the bond [30].

Further, several molecular orbitals (MOs) displayed $N_{lonepair}$–Ge interactions, lessening the propensity for Ge–Ge multiple bonding due to the electronic saturation of the vacant *p*-orbital at germanium. This amido-digermyne was not accessible via alkali-metal reduction routes, contrary to aryl-derivatives, but was synthesised by reduction with $\{(^{Mes}nacnac)Mg\}_2$, which, as described in Chap. 1, has seen great synthetic utility in reduction chemistry.

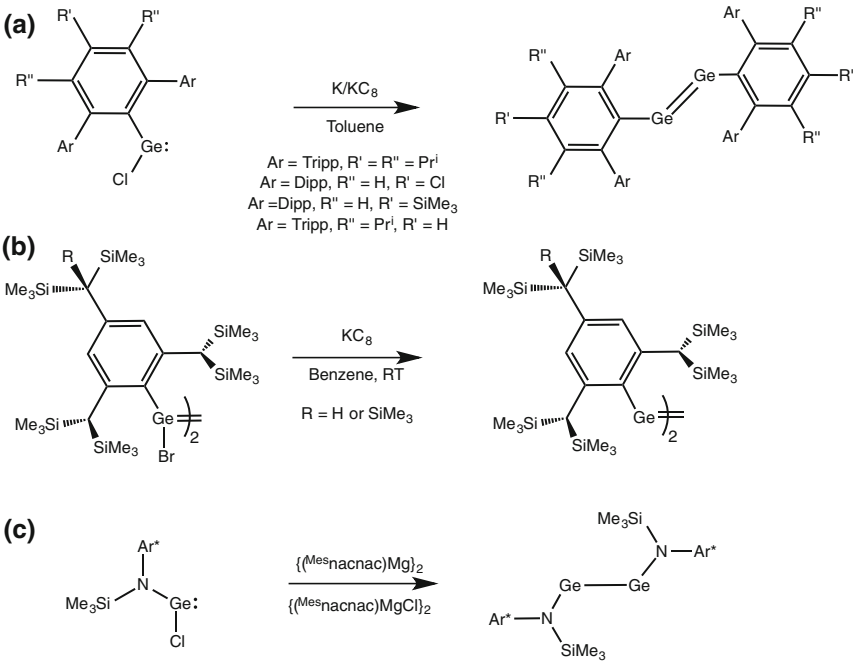

Scheme 3.4 **a**, **b** The synthesis of aryl-ligated digermynes. **c** The synthesis of an amido digermyne

The chemistry of the digermynes has been extremely fruitful, and for ease of discussion will be broken down into two parts: discrete small molecule activations and coordination; and reactions involving olefin addition and activation reactions.

3.1.2.2 Reactivity of 2-Coordiante Digermynes Towards H_2 and Lewis-Bases

Initial reactivity studies of Power's digermyne, $\{(^{Dipp}Terph)Ge\}_2$, led to chemistry never before observed for *p*-block elements: the homolytic cleavage of H_2. Addition of one, two, or three equivalents of H_2 to $\{(^{Dipp}Terph)Ge\}_2$ at ambient temperature resulted in the formation of a mixture of compounds containing Ge(II), Ge(III), and Ge(IV) hydride complexes (Scheme 3.5) [31]. This facile activation of a relatively benign small molecule suggested a new vista for the chemistry of such low-oxidation state elements, and has brought them comparisons with transition elements [2]. It has been speculated that this reaction occurs via donation of a Ge–Ge based π-orbital to the σ*-orbital on the H_2 molecule, with concomitant donation from the σ-orbital of H_2 to the n_+-orbital of the digermyne. This interaction is aided by the narrow HOMO-LUMO gap of ∼2 eV in the digermyne. Subsequent DFT studies suggested a complex set of mechanisms for the formation of these various

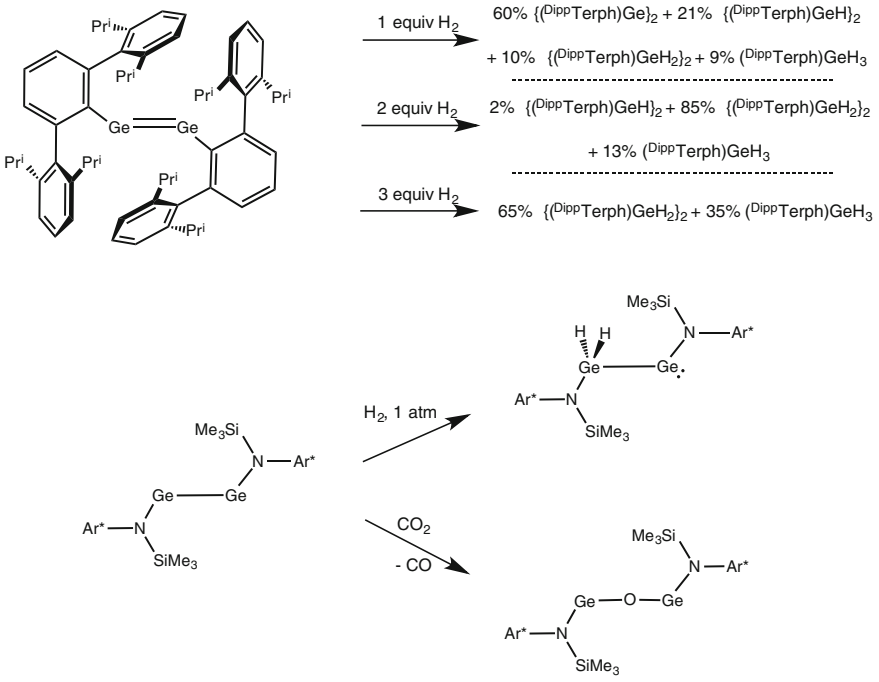

Scheme 3.5 *Above* Reaction of $\{(^{Dipp}Terph)Ge\}_2$ with varying stoichiometries of H_2. *Below* Reaction of an amido-digermyne, $\{(^{TMS}L^*)Ge\}_2$, with H_2 and CO_2

germanium hydride species, which included this initial interaction [32]. Notably, the formation of monomeric (^{Dipp}Terph)(H)Ge: and its reactivity with H_2, leading to (^{Dipp}Terph)GeH_3, was not found to be favourable (vide infra) [32]. Rather, the asymmetric {(^{Dipp}Terph)GeGe(H)$_2$(^{Dipp}Terph)} compound has been postulated as an intermediate, a hypothesis supported by the formation of this species upon coordination with PMe_3 [33]. Outside of this example, no other aryl-digermynes have been described to activate H_2. It is worthy of note that {(^{Dipp}Terph)GeH}$_2$ can also be accessed via the salt-metathesis reaction of Li[BBu$^s{}_3$H] with (^{Dipp}Terph)GeCl [33].

The amido-digermyne, {(^{TMS}L*)Ge}$_2$, is also highly reactive towards H_2, yet shows somewhat differing reactivity than that of {(^{Dipp}Terph)Ge}$_2$. Under one atmosphere of H_2, at ambient temperature, only one product was quantitatively formed, with the reaction occurring in both solution and the solid state [30]. The ^{1}H NMR spectrum of the product reportedly showed very broad peaks, hypothesised to demonstrate an equilibrium between two isomeric forms of a Ge(II) hydride species, as was further implied by variable temperature (VT) ^{1}H NMR spectroscopic studies. The solid state structure of the product revealed it to be a mixed valence Ge(I)/Ge(III) hydride, {(^{TMS}L*)GeGe(H)$_2$(^{TMS}L*)}, which likely undergoes isomerisation between this species and the symmetrical {(^{TMS}L*)GeH}$_2$ in solution. Indeed, DFT calculations have shown such an isomerisation to be thermodynamically viable [34]. The same amido-digermyne exhibited the ability to quantitatively reduce CO_2 to CO, with formation of a germanium(II) ether derivative, (^{TMS}L*)GeOGe(^{TMS}L*) [35]. Such reactivity has only recently been observed for a number of low-oxidation state main-group systems, such as intramolecularly donor-stabilized silylenes [36], a disilyne [37], N-heterocyclic carbenes (NHCs) [38], and a magnesium(I) dimer [39]. However, traditionally, examples of CO_2 reduction, be they stoichiometric or catalytic, are widely derived from *d*- or *f*-block elements [40–44].

Given the presence of a vacant *p*-orbital at the germanium(I) centres in these systems, their coordination with Lewis bases has been investigated. The aryl-digermyne {(^{Dipp}Terph)Ge}$_2$ (Ge-Ge bond = 2.2850(6) Å) was shown to coordinate one Bu^{t}NC: molecule at one Ge centre, forming an asymmetrically substituted digermyne with a formal double bond that was slightly longer than in the parent digermyne (Ge–Ge distance = 2.3432 Å, ∼3% lengthening). However, adding two equivalents of MesNC: resulted in coordination of both Ge centres, and the formation of a much longer, formally single Ge–Ge bond (2.6626(8) Å, ∼14% lengthening). As such, this is Lewis-base-induced tuning of the bond order in this digermyne [45]. Converse to this observation, coordination of the two germanium centres in {(^{TMS}L*)Ge}$_2$ with two molecules of dimethylamino pyridine (DMAP) results in the formation of a bis-adduct, with one DMAP molecule at each centre, which holds a *shorter* Ge–Ge bond than in the parent digermyne (∼2.5% shortening, Scheme 3.6) This has been explained through increased *s*-character in the Ge–Ge bond, manifested by the more open N–Ge–Ge angles in the product (103.50(6)°), compared to those in {(^{TMS}L*)Ge}$_2$ (100.09(6)°). Nevertheless, both distances represent single bonds [46].

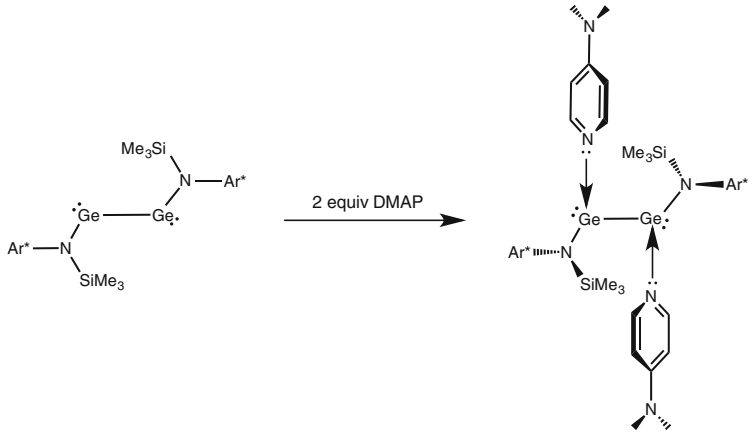

Scheme 3.6 Adduct formation upon the addition of DMAP to $\{(^{TMS}L^*)Ge\}_2$

3.1.2.3 Reactions of 2-Coordinate Digermynes with Unsaturated Molecules and Olefin Activation/Addition

The chemistry of the activation of C–C double bonds by digermynes has seen considerable attention since the initial synthesis of a digermyne, with modes of reactivity involving CH-activation, reversible C–C bond cleavage, and cycloaddition processes. The vast majority of this work has been carried out by the group of Power [47, 48]. Further, reactivity with molecules containing N–N multiple bonds has also seen a large amount of attention. More recently, examples of this chemistry utilising $\{(^{TMS}L^*)Ge\}_2$ have been reported, with other isolated examples from the group of Tokitoh (vide infra).

N–N Unsaturates

Power and co-workers have reported on the reactivity of $\{(^{Dipp}Terph)Ge\}_2$ with many unsaturated molecules involving N–N multiple bonds. Although the list here is more exhaustive, comparisons can be drawn with disilyne chemistry, where either cycloaddtion (with azobenzene) or reductive coupling (with benzonitrile) is observed. However, more complex reactivity is seen with other such unsaturates (Scheme 3.7) [49]. Interestingly, the reaction of $\{(^{Dipp}Terph)Ge\}_2$ with two equivalents of (TMS)azide results in loss of two N_2 molecules, and generation of a cyclic diradicaloid, with two 3-coordinate germanium centres, each of which is pyramidal, suggesting the presence of localised electron density at these centres [49]. Reaction of the same digermyne with three equivalents of (TMS)diazomethane results in complete Ge–Ge bond cleavage, giving a species with two 4-coordinate germanium(IV) centres, with 3 differing bridging modes: one $(TMS)C(H)N_2$ unit has lost N_2, forming an alkylidene bridge, one $(TMS)C(H)N_2$

unit bridges through both N-atoms, and the final (TMS)C(H)N_2 unit bridges through only the terminal N-atom [49]. Reaction of $\{(^{Dipp}Terph)Ge\}_2$ with three equivalents of tetracyanoethylene (TCE) results in a complex cage structure, again with all Ge–Ge interactions of the digermyne reactant broken. The formulation of these species can be seen in Scheme 3.7 [49].

The only related reaction of an N–N unsaturate carried out with $\{(^{TMS}L^*)Ge\}_2$ was that with azobenzene, which gave a similar result to the aryl-substituted digermyne, $\{(^{Dipp}Terph)Ge\}_2$ [46]. Interestingly, however, the reactions of aryl-digermyne $\{(^{Dipp}Terph)Ge\}_2$ and amido-digermyne $\{(^{TMS}L^*)Ge\}_2$ with N_2O differ somewhat, with the former yielding a novel germanium(IV) oxo-peroxo-bridged species, and the later forming a germanium(II) oxo-bridged ether analogue, i.e. the same product as seen from the reduction of CO_2 by the amido-digermyne [35]. It is likely that the mechanism for the formation of the former proceeds similarly to that of the later in the initial stages, and that the generated oxo-bridged compound is highly reactive towards oxidation, likely due to differences in ligand electronics and steric encumbrance (Scheme 3.7).

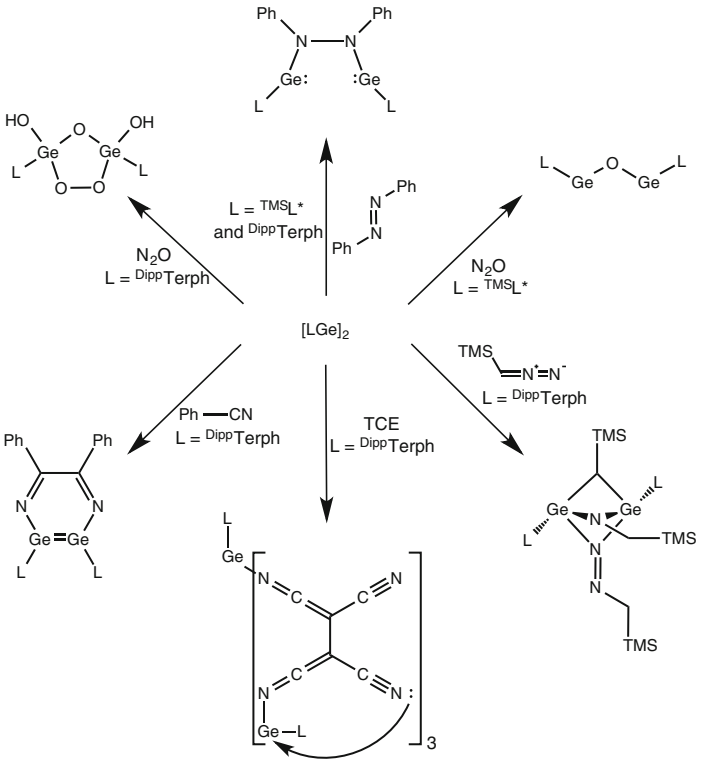

Scheme 3.7 Some reactions of the digermynes $\{(^{Dipp}Terph)Ge\}_2$ and $\{(^{TMS}L^*)Ge\}_2$ with molecules involving N–N unsaturated bonds

Alkynes

Power has reported on the reactivity of $\{(^{Dipp}Terph)Ge\}_2$ with diphenylacetylene and (TMS)acetylene, both of which react in a 1:1 ratio to yield the first two examples of digermacyclobutene analogues (Scheme 3.8) [50]. This is in contrast to reported disilyne species, which were shown effective in the reductive coupling of alkynes (vide supra). It was also mentioned that $\{(^{Dipp}Terph)Ge\}_2$ reacts with two equivalents of (TMS)acetylene yielding a 6-membered diradicaloid intermediate, which subsequently undergoes cycloaddition with one flanking phenyl group of the ligand (Scheme 3.8). One example of alkyne reactivity is reported for the $\{(^{TMS}L^*)Ge\}_2$ system, utilising bis(TMS)-1,3-butadiyne [46]. This species undergoes cycloaddition at one alkyne moiety only, likely due to the great steric bulk of its substituents (Scheme 3.8). Further, no reductive alkyne-coupling is observed. Notably, in this later example the Ge–Ge interaction is cleaved, whereas the aryl-digermyne examples retained Ge–Ge double bonds. This is likely due to the *p*-based N-donation to the empty *p*-orbital at the Ge centres in the amido-substituted example.

Linear Alkenes

Both the groups of Tokitoh and Power have shown that aryl-digermynes react with alkenes. The former reacted $\{(Bbt)Ge\}_2$ with 2,3-dimethyl-1,3-butadiene: one equivalent yielded an {(aryl)germyl}germylene through a [4 + 1] reaction at one germanium centre, with a second equivalent also undergoing a [4 + 1] reaction at the second germanium centre, yielding a digermene (Scheme 3.9) [29]. Worthy of note is the reactivity of the intermediate asymmetric germylene (see Scheme 3.9),

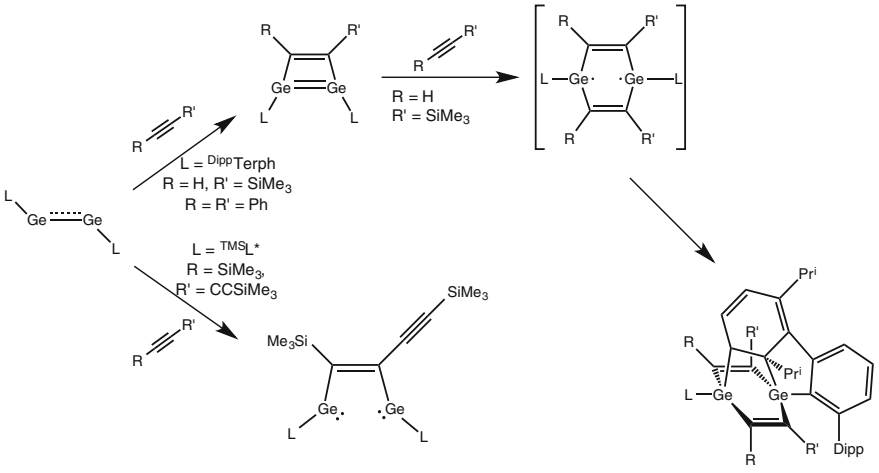

Scheme 3.8 Reactions of $\{(^{Dipp}Terph)Ge\}_2$ and $\{(^{TMS}L^*)Ge\}_2$ with acetylene derivatives

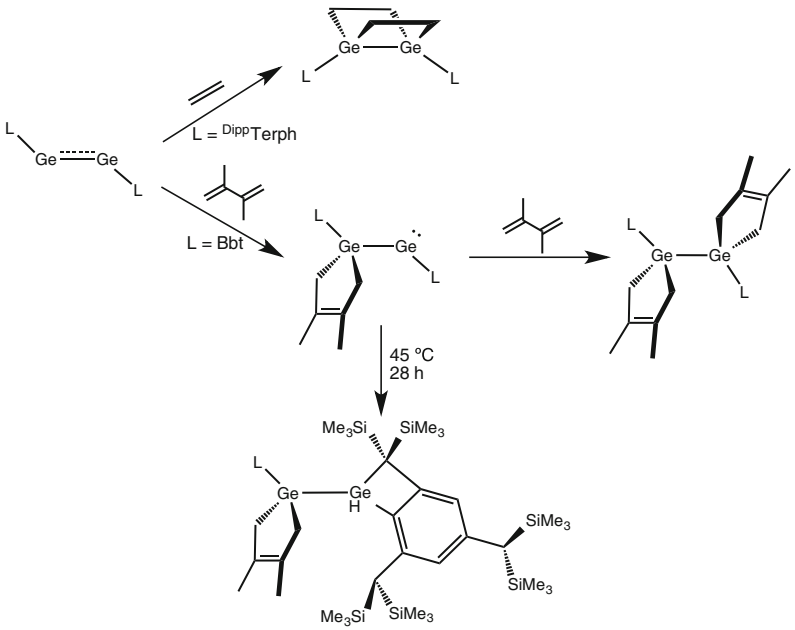

Scheme 3.9 Reactions of aryl-digermynes, $\{(^{Dipp}Terph)Ge\}_2$ and $\{(Bbt)Ge\}_2$, with acyclic alkenes

which CH-activates the ligand upon heating to 45 °C for 28 h. Power reported that $\{(^{Dipp}Terph)Ge\}_2$ reacts with excess ethylene gas to yield a bis(ethylene)-bridged germane (Scheme 3.9) [51]. It is likely that this reaction occurs via two [1 + 2] cycloaddtions, one at each germanium, due to [2 + 2] cycloadditions being symmetry-disallowed. This species would then rearrange giving the observed product. In a related reaction, it was shown that one equivalent of 1,6-heptadiene reacts with one equivalent of $\{(^{Dipp}Terph)Ge\}_2$ in a similar manner to ethylene, giving a bis-bridged digermane species [52].

Cycloalkenes

The reactivity of digermynes with cycloalkenes has been a major topic of study. The majority of work in the area has come from the groups of Power and Jones.

Power and co-workers have observed that the addition of cyclic alkenes to the $\{(^{Dipp}Terph)Ge\}_2$ system yielded, in all cases, products involving CH-activation. The alkenes studied were cyclopentene, cyclopentadiene (CpH), and 1,4-cyclohexadiene (1,4-CHD, Scheme 3.10). The reaction with cyclopentene was found to be relatively straight forward: $\{(^{Dipp}Terph)Ge\}_2$ reacted with one equivalent of cyclopentene generated the known $\{(^{Dipp}Terph)GeH\}_2$ hydride species and CpH. In the presence of an excess of cyclopentene, two products were observed:

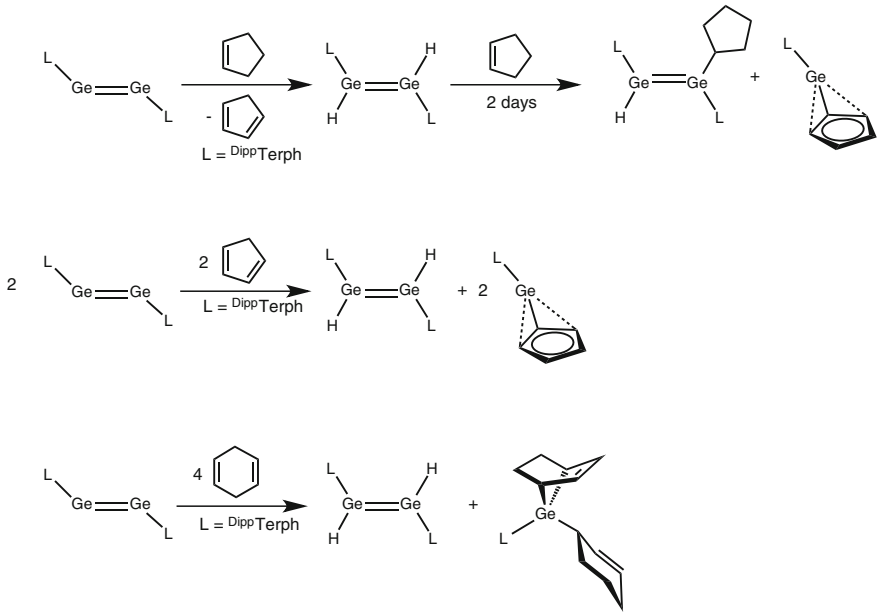

Scheme 3.10 Reactions of $\{(^{Dipp}Terph)Ge\}_2$ with cycloalkenes

one resulting from the hydrogermylation of cyclopentene by $\{(^{Dipp}Terph)GeH\}_2$, and one from the CH-activation of CpH by $\{(^{Dipp}Terph)GeH\}_2$, with the release of H_2. Further, $\{(^{Dipp}Terph)Ge\}_2$ reacted near quantitatively with two equivalents of cyclopentadiene to give H_2 and two equivalents of $(^{Dipp}Terph)GeCp$, suggesting the generation of $\{(^{Dipp}Terph)GeH\}_2$ in the initial stages of the reaction. The digermyne also dehydroaromatised 1,4-cyclohexadiene, generating benzene, $\{(^{Dipp}Terph)GeH\}_2$, and a germanium(IV) species. These reactions are summarised in Scheme 3.10. Such CH-activation reactions had not been observed prior to this study for germanium, further reinforcing the importance and novelty of this low-oxidation state group 14 element chemistry [52, 53].

Further to these CH-activation reactions, an intriguing reaction of $\{(^{Dipp}Terph)Ge\}_2$ with cyclooctatetraene (COT) was observed, whereby initially a kinetically stable inverse sandwich complex was formed (i.e. $\{(^{Dipp}Terph)Ge(\mu\text{-}COT)Ge(^{Dipp}Terph)\}$), through double reduction of the COT ring (Scheme 3.11). The

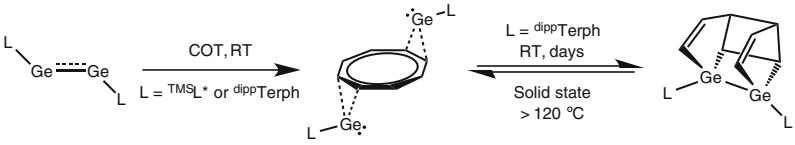

Scheme 3.11 The reaction of digermynes with COT

$[COT]^{2-}$ ligand is bound through π-interactions, with no remaining Ge–Ge interactions. Over time at ambient temperature, this isomerised to the thermodynamic product, a tetracylic diene-digermane, in which a Ge–Ge bond had inserted into one of the double bonds of the COT unit, formally cleaving the C–C bond. This process was reversed by heating crystals of the kinetic product at >120 °C. Again, this is the first example of such reactivity occurring at a group 14 element centre [54].

The amido-digermyne, $\{(^{TMS}L^*)Ge\}_2$, was also shown to react with COT, yielding the inverse sandwich complex, $(^{TMS}L^*)Ge(\mu\text{-}COT)Ge(^{TMS}L^*)$, with complete cleavage of Ge–Ge bonding (Scheme 3.11) [46]. However, this was not seen to undergo isomerisation over extended time periods, highlighting differences between the aryl- and amido-stabilised Ge(I) species. The same digermyne also undergoes cycloaddition with one equivalent of norbornadiene, with no further reaction observed in the presence of excess alkene, likely due to its bulk [46].

3.1.3 Tin Analogues of Alkynes

3.1.3.1 Synthesis of 2-Coordinate Distannynes

The first distannyne to be structurally characterised was reported by Power and co-workers in 2002, and was stabilised by the same ^{Dipp}Terph ligand used to stabilise the first digermyne [55]. The Sn–Sn distance in the solid state is 2.667 Å, which is considerably shorter than the average Sn–Sn double bond (2.801 Å), but in the lower range of known Sn–Sn double bond lengths (shortest = 2.668 Å) [55]. The distannyne was prepared by the reduction of $(^{Dipp}$Terph)SnCl with finely divided potassium metal over the course of two days in benzene, and was isolated in a moderate yield (Scheme 3.12). Since this initial report, several derivatives of aryl-distannynes have been reported by Power, utilising slightly modified terphenyl ligands, with a broad range of Sn–Sn bond lengths (2.6461(3)–3.0753(8) Å) [28, 56]. Here, the shorter bond lengths infer multiple Sn–Sn bonding character, whilst the longer Sn–Sn bonds infer a single bond. Interestingly, where the Sn–Sn distance is shorter (2.6–2.7 Å), the central phenyl ring of the ligand lies in plane with the C–Sn–Sn–C core, whilst where the Sn–Sn distance is longer (3.0–3.1 Å), the central phenyl ring lies perpendicular to the central C–Sn–Sn–C core. Calculations showed the energy difference between such singly and multiply bonded isomers to be very small (*ca.* 5 kcal mol^{-1}), suggesting this isomerisation can be affected by packing forces. Hence, minor changes in the ligand afford seemingly drastic changes in the Sn–Sn bonding mode [57, 58]. All distannynes were synthesised by reduction of Sn(II) halide precursor complexes with potassium or KC_8 (Scheme 3.12).

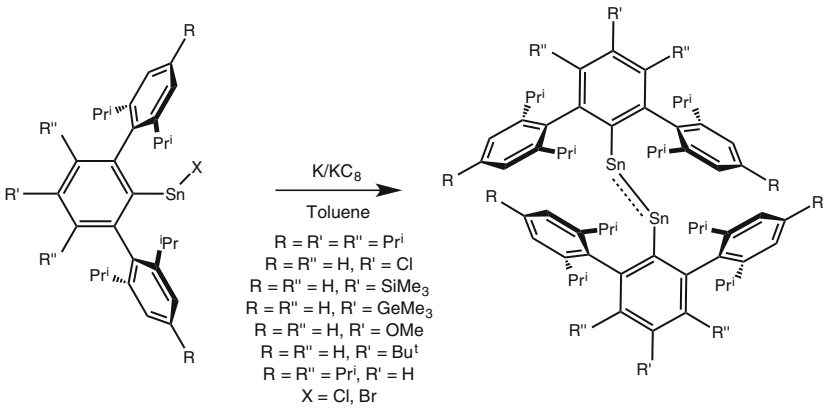

Scheme 3.12 Synthesis of terphenyl-stabilised distannynes

3.1.3.2 Reactivity of 2-Coordinate Distannynes

Similar to their Ge-based counterparts, the described aryl-distannynes are also capable of H_2 activation under atmospheric pressure [59]. However, in all cases the only observable products are Sn(II) hydride complexes, highlighting the stability of Sn(II) relative to Ge(II) for these terphenyl substituted systems. It was shown that such species are also accessible via the reaction of the aryl Sn(II) halide precursor complexes with hydride sources (e.g. $LiBH_4$), or by σ-metathesis of a Sn(II) amide complex with BH_3.THF (vide infra). All of the isolated Sn(II) hydride complexes are dimeric in the solid state, with all bar one example featuring bridging hydrides, with the single outlying example forming a mixed valence isomer, $LSnSn(H)_2L$ (L = $^{Dipp}Terph^{Tripp}$, 3,5-Pr^i_2-C_6H-2,6-(C_6H_2-2,4,6-Pr^i_3)$_2$) [60]. Prior to Power's report of these hydrides, Trinquier had calculated the hydride-bridge isomer to be most stable, with the asymmetric isomer being only slightly higher in energy (1.3–7 kcal mol^{-1}, depending on the calculation method used) [61, 62]. Therefore, similar to the isomeric forms of the aryl-distannynes, slight modification of the ligand, and hence modification of crystal packing forces, may align with isomerisation of the Sn(II) hydride species, as observed here.

Similar to the germanium derivative, the distannyne {($^{Dipp}Terph$)Sn}$_2$ was shown to coordinate the isocyanides, Bu^tNC: and MesNC:, with one isocyanide coordinating each Sn center (Scheme 3.13) [63]. Further, the process showed reversibility, with dissociation being temperature and pressure dependant. In keeping with the small energy difference between singly and multiply bonded distannynes, this coordination leads to a single bond between the two Sn atoms, with the bond lengths being at the higher end of known Sn–Sn single bonds (Bu^tNC: = 2.9282(6) Å, MesNC: = 3.0412(3) Å).

Remarkable reactivity of distannynes with unsaturated C–C bonds has been displayed by Power and co-workers, including CH-activation and cycloaddition

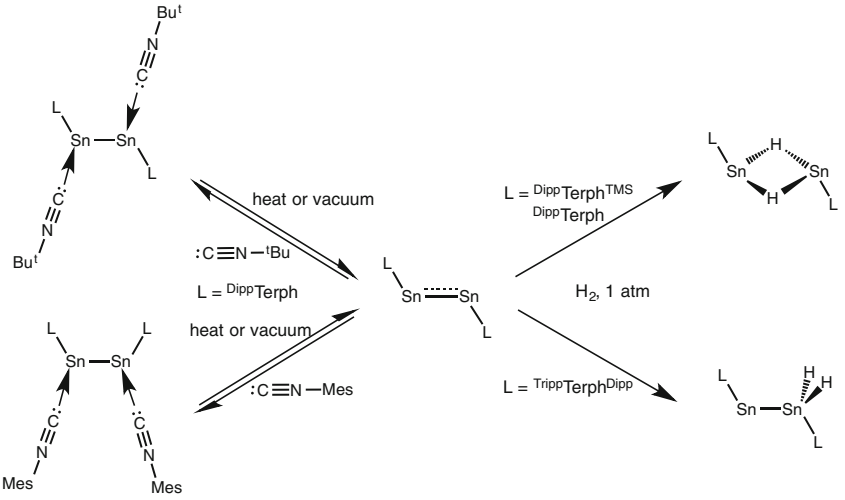

Scheme 3.13 The reactivity of aryl-distannynes towards isocyanides and H_2

(summarised in Scheme 3.14), similar to Ge-based examples. The addition of ethylene to $\{(^{Dipp}Terph)Sn\}_2$ and $\{(^{Tripp}Terph^{Dipp})Sn\}_2$ was shown to occur rapidly under ambient conditions, but more interestingly, was also shown to be quantitatively reversible when the ethylene atmosphere was removed [51]. Similar reversible reactivity was observed where the olefin employed was norbornadiene. The low experimental enthalpies of dissociation ($\{(^{Dipp}Terph)Sn\}_2$ = −48(4) kJ mol^{-1}, $\{(^{Tripp}Terph^{Dipp})Sn\}_2$ = −27(3) kJ mol^{-1}) for the addition of ethylene to the distannynes highlights the weak interaction between the tin centres and the bound ethylene molecules. Nevertheless, the long C–C distances (i.e. 1.528(8) Å and 1.552(8) Å for $(^{Dipp}Terph)Sn(\mu\text{-}C_2H_4)_2Sn(^{Dipp}Terph)$) and normal Sn–C distances (i.e. 2.184(6) Å, 2.191(6) Å, 2.202(6) Å, and 2.178(6) Å for $(^{Dipp}Terph)Sn(\mu\text{-}C_2H_4)_2Sn(^{Dipp}Terph)$) of the bridging ethylene moieties are indicative of formal C–C and Sn–C single bonds. The inherent reversibility of the reaction has been attributed to the geometry of the complexes, which show considerable strain. That is, despite being 4-coordinate, the two Sn centres show considerable deviation from a tetrahedral geometry, with both bulky ligands sitting *cis* to the Sn–Sn bond. This results in a Sn(III) system which is unstable relative to the Sn(I) starting material. Note that these are the first and only known examples of reversible olefin addition to a Sn(I) species.

The distannyne, $\{(^{Dipp}Terph)Sn\}_2$, was also shown to react with the cyclic olefins COT and CpH in a similar manner to $\{(^{Dipp}Terph)Ge\}_2$ (Scheme 3.14) [53, 64]. The former formed an inverse sandwich complex, although no isomerisation to a second product was observed. The latter reaction cleanly formed $(^{Dipp}Terph)SnCp$, with loss of H_2, suggesting first the formation of $\{(^{Dipp}Terph)SnH\}_2$ followed by CH-activation of CpH, via a similar mechanism to those observed for the related Ge(I) system (vide supra) [52, 53].

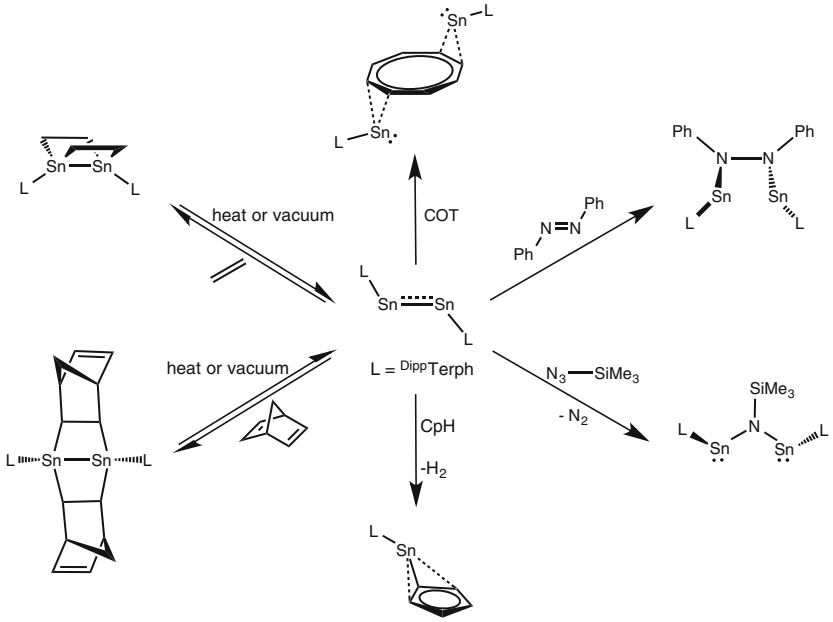

Scheme 3.14 Reactivity of an aryl-distannyne, $\{(^{Dipp}Terph)Sn\}_2$, with unsaturated organic molecules

Reactions of $\{(^{Dipp}Terph)Sn\}_2$ with N-based unsaturates, (TMS)azide and azobenzene, have also been described by Power (Scheme 3.14) [49]. The expected cycloaddition product is observed for azobenzene, $\{(^{Dipp}Terph)SnN(Ph)\}_2$, with complete cleavage of the Sn–Sn interaction, with the two Sn-centres bridged by the $[(NPh)_2]^{2-}$ unit. The reaction with (TMS)azide gave one clean Sn(II) product, an amide bridged bis(stannylene), $\{(^{Dipp}Terph)Sn\}_2N(TMS)$. This is in contrast with the Ge-based derivative, which underwent reaction with two equivalents of the azide, forming a cyclic Ge_2N_2 biradicaloid (vide supra), again highlighting the stability of Sn(II) relative to Ge(II) in these systems.

3.1.4 Lead Analogues of Alkynes

3.1.4.1 Synthesis and Reactivity of a 2-Coordinate Diplumbyne

The synthesis of the only 2-coordinate diplumbyne, reported by Power in 2000, marked the beginning of heavier alkyne chemistry [6]. Interestingly, this was not synthesised through reductive methods, but rather serendipitously through the attempted synthesis of a Pb(II) hydride (Scheme 3.15). As such, $LiAlH_4$ was added to $(^{Tripp}Terph)PbBr$ in diethyl ether. Following work up, a small amount (*ca* 10%

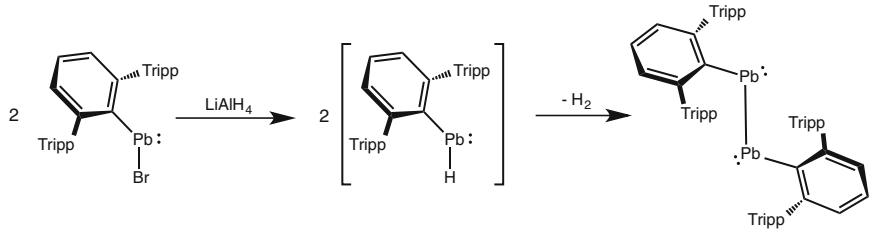

Scheme 3.15 Synthesis of an aryl-diplumbyne, $\{(^{Tripp}Terph)Pb\}_2$

yield) of the diplumbyne, $\{(^{Tripp}Terph)Pb\}_2$, was isolated. It is likely that the lead hydride is first formed, which undergoes elimination of H_2 forming the lead(I) dimer (Scheme 3.15). The diplumbyne features a long Pb–Pb single bond (3.1881 (1) Å, average Pb–Pb single bond = *ca* 3.1 Å) [11], and a Pb–Pb–C angle of 94.26 (4)°, in keeping with minimal or no hybridisation of the 6 *s*- and 6*p*-orbitals at lead, and indicative of a lone-pair of electrons residing at each lead(I) centre, as a result of the inert pair effect [65]. These values are consistent with subsequent computational data, which suggested the stability of the strongly *trans*-bent conformation likely lies with the steric bulk of the ^{Tripp}Terph ligand, which effectively destabilises alternative geometries [66].

Presumably due to the low yield of $\{(^{Tripp}Terph)Pb\}_2$ from the reported synthetic procedure, very few reactivity studies have been forthcoming. Only one example, whereby $\{(^{Tripp}Terph)Pb\}_2$ was reacted with (TMS)azide, has been published [67]. The observed product, a plumbylplumbylene, was likely formed through a radical process. The solid state structure shows that one of the Me groups of a flanking Pr^i group of each ligand has been activated by the same Pb-centre, giving a mixed-valence product (Scheme 3.16). The formation of this mixed-valence species is surprising given the presumed instability of such a species relative to one of symmetric valence (i.e. two Pb(II) centres). The mechanism for its formation is unknown.

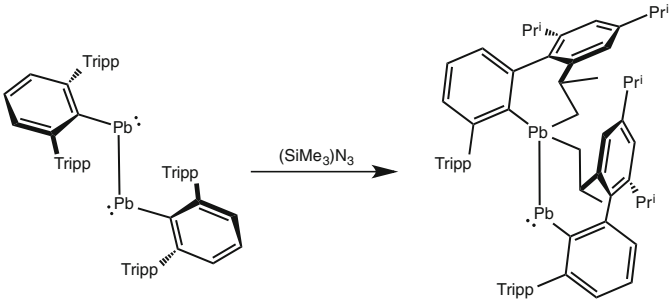

Scheme 3.16 Reaction of an aryl-diplumbyne, $\{(^{Tripp}Terph)Pb\}_2$, with (TMS)azide

3.1.5 *Low-Oxidation State Group 14 Element Hydride Complexes*

The area of heavier group 14 element(II) hydride chemistry has seen marked growth over the past two decades, with the first example of such a species being the Sn(II) hydride complex reported by Power and co-workers in 2000, $\{(^{Tripp}Terph)SnH\}_2$ [68]. Since this seminal discovery, numerous examples of 3-coordinate Ge(II) and Sn(II) hydride complexes have been published, as well as isolated examples of 3- and 4-coordinate Si(II) hydrides. These vary between mononuclear and dinuclear, generally depending on the ligand used. As well as these examples, which use mono-anionic ligands, the parent silylene, germylene, and stannylene have all been reported using neutral 'push-pull' stabilisation [69], whereby neutral Lewis-acid/Lewis-base ligands are used to accept the lone pair of *s*-electrons and coordinate the empty *p*-orbital, respectively, at the element(II) centres. Prior to this thesis, there had been no reports of monomeric, 2-coordinate group 14 element(II) hydrides. Also worthy of note is the lack of any structurally characterised lead hydrides, be they in the +2 or +4 oxidation state. Here, the synthesis and interesting characteristics of group 14 element(II) hydrides will briefly be discussed.

3.1.5.1 Parent Heavier Methylenes

The free heavier parent-tetrylenes are unknown, due to the inability of two H^- ligands to stabilise the E(II) (E = Si–Pb) centres, on both thermodynamic and steric grounds. Methylene has been known as a TM-stabilised fragment for some time [70–73], but, until recently, isolable derivatives of the heavier members of group 14 were unknown [69]. In 2009, Rivard and co-workers reported on the isolation of GeH_2 through 'push-pull' stabilisation, whereby the reaction of IPr.$GeCl_2$ with $LiBH_4$ yielded the product germylene, IPr.GeH_2.BH_3, in good yield (Scheme 3.17) [74]. Subsequent work by the same group has led to the isolation of a tin(II) derivative through the use of a neutral Lewis-acidic TM-fragment, $W(CO)_5$. In this case, $LiBH_4$ was reacted with the 'pre-coordinated' IPr.$SnCl_2$.$W(CO)_5$, yielding the push-pull stabilised IPr.SnH_2.$W(CO)_5$ in high yield (Scheme 3.17). The corresponding TM-stabilised GeH_2 complex was published concordantly, accessed via a similar route (Scheme 3.16) [75]. It followed that the related SiH_2 fragment could also be stabilised in a similar fashion, and this was isolated from the reaction of IPr.$SiCl_2$.BH_3 with $LiAlH_4$ in good yield (Scheme 3.17) [76]. It is worth noting that, prior to this work, Robinson and co-workers reported on the somewhat serendipitous synthesis of a parent silylene, through the insertion of BH_3 into the double bond of $(IPr.Si:)_2$ [77, 78].

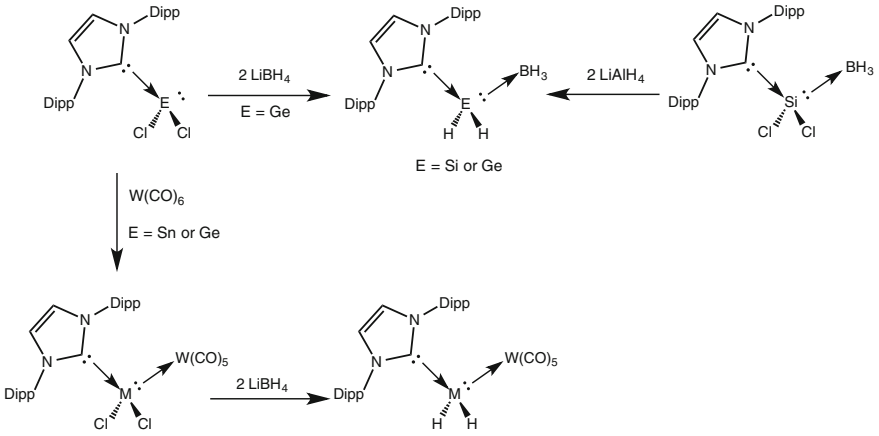

Scheme 3.17 Synthesis of 'push-pull' stabilised parent heavier tetrylenes, SiH_2, GeH_2, and SnH_2

3.1.5.2 Di-nuclear Low-Oxidation State Group 14 Element Hydride Complexes

To date, the large majority of this class of group 14 element hydride compounds have been reported by Power and co-workers, as discussed in Sect. 3.1.2.2 [60, 79]. As described, these have been accessed through H_2 activation, salt-metathesis, or σ-metathesis routes, and were the first examples of group 14 element(II) hydrides. The amido Ge(II) hydride complex, (^{TMS}L*)GeGe(H)$_2$(^{TMS}L*), can also be synthesised via a salt metathesis route, although an amount of the Ge(III) hydride, {(^{TMS}L*)Ge(H)$_2$}$_2$, is also formed [30].

Due to the lack of examples of H_2 activation by a Si(I) dimer, such a route to a Si (II) hydride has as yet eluded chemists. Nevertheless, examples of dimeric Si(II) hydrides have been reported, with the first reported example from the group of Tokitoh in 2012: the double reduction of (Bbt)Si(H)Br$_{2-}$ with lithium naphthalenide led to the formation of {(Bbt)SiH}$_2$ in moderate yields (Scheme 3.18) [80]. This species contains a Si–Si double bond, with a Si–Si distance of 2.1708(6) Å, slightly shorter than the mean of known Si–Si double bond lengths (mean = *ca.* 2.195 Å). As predicted by Trinquier [61], the disilene has a *trans*-bent structure, with a *trans*-bending angle of 6.3°, although somewhat lesser in its bending out of the plane than was predicted for parent disilene, Si_2H_4 (θ = 36°). Nevertheless, DFT calculations by the publication's authors predicted a Si–Si distance (2.157 Å) and a *trans*-bending angle (θ = 2.9°), in good agreement with those observed experimentally. Although stable at ambient temperature, {(Bbt)SiH}$_2$ undergoes ligand CH-activation in a very similar manner to the previously discussed {(Bbt)SiBr}$_{2-}$ at 80 °C (Scheme 3.18). This was hypothesised to occur via a similar ligand-migration to that previously described [81].

One other example of a dimeric Si(II) hydride has been reported by Inoue and co-workers, whereby the addition of Ni(COD)$_2$ to a solution of (Bu$^t_3$Si)SiH.TMC

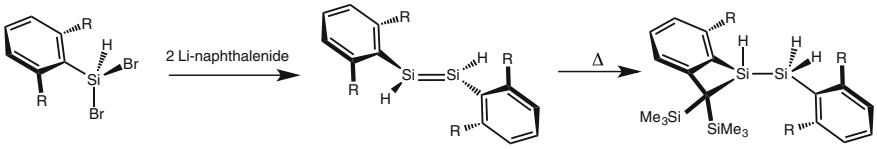

Scheme 3.18 Synthesis of, and thermal CH-activation by, a 1,2-bis(hydrido)disilene. R = C(H)$(TMS)_2$

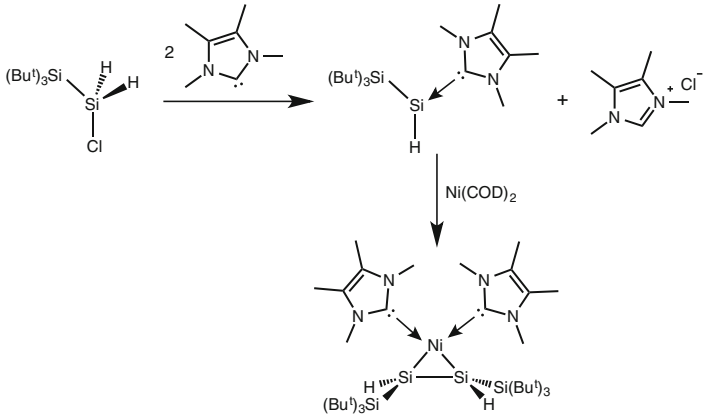

Scheme 3.19 Dimerisation of a monomeric silicon(II) hydride through reaction with $Ni(COD)_2$

(vide infra) (TMC = :C{N(Me)C(Me)}$_2$) resulted in the formation of a Si–Si bound dimer, with a Ni.$(TMC)_2$ unit coordinating both Si-centres (Scheme 3.19) [82]. On the basis of the relatively long Si–Si bond (2.2574(6) Å), the *cis*-bending angles at the silicon centres (θ = 35.05° and 34.7°), and the highly shielded ^{29}Si NMR signal (δ = −115.0 ppm), the species was regarded as a disila-metallacyclopropane, as opposed to a π-complex of a disilene.

Higher-coordinate group 14 element(II) hydride systems tend not to dimerise due to occupation of the elements empty *p*-orbital and/or coordination of its lone-pair of electrons, both of which are generally utilised in bonding between two E(II) centres [83].

3.1.5.3 Monomeric Low-Oxidation State Group 14 Element Hydride Complexes

Such species, prior to this thesis, contained three or higher coordinate group 14 element(II) centres, utilising chelating ligands, and/or Lewis acids and bases, the synthesis of which is discussed herein.

Monomeric Silicon (II) Hydride Complexes

The first example of a monomeric Si(II) hydride was reported by Roesky and co-workers in 2011, and this utilised the chelating amidinate ligand, ^{tBu}Am (^{tBu}Am = [PhC{N(Bu^t)}$_2$]$^-$) (Scheme 3.20a). Although a Si(II) hydride could not be directly synthesised from the Si(II) chloride precursor, (^{tBu}Am)SiCl, prior addition of BH_3 followed by K[BBu$^s_3$H] yielded the desired hydride product, (^{tBu}Am)SiH.BH_3, as a 4-coordinate monomer [84]. The Si–*H* resonance in its ^{1}H NMR spectrum was reported as broad, at δ = 6.12 ppm. Presumably the broadness precluded the observation of ^{29}Si satellites. Since this publication, two related examples of monomeric 4-coordinate Si(II) hydrides have been reported. The group of So reported on the reduction of (^{tBu}Am)Si(H)Cl_2 with two or four equivalents of KC_8: the former yielded a product hypothesised to result from the hydrosilylation of intermediate (^{tBu}Am)SiCl, yielding (^{tBu}Am)Si–Si(Cl)[{N(Bu^t)}$_2$CHPh]. The latter was formed from the hydrosilylation of the generated (^{tBu}Am)SiH by itself, yielding the silylene-stabilised Si(II) hydride, (^{tBu}Am)Si–Si(H)[{N(Bu^t)}$_2$C(H)Ph] (Scheme 3.20b) [85]. The yield for this latter reaction, however, was reported to be very low (1.6%), and so it being present as a major product is doubtful. Nevertheless, the ^{1}H NMR spectrum of the product was reported, with the Si-*H* resonance being observed at δ = 6.70 ppm, with $^1J_{SiH}$ = 146 Hz, in keeping with known Si-H coupling constants. The final example of such a monomeric Si(II) hydride was reported by Driess and co-workers. This involved a chelating β-diketiminate ligand, and a Lewis-acidic [Ni(CO)$_3$] fragment, and was synthesised by first coordination of Ni(CO)$_3$ to the known silylene, (^{Dipp}nacnac′)Si: (^{Dipp}nacnac′ = [CH[(C=CH$_2$)CMe{N(Dipp)}$_2$]]$^-$). From this adduct, the hydride, [(^{Dipp}nacnac)Si(H).BH_3] (^{Dipp}nacnac = [CH{(Dipp)NC(Me)}$_2$]$^-$), could be generated in two steps by reaction with HCl followed by Li[BEt$_3$H], or in one step by addition of NH_3.BH_3. Both routes gave the compound in good yield (Scheme 3.20c) [86]. The ^{1}H NMR signal for the Si-*H* moiety is in keeping with the two previously described Si(II) hydrides (δ = 6.15 ppm, $^1J_{SiH}$ = 154 Hz).

There are also three reported 3-coordinate monomeric Si(II) hydrides, from the groups of Baceiredo (2 examples) and Inoue (1 example) (Scheme 3.21). The former involve derivatives of a rather interesting chelating amide ligands (^{PN1}L and ^{PN2}L, Scheme 3.21a), containing a pendant phosphine moiety, which coordinates the element to which the ligand is bound [87]. From the precursors (^{PN1}L)Si(H)Cl_2 and (^{PN2}L)Si(H)Cl_2, the target hydrides were easily accessed in good yield, through reduction with Mg metal in THF. Their ^{1}H NMR spectra show Si-*H* resonances in keeping with previously described, higher coordinate Si(II) hydride species ((^{PN1}L)SiH: δ = 5.99 ppm; (^{PN2}L)SiH: δ = 5.79 ppm), whilst their $^1J_{SiH}$ coupling constants are much smaller ((^{PN1}L)SiH: $^1J_{SiH}$ = 85.1 Hz; (^{PN2}L)SiH: $^1J_{SiH}$ = 85.7 Hz). The final example simply utilises the known Bu$^t_3$Si-ligand, and TMC as both a reductant and Lewis-base (Scheme 3.21b): addition of two equivalents of TMC to (Bu$^t_3$Si)SiH_2Cl yielded (Bu$^t_3$Si)SiH.TMC in moderate yield, with loss of TMC. HCl as an insoluble solid [82]. The surprisingly up-field shift of the Si-*H* ^{1}H NMR

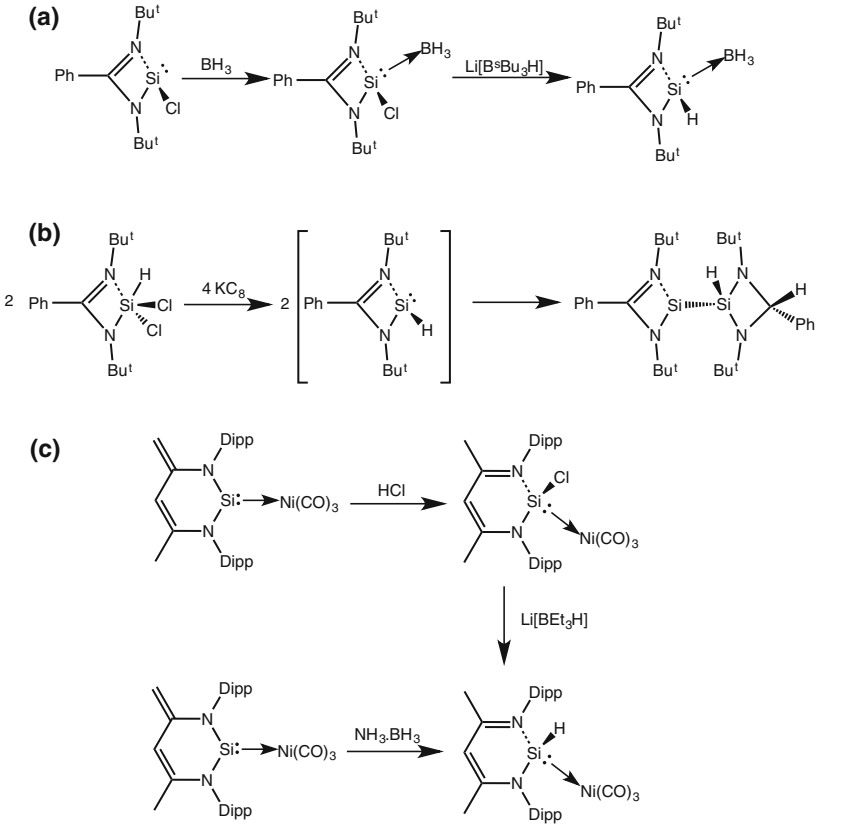

Scheme 3.20 Synthesis of (transient) 4-coordinate monomeric silicon(II) hydrides, and related Si (III) hydrides utilising chelating ligands

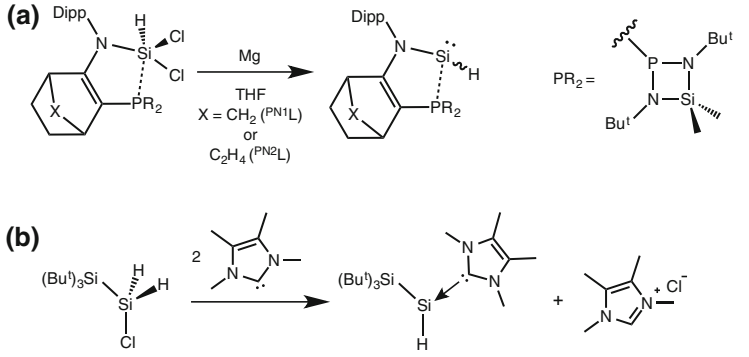

Scheme 3.21 Synthesis of 3-coordinate monomeric silicon(II) hydrides

resonance (δ = 3.17 ppm, $^{1}J_{SiH}$ = 101 Hz) is possibly a result of the strong σ-donation of the carbene and the inductive effects of the $Bu^{t}_{3}Si$-group, leading to a highly shielded Si-H moiety.

Monomeric Germanium(II) Hydride Complexes

The first example of a monomeric Ge(II) hydride complex was reported in 2001 by Roesky and co-workers [88]. This features the chelating ^{Dipp}nacnac ligand, and a coordinated BH_3 molecule, remaining from its synthesis, which involved the addition of $NaBH_4$ to a solution of (^{Dipp}nacnac)GeCl (Scheme 3.22a). No resonance for the Ge–*H* moiety was reported for this species. Further, although the BH_3 could be removed using PMe_3, the potential 3-coordinate Ge(II) hydride complex was not structurally characterised in this report, and hence its solid-state structure could not be commented on. However, in a subsequent publication by the same group, the monomeric nature of the 3-coordinate (^{Dipp}nacnac)GeH was confirmed [89]. In this case the hydride compound was generated via an alternative route, from (^{Dipp}nacnac)GeCl and [AlH_3.NMe_3], in good yield (Scheme 3.22a). The ^{1}H NMR spectrum reportedly showed a resonance attributable to the Ge–H moiety at δ = 8.08 ppm, which is dramatically shifted down-field relative to that for the first dimeric Ge(II) hydride complex, {(^{Dipp}Terph)GeH}$_2$ (δ = 3.48 ppm) [33]. The related (^{Mes}nacnac)GeH complex (^{Mes}nacnac = CH[(C=CH_2)CMe{N(Mes)}$_2$]) was subsequently reported by Jones and co-workers in 2011, arising from the reaction of (^{Mes}nacnac)GeCl with K[BEt_3H] [90]. This complex is also monomeric in the solid state, and has a similar shift in its ^{1}H NMR spectrum for the Ge–*H* moiety (δ = 8.25 ppm). Roesky and co-workers have reported on the synthesis of a 4-coordinate Ge(II) hydride complex, which utilises a bulky bis(imino)phenyl pincer-type ligand, ^{pinc}L (^{pinc}L = [{DippNCMe}$_2$$C_6H_3$]$^-$) (Scheme 3.22b) [91]. This species has a more upfield shifted Ge–*H* resonance (δ = 6.69 ppm), relative to

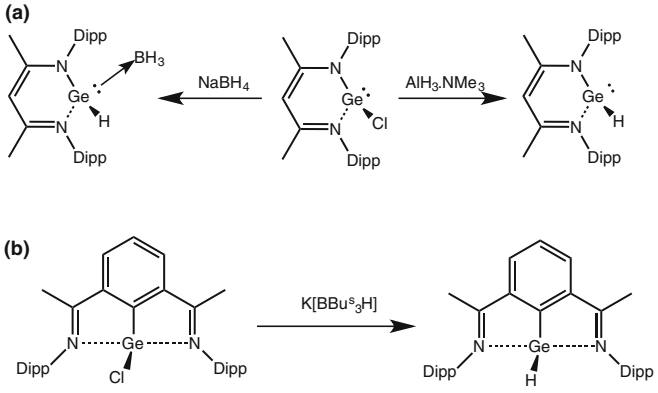

Scheme 3.22 Synthesis of 3- and 4-coordinate germanium(II) hydrides

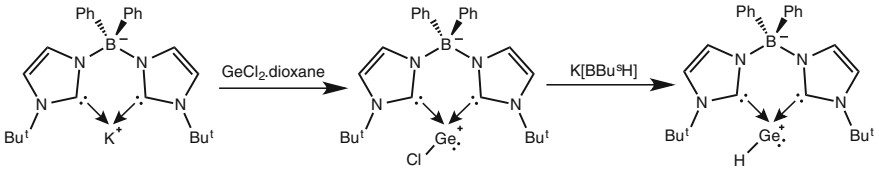

Scheme 3.23 Synthesis of a 3-coordinate cationic germanium(II) hydride

the other monomeric divalent germanium hydrides described. This likely arises from the higher coordination environment at Ge, resulting a more shielded Ge-centre.

In related work, Driess and co-workers reported on a cationic three-coordinate Ge (II) hydride complex, or a germyliumylidene hydride, stabilised by a borate-bridged anionic biscarbene ligand, $^{Ph}B(NHC)_2$ ($^{Ph}B(NHC)_2 = Ph_2B(^{tBu}NHC)_2$, ^{tBu}NHC = :C[N(Bu^t){C(H)}$_2$N]$^-$, Scheme 3.23) [92]. This was synthesised by reaction of the Ge(II) chloride precursor complex with K[BBu^s$_3$H], quantitatively yielding the product hydride, $[Ph_2B(^{tBu}NHC)_2]^-[GeH]^+$ (Scheme 3.23). The Ge–*H* resonance in its ^{1}H NMR spectrum (δ = 5.69 ppm) is surprisingly up-field relative to other discussed monomeric Ge(II) hydride complexes, likely due to the high electron density on the Ge-centre arising from the strong σ-donation of the NHC-based ligand.

Monomeric Tin(II) Hydride Complexes

The initial report of a monomeric tin(II) hydride species was published along side the Ge(II) analogue, (^{Dipp}nacnac)GeH, using the same ligand, and the same synthetic methodology. Hence, reaction of (^{Dipp}nacnac)SnCl with [AlH$_3$.NMe$_3$] afforded the target hydride, (^{Dipp}nacnac)SnH, in high isolated yield [89]. In line with related relativistic spin-orbit coupling effects, which have been shown to greatly deshield hydrides in the ^{1}H NMR spectra of heavier d^{10} element systems (i.e. Zn(II), Cd(II), and Hg(II) hydrides) [93], the Sn–*H* resonance for (^{Dipp}nacnac)SnH is considerably down-field relative to the Ge(II) analogue (δ = 13.83 ppm). The same group also reported on the synthesis of a bis(imino)phenyl pincer-ligated Sn(II) hydride complex, (^{pinc}L)SnH, along side the Ge(II) derivative, again via a similar synthetic route. This complex also shows a rather downfield shift for the Sn–*H* fragment in its ^{1}H NMR spectrum (δ = 10.57 ppm) [91]. A related species, utilising a bis(imino)phenyl pincer ligand, [2,6-(Me$_2$NCH$_2$)$_2$C$_6$H$_3$]$^-$, was reported by Jurkschat, although in this case the species was also stabilised by a Lewis-basic W(CO)$_5$ moiety. The synthesis involved the addition of K[BBu^s$_3$H] to [{2,6-(Me$_2$NCH$_2$)$_2$C$_6$H$_3$}Sn(Cl){W(CO)$_5$}], affording the product hydride in good yield [94]. A recent example of a monomeric 3-coordinate Sn(II) hydride complex has also been reported, utilising a terphenyl ligand and a coordinated NHC, MeEtC (MeEtC = :C{N(Et)C(Me)}$_2$). This species was synthesised in a rather novel manner, by H$_2$ abstraction from a terphenyl stannane. Thus, the addition of two

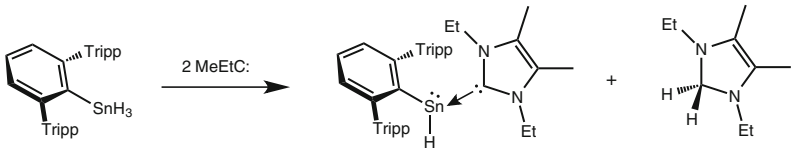

Scheme 3.24 Hydrogen abstraction from (^{Tripp}Terph)SnH_3, yielding a 3-coordinate tin(II) hydride

equivalents of MeEtC to (^{Tripp}Terph)SnH_3 afforded the Sn(II) hydride complex, (^{Tripp}Terph)(H)Sn.(MeEtC), and the hydrogenated carbene, $MeEtCH_2$, in near quantitative yield (Scheme 3.24) [95]. The Sn–*H* resonance in the ^{1}H NMR spectrum of that compound is surprisingly upfield (δ = 5.69 ppm), possibly due to shielding from the strongly σ-donating NHC ligand. Note that the less-bulky Sn(II) hydride complex, (Tripp)SnH.MeEtC, was synthesised by a similar method, but its solid state structure not acquired, hence its monomeric nature cannot be confirmed.

Reported reactivity of the heavier group 14 element(II) hydrides described in this section will be discussed in Chap. 4.

3.2 Research Proposal

As can be seen from literature examples presented in this chapter, monodentate ligands have been used to great effect in low-oxidation state group 14 element chemistry, with a sizeable portion of the results being generated through application of the terphenyl ligand system. However, very few comparative results have been seen from the use of bulky monodentate amide ligands, the synthesis of which has seen fruitful development in our group. Although a novel, singly bonded amido digermyne has been reported using this amide ligand system, no other examples of 2-coordinate amido-digermynes exist, and hence the effects of ligand electronics and bulk on the bonding in these species is unknown. It follows that related studies are lacking in regards to other group 14 element(I) dimers stabilised by the bulky amide ligands developed in our group, as are examples of low-oxidation state group-14 hydride species utilising these ligands, with only one Ge(II) hydride complex known to be stabilised by this ligand system. Contrary to this, group 14 element(I) chemistry and group 14 element(II) hydride chemistry has been widely studied for the terphenyl stabilised systems, with terphenyl Ge(I), Sn(I), and Pb(I) dimers fully characterised, alongside a plethora of Ge(II) and Sn(II) hydride complexes using related ligands. Reactivity studies involving amido-stabilised germylynes is also lacking somewhat relative to terphenyl-stabilised systems, as are any reactivity studies utilising the described amido Ge(II) hydride complex, (^{TMS}L*)GeGe(H)$_2$(^{TMS}L*).

Hence, our goal was to utilise the ligands discussed in Chap. 2 in low-oxidation state group 14 element chemistry, and to observe any effects on E–E bond orders

and dynamic solution-based effects (i.e. hydride complex isomerisation). We aimed to further study the reactivity of the digermyne system, which is a field largely dominated by terphenyl-ligated Ge(I) dimers. We also aimed to apply these bulky amide ligands to the chemistry of the other heavier elements of group 14, so as to draw comparisons between structural and electronic characteristics between these species.

3.3 Results and Discussion

3.3.1 Reduction of Amido Germanium(II) Chloride Complexes

The first synthetic targets of this study were amido-digermynes utilising the monodentate bulky amide ligands described in Chap. 2. As no bis(aryl)amide ligands had been used to stabilise Ge(I) species to date, the reduction of the bis(aryl)amido Ge(II) chloride complexes, **1–6** (Scheme 3.25), was first pursued. The reactions were attempted with $\{(^{Mes}nacnac)Mg\}_2$ (**7**) as a reducing agent, but were unsuccessful in the majority of cases, yielding intractable mixtures of products. However, where Mes-substituted amides were employed (**3**, **4**, and **5**) deep green solutions were obtained, which discoloured rapidly above −25 °C. Attempts to crystallise the products resulted in either decomposition or isolation of small green ball-like crystals which were not suitable for crystal-structure determination. On one occasion a bis(amido)germylene was isolated, likely as a product of disproportionation of an amido Ge(I) species. Its structure is shown in Fig. 3.1. The smaller Mes-groups take up "endo" positions relative to the Ge(II) centre, likely due to the bulk of the $Ar^{\dagger}$ group. The N–Ge–N angle (112.12°, average of reported $(N–Ge–N)_{acyclic}$ angles = 103.38°) is indicative of a lone-pair of electrons at Ge1, and is in fact more obtuse than that of any previously reported example of an acyclic bis(amido) germylene, likely due to the extreme bulk of the $^{Mes}L^{\dagger}$ ligand. Although this species was isolated as a by-product, it is currently the target of direct synthesis, so as to investigate its potential reactivity.

As the bis(aryl)amide ligands did not seem capable of stabilising of Ge(I) species, our attention turned to aryl/silyl amide ligands, and the respective Ge(II) chloride precursor complexes. Given the success of the previously reported $^{TMS}L^{*}$ ligand in this regard, it seemed this ligand class may be better suited to low oxidation state group 14 element chemistry. Hence, the reductions of **8–13** with **7** were attempted (Scheme 3.26).

It was apparent that the bulk of the ligands containing the $(Bu^{t}O)_3Si$ group was too great, and likely prevented the formation of Ge(I) dimers. In these cases only intractable product mixtures were observed (reduction of precursors **11–13**, Scheme 3.26). A similar result was obtained for precursor **9**. However, the remaining two precursors containing the $Pr^{i}{}_3Si$ group (**8** and **10**) were successfully

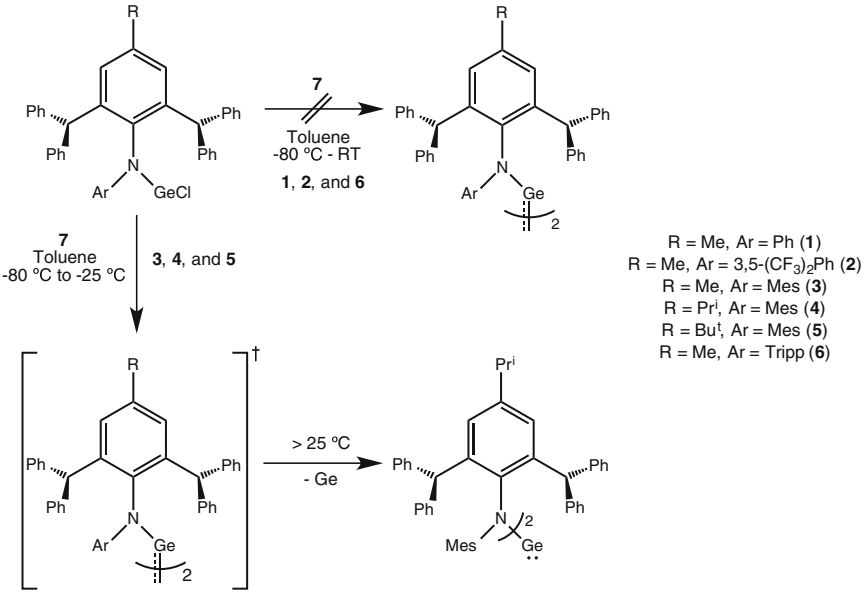

Scheme 3.25 Attemped reductions of bis(aryl)amido germanium(II) chloride compounds

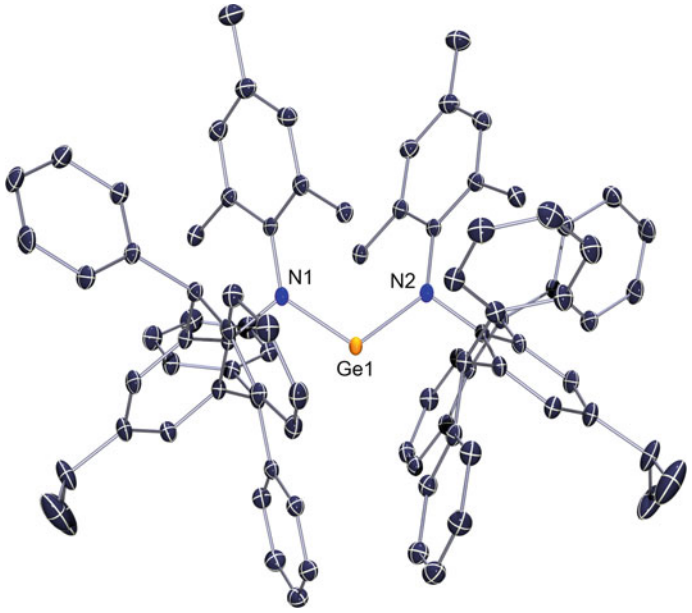

Fig. 3.1 ORTEP representation of $(^{Mes}L^{\dagger})_2Ge$: (30% ellipsoids; hydrogen atoms omitted). Relevant bond lengths (Å) and angles (°): N1–Ge1 1.890(2), Ge1–N2 1.890(2), N1–Ge–N2 112.12(1)

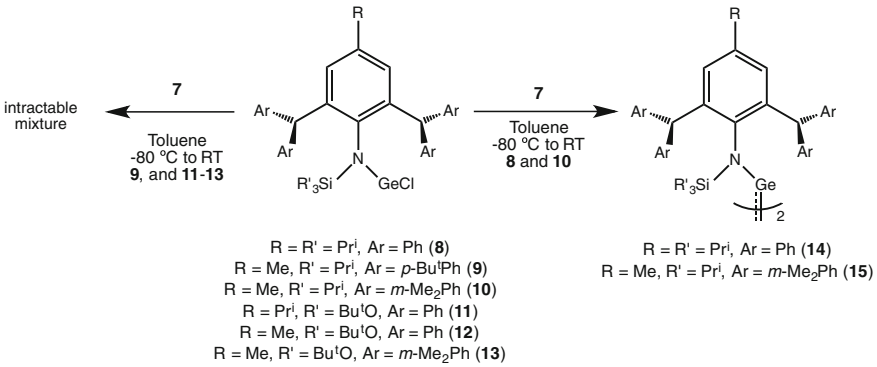

Scheme 3.26 Reactions of silyl aryl amido germanium(II) chlorides **8–13** with $\{(^{Mes}\text{nacnac})\text{Mg}\}_2$, yielding $\{(^{iPr}L^{\dagger})\text{Ge}\}_2$ (**14**) and $\{(^{iPr}L^{\ominus})\text{Ge}\}_2$ (**15**)

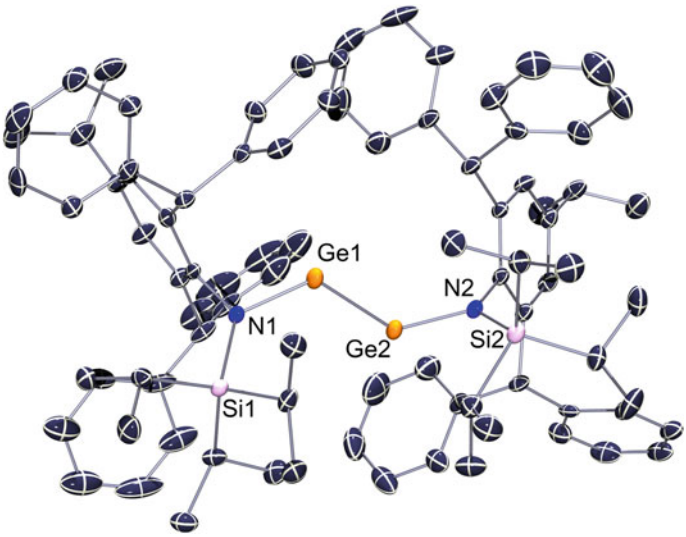

Fig. 3.2 ORTEP representation of **14** (50% ellipsoids; hydrogen atoms omitted). Relevant bond lengths (Å) and angles (°) (Calculated values at BP86 + D3/def2-TZVPP in square brackets): Ge1–Ge2 2.3568(3) [2.362], Ge1–N1 1.8601(14) [1.886], Ge2–N2 1.8631(14) [1.886], N1–Ge1–Ge2 120.39(4) [116.86], N2–Ge2–Ge1 121.03(4) [116.91], C1–N1–Si1 125.22(11) [121.91], C45–N2–Si2 126.44(11) [121.90]

reduced by **7**, affording good isolated yields of the amido-digermynes **14** and **15** (Scheme 3.26) after recrystallisation from Et_2O. Interestingly, powdered **15** is turquoise in colour, whilst solutions of this compound in organic solvents are deep orange. The solid-state structures of these two compounds [Fig. 3.2 (**14**) and Fig. 3.3 (**15**)] reveal them to be isostructural, with similar bond lengths and angles (Table 3.1).

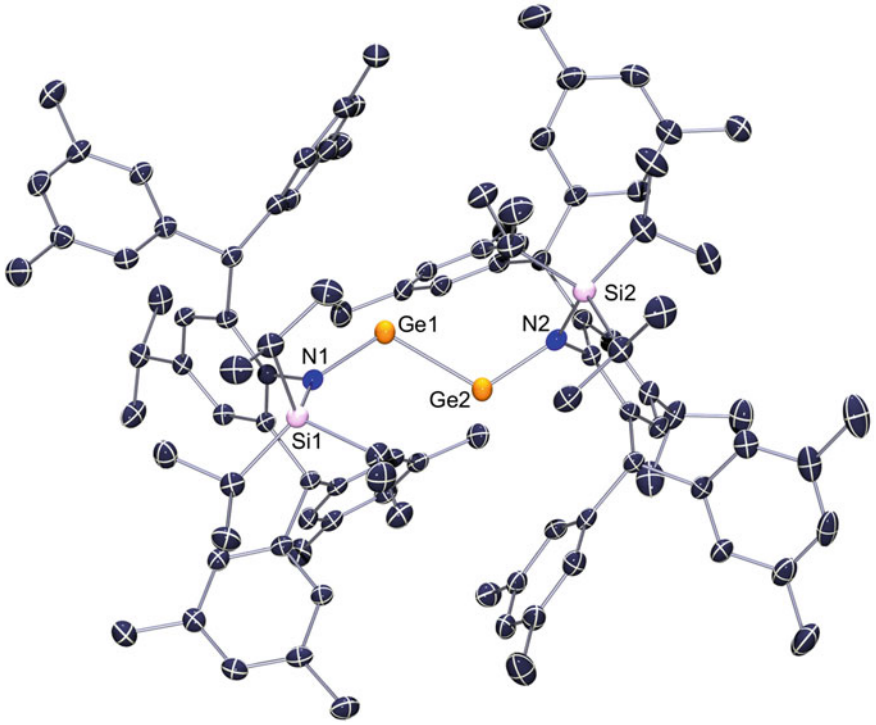

Fig. 3.3 ORTEP representation of **15** (50% ellipsoids; hydrogen atoms omitted). Relevant bond lengths (Å) and angles (°): Ge1–Ge2 2.3667(6), Ge1–N1 1.853(2), Ge2–N2 1.861(2), N1–Ge1–Ge2 119.01(8), N2–Ge2–Ge1 118.74(8), C1–N1–Si1 125.22(2), C45–N2–Si2 126.21(2)

Table 3.1 Comparison of selected bond lengths and angles in amido digermynes **14**, **15**, and $\{(^{TMS}L^*)Ge\}_2$ [30]

	Ge1–Ge2 dist. (Å)	Ge–N dist. (average, Å)	N1–Ge1–Ge2 ang. (°)	N2–Ge2–Ge1 ang. (°)	N1–Ge1–Ge2–N2 torsion (°)
14	2.3668(6)	1.863(4)	119.61(1)	122.64(1)	22.09(1)
15	2.3667(6)	1.857(4)	119.01(8)	118.74(8)	20.29(1)
$\{(^{TMS}L^*)Ge\}_2$	2.7093(7)	1.872(2)	100.09(6)	100.09(6)	0

The Ge–Ge bond lengths in **14** and **15** are slightly greater than the mean reported Ge–Ge double bond length (*ca*. 2.332 Å), which suggests some singlet-biradicaloid character, as with previously reported examples of aryl substituted species [2, 5]. That is, these bonds are only marginally longer than those in known terphenyl digermynes (e.g. 2.2850(8) Å for $\{(^{Dipp}Terph)Ge\}_2$), while their N–Ge–Ge angles (119.61° (**14**) and 119.01° (**15**) average, cf. 100.09(6)° for $\{(^{TMS}L^*)Ge\}_2$) [30] are slightly more acute than terphenyl-digermyne C–Ge–Ge angles (e.g. 128.67(8)° in

$\{(^{Dipp}Terph)Ge\}_2$) [26]. Therefore, despite the greater apparent bulk of the $^{iPr}L^{\dagger}$ and $^{iPr}L^{\partial}$ ligands relative to $^{TMS}L^*$, these two digermynes have Ge–Ge multiple bonds, whilst $\{(^{TMS}L^*)Ge\}_2$ has a long Ge–Ge single bond. This can be attributed to the differences in torsion angles for the species. The greater bulk of the former ligands leads to torsion of the central Ge_2N_2 unit away from planarity (**14** = 22.09(1)°, **15** = 20.29(1)°), whilst $\{(^{TMS}L^*)Ge\}_2$ has a planar central Ge_2N_2 unit. This prevention in planarisation of Ge_2NSiC fragments in **14** and **15** thereby disallows N–Ge π-bonding, as is present in $\{(^{TMS}L^*)Ge\}_2$ [30]. Another intriguing feature of the structure of **14** is the fact that its Pr^i_3Si groups take up *cis* positions relative to the Ge_2N_2 plane, presumably to minimise steric repulsion within the compound. The UV/Vis spectrum of **14** exhibits two absorption bands [λ_{max} = 399 nm (ε = 3920 L mol^{-1} cm^{-1}) and λ_{max} = 472 nm (ε = 650 L mol^{-1} cm^{-1})] at similar wavelengths, and of comparable intensities, to the π–π* and n_-–n_+ transitions reported for other multiply bonded digermynes [28, 29].

So as to compare the electronic structure of **14** with that reported for $\{(^{TMS}L^*)Ge\}_2$ in the gas phase, DFT calculations were carried out on **14**. The calculated and experimental (Fig. 3.2) geometries of the compound agree very well, although the slight deviations between the bond angles might arise from intermolecular interactions for the latter in the solid state. An analysis of the frontier orbitals of **14** (Fig. 3.4) reveals its electronic structure to be similar to those previously reported

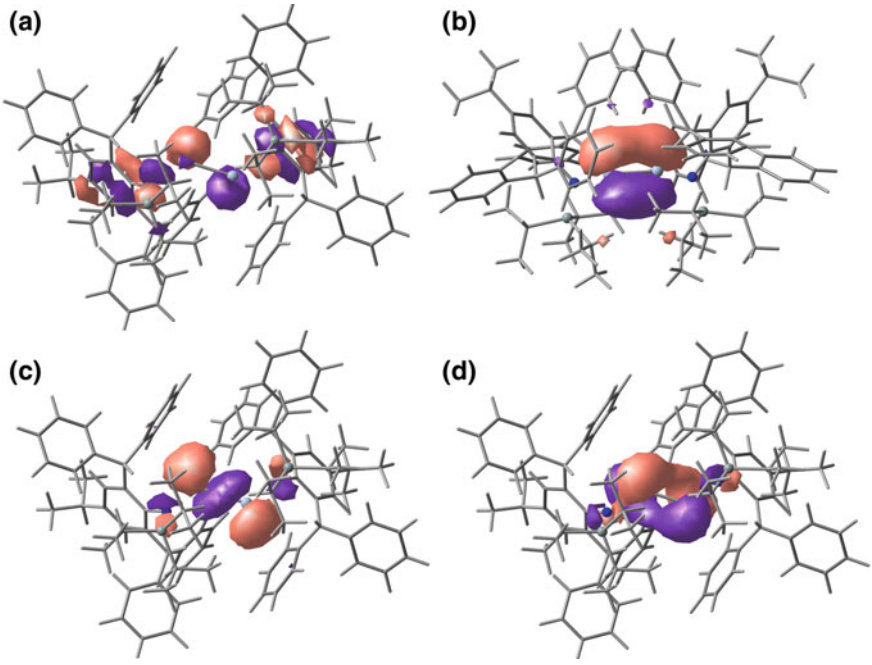

Fig. 3.4 **a** HOMO-1 (−5.18 eV), **b** HOMO (−3.92 eV), **c** LUMO (−3.13 eV) and **d** LUMO + 1 (−2.11 eV) of $\{(^{iPr}L^{\dagger})Ge\}_2$, **14**

for multiply bonded digermynes. That is, its HOMO largely comprises a π-bond orthogonal to the Ge_2N_2 fragment, whereas the HOMO-1 is comparable to the essentially non-bonding, or "slipped", π orbital that lies in the Ge_2C_2 plane of the terphenyl digermynes, and is thought to give rise to their singlet biradicaloid character. The LUMO + 1 and LUMO represent the antibonding counterparts of these two orbitals, and no MO exhibits any N-Ge π-bonding. Taken as a whole, these results suggest that **14** possesses a Ge–Ge interaction that is close to a double bond, a view consistent with the Wiberg bond index (WBI) of 1.75. Importantly, the HOMO-LUMO gap of **14** is very narrow (0.79 eV), suggesting that it is likely highly reactive in regards to small-molecule activation processes (vide infra).

3.3.2 *Reduction of Amido Tin(II) Halide Complexes*

As with their germanium counterparts, bis(aryl)amido Sn(II) halide complexes gave poor results when reduced with **7**. Generally large amounts of elemental tin formed, even at low temperature, with only protonated ligand observed in ^{1}H NMR spectra of crude reaction mixtures. Hence, attempts at using such ligands for the stabilisation of Sn(I) species were abandoned. Where the bulky silyl-aryl amide, $^{iPr}L^{\dagger}$, was used, results were somewhat more promising. Solutions of ($^{iPr}L^{\dagger}$)SnCl (**16**) in toluene quickly became orange/brown at −80 °C upon addition of **7**. Attempted isolation of reduced products, however, resulted in formation of dark precipitates, and isolation of only starting materials and protonated ligand. Fortuitously, reduction of ($^{iPr}L^{\dagger}$)SnBr (**17**), as opposed to the chloride derivative, formed dark green toluene solutions upon addition of **7** at −80 °C. It was noted that this colour began to dissipate, with the formation of a dark precipitate, at −20 °C, and hence repeat reactions were kept below this temperature. Stirring a mixture of **7** and **17** from −80 to −25 °C for 5 h (Fig. 3.5), followed by low-temperature work-up, afforded good yields of the first amido-distannyne, **18**, as dichroic green/orange blocks.

In the solid state the compound is thermally stable for weeks, whilst in solution its decomposition is complete within 48 h at ambient temperature, yielding tin metal and protonated ligand. The ^{1}H and ^{13}C{^{1}H} NMR spectra of **18** both display one set of amide signals, which implies the compound has a symmetrical structure in solution. No signal was observed in the ^{119}Sn{^{1}H} NMR spectrum, presumably as a result of large chemical shift anisotropies arising from the two-coordinate tin environments [28]. Only one distinguishable absorption band (λ_{max} = 409 nm, ε = 6500 L mol^{-1} cm^{-1}) was observed in the UV/Vis spectrum of **18**, which contrasts with terphenyl distannynes, all of which display moderately intense π–π* absorption bands at *ca.* λ_{max} 600 nm, and are, therefore, thought to possess Sn–Sn multiple bonds in solution [28, 56].

In order to shed light on the nature of the Sn–Sn bonding in **18** in the solid state, its X-ray crystal structure was determined (Fig. 3.5). The compound displays a *trans*-bent structure with a Sn–Sn bond (3.1429(7) Å, cf. 3.038 Å calculated for (L′

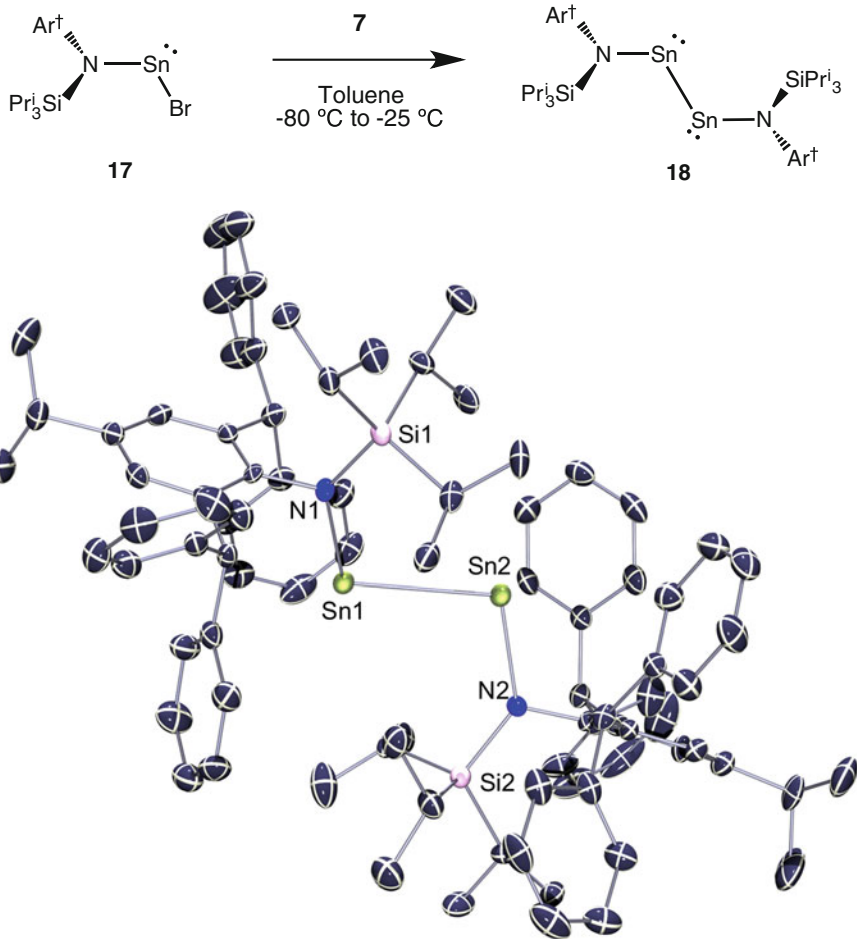

Fig. 3.5 *Above* Scheme for the synthesis of the amido distannyne, $\{(^{iPr}L^{\dagger})Sn\}_2$ (**18**); *Below* ORTEP representation of **18** (50% thermal ellipsoids; hydrogen atom omitted). Selected bond lengths (Å) and angles (°): Sn(1)–N(1) 2.128(4), Sn(1)–Sn(2) 3.1434(5), Sn(2)–N(2) 2.118(4), N (1)–Sn(1)–Sn(2) 104.53(10), N(2)–Sn(2)–Sn(1) 103.48(11)

$Sn)_2$ (L′ = $[Me_2N]^-$)) [34] that is longer than in any previously reported distannyne. This, combined with the rather narrow N–Sn–Sn angles (104.00° mean, cf. 94.4° calculated for $(L'Sn)_2$) [34], clearly signifies that **18** possesses a Sn–Sn single bond. It is likely that Sn–Sn multiple bonding in the distannyne is frustrated by its essentially planar Sn_2NSiC fragments, which presumably allows for a degree of N-Sn π-donation, similar to that observed in $\{(^{TMS}L^*)Ge\}_2$ (vide supra). A similar planarisation of the Ge_2NSiC fragments in the multiply bonded digermyne analogue of **18**, viz. **14**, is doubtless prevented by greater steric buttressing between the amide ligands, which occurs because of the smaller covalent radius of Ge (1.20 Å)

versus Sn (1.39 Å) [96]. Despite this, there is still significant steric crowding in **18**, as evidenced by the marked torsion in its Sn_2N_2 fragment (148.6°).

3.3.3 *Reactivity of a Doubly-Bonded Amido-Digermyne*

3.3.3.1 With H_2

Due to the differences between **14** and previously reported terphenyl-digermynes, we sought to compare the reactivity of the former to the latter. This initially involved the reaction of **14** with H_2. Similar to $\{(^{TMS}L^*)Ge\}_2$, **14** rapidly reacted with H_2 at ambient temperature, with complete conversion to one new product (**19**) within 20 min, with a concomitant colour change from dark brown to bright orange (Scheme 3.27). The generation of just one product is in stark contrast to previously reported reactivity of terphenyl digermynes with H_2 (vide supra), but in keeping with the reactivity of $\{(^{TMS}L^*)Ge\}_2$. However, X-ray crystallographic analysis of **19** showed that it exists as a symmetrical doubly-bonded isomer, $(^{iPr}L^{\dagger})Ge(H)=Ge(H)(^{iPr}L^{\dagger})$, in the solid state, as opposed to the unsymmetrical product observed from the reaction of $\{(^{TMS}L^*)Ge\}_2$ with H_2, viz. $(^{TMS}L^*)GeGe(H)_2(^{TMS}L^*)$. The ^1H NMR spectrum of **19** displays one set of ligand signals, suggestive of a symmetrical formulation in solution. The Ge–*H* resonance in its ^1H NMR spectrum, however, was observed as a broad peak at δ = 8.21 ppm, which is closer to reported monomeric Ge(II) hydride species than dimeric derivatives (e.g. $(^{Dipp}$nacnac$)GeH$: δ = 8.08 ppm, $\{(^{Dipp}$Terph$)GeH\}_2$: δ = 5.87 ppm). To observe whether this was related to isomerisation between symmetrical and asymmetrical forms of **19**, a VT

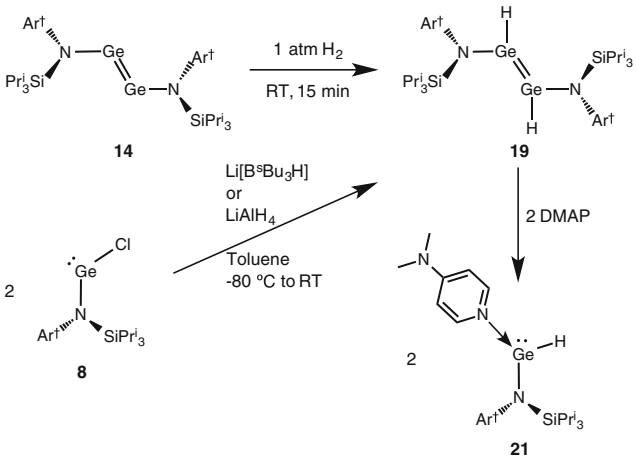

Scheme 3.27 Synthesis of **19** via H_2 activation or salt metathesis routes; and formation of **21** through coordination of DMAP to **19**

^{1}H NMR spectroscopic study was carried out on a d_8-toluene solution of the compound (Fig. 3.6).

No evidence was seen for such an isomerisation, but the Ge–*H* resonance was seen to shift considerably, and reversibly, to δ = 10.60 ppm at 100 °C. Such an observation is related to a colour change from deep orange at low temperatures to pale yellow at high temperatures. Such thermochromicity has been quantified by VT UV/Vis spectroscopy, which revealed that an absorption band centered at

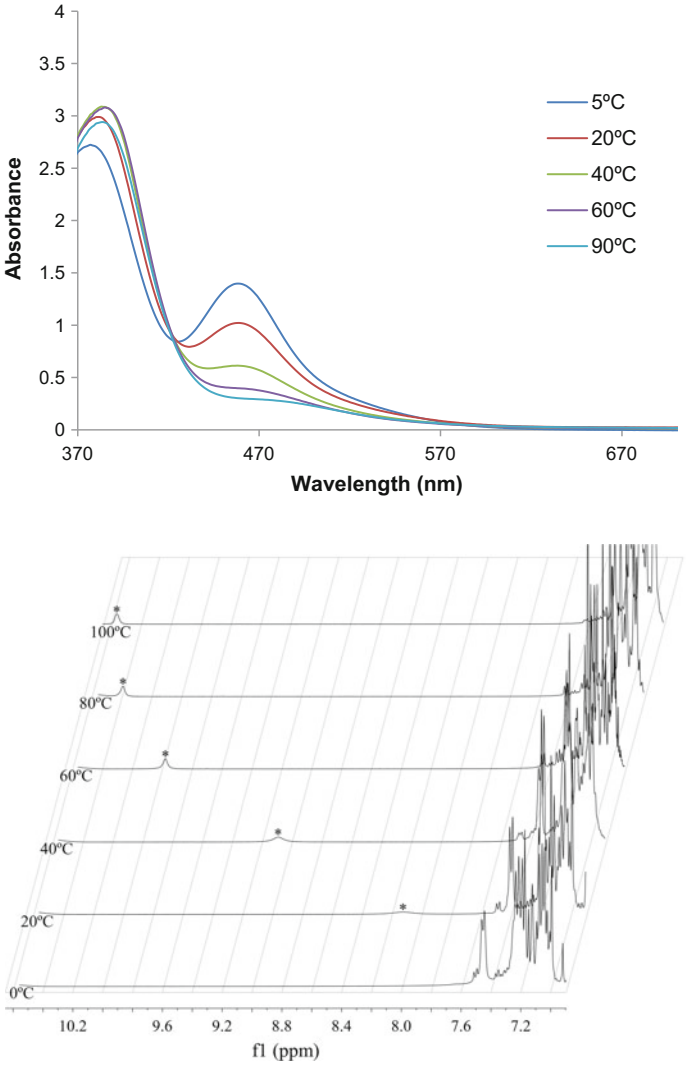

Fig. 3.6 *Above* VT UV/Vis spectra of **19** acquired from 5 to 90 °C in toluene (2.15×10^{-3} M). *Below* VT ^{1}H NMR spectra of a d_8-toluene solution of **19**, showing temperature variance of the Ge-*H* resonance (marked by *asterisk*), from 0 to 100 °C

λ_{max} = 460 nm (0 °C, assigned as the $n_- - n_+$ transition) had almost completely diminished at 100 °C (Fig. 3.6). An isosbestic point was observed in the spectrum at λ = 420 nm, which gives strong evidence that there is an equilibrium between only two species in solution. We contend that this equilibrium is between **19** and the two-coordinate hydrido-germylene, ($^{iPr}L^{\dagger}$)(H)Ge:, similar to that previously reported for the 1,2-dibromodigermene, {(Bbt)Ge(Br)}$_2$ [81]. The solid state structure of **19** (Fig. 3.7) reveals a Ge–Ge bond distance of 2.4864(4) Å, which is

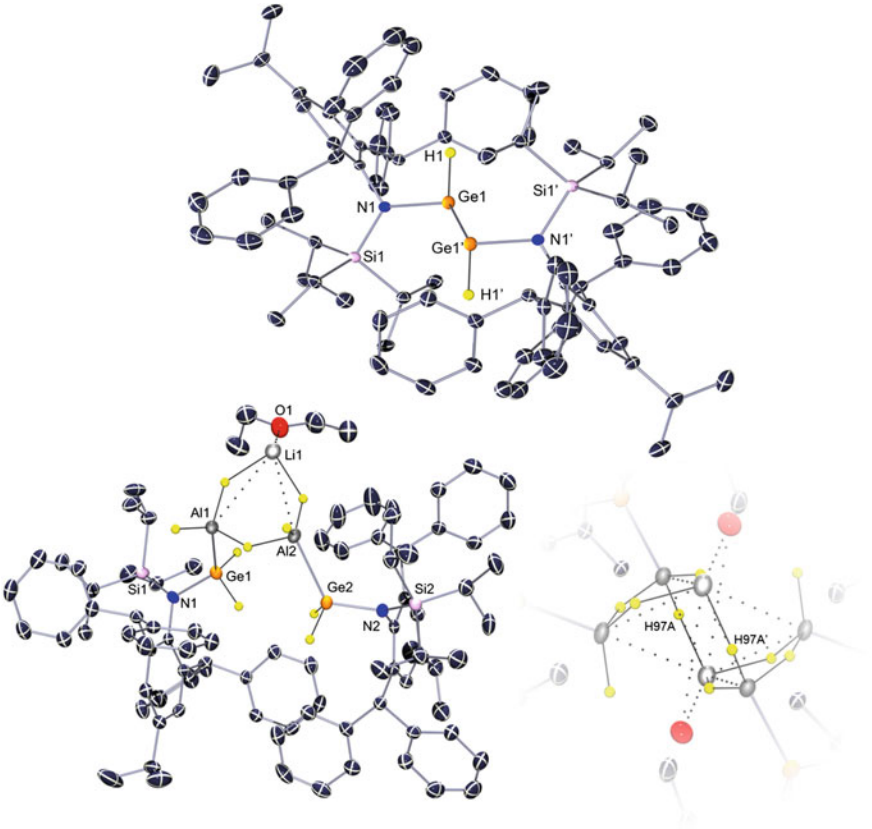

Fig. 3.7 *Above* ORTEP representation of **19** (thermal ellipsoids at 50% probability, hydrogen atoms omitted aside from terminal hydride ligands, H1 and H1′). Relevant bond lengths (Å) and angles (°) (Calculated values at BP86 + D3/def2 TZVPP in square brackets): Ge1–N1 1.8564(13) [2.510], Ge1–Ge1′ 2.4864(4) [2.510], Ge1–H1 1.470(8) [1.572], N1–Ge1–Ge1′ 117.85(4) [116.18], N1-Ge1-H1 98.2(9) [97.22], C1-N1-Si1 116.58(10) [119.19]. *Below* ORTEP representation of **20** (thermal elipsoids at 30% probability, hydrogen atoms omitted aside from hydride ligands; zoom of hydride cluster inlayed). Relevant bond lengths (Å) and angles (°): N1–Ge1 1.881(3), N2–Ge2 1.890(2), Ge1–Al1 2.495 (1), Ge2–Al2 2.465(1), Al1–H98 1.633(2), Al1–H97A 1.568(4), Al1–H97B 1.508(3), Al2–H98 1.719(3), Al2–H96A 1.566(3), Al2–H96B 1.492 (4), Li1–H96B 1.919(4), Li–H97B 1.918(3), Li1–H97A' 1.852(4), N1–Ge1–Al1 122.51(8), N2–Ge2–Al2 123.57(8)

in fact longer than a large number of reported Ge–Ge single bonds. The only longer reported Ge–Ge double bond exists in (Bbt)Ge(Br)=Ge(Br)(Bbt) (2.509 Å) [81]. The dimer is *trans*-bent, and interestingly has a more obtuse *trans*-bending angle (θ = 54°) than the related $\{(^{Dipp}Terph)GeH\}_2$ (θ = 45°). This suggests that the Ge–Ge bond in **19** has much less π-character than the latter. It is likely that the degree of Ge–Ge π-bonding in **19** is frustrated by π-overlap of lone-pairs on each N atom with empty *p*-orbitals on each Ge atom. The geometry at each Ge center (dihedral angle between H–Ge–N and C–N–Si planes = 7.6°) is certainly amenable to such an overlap.

Note that compound **19** can also be synthesised via two alternative routes: either the slow addition of $Li[BBu^s{}_3H]$ to a toluene solution of **8**, followed by slow warming to ambient temperature, or the addition of toluene to a solid mixture of **8** and $LiAlH_4$, followed by stirring for 4 days (Scheme 3.27).

Both of these routes afford moderate yields of **19**, however neither route is as efficient as the generation of **19** from **14** and H_2 gas. It is also worth noting that the reaction of **8** with solutions of $LiAlH_4$ in Et_2O results in the formation of $[\{^{iPr}L^{\dagger}GeH_2AlH_2\}_2LiH.Et_2O]_2$ (**20**), which is an example of an amidogermane-stabilised lithium aluminium-hydride cluster. Based on a survey of the CCDC, this is the first of its kind. It is likely that this species forms from initial generation of **19**, with subsequent oxidative addition of $LiAlH_4$, or generated AlH_3, across the Ge(II) centre. Attempts to generate such a species by addition of AlH_3 to solutions of **19** were unsuccessful, and yielded complex product mixtures. The solid-state structure of **20** (Fig. 3.7) features a central Al_2Li unit bridged by three hydrides, with Li1 coordinated by an Et_2O molecule. Both Al1 and Al2 are bound by a $[(^{iPr}L^{\dagger})Ge(H)_2]^-$ unit. Two of the $\{^{iPr}L^{\dagger}GeH_2AlH_2\}_2LiH.Et_2O$ units (see Fig. 3.7) bridge via H97A and H97A', bound to Al2 and Al2', respectively (Fig. 3.7, inset), giving the full molecule, $[\{^{iPr}L^{\dagger}GeH_2AlH_2\}_2LiH.Et_2O]_2$.

The mechanism for the addition of H_2 to both terphenyl digermynes and amido digermynes has been the subject of DFT analyses [97–99]. Frenking and co-workers found that the primary transition state in the addition of H_2 to both $\{(^{TMS}L^*)Ge\}_2$ and **14** involves the approach of an H_2 molecule to one Ge(I) centre [98, 99]. The H–H bond is cleaved through interaction of the HOMO (π) and LUMO (n_+) of **14** with the LUMO (σ*) and HOMO (σ) on H_2, respectively (Scheme 3.28). A similar result is found for $\{(^{TMS}L^*)Ge\}_2$, via different initial orbital interactions [98]. In both cases, the mono-hydride bridged dimeric intermediates, $(^{TMS}L^*)Ge(\mu\text{-}H)Ge(H)(^{TMS}L^*)$ and $(^{iPr}L^{\dagger})Ge(\mu\text{-}H)Ge(H)(^{iPr}L^{\dagger})$ are generated. The $(^{TMS}L^*)Ge(\mu\text{-}H)Ge(H)(^{TMS}L^*)$ intermediate has a relatively large barrier to the lower energy symmetrical isomer, $\{(^{TMS}L^*)GeH\}_2$ (7 kcal mol^{-1}, Fig. 3.8a). On the other hand, the $^{iPr}L^{\dagger}$ stabilised congener has a negligible barrier to the symmetrical dimer, $\{(^{iPr}L^{\dagger})GeH\}_2$ (0.7 kcal mol^{-1}, Fig. 3.8b), and no barrier to the mixed valence isomer, $(^{iPr}L^{\dagger})GeGe(H)_2(^{iPr}L^{\dagger})$ (−0.8 kcal mol^{-1}). The symmetrical $\{(^{iPr}L^{\dagger})GeH\}_2$ is the lowest energy isomer for this system [98, 99]. These results shed light on the isolated species in the hydrogenations of $\{(^{TMS}L^*)Ge\}_2$ and **14**. Whilst the mixed valence isomer $((^{TMS}L^*)GeGe(H)_2(^{TMS}L^*))$ is preferred for the $^{TMS}L^*$ system, the energy separation between this isomer and the

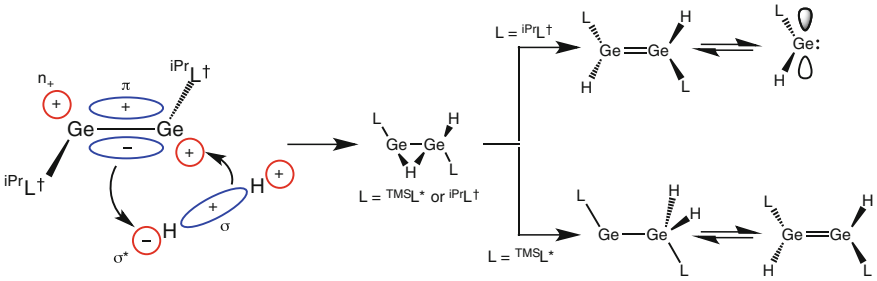

Scheme 3.28 The interactions involved in the activation of H_2 by $\{(^{iPr}L^{\dagger})Ge\}_2$ (**14**), and intermediates and isomeric forms of related Ge(II) hydride complexes stabilised by $^{TMS}L^*$ and $^{iPr}L^{\dagger}$

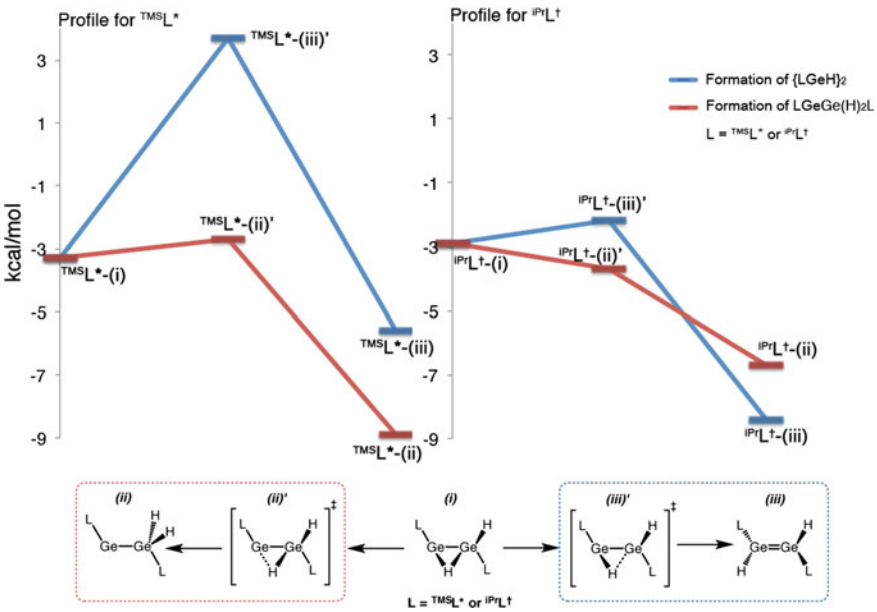

Fig. 3.8 Energy profile for the isomerisation of LGe(μ-H)Ge(H)L to $LGeGe(H)_2L$ (*red*) or $(LGeH)_2$ (*blue*). (a) L = $^{TMS}L^*$, (b) L = $^{iPr}L^{\dagger}$)

symmetrical dimer is very small (Fig. 3.8a). The slight ligand modification (i.e. using $^{iPr}L^{\dagger}$) leads to significant stabilisation of the symmetrical dimer, $\{(^{iPr}L^{\dagger})GeH\}_2$ (Fig. 3.8b), relative to the mixed valence species, making this the most stable isomer for **19**.

Further to these discussed results, a large barrier to the formation of Ge(III) and Ge(IV) products, through further H_2 activation by $\{(^{TMS}L^*)GeH\}_2$ (27.4 kcal mol^{-1}) or $(^{TMS}L^*)GeGe(H)_2(^{TMS}L^*)$ (25 kcal mol^{-1}) was found [98], explaining

the stability of the amido Ge(II) hydride complexes in this regard. Conversely, lower barriers to the formation of Ge(III) (19.3 kcal mol^{-1}) and Ge(IV) (19.6 kcal mol^{-1}) hydride complexes were found for the hydrogenation of the terphenyl digermyne, $\{(^{Dipp}Terph)Ge\}_2$, by Schleyer and co-workers, justifying the observations of such species in the experimental addition of H_2 to $\{(^{Dipp}Terph)Ge\}_2$.

DFT analyses on the equilibrium between **19** and $(^{iPr}L^{\dagger})(H)Ge$:, were also carried out as part of this study by Frenking and co-workers [99]. Surprisingly, where dispersion forces were included (i.e. at the BP86 + D3/def2-TZVPP level) the dissociation of $\{(^{iPr}L^{\dagger})GeH\}_2$ to two $(^{iPr}L^{\dagger})(H)Ge$: units was found to have a ΔG°_{298} that is considerably endergonic (19.4 kcal mol^{-1}), which decreased slightly to a still endergonic value (16.1 kcal mol^{-1}) where solvent effects were taken into consideration (i.e. using the COSMO model [100]). These values are too high to account for the readily established equilibrium between **19** and $(^{iPr}L^{\dagger})(H)Ge$: in hydrocarbon solvents [99]. However, where both dispersion forces and solvent effects were ignored (i.e. at the BP86/def2-TZVPP level) an exergonic value of −10.5 kcal mol^{-1} was found for ΔG°_{298}, suggesting inaccuracies in the estimates of dispersion forces using Grimme's D3 term [101] in this case.

As a means to provide further evidence for the equilibrium between **19** and $(^{iPr}L^{\dagger})(H)Ge$:, we sought to form a Lewis-base adduct of the monomeric species. To this end, DMAP was added to a C_6D_6 solution of **19** (Scheme 3.27). The solution instantly became pale yellow, with a concomitant shift in the major ligand-based peaks in its ^1H NMR spectrum. Further, the DMAP resonances had shifted from those for free DMAP, as had that of the Ge–*H* unit (δ = 9.04 ppm, viz. $(^{Dipp}nacnac)GeH$, Ge–*H*: δ = 8.08 ppm). Scale-up of this reaction afforded **21**, X-ray crystallographic analysis of which revealed it to be a DMAP adduct of a monomeric Ge(II) hydride unit, $(^{iPr}L^{\dagger})(H)Ge$.DMAP. This represents the first example of an acyclic 3-coordinate Ge(II) hydride complex. This observed reactivity contrasts with Power's report of isomerisation of $\{(^{Dipp}Terph)Ge(H)\}_2$ to the unsymmetrical isomer, $(^{Dipp}Terph)(PMe_3)GeGe(H)_2(^{Dipp}Terph)$, upon PMe_3 coordination, rather than dissociation to two equivalent monomeric hydride species [33]. The solid state structure of **21** (Fig. 3.9) shows it to have a *pseudo*-tetrahedral Ge geometry, with the "vacant" site being occupied by a lone-pair of electrons. Importantly, the Ge1–N2 distance, that is the distance from Ge to the coordinated DMAP molecule, is quite long at 2.204(4) Å, in keeping with a dative bond. The terminal Ge–*H* atom was located and freely refined during crystal structure determination, with a Ge–H distance of 1.494(8) Å.

3.3.3.2 With Olefins

Reactivity studies of **14** towards olefins were pursued so as to draw comparisons between it and the terphenyl ligated analogue, $\{(^{Dipp}Terph)Ge\}_2$, which has been extremely widely studied in this regard. To this end, **14** was reacted with ethylene,

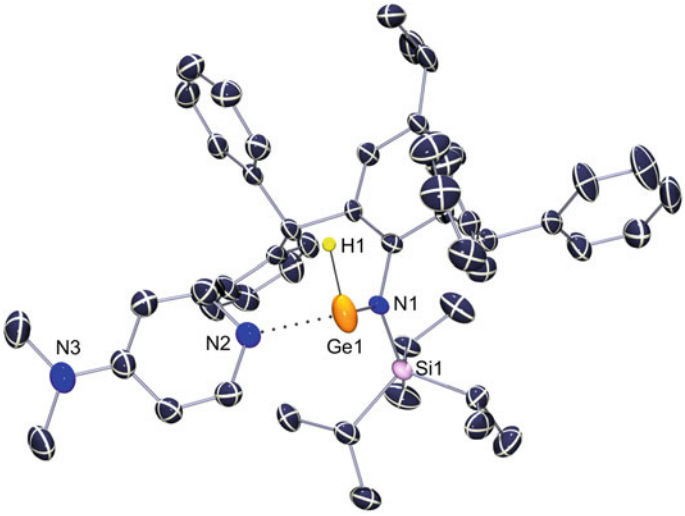

Fig. 3.9 Relevant bond lengths (Å) and angles (°) for **21** (Calculated values at BP86 + D3/def2-TZVPP in square brackets): Ge1–N1 1.933(3) [1.983], Ge1–N2 2.204(4) [2.241], Ge1–H1 1.494(8) [1.607], N1–Ge1–N2 107.98(13) [104.33], N1–Ge1–H1 99.9(14) [102.73], N2–Ge1–H1 89.5(13) [91.96], C1–N1–Si1 120.8(3) [116.48]

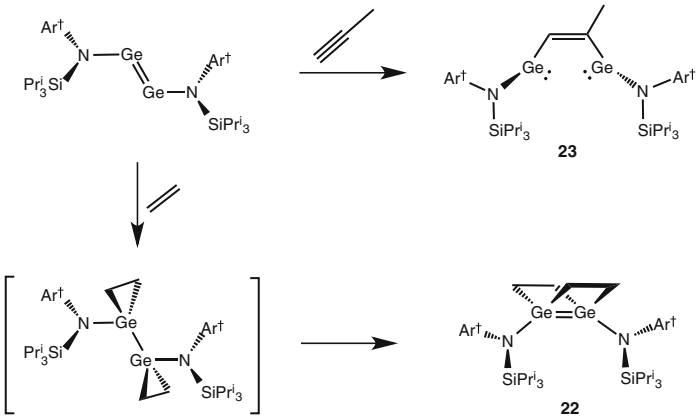

Scheme 3.29 Reactions of **14** with ethylene and propyne

propyne, COD, and 1,3-cyclohexadiene (1,3-CHD), with both similar and differing resultant paths of reactivity seen for **14**, relative to $\{(^{Dipp}Terph)Ge\}_2$.

The addition of ethylene to **14** occurs readily at one atmosphere of pressure and ambient temperature, yielding a solution which quickly dissipates in colour to yellow/orange (Scheme 3.29). Removal of volatiles in vacuo resulted in no colour change, suggesting the reaction is irreversible (cf. the reversible addition of ethylene to $\{(^{Dipp}Terph)Sn\}_2$) [51]. A ^1H NMR spectroscopic analysis of the reaction mixture

revealed the formation of a single product with a broad resonance at δ = −0.63 ppm, likely corresponding to bridging $[C_2H_4]^{2-}$ ligands. The remainder of the spectrum was in keeping with one symmetrical ligand environment. Crystallisation of the reaction mixture yielded yellow blocks of the product in low yield, likely due to the high solubility of this species. X-ray structural analysis of the product revealed it to be a doubly C_2H_4-bridged digermabicyclo[2.2.0]hexane, ($^{iPr}L^{\dagger}$)Ge(μ-C_2H_4)$_2$Ge($^{iPr}L^{\dagger}$) (**22**, Fig. 3.10), formed via a formal [2+2+2] cycloaddition of ethylene to **14**. Compound **22** is very similar to the product reported by Power [51], in that it has a puckered bicyclic Ge_2C_4 core (dihedral angle between Ge_2C_2 least squares planes = 74.6°), with Ge–Ge and Ge–C distances (2.5102(10) Å and 1.99 Å (mean) respectively) that are in the normal single bonded ranges. Considering that [2+2] cycloaddition reactions are symmetry forbidden, according to the Woodward-Hoffman rules [102], it is unlikely that the mechanism of the facile formation of **22** involves two concerted [2+2] processes. Instead, the mechanism is likely to be similar to that proposed for the closely related compounds, (^{Dipp}Terph)E(μ-C_2H_4)$_2$E(^{Dipp}Terph) (E = Ge or Sn) [51], and that calculated for the formal [2+2] cycloaddition of ethylene with a disilyne [103]. That is, the C–C bond of each ethylene molecule interacts with a Ge center of **14** (via *quasi*-[1+2] cycloaddition reactions), to give an intermediate with two GeC_2 three-membered rings. This intermediate then rearranges to give **22**, as previously discussed in this chapter.

The reaction of **14** with one atmosphere of propyne yields the monobridged product, ($^{iPr}L^{\dagger}$)Ge{μ-C_2H_2(Me)}Ge($^{iPr}L^{\dagger}$) (**23**, Scheme 3.29), which was isolated as large deep-red clusters of plate-like crystals, which have high thermal stability (decomp. above 211 °C). The ^{1}H NMR spectrum of the product shows two differing ligand environments, as indicated by coalescence of ligand signals.

The bridging C–C distance of 1.351(4) Å is concordant with a C–C double bond, whilst the two Ge–C distances (1.945(3) Å and 2.039(2) Å) are in the known range of Ge–C single bonds. The two germylene fragments are aligned such that the Ge lone pair of one is apparently directed towards the empty Ge *p*-orbital of the other, giving rise to a fairly close, and possibly partially bonding, Ge···Ge interaction (3.127(2) Å). Interestingly, the addition of diphenylacetylene to Power's digermyne, {(^{Dipp}Terph)Ge}$_2$, yielded a product with an intact Ge–Ge double bond. This provides further evidence for donation of the N lone-pair of the ligand to the empty *p*-orbital of Ge in **23**, weakening any π-interaction between the two Ge-centres.

Following the addition of monounsaturated species to **14**, we sought to investigate the products of reactions of polyunsaturates with **14**, given the various CH-activation and C–C bond cleavage reactions observed by Power in this regard (vide supra) [52, 53]. Primarily, the addition of approximately two equivalents of 1,3-CHD to **14** yielded a single product as determined by ^{1}H NMR spectroscopic analysis. That is, the spectrum showed broadened resonances for the majority of the ligand peaks, and two separate peaks for the ligand Ph_2CH moieties, as well as a new broad singlet at δ = 4.89 ppm. Further, approximately one equivalent of unreacted 1,3-CHD remained in the mixture. Upon heating the sample to 70 °C for 5 min, followed by cooling to room temperature, the ^{1}H NMR spectrum of the reaction mixture showed the presence of a single new product, concomitant with the

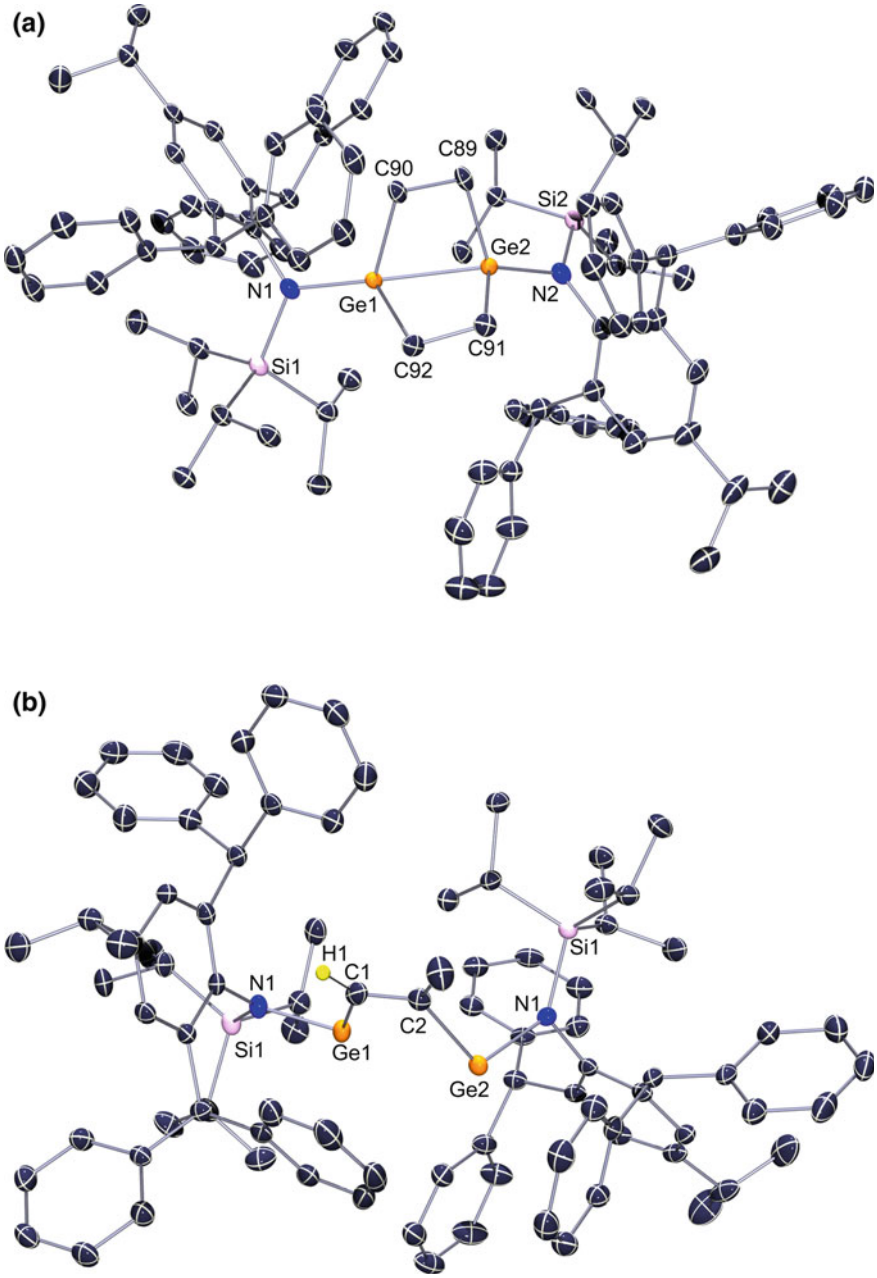

Fig. 3.10 Thermal ellipsoid plots (30% probability surface) of *a* **22** and *b* **23** (hydrogens omitted, aside from H1 in **23**). Selected interatomic distances (Å) and angles (°) for **22**: Ge1–N1 1.877(5), Ge1–C89 1.996(5), Ge1–C91 2.002(6), Ge1–Ge2 2.5102(10), Ge2–N2 1.889(5), Ge2–C92 1.971 (6), Ge2–C90 2.003(6), N1–Ge1–Ge2 154.54(14), N2–Ge2–Ge1 154.88(14); **23**: Ge1–N1 1.876 (2), Ge1–C1 1.945(3), Ge2–N2 1.8927(19), Ge2–C2 2.039(2), C1–C2 1.351(4), N1–Ge1–C1 105.06(10), N2–Ge2–C2 110.22(9), C2–C1–Ge1 113.40(18), C1–C2–Ge2 118.31(18)

appearance of a large C_6H_6 peak. Moreover, the excess 1,3-CHD had been consumed. We speculate that the first product is that of a Ge–Ge bond cleaved [4+2] cycloadduct of 1,3-CHD and **14**, which CH-activates upon heating, to generate **19** and C_6H_6. The excess 1,3-CHD may then react with the in situ generated **19**, through hydrogermylation. Scale up of the room temperature addition reaction of

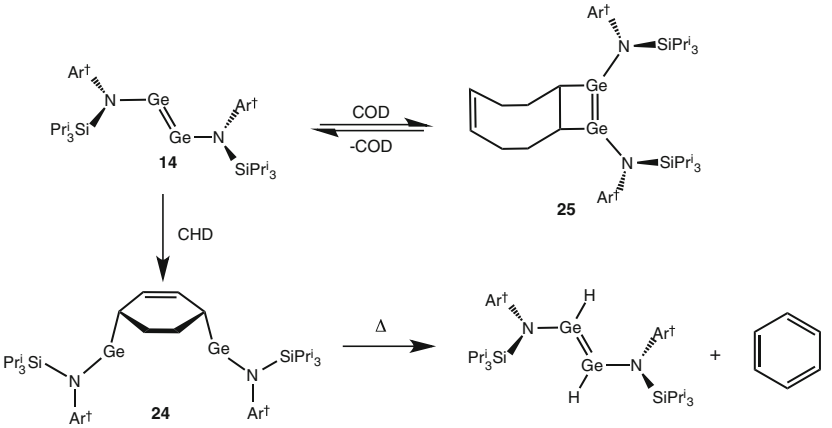

Scheme 3.30 Reactions of **14** with 1,3-CHD and COD

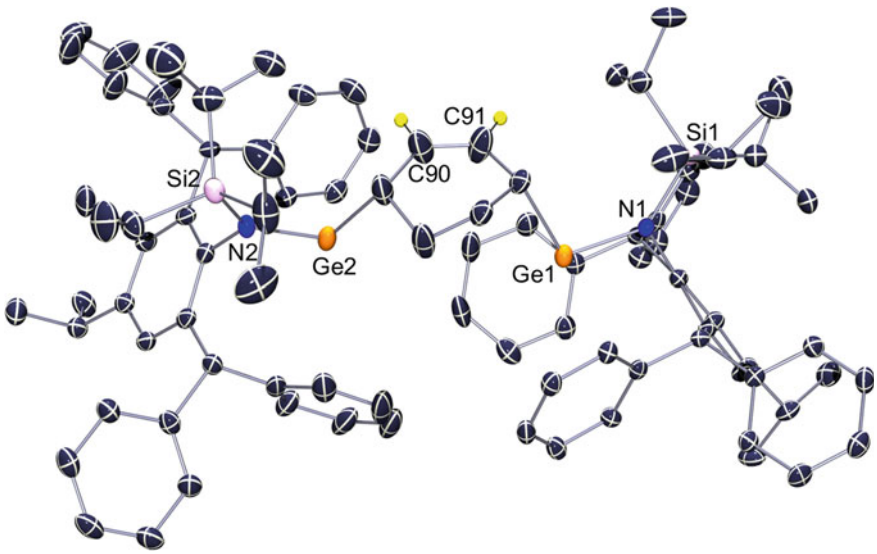

Fig. 3.11 Thermal ellipsoid plot (30% probability surface) of **24** (hydrogen atoms, except those on the reduced 1,3-CHD unit, omitted). Selected interatomic distances (Å) and angles (°): Ge1–N1 1.918(4), Ge1–C92 2.053(5), Ge2–N2 1.900(4), Ge2–C89 2.039(7), C90–C91 1.308(9), N1–Ge1–C92 105.55(19), N2–Ge2–C89 104.9(2)

1,3-CHD to **14** yielded, after crystallisation, the "[4+2] addition" product, (^{iPr}L†)Ge(μ-C_6H_8)Ge(^{iPr}L†) (**24**, Scheme 3.30, Fig. 3.11) in which two germylene fragments are bound at the 1,4-positions of a central cyclohexenediyl unit. Although the two germylene fragments adopt *cis*-positions relative to the bridging organic unit, it is unlikely that there is any "cross-ring" Ge···Ge interaction, given the large separation between the two metal centers (5.246(2) Å). The Ge1–C92 (2.053(5) Å) and Ge2–C89 (2.039(7) Å) distances are in the standard single bond range, whilst there is one clear double bond in the bridging cyclohexyl unit (C90–C91 1.308(9) Å).

The thermal degradation of **24** was confirmed by heating a sample of the pure compound in the absence of excess 1,3-CHD. Heating to 70 °C in C_6D_6, followed by cooling to ambient temperature, resulted in the formation of several products. These included benzene and the Ge(II) hydride species, **19**. The other observed products comprised a complex mixture of species. It was also shown that **19** cleanly reacts with 1,3-CHD to yield a single product, the ^{1}H NMR spectrum of which is in keeping with that observed when heating **24** in the presence of excess 1,3-CHD. Therefore, it is likely that the previously speculated reaction route is accurate. That is, primarily a [4+2] cycloaddition reaction of 1,3-CHD to **14** occurs, yielding **24**. Each Ge-centre can then undergo β-hydride elimination with the cyclohexendiyl ring, generating {(^{iPr}L†)GeH}$_2$ and benzene (Scheme 3.30). The gain in aromatisation of the cyclohexyl ring to benzene likely aids in driving the reaction. Overall this process can be considered as the CH-activation of 1,3-CHD by **14**, or equally, the transfer hydrogenation of **14** by 1,3-CHD.

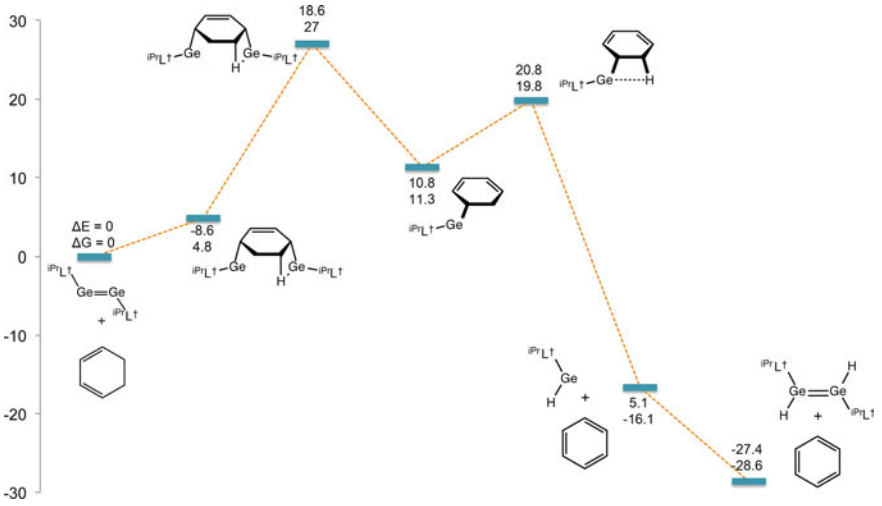

Fig. 3.12 Calculated reaction profile (TPSS + D3(ABC)/def2-TZVPP//TPSS + D3(BJ)/def2-SVP) for the transfer hydrogenation of {(^{iPr}L†)Ge}$_2$, **14**, with 1,3-cyclohexadiene, yielding **24**, and giving rise to subsequent benzene elimination

This proposed mechanism was probed using computational studies, carried out at several levels of theory, on the full molecules employed in the reaction (Fig. 3.12). These studies firstly showed good agreement between the experimental geometry of **24**, and that calculated for it (e.g. Ge···Ge 5.114 Å; Ge–C 2.087 Å, 2.106 Å; Ge–N 1.931, 1.932 Å at TPSS + D3/def2-SVP). More importantly, the calculations revealed that, in contrast to our prediction, there is no [4+2] cycloaddition intermediate on the reaction pathway to **24**. In addition, the reaction was calculated to be slightly endergonic (ΔG = 2.6 kcal mol^{-1} at BP86 + D3 (ABC)/def2-TZVPP//BP86 + D3/def2-SVP), though an exergonic outcome here is certainly within the error of the computational technique. The formation of **19** from **24** is quite exergonic (ΔG = −24.4 kcal mol^{-1}), and proceeds via stepwise β-hydrogen elimination steps. This sees the reaction passing through two transition states, the first of which has a quite high energy of activation ($\Delta G^{\ddagger}$ = 22.2 kcal mol^{-1}), which is consistent with the relatively high temperatures required (*ca.* 70 °C) for the formation of **19** and benzene from **24**.

Treatment of the amido-digermyne, **14**, with an excess of 1,5-COD afforded a moderate yield of the purple-red digermacyclobutene complex, **25**, via a formal [2+2] cycloaddition process. This contrasts with {(^{Dipp}Terph)Ge}$_2$, which does not react with 1,5-COD, perhaps highlighting the greater reactivity of amido-digermynes relative to that of their terphenyl substituted counterparts. Addition of only one equivalent of 1,5-COD to a C_6D_6 solution of **14** results in negligible change in colour of the solution or consumption of **14**. However, upon addition of a large excess of 1,5-COD the solution becomes deep purple. Further, the colour of the solution reversibly dissipated to deep brown/orange (i.e. that of **14**) with heating to 60 °C.

In a scale-up reaction, a 15 fold excess of 1,5-COD was added to a toluene solution of **14**, and the solution colour instantly became purple. Careful concentration, further addition of 1,5-COD, and addition of hexane, followed by filtration, resulted in the crystallisation of purple/red crystals of **25** in a moderate yield. Dissolution of a pure sample of **25** in C_6D_6 at ambient temperature resulted in near complete (95%) dissociation of **25** into **14** and 1,5-COD. This suggests that the cycloaddition reaction that yielded **25** is a reversible process in solution under mild conditions. Although the room temperature reversible cycloaddition of olefins to distannynes and silylenes has been reported [51, 104, 105], to the best of our knowledge, such reactivity is unknown for low-valent germanium systems. Cooling d_8-toluene solutions containing equilibrium mixtures of **25**, **14** and 1,5-COD led to an increase in the amount of **25** in the sample, at the expense of **14** and 1,5-COD. Heating the mixture resulted in complete dissociation of **25** at *ca.* 40 °C. Attempts to ascertain the enthalpy of 1,5-COD association in **25** using a Van't Hoff analysis of the variable temperature ^{1}H NMR spectra of the compound were thwarted by overlapping of key signals for **25** and **14**, making accurate integration of those signals problematic. Presumably, however, the dissociation of COD from **24** is a low energy process.

The molecular structure of **25** (Fig. 3.13) shows it to be a formal [2+2] cycloadduct between **14** and 1,5-COD, with the two Ge centers coordinated to the

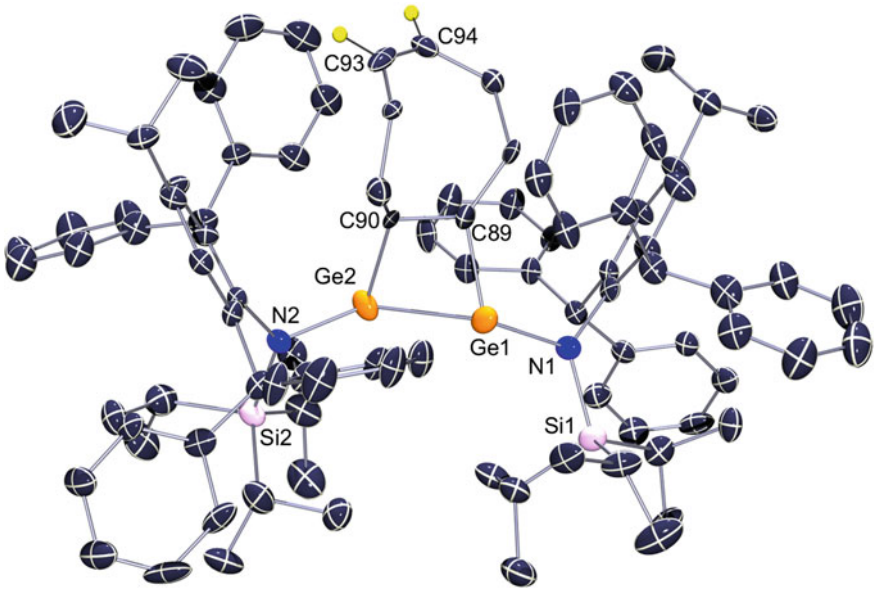

Fig. 3.13 ORTEP representation of **25** (30% probability surface; hydrogen atoms, except those on the olefinic moiety of the reduced COD unit, omitted). Selected interatomic distances (Å) and angles (°): Ge1–N1 1.883(6), Ge1–C89 1.969(8), Ge1–Ge2 2.5177(14), Ge2–N2 1.872(6), Ge2–C90 1.944(9), C89–C90 1.506(11), N1–Ge1–Ge2 140.65(19), N2–Ge2–Ge1 140.68(18), C89–Ge1–Ge2 72.2(2), C90–Ge2–Ge1 71.1(2), C90–C89–Ge1 97.7(5), C89–C90–Ge2 101.3(6)

carbocycle with a *cis*-disposition relative to each other. The strained nature of the Ge_2C_2 ring in the compound is manifested by the length of the formal Ge–Ge double bond (2.5177(14) Å) which is longer than any such interaction in digermenes (range: 2.21–2.51 Å [11]). It is, in fact, longer than the Ge–Ge single bond in **22**, yet has not cleaved. That said, the Ge–C distances in the compound (1.96 Å mean) are close to the mean value for all crystallographically characterised Ge–C single bonds (1.97 Å [11]), which is seemingly at odds with the facile dissociation of 1,5-COD from the compound in solution at ambient temperatures. It is important to note, however, that the atomic positions of the 1,5-COD ligand in **25** are disordered over two positions, and so the accuracy of the Ge–C distances in the molecule may be compromised to some extent. With that said, the distannyne-ethylene cycloadduct, (^{Dipp}Terph)Sn(μ-C_2H_4)$_2$Sn(^{Dipp}Terph), has been reported to display normal Sn–C bond lengths, yet dissociates ethylene in solution at ambient temperature [51].

In order to explore the strength of the association between **14** and 1,5-COD in the cycloadduct, **25**, computational studies were carried out on the full molecules at several levels of theory. These studies revealed that the optimized geometry of **25** is broadly similar to that determined in the solid state (e.g. Ge–Ge 2.512 Å; Ge–N 1.905 Å, 1.896 Å; N–Ge–Ge 142.8°, 135.6° at TPSS + D3/def2-TZVPP), with the

exception of the Ge–C bonds in the compound, which are approximately 0.1 Å longer (e.g. 2.071 Å, 2.051 Å at TPSS + D3/def2-TZVPP) than in the experimental situation. This discrepancy could result from the aforementioned inaccuracy arising from disorder in 1,5-COD ring atomic positions in the X-ray crystal structure of **25**. With regard to the free energy of association of 1,5-COD and **14** (to give **25**), this was calculated to be very low ($\Delta G_{assoc} = -3.9$ kcal mol^{-1} at TPSS + D3/def2-TZVPP), which is fully consistent with the facile dissociation of 1,5-COD from **25** that was observed in the solution state. This value can be compared with the experimental enthalpy of association which was determined for the reaction between $\{(^{Dipp}Terph)Sn\}_2$ and two molecules of ethylene (i.e. $\Delta H_{assoc} = -11.4(9)$ kcal mol^{-1}) [51]. Similar to what was proposed for that reaction, there is likely a fine balance between the energy gained from the formation of two Ge–C bonds in **25**, and the loss of one C–C π-bond from the 1,5-COD molecule in the same process.

These results for the activation of C–C unsaturates by an amido-digermyne highlight both similarities and significant differences between the reactivities of amido-digermynes and their terphenyl substituted counterparts. In this respect, several novel patterns of reactivity have been identified for digermynes, which include unprecedented examples of their reversible formal cycloaddition and transfer hydrogenation reactions with diolefins under mild conditions.

3.3.4 *Reactivity of an Amido Distannyne with H_2, CO_2, and Bu^{t}NC*

Following reactivity studies of **14**, we sought to study some related reactivity of **18**. With the amido-distannyne in hand, its reactivity towards H_2 was investigated by placing a solution of the compound, in C_6D_6, under an atmosphere of dihydrogen at ambient temperature and atmospheric pressure. Monitoring the reaction by ^{1}H NMR spectroscopy showed that, after three hours, *ca.* 30% of **18** had converted to a new product, with a broadened singlet resonance at *ca.* δ = 17.9 ppm tentatively assigned to a Sn–*H* moiety (Scheme 3.31). After 24 h the reaction was *ca.* 70% complete, though because of the low thermal stability of **18** and the apparent tin hydride product, an amount of $^{iPr}L^{\dagger}H$ and tin metal were also present in the reaction mixture at that time. Therefore, although **18** does react with H_2, this reaction is considerably slower than that for the corresponding digermyne, **14**, which is complete after 20 min. To ascertain whether the formed product was a Sn(II) hydride complex, the species $(^{iPr}L^{\dagger})Sn(\mu\text{-}H)_2Sn(^{iPr}L^{\dagger})$ (**26**) was generated by the reaction of **16** ($(^{iPr}L^{\dagger})SnCl$) with $Li[BBu^s{}_3H]$ in toluene, from −80 °C to ambient temperature. The colourless solution became intensely yellow instantaneously at −80 °C, and remained unchanged until temperatures above −20 °C, whereby a dark precipitate formed, and the solution became dark brown. At this temperature ^{1}H NMR spectroscopic analysis showed the assumed Sn(II) hydride species was

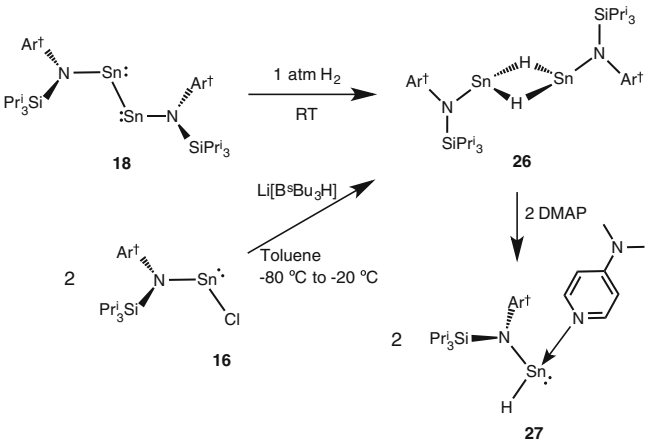

Scheme 3.31 Generation of a hydride-bridged amido stannylene, **26**, via H_2 activation by **18**, or salt metathesis; and coordination of **26** with DMAP to form a monomeric tin(II) hydride complex, **27**

present, alongside amounts (>30%) of protonated ligand. Keeping the reaction mixture below −20 °C during work-up allowed for the crystallisation of pure **26**, the ^{1}H NMR spectrum of which showed a similar broad singlet resonance at *ca.* δ = 17.5 ppm for its Sn–*H* fragment. Due to the broadness of this peak, no ^{119}Sn satellites could be observed, even after extended acquisition times. All other peaks in the spectrum were concordant with a single symmetrical ligand environment in solution. The NMR sample of **26** showed relatively rapid decomposition, being complete after 72 h. Interestingly, a large H_2 peak is present after this time, suggesting a potential decomposition pathway via the distannyne, **18**. Crystalline samples also decompose over the course of a few weeks if all lattice hexane is removed. However, they remain stable for longer periods if solvent is not completely removed in vacuo.

The molecular structure of **26** (Fig. 3.14) shows it to be an unsymmetrically hydride-bridged dimer that is closely related to several previously reported terphenyl-substituted systems, for example, $\{(^{Dipp}Terph)Sn(\mu\text{-}H)\}_2$ [60]. However, the Sn···Sn separation in **26** (3.35 Å) is considerably greater than in all of the terphenyl tin(II) hydrides, for example, 3.13 Å for $\{(^{Dipp}Terph)Sn(\mu\text{-}H)\}_2$. Similar to **19**, this difference likely results from some overlap of the *p*-orbital lone pairs of the N atoms of **26** with the empty *p*-orbitals of the Sn centers (dihedral angle between H–Sn–N and C–N–Si planes = 20.9°). This, in turn, could lead to a weakening of the hydride bridges in **26**, and its proposed equilibrium with ($^{iPr}L^{\dagger}$)(H)Sn: in solution (vide infra).

It was found that, similar to **19**, the Sn–*H* resonance of **26** in its ^{1}H NMR spectra is somewhat temperature dependant. A VT ^{1}H NMR spectroscopic study of **26** showed that over the temperature range −60–80 °C the peak assigned to the Sn–*H* moiety shifted from δ = 13.6 to δ = 20.6 ppm. Although **26** had completely

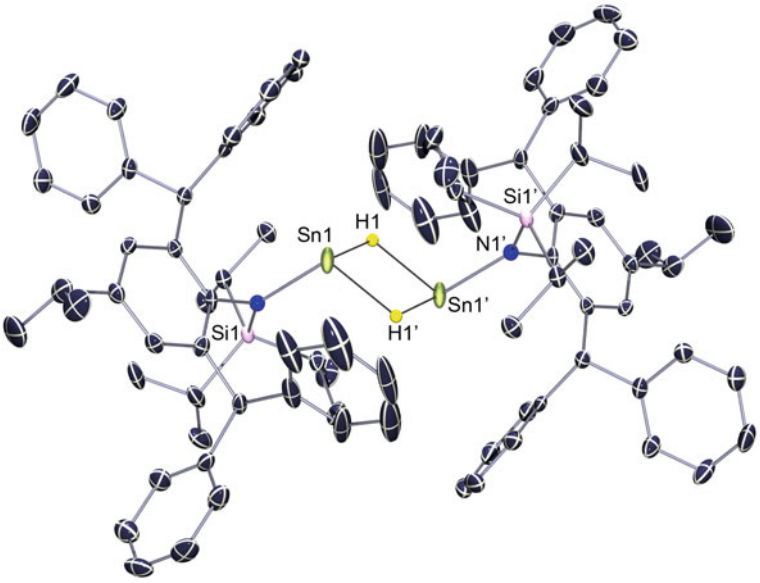

Fig. 3.14 ORTEP diagram of **26** (50% thermal ellipsoids; hydrogen atoms omitted aside from bridging hydride ligands). Selected bond lengths (Å) and angles (°): Sn1–N1 2.133(2), Sn1–H1 1.89(3), Sn1–H1–Sn1′ 115(1), H1–Sn1–H1′ 65(1), N1–Sn1–H1 103.0(10), C1–N1–Si1 121.22 (18)

decomposed upon cooling from 80 °C due to its thermal instability, a further experiment revealed that the process giving rise to the hydride resonance temperature dependence is reversible. That is, a solution of **26** was warmed to 40 °C, a ^{1}H NMR spectrum collected, and the solution rapidly cooled to −20 °C, followed by the collection of another ^{1}H NMR spectrum. This confirmed the reversibility of the process. Even over this temperature range the Sn–*H* resonance shifts considerably (40 °C: δ = 19.20 ppm). This led us to believe that, as for **19**, **26** is in equilibrium with the monomeric species, (^{iPr}L†)(H)Sn:, in solution.

We sought to verify this through the coordination of **26** with DMAP, which, as was the case with **19**, led to the isolation of the DMAP adduct, (^{iPr}L†)(H)Sn.DMAP (**27**). The ^{1}H NMR spectrum of **27** has a slightly broadened resonance at δ = 15.01 ppm, assigned to the Sn–*H* unit, which is even further down-field than that for the comparable monomeric Sn(II) hydride complex, (^{Dipp}nacnac)SnH (δ = 13.83 ppm). Peaks relating to the ^{iPr}L† ligand shifted slightly relative to **26**. Despite the base-coordination in **27**, C_6D_6 solutions of the compound decomposed over the course of 24 h at ambient temperature, with pure crystalline samples also decomposing rapidly in the solid state. The solid state structure of **27** revealed it to be the first example of an acyclic monomeric Sn(II) hydride complex (Fig. 3.15). The structure is very similar to that of the Ge centred analogue, **21**, in that the Sn-centre is in a *pseudo*-tetrahedral geometry, formed by the hydride ligand, ^{iPr}L†, the coordinated DMAP molecule, and a lone-pair of electrons. The Sn1–N1

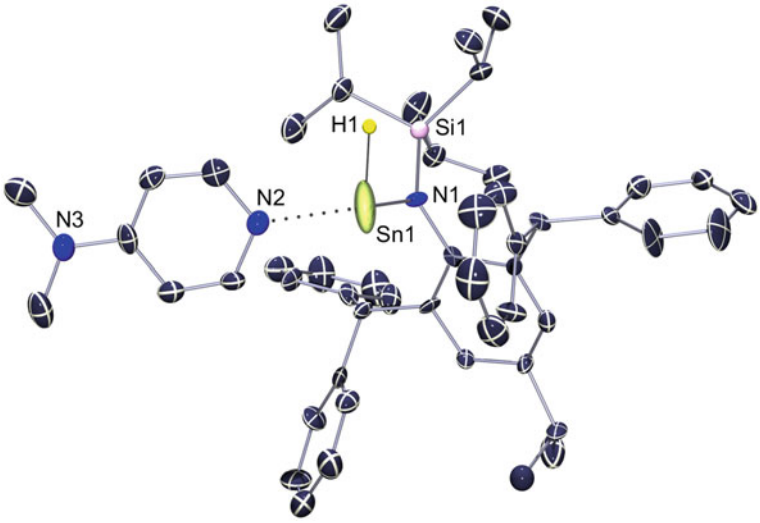

Fig. 3.15 ORTEP diagram of **27** (50% thermal ellipsoids; hydrogen atoms omitted aside from the terminal Sn-H ligand, H1). Relevant bond lengths (Å) and angles (°) for **27**: Sn1–N1 2.151(6), Sn1–N2 2.388(6), N1–Sn1–N2 106.08(2), N1–Sn1–H1 82.15(4), N2–Sn1–H1 100.22(4), C1–N1–Si1 123.68(3)

distance (2.151(6) Å) is in keeping with a covalent bond, with the longer Sn1–N2 bond (2.388(6) Å) being reminiscent of a dative interaction. As H1 could not be freely refined, bond lengths and angles related to it are inaccurate, and so shall not be discussed here.

Following the reactivity of **18** with H_2, its reactivity with CO_2 was ascertained as a comparison to that with $\{(^{TMS}L^*)Ge\}_2$, which formally reduces CO_2 with the release of CO gas, generating $\{(^{TMS}L^*)Ge\}_2O$ [35]. A deep green solution of **18** rapidly decolourises upon exposure to dry CO_2 at −80 °C, with no further colour change observed upon warming to ambient temperature. The ^1H NMR spectrum of the reaction mixture is consistent with the formation of a single product with two equally integrating ligand environments. X-ray structural analysis, although not to a publishable standard, ascertained the connectivity of the product, which, rather than a mono(oxo)-bridged species analogous to $\{(^{TMS}L^*)Ge\}_2O$, is a Sn(II) carbonate complex, $\{(^{iPr}L^\dagger)Sn(\mu\text{-}CO_3)Sn(^{iPr}L^\dagger)\}$ (**28**, Scheme 3.32). It is likely that in the reaction, an oxo-bridged bis(stannylene), $(^{iPr}L^\dagger)SnOSn(^{iPr}L^\dagger)$, is first formed, with the elimination of CO gas. The oxo-bridged species may then react with a further equivalent of CO_2, in an analogous fashion to previously reported uranium and magnesium species [39, 44]. This mechanism is a current point of study.

To further explore analogies between the reactivity of **18** and aryl-distannynes, the former was generated in situ and treated with two equivalents of the isocyanide, Bu^tNC:. Upon work-up, the adduct complex, **29**, was obtained in moderate isolated yield as dichroic orange/green crystals (Scheme 3.32). Unlike the corresponding

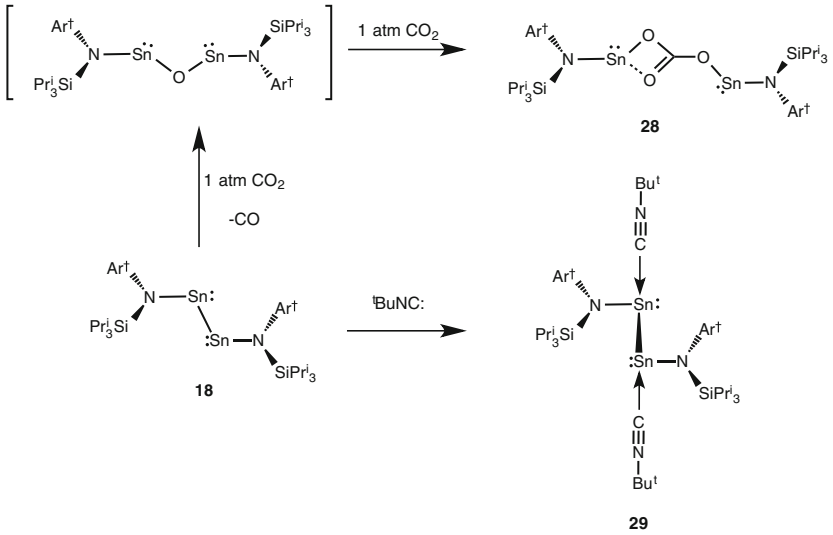

Scheme 3.32 The coordination of **18** with Bu^{t}NC:, and the reduction of CO_2 by **18**

aryl-distannyne complex, {(^{Dipp}Terph)(Bu^{t}NC:)Sn}$_2$, which fully dissociates to {(^{Dipp}Terph)Sn}$_2$ and Bu^{t}NC: in solution at 25 °C [59], compound **29** is stable in C_6D_6 solutions at room temperature (^{119}Sn{^{1}H} NMR: δ 241.8 ppm; cf. δ 181 ppm for {(^{Dipp}Terph)(Bu^{t}NC:)Sn}$_2$), and is returned when volatiles are removed from those solutions in vacuo.

This is perhaps surprising, as it might be thought that the isocyanide–Sn interactions in **29** would be weak, given the crowding around the tin centres of **18**, and the fact that the infrared spectrum of crystals of **29** exhibit a C≡N stretching mode at 2138 cm^{-1} (cf. 2162/2175 cm^{-1} for {(^{Dipp}Terph)(Bu^{t}NC:)Sn}$_2$) which is only slightly shifted relative to that for free Bu^{t}NC: (2134 cm^{-1}) [59]. It is also noteworthy that reaction of the related singly bonded digermyne, {(^{TMS}L*)Ge}$_2$, with Bu^{t}NC: did not give a stable adduct complex, but instead led to facile reductive coupling of two Bu^{t}NC: molecules [35], indicating that {(^{TMS}L*)Ge}$_2$ is notably more reducing than **18**.

The apparent weakness of the isocyanide–Sn interactions in **29** is borne out by its X-ray crystal structure (Fig. 3.16), which reveals NC: → Sn distances (2.325 (4) Å) that are longer than those in {(^{Dipp}Terph)(Bu^{t}NC:)Sn}$_2$ (2.301 Å mean) [59]. Moreover, the dative nature of those interactions is evidenced by the isocyanide CN bond lengths, 1.149(6) Å (cf. 1.159 Å mean in {(^{Dipp}Terph)(Bu^{t}NC:)Sn}$_2$), which are typical for triple bonds [106]. It is interesting to note that the Sn–Sn bond in **29** (3.0759(6) Å) is significantly shorter than that in **18**, presumably because the bond takes on more s-character (Σ angles at Sn1 = 287.4°) upon isocyanide coordination. This differs to coordination of {(^{Dipp}Terph)Sn}$_2$ by Bu^{t}NC:, which leads to a lengthening of its Sn–Sn bond by 0.374 Å, due to loss of multiple bond character for that bond. Somewhat related is the fact that any N–Sn multiple bond character in

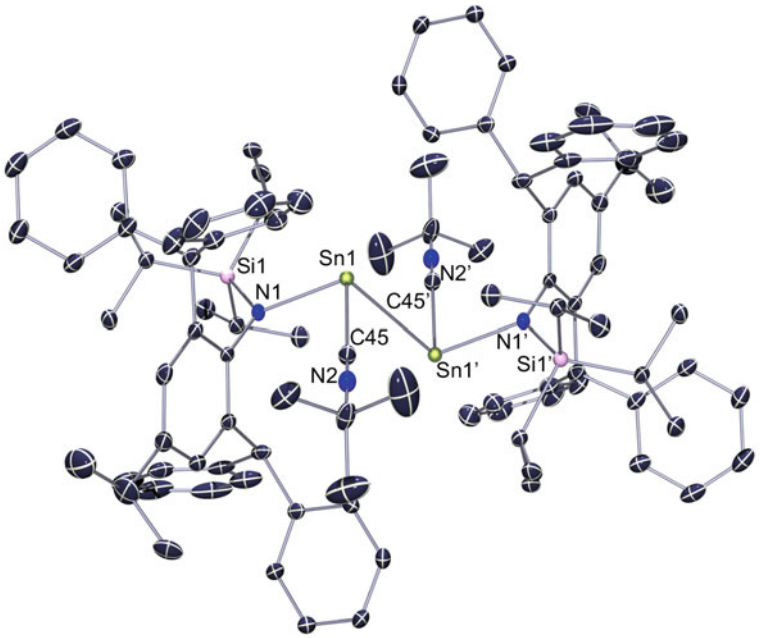

Fig. 3.16 Molecular structure of **29** (30% thermal ellipsoids; hydrogen atoms omitted). Selected bond lengths (Å) and angles (°): Sn1–N1 2.202(3), Sn1–C45 2.325(4), Sn1–Sn1′ 3.0759(6), N2–C45 1.149(6), N1–Sn1–Sn1′ 105.76(10), C45–Sn1–Sn1′ 92.23(12), N1–Sn1–C45 89.39(14)

18 (Sn–N 2.123 Å mean) must be lost upon isocyanide coordination, as the planar NSiC fragments of **29** (Sn–N 2.202(3) Å) are essentially orthogonal to the Sn_2N_2 plane in that compound.

Although not exhaustive, these reactivity studies highlight both differences and similarities between aryl-distannynes and the first amido-distannyne, as well as differences in the reactivities of the amido-distannyne and amido-digermynes. Further work will be carried out on the reactivity of the amido-distannyne, in regards to the activation of unsaturated molecules and other potentially interesting small-molecules.

3.3.5 Monomeric, 2-Coordinate Group 14 Element(II) Hydride Complexes

Given the postulated equilibria between the dimeric forms of the Ge(II) and Sn(II) hydride complexes, **19** and **26**, and their monomeric counterparts (($^{iPr}L^{\dagger}$)(H)Ge:) and (($^{iPr}L^{\dagger}$)(H)Sn:) in solution, we hypothesised that an increase in the steric encumbrance of the amide ligand may lead to the monomeric species being the lowest energy isomeric form of such systems, leading to the monomeric species

being maintained in the solid state. A survey of the literature revealed the extremely large silyl chloride, $(Bu^tO)_3SiCl$, to be easily accessed in one synthetic step from readily available starting materials, and hence we were able to subsequently access the extremely bulky secondary amines, $^{tBuO}L^*H$ and $^{tBuO}L^{\dagger}H$ ($^{tBuO}L^*H$ = Ar*N(H)Si(OBu^t)$_3$; $^{tBuO}L^{\dagger}H$ = Ar†N(H)Si(OBu^t)$_3$), which can be deprotonated with KH and catalytic amounts of $(SiMe_3)_2NH$ (see Chap. 2). With these ligands in hand, we sought a synthetic route to the target monomeric hydride complexes.

Our initial focus was on the reduction of the amido element(II) halide complexes, LEX (L = $^{tBuO}L^{\dagger}$ or $^{tBuO}L^*$; E = Ge, X = Cl; E = Sn, X = Br), which proved problematic, as reductions yielded intractable mixtures of products. Further, salt metathesis with standard hydride sources (i.e. $LiAlH_4$, $NaBH_4$) led to the formation of large amounts of protonated ligand, and complicated reactions mixtures. Our efforts then moved toward a σ-metathesis route. To this end, the LEOBu^t (L = $^{tBuO}L^*H$ or $^{tBuO}L^{\dagger}H$, E = Ge or Sn) species were synthesised by in situ reaction of the generated amido element(II) halide complexes with KOBu^t. Both the Ge(II) species, ($^{tBuO}L^*$)GeOBu^t (**30**) and ($^{tBuO}L^{\dagger}$)GeOBu^t (**31**), were isolated in good yields as white crystalline solids (Scheme 3.33). The solid state structure of **30** can be seen in Fig. 3.17, and reveals the amido-alkoxy germylene to be monomeric, for two likely reasons. Both the amide and alkoxy ligands can potentially donate to the empty *p*-orbital on germanium, weakening any potential intermolecular Ge–Ge interactions. In addition, the sheer bulk of the amide ligand, and to a lesser degree, the OBu^t ligand, prevents the approach of two monomers to form a dimer. The presence of a lone-pair of electrons at Ge1 is demonstrated by the N1–Ge1–O1 angle (97.24°). Other bond lengths and angles are in keeping with what one would expect. For the related Sn(II) systems, large amounts (>50%) of protonated ligand (e.g. $^{tBuO}L^{\dagger}H$) formed alongside one other product presumed to be the target tin *tert*-butoxide species. However, purification was not possible due to the high solubility of both species in hydrocarbon solvents.

Reaction of **30** and **31** with the borane, HBcat (cat = catecholato), resulted in the formation of pale yellow solutions, each of which contained one clean product, as determined by ^{1}H NMR spectroscopy, after 15 min at ambient temperature. These were proposed to be the target 2-coordinate germylenes (Scheme 3.33). Broad resonances at δ = 10.00 (**32**) and 10.02 (**33**) ppm suggested the presence of a Ge–*H* moiety in each case; these shifts are similar to those observed for **19** at high

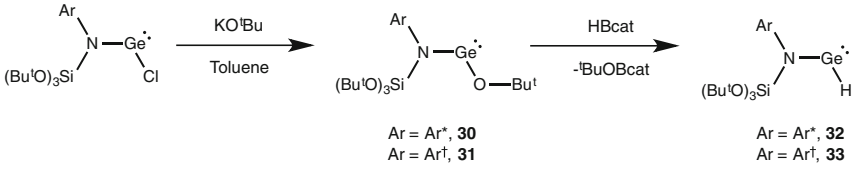

Scheme 3.33 Synthesis of germanium(II) alkoxides, **30** and **31**, and subsequent σ-metathesis with HBcat, to generate monomeric, 2-coordinate germanium(II) hydrides, **32** and **33**

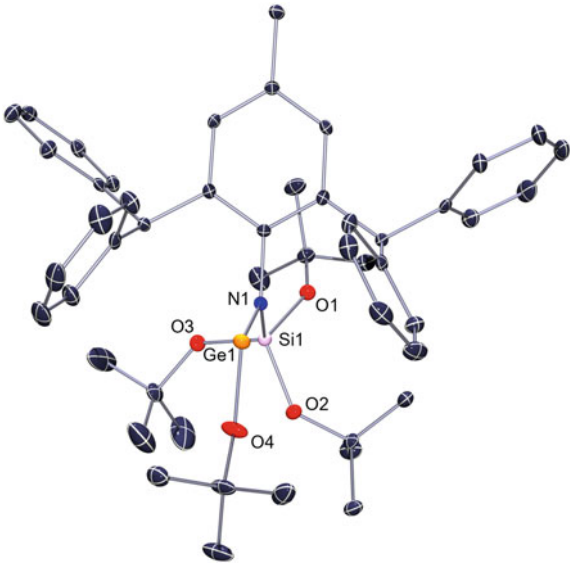

Fig. 3.17 ORTEP representation of **30** (30% thermal ellipsoids; hydrogen atoms omitted). Selected bond lengths (Å) and angles (°): Ge1–O4 1.796(2), Ge1–N1 1.877(2), O4–Ge1–N1 97.24 (9), C1–N1–Si1 117.02(16), C1–N1–Ge1 111.17(16), Si1–N1–Ge1 131.31(12)

temperature in d_8-toluene, where it is presumed the equilibrium lies in favour of the monomeric germylene, ($^{iPr}L^{\dagger}$)(H)Ge:.

A variable temperature ^{1}H NMR spectroscopic study of **33** (d_8-toluene) revealed its hydride resonance to shift from δ = 10.00 ppm to δ = 8.45 ppm over the temperature range, 20 to −50 °C. We do not believe that this indicates association of **33** to the digermene ($^{tBuO}L^{\dagger}$)(H)Ge = Ge(H)($^{tBuO}L^{\dagger}$) at low temperatures, as the solution remains pale yellow over the temperature range. This contrasts with the equilibrium mixture of **19** and ($^{iPr}L^{\dagger}$)(H)Ge: which is thermochromic, being deep orange at 20 °C, due to the presence of significant digermene in the solution, and essentially colourless at 100 °C, due to a high degree of digermene dissociation. Indeed a UV/Vis analysis of a toluene solution of related **32** showed no sign of an $n_- \rightarrow n_+$ transition, expected for a hydrido-digermene (cf. λ = 460 nm for **19**), suggesting the absence of a Ge=Ge bond.

The temperature dependence of the hydride resonance of **33** could possibly be due to transient intramolecular O → Ge coordination in solution, though there is no evidence of this in the crystal structure of the compound (vide infra). Consistent with this are the solid-state IR spectra of **32** and **33** which display Ge–H stretching bands at ν = 1887 cm^{-1} and 1923 cm^{-1} respectively. Although these lie in the normal range for higher coordinate germanium(II) hydrides [31], they are at considerably higher frequency than that for the closely related three-coordinate adduct complex, **21** (ν = 1812 cm^{-1}), as might be expected for two-coordinate species.

Both **32** and **33** were crystallographically characterised and found to be monomers in the solid state (Fig. 3.18). The hydride ligand of **33** was located from difference maps and freely refined, confirming the compound possesses a two-coordinate germanium centre. Interestingly, there are no O → Ge interactions

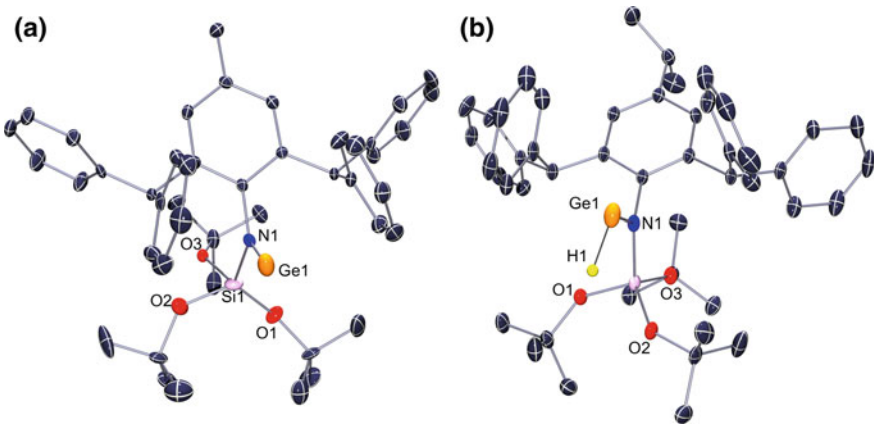

Fig. 3.18 ORTEP representation (30% probability surface) of **32** (*left*) and **33** (*right*) (hydrogen atoms omitted, aside from H1 in **33**). Selected bond lengths (Å) and angles (°) for **32**: Ge1–N1 1.877(4), N1–C1 1.427(6), Si1–N1 1.730(4), C1–N1–Si1 118.7(3), C1–N1–Ge1 119.9(3), Si1–N1–Ge1 120.5(2); **33**: Ge1–N1 1.886(3), Ge1–H1 1.45(1), N1–Ge1–H1 102(1), C1-N1–Si2 118.2 (2), C1–N1–Ge1 118.5(2), Si2–N1–Ge1 122.7(2)

in the compound, as is the case for **30**, and there are no contacts between the Ge centre and the flanking phenyl groups of the amide ligand that are less than 3.0 Å. The HGeNCSi fragment of the compound is close to planar which allows for the possibility of a N → Ge π-interaction (N–Ge 1.886(3) Å) in the compound. This, in addition to the considerable steric shielding of the Ge–H fragment, could help prevent its dimerisation. Given the angle at germanium (N–Ge–H 102(1)°), it can be concluded that there is a stereochemically active lone pair at that centre. It is worth noting that the structural characterisation of **32** and **33** represent the first for any two-coordinate, primary tetrylene, R(H)E:, E = C–Pb.

In order to shed light on the energies of dimerisation for the monomeric hydrido-germylenes, DFT calculations (M062X/cc-pVDZ) were carried out on the full molecule of **32**, and both its digermene, (^{tBuO}L*)(H)Ge = Ge(H)(^{tBuO}L*), and hydride bridged, (^{tBuO}L*)Ge(μ-H)$_2$Ge(^{tBuO}L*), associated forms (Table 3.2). The geometry of **32** in the gas phase optimised to be similar to that of the compound in the solid state, including the absence of any O → Ge interactions. Moreover, the dimerisation of the compound was found to be endergonic by 3.1 kcal mol^{-1} with respect to (^{tBuO}L*)(H)Ge = Ge(H)(^{tBuO}L*), and 16.5 kcal mol^{-1} with respect to

Table 3.2 Gibbs free energies of dimerisation (in kcal mol^{-1}) calculated at the M062X/cc-pVTZ and HF/cc-pVTZ levels of theory

Dimers	ΔG(M062X)	ΔG(HF)
^{tBuO}L*(H)Ge=Ge(H)^{tBuO}L*	3.1	44.2
L°(H)Ge=Ge(H)L°	−8.3	31.6
^{tBuO}L*Ge(μ-H)2Ge^{tBuO}L*	16.5	64.1

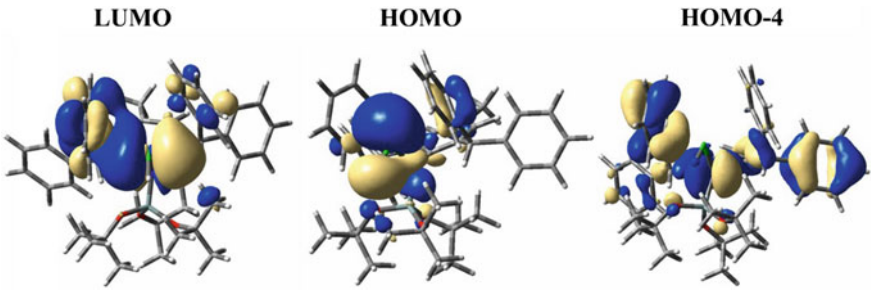

Fig. 3.19 LUMO, HOMO, and HOMO-4 of the optimised structure of **32**. Reproduced from *Chem. Commun.*, **2015**, *51*, 6854, with permission from The Royal Society of Chemistry

(^{tBuO}L*)Ge(μ-H)$_2$Ge(^{tBuO}L*). These results are consistent with the steric bulk of the amide ligands of both **32** and **33** preventing their dimerisation in the solid state. For sake of comparison, calculations were also carried out (at the same level of theory) on a slightly modified form of the less bulky hydrido-germylene, (^{iPr}L†)(H)Ge:, viz. :Ge(H)(L°), and its dimer, (L°)(H)Ge=Ge(H)(L°) (L° = $^{-}$N(Ar*)(SiPr$^{i}_3$). These revealed that the dimerisation of (L°)(H)Ge: to the corresponding digermene is exergonic by 8.3 kcal mol^{-1}, a result which is in line with the experimentally observed dimerisation of (^{iPr}L†)(H)Ge: in the solid state. The electronic structure of **32** is similar to that reported for related germylenes, in that the Ge lone pair of the compound is associated the HOMO, whilst the LUMO exhibits considerable Ge *p*-orbital character (Fig. 3.19). In addition, the N *p*-orbital lone pair (HOMO-4) appears to be engaged in a small degree of N → Ge π-bonding, which is likely partly responsible for the resistance of the compound towards dimerisation, as mentioned above.

3.4 Conclusion

We have utilised a number of new ligands in the synthesis of a variety of novel low-oxidation state species of tin and germnaium. These include the first example of an amido-distannyne, the first example of a 1,2-hydridodigermene that dissociates to monomeric species in solution, and the first examples of 2-coordinate germanium(II) hydrides. These discoveries have been realised through utilisation of novel super-bulky monodentate amide ligands, which show diverse electronic and steric properties.

Further, we have studied the reactivity of a novel digermyne towards a variety of unsaturated small-molecules, highlighting reactivities previously unknown for Ge (I) species. These include the reversible cycloaddition to, and clean transfer-hydrogenation of a digermyne, both of which bring further comparisons between this earth-abundant element and the transition metals.

These results, along side in-depth computational analyses of these systems, have led us to a greater understanding of the electronic characteristics of such species. This in turn aids us in the design of systems that may be employed in further stimulating reactivity studies, such as reversible chemistries and catalysis. This work highlights the importance of ligand design in studying the fine details of chemical behaviour in organometallic synthesis.

3.5 Experimental

{(^{iPr}L†)Ge}$_2$ (14) A solution of {(^{Mes}Nacnac)Mg}$_2$ (488 mg, 0.70 mmol) in toluene (10 mL) was added to a solution of (^{iPr}L†)GeCl (1.0 g, 1.4 mmol) in toluene (60 mL) at −80 °C. The reaction mixture was warmed to 20 °C over 5 h. It was then filtered and volatiles removed from the filtrate in vacuo. The solid residue was washed with cold hexane (10 mL) to afford and orange/brown powder. This was recrystallised from the minimum volume of hot hexane to yield {(^{iPr}L†)Ge}$_2$ as a dark brown/orange crystalline solid (765 mg, 77%). M.p. 128–132 °C; ^{1}H NMR (C_6D_6, 500 MHz, 298 K): δ = 0.96 (d, $^3J_{HH}$ = 6.8 Hz, 6H, Ar†-*p*-CH(C*H*$_3$)$_2$), 1.08 (br d, 18H, SiPr$^i_3$-CH(C*H*$_3$)$_2$), 1.50 (br sept, 3H, SiPr$^i_3$-C*H*(CH$_3$)$_2$), 2.51 (sept, $^3J_{HH}$ = 6.8 Hz, 1H, Ar†-*p*-C*H*(CH$_3$)$_2$), 6.23 (s, 2H, C*H*Ph$_2$), 6.96–7.49 (m, 22H, Ar-*H*); ^{13}C{^{1}H} NMR (C_6D_6, 75.5 MHz): δ = 19.1 (SiPr$^i_3$-*C*H(CH$_3$)$_2$), 19.7 (SiPr$^i_3$-CH(*C*H$_3$)$_{2-}$), 24.0 (Ar†-*p*-CH(*C*H$_3$)$_2$), 33.5 (Ar†-*p*-*C*H(CH$_3$)$_2$), 51.6 (*C*HPh$_2$), 126.7, 126.8, 129.3, 130.5, 130.7, 140.6, 143.9, 145.0, 146.5, 148.4 (Ar-*C*); ^{29}Si{^{1}H} NMR (C_6D_6, 80 MHz, 298 K): δ = 9.4; UV/Vis (toluene), λ_{max}, nm (ε, Lcm^{-1}mol^{-1}): 472 (650), 399 (3920); IR, ν/cm^{-1} (ATR): 3060(w), 3025(w), 1599(w), 1378(m), 1198(m), 877(m), 797(s), 723(s), 664(s); MS/EI + , *m/z* (%): 624.3 (^{iPr}L$^{\dagger+}$, 32), 580.3 (^{iPr}L†-Pr^{i+}, 62), 467.2 (^{iPr}L†-SiPr$^i_3{}^+$, 100), 167.0 (Ph$_2$C$^+$, 66); anal. calc. for $C_{88}H_{104}Ge_2N_2Si_2$: C, 75.97%; H, 7.54%; N, 2.01%; found: C, 75.92%; H, 7.43%; N, 2.13%.

{(^{iPr}L$^{\partial}$)Ge}$_2$ (15) This compound was synthesised in an equivalent procedure to that for **14**, but using (^{iPr}L$^{\partial}$)GeCl (500 mg, 0.68 mmol) and {(^{Mes}nacnac)Mg}$_2$ (244 mg, 0.34 mmol). The product was isolated by storing a concentrated Et$_2$O solution at 4 °C for 2 days, as a turquoise powder (350 mg, 74%). X-ray quality crystals were formed upon refluxing of a hexane solution of **15**, followed by slow cooling to ambient temperature. M.p. 145–152 °C; ^{1}H NMR (C_6D_6, 400 MHz, 298 K): δ = 0.90 (br, 3H, SiPr$^i_3$-C*H*(CH$_3$)$_2$), 1.03 (d, $^3J_{HH}$ = 6.8 Hz, 6H, Ar$^{\partial}$-*p*-CH(C*H*$_3$)$_2$), 1.20–1.30 (br m, 18H, SiPr$^i_3$-CH(C*H*$_3$)$_2$), 2.05 (s, 12H, Xyl-*m*-C*H*$_3$), 2.23 (s, 12H, Ar$^{\partial}$-*m*-C*H*$_3$), 2.59 (sept, $^3J_{HH}$ = 6.8 Hz, 1H, Ar$^{\partial}$-*p*-C*H*(CH$_3$)$_2$), 6.22 (s, 2H, C*H*Ph$_2$), 6.74 (s, 2H, Xyl-*p*-C*H*), 6.80 (s, 2H, Xyl-*p*-C*H*), 7.05 (s, 4H, Xyl-*o*-C*H*), 7.25 (s, 4H, Xyl-*o*-C*H*), 7.35 (s, 2H, Ar$^{\partial}$-*m*-C*H*); ^{13}C{^{1}H} NMR (C_6D_6, 75.5 MHz): δ = 17.3 (SiPr$^i_3$-*C*H(CH$_3$)$_2$), 19.6 (SiPr$^i_3$-CH(*C*H$_3$)$_2$), 21.6 (Xyl-*m*-*C*H$_3$), 24.0 (Ar$^{\partial}$-*p*-CH(*C*H$_3$)$_2$), 33.7 (Ar$^{\partial}$-*p*-*C*H(CH$_3$)$_2$), 51.4 (*C*HPh$_2$), 128.0,

128.2, 128.4, 129.0, 129.1, 129.5, 137.4, 137.5, 140.2, 143.5, 144.2, 147.0 (Ar-*C*); $^{29}Si\{^1H\}$ NMR (C_6D_6, 80 MHz, 298 K): δ = 8.8; IR, ν/cm^{-1} (ATR): 1890 (w), 1594 (s), 1376 (m), 1280 (w), 1197 (m), 1114 (m), 1036 (w), 983 (w), 849 (s), 809 (s), 767 (m), 657 (s).

{(^{iPr}L†)Sn}$_2$ (18) (^{iPr}L†)SnBr (1.00 g, 1.22 mmol) was dissolved in a toluene/diethyl ether mix (5 mL/20 mL), and the solution cooled to −80 °C. To this was added a solution of {(^{Mes}Nacnac)Mg}$_2$ (435 mg, 0.61 mmol) in diethyl ether (20 mL). The reaction mixture was slowly warmed to −20 °C during which time it took on a deep green colour. Volatiles were removed from the mixture in vacuo at −20 °C, and the residue was then extracted into pre-cooled (−20 °C) hexane (20 mL), before the extract was filtered. The deep green filtrate was concentrated in vacuo and stored at −30 °C for 24 h to afford large orange/green crystals of {(^{iPr}L†)Sn}$_2$ (410 mg, 45%). N.B. Crystals of the compound suitable for the X-ray diffraction experiment were grown from a toluene/hexane solution. M.p.: 96–100 °C (melt and decomp.); ^1H NMR (C_6D_6, 400 MHz, 298 K), δ = 1.01 (d, $^3J_{HH}$ = 6.8 Hz, 6H, Ar†-*p*-CH(C*H*$_3$)$_2$), 1.22 (d, $^3J_{HH}$ = 6.8 Hz, 18H, CH(C*H*$_3$)$_2$), 1.42 (sept, $^3J_{HH}$ = 6.8 Hz, 3H, C*H*(CH$_3$)$_2$), 2.59 (sept, $^3J_{HH}$ = 6.8 Hz, 1H, Ar†-*p*-C*H*(CH$_3$)$_2$), 6.40 (s, 2H, Ph$_2$C*H*), 6.97 (m, 2H, Ar†-*m*-C*H*), 7.00–7.48 (m, 20H, Ar-*H*); $^{13}C\{^1H\}$ NMR (C_6D_6, 75.5 MHz, 298 K), δ = 17.3 (SiPr$^i_3$-*C*H(CH$_3$)$_2$), 20.0 (SiPr$^i_3$-CH(*C*H$_3$)$_2$), 24.3 (Ar†-*p*-CH(*C*H$_3$)$_2$), 33.5 (Ar†-*p*-*C*H(CH$_3$)$_2$), 51.9 (Ph$_2$*C*H), 126.6, 127.1, 128.5, 128.7, 129.3, 130.1, 130.4, 140.9, 142.4, 144.9, 146.5, 152.5 (Ar-*C*); $^{29}Si\{^1H\}$ NMR (C_6D_6, 80 MHz, 298 K), δ = 6.00; $^{119}Sn\{^1H\}$ NMR (C_6D_6, 149.2 MHz, 298 K): no signal observed; UV/Vis, λ_{max}, nm (ε, Lcm^{-1}mol^{-1}): 409 (6500); IR, ν/cm^{-1} (ATR): 3058 (w), 3025 (w), 1943 (w), 1870 (w), 1802 (w), 1599 (w), 1388 (m), 1365 (m), 1223 (m), 1116 (w), 1074 (w), 1031 (w), 881 (m), 759 (s), 657 (s); anal. calc. for $C_{88}H_{104}Sn_2N_2Si_2$: C, 71.25%; H, 7.07%; N, 1.89%; found: C, 71.18%; H, 7.17%; N, 1.88%.

{(^{iPr}L†)GeH}$_2$ (19). Route (a) A solution of **14** (700 mg, 0.50 mmol) in toluene (40 mL) was vigorously stirred under an atmosphere of ultra-high purity H_2 for 1 h. A colour change from orange-brown to bright orange was seen to occur in the initial stages of the experiment. Volatiles were subsequently removed in vacuo, and the solid residue washed with a small volume of hexane. The remaining solid was dried under vacuum to yield analytically pure **19**. X-ray quality orange crystals of the compound were grown at 4 °C by recrystallization from a minimum volume of hexane (536 mg, 77%). N.B. following the reaction by ^1H NMR spectroscopy showed the reaction to be essentially quantitative after 20 min.

Route (b) A solution of L-Selectride (1.37 mL, 1 M solution, 1.37 mmol) was added to a solution of (^{iPr}L†)GeCl (1.0 g, 1.37 mmol) in toluene (50 mL) at −80 °C. The reaction mixture was warmed to 20 °C over 4 h. It was subsequently filtered, and the filtrate concentrated. Hexane was added to the solution to the point of incipient crystallization. Placement of the resulting solution at 4 °C yielded {(^{iPr}L†)GeH}$_2$ as an orange crystalline material (496 mg, 52%).

Route (c) To a mixture of (^{iPr}L†)GeCl (1 g, 1.37 mmol) and $LiAlH_4$ (70 mg, 1.78 mmol) in a Schlenk flask was added toluene (30 mL) at ambient temperature. The suspension was stirred at this temperature for 4 days, over which time it became bright orange. The reaction was subsequently filtered, all solvents removed from the filtrate, and hexane (5 mL) added. The extract was left at ambient temperature overnight, yielding large orange crystals of {(^{iPr}L†)GeH}$_2$ (380 mg, 40%). M.p. 186–188 °C (dec.); ^{1}H NMR (C_6D_6, 500 MHz, 298 K): δ = 0.97 (d, $^3J_{HH}$ = 6.8 Hz, 6H, Ar†-*p*-CH(C*H*$_3$)$_2$), 1.17 (br. d, $^3J_{HH}$ ≈ 8 Hz, 18H, SiPr$^i_3$-CH(C*H*$_3$)$_2$), 1.51 (sept, $^3J_{HH}$ = 7.6 Hz, 3H, SiPr$^i_3$-C*H*(CH$_3$)$_2$), 2.49 (sept, $^3J_{HH}$ = 6.8 Hz, 1H, Ar†-*p*-C*H*(CH$_3$)$_2$), 6.26 (s, 2H, C*H*Ph$_2$), 6.99–7.42 (m, 22H, Ar-*H*), 8.21 (br s, 1H, Ge-*H*); ^{13}C{^{1}H} NMR (C_6D_6, 75.5 MHz, 298 K): δ = 15.2 (SiPr$^i_3$-*C*H(CH$_3$)$_2$), 19.7 (SiPr$^i_3$-CH(*C*H$_3$)$_2$), 24.0 (Ar†-*p*-CH(*C*H$_3$)$_2$), 33.64 (Ar†-*p*-*C*H(CH$_3$)$_2$), 54.9 (*C*HPh$_2$), 126.6, 127.1, 128.5, 128.8, 130.1, 130.2, 140.6, 144.5, 145.0, 146.0 (Ar-*C*); ^{29}Si{^{1}H} NMR (C_6D_6, 80 MHz, 298 K): δ = 9.48; UV/Vis (toluene, 298 K), λ_{max}, nm (ε, L cm^{-1} mol^{-1}): 458 (650), 385 (1260); IR, ν/cm^{-1} (ATR): 3057(w), 3022(w), 2947(m), 1961(s, Ge-H), 1492(m), 1198(w), 1119(w), 895(m), 827(m), 700(s); MS/EI *m/z* (%): 623 (^{iPr}L$^{\dagger+}$, 48), 580 (^{iPr}L$^{\dagger+}$-Pr^i, 100); anal. calc. for $C_{88}H_{106}Ge_2N_2Si_2$: C, 75.86%; H, 7.67%; N, 2.01%. Found: C, 75.67%; H, 7.50%; N, 1.93%.

{(^{iPr}L†)GeD}$_2$ This compound was synthesised by an equivalent procedure (route a) to that which generated {(^{iPr}L†)GeH}$_2$, but using D_2 in place of H_2. ^{1}H NMR (C_6D_6, 500 MHz, 298 K): identical to that of **19**, with the exception of the broad Ge-*H* resonance at δ = 8.21 ppm, which is absent; ^{2}H NMR (C_6D_6, 61.4 MHz, 298 K): δ = 8.32; IR, ν/cm^{-1} (ATR): identical to that of {(^{iPr}L†)GeH}$_2$, with the exception that the Ge-H stretching band centred at ν = 1961 cm^{-1} is absent, and a Ge-D stretching band centered at ν = 1377 cm^{-1} is present.

N.B. when C_6D_6 solutions of {(^{iPr}L†)GeD}$_2$ at 20 °C are placed under an atmosphere of excess H_2, the hydride resonance for {(^{iPr}L†)GeH}$_2$ slowly grows into the ^{1}H NMR spectrum of the compound. After approximately 7 days, the apparent H/D exchange reaction is essentially complete.

[{(^{iPr}L†)Ge(H)$_2$Al(H)$_2$}$_2$LiH.OEt$_2$]$_2$ (20) To a solution of (^{iPr}L†)GeCl (0.5 g, 0.68 mmol) in toluene (20 mL) at −80 °C was added a solution of $LiAlH_4$ (30 mg, 0.80 mmol) in Et_2O (10 mL), dropwise. An initial colour change to pale orange was seen, which reverted to colourless after 5 min. The reaction mixture was allowed to warm to ambient temperature over the course of 2 h, after which time all volatiles were removed in vacuo, and the residue extracted in hexane (30 mL). The extract was filtered, and the filtrate stored at ambient temperature overnight, after which time large colourless blocks of [{(^{iPr}L†)Ge(H)$_2$Al(H)$_2$}$_2$LiH.OEt$_2$]$_2$ had formed (120 mg, 23%). M.p.: 156–162 °C (decomp.); ^{1}H NMR (C_6D_6, 400 MHz, 298 K): δ = 0.63 (br t, $^3J_{HH}$ = 6 Hz, 6H, Li-O(CH$_2$C*H*$_3$)), 1.02 (overlapping d, $^3J_{HH}$ = 6.8 Hz, 12H, Ar†-*p*-CH(C*H*$_3$)$_2$), 1.20 (overlapping br d, $^3J_{HH}$ = 6.8 Hz, 36H, SiPr$^i_3$-CH(C*H*$_3$)$_2$), 1.40 (br sept, $^3J_{HH}$ = 6.8 Hz, 6H, SiPr$^i_3$-C*H*(CH$_3$)$_2$), 2.57 (sept, $^3J_{HH}$ = 6.8 Hz, 2H, Ar†-*p*-CH(C*H*$_3$)$_2$), 2.96 (br, 4H, Li-O(C*H*$_2$CH$_3$)), 5.21

(br s, 2H, Al-*H*), 5.46 (br s, 2H, Al-*H*), 6.76 (s, 4H, Ph_2CH), 7.09 (m, 4H, Ge-*H*), 6.83–7.61 (m, 40H, Ar-*H*); $^{13}C\{^1H\}$ NMR (C_6D_6, 75.5 MHz): δ = 14.1 and 15.5 ($SiPr^i_3$-*C*H(CH_3)$_2$), 19.9 and 20.0 ($SiPr^i_3$-CH(*C*H_3)$_2$), 23.1 (Li-O(CH_2*C*H_3)$_2$), 24.0 ($Ar^†$-*p*-CH(*C*H_3)$_2$), 32.0 (Li-O(*C*H_2CH$_3$)$_2$), 33.5 (br, $Ar^†$-*p*-*C*H(CH_3)$_2$), 51.2 and 51.4 (*C*HPh_2), 125.7, 125.9, 126.3, 126.5, 129.9, 130.1, 130.5, 131.1, 131.2, 141.8, 142.0, 144.9, 145.6, 149.3 (Ar-*C*); $^{29}Si\{^1H\}$ NMR (C_6D_6, 80 MHz, 298 K): δ = 6.3; IR, ν/cm^{-1} (ATR): 3060 (w), 3025 (w), 2055 (w, LiH), 2008 and 1947 (m, GeH), 1802 (v br, s, AlH), 1599 (m), 1222 (m), 1120 (m) 1063 (m), 1032 (m), 987 (m), 916 (s), 876 (s), 817 (m), 744 (s), 661 (s); MS/EI + , *m/z* (%): 623.7 (15%, $^{iPr}L^{†+}$), 167.2 (100%, Ph_2C^+).

N.B. the Li-*H* resonance could not be observed in the ^1H NMR spectrum. After four attempts only elemental analyses with low C values couple be obtained.

($^{iPr}L^†$)(H)Ge.(DMAP) (21) DMAP (53 mg, 0.42 mmol) was added to a solution of {($^{iPr}L^†$)GeH}$_2$ (200 mg, 0.14 mmol) in toluene (30 mL) at 20 °C, and the reaction mixture stirred for 3 h. Volatiles were subsequently removed in vacuo and the residue was extracted with hexane and filtered. The bright orange filtrate was placed at 3 °C overnight, yielding ($^{iPr}L^†$)(H)Ge.(DMAP) as a pale yellow crystalline solid (64 mg, 27%). M.p. 130–132 °C (dec.); ^1H NMR (C_6D_6, 400 MHz, 298 K): δ = 1.01 (d, $^3J_{HH}$ = 6.8 Hz, 6H, $Ar^†$-*p*-CH(C*H*$_3$)$_2$), 1.21 (d, $^3J_{HH}$ = 7.6 Hz, 18H, $SiPr^i_3$-CH(C*H*$_3$)$_2$), 1.59 (br. sept, $^3J_{HH}$ ≈ 7 Hz, 3H, $SiPr^i_3$-C*H*(CH_3)$_2$), 2.12 (s, 6H, DMAP-N(C*H*$_3$)$_2$), 2.57 (sept, $^3J_{HH}$ = 6.8 Hz, 1H, $Ar^†$-*p*-C*H*(CH_3)$_2$), 5.96 (d, 2H, DMAP-*m*-Ar-*H*), 6.43 (s, 2H, C*H*Ph_2), 6.98–7.47 (m, 22H, Ar-*H*), 8.42 (d, 2H, DMAP-*o*-Ar-*H*), 9.04 (br s, 1H, Ge-*H*); $^{13}C\{^1H\}$ NMR (C_6D_6, 75.5 MHz, 298 K): δ = 15.3 ($SiPr^i_3$-*C*H(CH_3)$_2$), 19.9 ($SiPr^i_3$-CH(*C*H_3)$_2$), 24.2 ($Ar^†$-*p*-CH(*C*H_3)$_2$), 33.6 ($Ar^†$-*p*-*C*H(CH_3)$_2$), 38.2 (DMAP-N(*C*H_3)$_2$), 51.7 (*C*HPh_2), 106.7 (DMAP-*o*-*C*H), 126.4, 126.5, 126.6, 130.1, 130.6 (Ar-*C*), 130.7 (DMAP-*m*-*C*H), 141.1, 144.9 (Ar-*C*), 145.0 (DMAP-Me_2N*C*), 147.2, 150.3, 154.3 (Ar-*C*); $^{29}Si\{^1H\}$ NMR (C_6D_6, 80 MHz, 298 K): δ = 6.11; IR, ν/cm^{-1} (ATR): 3095 (w), 1812(m, Ge-H), 1598(m), 1493(m), 1065(w), 1010(m), 916(m), 881(m), 804(s), 758(s); MS/EI *m/z* (%): 692.2 (M^+-DMAP, 5), 654.2 (M^+-DMAP-Pr^i, 13), 624 ($^{iPr}L^{†+}$, 26), 121.3 (DMAP$^+$, 100); anal. calc. for $C_{51}H_{63}N_3Si_1Ge_1$: C, 74.81%; H, 7.76%; N, 5.13%; found: C, 74.64%; H, 7.82%; N, 5.01%.

($^{iPr}L^†$)Ge(μ-C_2H_4)$_2$Ge($^{iPr}L^†$) (22) A solution of {($^{iPr}L^†$)Ge}$_2$ (0.1 g, 0.07 mmol) in toluene (25 mL) was placed under an atmosphere of high purity ethylene gas in a Schlenk tube, which was subsequently sealed. The mixture was stirred at room temperature for 2 h, whereupon all volatiles were removed in vacuo, and the solid residue washed with hexane to give ($^{iPr}L^†$)Ge(μ-C_2H_4)$_2$Ge($^{iPr}L^†$) as a pale yellow solid. X-ray quality crystals of the compound were grown from a concentrated hexane solution, held at −30 °C for 1 week (30 mg, 29%). M.p.: 109–122 °C; ^1H NMR (C_6D_6, 400 MHz, 298 K), δ = −0.63 (br, 8H, Ge(C_2H_4)$_2$Ge), 1.15 (d, $^3J_{HH}$ = 7.0 Hz, 12H, $Ar^†$-*p*-CH(C*H*$_3$)$_2$), 1.23 (d, $^3J_{HH-}$ = 7.2 Hz, 36H, $SiPr^i_3$-CH(C*H*$_3$)$_2$), 1.61 (sept, $^3J_{HH-}$ = 7.2 Hz, 6H, $SiPr^i_3$-C*H*(CH_3)$_2$), 2.74 (sept, $^3J_{HH-}$ = 7.0 Hz, 2H, $Ar^†$-*p*-C*H*(CH_3)$_2$), 6.08 (s, 4H, C*H*Ph_2), 6.88–7.50 (m, 44H, Ar-

H); $^{13}C\{^1H\}$ NMR (C_6D_6, 75.5 MHz, 298 K), δ = 14.4 (br, Ge(C_2H_4)$_2$Ge), 14.9 (SiPr$^i_3$-CH(CH_3)$_2$), 19.1 (br, SiPr$^i_3$-$CH(CH_3)_2$), 23.9 (Ar†-*p*-CH(CH_3)$_2$)), 33.4 (Ar†-*p*-$CH(CH_3)_2$)), 51.6 ($CHPh_2$), 125.7, 126.5, 126.6, 128.4, 128.5, 129.3, 130.6, 131.0, 142.3, 142.9, 145.0, 146.3 (Ar-*C*); $^{29}Si\{^1H\}$ NMR (C_6D_6, 80 MHz, 298 K), δ = 9.28; IR, ν/cm^{-1} (ATR): 3060 (w), 3025 (bw), 1599 (w), 1378 (m), 1259 (m), 1200 (m), 1117 (w), 1031 (w), 881 (m), 807 (m), 732 (m), 662 (s); MS/EI *m/z* (%): 695.6 ((^{iPr}L†)Ge$^+$, 3), 623.6 (^{iPr}L$^{\dagger+}$, 23), 580.5 (^{iPr}L†-Pr^{i+}, 66), 167.1 (Ph_2C^+, 100). N.B. A reproducible microanalysis could not be obtained, as samples contained variable amounts of hexane of crystallization which could not be completely removed by placing the sample under reduced pressure for several hours.

(^{iPr}L†)Ge{μ-HC=C(Me)}Ge(^{iPr}L†) (23) A solution of {(^{iPr}L†)Ge}$_2$ (150 mg, 0.11 mmol) in toluene (25 mL) was cooled to −40 °C and the head space of the reaction flask purged with an excess of propyne, and then sealed. The reaction mixture was warmed to room temperature and stirred for 2 h. All volatiles were subsequently removed in vacuo, the residue extracted into hexane (20 mL), and filtered. Concentration of the filtrate to 10 mL and storage at 4 °C for 1 week yielded deep orange/red plates of (^{iPr}L†)Ge{μ-HC=C(Me)}Ge(^{iPr}L†) (65 mg, 42%). M.p.: 211–225 °C (decomp.); ^1H NMR (C_6D_6, 400 MHz, 298 K), δ = 1.02 (2 × coincidental d, $^3J_{HH}$ = 7.2 Hz, 12H, Ar†-*p*-CH(CH_3)$_2$), 1.10 (br, 36H, SiPr$^i_3$-CH(CH_3)$_2$), 1.24 (br s, 3H, GeCHC(CH_3)Ge), 1.45 (br sept, $^3J_{HH}$ ≈ 7 Hz, 6H, SiPr$^i_3$-C*H*(CH_3)$_2$), 2.60 (br sept, $^3J_{HH}$ ≈ 7 Hz, 2H, Ar†-*p*-C*H*(CH_3)$_2$), 6.21 (br s, 2H, C*H*Ph$_2$), 6.40 (br s, 2H, C*H*Ph$_2$), 7.04–7.42 (m, 44H, Ar-C*H*), GeC*H* obscured by aromatic region; $^{13}C\{^1H\}$ NMR (C_6D_6, 75.5 MHz, 298 K), δ = 14.3 (SiPr$^i_3$-*C*H(CH_3)$_2$), 14.7 (br, SiPr$^i_3$-*C*H(CH_3)$_2$), 19.3 (br, SiPr$^i_3$-CH(*C*H_3)$_2$), 19.7 (br, SiPr$^i_3$-CH(*C*H_3)$_2$), 23.9 (br, Ar†-*p*-CH(*C*H_3)$_2$), 33.6 (br, GeC*C*H_3), 33.7 (br, Ar†-*p*-*C*H(CH_3)$_2$), 51.7, 52.0 (*C*HPh$_2$), 126.7, 127.3 (Ge*C*H and Ge*C*CH$_3$), 126.5, 126.6, 128.3, 129.3, 129.7, 130.1, 130.2, 130.3, 130.4, 130.7, 130.8, 143.4, 144.7, 145.0, 146.5, 146.7, 147.4, 147.5 (all br, Ar-*C*); $^{29}Si\{^1H\}$ NMR (C_6D_6, 80 MHz, 298 K): signal too broad to be observed; IR, ν/cm^{-1} (ATR): 3058 (w), 3024 (w), 2100 (b), 1943 (w), 1877 (w), 1598 (m), 1381 (w), 1363 (w), 1244 (w), 1196 (w), 1116 (m), 1031 (m), 878 (s), 841 (m), 804 (m), 758 (s), 727 (s); MS/EI *m/z* (%): 737.5 (M-^{iPr}L†Ge$^+$, 1), 695.6 (^{iPr}L†Ge$^+$, 2), 623.6 (^{iPr}L$^{\dagger+}$, 16), 580.5 (^{iPr}L†-Pr^{i+}, 43), 167.1 (Ph_2C^+, 100); anal. calc. for $C_{91}H_{108}Ge_2N_2Si_2$: C 76.36%, H 7.61%, N 1.96%; found: C 76.23%, H 7.78%, N 1.98%.

(^{iPr}L†)Ge(μ-C_6H_8)Ge(^{iPr}L†) (24) To a solution of {(^{iPr}L†)Ge}$_2$ (150 mg, 0.11 mmol) in toluene (20 mL) at room temperature was added 1,3-cyclohexadiene (15 μL, 0.16 mmol). The reaction mixture was stirred for 2 h, after which time all volatiles are removed in vacuo, and the residue extracted into hexane (30 mL). Filtration of the extract, concentration of the filtrate to 15 mL, and storage at 4 °C for 3 days yields large orange/red dichroic crystals of (^{iPr}L†)Ge(μ-C_6H_8)Ge(^{iPr}L†) (45 mg, 28%). M.p.: 160–171 °C (decomp.); ^1H NMR (C_6D_6, 400 MHz, 298 K) δ = 1.01 (d overlapping m, $^3J_{HH}$ = 7.2 Hz, 12H, Ar†-*p*-CH(CH_3)$_2$; and 2H, GeC*H*), 1.23 (virtual t, $^3J_{HH}$ = 7.2 Hz, 36H, SiPr$^i_3$-CH(CH_3)$_2$), 1.63 (sept, $^3J_{HH}$ = 7.2 Hz,

6H, SiPr$^{i}_{3}$-C*H*(CH$_3$)$_2$), 2.48 (br m, 4H, GeCHC*H*$_2$), 2.56 (sept, $^{3}J_{HH}$ = 7.2 Hz, 2H, Ar†-*p*-CH(C*H*$_3$)$_2$), 4.89 (br s, 2H, GeCHC*H*), 6.23 (s, 2H, C*H*Ph$_2$), 6.34 (s, 2H, C*H*Ph$_2$), 6.95–7.42 (m, 44H, Ar-C*H*); ^{13}C{^{1}H} NMR (C$_6$D$_6$, 75.5 MHz, 298 K), δ = 15.3 (SiPr$^{i}_{3}$-*C*H(CH$_3$)$_2$), 19.9 (SiPr$^{i}_{3}$-CH(*C*H$_3$)$_2$), 24.0 (Ar†-*p*-CH(*C*H$_3$)$_2$), 21.3 (br, Ge*C*H), 33.6 (Ar†-*p*-*C*H(CH$_3$)$_2$), 51.6 (*C*HPh$_2$), 51.8 (CHD-*C*H$_2$), 125.6 (CHD-*C*H), 126.3, 129.4, 130.0, 130.2, 130.3, 130.7, 131.4, 142.9, 145.3, 145.4, 145.7, 148.0 (Ar-*C*); ^{29}Si{^{1}H} NMR (C$_6$D$_6$, 80 MHz, 298 K), δ = 9.05; IR, ν/cm^{-1} (ATR): 3058 (bw), 3023 (bw), 2069 (b), 1598 (w), 1318 (w), 1803 (w), 1223 (m), 1197 (m), 1155 (m), 1119 (m), 1072 (w), 1032 (w), 1002 (w), 880 (m), 862 (m), 827 (m), 812 (m), 733 (s), 661 (s); MS/EI *m/z* (%): 695.6 (^{iPr}L†Ge^{+}, 2), 623.6 (^{iPr}L$^{\dagger+}$, 20), 580.5 (^{iPr}L†-Pr^{i+}, 42), 167.1 (Ph$_2$C^{+}, 100); anal. calc. for C$_{94}$H$_{112}$Ge$_2$N$_2$Si$_2$: C 76.74%, H 7.67%, N 1.90%; found: C 76.50%, H 7.58%, N 1.82%.

(^{iPr}L†)Ge $\lceil\overline{\text{COD}}\rceil$ Ge(^{iPr}L†) (25) To a solution of {(^{iPr}L†)Ge}$_2$ (200 mg, 0.14 mmol) in diethyl ether (30 mL) was added 1,5-cyclooctadiene (60 μL, 0.48 mmol) at room temperature. An instant colour change from dark brown/orange to intense purple was observed. The reaction mixture was then stirred for 1 h, after which time its volume was reduced to *ca.* 1 mL. Hexane (20 mL) was added and the solution filtered. Concentration of the filtrate to 7 mL and storage at 4 °C for 2 days yielded small purple/red dichroic plates of (^{iPr}L†)Ge $\lceil\overline{\text{COD}}\rceil$ Ge(^{iPr}L†) (92 mg, 43%). M.p. 133–145 °C (decomp.); ^{1}H NMR (*d*$_8$-toluene, 400 MHz, 253 K) δ = −1.15 (br m, 2H, COD-GeC*H*), 0.41 (br d, $^{3}J_{HH}$ ≈ 7 Hz, 6H, Ar†-*p*-CH(C*H*$_3$)$_2$), 0.54 (br d, $^{3}J_{HH}$ ≈ 7 Hz, 6H, Ar†-*p*-CH(C*H*$_3$)$_2$), 0.72–1.47 (v br overlapping m, 38H, SiPr$^{i}_{3}$-CH(C*H*$_3$)$_2$ and COD-C*H*$_2$), 1.69 (v br m, 6H, SiPr$^{i}_{3}$-C*H*(CH$_3$)$_2$), 2.46 (br m, 2H, COD-C*H*$_2$), 2.80 (sept, $^{3}J_{HH}$ = 6.8 Hz, 1H, Ar-C*H*(CH$_3$)$_2$), 2.86 (sept, $^{3}J_{HH}$ = 6.8 Hz, 1H, Ar-C*H*(CH$_3$)$_2$), 3.30 (br m, 2H, COD-C*H*$_2$), 4.04 (br m, 2H, COD-C*H*$_2$), 4.69 (br m, 2H, COD-C*H*), 6.22 (br s, 4H, C*H*Ph$_2$), 6.62–8.04 (m, 44H, Ar-C*H*); ^{13}C{^{1}H} NMR (*d*$_8$-toluene, 75.5 MHz, 253 K), δ = 15.0 (br, SiPr$^{i}_{3}$-*C*H(CH$_3$)$_2$), 19.5 (br, SiPr$^{i}_{3}$-CH(*C*H$_3$)$_2$), 24.0 (br, Ar†-*p*-CH(*C*H$_3$)$_2$), 33.9 (br, Ar†-*p*-*C*H(CH$_3$)$_2$), 51.3 (br, *C*HPh$_2$), 19.0 (Ge*C*H), 25.9, 33.5 (COD-*C*H$_2$), 126.1 (COD-*C*H), 126.6, 128.3, 129.1, 129.5, 129.8, 130.3, 130.4, 131.1, 131.4, 131.6, 137.7, 138.6, 139.1, 140.4, 142.6, 142.0, 143.5, 143.6, 144.8, 146.2, 147.0, 147.4 (Ar-*C*); ^{29}Si{^{1}H} NMR (C$_6$D$_6$, 80 MHz, 298 K): signal too broad to be observed; IR, ν/cm^{-1} (ATR): 3061 (bw), 3025 (bw), 1945 (w), 1882 (w), 1599 (m), 1380 (w), 1227 (m), 1118 (m), 1071 (w), 879 (s), 860 (s), 793 (s), 718 (s), 661 (s); MS/EI *m/z* (%): 695.6 (^{iPr}L†Ge^{+}, 18), 623.6 (^{iPr}L$^{\dagger+}$, 60), 580.5 (^{iPr}L†-Pr^{i+}, 100); anal. calc. for C$_{96}$H$_{116}$Ge$_2$N$_2$Si$_2$: C 76.90%; H 7.80%; N 1.87%; found: C 76.84%; H 7.92%; N 1.93%. N.B. Solutions of compound (^{iPr}L†)Ge $\lceil\overline{\text{COD}}\rceil$ Ge(^{iPr}L†) exist in equilibrium with significant amounts of free COD and the digermyne {(^{iPr}L†)Ge}$_2$, even at 253 K. As a result, the assignment of the NMR spectra of (^{iPr}L†)Ge $\lceil\overline{\text{COD}}\rceil$ Ge(^{iPr}L†) was complicated by overlap of some signals for the three species in solution.

{(^{iPr}L†)Sn(μ-H)}$_2$ (26) A solution of L-Selectride (1.29 mL, 1 M solution, 1.29 mmol) was added to a solution of (^{iPr}L†)SnCl (1.0 g, 1.29 mmol) in toluene (40 mL) at −80 °C. The reaction mixture was warmed to −20 °C over 3 h. At this temperature, all volatiles are removed in vacuo to afford an orange/brown residue which was extracted with diethyl ether (30 mL), and the extract filtered. The filtrate was concentrated to 5 mL and stored at −20 °C overnight to yield large dichroic yellow/orange blocks of {(^{iPr}L†)Sn(μ-H)}$_2$ (489 mg, 51). M.p. = 75–82 °C; ^{1}H NMR (C_6D_6, 500 MHz, 298 K): δ = 1.00 (d, $^3J_{HH}$ = 6.8 Hz, 6H, Ar†-*p*-CH(C*H*$_3$)$_2$), 1.30 (d, $^3J_{HH}$ = 7.6 Hz, 18H, SiPr$^i_3$-CH(C*H*$_3$)$_2$), 1.69 (sept, $^3J_{HH}$ = 7.6 Hz, 3H, SiPr$^i_3$-C*H*(CH$_3$)$_2$), 2.56 (sept, $^3J_{HH}$ = 6.8 Hz, 1H, Ar†-*p*-C*H*(CH$_3$)$_2$), 6.46 (s, 2H, C*H*Ph$_2$), 6.97–7.36 (m, 22H, Ar-*H*), 17.20 (br s, Sn-*H*, no $^{117/119}$Sn satellites observed), N.B. the broad SnH resonance appears at δ = 19.20 ppm at 313 K; ^{13}C{^{1}H} NMR (C_6D_6, 75.5 MHz, 298 K): δ = 16.0 (SiPr$^i_3$-*C*H(CH$_3$)$_2$), 20.0 (SiPr$^i_3$-CH(*C*H$_3$)$_2$), 24.2 (Ar†-*p*-CH(*C*H$_3$)$_2$), 33.6 (Ar†-*p*-*C*H(CH$_3$)$_2$), 52.0 (*C*HPh$_2$), 126.5, 128.5, 129.4, 130.0, 130.1, 141.3, 142.4, 145.0, 145.3, 145.6 (Ar-*C*); ^{29}Si{^{1}H} NMR (C_6D_6, 80 MHz, 298 K): δ = 4.70; ^{119}Sn{^{1}H} NMR (C_6D_6, 149 MHz, 273 K): no signal observed, even for a concentrated sample and long acquisition time; IR, ν/cm^{-1} (ATR): 3058(w), 3024(w), 1598(m), 1379(w), 1200(w), 1119(m), 886(m), 809(m), 802(m), 755(m); No Sn(μ-H)Sn band could be assigned, presumably as this lies in the "fingerprint" region; IR, ν/cm^{-1} (solution in cyclohexane): similar to that of a solid sample, but with a broad peak at ν 1800 cm^{-1}, tentatively assigned as the Sn-H$_{terminal}$ stretching band of monomeric (^{iPr}L†)SnH; MS/EI *m/z* (%): 623.4 (^{iPr}L$^{\dagger+}$, 68), 580.3 (^{iPr}L$^{\dagger+}$-Pr^i, 100), 167.0 (Ph$_2$C$^+$, 46); anal. calc. for $C_{88}H_{106}Sn_2N_2Si_2$: C, 71.16%; H, 7.19%; N, 1.89%. found: C, 71.05%; H, 7.22%; N, 1.96%;

N.B. Pure samples of {(^{iPr}L†)Sn(μ-H)}$_2$ dissolved in C_6D_6 decomposed over the course of 2 days at room temperature, to yield tin metal and ^{iPr}L†H. The thermal instability of the compound in solution precluded meaningful UV/visible spectra being acquired above 40 °C.

(^{iPr}L†)(H)Sn.(DMAP) (27) DMAP (49 mg, 0.40 mmol) was added to a solution of **26** (100 mg, 0.13 mmol) in diethyl ether (30 mL) at −40 °C, and the reaction mixture stirred for 3 h. The mixture was subsequently concentrated in vacuo to *ca.* 4 mL and filtered. Storage of the filtrate at −20 °C overnight yield colourless crystalline blocks, and a brown precipitate. Crystals were isolated by suspension of the dark precipitate by agitation, followed by decanting of the suspension (21 mg, 18%); M.p.: 118–123°C (dec.); ^{1}H NMR (C_6D_6, 500 MHz, 298 K): δ = 1.06 (d, $^3J_{HH}$ = 6.8 Hz, 6H, Ar†-*p*-CH(C*H*$_3$)$_2$), 1.25 (d, $^3J_{HH}$ = 7.6 Hz, 18H, SiPr$^i_3$-CH(C*H*$_3$)$_2$), 1.56 (sept, $^3J_{HH}$ = 7.6 Hz, 3H, SiPr$^i_3$-C*H*(CH$_3$)$_2$), 1.94 (s, 6H, DMAP-N(C*H*$_3$)$_2$), 2.62 (sept, $^3J_{HH}$ = 6.8 Hz, 1H, Ar†-*p*-C*H*(CH$_3$)$_2$), 5.73 (d, 2H, DMAP-*o*-C*H*), 6.90 (s, 2H, C*H*Ph$_2$), 7.10–7.61 (m, 22H, Ar-*H*), 8.30 (d, 2H, DMAP-*m*-C*H*), 15.01 (br d, 1H, Sn-*H*, no $^{117/119}$Sn satellites observed); ^{13}C{^{1}H} NMR (C_6D_6, 75.5 MHz, 298 K): δ = 16.2 (SiPr$^i_3$-*C*H(CH$_3$)$_2$), 20.1 (SiPr$^i_3$-CH(*C*H$_3$)$_2$), 24.3 (Ar†-*p*-CH(*C*H$_3$)$_2$), 33.6 (Ar†-*p*-*C*H(CH$_3$)$_2$), 38.1 (DMAP-N(*C*H$_3$)$_2$), 51.5 (*C*HPh$_2$),

106.7 (DMAP-*o*-*C*H), 126.2, 126.6, 128.2, 128.6, 129.4, 130.7 (Ar-*C*), 131.2 (DMAP-*m*-*C*H), 141.7 (br), 145.7, (Ar-*C*), 148.0 (DMAP-Me_2N-*C*), 150.6, 154.2 (Ar-*C*); $^{29}Si\{^1H\}$ NMR (C_6D_6, 80 MHz, 298 K): δ = 6.11; IR, ν/cm^{-1} (ATR): 3059(w), 3025(w), 1759(Sn-H, br. m), 1609(s), 1540(m), 1493(m), 1444(s), 1381 (m), 1224(s), 1119(m), 1062(m), 1030(m), 1001(m), 884(m), 806(m), 758(w), 655 (s); MS/EI *m/z* (%):623.4 ($^{iPr}L^{\dagger+}$, 28), 580.4 ($^{iPr}L^{\dagger+}$-Pr^i, 48), 121.0 ($DMAP^+$, 100).

N.B. Pure samples of ($^{iPr}L^{\dagger}$)(H)Sn.DMAP dissolved in C_6D_6 decompose over the course of 24 h at room temperature, to yield tin metal and $^{iPr}L^{\dagger}H$. Crystalline samples of the compound slowly decompose at 20 °C.

($^{iPr}L^{\dagger}$)Sn(CO_3)Sn($^{iPr}L^{\dagger}$) (28) A deep green solution of **18** (200 mg, 0.13 mmol) was stirred under an atmosphere of dry CO_2 at −60 °C, whereupon the reaction mixture became colourless. The mixture was warmed, with stirring, to ambient temperature, an all volatiles removed in vacuo. The solid residue was extracted in warm hexane (15 mL), and the extract filtered. The filtrate was concentrated to ∼5 mL in vacuo, and stored at room temperature for 2 days, yielding large colourless blocks of **28** (130 mg, 65%). M.p.: 112–120 °C (bubbles), 162 °C (decomp.); ^1H NMR (C_6D_6, 400 MHz, 298 K), δ = 0.99 (d, $^3J_{HH}$ = 6.8 Hz, 6H, $Ar^{\dagger}$-*p*-CH(CH_3)$_2$), 1.36 (d, $^3J_{HH}$ = 6.8 Hz, 18H, CH(CH_3)$_2$), 1.74 (sept, $^3J_{HH}$ = 6.8 Hz, 3H, C*H*(CH_3)$_2$), 2.54 (sept, $^3J_{HH}$ = 6.8 Hz, 1H, $Ar^{\dagger}$-*p*-C*H*(CH_3)$_2$), 6.29 (s, 2H, Ph_2CH), 6.97–7.26 (m, 22H, Ar-*H*); $^{13}C\{^1H\}$ NMR (C_6D_6, 75.5 MHz, 298 K), δ = 15.4 ($SiPr^i_3$-*C*H(CH_3)$_2$), 19.9 ($SiPr^i_3$-CH(*C*H_3)$_2$), 24.2 ($Ar^{\dagger}$-*p*-CH(*C*H_3)$_2$), 33.8 ($Ar^{\dagger}$-*p*-*C*H(CH_3)$_2$), 52.2 (Ph_2CH), 126.7, 127.6, 128.8, 129.9, 130.1, 131.5, 140.8, 143.4, 144.4, 145.0, 145.6, 145.7, 152.5 (Ar-*C*), 167.4 (Sn-(*C*O_3)-Sn); $^{29}Si\{^1H\}$ NMR (C_6D_6, 80 MHz, 298 K), δ = 7.4; $^{119}Sn\{^1H\}$ NMR (C_6D_6, 149.2 MHz, 298 K): −209; MS/EI *m/z* (%): 741.5 (($^{iPr}L^{\dagger}$)Sn^+, 0.5), 580.6 ($^{iPr}L^{\dagger+}$-Pr^i, 50), 167.2 (Ph_2C^+, 100); anal. calc. for $C_{89}H_{104}Sn_2N_2O_3Si_2$: C, 69.13%; H, 6.97%; N, 1.81%; found: C, 69.01%; H, 6.93%; N, 1.87%.

($^{iPr}L^{\dagger}$)(Bu^tNC)SnSn($CNBu^t$)($^{iPr}L^{\dagger}$) (29) The procedure for the synthesis of {($^{iPr}L^{\dagger}$)Sn}$_2$ was followed, using ($^{iPr}L^{\dagger}$)SnBr (250 mg, 0.30 mmol) and {(^{Mes}Nacnac)Mg}$_2$ (109 mg, 0.15 mmol) in a toluene/diethyl ether mixture (5 mL/10 mL), followed by the addition of neat Bu^tNC (38 μL, 0.33 mmol) to the solution of in situ generated {($^{iPr}L^{\dagger}$)Sn}$_2$. After stirring the reaction mixture for 1 h at −20 °C, volatiles were removed in vacuo and the residue was extracted in hexane. The extract was filtered and concentrated to incipient crystallisation, then placed at −30 °C for 1 week to afford large dark orange/green crystals of ($^{iPr}L^{\dagger}$)(Bu^tNC)SnSn($CNBu^t$)($^{iPr}L^{\dagger}$) (90 mg, 36%). M.p.: 101–108 °C (melt and decomp.); ^1H NMR (C_6D_6, 400 MHz, 298 K), δ = 0.86 (s, 9H, CNC(CH_3)$_3$), 1.02 (d, $^3J_{HH}$ = 6.8 Hz, 6H, $Ar^{\dagger}$-*p*-CH(CH_3)$_2$), 1.22 (d, $^3J_{HH}$ = 6.8 Hz, 18H, $SiPr^i_3$-CH(CH_3)$_2$), 1.40 (sept, $^3J_{HH}$ = 6.8 Hz, 3H, $SiPr^i_3$-C*H*(CH_3)$_2$), 2.60 (sept, $^3J_{HH}$ = 6.8 Hz, 1H, $Ar^{\dagger}$-*p*-C*H*(CH_3)$_2$), 6.43 (s, 2H, Ph_2CH), 6.93 (m, 2H, $Ar^{\dagger}$-*m*-C*H*), 6.96–7.46 (m, 20H, Ar-*H*); $^{13}C\{^1H\}$ NMR (C_6D_6, 75.5 MHz, 298 K), δ = 17.0 ($SiPr^i_3$-*C*H(CH_3)$_2$), 20.0 ($SiPr^i_3$-CH(*C*H_3)$_2$), 24.2 ($Ar^{\dagger}$-*p*-CH(*C*H_3)$_2$), 30.3 (CNC(*C*H_3)$_3$), 33.5 ($Ar^{\dagger}$-*p*-*C*H(CH_3)$_2$), 51.8 (Ph_2CH), 53.7 (CN*C*(CH_3)$_3$); 125.7,

126.5, 127.0, 128.4, 128.6, 130.4, 137.8, 141.0, 142.0, 145.0, 146.9, 152.6 (Ar-*C*), *C*NC$(CH_3)_3$ resonance not observed; $^{29}Si\{^1H\}$ NMR (C_6D_6, 80 MHz, 298 K), δ = 5.4; ^{119}Sn NMR (C_6D_6, 149.2 MHz, 298 K): δ = 241 (p.w. at 1/2 peak height: 90 Hz), $^{117/119}Sn$ satellites not observed; UV/Vis, λ_{max}, nm (ε, $Lcm^{-1}mol^{-1}$): 420 (5200); IR, ν/cm^{-1} (ATR): 3060 (w), 3026 (w), 2786 (w), 2138 (s, CN) 1944 (w), 1890 (w), 1802 (w), 1599 (m), 1426 (m), 1210 (s), 1192 (m), 1120 (m), 1031 (m), 896 (s), 786 (s), 761 (s), 716 (s), 679 (s); anal. calc. for $C_{98}H_{122}Sn_2N_4Si_2$: C, 71.35%; H, 7.45%; N, 3.40; found: C, 71.12%; H, 7.40%; N, 3.51%.

(^{tBuO}L*)GeOBu^t (30) This compound was prepared following a method similar to that used for (^{tBuO}L†)GeOBu^t, using (^{tBuO}L*)K (1.0 g, 1.38 mmol), $GeCl_2$.dioxane (336 mg, 1.45 mmol), and KOBu^t (186 mg, 1.66 mmol). The product was isolated as a colourless micro-crystalline powder. Recrystallisation from hexane yielded X-ray quality colourless crystals. (940 mg, 82%). M.p.: 225–230 °C (decomp.); ^1H NMR (C_6D_6, 400 MHz, 298 K), δ = 1.14 (s, 9H, GeOC(CH_3)$_3$), 1.56 (s, 27H, SiOC(CH_3)$_3$), 1.94 (s, 3H, Ar*-*p*-*Me*), 6.55 (s, 2H, Ph_2CH), 6.92 (m, 2H, Ar*-*m*-Ar-*H*), 7.06–7.56 (m, 20H, Ar-*H*); $^{13}C\{^1H\}$NMR (C_6D_6, 75.5 MHz, 298 K), δ = 21.3 (Ar*-*p*-*Me*), 32.8 (SiOC(*C*H_3)$_3$), 34.6 (GeOC(*C*H_3)$_3$), 52.0 (Ph_2*C*H), 73.1 (GeO*C*$(CH_3)_3$), 74.4 (SiO*C*$(CH_3)_3$), 126.4, 126.9, 128.9, 129.7, 130.5, 131.1, 131.2, 133.0, 142.6, 144.6, 145.4, 145.5 (Ar-*C*); $^{29}Si\{^1H\}$ NMR (C_6D_6, 80 MHz, 298 K), δ = −96.2; IR, ν/cm^{-1} (ATR): 3059 (w), 3025 (w), 1947 (w), 1810(w), 1598 (m), 1361 (m), 1238 (m), 1182 (s), 1049 (s), 1020 (s), 901 (m), 842 (m), 744 (m); MS/EI *m/z* (%): 831.7 (M^+, 1), 757.6 (M^+-OBu^t, 3), 167.2 (Ph_2C^+, 100); anal. calc. for $C_{49}H_{63}GeNO_4Si$: C, 70.84%; H, 7.64%; N, 1.69%; found: C, 71.11%; H, 7.51%; N, 1.73%.

(^{tBuO}L†)GeOBu^t (31) A solution of (^{tBuO}L†)K (1.5 g, 2.00 mmol) in THF (50 mL) was added to a stirred solution of $GeCl_2$.dioxane (486 mg, 2.10 mmol) in THF (15 mL) at −80 °C. The reaction mixture was stirred for 30 min before being warmed to ambient temperature and stirred for a further 2 h. Subsequently, all volatiles were removed in vacuo and the residue extracted into toluene (40 mL). The extract was filtered onto a suspension of KOBu^t (268 mg, 2.40 mmol) in toluene (20 mL) at −80°C, and the mixture warmed to ambient temperature, then stirred for 3 h. Volatiles were subsequently removed in vacuo, the residue extracted into hot hexane (50 mL), and the extract filtered, yielding a pale yellow solution. Removal of volatiles from the filtrate and washing the residue with a minimum amount of hexane yielded (^{tBuO}L†)GeOBu^t as an analytically pure off-white powder (900 mg, 53%). M.p.: 217–221 °C (decomp.); ^1H NMR (C_6D_6, 400 MHz, 298 K), δ = 1.00 (d, $^3J_{HH}$ = 6.8 Hz, 6H, Ar†-*p*-CH(CH_3)$_2$), 1.16 (s, 9H, GeOC(CH_3)$_3$), 1.55 (s, 27H, SiOC(CH_3)$_3$), 2.57 (sept, 1H, Ar†-*p*-C*H*$(CH_3)_2$), 6.62 (s, 2H, Ph_2CH), 6.93 (m, 2H, Ar†-*m*-C*H*), 7.07–7.56 (m, 20H, Ar-*H*); $^{13}C\{^1H\}$NMR (C_6D_6, 75.5 MHz, 298 K), δ = 24.3 (Ar†-*p*-CH(*C*H_3)$_2$), 32.8 (SiOC(*C*H_3)$_3$), 34.0 (Ar†-*p*-*C*H$(CH_3)_2$), 34.6 (GeOC(*C*H_3)$_3$), 52.2 (Ph_2*C*H), 73.1 (GeO*C*$(CH_3)_3$), 74.4 (SiO*C*

$(CH_3)_3$), 126.4, 126.9, 127.0, 128.2, 129.0, 131.0, 131.1, 142.9, 144.1, 144.5, 145.5, 145.6 (Ar-*C*); $^{29}Si\{^1H\}$ NMR (C_6D_6, 80 MHz, 298 K), δ = −96.4; IR, ν/cm^{-1} (ATR): 3062 (w), 3029 (w), 1598 (w), 1359 (s), 1238 (m), 1182 (s), 1074 (s), 1041 (s), 932 (m), 905 (s), 838 (s), 748 (s); MS/EI *m/z* (%): 859.7 (M^+, 1), 785.7 (M^+-OBu^t, 5), 167.2 (Ph_2C^+, 100); anal. calc. for $C_{51}H_{67}GeNO_4Si$: C, 71.33%; H, 7.86%; N, 1.63%; found: C, 71.12%; H, 7.90%; N, 1.71%.

(^{tBuO}L*)GeH (32) This compound was prepared following a method similar to that used for (^{tBuO}L†)GeH, but using (^{tBuO}L*)GeOBu^t (250 mg, 0.30 mmol) and HBcat (34 μL, 0.32 mmol). The product was isolated as pale-yellow crystalline blocks, grown by slow-cooling of a concentrated hexane solution (110 mg, 48%). M.p.: 155–160 °C (decomp.); ^1H NMR (C_6D_6, 400 MHz, 298 K), δ = 1.49 (s, 27H, OC(CH_3)$_3$), 2.00 (s, 3H, Ar*-*p*-*Me*), 6.50 (s, 2H, Ph_2CH), 6.92–7.54 (m, 22H, Ar-*H*), 10.00 (v br, 1H, Ge*H*); $^{13}C\{^1H\}$NMR (C_6D_6, 75.5 MHz, 298 K), δ = 21.4 (Ar*-*p*-*Me*), 32.6 (OC(CH_3)$_3$), 52.1 (Ph_2CH), 74.7 (O*C*(CH_3)$_3$), 122.4, 126.4, 128.8, 129.1, 129.3, 130.0, 130.5, 130.8, 133.2, 144.8, 145.3, 145.5 (Ar-*C*); $^{29}Si\{^1H\}$ NMR (C_6D_6, 80 MHz, 298 K), δ = −94.0; UV/Vis (toluene, 298 K), λ_{max}, nm (ε, Lcm^{-1}mol^{-1}): 330 (700); IR, ν/cm^{-1} (ATR): 3060 (w), 3026 (w), 1923 (w, Ge-H), 1751 (m), 1597 (m), 1386 (m), 1363 (m), 1181 (s), 1039 (s), 925 (s), 853 (m), 737 (m); MS/EI *m/z* (%): 757.6 (M^+, <1), 167.2 (Ph_2C^+, 100); anal. calc. for $C_{45}H_{55}GeNO_3Si$: C, 71.24%; H, 7.31%; N, 1.85%; found: C, 71.05%; H, 7.20%; N, 1.93%.

(^{tBuO}L†)GeH (33) To a colourless solution of (^{tBuO}L†)GeOBu^t (200 mg, 0.23 mmol) in toluene (20 mL) was added HBcat (23 μL, 0.24 mmol) at ambient temperature, with stirring. The reaction mixture immediately became pale yellow in colour. The mixture was then stirred for 2 h, after which time all volatiles were removed in vacuo and the residue extracted into warm hexane (30 mL). The extract was filtered, and the filtrate concentrated to incipient crystallisation, before being stored at 6°C for 2 days to yield (^{tBuO}L†)GeH as small pale yellow plates (80 mg, 44%). M.p.: 97–102 °C (melt), 148–153 °C (decomp.); ^1H NMR (C_6D_6, 400 MHz, 298 K), δ = 1.01 (d, $^3J_{HH}$ = 6.8 Hz, 6H, Ar†-*p*-CH(CH_3)$_2$), 1.48 (s, 27H, OC(CH_3)$_3$), 2.60 (sept, 1H, Ar†-*p*-C*H*(CH_3)$_2$), 6.51 (s, 2H, Ph_2CH), 6.75 (m, 2H, Ar†-*m*-C*H*), 7.01–7.55 (m, 20H, Ar-*H*), 10.02 (v br, 1H, Ge*H*); $^{13}C\{^1H\}$NMR (C_6D_6, 75.5 MHz, 298 K), δ = 24.5 (Ar†-*p*-CH(*C*H_3)$_2$), 32.4 (Ar†-*p*-*C*H(CH_3)$_2$), 32.6 (OC(CH_3)$_3$), 52.3 (Ph_2CH), 74.7 (O*C*(CH_3)$_3$), 122.3, 126.3, 126.4, 127.4, 129.1, 129.3, 130.7, 143.1, 144.9, 145.6, 146.5, 148.6 (Ar-*C*); $^{29}Si\{^1H\}$ NMR (C_6D_6, 80 MHz, 298 K), δ = −93.1; IR, ν/cm^{-1} (ATR): 3061 (w), 3026 (w), 1887 (br m, Ge-H), 1772 (m), 1599 (w), 1521 (w), 1326 (m), 1237 (m), 1182 (s), 1065 (s), 1041 (s), 925 (s), 871 (m), 742 (s); MS/EI *m/z* (%): 713.7 (^{iPr}L$^{†+}$, 10), 167.2 (Ph_2C^+, 100); anal. calc. for $C_{47}H_{59}GeNO_3Si$: C, 71.76%; H, 7.56%; N, 1.78%; found: C, 71.66%; H, 7.67%; N, 1.83%.

References

1. Asay M, Jones C, Driess M (2011) N-heterocyclic carbene analogues with low-valent group 13 and group 14 elements: syntheses, structures, and reactivities of a new generation of multitalented ligands. Chem Rev 111:354
2. Power PP (2010) Main-group elements as transition metals. Nature 463:171
3. Caputo CA, Power PP (2013) Heavier main group dimetallene reactivity: effects of frontier orbital symmetry. Organometallics 32:2278
4. Lee VY, Sekiguchi A (2007) Stable silyl, germyl, and stannyl cations, radicals, and anions: heavy versions of carbocations, carbon radicals, and carbanions. Acc Chem Res 40:410
5. Rivard E, Power PP (2007) Multiple bonding in heavier element compounds stabilized by bulky terphenyl ligands. Inorg Chem 46:10047
6. Pu L, Twamley B, Power PP (2000) Synthesis and characterization of 2,6-Trip2H3C6PbPb C6H3-2,6-Trip2 (Trip = C6H2-2,4,6-i-Pr3): a stable heavier group 14 element analogue of an alkyne. J Am Chem Soc 122:3524
7. Power PP (2007) Bonding and reactivity of heavier group 14 element alkyne analogues. Organometallics 26:4362
8. Sekiguchi A, Kinjo R, Ichinohe M (2004) A stable compound containing a silicon-silicon triple bond. Science 305:1755
9. Mulliken RS (1950) Overlap integrals and chemical binding. J Am Chem Soc 72:4493
10. Pitzer KS (1948) Repulsive forces in relation to bond energies, distances and other properties. J Am Chem Soc 70:2140
11. As determined by a survey of the Cambridge Crystallographic Database
12. Nagase S, Kobayashi K, Takagi N (2000) Triple bonds between heavier group 14 elements. A theoretical approach. J Organomet Chem 611:264
13. Colegrove BT, Schaefer HF (1990) Disilyne (Si2H2) revisited. J Phys Chem 94:5593
14. Hühn MM, Amos RD, Kobayashi R, Handy NC (1993) Structure and properties of disilyne. J. Chem Phys 98:7107
15. Goubeau J (1957) Mehrfachbindungen in der anorganischen chemie. Angew Chem 69:77
16. Jutzi P (1975) New element-carbon (p-p)π bonds. Angew Chem Int Ed 14:232
17. Murata Y, Ichinohe M, Sekiguchi A (2010) Unsymmetrically substituted disilyne $Dsi_2{}^{i}PrSi$—Si≡Si—$SiNpDsi_2$ (Np = CH_2tBu): synthesis and characterization. J Am Chem Soc 132:16768
18. Ishida S, Sugawara R, Misawa Y, Iwamoto T (2013) Palladium and platinum η2-disilyne complexes bearing an isolable dialkyldisilyne as a ligand. Angew Chem 125:13107
19. Sasamori T, Hironaka K, Sugiyama Y, Takagi N, Nagase S, Hosoi Y, Furukawa Y, Tokitoh N (2008) Synthesis and reactions of a stable 1,2-diaryl-1,2-dibromodisilene: a precursor for substituted disilenes and a 1,2-diaryldisilyne. J Am Chem Soc 130:13856
20. Sekiguchi A, Ichinohe M, Kinjo R (2006) The chemistry of disilyne with a genuine Si–Si triple bond: synthesis, structure, and reactivity. Bull Chem Soc Jpn 79:825
21. Takeuchi K, Ichinohe M, Sekiguchi A (2008) Reactivity of the disilyne RSi≡SiR (R = $Si^{i}Pr[CH(SiMe_3)_2]_2$) toward silylcyanide: two pathways to form the bis-adduct [RSiSiR $(CNSiMe_3)_2$] with some silaketenimine character and a 1,4-diaza-2,3-disilabenzene analogue. J Am Chem Soc 130:16848
22. Kinjo R, Ichinohe M, Sekiguchi A, Tagaki N, Sumimoto M, Nagase S (2007) Reactivity of a disilyne RSi≡SiR (R = $Si^{i}Pr[CH(SiMe_3)_2]_2$) toward π-bonds: stereospecific addition and a new route to an isolable 1,2-disilabenzene. J Am Chem Soc 129:7766
23. Takeuchi K, Ichinohe M, Sekiguchi A (2011) Hydroboration of disilyne RSi≡SiR (R = $Si^{i}Pr[CH(SiMe_3)_2]_2$), giving boryl-substituted disilenes. Organometallics 30:2044
24. Han JS, Sasamori T, Mizuhata Y, Tokitoh N (2010) Reactivity of an aryl-substituted silicon −silicon triple bond: reactions of a 1,2-diaryldisilyne with alkenes. J Am Chem Soc 132:2546

25. Han JS, Sasamori T, Mizuhata Y, Tokitoh N (2010) Reactivity of an aryl-substituted silicon–silicontriple bond: 1,2-disilabenzenes from the reactions of a 1,2-diaryldisilyne with alkynes. Dalton Trans 39:9238
26. Stender M, Phillips AD, Wright RJ, Power PP (2002) Synthesis and characterization of a digermanium analogue of an alkyne. Angew Chem 114:1863
27. Takagi N, Nagase S (2001) Substituent effects on germanium−germanium and tin−tin triple bonds. Organometallics 20:5498
28. Peng Y, Fischer RC, Merrill WA, Fischer J, Pu L, Ellis BD, Fettinger JC, Herber RH, Power PP (2010) Substituent effects in ditetrel alkyne analogues: multiple vs. single bonded isomers. Chem Sci 1:461
29. Sugiyama Y, Sasamori T, Hosoi Y, Furukawa Y, Takagi N, Nagase S, Tokitoh N (2006) Synthesis and properties of a new kinetically stabilized digermyne: new insights for a germanium analogue of an alkyne. J Am Chem Soc 128:1023
30. Li J, Schenk C, Goedecke C, Frenking G, Jones C (2011) A digermyne with a Ge–Ge single bond that activates dihydrogen in the solid state. J Am Chem Soc 133:18622
31. Spikes GH, Fettinger JC, Power PP (2005) Facile activation of dihydrogen by an unsaturated heavier main group compound. J Am Chem Soc 127:12232
32. Zhao L, Huang F, Lu G, Wang ZX, Schleyer PR (2012) Why the mechanisms of digermyne and distannyne reactions with H2 differ so greatly. J Am Chem Soc 134:8856
33. Richards AF, Phillips AD, Olmstead MM, Power PP (2003) Isomeric forms of divalent heavier group 14 element hydrides: characterization of Ar‘(H)GeGe(H)Ar‘ and Ar‘$(H)_2$GeGeAr‘·PMe_3 (Ar‘ = C_6H_3-2,6-$Dipp_2$; Dipp = C_6H_3-2,6-Pr^i_2). J Am Chem Soc 125:3204
34. Hermann M, Goedecke C, Jones C, Frenking G (2013) Reaction pathways for addition of H2 to amido-ditetrylynes R_2N–EE–NR_2 (E = Si, Ge, Sn). A theoretical study. Organometallics 32:6666
35. Li J, Hermann M, Frenking G, Jones C (2012) The facile reduction of carbon dioxide to carbon monoxide with an amido-digermyne. Angew Chem Int Ed 51:8611
36. Yao S, Xiong Y, Brym M, Driess M (2007) An isolable silanoic ester by oxygenation of a stable silylene. J Am Chem Soc 129:7268
37. Gau D, Rodriguez R, Kato T, Saffon-Merceron N, de Cozar A, Cossio FP, Baceiredo A (2011) Synthesis of a stable disilyne bisphosphine adduct and its non-metal-mediated CO_2 reduction to CO. Angew Chem Int Ed 50:1092
38. Gu L, Zhang Y (2010) Unexpected CO_2 splitting reactions to form CO with N-heterocyclic carbenes as organocatalysts and aromatic aldehydes as oxygen acceptors. J Am Chem Soc 132:914
39. Lalrempuia R, Stasch A, Jones C (2013) The reductive disproportionation of CO_2 using a magnesium(I) complex: analogies with low valent *f*-block chemistry. Chem Sci 4:4383
40. Lam OP, Meyer K (2012) Metal mediated transformations of CO_2. Polyhedron 32:1
41. Cokoja M, Bruckmeier C, Rieger B, Herrmann WA, Kühn FE (2011) Transformation of carbon dioxide with homogeneous transition-metal catalysts: a molecular solution to a global challenge? Angew Chem Int Ed 50:8510
42. Silvia JS, Cummins CC (2010) Ligand-based reduction of CO_2 to CO mediated by an anionic niobium nitride complex. J Am Chem Soc 132:2169
43. Noor A, Qayyum S, Bauer T, Schwarz S, Weber B, Kempe R (2014) CO_2 and SO_2 activation by a Cr–Cr quintuple bond. Chem Commun 50:13127
44. Mougel V, Camp C, Pécaut J, Copéret C, Maron L, Kefalidis CE, Mazzanti M (2012) Siloxides as supporting ligands in uranium(III)-mediated small-molecule activation. Angew Chem Int Ed 51:12280
45. Spikes GH, Power PP (2007) Lewis base induced tuning of the Ge–Ge bond order in a “digermyne”. Chem Commun 1:85
46. Hadlington TJ, Li J, Hermann M, Davey A, Frenking G, Jones C (2015) Reactivity of amido-digermynes, LGeGeL (L = Bulky Amide), toward olefins and related molecules:

facile reduction, C–H activation, and reversible cycloaddition of unsaturated substrates. Organometallics 34:3175
47. Power PP (2011) Interaction of multiple bonded and unsaturated heavier main group compounds with hydrogen, ammonia, olefins, and related molecules. Acc Chem Res 44:627
48. Power PP (2005) Synthesis and some reactivity studies of germanium, tin and lead analogues of alkynes. Appl Organometal Chem 19:488
49. Cui C, Olmstead MM, Fettinger JC, Spikes GH, Power PP (2005) Reactions of the heavier group 14 element alkyne analogues Ar‘EEAr‘ (Ar‘ = C_6H_3-2,6(C_6H_3-2,6-Pr^i_2)$_2$; E = Ge, Sn) with unsaturated molecules: probing the character of the EE multiple bonds. J Am Chem Soc 127:17530
50. Cui C, Olmstead MM, Power PP (2004) Reactivity of Ar‘GeGeAr‘ (Ar‘ = C_6H_3-2,6-$Dipp_2$, Dipp = C_6H_3-2,6-$^iPr_2$) toward alkynes: isolation of a stable digermacyclobutadiene. J Am Chem Soc 126:5062
51. Peng Y, Ellis BD, Wang X, Fettinger JC, Power PP (2009) Reversible reactions of ethylene with distannynes under ambient conditions. Science 325:1668
52. Summerscales OT, Caputo CA, Knapp CE, Fettinger JC, Power PP (2012) The role of group 14 element hydrides in the activation of C–H bonds in cyclic olefins. J Am Chem Soc 134:14595
53. Summerscales OT, Fettinger JC, Power PP (2011) C–H activation of cycloalkenes by dimetallynes (M = Ge, Sn) under ambient conditions. J Am Chem Soc 133:11960
54. Summerscales OT, Jiménez-Halla JOC, Merino G, Power PP (2011) Unusual electrocyclic rearrangements with group 14 element compounds: reversible isomerization of a π-aromatic digermyl complex with carbon−carbon and germanium−germanium multiple bond cleavage. J Am Chem Soc 133:180
55. Phillips AD, Wright RJ, Olmstead MM, Power PP (2002) Synthesis and characterization of 2,6-$Dipp_2$-$H_3C_6SnSnC_6H_3$-2,6-$Dipp_2$(Dipp = C_6H_3-2,6-Pr^i_2): a tin analogue of an alkyne. J Am Chem Soc 124:5930
56. Fischer RC, Pu L, Fettinger JC, Brynda MA, Power PP (2006) Very large changes in bond length and bond angle in a heavy group 14 element alkyne analogue by modification of a remote ligand substituent. J Am Chem Soc 128:11366
57. Takagi N, Nagase S (2007) Tin analogues of alkynes. Multiply bonded structures vs singly bonded structures. Organometallics 26:469
58. Jung Y, Brynda M, Power PP, Head-Gordon M (2006) Ab initio quantum chemistry calculations on the electronic structure of heavier alkyne congeners: diradical character and reactivity. J Am Chem Soc 128:7185
59. Peng Y, Brynda M, Ellis BD, Fettinger JC, Rivard E, Power PP (2008) Addition of H2 to distannynes under ambient conditions. Chem Commun 45:6042
60. Rivard E, Fischer RC, Wolf R, Peng Y, Merrill WA, Schley ND, Zhu Z, Pu L, Fettinger JC, Teat SJ, Nowik I, Herber RH, Takagi N, Nagase S, Power PP (2007) Isomeric forms of heavier main group hydrides: experimental and theoretical studies of the $[Sn(Ar)H]_2$ (Ar = Terphenyl) system. J Am Chem Soc 129:16197
61. Trinquier G (1991) Singly bridged arrangements on Group 14 X_2H_4 potential surfaces. J Am Chem Soc 113:144
62. Balasubramanian K (1988) Relativistic configuration interaction calculations for polyatomics: applications to PbH_2, SnH_2, and GeH_2. J Chem Phys 89:5731
63. Peng Y, Wang X, Fettinger JC, Power PP (2010) Reversible complexation of isocyanides by the distannyne Ar′SnSnAr′ (Ar′ = C_6H_3-2,6(C_6H_3-2,6-$^iPr_2$)$_2$). Chem Commun 46:943
64. Summerscales OT, Wang X, Power PP (2010) Cleavage of the Sn-Sn multiple bond in a distannyne by cyclooctatetraene: formation of the π-bound inverse sandwich complex [(Ar′Sn)$_2$(μ_2-η^2:η^3-cot)]. Angew Chem Int Ed 49:4788
65. Power PP (1999) π-bonding and the lone pair effect in multiple bonds between heavier main group elements. Chem Rev 99:3463

66. Chen Y, Hartmann M, Diedenhofen M, Frenking G (2001) Turning a transition state into a minimum—the nature of the bonding in diplumbylene compounds RPbPbR (R=H, Ar). Angew Chem Int Ed 40:2051
67. Hino S, Olmstead MM, Power PP (2005) Characterization of a plumbylplumbylene: an isomeric form of a "Diplumbene". Organometallics 24:5484
68. Eichler BE, Power PP (2000) [2,6-$Trip_2H_3C_6Sn(\mu\text{-}H)]_2$ (Trip = C_6H_2-2,4,6-^{i}-Pr_3): synthesis and structure of a divalent group 14 element hydride. J Am Chem Soc 122:8785
69. Rivard E (2014) Donor–acceptor chemistry in the main group. Dalton Trans 43:8577
70. Schrock RR (1979) Alkylidene complexes of niobium and tantalum. Acc Chem Res 12:98
71. Tebbe FN, Parshall GW, Ovenall DW (1979) Titanium-catalyzed olefin metathesis. J Am Chem Soc 101:5074
72. Schwab P, France MB, Ziller JW, Grubbs RH (1995) A series of well-defined metathesis catalysts–synthesis of [RuCl2(=CHR′)$(PR_3)_2$] and Its reactions. Angew Chem Int Ed 34:2039
73. Scott J, Mindiola DJ (2009) A tribute to frederick nye tebbe. Lewis acid stabilized alkylidyne, alkylidene, and imides of 3d early transition metals. Dalton Trans 40:8463
74. Thimer KC, Al-Rafia SMI, Ferguson MJ, McDonald R, Rivard E (2009) Donor/acceptor stabilization of Ge(II) dihydride. Chem Commun 46:7119
75. Al-Rafia SMI, Malcolm AC, Liew SK, Ferguson MJ, Rivard E (2011) Stabilization of the heavy methylene analogues, GeH_2 and SnH_2, within the coordination sphere of a transition metal. J Am Chem Soc 133:777
76. Al-Rafia SMI, Malcolm AC, McDonald R, Ferguson MJ, Rivard E (2012) Efficient generation of stable adducts of Si(II) dihydride using a donor–acceptor approach. Chem Commun 48:1308
77. Wang Y, Xie Y, Wei P, King RB, Schaefer HF III, Schleyer PR, Robinson GH (2008) A stable silicon(0) compound with a Si=Si double bond. Science 321:1069
78. Abraham MY, Wang Y, Xie Y, Wei P, Schaefer HF III, Schleyer PR, Robinson GH (2011) Cleavage of carbene-stabilized disilicon. J Am Chem Soc 133:8874
79. Rivard E, Power PP (2008) Recent developments in the chemistry of low valent Group 14 hydrides. Dalton Trans 33:4336
80. Agou T, Sugiyama Y, Sasamori T, Sakai H, Furukawa Y, Takagi N, Guo JD, Nagase S, Hashizume D, Tokitoh N (2012) Synthesis of kinetically stabilized 1, 2-dihydrodisilenes. J Am Chem Soc 134:4120
81. Sasamori T, Sugiyama Y, Takeda N, Tokitoh N (2005) Structure and properties of an overcrowded 1,2-dibromodigermene. Organometallics 24:3309
82. Inoue S, Eisenhut C (2013) A dihydrodisilene transition metal complex from an n-heterocyclic carbene-stabilized silylene monohydride. J Am Chem Soc 135:18315
83. Fischer RC, Power PP (2010) π-bonding and the lone pair effect in multiple bonds involving heavier main group elements: developments in the new millennium. Chem Rev 110:3877
84. Jana A, Leusser D, Objartel I, Roesky HW, Stalke D (2011) A stable silicon(II) monohydride. Dalton Trans 40:5458
85. Zhang SH, Yeong HX, Xi HW, Lim KH, So CW (2010) Hydrosilylation of a silicon(II) hydride: synthesis and characterization of a remarkable silylsilylene. Chem Eur J 16:10250
86. Stoelzel M, Präsang C, Inoue S, Enthaler S, Driess M (2012) Hydrosilylation of alkynes by $Ni(CO)_3$-stabilized silicon(II) hydride. Angew Chem Int Ed 51:399
87. Rodriguez R, Gau D, Contie Y, Kato T, Saffon-Merceron N, Baceiredo A (2011) Synthesis of a phosphine-stabilized silicon(II) hydride and its addition to olefins: a catalyst-free hydrosilylation reaction. Angew Chem Int Ed 50:11492
88. Ding Y, Hao H, Roesky HW, Noltemeyer M, Schmidt HG (2001) Synthesis and structures of germanium(II) fluorides and hydrides. Organometallics 20:4806
89. Pineda LW, Jancik V, Starke K, Oswald RB, Roesky HW (2006) Stable monomeric germanium(II) and tin(II) compounds with terminal hydrides. Angew Chem 118:2664

90. Choong SL, Woodul WD, Schenk C, Stasch A, Richards AF, Jones C (2011) Synthesis, characterization, and reactivity of an N-heterocyclic germanium(II) hydride: reversible hydrogermylation of a phosphaalkyne. Organometallics 30:5543
91. Khan S, Samuel PP, Michel R, Dieterich JM, Mata RA, Demers JP, Lange A, Roesky HW, Stalke D (2012) Monomeric Sn(II) and Ge(II) hydrides supported by a tridentate pincer-based ligand. Chem Commun 48:4890
92. Xiong Y, Szilvási T, Yao S, Tan G, Driess M (2014) A cyclic germadicarbene ("Germylone") from germyliumylidene. J Am Chem Soc 136:11300
93. Hrobárik P, Hrobáriková V, Meier F, Repisky M, Komorovsky S, Kaupp M (2011) Relativistic four-component DFT calculations of ^{1}H NMR chemical shifts in transition-metal hydride complexes: unusual high-field shifts beyond the buckingham–stephens model. J Phys Chem A 115:5654
94. Jambor R, Herres-Pawlis S, Schürmann M, Jurkschat K (2011) [{2,6-$(Me_2NCH_2)_2C_6H_3$}Sn(μ-OH)$W(CO)_5]_2$: a transition-metal-coordinated organotin(II) hydroxide. Eur J Inorg Chem 3:344
95. Sindlinger SP, Wesemann L (2014) Hydrogen abstraction from organotin di- and trihydrides by N-heterocyclic carbenes: a new method for the preparation of NHC adducts to tin(II) species and observation of an isomer of a hexastannabenzene derivative [R_6Sn_6]. Chem Sci 5:2739
96. Cordero B, Gomez V, Platero-Prats AE, Reves M, Echeverria J, Cremades E, Barragan F, Alvarez S (2008) Covalent radii revisited. Dalton Trans 21:2832
97. Zhao L, Huang F, Lu G, Wang Z-X, Schleyer PR (2012) Why the mechanisms of digermyne and distannyne reactions with H_2 differ so greatly. J Am Chem Soc 134:8856
98. Hermann M, Goedecke C, Jones C, Frenking G (2013) Reaction pathways for addition of H_2 to amido-ditetrylynes $R_2N–EE–NR_2$(E = Si, Ge, Sn). A theoretical study. Organometallics 32:6666
99. Hermann M, Jones C, Frenking G (2014) Reaction mechanisms of small-molecule activation by amidoditetrylynes $R_2N–EE–NR_2$ (E = Si, Ge, Sn). Inorg Chem 53:6482
100. Klamt A, Schüürmann G (1993) COSMO: a new approach to dielectric screening in solvents with explicit expressions for the screening energy and its gradient. J Chem Soc Perkin Trans 2:799
101. Grimme S, Antony J, Ehrlich S, Krieg H (2010) A consistent and accurate ab initio parametrization of density functional dispersion correction (DFT-D) for the 94 elements H-Pu. J Chem Phys 132:154104
102. Woodward RB, Hoffmann R (1970) The conservation of orbital symmetry. VCH, Weinheim
103. Kinjo R, Ichinohe M, Sekiguchi A, Takagi N, Sumimoto M, Nagase S (2007) Reactivity of a disilyne RSi≡SiR (R = SiiPr[CH(SiMe3)2]2) toward π-bonds: stereospecific addition and a new route to an isolable 1,2-disilabenzene. J Am Chem Soc 129:7766
104. Rodriguez R, Gau D, Kato T, Saffon-Merceron N, De Cózar A, Cossío FP, Baceiredo A (2011) Reversible binding of ethylene to silylene–phosphine complexes at room temperature. Angew Chem Int Ed 50:10414
105. Lips F, Fettinger JC, Mansikkamäki A, Tuononen HM, Power PP (2014) Reversible complexation of ethylene by a silylene under ambient conditions. J Am Chem Soc 136:634
106. Green JA, Hoffmann PT (1971) Isonitrile chemistry. Org Chem ed Ugi I 20:1

Chapter 4
Reactivity of Low-Coordinate Group 14 Element(II) Hydride Complexes

4.1 Introduction

The addition of element-hydrogen bonds across unsaturations (i.e. hydroelementation) is of paramount importance in organic synthesis. The application of group 14 element-hydrogen (E–H) bonds in this regard, however, has largely relied upon transition-metal (TM) catalysts or radical mechanisms [1]. In contrast, *s*-block hydrides, which have been extensively studied [2, 3], are generally highly reactive due to the polar nature of their E–H bonds and the non-directionality of their valence *s*-orbitals, leading to facile substrate coordination. The reactivity of group 13 hydride species is similarly aided by the Lewis-acidity of these elements, exemplified by the seminal work of Brown on the synthesis and reactivity of borane and its derivatives [4]. Well defined molecular hydrides of the early main group elements have hence seen applications in hydroelementation [5–7], and, in some cases, catalytic reductions of unsaturated organic molecules [8–11]. The renaissance in low-oxidation state and low-coordinate group 14 chemistry has led to the isolation of stable unsaturated group 14 element(II) hydrides, discussed in Chap. 3, which have shown hydridic reactivity that was previously unknown for these elements in the absence of a catalyst or radical initiator. Interest in such reactivity can be understood on the basis of the importance of hydroelementation reactions in catalytic cycles, with the current push by chemists away from traditional precious TM catalysts, and towards more affordable and abundant elements for these transformations. Steps towards this effort shall be discussed here.

T.J. Hadlington, *On the Catalytic Efficacy of Low-Oxidation State Group 14 Complexes*, Springer Theses, DOI 10.1007/978-3-319-51807-7_4

4.1.1 Reactivity of Group 14 Element(II) Hydride Complexes with Unsaturated Carbon-Heteroatom Bonds

Broadly, well defined 'reactive hydride' chemistry has largely evaded the group 14 elements (E), until recently. This is arguably due to a distinct lack of a vacant coordination site at the E centre when in the +4 oxidation state. Additions of these E(IV)–H bonds to unsaturates has typically relied on radical or catalytic activation [1].

Known E(II)–H species, however, can hold a stereo-active lone pair of electrons, and are generally low-coordinate. This can hypothetically lead to substrate coordination/activation, followed by hydride insertion. Indeed, Sakaki and co-workers showed this to be the case through DFT calculations, showing theoretically that the known (^{Dipp}nacnac)GeH (^{Dipp}nacnac = [CH{N(2,6-Pr^i_2Ph)C(Me)}$_2$]$^-$) [12] could hydrogermylate unsaturated C=O bonds through pre-coordination of the substrate to the Ge centre of the Ge(II) hydride, followed by insertion into the Ge–H bond (note, similar transition states were found for the addition of a Rh–H bond across a C=O bond as part of the same study) [13], giving evidence for the importance of coordinative substrate activation in hydroelementation reactions. In this case, due to the chelating ligand, the coordination is likely favoured due to the oxophilic Ge centre, and the propensity for O to coordinate, as the ^{Dipp}nacnac chelating ligand saturates the otherwise vacant 3*p*-orbital at the Ge(II) centre in (^{Dipp}nacnac)GeH. Nevertheless, this study underlined the key substrate coordination step in such a group 14 element(II) based hydroelementation.

4.1.1.1 Reactivity of Group 14 Element(II) Hydride Complexes with C=O Bonds

Roesky et al. [14] have reported on many applications of both (^{Dipp}nacnac)GeH and (^{Dipp}nacnac)SnH in hydroelementation chemistry. In 2009, that group reported on initial studies of the reactivity of (^{Dipp}nacnac)GeH, which included the first examples of hydrogermylation of C=O bonds, including those in CO_2, by a low-valent germanium hydride complex [15]. Prior to this publication, the only reports of the hydroelemention of CO_2 by a group 14 hydride involved Sn(IV) hydrides [16] and Si(IV) hydrides [17, 18], yet (^{Dipp}nacnac)GeH was shown to react with CO_2 at one atmosphere of pressure and at ambient temperature within 15 min, yielding the Ge(II) formate, (^{Dipp}nacnac)GeOC(H)O (Scheme 4.1). The analogous reaction for (^{Dipp}nacnac)SnH was subsequently reported by the same group, and proceeded equally as rapidly, to give the related (^{Dipp}nacnac)SnOC(H)O (Scheme 4.1) [19]. It was later shown that (^{Dipp}nacnac)GeOC(H)O cleanly reacts with Li[$H_2N{\cdot}BH_3$], or somewhat less cleanly with $NH_3{\cdot}BH_3$, regenerating the (^{Dipp}nacnac)GeH starting material (Scheme 4.1) [20]. Although this was very promising, no catalytic studies were described. Similar studies were more recently

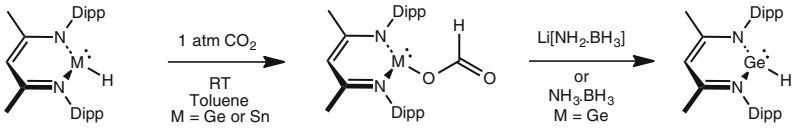

Scheme 4.1 The reaction of β-diketiminate-stabilised Ge(II) and Sn(II) hydrides with CO_2

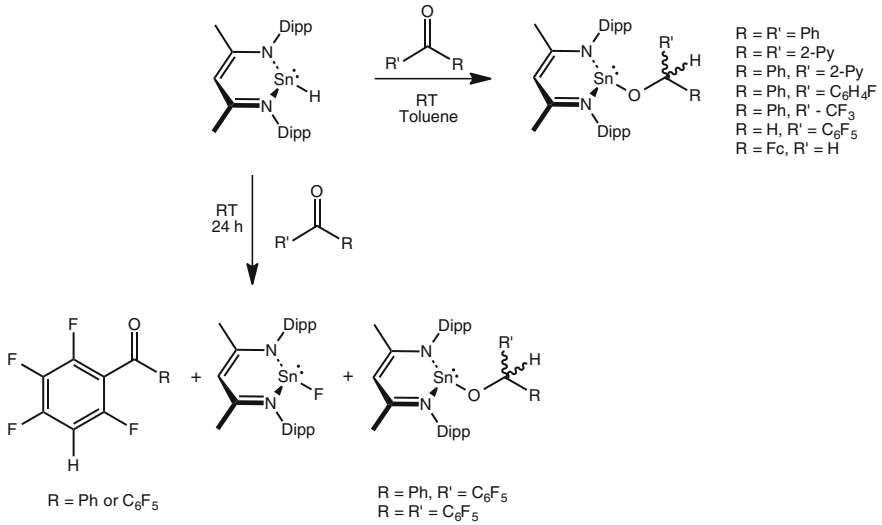

Scheme 4.2 Reactions of (^{Dipp}nacnac)SnH with inactivated ketones and aldehydes, and CF-activation of fluorinated aromatic substituents by (^{Dipp}nacnac)SnH

Scheme 4.3 Reactions of (^{Dipp}nacnac)GeH with activated ketones

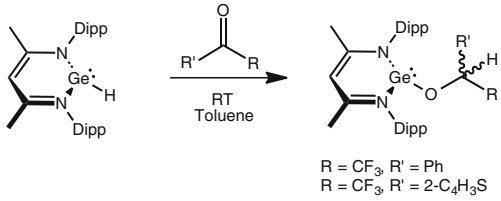

reported by Driess and co-workers, whereby the reaction of (^{Dipp}nacnac)GeOC(H)O with AlH_3 yielded (^{Dipp}nacnac)GeH, amongst other products. These reactions will be discussed further where relevant in Chap. 5; [21].

Both ^{Dipp}nacnac group 14 element(II) hydride species, (^{Dipp}nacnac)GeH and (^{Dipp}nacnac)SnH, were also reacted with various ketones. Whilst (^{Dipp}nacnac)SnH reacted with unactivated ketones at ambient temperature, yielding Sn(II) alkoxides (Scheme 4.2) [19], (^{Dipp}nacnac)GeH did not. Rather, only the activated ketones, $(CF_3)(Ph)C{=}O$ and $(CF_3)(2\text{-}C_4H_3S)C{=}O$, were hydrogermylated (Scheme 4.3)

[22]. Interestingly, the reactivity of (^{Dipp}nacnac)SnH was complicated by the presence of C_6F_5-substituted ketones (Scheme 4.2). The reaction of either (C_6F_5)(Ph)C=O or $(C_6F_5)_2$C=O with (^{Dipp}nacnac)SnH led to reaction mixtures containing both the expected hydrostannylation products and the somewhat unexpected (^{Dipp}nacnac)SnF [23]. Further, the products from nucleophilic substitution of the C_6F_5-substitents, (C_6F_4H)(Ph)C=O or $(C_6F_4H)_2$C=O, were also present, justifying the presence of (^{Dipp}nacnac)SnF, which arises from nucleophilic substitution of C–F bond with the Sn–H bond of (^{Dipp}nacnac)SnH. Whilst not conducive to the hydrostannylation of these fluorinated ketones, this brief study highlights the impressive nucleophilicity of the tin centre in (^{Dipp}nacnac)SnH.

In related work, Rivard and co-workers have reported on the facile hydrosilylation and hydrostannylation of ketones by donor-acceptor stabilised inorganic ethylene ([IPr·Si(H)$_2$=Ge(H)$_2$·W(CO)$_5$]) and stannene ([IPr·SnH$_2$·W(CO)$_5$]; IPr=:C{N(Dipp)C(H)}$_2$; Scheme 4.4) analogues. In the former example, the addition of acetyl acetone to [IPr·Si(H)$_2$=Ge(H)$_2$·W(CO)$_5$] yielded an enolate-coordinated anionic adduct, [{MeC(O)H–C(H)=C(Me)O}SiH=GeH$_2$·W(CO)$_5$]$^-$, as a salt with the known imidazolium cation, [IPrH]$^+$ (Scheme 4.4a) [24]. The parent stannylene, [IPr·SnH$_2$·W(CO)$_5$], showed increased reactivity relative to the described silicon(II) species, hydrostannylating two equivalents of acetophenone, with one further equivalent inserting into the IPr–Sn bond (Scheme 4.4b), highlighting the increased polarity of Sn–H bond relative to that of the lighter congeners [25].

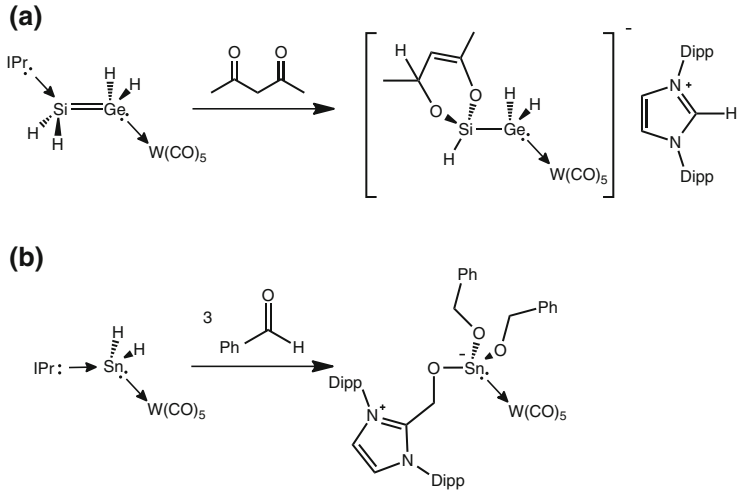

Scheme 4.4 Reaction of **a** a push-pull stabilised inorganic parent ethylene analogue with acetyl acetone and **b** reaction of push-pull stabilised parent stannylene with 3 equivalents of acetophenone

4.1.1.2 Reactivity of Group 14 Element(II) Hydride Complexes with Compounds Containing C=N and Unsaturated N–N Bonds

The majority of the reported reactivity of low-valence group 14 hydride complexes with unsaturated C–N and N–N bonds come from the group of Roesky [15]. The insertion of diethyl azodicarboxylate into the Ge–H moiety of (^{Dipp}nacnac)GeH proceeded readily at ambient temperature, forming the end-on insertion product ((^{Dipp}nacnac)GeN(CO_2Et)N(H)(CO_2Et), Scheme 4.5) [26]. In a related reaction, substituted diazomethane species were shown to undergo end-on insertion into the Ge–H bond of (^{Dipp}nacnac)GeH, subsequently rearranging to form Ge(II) hydrazone derivatives. Remarkably, in neither of these cases was any reactivity with the CO_2Et moiety been observed, despite the previously described insertion of the Ge–H moiety of (^{Dipp}nacnac)GeH into unsaturated C–O bonds (Scheme 4.5) [26].

The (^{Dipp}nacnac)GeH compound also underwent reaction with (TMS)N_3, and nitrous oxide (N_2O, Scheme 4.6) [22]. The former yielded a 1:1 mixture of two products; a Ge(II) azide, (^{Dipp}nacnac)GeN_3, and a tetra(amido) Ge(IV) species (Scheme 4.6). The terminal Ge(II) azide product likely forms through metathesis of the N–(TMS) fragment of the reactant with the Ge–H moiety. The latter is likely generated via sequential reaction of two equivalents of (TMS)N_3, both of which lose N_2 forming the nitrene, :N(TMS). The first equivalent inserts into the Ge–H bond, whilst the second equivalent activates the ligand, abstracting a proton from its backbone, oxidising the Ge(II) centre to the +4 oxidation state.

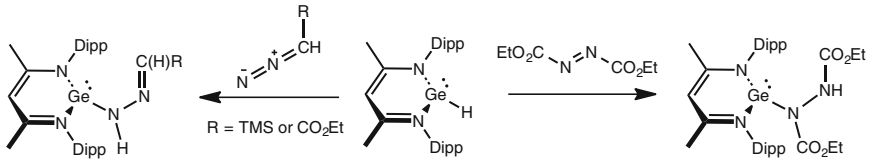

Scheme 4.5 The reaction of (^{Dipp}nacnac)GeH with unsaturated N–N bonds

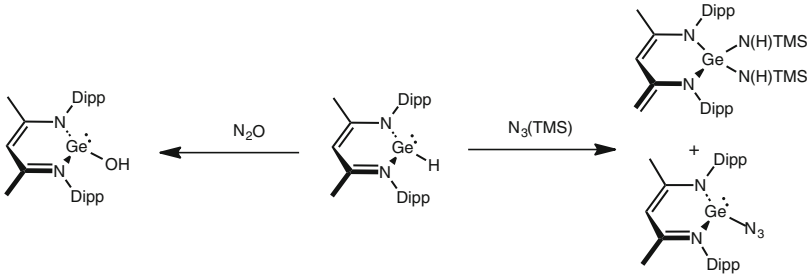

Scheme 4.6 Reactivity of (^{Dipp}nacnac)GeH with nitrous oxide and (trimethylsilyl)azide

Scheme 4.7 The reaction of (^{Dipp}nacnac)SnH with a carbodiimide

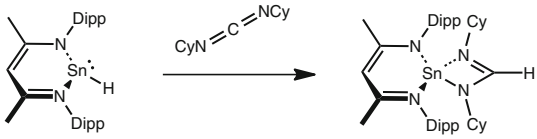

The same group also showed that the Sn(II) hydride, (^{Dipp}nacnac)SnH, hydrostannylated the C=N bond of carbodimides [19]. The reaction proceeded rapidly at ambient temperature to quantitatively yield the bicyclic product, (^{Dipp}nacnac)Sn(^{Cy}Am) (^{Cy}Am=CH{N(Cy)}$_2$, Cy=cyclohexyl; Scheme 4.7).

4.1.1.3 Reactivity of Group 14 Element(II) Hydride Complexes with Compounds Containing Unsaturated C–C Bonds

The hydroelementation of unsaturated C–C bonds, and in particular C–C double bonds, is one of the most challenging organic transformations, and is of paramount importance in numerous chemical fields. Until very recently, addition of group 14 element(II) E–H bonds across such unsaturations were unknown, whilst related reactions of group 14 element(IV) species require catalysts or a radical initiator [27–29]. However, remarkable developments in low-coordinate low-valent group 14 hydride chemistry has lead to such species being effective in uncatalysed hydrosilylation, hydrogermylation, and hydrostannylation of unsaturated C–C bonds.

Initial examples of hydrogermylation and hydrostannylation of alkynes were reported by Roesky and co-workers, using (^{Dipp}nacnac)GeH and (^{Dipp}nacnac)SnH. These reactions were rapid, being complete at ambient temperature in under an hour [15, 19, 22, 30]. The reactions of (^{Dipp}nacnac)GeH with alkynes yielded only (*E*)-isomers of the product alkenyl tetrelenes, as air-stable solids (Scheme 4.8). In the presence of functional groups (e.g. ester-substituted alkynes), only addition across the C–C triple bond was observed [15, 22]. Further, in reaction with the acetylene derivative, HCC(CO_2Et), no H_2 generation was observed through the formation of acetylide species, again with only the product of hydrogermylation of the alkyne moiety being observed. The case was similar with the Sn(II) species, (^{Dipp}nacnac)SnH, which rapidly underwent addition reactions with several functionalised alkynes (Scheme 4.8) [19, 30]. However, conversely to Ge(II) examples, the stannylene-substituted alkene products were formed as both (*E*) and (*Z*) isomers, in differing ratios. This may be due to the increased covalent radius of Sn relative to Ge, rendering the ligand's bulk more effective in directing the selectivity of the reactions for (^{Dipp}nacnac)GeH.

The related Si(II) hydride, (^{Dipp}nacnac)(H)Si·Ni$(CO)_3$, is also reactive towards alkynes, as demonstrated in the first published example of an uncatalysed hydrosilylation of an unsaturated C–C bond [31]. The reaction of this Si(II) hydride complex with disubstituted alkynes (e.g. PhCCPh) proceeded at 90 °C in toluene,

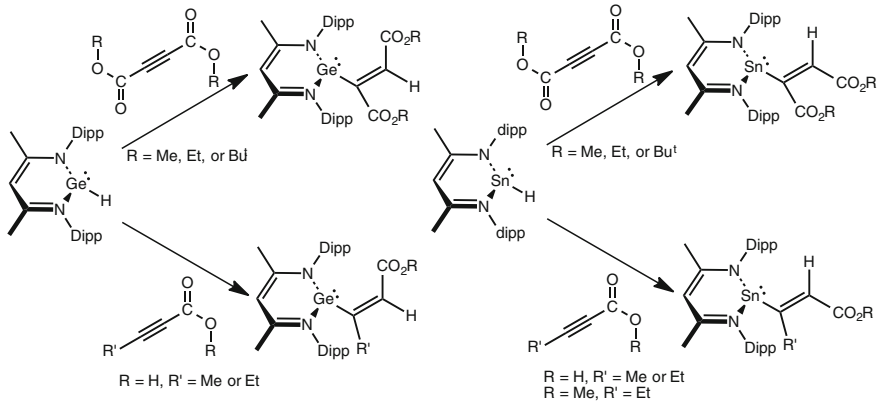

Scheme 4.8 Reactions of (^{Dipp}nacnac)GeH and (^{Dipp}nacnac)SnH with alkynes

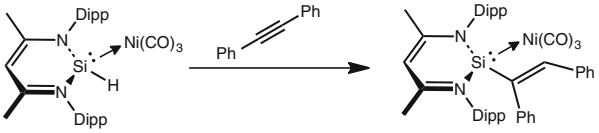

Scheme 4.9 The reaction of (^{Dipp}nacnac)Si(H)·Ni(CO)$_3$ with diphenylacetylene

yielding exclusively (*Z*) alkene products (Scheme 4.9). Although this occurs in the absence of an added catalyst, computational studies revealed that initial substrate coordination to the Ni(CO)$_3$ moiety occurs, followed by migration and insertion into the Si–H bond. This was confirmed by attempting the addition of (^{Dipp}nacnac)Si(H)·Ni(CO)$_3$ to diphenylacetylene under an atmosphere of CO, whereby no reaction was observed. Thus, in this example, it seems likely that the Ni(CO)$_3$ acts to activate the alkyne, and hence can be considered as intramolecularly catalysed hydrosilylation.

Baceiredo and co-workers have also reported on the reactivity of a Si(II) hydride, (^{P1}L)SiH, towards olefins, stabilised by a bidentate amide ligand featuring a pendant phosphine moiety (Scheme 4.10). Although somewhat forcing conditions were required (e.g. 8 equivalents of cyclopentene, 110 °C), the quantitative uncatalysed hydrosilylation of both terminal and internal unactivated alkenes was achieved [32]. Importantly, the reversible complexation of (TMS)ethylene to (^{P1}L)SiH was observed, forming a silirane ((^{P1}L)Si(H){η^2-C_2H_4(TMS)}, Scheme 4.10). It was found that heating this species, generated through the [2+1] cycloaddition of an alkene to the Si(II) centre of (^{P1}L)SiH, led to the migration of the hydride onto one of the α-carbons of the silirane intermediate, forming (^{P1}L)Si{C_2H_4(TMS)} as a mixture of regio-isomers in the effective hydrosilyation of an alkene (Scheme 4.10). This observation highlights the importance of coordinative substrate activation for such group 14 element(II) hydride systems, and further suggests that lower

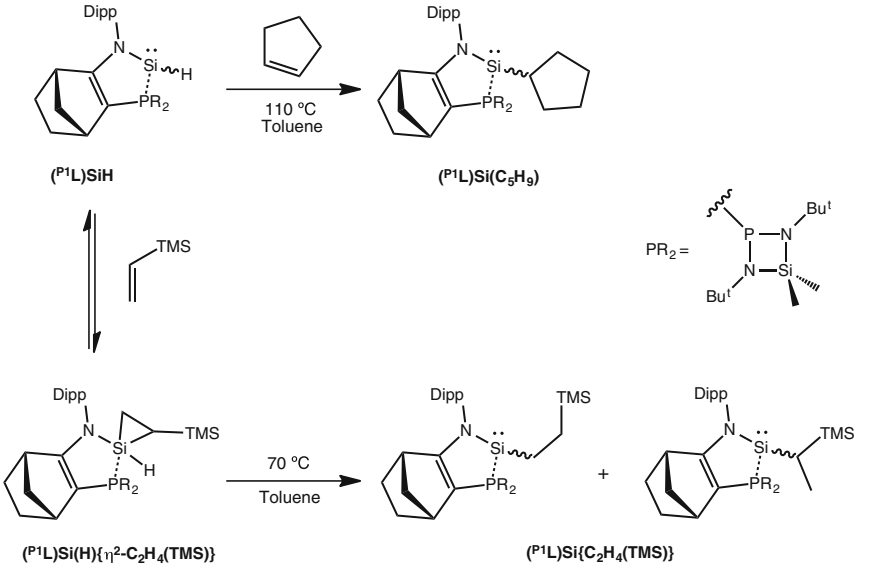

Scheme 4.10 The reaction of (^{P1}L)SiH with cyclopentene and (TMS)ethylene

coordinate systems are likely to be more reactive in the hydroelementation of unsaturated bonds.

Finally, Power and co-workers reported on examples of hydroelementation by dimeric group 14 element(II) hydride species. Here, the dimeric hydrides, $\{(^{Dipp}Terph)GeH\}_2$ and $\{(^{Dipp}Terph)Sn(\mu\text{-}H)\}_2$ (^{Dipp}Terph = 2,6-(Dipp)Ph), were reacted with (TMS)ethylene [33]. The former reaction mixture, after 48 h, contained two products: the known Ge(IV) hydride species, (^{Dipp}Terph)GeH_3, and a second product whose ^{1}H NMR spectrum was consistent with (^{Dipp}Terph)Ge$\{C_2H_4(TMS)\}$, i.e. the product of hydrogermylation of (TMS)ethylene. The latter Sn(II) hydride complex yielded one product quantitatively when reacted with (TMS)ethylene, after 48 h, presumed (^{Dipp}Terph)Sn$\{C_2H_4(TMS)\}$ again based on its ^{1}H NMR spectrum. Although neither of these compounds were structurally characterised, it was also shown that $\{(^{Dipp}Terph)GeH\}_2$ reacts with cyclopentene over the course of 48 h, giving the structurally characterised dimeric product, (^{Dipp}Terph)(C_5H_9)GeGe(H)(^{Dipp}Terph) (Scheme 4.11). This shows that only one hydride moiety had undergone addition to an olefin. Given that only this product is observed, it is highly unlikely that $\{(^{Dipp}Terph)GeH\}_2$ has any significant degree of dissociation in solution, unlike the previously discussed amido Ge(II) hydride, $\{(^{iPr}L^{\dagger})GeH\}_2$ ($^{iPr}L^{\dagger}$ = $[(Ar^{\dagger})N(SiPr^i_3)]^-$, $Ar^{\dagger}$ = 2,6-$(Ph)_2$CH-4-Pr^iPh; **1**), which we have shown dissociates readily at ambient temperature in hydrocarbon solvents (see Chap. 3).

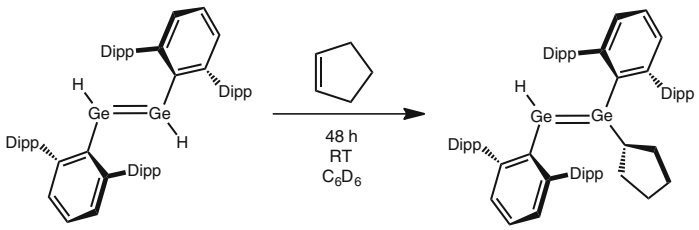

Scheme 4.11 Reaction of $\{(^{Dipp}Terph)GeH\}_2$with cyclopentene

4.2 Research Proposal

Although there are known examples of the reactivity of low-oxidation state group 14 hydride complexes, as discussed in Sect. 4.1, these studies are by no means exhaustive. Further, only higher-coordinate examples (i.e. coordination number ≥3) of group 14 element(II) hydride complexes have previously been known, where potential substrate coordination sites are quenched by either a chelating ligand, a Lewis acid, or a Lewis base. As discussed in Chap. 3, the Ge(II) and Sn(II) hydrides, **1** and **2** (**2** = $\{(^{iPr}L^{\dagger})Sn(\mu\text{-}H)\}_2$), readily dissociate when dissolved in hydrocarbon solvents, forming 2-coordinate Ge(II) and Sn(II) hydrides, $(^{iPr}L^{\dagger})(H)M$: (M = Ge or Sn). As such, **1** and **2** can be considered *pseudo*-2-coordinate Ge(II) and Sn(II) hydrides, and therefore possess a lone-pair of electrons and an empty *p*-orbital at their group 14 element centres. On this basis, we hypothesised that their reactivity may be increased relative to that of the previously discussed higher coordinate group 14 element(II) hydride complexes, due to a greater ability to coordinately activate unsaturated substrates. Indeed, the lower valent group 14 hydrides have already shown a greater hydridic potency when compared with group 14 element(IV) hydrides. Hence, the hydroelementation of unsaturates by hydrides **1** and **2** has been investigated.

4.3 Results and Discussion

4.3.1 Hydroelementation of Unsaturated C=O Bonds by Amido Group 14 Element(II) Hydride Complexes

Our initial studies in regard to the reactivity of **1** and **2** focused on the hydroelementation of C=O bonds, given the success in hydrogermylation and hydrostannylation of these bonds by low-oxidation state group 14 hydride complexes seen previously [14]. A deep orange sample of **1** in C_6D_6 instantly became colourless upon the addition of one equivalent of either *para*-methoxybenzaldehyde or

2,4-dimethyl-3-pentanone. ^{1}H NMR spectroscopic analyses of the crude reactions revealed quantitative formation of single products, with concomitant disappearance of the characteristic Ge–H hydride resonance, ordinarily observed at δ ~8.2 ppm at ambient temperature. For the former reaction, a new 2H methylene singlet was observed at δ = 4.58 ppm, whilst the latter reaction displayed a characteristic 1H methine triplet at 2.88 ppm, consistent with the formation of (^{iPr}L†)GeO{(CH_2)-*p*-MeOPh} (**3**) and (^{iPr}L†)GeOC(H)Pr$^i_2$ (**4**), respectively (Scheme 4.12). Scale-up of these two reactions, followed by recrystallisation of the products from cold hexane solutions led to the isolation of **3** and **4** in good yields. The ^{1}H NMR spectra of the crystalline species was in accordance with those of the NMR scale reactions described. The solid state structures of **3** and **4** revealed both compounds to be monomeric (Fig. 4.1), giving further evidence for the hydrido-germylene, (^{iPr}L†)(H)Ge:, being the true reactive species in solution. The Ge–O bond distances (**3**: 1.797 (3) Å, **4**: 1.8120(19) Å) are in keeping with those previously reported for alkoxy-germanium species (mean of reported Ge–O distances = 1.832 Å), whilst the N–Ge–O angles of those species (99.44(14) and 97.49(9)°, respectively) are concordant with the presence of a lone pair of electrons at the Ge(II) centres. Other bond lengths and angles are as would be expected, and are listed in Fig. 4.1.

Subsequently, related chemistry was carried out using **2**. The Sn(II) hydride immediately reacted with both *para*-methoxybenzaldehyde or 2,4-dimethyl-3-pentanone at ambient temperature, with the intense yellow solution in C_6D_6 decolourising instantly upon addition of the unsaturated species. The ^{1}H NMR spectra of the two reaction mixtures displayed single sets of ligand resonances which were similar to those observed for **3** and **4**, with no remaining aldehyde/ketone starting materials. That is, the spectrum of the reaction mixture of **2** with *para*-methoxybenzaldehyde displayed a singlet at δ = 4.90 ppm, consistent with

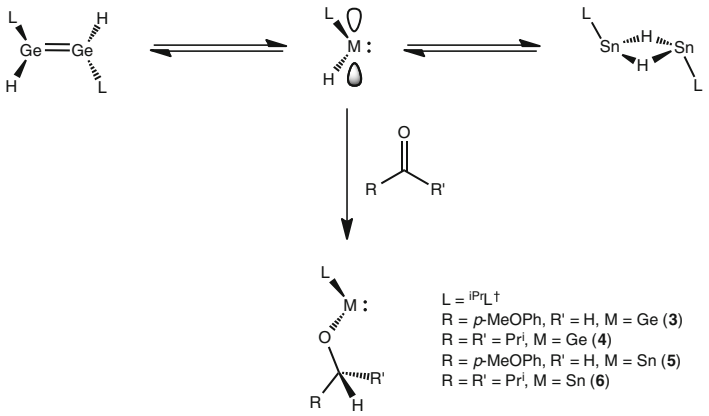

Scheme 4.12 The reactions of **1** and **2** with ketones and aldehydes

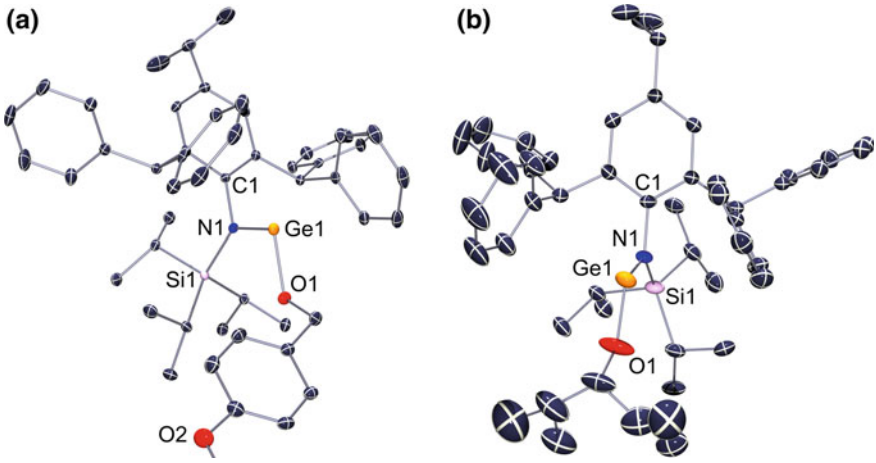

Fig. 4.1 ORTEP representations of **a** ($^{iPr}L^{\dagger}$)GeO{(CH_2)-*p*-MeOPh} (**3**), and **b** ($^{iPr}L^{\dagger}$)GeOC(H)Pr^{i}_2 (**4**) (hydrogen atoms omitted). Selected bond lengths (Å) and angles (°) for **3/4**: Ge1–O1 1.797(3)/1.8120(19), Ge1–N1 1.883(3)/1.877(2), Si1–N1 1.788(2)/1.789(2), O1–Ge1–N1 99.44(14)/97.49(9), C1–N1–Si1 116.28(2)/118.33(2), C1–N1–Ge1 110.36(2)/108.20(2), Si1–N1–Ge1 133.32(1)/133.46(2)

the formation of ($^{iPr}L^{\dagger}$)SnO{(CH_2)-*p*-MeOPh} (**5**), whilst that of the reaction mixture of **2** with 2,4-dimethyl-3-pentanone displayed a triplet at δ = 2.89 ppm, consistent with the formation of ($^{iPr}L^{\dagger}$)SnOC(H)Pr^{i}_2 (**6**) (Scheme 4.12). Both products were isolated as colourless crystalline solids upon scale-up of these two reactions. The solid state structures of **5** and **6** revealed them to be monomeric, as with the Ge(II) analogues, **3** and **4**. Their structures are shown in Fig. 4.2. As with **3** and **4**, the Sn–O bond lengths are in keeping with reported values (**5**: 1.998(4) Å, **6**: 2.020(5) Å, mean of reported Sn–O distances = 2.187 Å), whilst the N–Sn–O angles in both species are concordant with a lone-pair of electrons at the Sn(II) centres (**5**: 96.86(14)°, **6**: 94.2(2)°). Other bond lengths and angles are as would be expected, and are listed in Fig. 4.2.

This reactivity of **1** and **2** can be compared to that of the only other group 14 metal(II) hydride species, (^{Dipp}nacnac)EH (E = Ge or Sn), that are known to undergo addition with ketones. Whilst **1** and **2** rapidly reduce the bulky unactivated ketone, 2,4-dimethyl-3-pentanone, at ambient temperature, (^{Dipp}nacnac)GeH reacts only slowly (over 12 h) with activated ketones (e.g., O=C(Ph)(CF3)) [22], and forcing conditions (110 °C, 12 h) are required for (^{Dipp}nacnac)SnH to hydrostannylate the bulky aliphatic ketone, O=C(cyclopropyl)$_2$ [30]. It seems that, as hypothesised, the empty *p*-orbital available at the metal centres of **1** and **2** gives rise to their markedly enhanced reactivity, relative to the *intra*-molecularly base stabilised (^{Dipp}nacnac)EH species.

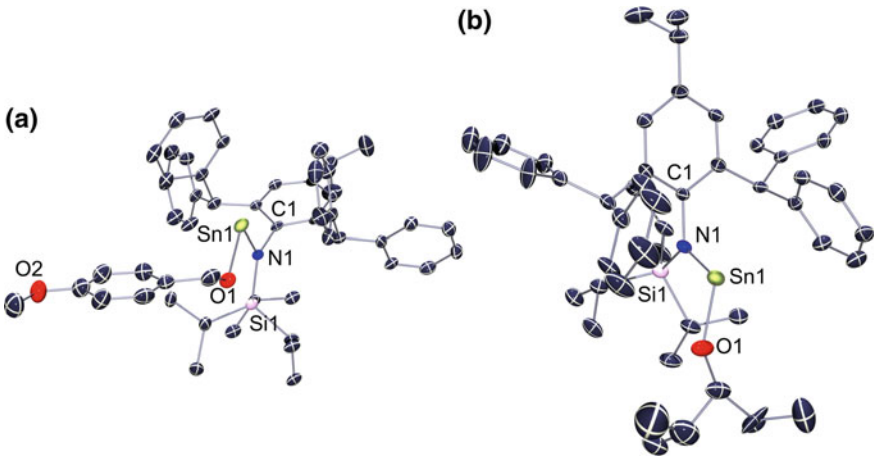

Fig. 4.2 ORTEP representations of **a** ($^{iPr}L^{\dagger}$)SnO{(CH_2)-*p*-MeOPh} (**5**), and **b** ($^{iPr}L^{\dagger}$)SnOC(H)Pr^{i}_2 (**6**) (hydrogen atoms omitted). Selected bond lengths (Å) and angles (°) for **5/6**: Sn1–O1 1.998(4)/2.020(5), Sn1–N1 2.113(3)/2.096(6), Si1–N1 1.771(4)/1.783(6), O1–Sn1–N1 96.86(14)/94.2(2), C1–N1–Si1 119.2(3)/116.9(4), C1–N1–Sn1 107.1(2)/110.3(4), Si1–N1–Sn1 133.6(2)/132.8(3)

4.3.2 Hydroelementation of Unsaturated C–C Bonds by Amido Group 14 Element(II) Hydride Complexes

Following the reactivity studies of **1** and **2** with C=O bonds, we sought to investigate the hydroelementation of less reactive C–C unsaturations. As an initial test, one equivalent of styrene was added to a sample of **1** dissolved in C_6D_6. The colour of the solution rapidly became bright yellow. A ^{1}H NMR spectroscopic analysis of the reaction mixture showed quantitative conversion to one new product, with consumption of the styrene and disappearance of the characteristic Ge–*H* resonance ($\delta = \sim 8.2$ ppm). The new signals suggested the presence of a single new ligand environment, with two new resonances: a broad peak at $\delta = -0.60$ ppm, and a multiplet at $\delta = 2.15$ ppm, each integrating to 2H. These were tentatively assigned to the terminal Ge–CH_2 and *β*–CH_2, respectively, of the product of hydrogermylation of styrene (Scheme 4.13), ($^{iPr}L^{\dagger}$)Ge$(CH_2)_2$Ph (**7**). Scale-up of the reaction, followed by recrystallisation from hexane at 4 °C yielded deep yellow crystals, the ^{1}H NMR spectrum of which was in keeping with the NMR scale reaction carried out prior. The IR spectrum of the crystals displayed no characteristic Ge–H stretches, expected at around 1800 cm^{-1}, implying no remaining Ge–H moiety, in contrast to that of the reaction of Power's {(^{Dipp}Terph)GeH}$_2$ with cyclopentene (vide supra) [33]. An X-ray crystallographic study of the crystalline product revealed it to be monomeric in the solid state, much like compounds **3–6**. The N1–Ge1–C45 angle of 106.08° is indicative of a stereoactive lone-pair of electrons at germanium. The Ge1–C45 distance (1.991(2) Å) is in keeping with previously reported Ge–C^{sp3} distances (mean of reported Ge–C^{sp3} distances = 1.969 Å),

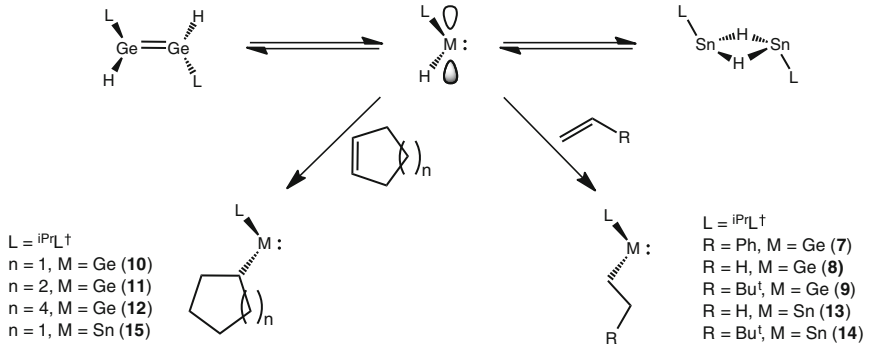

Scheme 4.13 Reactions of **1** and **2** with linear and cyclic unactivated alkenes

although two-coordinate species containing such bonds are to date very rare [34, 35]. The closest Ge···$C_{ortho\text{-}Ph}$ contact in the compound is 3.664(2) Å (Ge1–C45), which is only just within the sum of the van der Waals radii of the two elements (3.68 Å [36]). It is therefore highly unlikely that such a distance accounts for any real contact or degree of stabilisation. The N1 atom sits in a trigonal planar geometry (sum of angles around N1 = 359.89°), which is co-plannar with the central SiNGeC unit (Si1–N1–Ge1–C45 torsion = 2.27°), and hence the N-*p*-orbital lone pair likely overlaps with the empty *p*-orbital at Ge1. This could aid in stabilising the monomeric nature of **7** by decreasing the propensity for intermolecular donor-acceptor bonding between two monomeric germylenes.

Subsequently, several unactivated alkenes were reacted with **1**, with equally facile reactivity observed in all cases. The olefins studied were ethylene, 3,3-dimethyl-1-butene, cyclopentene, cyclohexene, and cyclooctene (Scheme 4.13). All stoichiometric reactions were complete in well under 10 min at ambient temperature, with no observable by-products (viz. CH-activation reactions of{(^{Dipp}Terph)GeH}$_2$ with cyclic alkenes) [33, 34]. All amido-alkyl germylenes were crystallographically characterised, and are monomeric in the solid state (Fig. 4.3), being the first examples of such species to date; metrical parameters are summarised in Table 4.1. Generally, there are no major deviations in the bond lengths and angles between these species. Not surprisingly, the cyclic alkyl species display slightly longer Ge1–C45 distances (cyclic alkyls generally >2 Å, with linear alkyls <2 Å), due to the greater effective bulk of these alkyl moieties over the linear alkyl derivatives. Further, likely due to steric demands, the Pr^i_3Si and alkyl moieties sit "*cis*" to the central N–Ge unit for all cyclic alkyl species, with the opposite being true for the linear alkyl species. In turn, this allows for considerably closer Ge···$C_{ortho\text{-}Ph}$ contacts in the former compounds (3.257(3), 3.307(3), 3.330(3) Å; cyclopentyl (**10**), cyclohexyl (**11**), cyclooctyl (**12**)), which may account for some energy gain in this conformation preference [36]. It is likely this conformational preference causes the slightly increased N1–Ge1–C45 angles in the bulkier cyclic-alkyl species (average of N–Ge–C for **8–9**: 105.54°, and for **10–12**: 109.45°),

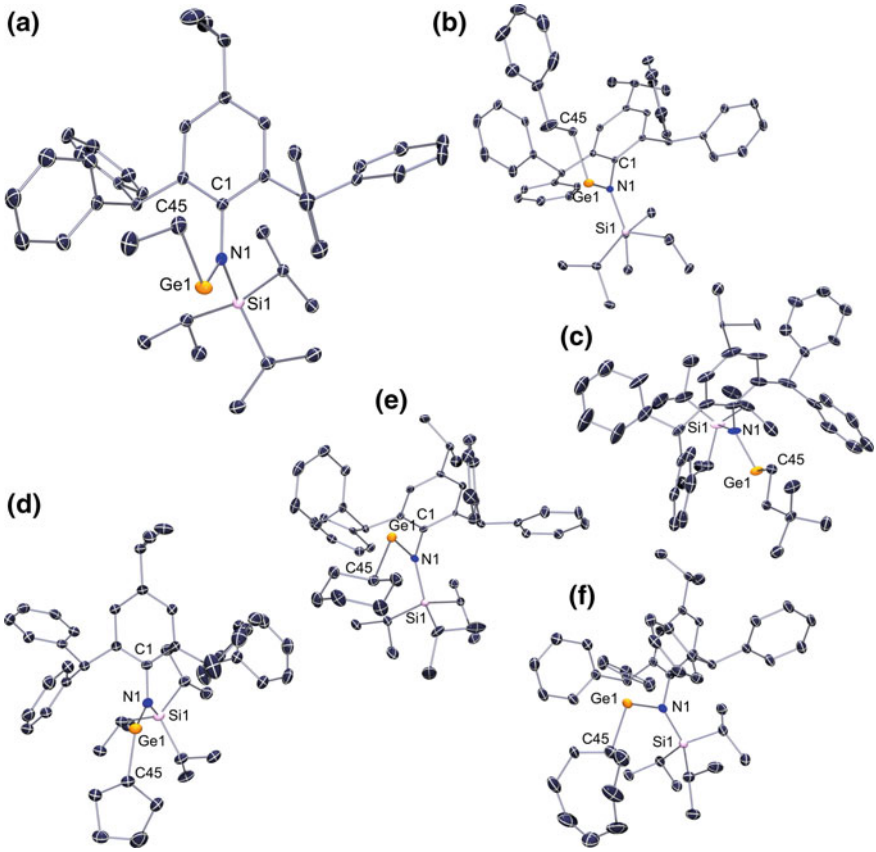

Fig. 4.3 ORTEP represenations of **a** ($^{iPr}L^{\dagger}$)GeEt (**8**), **b** ($^{iPr}L^{\dagger}$)Ge$(CH_2)_2$Ph (**7**), **c** ($^{iPr}L^{\dagger}$)Ge$(CH_2)_2$Bu^t (**9**), **d** ($^{iPr}L^{\dagger}$)Ge(C_5H_9) (**10**), **e** ($^{iPr}L^{\dagger}$)Ge(C_6H_{11}) (**11**), and **f** ($^{iPr}L^{\dagger}$)Ge(C_8H_{15}) (**12**) (ellipsoids at 30% probability, hydrogen atoms omitted). For relevant bond lengths (Å) and angles (°), see Table 4.1

Table 4.1 Bond distances (Å) and angles (°) for compounds **7**–**12**

	8	**7**	**9**	**10**	**11**	**12**
Ge–N	1.874(2)	1.865(2)	1.875(8)	1.885(3)	1.904(2)	1.898(2)
Ge–C	1.990(3)	1.991(2)	1.991(7)	1.999(4)	2.031(3)	2.054(5)
N–Ge–C45	105.42(1)	106.80(8)	104.41(3)	110.62(1)	107.97(1)	109.77(2)
SiNGeC45	5.43(1)	2.27(1)	2.14(4)	10.68(3)	3.24(2)	1.32(3)
Ge···$C^a_{ortho\text{-Ph}}$	3.461(3)	3.664(2)	3.532(1)	3.257(3)	3.307(3)	3.330(3)

The corresponding ORTEP diagrams for these compounds can be found in Fig. 4.3
[a]The closest contact is given

relative to the related angles in the linear species. It is worthy of note that previously reported low-coordinate Ge(II) species, such as *pseudo*-one-coordinate germanium (II) cations (e.g. $[(^{TMS}L^*)Ge]^+$, $^{TMS}L^*$ = [(TMS)N(Ar*)]$^-$, Ar* = 2,6-$(Ph_2CH)_2$-4-MePh) [37] have much shorter Ge···Aryl contacts ($[(^{TMS}L^*)Ge]^+$: Ge···C_{Aryl} = 2.65 Å mean), and are not considered as highly stabilising interactions. Hence, such interactions in **8–12** are likely not important in stabilising these low-coordinate species. Note that pure samples of the cyclic alkyls, **11** and **12**, showed small amounts of $\{(^{iPr}L^\dagger)GeH\}_2$ when dissolved in C_6D_6 at ambient temperature, suggesting some reversible character in the reactions that yielded them (vide infra). It is clear that the reactions involving **1** are far more rapid than any previously reported analogous reactions (e.g. the reaction of $\{(^{Dipp}Terph)GeH\}_2$ with cyclopentene or (TMS)ethylene [33]), giving further substantiation to the hypothesised importance of a low-coordination environment in the activation, and further hydroelementation of unsaturated species by such group 14 element(II) hydride complexes.

Given the unprecedented reactivity of **1** towards unsaturated C–C bonds, we also wished to study the reactivity of the Sn(II) hydride complex, **2**, towards similar alkenes. As was the case with **1**, **2** reacts with unactivated alkenes rapidly at ambient temperature, as observed by ^{1}H NMR spectroscopy. This was clearly demonstrated by reaction of a sample of **2** dissolved in C_6D_6 with dry ethylene gas. The ^{1}H NMR spectrum of the reaction mixture clearly indicated the formation of one major product, with small (<10%) amounts of protonated ligand ($^{iPr}L^\dagger H$) and also H_2, due to the thermal instability of **2**. A characteristic broad resonance at $\delta = -0.82$ ppm in the ^{1}H NMR spectrum of the reaction mixture, which integrated to 2H, was suggestive of a Sn–CH_2 moiety in the putative ($^{iPr}L^\dagger$)SnEt product (**13**), formed through hydrostannylation of ethylene (viz. ($^{iPr}L^\dagger$)GeEt). Concomitantly, the Sn–*H* resonance of **2**, typically observable at $\delta = \sim 17$ ppm at ambient temperatures, had entirely diminished. Repeating the reaction in toluene on a preparative scale yielded large yellow crystals, the ^{1}H NMR spectrum of which was consistent with the NMR scale reaction. Structural analysis of this product, as well as analysis of those from analogous reactions with the terminal alkene 3,3-dimethylbut-1-ene (($^{iPr}L^\dagger$)Sn(CH_2CH_2)Bu^t, **14**), and cyclopentene (($^{iPr}L^\dagger$)Sn(C_5H_9), **15**), revealed them to be the first examples of structurally characterised monomeric alkyl-amido stannylenes (Fig. 4.4) [38].

As with the Ge(II) species, the amido-alkyl Sn(II) derivatives exhibit stereoactive lone-pairs of electrons at the Sn(II) centres, as indicated by their N1–Sn1–C45 angles (101.74(1)–105.7(6)°). All display terminal Sn–C bond lengths (2.168(5)–2.208(2) Å) consistent with those previously published for tin alkyl species (mean of previously reported Sn–C distances = 2.140 Å). Significant metrical data can be found in Table 4.2. Sn1–C45 distances are expectedly longer than the germanium analogues, due to the greater covalent radius of Sn(II) relative to Ge(II). The closest Sn···$C_{ortho\text{-}Ph}$ contacts are much shorter for the Sn(II) alkyls, **13–15** (e.g. ($^{iPr}L^\dagger$)SnEt: Sn···$C_{ortho\text{-}Ph}$ = 3.173(6) Å), than those for the Ge(II) derivatives, **8–10** (e.g. ($^{iPr}L^\dagger$)GeEt: Ge···$C_{ortho\text{-}Ph}$ = 3.461(3) Å), and lie well within the sum of the van der Waals radii of the two elements (3.86 Å [36]). This makes stabilising Sn···$C_{ortho\text{-}Ph}$

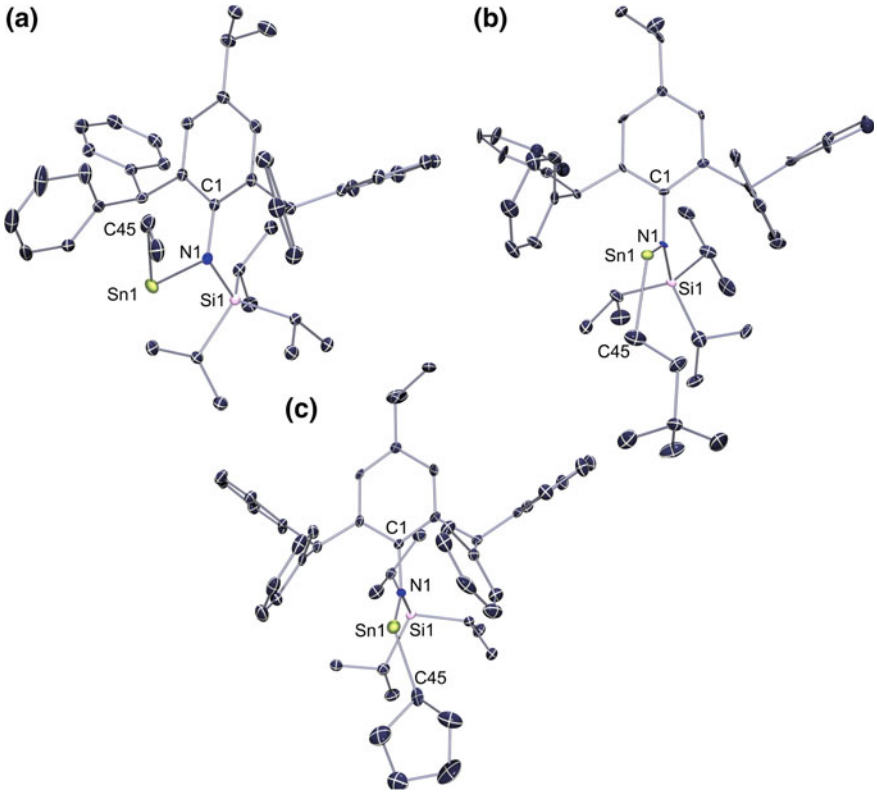

Fig. 4.4 ORTEP representations of **a** ($^{iPr}L^{\dagger}$)SnEt (**13**), **b** ($^{iPr}L^{\dagger}$)Sn(C_2H_4)Bu^t (**14**), and **c** ($^{iPr}L^{\dagger}$)Sn(C_5H_7) (**15**) (ellipsoids at 30% probability, hydrogen atoms omitted). For relevant bond lengths and angles see Table 4.2

Table 4.2 Bond distances (Å) and angles (°) for compounds **13–15**

	13	**14**	**15**
Sn–N	2.123(3)	2.127(1)	2.127(4)
Sn–C45	2.182(3)	2.208(2)	2.168(5)
N–Sn–C45	101.74(1)	105.7(6)	102.80(2)
SiNSnC45 (torsion)	18.19(1)	4.22(1)	13.55(3)
Sn···$C^a_{ortho\text{-}Ph}$	3.239(3)	3.263(2)	3.173(6)

The corresponding ORTEP diagrams for these compounds can be found in Fig. 4.4

[a]The closest contact is given

contacts in the former systems more likely than in the latter. As with the Ge(II) alkyls, **7–12**, the overlap of the *p*-based lone pair of N1 with the empty *p*-orbital on Sn1 likely aids in stabilising the monomeric character of **13–15**, with the sum of angles around the trigonal planar N1 being close to 360° in all cases.

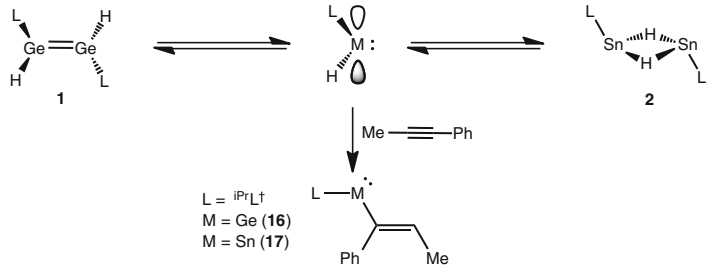

Scheme 4.14 The hydrometallation of 1-phenylpropyne by **1** and **2**

Finally, to observe whether the double-hydroelementation of alkynes was possible, **1** and **2** were both reacted with 1-phenyl-1-propyne, in a 2:1 stoichiometry. In both cases, only the mono-addition product could be observed and isolated, which is not surprising considering the pronounced steric bulk of the amide ligand involved. A ^{1}H NMR spectroscopic analysis of the reaction mixture indicated consumption of both the hydride and the alkyne starting materials, with a single new product for both the Ge(II) and Sn(II) systems observed after 15 min at ambient temperature. This rapid reactivity is in accordance with previous examples of group 14 element(II) alkyne hydroelementations [15, 19, 22, 30]. Both spectra displayed a broadened down-field resonance attributable to a single alkenyl proton. However, discerning between the presence of either the potential (*E*) or (*Z*) isomers, or either regio-isomers was not possible by this NMR spectroscopic study. Both compounds were recrystallised from concentrated hexane solutions at 4 °C, yielding large yellow blocks of **16** ((^{iPr}L†)GeC(Ph)C(Me)H) and **17** ((^{iPr}L†)SnC(Ph)C(Me)H) (Scheme 4.14). X-ray structural analysis confirmed both tin and germanium derivatives to have hydrometalated the alkyne only once (Fig. 4.5), with the phenyl group present at the metal bound carbon in both cases (Scheme 4.14). As one would expect, the αβ-CC distances are indicative of double bonds (Sn = 1.324 (1) Å, Ge = 1.348(2) Å). Further evidence of this is the planarity of this fragment, clearly highlighting the sp^2 character of the bonding between C45 and C46. Aside from these structural characteristics, all other distances/angles are similar to those of the alkyl derivatives, and do not warrant an in-depth discussion, but can be found in Fig. 4.5.

4.3.2.1 Reversible Alkene Hydroelementation and Alkene Isomerisation

It was observed that dissolving pure samples of **11** and **12** in C_6D_6 led to small amounts of {(^{iPr}L†)GeH}$_2$ in their ^{1}H NMR spectra. Further, following work-up, hexane solutions of **10**, **11**, and **12** yielded small amounts of starting material, **1**, despite confirming full conversion to products by ^{1}H NMR spectroscopic analyses of the crude reaction mixtures. For the Sn(II) alkyl compound, (^{iPr}L†)Sn(C_5H_9)

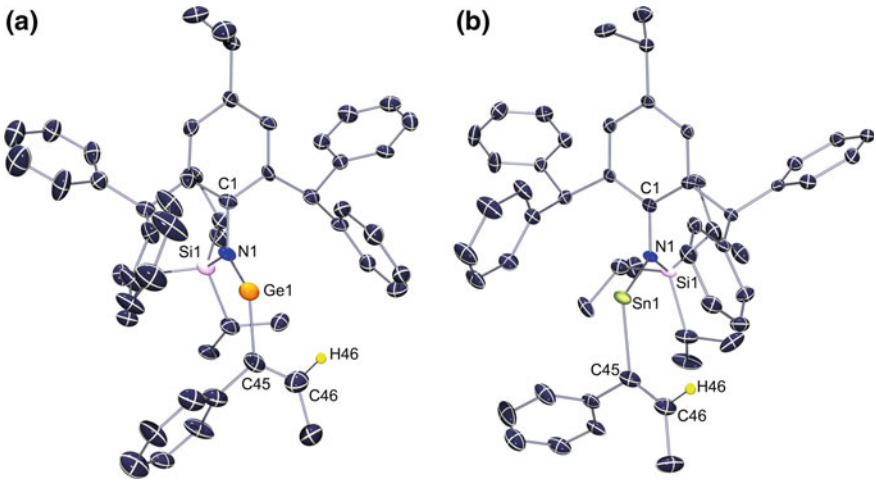

Fig. 4.5 ORTEP representations of **a** ($^{iPr}L^{\dagger}$)GeC(Ph)C(Me)H (**16**), and **b** ($^{iPr}L^{\dagger}$)SnC(Ph)C(Me)H (**17**) (ellipsoids at 30% probability, hydrogen atoms omitted, aside from the H46). Selected bond lengths and angles for **16**: Ge1–N1 1.882(5), Ge1–C45 1.991(9), C45–C46 1.348(2), Ge···$C_{ortho\text{-}Ph}$ 3.271(8), N1–Ge1–C45 110.28(4), Si1–N1–Ge1–C45 7.61(6). **17**: Sn1–N1 2.122(5), Sn1–C45 2.229(9), C45–C46 1.324(1), Sn···$C_{ortho\text{-}Ph}$ 3.256(7), N1–Sn1–C45 107.13(3), Si1–N1–Sn1–C45 8.84(5)

(**15**), slow decomposition in C_6D_6 solution was observed (complete after 4 days at ambient temperature), yielding largely $^{iPr}L^{\dagger}H$ and cyclopentene as soluble products, alongside H_2, as assessed by NMR spectroscopy. The same species is stable for extended periods in the presence of a ten fold excess of cyclopentene, even with heating at 80 °C. These observations strongly suggest reversibility in the addition of the hydride complexes **1** and **2** to cyclic alkenes (Scheme 4.15).

The postulated reversibility was confirmed by a VT ^{1}H NMR spectroscopic study of **11**. Using an alternative synthesis of this compound via addition of the Grignard reagent, (cyclohexyl)MgBr, to ($^{iPr}L^{\dagger}$)GeCl, pure **11** was isolated in good yields, to ensure no {($^{iPr}L^{\dagger}$)GeH}$_2$ was present. A sample of this dissolved in C_6D_6 was then heated to 60 °C for 10 min, allowing any dynamic processes to equilibrate. A subsequent ^{1}H NMR spectrum collected at this temperature showed the appearance of a new set of signals corresponding to both cyclohexene and **1**.

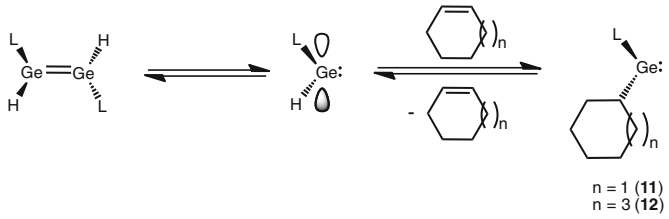

Scheme 4.15 The revesible hydrogermylation of cyclic alkenes by {($^{iPr}L^{\dagger}$)GeH}$_2$ (**1**)

Subsequently cooling the solution to ambient temperature for one hour resulted in near quantitative regeneration of **11**. As expected, a similar effect was seen for **12**, although a quantitative study was not carried out on this species. We contend that such reversibility arises from the β-hydride elimination from the alkyl substituent in **11** and **12**. This compares to one related reversible reaction between (^{Mes}nacnac)GeH and a phosphalkyne, whereby a P–H bond of the phophalkenyl hydrogermylation product is reversibly cleaved [39]. Note that direct observation of the reversibility of tin(II) hydride addition to cyclopentene was thwarted by the instability of **2**, resulting in decomposition of this species and the eventual presence of just ^{iPr}L†H and cyclopentene in the reaction mixture. However, linear Sn(II) alkyls, **13** and **14**, showed surprising thermal stability in solution, with no observable decomposition after heating at 80 °C for 18 h, without the presence of excess alkene. This implies that the instability of **15** is due to its dissociation into cyclopentene and the thermally unstable **2**, through β-hydride elimination. This phenomenon may be attributable to the relatively close E···β-H contacts in these amido-alkyl terelenes, estimates of which can be taken from their solid state structures (Table 4.3). In all cases, these distances are somewhat smaller than the sum of the van der Waals radii of E and H (i.e. sum of Ge and H = 3.21 Å, sum of Sn and H = 3.35 Å).

In order to quantify the propensity for **11** to dissociate to **1** and cyclohexene, a Van't Hoff analysis of this process was carried out over the temperature range 304–314 K in 2 K increments, on a solution of **11** in C_6D_6 (Fig. 4.6). This revealed the reaction to be exothermic ($\Delta H^{\circ} = -172$ kJ mol^{-1}). The reaction has a large entropic factor ($\Delta S^{\circ} = 395$ J mol^{-1}), which may be expected given the bimolecular nature of the reaction. These values give a Gibbs free energy of −54 kJ mol^{-1} at 298 K, which, being mildly exergonic, is in keeping with the equilibrium favouring **11** at ambient temperatures, and the need for higher temperatures to induce any notable quantities of free cyclohexene and **1**. A DFT analysis of the reaction pathway for the dissociation of (^{iPr}L†)Ge(C_6H_{11}) to (^{iPr}L†)(H)Ge: and cyclohexene confirms that the mechanism likely occurs via a β-hydride elimination, through interaction of the β-hydrogen of the cyclic alkyl moiety with the empty *p*-orbital at the Ge(II) centre. The computed value for ΔG_{298}° is −44 kJ mol^{-1}, concordant with the experimental value of −54 kJ mol^{-1}. Whilst the DFT study (at the M062X+D3

Table 4.3 Distances between the group 14 element (E) centres and cyclic alkyl β-hydrogens in amido-alkyl tetrelenes, (^{iPr}L†)ER (E = Ge or Sn, R = a cyclic alkyl)

E	R	E···β-H distance (Å)[a]
Ge	C_5H_9	2.702
Ge	C_6H_{11}	2.825
Ge	C_8H_{15}	2.620
Ge	C_8H_{13}	2.888
Sn	C_5H_9	2.994

[a]The closest contact is given

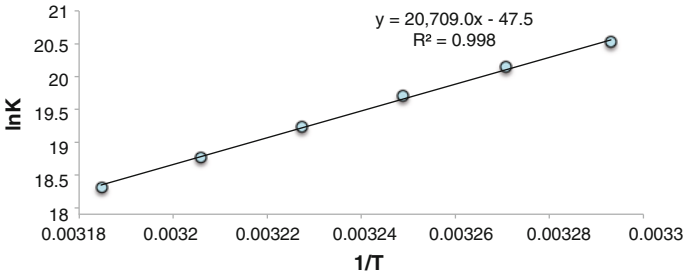

Fig. 4.6 Graphical representation of a Van't Hoff analysis of the reversible hydrogermylation of cyclohexene by **1**

(ABC)/def2-TZVPP level of theory) included dispersion forces (i.e. the D3 term), which likely play a part in this equilibrium, they don't account for solvent effects. This may help explain the slight discrepancy observed between the experimental and theoretical values.

Further evidence for the reversible hydrogermylation of cyclic alkenes by **1** and **2**, and perhaps more so for the hypothesised β-hydride elimination mechanism, came from the reactions of **1** with 1,5-cyclooctadiene and 2-methyl-2-butene. In both of these cases, the expected direct addition products were not observed. Instead, species with isomerised alkyl moieties were isolated (Scheme 4.16). However, in each case, ^{1}H NMR spectroscopic analysis of the reaction mixture suggested two products after addition of the alkenes, and a single product after a further 18 h. Although difficult to ascertain the connectivity of the final 1,5-cyclooctadiene product from this ^{1}H NMR spectrum, it was noted that a C=C bond remained in the product. That is, alkenyl multiplets were observed at $\delta = 4.23$ ppm and 4.99 ppm, each integrating to 1H, implying only mono-hydrogermylation of the diene. However, from the ^{1}H NMR spectrum of the reaction with 2-methyl-2-butene, it was clear that the direct Markovnikov or anti-Markovnikov products were not formed due to the absence of key expected resonances. Scale-up and isolation of crystals of products from both reactions confirmed that in both cases alkene isomerisation had occurred, through X-ray crystallographic analyses (Fig. 4.7). The structure of the product from the reaction of **1** with 1,5-cyclooctadiene suggests that the cyclic diene effectively isomerised to 1,3-cyclooctadiene, which, after subsequent hydrogermylation by **1**, yields the 1-amidogermyl-cycloocta-2-ene (**18**, Scheme 4.16). This is clear due to the one considerably shorter C=C bond at the 2-position of the cyclooctyl ring of **18**. As outlined in Scheme 4.16, this reaction may proceed through sequential β-hydride elimination reactions, causing the isomerisation of 1,5-cyclooctadiene to 1,3-cyclooctadiene. The observation of **18** as the sole reaction product is understandable given that β-hydride elimination of its alkyl substituent can only yield 1,3-COD, and may act as a 'sink' for this isomerisation reaction. In the attempted

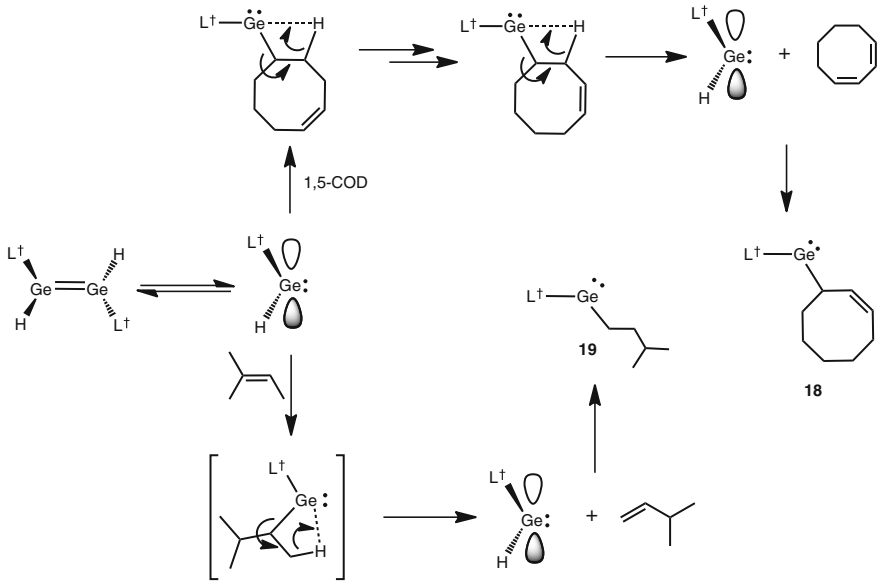

Scheme 4.16 The isomerisation and hydrogermylation of 1,5-COD and 2-methyl-2-butene by {($^{iPr}L^{\dagger}$)GeH} (**1**)

hydrogermylation of 2-methyl-2-butene, the isolated product was in fact 1-amidogermyl-3-methyl-butane, ($^{iPr}L^{\dagger}$)Ge(C_2H_4)Pr^i (**19**, Scheme 4.16), which likely occurs via first hydrogermylation of the alkene, β-hydride elimination generating 3-methyl-1-butene and **1**, and subsequent hydrogermylation of this isomerised alkene. Although only stoichiometric, such isomerisation has only been observed in TM systems [40–42], and highlights a potential novel application for such MG species in olefin isomerisation. Note that, due to the likely reversibility in the initial stages of these reactions, products were not attainable for the related Sn (II) system, again due to the instability of **2**. As with all other germylenes discussed, both **18** and **19** are monomeric in the solid state. The cyclooctyl ring of **18** features one short sp^2-hybridised C–C bond (C46–C47 = 1.372(6) Å), with all remaining distances in this ring in keeping with sp^3-hybridised C–C bonding. The Ge1–C45 distances of **18** (2.034(3) Å) and **19** (1.988(2) Å) are similar to previously discussed alkyl germylenes (**10**–**12**), as are their N1–Ge1–C45 angles (**18**: 108.69(1)°, **19**: 105.57(1)°), which is indicative of a lone-pair of electrons at the germanium centres. Neither compound shows signs of close Ge···Aryl contacts. All other distances and angles are as one would expect, and are given in Fig. 4.7.

The hydrometallation of tetrasubstituted alkenes was also attempted, using both 1,1,2,2-tetraphenylethylene and 2,3-dimethylbutene, but for both **1** and **2** no reaction was observed. This is likely a result of the bulk of both the alkene and the ligand, $^{iPr}L^{\dagger}$, which prevents the coordination of the alkene to the element(II)

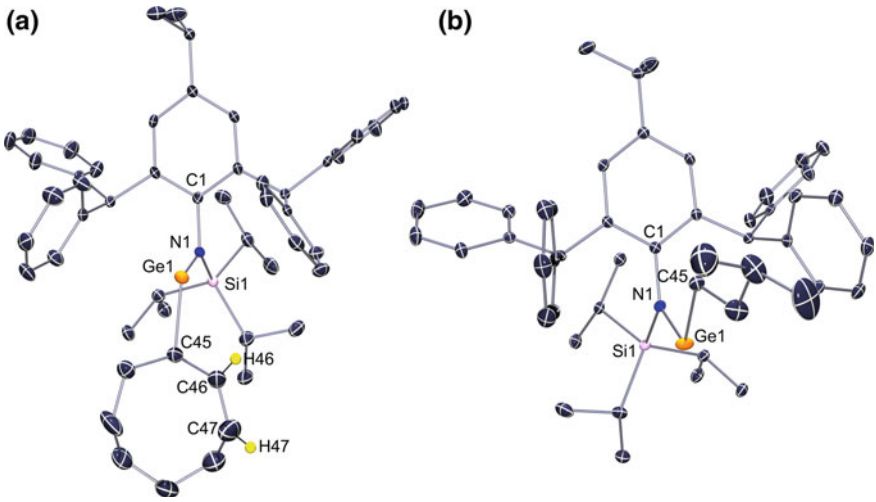

Fig. 4.7 ORTEP representation of **a** ($^{iPr}L^{\dagger}$)Ge($C_{8\text{-}}H_{11}$) (**18**), and **b** ($^{iPr}L^{\dagger}$)Ge(C_2H_4)Pr^i (**19**) (ellipsoids at 30% probability, hydrogen atoms, aside from H46 and H47 of **18**, omitted). Selected bond lengths and angles for **18**: Ge1–N1 1.890(2), Ge1–C45 2.034(3), C46–C47 1.372(6), Ge···$C_{ortho\text{-}Ph}$ 3.326(3), N1–Ge1–C45 108.69(1), Si1–N1–Ge1–C45 3.28(2); **19**: Ge1–N1 1.871 (3), Ge1–C45 1.988(2), Ge···$C_{ortho\text{-}Ph}$ 3.641(3), N1–Ge1–C45 105.57(1), Si1–N1–Ge1–C45 1.04 (1)

centres in **1** and **2**. Nevertheless, the hydrometallation reactions that have been discussed represent the only uncatalysed group 14 examples which occur readily at ambient temperature.

4.4 Conclusion

As demonstrated by the chemistry discussed in this chapter, the reactivity of the *pseudo*-2-coordinate hydrido terylenes, {($^{iPr}L^{\dagger}$)GeH}$_2$ (**1**) and {($^{iPr}L^{\dagger}$)Sn(μ-H)}$_2$ (**2**), is greatly increased through their low-coordinate nature in solution when compared to previously reported examples of higher coordinate group 14 element (II) hydride complexes. As such, we have demonstrated the first examples of the facile, room temperature hydrogermylation and hydrostannylation of unactivated terminal and internal alkenes. Further, and again aided by the low-coordinate nature of **1** and **2** in solution, the reversible hydrometallation of cyclic alkenes has been observed and quantified. This phenomenon has allowed for the facile stoichiometric isomerisation of alkenes at a main-group centre. This display of reactivity highlights the potential group 14 elements have in functionalisation chemistry, and stand as a promising platform for the investigation of the potential applications of these elements to catalytic transformations.

4.5 Experimental

(^{iPr}L†)GeOCH$_2$(4-OMePh) (3) To a solution of {(^{iPr}L†)GeH}$_2$ (0.20 g, 0.14 mmol) in toluene (15 mL) was added *p*-anisaldehyde (26 μL, 0.21 mmol) and the reaction mixture stirred at room temperature for 3 h. Volatiles were subsequently removed in vacuo, the residue extracted into hexane (20 mL), and the extract filtered and concentrated to *ca.* 10 mL. Storage at −30 °C for 3 days yielded large pale yellow crystals of **3** (185 mg, 62%). M.p.: 63–73 °C; ^{1}H NMR (C_6D_6, 400 MHz, 298 K), δ = 0.99 (d, $^3J_{HH}$ = 6.8 Hz, 6H, Ar†-*p*-CH(C*H*$_3$)$_2$), 1.33 (d, $^3J_{HH}$ = 7.6 Hz, 18H, SiPr$^i_3$-CH(C*H*$_3$)$_2$), 1.99 (sept, $^3J_{HH}$ = 7.6 Hz, 3H, SiPr$^i_3$-C*H*(CH$_3$)$_2$), 2.53 (sept, $^3J_{HH}$ = 6.8 Hz, 1H, Ar†-*p*-C*H*(CH$_3$)$_2$), 3.35 (s, 3H, GeOC(H)-$_2$-*p*-*Me*OPh), 4.58 (s, 2H, GeOC*H*-$_2$), 6.37 (s, 2H, C*H*Ph$_2$), 6.82–7.39 (m, 22H, Ar-C*H*); ^{13}C{^{1}H} NMR (C_6D_6, 75.5 MHz, 298 K), δ = 15.2 (SiPr$^i_3$-*C*H(CH$_3$)$_2$), 20.0 (SiPr$^i_3$-CH(*C*H$_3$)$_2$), 24.1 (Ar†-*p*-CH(*C*H$_3$)$_2$), 33.8 (Ar†-*p*-*C*H(CH$_3$)$_2$), 52.3 (*C*HPh$_2$), 54.8 (GeOCH$_2$-*p*-*Me*OPh), 65.5 (GeO*C*H$_2$), 113.8, 126.6, 127.4, 128.7, 128.9, 129.0, 130.2, 131.3, 135.2, 142.7, 144.3, 144.5, 145.1, 159.3 (Ar-*C*); ^{29}Si{^{1}H} NMR (C_6D_6, 80 MHz, 298 K), δ = 8.3; IR, ν/cm^{-1} (ATR): 3060 (w), 3026 (w), 1942 (w), 1869 (w), 1600 (bm), 1511 (m), 1448 (s), 1430 (m), 1245 (s), 1228 (m), 1116 (m), 1038 (s), 1007 (m), 876 (s), 828 (s), 737 (s), 655 (s); MS/EI *m/z* (%): 790.3 (M$^+$-Pr^i, 7), 623.4 (^{iPr}L$^{\dagger+}$, 61), 580.3 (^{iPr}L$^{\dagger+}$-Pr^i, 100).

(^{iPr}L†)GeOC(H)Pr-$^i_2$ (4) This compound was prepared in a similar manner to (^{iPr}L†)GeOCH$_2$(4-OMePh), but using {(^{iPr}L†)GeH}$_2$ (0.20 g, 0.14 mmol) and 2,4-dimethyl-3-pentanone (41 μL, 0.29 mmol). The product was isolated by extraction of the crude reaction residue into hexane (20 mL), and the extract filtered and concentrated to *ca.* 10 mL. Storage of the filtrate at −30 °C for 3 days yielded large pale yellow crystals of **4** (70 mg, 30%). M.p.: 194–204 °C; ^{1}H NMR (C_6D_6, 400 MHz, 298 K), δ = 0.70 (d, $^3J_{HH}$ = 6.8 Hz, 6H, GeOC(H)(C(H)C*H*$_3$)$_2$), 0.77 (d, $^3J_{HH}$ = 6.8 Hz, 6H, GeOC(H)(C(H)(C*H*$_3$)$_2$), 0.97 (d, $^3J_{HH}$ = 6.8 Hz, 6H, Ar†-*p*-CH(C*H*$_3$)$_2$), 1.36 (b, 18H, SiPr$^i_3$-CH(C*H*$_3$)$_2$), 1.61 (v. oct, $^3J_{HH}$ = 5.2 Hz, $^3J_{HH}$ = 5.2 Hz, 2H, GeOC(H)(C(*H*)(CH$_3$)$_2$)$_2$), 2.24 (b, 3H, SiPr$^i_3$-C*H*(CH$_3$)$_2$), 2.52 (sept, $^3J_{HH}$ = 5.2, 1H, Ar†-*p*-C*H*(CH$_3$)$_2$), 2.88 (t, $^3J_{HH}$ = 5.0 Hz, 1H, GeOC(*H*)(C(H)(CH$_3$)$_2$)$_2$), 6.43 (s, 2H, C*H*Ph$_2$), 6.94–7.38 (m, 22H, Ar-C*H*); ^{13}C{^{1}H} NMR (C_6D_6, 75.5 MHz, 298 K), δ = 14.6 (SiPr$^i_3$-CH(*C*H$_{3-}$)$_2$), 19.6 (d, GeOC(H)(C(H)*C*H$_3$)$_2$), 19.7 (SiPr$^i_3$-*C*H(CH$_{3-}$)$_2$), 24.0 (Ar†-*p*-C(H)(*C*H$_3$)$_2$), 31.3 (GeOC(H)(*C*(H)CH$_3$)$_2$), 33.8 (Ar†-*p*-*C*(H)(CH$_3$)$_2$), 52.0 (*C*(H)Ph$_2$), 83.7 (GeO*C*(H)(C(H)CH$_3$)$_2$), 126.6, 127.1, 127.93, 128.2, 128.4, 128.6, 129.0, 130.3, 131.2, 142.5, 144.2, 144.6, 145.2, 145.8 (Ar-*C*); ^{29}Si{^{1}H} NMR (C_6D_6, 80 MHz, 298 K), δ = 8.8; IR, ν/cm^{-1} (ATR): 3060 (w), 3028 (w), 2362 (w), 1801 (w), 1701 (w), 1653 (w), 1599 (w), 1387 (m), 1365 (s), 1228 (m), 1158 (m), 1033 (m), 987 (m), 972 (m), 880 (s), 832 (s), 756 (s), 662 (s); MS/EI *m/z* (%): 811.5 (M$^+$, 2), 768.3 (M$^+$-Pr^i, 15); anal. calc. for $C_{51}H_{67}GeNOSi$: C, 75.55%; H, 8.33%; N, 1.73%; found: C, 75.46%; H, 8.34%; N, 1.82%.

(^{iPr}L†)SnOCH$_2$(4-MeOPh) (5) This compound was prepared similarly to (^{iPr}L†)GeOCH$_2$(4-OMePh), but using {(^{iPr}L†)Sn(μ-H)}$_2$ (0.20 g, 0.27 mmol), and *p*-anisaldehyde (38 mg, 0.28 mmol). The reaction residue, following removal of solvents in vacuo, was extracted into warm hexane, and filtered. The filtrate was concentrated to ~2 mL and stored at −30 °C for 1 week to afford large clusters of colourless plates (100 mg, 47%). M.p.: 64–74 °C; ^{1}H NMR (C_6D_6, 400 MHz, 298 K), δ = 0.99 (d, $^3J_{HH}$ = 6.8 Hz, 6H, Ar†-*p*-CH(C*H*$_3$)$_2$), 1.43 (d, $^3J_{HH}$ = 7.6 Hz, 18H, SiPr$^i_3$-CH(C*H*$_3$)$_2$), 2.17 (sept, $^3J_{HH}$ = 7.6 Hz, 3H, SiPr$^i_3$-C*H*(CH$_3$)$_2$), 2.54 (sept, $^3J_{HH}$ = 5.2 Hz, 1H, Ar†-*p*-C*H*(CH$_3$)$_2$), 3.37 (s, 3H, Ar-*p*-O*Me*), 4.90 (s, 2H, SnOC*H*$_2$), 6.29 (s, 2H, C*H*Ph$_2$), 6.87–7.35 (m, 22H, Ar-C*H*); ^{13}C{^{1}H} NMR (C_6D_6, 75.5 MHz, 298 K), δ = 15.6 (SiPr$^i_3$-*C*H(CH$_3$)$_2$), 20.2 (SiPr$^i_3$-CH(*C*H$_3$)$_2$), 24.2 (Ar†-*p*-CH(*C*H$_3$)$_2$), 33.8 (Ar†-*p*-*C*H(CH$_3$)$_2$), 52.3 (*C*HPh$_2$), 54.9 (Ar-*p*-O*Me*), 65.6 (SnO*C*H$_2$), 113.9, 126.6, 127.3, 128.5, 128.6, 128.8, 129.6, 130.3, 131.5, 138.1, 143.0, 144.6, 144.8, 145.6, 159.1 (Ar-*C*); ^{29}Si{^{1}H} NMR (C_6D_6, 80 MHz, 298 K), δ = 7.0; ^{119}Sn{^{1}H} NMR (C_6D_6, 149 MHz, 298 K): δ = 193.6; IR, ν/cm^{-1} (ATR): 3059 (w), 3025 (w), 1945 (w), 1876 (w), 1600 (m), 1360 (m), 1300 (w), 1246 (s), 1057 (s), 1032 (s), 878 (s), 831 (s), 759 (m), 719 (s); MS/EI *m/z* (%): 697.3 ((^{iPr}L†)Sn$^+$-Pr^i, 100); anal. calc. for $C_{52}H_{61}NO_2SiSn$: C, 71.07%; H, 7.00%; N, 1.59%; found: C, 70.93%; H, 6.94%; N, 1.55%.

(^{iPr}L†)SnOC(H)Pr$^i_2$ (6) This compound was prepared similarly to (^{iPr}L†)GeOCH$_2$(4-OMePh), but using {(^{iPr}L†)Sn(μ-H)}$_2$ (0.20 g, 0.27 mmol), and 2,4-dimethyl-3-pentanone (40 μL, 0.28 mmol). The reaction residue, following removal of solvents in vacuo, was extracted into a diethyl ether/hexane mix (5 mL:10 mL), and this extract concentrated in vacuo until crystalline solid was seen to form. The solution was then warmed to redissolve the solid, and stored at −30 °C to induce crystallisation. Storage overnight afforded small colourless crystals (50 mg, 24%). M.p.: 172–186 °C; ^{1}H NMR (C_6D_6, 400 MHz, 298 K), δ = 0.79 (d, $^3J_{HH}$ = 6.8, 6H, SnOCH(CH(C*H*$_3$)$_2$)), 0.87 (d, $^3J_{HH}$ = 6.8 Hz, 6H, SnOCH(CH(C*H*$_3$)$_2$)), 0.98 (d, $^3J_{HH}$ = 6.8, 6H, Ar†-*p*-CH(C*H*$_3$)$_2$), 1.38 (br, 18H, SiPr$^i_3$-CH(C*H*$_3$)$_2$), 1.68 (v. oct, $^3J_{HH}$ = 5.2 Hz, $^3J_{HH}$ = 5.2 Hz, 2H, SnOCH(C*H*(CH$_3$)$_2$)$_2$), 2.32 (br, 3H, SiPr$^i_3$-C*H*(CH$_3$)$_2$), 2.54 (sept, $^3J_{HH}$ = 5.2 Hz, 1H, Ar†-*p*-C*H*(CH$_3$)$_2$), 2.89 (t, $^3J_{HH}$ = 5.0 Hz, 1H, GeOC*H*(CH(CH$_3$)$_2$)$_2$), 6.52 (s, 2H, C*H*Ph$_2$), 6.94–7.38 (m, 22H, Ar-C*H*); ^{13}C{^{1}H} NMR (C_6D_6, 75.5 MHz, 298 K), δ = 15.0 (SiPr$^i_3$-CH(*C*H$_3$)$_2$), 19.6 (s, SnOCH(CH(*C*H$_3$)$_2$), 19.8 (SiPr$^i_3$-*C*H(CH$_3$)$_2$), 21.0 (s, SnOCH(CH(*C*H$_3$)$_2$), 24.2 (Ar†-*p*-CH(*C*H$_3$)$_2$), 32.0 (SnOCH(*C*H(CH$_3$)$_2$), 33.77 (Ar†-*p*-*C*H(CH$_3$)$_2$), 52.0 (*C*HPh$_2$), 83.1 (SnO*C*H(CH(CH$_3$)$_2$), 126.6, 127.6, 127.8, 128.7, 129.8, 130.1, 131.3, 143.2, 144.3, 145.3, 145.4, 145.9 (Ar-*C*); ^{29}Si{^{1}H} NMR (C_6D_6, 80 MHz, 298 K), δ = 7.8; ^{119}Sn{^{1}H} NMR (C_6D_6, 149 MHz, 298 K): δ = 193.1; IR, ν/cm^{-1} (ATR): 3059 (w), 3025 (w), 1944 (w), 1803 (w), 1598 (m), 1381 (m), 1259 (m), 1098 (s), 1075 (w), 1014 (s), 882 (s), 801 (s), 758 (m), 746 (m), 686 (s), 657(s); MS/EI *m/z* (%): 857.4 (M$^+$, 1), 580.4 (^{iPr}L$^{\dagger+}$-Pr^i, 100). N.B. Thermal instability of the compound in the solid state precluded the collection of meaningful microanalysis data. However, a trace of the target compound was observed in the EI+ mass spectrum.

General procedure for the synthesis of (^{iPr}L†)Ge-(alkyl/alkenyl) species To a stirred solution of {(^{iPr}L†)GeH}$_2$ in toluene at ambient temperature was added the alkene or alkyne (typically 1.3 equiv.). The colour of the reactions rapidly changed from bright orange to yellow. The reaction mixture was stirred for 1 h, after which time all volatiles are removed. The residue was extracted in warm hexane and filtered. N.B. For cyclic alkyl species (i.e. **10**, **11**, **12**, and **18**), 5 equivalents of the relevant alkene were added prior to extraction to hinder equilibration, and subsequent crystallisation of the {(^{iPr}L†)GeH}$_2$ starting material.

(^{iPr}L†)Ge(CH$_2$)$_2$Ph (7) Using {(^{iPr}L†)GeH}$_2$ (0.20 g, 0.14 mmol), and styrene (0.34 mmol, 40 μL). The product was recrystallised from 10 mL hexane at 4 °C (115 mg, 51%). ^{1}H NMR (C_6D_6, 400 MHz, 298 K): δ = −0.60 (br, 2H, Ge-CH_2), 1.02 (d, $^3J_{HH}$ = 6.8 Hz, 6H, Ar†-*p*-CH(CH_3)$_2$), 1.26 (d, $^3J_{HH}$ = 7.6 Hz, 18H, SiPr$^i_3$-CH(CH_3)$_2$), 1.76 (sept, $^3J_{HH}$ = 7.6 Hz, 3H, SiPr$^i_3$-C*H*(CH$_3$)$_2$), 2.15 (m, 2H, Ge-CH$_2$CH_2), 2.57 (sept, $^3J_{HH}$ = 6.8 Hz, 1H, Ar†-*p*-C*H*(CH$_3$)$_2$), 6.16 (s, 2H, C*H*Ph$_2$), 6.73–7.40 (m, 27H, Ar-*H*); ^{13}C{^{1}H} NMR (C_6D_6, 75.5 MHz, 298 K): δ = 14.3 (SiPr$^i_3$-*C*H(CH$_3$)$_2$), 19.7 (SiPr$^i_3$-CH(*C*H$_3$)$_2$), 24.0 (Ar†-*p*-CH(*C*H$_3$)$_2$), 29.7 (Ge-*C*H$_2$), 33.6 (Ar†-*p*-*C*H(CH$_3$)$_2$), 46.8 (Ge-CH$_2$*C*H$_2$), 52.3 (*C*HPh$_2$), 125.4, 126.4, 127.4, 128.2, 128.8, 129.0, 129.6, 129.7, 129.9, 130.2, 137.9, 142.9, 145.1, 145.2, 146.1, 148.8 (Ar-*C*); ^{29}Si{^{1}H} NMR (C_6D_6, 80 MHz, 298 K): δ = 10.7; IR, ν/cm^{-1} (ATR): 3057 (w), 3024 (w), 1944 (w), 1871 (w), 1802 (w), 1597 (m), 1379 (m), 1258 (m), 1113 (m), 1031 (s), 877 (s), 809 (s), 744 (s), 661 (s); MS/EI m/z (%): 696.4 (M$^+$-(CH$_2$)$_2$Ph, 1), 623.4 (^{iPr}L$^{\dagger+}$, 55), 580.4 (^{iPr}L$^{\dagger+}$-Pr^i, 100); anal. calcd. for $C_{52}H_{61}GeNSi$: C, 78.00%; H, 7.68%; N, 1.75%; found: C, 77.90%; H, 7.75%; N, 1.82%.

(^{iPr}L†)GeEt (8) Using {(^{iPr}L†)GeH}$_2$ (0.3 g, 0.22 mmol), and ethylene (1 atm). The product was recrystallised from 5 mL hexane at 4 °C (215 mg, 68%).

Alternative synthesis of (^{iPr}L†)GeEt To a suspension of flame-dried fine Mg turnings (43 mg, 1.77 mmol) in Et$_2$O (15 mL) was added EtBr (112 μL, 1.50 mmol), and the reaction heated at 40 °C for 4 h. The resulting suspension was cooled and filtered into a cold (−80 °C) solution of (^{iPr}L†)GeCl (1 g, 1.38 mmol) in THF (40 mL). The cold bath was removed, the reaction allowed to warm to ambient temperature, and stirred for a further 30 min. Over this time the reaction became bright yellow. A ^{1}H NMR spectroscopic analysis showed quantitative conversion to the desired (^{iPr}L†)GeEt by this time. All volatiles were subsequently removed in vacuo, and the residue extracted in hot hexanes, followed by filtration. Removal of volatiles in vacuo resulted in **8** as a free-flowing analytically pure micro-crystalline yellow powder (800 mg, 80%).

M.p. 92–100 °C (melt); ^{1}H NMR (C_6D_6, 400 MHz, 298 K): δ = −1.02 (br m, 2H, Ge-CH_2), 0.55 (t, $^3J_{HH}$ = 7.2 Hz, 3H, Ge-CH$_2$CH_3), 1.04 (d, $^3J_{HH}$ = 6.8 Hz, 6H, Ar†-*p*-CH(CH_3)$_2$), 1.27 (d, $^3J_{HH}$ = 7.6 Hz, 18H, SiPr$^i_3$-CH(CH_3)$_2$), 1.77 (sept, $^3J_{HH}$ = 7.6 Hz, 3H, SiPr$^i_3$-C*H*(CH$_3$)$_2$), 2.60 (sept, $^3J_{HH}$ = 6.8 Hz, 1H, Ar†-*p*-C*H*(CH$_3$)$_2$), 6.17 (s, 2H, C*H*Ph$_2$), 7.07–7.41 (m, 22H, Ar-*H*); ^{13}C{^{1}H} NMR (C_6D_6, 75.5 MHz, 298 K): δ = 8.0 (Ge-CH$_2$*C*H$_3$), 14.9 (SiPr$^i_3$-*C*H(CH$_3$)$_2$), 20.3 (SiPr$^i_3$-CH(*C*H$_3$)$_2$), 24.6 (Ar†-*p*-CH(*C*H$_3$)$_2$), 34.2 (Ar†-*p*-*C*H(CH$_3$)$_2$), 37.2 (Ge-*C*H$_2$CH$_3$),

51.9 (*C*HPh$_2$), 126.9, 127.7, 128.7, 129.5, 130.0, 130.3, 138.5, 143.3, 145.6, 145.9, 146.7, 149.4 (Ar-*C*); ^{29}Si{^{1}H} NMR (C_6D_6, 80 MHz, 298 K): δ = 10.4; IR, ν/cm^{-1} (ATR): 3058 (w), 3028 (w), 1944 (w), 1872 (w), 1802 (w), 1597 (m), 1379 (m), 1226 (m), 1201 (m), 1118 (s), 1031 (s), 882 (s), 816 (s), 659 (s); MS/EI m/z (%): 696.3 (M$^+$-C_2H_5, 80), 580.3 (^{iPr}L$^{\dagger+}$-Pr^i, 100); anal. calcd. for $C_{46}H_{57}$GeNSi: C, 76.24%; H, 7.93%; N, 1.93%; found: C, 76.60%; H, 8.04%; N, 2.02%.

(^{iPr}L†)Ge(CH$_2$)$_2$Bu^t (9) Using {(^{iPr}L†)GeH}$_2$ (0.20 g, 0.14 mmol), and 3,3-dimethyl-1-butene (0.18 mmol, 23 μL). The product was recrystallised from 5 mL hexane at 4 °C (90 mg, 38%); M.p. 122–128 °C (melt); ^{1}H NMR (C_6D_6, 500 MHz, 298 K): δ = −0.72 (br, 2H, Ge-C*H*$_2$), 0.48 (s, 9H, Ge-CH$_2$CH$_2$C(C*H*$_3$)$_3$), 0.86 (m, 2H, Ge-CH$_2$C*H*$_2$), 1.05 (d, $^3J_{HH}$ = 6.8 Hz, 6H, Ar†-*p*-CH(C*H*$_3$)$_2$), 1.24 (d, $^3J_{HH}$ = 7.6 Hz, 18H, SiPr$^i_3$-CH(C*H*$_3$)$_2$), 1.67 (sept, $^3J_{HH}$ = 7.6 Hz, 3H, SiPr$^i_3$-C*H*(CH$_3$)$_2$), 2.62 (sept, $^3J_{HH}$ = 6.8 Hz, 1H, Ar†-*p*-C*H*(CH$_3$)$_2$), 6.18 (s, 2H, C*H*Ph$_2$), 6.95–7.48 (m, 22H, Ar-*H*); ^{13}C{^{1}H} NMR (C_6D_6, 75.5 MHz, 298 K): δ = 14.3 (SiPr$^i_3$-*C*H(CH$_3$)$_2$), 19.7 (SiPr$^i_3$-CH(*C*H$_3$)$_2$), 24.1 (Ar†-*p*-CH(*C*H$_3$)$_2$), 29.2 (Ge-CH$_2$CH$_2$C(*C*H$_3$)$_3$), 31.5 (Ar†-*p*-CH(CH$_3$)$_2$), 33.8 (Ge-CH$_2$*C*H$_2$), 36.5 (Ge-*C*H$_2$), 41.8 (Ge-CH$_2$CH$_2$*C*(CH$_3$)$_3$), 51.0 (*C*HPh$_2$), 126.3, 127.1, 129.5, 130.0, 130.1, 137.4, 140.8, 142.7, 145.0, 145.9, 146.2, 149.1 (Ar-*C*); ^{29}Si{^{1}H} NMR (C_6D_6, 80 MHz, 298 K): δ = 10.5; IR, ν/cm^{-1} (ATR): 3059 (w), 3024 (w), 1945 (w), 1872 (w), 1804 (w), 1752 (w), 1597 (m), 1360 (m), 1231 (s), 1117 (m), 1031 (m), 879 (s), 808 (s), 729 (s), 655 (s); MS/EI m/z (%): 696.3 (M$^+$-(3,3-Me$_2$Bu), 3), 623.4 (^{iPr}L$^{\dagger+}$, 44), 580.3 (^{iPr}L$^{\dagger+}$-Pr^i, 100); anal. calcd. for $C_{50}H_{65}$GeNSi: C, 76.92%; H, 8.39%; N, 1.79%; found: C, 75.92%; H, 7.43%; N, 2.13%.

(^{iPr}L†)Ge(C$_5$H$_9$) (10) Using {(^{iPr}L†)GeH}$_2$ (0.20 g, 0.14 mmol), and cyclopentene (0.18 mmol, 16 μL). The product was recrystallised from 5 mL hexane, with additional cyclopentene (80 μL) at −30 °C (190 mg, 73%). M.p. 137–146 °C (melt); ^{1}H NMR (C_6D_6, 400 MHz, 298 K): δ = 0.92 (br m, 3H, Ge–(C$_5$H$_9$)-C*H*$_2$), 1.01 (d, $^3J_{HH}$ = 6.8 Hz, 6H, Ar†-*p*-CH(C*H*$_3$)$_2$), 1.21 (br m, 1H, Ge–C*H*), 1.28 (d, $^3J_{HH}$ = 7.6 Hz, 18H, SiPr$^i_3$-CH(C*H*$_3$)$_2$), 1.42 (br m, 5H, Ge–(C$_5$H$_9$)-C*H*$_2$), 1.77 (sept, $^3J_{HH}$ = 7.6 Hz, 3H, SiPr$^i_3$-C*H*(CH$_3$)$_2$), 2.57 (sept, $^3J_{HH}$ = 6.8 Hz, 1H, Ar†-*p*-C*H*(CH$_3$)$_2$), 6.27 (s, 2H, C*H*Ph$_2$), 6.96–7.38 (m, 22H, Ar-*H*); ^{13}C{^{1}H} NMR (C_6D_6, 75.5 MHz, 298 K): δ = 15.7 (SiPr$^i_3$-*C*H(CH$_3$)$_2$), 20.0 (SiPr$^i_3$-CH(*C*H$_3$)$_2$), 24.1 (Ar†-*p*-CH(*C*H$_3$)$_2$), 25.9 (Ge–(C$_5$H$_9$)-C*H*$_2$), 27.4 (Ge–(C$_5$H$_9$)-C*H*$_2$), 33.7 (Ar†-*p*-*C*H(CH$_3$)$_2$), 50.2 (Ge–*C*H), 52.3 (*C*HPh$_2$), 126.5, 127.1, 128.5, 128.7, 129.0, 130.2, 130.8, 141.5, 143.4, 144.4, 145.7, 147.8 (Ar-*C*); ^{29}Si{^{1}H} NMR (C_6D_6, 80 MHz, 298 K): δ = 7.4; IR, ν/cm^{-1} (ATR): 3058 (w), 1876 (w), 1801 (w), 1596 (w), 1190 (m), 1069 (m), 1001 (m), 881 (s), 761(s), 714 (s), 646 (s); MS/EI m/z (%): 696.3 ((^{iPr}L†)Ge$^+$, 5), 623.4 (^{iPr}L$^{\dagger+}$, 40), 580.3 (^{iPr}L$^{\dagger+}$-Pr^i, 75), 167.0 (Ph$_2$C$^+$, 100); anal. calcd. for $C_{49}H_{61}$GeNSi: C, 76.96%; H, 8.04%; N, 1.84%; found: C, 76.81%; H, 8.13%; N, 1.91%.

(^{iPr}L†)Ge(C$_6$H$_{11}$) (11) Using {(^{iPr}L†)GeH}$_2$ (0.20 g, 0.14 mmol), and cyclohexene (0.18 mmol, 16 μL). The product was recrystallised from 4 mL hexane, with additional cyclohexene (80 μL), at 4 °C (95 mg, 42%).

Alternative synthesis of (^{iPr}L†)Ge(C_6H_{11}) To a suspension of flame-dried fine Mg turnings (22 mg, 0.89 mmol) in THF (15 mL) was added CyCl (89 μL, 0.75 mmol), and the reaction mixture heated at 40 °C for 4 h. The resulting suspension was cooled and filtered directly into a cold (−80 °C) stirred solution of (^{iPr}L†)GeCl (0.50 g, 0.69 mmol) in THF (25 mL). The reaction was allowed to warm to ambient temperature, and stirred for a further 30 min, over which time the mixture became bright yellow. A ^{1}H NMR spectroscopic analysis showed quantitative conversion to the desired (^{iPr}L†)Ge(C_6H_{11}) by this time. All volatiles were subsequently removed in vacuo, and the residue extracted in hexanes, and filtered. Concentration to 2 mL in vacuo, and storage overnight at 4 °C results in the formation of a deep yellow-orange crystalline solid (390 mg, 73%).

M.p. 127–133 °C (melt); ^{1}H NMR (C_6D_6, 400 MHz, 298 K): δ = 0.82 (m, 1H, Ge–C*H*), 1.02 (d, $^3J_{HH}$ = 6.8 Hz, 6H, Ar†-*p*-CH(CH_3)$_2$), 1.10 (m, 5H, Ge–(C_6H_{11})-CH_2), 1.24 (m, 5H, Ge–(C_6H_{11})-CH_2), 1.29 (d, $^3J_{HH}$ = 7.6 Hz, 18H, SiPr$^i_3$-CH(CH_3)$_2$), 1.71 (sept, $^3J_{HH}$ = 7.6 Hz, 3H, SiPr$^i_3$-C*H*(CH$_3$)$_2$), 2.58 (sept, $^3J_{HH}$ = 6.8 Hz, 1H, Ar†-*p*-C*H*(CH$_3$)$_2$), 6.25 (s, 2H, C*H*Ph$_2$), 6.93–7.36 (m, 22H, Ar-*H*); ^{13}C{^{1}H} NMR (C_6D_6, 75.5 MHz, 298 K): δ = 15.7 (SiPr$^i_3$-*C*H(CH$_3$)$_2$), 20.0 (SiPr$^i_3$-CH(*C*H$_3$)$_2$), 23.1 (Ar†-*p*-CH(*C*H$_3$)$_2$), 26.3 (Ge–(C_6H_{11})-CH_2), 27.2 (Ge–(C_6H_{11})-CH_2), 28.2 (Ge–(C_6H_{11})-CH_2), 33.8 (Ar†-*p*-CH(CH$_3$)$_2$), 52.4 (*C*HPh$_2$), 52.8 (Ge–*C*H), 126.5, 127.1, 128.5, 129.0, 130.1, 130.8, 140.8, 143.5, 144.5, 145.0, 14585, 148.1 (Ar-*C*); ^{29}Si{^{1}H} NMR (C_6D_6, 80 MHz, 298 K): δ = 7.8; IR, ν/cm^{-1} (ATR): 3063 (w), 3025 (w), 1941 (w), 1870 (w), 1799 (w), 1600 (w), 1379 (m), 1225 (m), 1199 (m), 1031 (m), 876 (s), 834 (s), 734 (s), 729 (s), 656 (s); MS/EI m/z (%): 696.4 ((^{iPr}L†)Ge$^+$, 3), 623.4 (^{iPr}L$^{\dagger+}$, 32), 580.3 (^{iPr}L$^{\dagger+}$-Pr^i, 75), 167.0 (Ph_2C^+, 100); anal. calcd. for $C_{50}H_{63}$GeNSi: C, 77.11%; H, 8.15%; N, 1.80%; found: C, 76.99%; H, 8.26%; N, 1.87%.

(^{iPr}L†)Ge(C_8H_{15}) (12) Using {(^{iPr}L†)GeH}$_2$ (0.20 g, 0.14 mmol), and cyclooctene (0.18 mmol, 23 μL). The product was recrystallised from 4 mL hexane, in the presence of additional cyclooctene (120 μL), at −30 °C (120 mg, 53%). M.p. 112–118 °C (dec.); ^{1}H NMR (C_6D_6, 400 MHz, 298 K): δ = 1.00 (d, $^3J_{HH}$ = 6.8 Hz, 6H, Ar†-*p*-CH(CH_3)$_2$), 1.10–1.62 (br m, 15H, Ge–(C_8H_{15})-CH_2/C*H*), 1.29 (br m, 18H, SiPr$^i_3$-CH(CH_3)$_2$), 1.78 (sept, $^3J_{HH}$ = 7.6 Hz, 3H, SiPr$^i_3$-C*H*(CH$_3$)$_2$), 2.56 (sept, $^3J_{HH}$ = 6.8 Hz, 1H, Ar†-*p*-C*H*(CH$_3$)$_2$), 6.29 (s, 2H, C*H*Ph$_2$), 6.95–7.36 (m, 22H, Ar-*H*); ^{13}C{^{1}H} NMR (C_6D_6, 75.5 MHz, 298 K): δ = 15.8 (SiPr$^i_3$-CH(*C*H$_3$)$_2$), 19.0 (Ge–(C_8H_{15})-CH_2), 19.9 (SiPr$^i_3$-*C*H(CH$_3$)$_2$), 24.1 (Ar†-*p*-CH(*C*H$_3$)$_2$), 26.3, 26.9, and 27.4 (Ge–(C_8H_{15})-CH_2), 33.8 (Ar†-*p*-*C*H(CH$_3$)$_2$), 52.0 (*C*HPh$_2$), 52.8 (Ge–*C*H), 126.5, 127.1, 128.5, 128.8, 130.1, 130.2, 130.4, 130.8, 131.2, 145.0, 146.0, 147.6 (Ar-C); ^{29}Si{^{1}H} NMR (C_6D_6, 80 MHz, 298 K): δ = 7.2; IR, ν/cm^{-1} (ATR): 3061 (w), 3025 (w), 1802 (w), 1599 (w), 1377 (m), 1224 (w), 1196 (m), 1115 (m), 1033 (m), 879 (s), 833 (s), 727 (s), 699 (s), 659 (s); MS/EI m/z (%): 696.3 ((^{iPr}L†)Ge$^+$, 18), 623.3 (^{iPr}L$^{\dagger+}$, 48), 580.3 (^{iPr}L$^{\dagger+}$-Pr^i, 100); anal. calcd. for $C_{52}H_{67}$GeNSi: C, 77.41%; H, 8.37%; N, 1.74%; found: C, 77.34%; H, 8.48%; N, 1.81%.

General synthesis of (^{iPr}L†)Sn-(alkyl/alkenyl) species These compounds were synthesised by two routes:
Route (a): To a cold (−80 °C) solution of {(^{iPr}L†)Sn(μ-H)}$_2$ in toluene was added the relevant alkene or alkyne (1.5 equiv. for alkynes/linear alkenes, 6 equiv. for cyclic alkenes), the cold bath removed and the reaction stirred at ambient temperature for 1 h. Subsequently, all volatiles were removed in vacuo, and the residue extracted in hexane, and filtered.
Route (b): To a cold (−30 °C) solution of (^{iPr}L†)SnOBu^t in toluene was added HBpin, and the relevant alkene (1.5 equiv. for alkynes/linear alkenes, 6 equiv. for cyclic alkenes). The reaction mixture was slowly warmed to ambient temperature overnight, resulting in a deep yellow/brown solution. Volatiles were removed in vacuo, the solid residue extracted in hexane, and filtered.

(^{iPr}L†)SnEt (13)
Route (a): Using {(^{iPr}L†)Sn(μ-H)}$_2$ (0.20 g, 0.27 mmol) and ethylene (1 atm). The product was recrystallised at 4 °C from a concentrated (∼5 mL) hexane solution, yielding large yellow orange blocks (125 mg, 60%).
Route (b): Using (^{iPr}L†)SnOBu^t (0.3 g, 0.37 mmol), HBpin (60 μL, 0.41 mmol), and ethylene (1 atm). The product was isolated as an analytically pure deep yellow powder, through removal of volatiles in vacuo from the hexane extract, and washing the solid residue with pentane (∼10 mL) then drying in vacuo (210 mg, 73%).

M.p. 132–143 °C (melt); ^{1}H NMR (C_6D_6, 400 MHz, 298 K): δ = −0.82 (br, 2 H, Sn-CH_2), 0.83 (t, $^3J_{HH}$ = 7.2 Hz, 3H, Sn-CH$_2$CH_3), 1.04 (d, $^3J_{HH}$ = 6.8 Hz, 6H, Ar†-*p*-CH(CH_3)$_2$), 1.31 (d, $^3J_{HH}$ = 7.6 Hz, 18H, SiPr$^i_3$-CH(CH_3)$_2$), 1.73 (sept, $^3J_{HH}$ = 7.6 Hz, 3H, SiPr$^i_3$-C*H*(CH$_3$)$_2$), 2.61 (sept, $^3J_{HH}$ = 6.8 Hz, 1H, Ar†-*p*-C*H*(CH$_3$)$_2$), 6.37 (s, 2H, C*H*Ph$_2$), 6.91–7.32 (m, 22H, Ar-*H*); ^{13}C{^{1}H} NMR (C_6D_6, 75.5 MHz, 298 K): δ = 7.7 (Sn-CH$_2$*C*H$_3$), 14.9 (SiPr$^i_3$-*C*H(CH$_3$)$_2$), 19.1 (SiPr$^i_3$-CH(*C*H$_3$)$_2$), 24.0 (Ar†-*p*-CH(*C*H$_3$)$_2$), 33.7 (Ar†-*p*-*C*H(CH$_3$)$_2$), 49.1 (Sn-*C*H$_2$CH$_3$), 51.9 (*C*HPh$_2$), 126.6, 127.6, 128.6, 129.7, 129.8, 129.9, 130.1, 140.8, 143.3, 145.0, 145.9, 150.9 (Ar-*C*); ^{29}Si{^{1}H} NMR (C_6D_6, 80 MHz, 298 K): δ = 6.2; IR, ν/cm^{-1} (ATR): 3058 (w), 3026 (w), 1943 (w), 1802 (w), 1597 (m), 1379 (m), 1221 (s), 1201 (s), 1116 (s), 1031 (m), 982 (m), 881 (s), 831 (s), 759 (s); MS/EI m/z (%): 770.5 (M$^+$, 0.5), 742.6 ((^{iPr}L†)Sn$^+$, 2), 167.2 (Ph$_2$C$^+$, 0.5); anal. calcd. for C_{46}H$_{57}$NSiSn: C, 71.68%; H, 7.45%; N, 1.82%; found: C, 71.59%; H, 7.51%; N, 1.82%.

(^{iPr}L†)Sn(CH$_2$)$_2$Bu^t (14)
Route (a): Using {(^{iPr}L†)Sn(μ-H)}$_2$ (0.20 mg, 0.27 mmol) and 3,3-dimethyl-1-butene (52 μL, 0.41 mmol). The product was recrystallised at 4 °C from a concentrated (∼5 mL) hexane solution, yielding large red orange blocks (150 mg, 67%).
Route (b): Using (^{iPr}L†)SnOBu^t (0.3 g, 0.37 mmol), HBpin (60 μL, 0.41 mmol), and 3,3-dimethyl-1-butene (71 μL, 0.56 mmol). The product was recrystallised at 4 °C from a concentrated (∼8 mL) hexane solution, yielding large red orange blocks (200 mg, 66%).

M.p. 82–92 °C (melt); ^{1}H NMR (C_6D_6, 400 MHz, 298 K): δ = −0.42 (br, 2H, Sn-CH_2), 0.67 (s, 9H, Sn-$(CH_2)_2$C(C$H_3)_3$), 0.98 (m, 2H, Sn-CH_2CH_2), 1.07 (d, $^{3}J_{HH}$ = 6.8 Hz, 6H, Ar†-*p*-CH(C$H_3)_2$), 1.31 (d, $^{3}J_{HH}$ = 7.6 Hz, 18H, SiPr$^{i}_3$-CH(C$H_3)_2$), 1.67 (sept, $^{3}J_{HH}$ = 7.6 Hz, 3H, SiPr$^{i}_3$-C*H*(C$H_3)_2$), 2.64 (sept, $^{3}J_{HH}$ = 6.8 Hz, 1H, Ar†-*p*-C*H*(C$H_3)_2$), 6.41 (s, 2H, C*H*Ph$_2$), 6.93–7.36 (m, 22H, Ar-*H*); ^{13}C{^{1}H} NMR (C_6D_6, 75.5 MHz, 298 K): δ = 15.9 (SiPr$^{i}_3$-*C*H(C$H_3)_2$), 20.3 (SiPr$^{i}_3$-CH(*C*$H_3)_2$), 24.4 (Ar†-*p*-CH(*C*$H_3)_2$), 29.3 (Sn-CH_2CH_2C(*C*$H_3)_3$), 32.7 (Ar†-*p*-CH(C$H_3)_2$), 33.7 (Sn-CH_2CH_2), 37.6 (Sn-*C*H_2), 51.6 (*C*HPh$_2$), 53.7 (Sn-CH_2CH_2*C*$(CH_3)_3$), 126.3, 127.6, 128.6, 129.7, 129.9, 130.1, 130.3, 139.7, 141.8, 145.9, 146.2, 151.0 (Ar-*C*); ^{29}Si{^{1}H} NMR (C_6D_6, 80 MHz, 298 K): δ = 5.9; IR, ν/cm^{-1} (ATR): 3060 (w), 3026 (w), 1945 (w), 1598 (w), 1380 (m), 1363 (m), 1222 (m), 1155 (m), 1116 (m), 1031 (m), 878 (s), 830 (s), 759 (s); MS/EI m/z (%): 623.4 (^{iPr}L$^{\dagger+}$, 55), 580.4 (^{iPr}L$^{\dagger+}$-Pr^{i+}, 100); anal. calcd. for $C_{50}H_{65}NSiSn$: C, 72.63%; H, 7.92%; N, 1.69%; found: C, 72.49%; H, 8.10%; N, 1.79%.

(^{iPr}L†)Sn(C_5H_9) (15)

Route (a): Using {(^{iPr}L†)Sn(μ-H)}$_2$ (0.25 g, 0.34 mmol) and cyclopentene (180 μL, 2.04 mmol). The product was recrystallised at −30 °C from a concentrated (∼6 mL) hexane solution, in the presence of additional cyclopenetene (150 μL), yielding large red-orange blocks (125 mg, 45%).

Route (b): Using (^{iPr}L†)SnOBu^{t} (0.3 g, 0.37 mmol), HBpin (60 μL, 0.41 mmol), and cyclopentene (196 μL, 2.22 mmol). The product was recrystallised from a concentrated hexane solution (∼5 mL), with additional cyclopentene (150 μL), at −30 °C, yielding red-orange blocks (230 mg, 77%).

M.p. 96–106 °C (dec.); ^{1}H NMR (C_6D_6, 400 MHz, 298 K): 1.03 (d, $^{3}J_{HH}$ = 6.8 Hz, 6H, Ar†-*p*-CH(C$H_3)_2$), 1.32 (m, 3H, Sn–(C_5H_9)-CH_2), 1.36 (d, $^{3}J_{HH}$ = 7.0 Hz, 18H, SiPr$^{i}_3$-CH(C$H_3)_2$), 1.51 (br m, 1H, Sn–C*H*), 1.57 (br m, 5H, Sn–(C_5H_9)-CH_2), 1.83 (sept, $^{3}J_{HH}$ = 7.0 Hz, 3H, SiPr$^{i}_3$-C*H*(C$H_3)_2$) 2.58 (sept, $^{3}J_{HH}$ = 6.8 Hz, 1H, Ar†-*p*-C*H*(C$H_3)_2$), 6.44 (s, 1H, Ph_2C*H*), 6.88–7.39 (Ar-*H*); ^{13}C{^{1}H} NMR (C_6D_6, 75.5 MHz, 298 K): δ = 16.5 (SiPr$^{i}_3$-*C*H(C$H_3)_2$), 19.3 (SiPr$^{i}_3$-CH(*C*$H_3)_2$), 23.2 (Sn–*C*H), 24.6 (Ar†-*p*-CH(*C*$H_3)_2$), 26.9 and 27.9 (Sn–CH(C_2H_4)$_2$), 33.8 (Ar†-*p*-*C*H(C$H_3)_2$), 52.3 (*C*HPh$_2$), 126.5, 126.6, 128.6, 129.6, 130.0, 130.1, 140.8, 142.5, 144.6, 145.0, 145.4, 149.6; ^{29}Si{^{1}H} NMR (C_6D_6, 80 MHz, 298 K): δ = 4.7; IR, ν/cm^{-1} (ATR): 3058 (w), 3023 (w), 1949 (w), 1888 (w), 1808 (w), 1598 (m), 1378 (m), 1222 (m), 1195 (m), 1113 (m), 1031 (m), 916 (m), 877 (s), 843 (s), 805 (s), 743 (s), 671 (s); MS/EI m/z (%): 810.7 (M^{+}, 0.5), 742.6 ((^{iPr}L†)Sn^{+}, 7), 167.2 (Ph_2C^{+} 100); anal. calcd. for $C_{49}H_{61}NSiSn$: C, 72.58%; H, 7.58%; N, 1.73%; found: C, 72.57%; H, 7.67%; N, 1.85%.

(^{iPr}L†)GeC(Ph)=C(H)Me (16) Using {(^{iPr}L†)GeH}$_2$ (0.25 g, 0.18 mmol), and 1-phenyl-1-propyne (0.43 mmol, 54 μL). Crystallised from 5 mL hexane at −30 °C (120 mg, 44%). M.p. 146–158 °C (dec.); ^{1}H NMR (C_6D_6, 400 MHz, 298 K): δ = 1.04 (d, $^{3}J_{HH}$ = 6.8 Hz, 6H, Ar†-*p*-CH(C$H_3)_2$), 1.18 (d, $^{3}J_{HH}$ = 7.6 Hz, 18H, SiPr$^{i}_3$-CH(C$H_3)_2$), 1.66 (sept, $^{3}J_{HH}$ = 7.6 Hz, 3H, SiPr$^{i}_3$-C*H*(C$H_3)_2$), 1.66 (br, 3H, Ge(Ph)C=C(H)*Me*), 2.61 (sept, $^{3}J_{HH}$ = 6.8 Hz, 1H, Ar†-*p*-C*H*(C$H_3)_2$), 4.18 (v br, 1H, Ge(Ph)C=C(*H*)Me), 6.32 (s, 2H, C*H*Ph$_2$), 6.84–7.47 (m, 27H, Ar-*H*); ^{13}C{^{1}H}

NMR (C_6D_6, 75.5 MHz, 298 K): δ = 14.5 ($SiPr^i_3$-*C*H(CH_3)$_2$), 19.7 ($SiPr^i_3$-CH(*C*H_3)$_2$), 23.1 (Ge–C(Ph)=C(H)*Me*), 24.2 ($Ar^†$-*p*-CH(*C*H_3)$_2$), 33.8 ($Ar^†$-*p*-*C*H(CH_3)$_2$), 51.3 (*C*HPh_2), 80.5 (Ge–*C*(Ph)=C(H)Me), 86.1 (Ge–C(Ph=*C*(H)Me), 125.6, 126.4, 127.0, 128.5, 129.0, 129.9, 130.1, 130.8, 137.9, 138.1, 142.7, 143.4, 145.2, 145.8, 145.9, 147.9 (Ar-*C*); ^{29}Si{^{1}H} NMR (C_6D_6, 80 MHz, 298 K): δ = 10.7; IR, ν/cm^{-1} (ATR): 3059 (w), 3024 (w), 1878 (w), 1597(m), 1364 (m), 1224 (w), 1195 (w), 1113 (m), 1074 (m), 1030 (m), 878 (s), 831 (s), 756 (s), 662 (s); MS/EI m/z (%): 623.7 ($^{iPr}L^{†+}$, 30), 167.2 (Ph_2C^+, 100).

($^{iPr}L^†$)SnC(Ph)=C(H)Me (17) This compound was synthesised via Route (a) only, using {($^{iPr}L^†$)Sn(μ-H)}$_2$ (0.20 g, 0.13 mmol), and 1-phenyl-1-propyne (38 μL, 0.30 mmol). The product was recrystallised from hexane (∼3 mL) at −30 °C (105 mg, 47%). M.p. 115–120 °C (dec.); ^{1}H NMR (C_6D_6, 400 MHz, 298 K): δ = 1.02 (d, $^3J_{HH}$ = 6.8 Hz, 6H, $Ar^†$-*p*-CH(C*H*$_3$)$_2$), 1.21 (d, $^3J_{HH}$ = 7.6 Hz, 18H, $SiPr^i_3$-CH(C*H*$_3$)$_2$), 1.56 (br d, $^3J_{HH}$ = 6 Hz, 3H, Sn-C(Ph)=C(H)*Me*), 1.77 (sept, $^3J_{HH}$ = 7.6 Hz, 3H, $SiPr^i_3$-C*H*(CH_3)$_2$), 2.57 (sept, $^3J_{HH}$ = 6.8 Hz, 1H, $Ar^†$-*p*-C*H*(CH_3)$_2$), 5.26 (br quart, $^3J_{HH}$ = 6 Hz, 1H, Sn-C(Ph)=C(*H*)Me), 6.39 (s, 2H, C*H*Ph_2), 6.90–7.35 (m, 27H, Ar-*H*); ^{13}C{^{1}H} NMR (C_6D_6, 75.5 MHz, 298 K): δ = 15.3 ($SiPr^i_3$-*C*H(CH_3)$_2$), 16.6 (Sn-C(Ph)=C(H)*Me*), 19.5 ($SiPr^i_3$-CH(*C*H$_3$)$_2$), 24.3 ($Ar^†$-*p*-CH(*C*H_3)$_2$), 33.8 ($Ar^†$-*p*-*C*H(CH_3)$_2$), 52.8 (*C*HPh_2), 82.2 (Sn-*C*(Ph)=*C*(H)Me), 125.0, 126.6, 127.6, 128.6, 128.7, 129.7, 129.9, 130.1, 131.4, 131.5, 140.8, 142.5, 144.9, 145.0, 145.6, 148.6 (Ar-*C*); ^{29}Si{^{1}H} NMR (C_6D_6, 80 MHz, 298 K): δ = 6.8; IR, ν/cm^{-1} (ATR): 3059 (w), 3025 (w), 1597 (m), 1380 (m), 1257 (m), 1155 (m), 1071 (m), 1013 (m), 882 (s), 759 (s); MS/EI m/z (%): 742.6 ($^{iPr}L^†$)Sn$^+$, 3), 167.2 (Ph_2C^+, 100); anal. calcd. for $C_{53}H_{61}NSiSn$: C, 74.12%; H, 7.16%; N, 1.63%; found: C, 73.99%; H, 7.04%; N, 1.69%.

($^{iPr}L^†$)Ge(C_8H_{13}) (18) Using {($^{iPr}L^†$)GeH}$_2$ (0.20 g, 0.14 mmol), and 1,5-cyclooctadiene (0.18 mmol, 23 μL). The product was recrystallised from 3 mL hexane, with additional 1,5-cyclooctadiene (120 μL) at −30 °C (80 mg, 36%). M.p. 108–112 °C (melt); ^{1}H NMR (C_6D_6, 400 MHz, 298 K): δ = 0.99 (d, $^3J_{HH}$ = 6.8 Hz, 6H, $Ar^†$-*p*-CH(C*H*$_3$)$_2$), 1.29 (d, $^3J_{HH}$ = 7.6 Hz, 18H, $SiPr^i_3$–CH(C*H*$_3$)$_2$), 1.40 (m, 1H, Ge–C*H*), 1.52–1.68 (br m, 10H, Ge–(C_8H_{13})–C*H*$_2$), 1.79 (sept, $^3J_{HH}$ = 7.6 Hz, 3H, $SiPr^i_3$-C*H*(CH_3)$_2$), 2.56 (sept, $^3J_{HH}$ = 6.8 Hz, 1H, $Ar^†$-*p*-C*H*(CH_3)$_2$), 4.23 (m, 1H, Ge–(C_8H_{13})-CH=C*H*), 4.99 (m, 1H, Ge–(C_8H_{13})-CH=C*H*), 6.29 (s, 2H, C*H*Ph_2), 6.96–7.37 (m, 22H, Ar-*H*); ^{13}C{^{1}H} NMR (C_6D_6, 75.5 MHz, 298 K): δ = 15.7 ($SiPr^i_3$-*C*H(CH_3)$_2$), 19.9 ($SiPr^i_3$-CH(*C*H$_3$)$_2$), 23.8 (Ge–(C_8H_{13})-*C*H$_2$), 24.1 ($Ar^†$-*p*-CH(*C*H_3)$_2$), 27.5 (Ge–(C_8H_{13})-*C*H$_2$), 28.5 (Ge–(C_8H_{13})-*C*H$_2$), 29.0 (Ge–(C_8H_{13})-*C*H$_2$), 33.8 ($Ar^†$-*p*-CH(*C*H$_3$)$_2$), 52.1 (CHPh_2), 53.3 (Ge–*C*H), 91.4 (br, Ge–CH*C*H=*C*H), 126.5, 127.1, 128.5, 128.8, 129.0, 130.2, 131.1, 141.8, 143.6, 144.3, 145.8, 147.2 (Ar-*C*); ^{29}Si{^{1}H} NMR (C_6D_6, 80 MHz, 298 K): δ = 7.3; IR, ν/cm^{-1} (ATR): 3061 (w), 3025 (w), 1945 (w), 1882 (w), 1803 (w), 1599 (m), 1380 (m), 1227 (m), 1118 (s), 879 (s), 793 (s), 718 (s), 661 (s);

MS/EI m/z (%): 696.3 (M^+-Pr^i, 1), 623.3 ($^{iPr}L^{\dagger+}$, 15), 580.4 ($^{iPr}L^{\dagger+}$-Pr^i, 35) 167.2 (Ph_2C^+, 42).

N.B. The presence of small amounts of $\{(^{iPr}L^{\dagger})GeH\}_2$ in recrystallised $(^{iPr}L^{\dagger})Ge(C_8H_{13})$ (> 5%) precluded the acquisition of an accurate elemental analysis.

($^{iPr}L^{\dagger}$)Ge(CH_2)$_2$Pr^i (19) Using $\{(^{iPr}L^{\dagger})GeH\}_2$ (0.20 g, 0.14 mmol) and 2-methyl-2-butene (0.18 mmol, 19 μL). The product was recrystallised from a concentrated hexane solution (3 mL) at 4 °C (140 mg, 65%). M.p. 142–150 °C (melt); ^{1}H NMR (C_6D_6, 400 MHz, 298 K): δ = −0.89 (br, 2H, Ge–CH_2), 0.58 (d, $^3J_{HH}$ = 6.0 Hz, 6H, Ge–$(CH_2)_2$CH(CH_3)$_2$), 0.63 (m, 1H, Ge–$(CH_2)_2$CH(CH_3)$_2$), 0.81 (br m, 2H, Ge–CH_2CH_2), 1.04 (d, $^3J_{HH}$ = 6.8 Hz, 6H, Ar†-*p*-CH(CH_3)$_2$), 1.26 (d, $^3J_{HH}$ = 7.6 Hz, 18H, SiPr$^i_3$-CH(CH_3)$_2$), 1.73 (sept, $^3J_{HH}$ = 7.6 Hz, 3H, SiPr$^i_3$-CH(CH_3)$_2$), 2.60 (sept, $^3J_{HH}$ = 6.8 Hz, 1H, Ar†-*p*-CH(CH_3)$_2$), 6.17 (s, 2H, CHPh$_2$), 7.95–7.44 (m, 22H, Ar-*H*); ^{13}C{^{1}H} NMR (C_6D_6, 75.5 MHz, 298 K): δ = 8.0 (Ge-CH_2*C*H$_3$), 14.3 (SiPr$^i_3$-*C*H(CH_3)$_2$), 19.7 (SiPr$^i_3$-CH(*C*H$_3$)$_2$), 22.7 (Ge–$(CH_2)_2$CH(*C*H$_3$)$_2$), 24.1 (Ar†-*p*-CH(*C*H$_3$)$_2$), 31.1 (Ge–CH_2*C*H$_2$), 32.7 (Ge–$(CH_2)_2$*C*H(CH_3)$_2$), 33.7 (Ar†-*p*-*C*H(CH_3)$_2$), 43.9 (Ge-*C*H$_2$), 51.2 (*C*HPh$_2$), 126.3, 127.1, 128.2, 128.9, 129.5, 129.7, 129.9, 137.7, 142.7, 145.6, 146.2, 149.0 (Ar-*C*); ^{29}Si{^{1}H} NMR (C_6D_6, 80 MHz, 298 K): δ = 11.1; IR, ν/cm^{-1} (ATR): 3057 (w), 3026 (w), 1801 (w), 1598 (m), 1380 (m), 1362 (m), 1258 (m), 1225 (m), 1114 (m), 1073 (m), 1032 (m), 877 (s), 811 (s), 759 (s), 727 (s), 658 (s); MS/EI m/z (%): 695.6 ($(^{iPr}L^{\dagger})Ge^+$, 4), 580.6 ($^{iPr}L^{\dagger+}$-Pr^i, 23), 167.2 (PhC^+, 100); anal. calcd. for $C_{49}H_{63}GeNSi$: C, 76.76%; H, 8.28%; N, 1.83%; found: C, 76.61%; H, 8.37%; N, 2.01%.

References

1. Knochel P, Molander GA (2014) Comprehensive organic synthesis II. Elsevier Ltd.
2. Aldridge S, Downs AJ (2001) Hydrides of the main-group metals: new variations on an old theme. Chem Rev 101:3305
3. Harder S (2012) Molecular early main group metal hydrides: synthetic challenge, structures and applications. Chem Comm 48:11165
4. Pelter A, Smith K, Brown HC (1988) Borane reagents (best synthetic methods). Academic Press
5. Spielmann J, Harder S (2007) Hydrocarbon-soluble calcium hydride: a “worker-bee” in calcium chemistry. Chem Eur J 13:8928
6. Fettinger JC, Gray PA, Melton CE, Power PP (2014) Hydroalumination of alkenes and alkynes by primary aluminum hydrides under mild conditions. Organometallics 33:6232
7. Hill MS, MacDougall DJ, Mahon MF (2010) Magnesium hydride-promoted dearomatisation of pyridine. Dalton Trans 39:11129
8. Stephan DW (2015) Frustrated lewis pairs: from concept to catalysis. Acc Chem Res 48:306
9. Barrett AGM, Crimmin MR, Hill MS, Procopiou PA (2010) Heterofunctionalization catalysis with organometallic complexes of calcium, strontium and barium. Proc R Soc A 466:927
10. Arrowsmith M, Hill MS, Hadlington T, Kociok-Köhn G, Weetman C (2011) Magnesium-catalyzed hydroboration of pyridines. Organometallics 30:5556
11. Buch F, Brettar J, Harder S (2006) Early main group metal catalysis: how important is the metal? Angew Chem 118:2807

12. Pineda LW, Jancik V, Starke K, Oswald RB, Roesky HW (2006) Stable monomeric germanium(II) and tin(II) compounds with terminal hydrides. Angew Chem 118:2664
13. Takagi N, Sakaki S (2013) Theoretical study of reactivity of Ge(II)-hydride compound: comparison with Rh(I)-hydride complex and prediction of full catalytic cycle by Ge(II)-hydride. J Am Chem Soc 135:8955
14. Mandal SK, Roesky HW (2012) Group 14 hydrides with low valent elements for activation of small molecules. Acc Chem Res 45:298
15. Jana A, Ghoshal D, Roesky HW, Objartel I, Schwab G, Stalke D (2009) A germanium(II) hydride as an effective reagent for hydrogermylation reactions. J Am Chem Soc 131:1288
16. Albertin G, Antoniutti S, Castro J, García-Fontán S, Zanardo G (2007) Preparation and reactivity of stannyl complexes of manganese and rhenium. Organometallics 26:2918
17. Jansen A, Görls H, Pitter S (2000) trans-[$Ru^{II}Cl(MeCN)_5$][$Ru^{III}Cl_4(MeCN)_2$]: a reactive intermediate in the homogeneous catalyzed hydrosilylation of carbon dioxide. Organometallics 19:135
18. Deglmann P, Ember E, Hofmann P, Pitter S, Walter O (2007) Experimental and theoretical investigations on the catalytic hydrosilylation of carbon dioxide with ruthenium nitrile complexes. Chem Eur J 13:2864
19. Jana A, Roesky HW, Schulzke C, Döring A (2009) Reactions of Tin(II) hydride species with unsaturated molecules. Angew Chem Int Ed 48:1106
20. Jana A, Tavčar G, Roesky HW, John M (2010) Germanium(II) hydride mediated reduction of carbon dioxide to formic acid and methanol with ammonia borane as the hydrogen source. Dalton Trans 39:9487
21. Tan G, Wang W, Bloma B, Driess M (2014) Mechanistic studies of CO_2 reduction to methanol mediated by an N-heterocyclic germylene hydride. Dalton Trans 43:6006
22. Jana A, Roesky HW, Schulzke C (2010) Reactivity of germanium(II) hydride with nitrous oxide, trimethylsilyl azide, ketones, and alkynes and the reaction of a methyl analogue with trimethylsilyl diazomethane. Dalton Trans 39:132
23. Jana A, Roesky HW, Schulzke C, Samuel PP (2010) Reaction of Tin(II) hydride with compounds containing aromatic C−F bonds. Organometallics 29:4837
24. Al-Rafia SMI, Malcolm AC, McDonald R, Ferguson MJ, Rivard E (2011) Trapping the parent inorganic ethylenes H2SiGeH2 and H2SiSnH2 in the form of stable adducts at ambient temperature. Angew Chem 123:8504
25. Al-Rafia SMI, Malcolm AC, Liew SK, Ferguson MJ, Rivard E (2011) Stabilization of the heavy methylene analogues, GeH_2 and SnH_2, within the coordination sphere of a transition metal. J Am Chem Soc 133:777
26. Jana A, Sen SS, Roesky HW, Schulzke C, Dutta S, Pati SK (2009) End-on nitrogen insertion of a diazo compound into a germanium(II) hydrogen bond and a comparable reaction with diethyl azodicarboxylate. Angew Chem Int Ed 48:4246
27. Davies AG, Smith PJ (1982) Tin. In: Comprehensive organometallic chemistry, vol 2. Oxford, Pergamon, p 519
28. Rivière P, Rivière-Baudet M, Satgè J (1982) Germanium. In Comprehensive organometallic chemistry, vol 2. Oxford, Pergamon, p 39
29. Smith ND, Mancuso J, Lautens M (2000) Metal-catalyzed hydrostannations. Chem Rev 100:3257
30. Jana A, Roesky HW, Schulzke C (2009) Hydrostannylation of ketones and alkynes with LSnH [L = $HC(CMeNAr)_2$, Ar = 2,6-^{i}Pr2C_6H_3]. Inorg Chem 48:9543
31. Stoelzel M, Präsang C, Inoue S, Enthaler S, Driess M (2012) Hydrosilylation of alkynes by $Ni(CO)_3$-stabilized silicon(II) hydride. Angew Chem Int Ed 51:399
32. Rodriguez R, Gau D, Contie Y, Kato T, Saffon-Merceron N, Baceiredo A (2011) Synthesis of a phosphine-stabilized silicon(II) hydride and its addition to olefins: a catalyst-free hydrosilylation reaction. Angew Chem Int Ed 50:11492
33. Summerscales OT, Caputo CA, Knapp CE, Fettinger JC, Power PP (2012) The role of group 14 element hydrides in the activation of C–H bonds in cyclic olefins. J Am Chem Soc 134:14595

34. Summerscales OT, Fettinger JC, Power PP (2011) C–H activation of cycloalkenes by dimetallynes (M = Ge, Sn) under ambient conditions. J Am Chem Soc 133:11960
35. Jutzi P, Becker A, Stammler HG, Neumann B (1991) Synthesis and solid-state structure of $(Me_3Si)_3CGeCH(SiMe_3)_2$, a monomeric dialkylgermylene. Organometallics 10:1647
36. Bondi A (1964) van der Waals volumes and radii. J Phys Chem 68:441
37. Li J, Schenk C, Winter F, Scherer H, Trapp N, Higelin A, Keller S, Pöttgen R, Krossing I, Jones C (2012) Weak arene stabilization of bulky amido-germanium(II) and Tin(II) monocations. Angew Chem Int Ed 51:9557
38. Emsley J (1995) The elements, 2nd edn. Clarendon, Oxford
39. Choong SL, Woodul WD, Schenk C, Stasch A, Richards AF, Jones C (2011) Synthesis, characterization, and reactivity of an N-heterocyclic germanium(II) hydride: reversible hydrogermylation of a phosphaalkyne. Organometallics 30:5543
40. Hostetler MJ, Butts MD, Bergman RG (1993) Scope and mechanism of alkene hydrogenation/isomerization catalyzed by complexes of the type $R_2E(CH_2)_2M(CO)(L)$ (R = Cp, Me, Ph; E = phosphorus, tantalum; M = rhodium, iridium; L = CO, PPh_3). J Am Chem Soc 115:2743
41. Manzini S, Nelson DJ, Nolan SP (2013) A highly active cationic ruthenium complex for alkene isomerisation: a catalyst for the synthesis of high value molecules. Chem Cat Chem 5:2848
42. Ashworth IW, Hillier IH, Nelson DJ, Percy JM, Vincent MA (2012) Searching for the hidden hydrides: the competition between alkene isomerization and metathesis with grubbs catalysts. Eur J Org Chem 29:5673

Chapter 5
Stoichiometric Reactivity and Catalytic Applications of Heavier Tetrylene Derivatives

5.1 Introduction

Whilst the spotlight has been on the synthesis and reactivity of the heavier alkyne analogues (LEEL, E = Si–Pb) in regards to low-oxidation state group 14 chemistry, the reactivity of heavier carbene analogues (L_2E:) has also seen considerable interest. To date, there have been numerous reports of the facile, and in some cases reversible, activation of benign small molecules (e.g. CO, H_2, C_2H_4) at these element(II) centres [3]. These transformations are of great importance if the goal of true transition-metal (TM) catalyst mimicry is to be realised using low-oxidation state and low-coordinate main-group (MG) elements. The potential for group 14 species to achieve reactions such as oxidative addition (OA) and reductive elimination (RE) is clear, with countless examples of the OA of A–B (A = a cationic substituent, B = an anionic substituent) bonds to the heavier tetrelenes. Further, related small-molecule activation reactions involving Sn(II) often resolve with no oxidation state change at tin, hinting at a OA/RE mechanism. This, however, does not eliminate the possibility of such transformations occurring through σ-metathesis mechanisms so important in lanthanide and alkaline-earth catalysed transformations, which may also be a viable route to group 14 element(II) catalysed transformations. Herein, these areas will be discussed in the context of applying such reactions to the heavier group 14 elements in catalysis.

5.1.1 Reactivity of the Monomeric Tetrelenes

Initial reports of OA reactions to the heavier tetrelenes by Lappert and co-workers were seen as early as 1977 [4], with the addition of a range of C–X bonds (X = a halide) across Ge(II), Sn(II), and Pb(II) centres supported by bulky amide (e.g. $[N(TMS)_2]^-$; TMS = $[SiMe_3]^-$) or alkyl ($[CH(TMS)_2]^-$) ligands [4, 5]. Along with the

T.J. Hadlington, *On the Catalytic Efficacy of Low-Oxidation State Group 14 Complexes*, Springer Theses, DOI 10.1007/978-3-319-51807-7_5

addition of C–X bonds, the OA reactions of anhydrides, acid chlorides, and bromoamides with germylenes and stannylenes were also reported [4, 5], showing the broad scope of the OA chemistry of low-coordinate, low-oxidation state group 14 compounds. However, the activation of catalytically relevant small-molecules (e.g. benign unsaturated species (CO, CO_2) or (potentially) hydridic/protic species (NH_3, BH_3, H_2)) to these centres came much later.

5.1.1.1 Small-Molecule Activation by Carbenes

Whilst the activation of H_2 had been achieved by digermynes [6] and Frustrated Lewis Pairs (FLPs) [7] prior, Bertrand and co-workers, in 2007, reported on the first single-site, homolytic scission of the H–H bond of dihydrogen by a group 14 element (Scheme 5.1) [8]. The reactive species were alkyl-amino carbenes (AACs, i.e. C(II) species). Similar to the heavier tetrelenes (see Chap. 1), these carbenes have a stable singlet state, and hence hold an sp^2-character lone-pair and an empty *p*-orbital. Comparisons between this electronic configuration and that of non-d^{10} transition metal (TM) complexes can be drawn: such complexes hold an empty orbital at the metal centre, which can interact with the σ-orbital of an H_2 molecule, and filled *d*-orbitals, which can interact with the σ*-orbital of the H_2 molecule (Fig. 5.1) [9, 10]. Hypothetically, the former interaction is possible with the empty *p*-orbital at a singlet tetrelene, whilst the latter may involve the lone pair of the same species (Fig. 5.1).

It was also shown that these AACs reacted with ammonia and carbon monoxide (Schemes 5.1 and 5.2) [8, 11], which are challenging molecules to activate due to

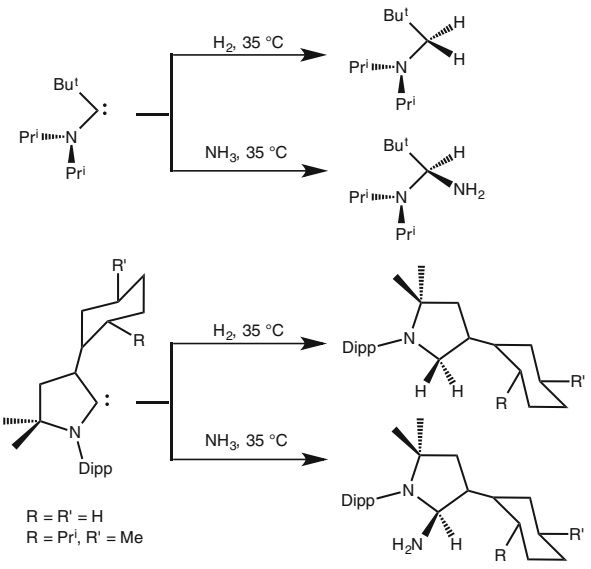

Scheme 5.1 The reactivity of singlet carbenes with H_2 and NH_3

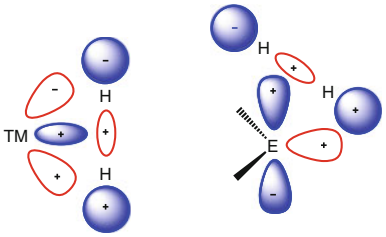

Fig. 5.1 The interaction of H_2 with (*left*) a TM fragment, and (*right*) a singlet tetrelene

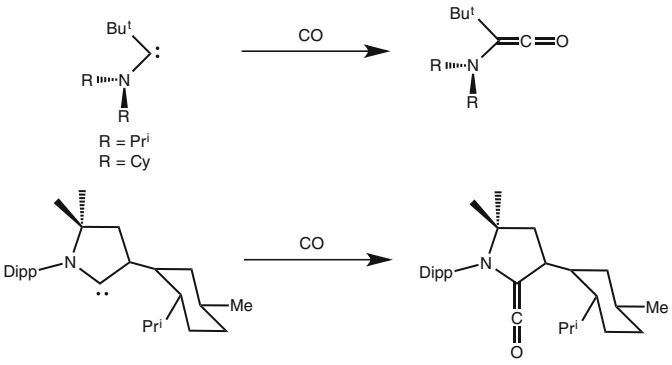

Scheme 5.2 The reactivity of alkyl-amino carbenes with carbon monoxide

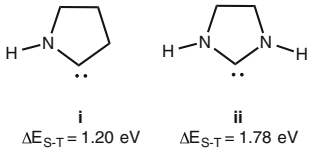

i $\Delta E_{S\text{-}T}$ = 1.20 eV **ii** $\Delta E_{S\text{-}T}$ = 1.78 eV

Fig. 5.2 The calculated singlet-triplet gap, $\Delta E_{S\text{-}T}$, of an alkyl-amino carbene and an N-heterocyclic carbene

their propensity to strongly ligate TM centres, rather than undergo bond-breaking reactions [12, 13]. Since these initial publications, further examples of the facile activation of ammonia and carbon monoxide by carbenes have been reported [14, 15].

This display of reactivity by monomeric carbon(II) species is largely related to the extremely narrow singlet-triplet gap ($\Delta E_{S\text{-}T}$) gap at the C(II) centre ($\Delta E_{S\text{-}T}$ = 1.20 eV, calculated for the model compound **i**, Fig. 5.2), compared to the far greater $\Delta E_{S\text{-}T}$ found in previously reported N-heterocyclic carbenes ($\Delta E_{S\text{-}T}$ = 1.78 eV, calculated for the model compound **ii**, Fig. 5.2) [8]. Further, the sp^2-character lone-pair of **i** was found to have high nucleophilicity, which in effect

activates the H_2 by first coordinating it, causing polarisation across the H_2 molecule. The second H atom, now hydridic, can donate to the low-lying LUMO of the C(II) centre, effecting the cleavage of the H–H bond. Overall, this reaction was found to be highly exergonic, with a calculated energy gain of 189 kJ mol^{-1} [8]. The C(II) centre can be seen as acting as a single-centre FLP, being concomitantly nucleophilic and electrophilic. This study demonstrates how the HOMO-LUMO gap of terelenes can be fine-tuned in order to increase or decrease the reactivity of these group 14 element(II) centres.

5.1.1.2 Small-Molecule Activation by the Heavier Tetrelenes

The facile homolytic cleavage of H_2 has also been achieved with the heavier tetrelenes, as has the activation of ammonia. Power and co-workers, in 2008, reported on the reactivity of the bulky bis(aryl) stannylene, $(^{Dipp}Terph)_2Sn$ ($^{Dipp}Terph$ = 2,6-$Dipp_2Ph$) with H_2 and NH_3, under non-forcing conditions (i.e. 65 °C, 1 atmosphere for the former; atmospheric temperature and pressure for the latter, Scheme 5.3) [16]. Again, these examples are comparable to transformations which have precedent to occur at TM centres [9, 10, 12, 13]. The observed products, however, were considerably different to the those observed from related reactions involving carbenes, in that only Sn(II) products were isolated. Further, for reactions with both H_2 and NH_3, one equivalent of protonated ligand was observed in the reaction mixtures. It transpired that the products formed were the known Sn (II) hydride complex, $\{(^{Dipp}Terph)Sn(\mu\text{-}H)\}_2$, and the novel amide-bridged Sn(II) complex, $\{(^{Dipp}Terph)Sn(\mu\text{-}NH_2)\}_2$, respectively. The mechanism for the addition of H_2 discussed above was shown to occur through initial partial OA of H_2 to the Sn (II) centre, forming $[(^{Dipp}Terph)_2SnH)\ldots(H)]$ as a transient species. This then spontaneously eliminates $^{Dipp}TerphH$, without first directly forming a stable Sn(IV) species. The mechanism is somewhat reminiscent of OA/RE cycles observed in TM catalysed transformations [17, 18].

Subsequently, related chemistry was reported which utilised Ge(II) species, and added plausibility to the hypothesised Sn(IV) intermediates in the reactions

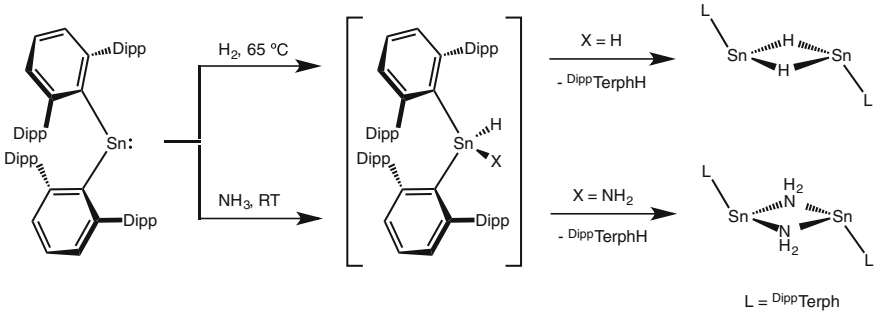

Scheme 5.3 Reaction of the stannylene, $(^{Dipp}Terph)_2Sn$, with dihydrogen and ammonia

described above. Addition of both H_2 and NH_3 readily occurred to two different bis (aryl) germylenes, (^{Dipp}Terph)$_2$Ge and (^{Mes}Terph)$_2$Ge (^{Mes}Terph = 2,6-Mes$_2$Ph; Mes = 2,4,6-Me$_3$Ph; Scheme 5.4) [19]. Both activated H_2 at 70 °C and atmospheric pressure, but different products were seen for the two reactions: the former yielded the arylgermane, (^{Dipp}Terph)GeH$_3$, with the elimination of one equivalent of ligand, whilst the latter formed the product of oxidative addition of a single equivalent of H_2, (^{Mes}Terph)$_2$GeH$_2$. The first of these reactions, involving (^{Dipp}Terph)$_2$Ge, likely follows the first two steps of the related Sn(II) reaction: OA of H_2, and RE of ^{Dipp}TerphH. However, transient [(^{Dipp}Terph)GeH] likely then undergoes further OA of a further equivalent of H_2. The reaction of (^{Mes}Terph)$_2$GeH$_2$ does not eliminate ^{Mes}TerphH, and hence it can be assumed that the greater bulk of the ^{Dipp}Terph ligand drives its elimination in the former reaction. Both bis(aryl) germylenes oxidatively add a single equivalent of ammonia with no ligand elimination in either case. These germanium-based reactions, therefore, give good evidence of an OA/RE mechanism in the generation of {(^{Dipp}Terph)Sn(μ-H)}$_2$ and {(^{Dipp}Terph)Sn(μ-NH$_2$)}$_2$ in the related Sn(II) reactions. The related asymmetrical bis(aryl) germylenes, (^{Mes}Terph)Ge(^{Dipp}Terph) and (^{Mes}Terph)Ge(^{Tripp}Terph) (^{Tripp}Terph = 2,6-Tripp$_2$Ph, Tripp = 2,4,6-^{i}Pr$_3$Ph) were shown to react rapidly with carbon monoxide at ambient temperature, likely through initial coordination of CO to the Ge(II) centre. However, in both reactions a ligand is activated through a C–C bond cleavage, revealing the presumed intermediary L$_2$Ge=C=O to be highly reactive. Whilst this CO activation reaction is unprecedented for group 14 complexes, the product has little relevance to further functionalisation reactivity.

The reactivity of heavier bis(aryl) tetrelenes towards various other HX bonds (X = CN$^-$, N$_3^-$, F$^-$, SO$_3$CF$_3^-$) has also been reported by Power and co-workers, with OA, forming E(IV) compounds (E = Ge or Sn), observed in all cases [20].

The reactivity of silylenes has perhaps seen the most attention of the heavier tetrelenes, with many N-heterocyclic and cyclic bis(alkyl) silylenes known. As the majority of this reactivity is outside of the context of this introduction, it will not be discussed here. Such research has, however, been the subject of several recent

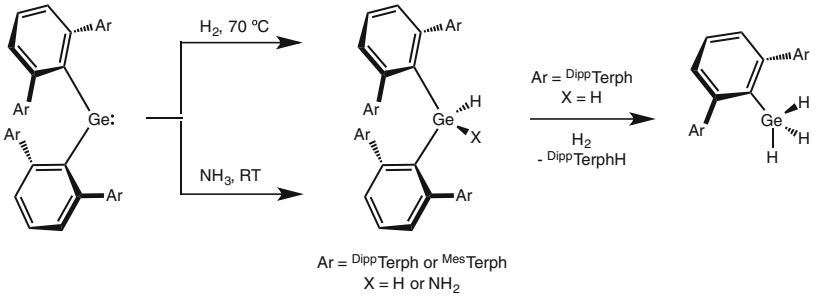

Scheme 5.4 Reactions of the germylenes, (^{Mes}Terph)$_2$Ge and (^{Dipp}Terph)$_2$Ge, with dihydrogen and ammonia

comprehensive review articles [21–23]. Highlights of this chemistry will be discussed in Chap. 6.

5.1.1.3 σ-Metathesis Reactions Involving Tetrelenes

Whilst the imitation of TM complexes by the heavier group 14 elements is a topic of pronounced significance, the mechanistic challenges of a well-defined OA/RE catalytic cycle are clear [17]. On the contrary, examples of well-defined MG catalysis that occurs via σ-metathesis type mechanisms are known, and take advantage of the polarity of A–X bonds (e.g. group 2 catalysed hydroboration, hydrosilylation, and hydrogenation; FLP catalysed hydrogenations; A = group 2 or group 13/15 element, X = H, C, O, N, etc.) [24–29]. Whilst the reactivity of E–X bonds (E = group 14 element(II), X = H, C, O, N, etc.) is not as pronounced as that of group 2 and group 13 congeners, their possession of a vacant *p*-orbital and a sp^2-character lone-pair of electrons at the element(II) centre can lead to substrate coordination and activation (vide supra). Indeed, such an effect has lead to highly reactive group 14 element(II) hydride species (see Chap. 4), and has led to the stoichiometric generation of group 14 element(II) hydrides from germanium(II) formates and tin(II) amides.

The generation of a group 14 element(II) hydride from the σ-metathesis reaction of a B–H bond with a tin(II) amide was reported by Power and co-workers, in the synthesis of $\{(^{Dipp}Terph)Sn(\mu\text{-}H)\}_2$ [30]. It was found that the optimal route to this compound was the first the synthesis of $(^{Dipp}Terph)SnNMe_2$. This amide, when reacted with $BH_3{\cdot}THF$, cleanly formed the aforementioned Sn(II) hydride in high yield (Scheme 5.5). The most logical route by which the reaction can proceed is first through coordination of a BH_3 molecule to the NMe_2 moiety, followed by σ-metathesis of one of its hydride ligands with the Sn–N bond, forming the Sn(II) hydride, $\{(^{Dipp}Terph)Sn(\mu\text{-}H)\}_2$, and Me_2NBH_2. Related reactions have been involved in the synthesis of $(^{Dipp}nacnac)EH$ complexes (E = Ge and Sn; $^{Dipp}nacnac = [CH\{N(Dipp)C(Me)\}]^-$), whereby element halide precursors were reacted with $NMe_3{\cdot}AlH_3$ (see Chap. 3) [31].

Beyond these examples, both the groups of Roesky and Driess independently reported on the reactivity of $(^{Dipp}nacnac)GeOC(H)O$ with hydride sources [32, 33]. In effect, this would regenerate the Ge(II) hydride, $(^{Dipp}nacnac)GeH$, which had

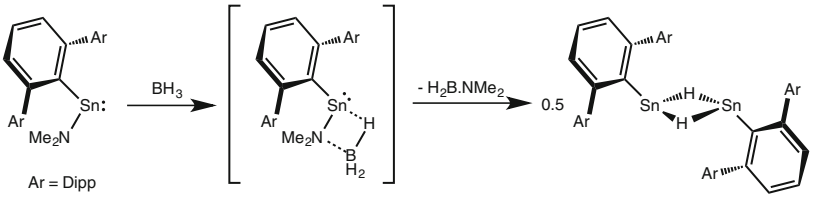

Scheme 5.5 The synthesis of $\{(^{Dipp}Terph)Sn(\mu\text{-}H)\}_2$ via σ-metathesis

been shown to readily react with CO_2 to quantitatively generate (^{Dipp}nacnac)GeOC(H)O (Scheme 5.6) [34]. Hence, the formation of the hydride starting material from (^{Dipp}nacnac)GeOC(H)O has an implicit relation to the mechanistic aspects of catalytic CO_2 reduction. The study published by Roesky and co-workers involved the addition of either $LiNH_2{\cdot}BH_3$ or $NH_3{\cdot}BH_3$ to the Ge(II) formate. The former cleanly reacted yielding the Ge(II) hydride, LiOC(H)O, and presumably NH_2BH_2, or a polymer thereof, almost quantitatively (Scheme 5.6) [32]. No mechanistic aspects of this reaction were discussed, but ^{1}H NMR spectroscopy clearly revealed the generation of up to 95% LiOC(H)O against a 1,4-dioxane standard. The latter reaction, with $NH_3{\cdot}BH_3$, proceeded slowly at ambient temperature, but was complete after ~20 h when carried out at 60 °C (Scheme 5.6). Although the generation of (^{Dipp}nacnac)GeH was observed, it made up only ~50% of the reaction mixture, along side ~30% of an unidentified product, and ~20% ^{Dipp}nacnacH. More interesting was the product resulting from the reduction of the formate moiety: the methanol derivative, $NH_3{\cdot}BH_2OCH_3$. Monitoring of the reaction through ^{13}C labelling of the formate unit did not yield concrete mechanistic details, but quenching of the complete reaction mixture with D_2O generated up to ~45% CH_3OD [32]. These results are in keeping with previously reported TM-catalysed CO_2 hydroborations, which tend to see the formation as R_2BOCH_3 (R = organic ligand) as the major product [35, 36].

The study by Driess and co-workers focused on reactions of $NMe_3{\cdot}AlH_3$ with the Ge(II) formate, (^{Dipp}nacnac)GeOC(H)O. Their investigation concentrated on the mechanistic aspects of the generation of (^{Dipp}nacnac)GeH and by-products occurring from this process (Scheme 5.7) [33]. It was found that, similar to reactions of the Ge(II) formate with $NH_3{\cdot}BH_3$, the related reaction with $NMe_3{\cdot}AlH_3$ formed (^{Dipp}nacnac)GeH, although much more rapidly (i.e. complete conversion of starting

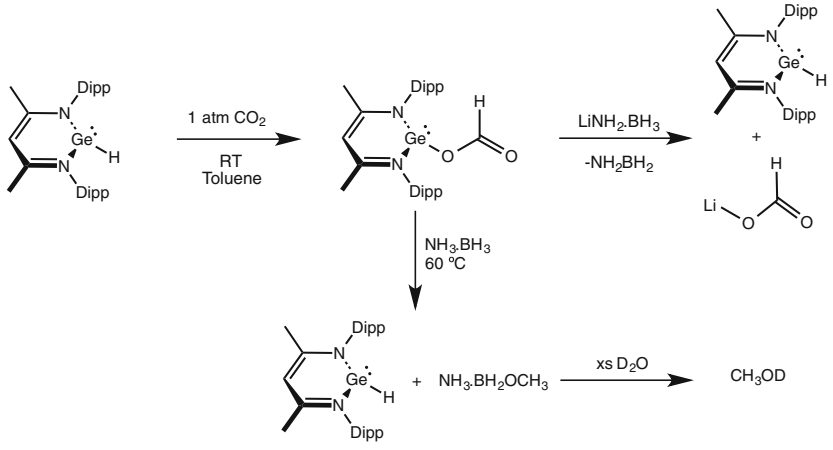

Scheme 5.6 Differing reactivities in the regeneration of (^{Dipp}nacnac)GeH from (^{Dipp}nacnac)GeOC(H)O and $LiNH_2{\cdot}BH_3$ or $NH_3{\cdot}BH_3$

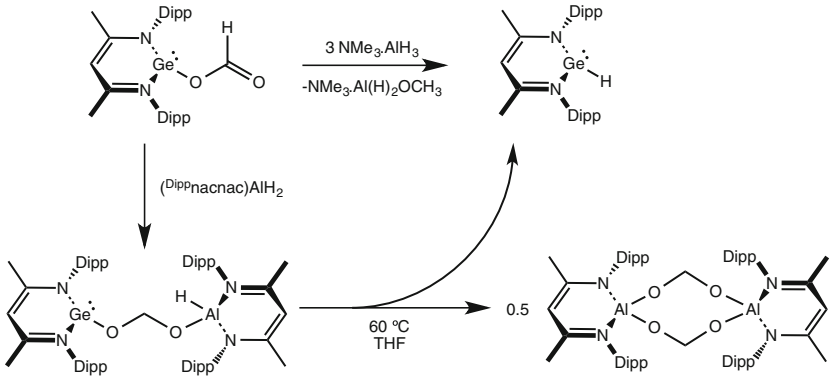

Scheme 5.7 The reaction of (^{Dipp}nacnac)GeOC(H)O with alane species

materials within two hours at ambient temperature). The yield of CH_3OD, after quenching the reaction mixture with D_2O, was in keeping with those reported by Roesky (i.e. 46%). Subsequently, reaction of (^{Dipp}nacnac)GeOC(H)O with the less reactive N-heterocyclic alane, (^{Dipp}nacnac)AlH_2, shed light on the intermediates in the former reaction. Addition of one equivalent of the N-heterocyclic alane to the Ge(II) formate led to the formation of a rare example of an OCH_2O-bridged bimetallic complex, (^{Dipp}nacnac)$GeOCH_2OAl(H)$(^{Dipp}nacnac), through effective hydroalumination of the C=O moiety of the Ge(II) formate (Scheme 5.7). Further, it was found that warming this species to 60 °C for three hours in THF led to the elimination of (^{Dipp}nacnac)GeH, and formation of a dimeric doubly-OCH_2O-bridged bis(N-heterocyclic alane), $\{(^{Dipp}nacnac)Al(OCH_2O)\}_2$. Whilst interesting, this study is perhaps too far removed from common catalytic CO_2 reduction reactions which involve monohydride reagents (e.g. HBpin, pin = pincolato), which cannot strictly follow the same route as was observed for the reaction between (^{Dipp}nacnac)GeOC(H)O and (^{Dipp}nacnac)AlH_2.

Outside of these examples, the reactivity of catalytically relevant H-sources with low-oxidation state group 14 element compounds through a σ-metathesis mechanism has not seen much attention in the literature.

5.1.2 Main-Group Catalysis

Although a relatively young field, MG catalysis has seen flourishing success over the past two decades, with countless group 2 and FLP catalysed transformations now known (e.g. CO_2 reduction, alkene hydroamination, carbonyl and imine hydroboration and hydrogenation, etc.), and related isolated examples from groups 1, 13, 14, and 15 [37–39]. Here, selected relevant examples will be discussed apropos of the results achieved in the original research contained in this chapter.

5.1.2.1 Group 12 Element Catalysed Functionalisation of Organic Unsaturations

Many TM catalysed transformations can involve complicated mechanisms with highly reactive intermediates, and as such, although impressive in their achieved transformations, can remain ill-defined. On the other hand, MG catalysed transformations often grow from stoichiometric reactivity studies, and in this regard can be seen as relatively well defined, where intermediates are fully characterised and their further reactivity in a catalytic regime documented. Further, group 2 complexes have seen comparison with lanthanide complexes, in that the metal ions form highly polarised ionic bonds that undergo σ-metathesis and insertion type reactivities of their M–X bonds (M = a trivalent lanthanide element/divalent group 2 element, X = a monoanionic σ-bonded substituent) [26, 40]. Thus, it has been postulated that sufficiently stable group 2 species, with discreet M–X moieties, would be capable of catalytic transformations already known for corresponding lanthanide complexes. Group 2 catalysed examples of such conversions will be briefly discussed.

The hydrocarbon-soluble Ca(II) hydride complex, (^{Dipp}nacnac)CaH·THF, has been shown effective in numerous stoichiometric hydrometalation reactions by Harder and co-workers [24]. Amongst these reactions were the addition to imines, ketones, and activated/conjugated alkenes (Scheme 5.8) [41]. The synthetic protocol for the generation of the hydride starting material suggested further reactivity of the products of these addition reactions may be possible, in that it involved the σ-metathesis of a Ca(II) amide with $PhSiH_3$ (Scheme 5.8) [42]. Thus, catalytic investigations using this calcium(II) hydride, and similar soluble calcium(II) species, have covered the hydrosilylation of ketones (Scheme 5.8) and the hydroboration of activated alkenes. Mechanisms for the former are thought to occur via hyper-coordinate silicon species, which are more reactive to insertion of unsaturated substrates, compared to tetra-coordinate silanes [43, 44]. The hydroboration of alkenes was found to not be true catalysis, but to instead form various reactive borane species (e.g. BH_4^-), via Ca(II) mediated degradation of HBcat (cat = catecholato). It is therefore unclear as to whether these catalytic transformations can be considered as proceeding via a σ-metathesis mechanism. However, the hydrogenation of activated alkenes, catalysed by hydrocarbon soluble Ca(II) species, has also been reported, and is thought to occur by the cleavage of H_2 through a σ-bond metathesis between a Ca–C bond and a H–H bond, and occurs at relatively low pressures of H_2 (20 bar). This suggests that such Ca(II) species can indeed be highly reactive and active in 'lanthanide-mimicking' σ-metathesis-based catalysis (Scheme 5.8).

The group of Hill has shown has given further evidence that catalytic mechanisms involving the heavier group 2 elements occur through a σ-metathesis mechanism [26]. For example, they have reported on the mechanism of magnesium and calcium catalysed hydroamination reactions reinforced by in-depth DFT calculations [45]. The mechanism of the cyclisation of alkenyl amines, for example, occurs through initial protonolysis of a heavier alkaline earth metal species, often an

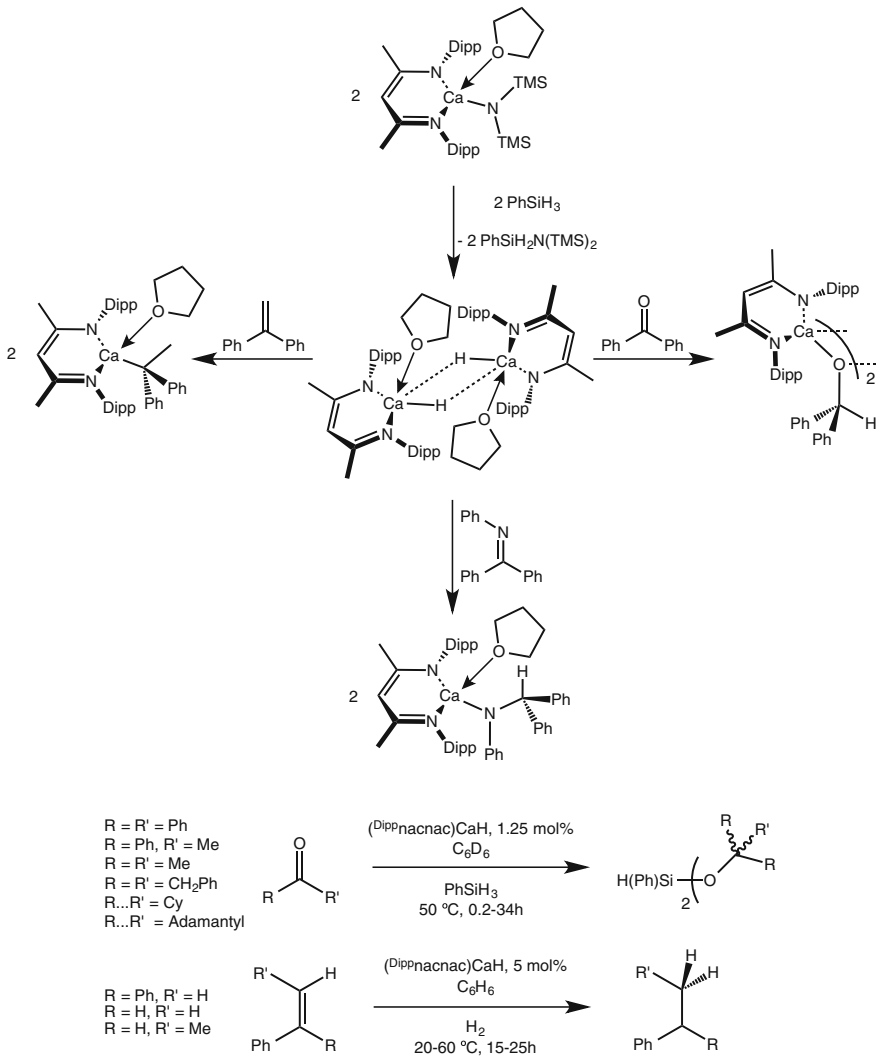

Scheme 5.8 *Above* Synthesis and examples of reactivity of $\{(^{Dipp}nacnac)CaH{\cdot}THF\}_2$; *Below* Examples of catalytic applications of $\{(^{Dipp}nacnac)CaH{\cdot}THF\}_2$

alkyl or amide complex (Scheme 5.9), by a alkenyl amine, forming a terminal amide. The alkenyl moiety of this amide can then orientate itself to form a four membered transition state (Scheme 5.9, *Transition* (a)), with subsequent σ-metathesis of the M–N bond. The newly formed M–C bond can then undergo protolysis with one more equivalent of the alkenyl amine substrate (Scheme 5.9, *Transition* (b)). Whilst Scheme 5.9 is indicative of a general mechanism for intramolecular hydroamination [46], the catalytic synthesis of numerous modified

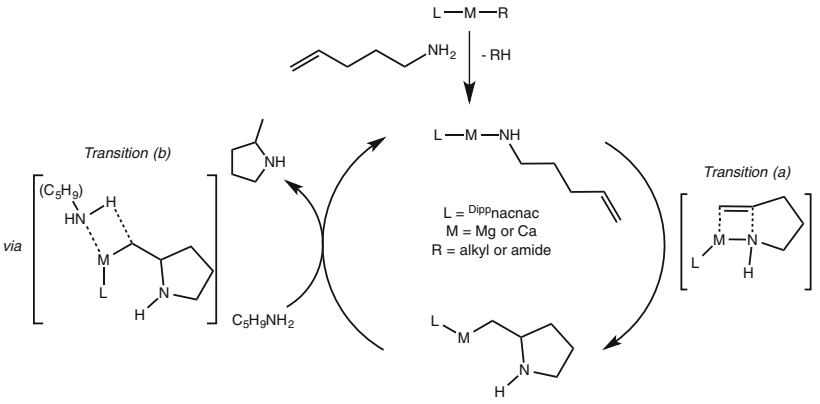

Scheme 5.9 A representative scheme for the mechanism of intramolecular hydroamination by heavier alkaline earth metal complexes

cyclised amines have been reported (e.g. 6-membered rings, tertiary and quaternary carbons incorporated into the ring, etc. [26]), as well as examples of intermolecular hydroamination examples, showing the broad synthetic utility of this group 2 catalysed transformation.

More recently, the group 2 element complex, (^{Dipp}nacnac)MgBu^{n}, has seen prominent application to the catalytic hydroboration of aldehydes, ketones, imines, and pyridine derivatives [25, 47, 48]. Similar to the described hydroamination examples, these hydroborations occur through σ-metathesis mechanisms. However, where the hydroamination reactions can be seen as protic, the hydroboration transformations are hydridic, with substrate insertion into a M–H bond, rather than a M–N bond. Although the mechanism has not been elucidated through computational studies, crystalline intermediates were structurally characterised, which exposed the propensity for the formation of Lewis-pair-like adducts (e.g. (^{Dipp}nacnac)MgOC(H)Ph$_2$.pinBOC(H)Ph$_2$, Scheme 5.10b) [25]. Further evidence for the σ-metathesis mechanism was illuminated through kinetic studies. It was found that addition of an excess of HBpin to catalytic reaction mixtures led to a notable decrease in reaction rate [48]. It was hypothesised that this phenomenon was due to coordination of HBpin to the in situ generated {(^{Dipp}nacnac)MgH}$_2$, forming either a coordination complex (i.e. {(^{Dipp}nacnac)MgH}$_2$.HBpin), or the borate, {(^{Dipp}nacnac)MgH(μ-pinBH$_2$)HMg(^{Dipp}nacnac)} (Scheme 5.10a), a compound which had previously been fully characterised [47]. These results further highlight the necessity of substrate coordination in such MG-based catalytic regimes. It is worthy of note that attempted catalytic hydrosilylation of related substrates (e.g. pyridines) was attempted, but proved unsuccessful, presumably due to lack of polarisation in the proposed metathetical transition state (e.g. Si–H/Mg–N metathesis). Nevertheless, the large majority of examples of these heterofunctionalisation catalyses had previously only seen congeners in TM-based systems [49–54].

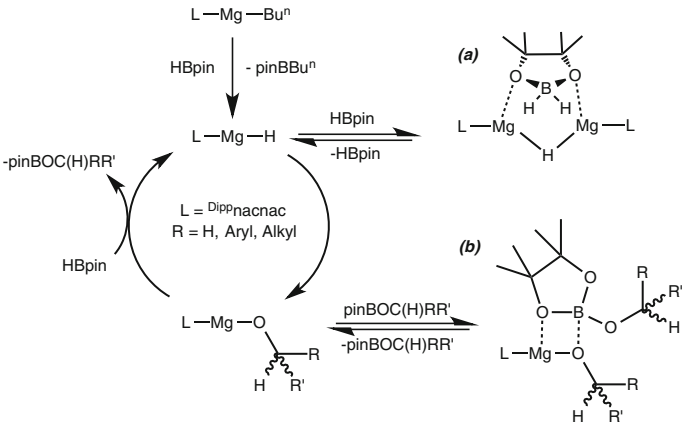

Scheme 5.10 Representative catalytic cycle for the hydroboration of C=O bonds catalysed by (^{Dipp}nacnac)MgH

5.1.2.2 Group 14 Element(II) Catalysed Functionalisation of Organic Unsaturations

Recently, Takagi and Sakaki reported on a comprehensive DFT analysis of the catalytic hydrosilylation of ketones by the Ge(II) hydride complex, (^{Dipp}nacnac)GeH [55], showing that such a regime is thermodynamically and kinetically plausible. The study revealed that activated silanes would favour this process, with viable reaction pathways found using F_3SiH. Importantly, the lowest energy transition-states involved in the stoichiometric reaction suggested coordination of both the ketone to (^{Dipp}nacnac)GeH, and F_3SiH to (^{Dipp}nacnac)GeOC(H)R_2, occurred in the catalytic cycle, further evidencing that lower-coordinate systems may be favourable in these transformations.

Examples of catalysis occurring at a group 14 element(II) centre are rare. Prior to the outset of this thesis, only one example of such a regime had been published. This example involved the use of tin(II) triflate, neutral N-donor ligands (e.g. TMEDA; TMEDA = *N*,*N*,*N*′,*N*′-tetramethylethylenediamine, 2,6-pyridine-bis (2H-oxazoline) (PYBOX, Scheme 5.11), and the polymeric silane, PMHS (PMHS = polymethylhydrosiloxane), in the hydrosilylation of aldehydes and ketones. Whist this is promising, catalyst loadings were high (10 mol%), and reactions were ill-defined, with no confident discussion of catalytic intermediates. It was postulated that the reaction occurred through a transient Sn–H complex, but again, no proof of this was given. It is worthy of note, however, that chiral ligands were successfully utilised in this synthetic procedure. Best results were found with Ph_2PYBOX (Scheme 5.11), which gave generally high conversions (77–99%) and average e.e. values (12–48%).

One further example of a group 14 element(II) catalysed transformation has very recently been published, by Siwatch and Nagendran. They found that an

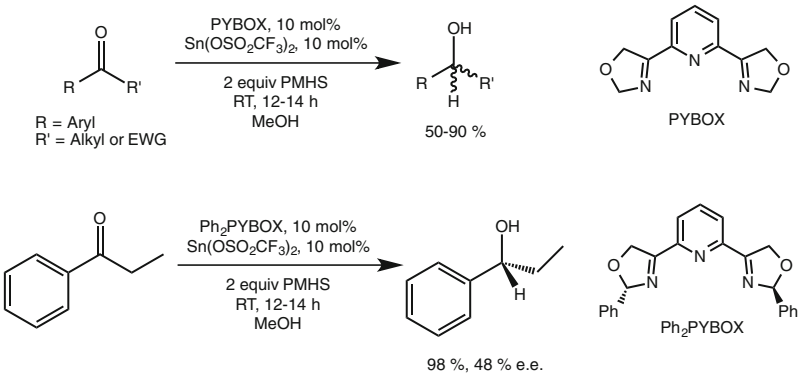

Scheme 5.11 *Above* The reduction of ketones, catalysed by Sn(II) triflate, by PMHS/MeOH, and *below*: and example of the steroselective reduction of a ketones catalysed by Sn(II) triflate

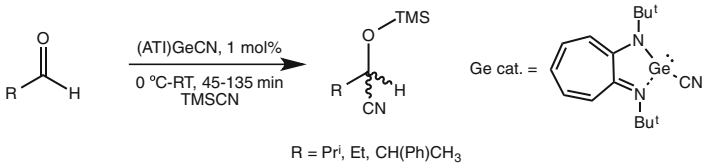

Scheme 5.12 The cyanosilylation of aldehydes catalysed by the Ge(II) complex, (ATI)GeCN

aminotroponiminate (ATI) Ge(II) cyanide complex, (ATI)GeCN, was capable of the cyano-silylation of aldehydes, rapidly (T = 45–135 min) at room temperature (Scheme 5.12). This stands as an important example of catalytic C–C bond formation. Unfortunately, whilst stoichiometric reaction studies characterised the overall transformation to some degree (e.g. isolation of (ATI)Ge-alkoxide complexes), DFT or kinetic studies were lacking. Further, such transformations have been achieved by numerous main-group systems, including metal-free examples (e.g. carbenes [56], thiourea [57]). Nevertheless, its expansion into low-oxidation state heavier group 14 chemistry may lead to investigations of related transformations occurring at such element centres, and a blossoming of this field.

5.1.2.3 Catalytic Reduction of CO_2 by Well-Defined Hydride Species

Despite the burgeoning acceptance of human-driven CO_2 generation as a prolific issue in the changes to our planet's climate [58], well-defined chemo-catalytic transformation of this molecule has only recently seen serious attention (note that electrocatalytic reduction of CO_2 has seen considerable attention for some time [59, 60], as has that by heterogeneous catalysis [61]). More recently, examples of the functionalisation of CO_2 to a range of C1 compounds (i.e. methane [62, 63],

CO [64, 65], and methanol derivatives [66, 67]), and in one case to higher carbon derivatives (C2 [68]), have been reported, using both TM and MG element catalysts, and reactants such as mild boranes (e.g. HBpin) and silanes (e.g. $PhSiH_3$). The formation of methanol is of particular interest, due to its potential direct use as a C1 feedstock in modern fuel technologies [69, 70]. The mechanism of its formation is complicated, and as yet has not been entirely elucidated experimentally, although hypotheses have been drawn based on the observation of generally fleeting intermediates (Scheme 5.14) [71]. Nevertheless, the overall transformation involves abstraction of one O atom, as, for example, R_2BOBR_2 in the case of hydroboration (Scheme 5.13). It seems logical that this abstraction results in a concomitant generation of formaldehyde. This can then react with the catalytically active hydride complex, forming an element methoxide, which can undergo σ-metathesis with the hydridic reagent (e.g. HBpin), thus forming the final methanol derivative, and regenerating the catalyst. As such, the CO_2 reduction can be seen as occurring in two steps: the reduction of CO_2 to formaldehyde, and the reduction of formaldehyde to methanol, as represented in Scheme 5.13, with HBpin as the hydride source.

The initial oxygen abstraction is accepted to occur through hydroelementation of CO_2, generating an element-formate. The steps that follow, however, are unclear. The formate species can undergo further hydroelementation by the hydride source (e.g. HBpin, cycle A, Scheme 5.14), or the hydrido catalyst complex (cycle B, Scheme 5.14). Further, the formate moiety can undergo σ-metathesis with the hydridic reagent, regenerating the hydride catalyst and forming a new element formate species (e.g. pinBOC(H)O, Scheme 5.14). The two potential OCH_2O-bridged species (e.g. $LMOCH_2OBpin$, $pinBOCH_2OBpin$) have been postulated to spontaneously eliminate formaldehyde, with concomitant formation of mono oxo-bridged species (e.g. LMOBpin, pinBOBpin). Presumably, if the former example, LMOBpin, was generated, it would undergo σ-metathesis with the hydride reagent to regenerate the active catalyst. Whilst these intermediates have been hypothesised, their isolation as part of a catalytic cycle is lacking, and as such the formation of formaldehyde via this mechanism is still hypothetical. This case is exacerbated by the high reactivity of formaldehyde. For example, a computational analysis of CO_2 hydroboration by HBcat, catalysed by an FLP, found that the

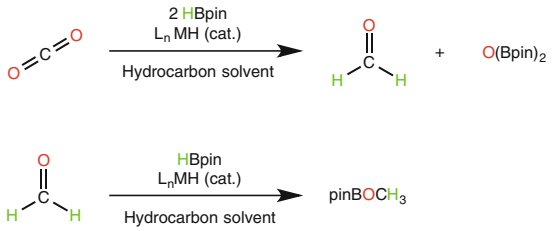

Scheme 5.13 The two steps of CO_2 reduction to pinBOMe by three equivalents of HBpin, catalysed by a general metal hydride complex, L_nMH (L = a typical mono- or poly-anionic ligand)

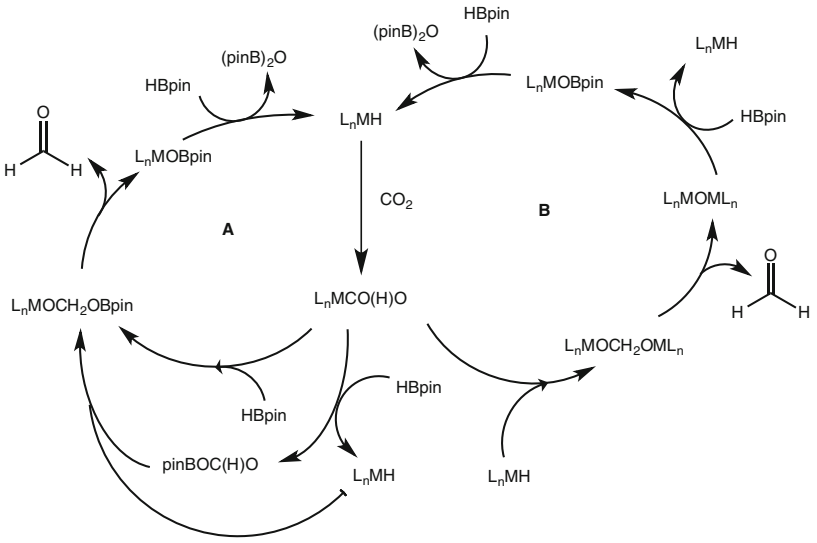

Scheme 5.14 Proposed competing catalytic cycles for the reduction of CO_2 to formaldehyde by HBpin, catalysed by a single-site metal hydride complex

catalyst-free addition of HBcat to formaldehyde is an exergonic reaction [72]. However, Sabo-Etienne and co-workers were successful in quantitatively isolating formaldehyde from the reduction of CO_2 with HBpin, catalysed by a Ru-complex, through trapping the formaldehyde with the bulky aniline, $DippNH_2$, proving at least that it is formed, if only transiently in the absence of a trapping agent [73].

Whilst FLPs and TMs have been applied to the catalytic reduction of CO_2, relatively few single-site MG element hydride species have seen use in this relatively undeveloped area, with one example for each magnesium(II) [71], Ca(II) [71], and Ga(III) [74]. These single-site MG-catalysed reductions have low TOFs (TOF = turn over frequency) (e.g. Mg(II) = 0.07 h^{-1}, Ga(III) = 2.5 h^{-1}, Scheme 5.15), with TM-catalysed derivatives being somewhat more rapid (e.g. Ru-hydride: TOF = ~20 h^{-1}). More active catalysts are known, but generally only in systems incorporating more reactive boranes (relative to HBpin) and higher temperatures (e.g. BH_3, 70 °C, TOF ~740 h^{-1} [75]), and so are out of the context of this discussion.

It is worthy of note that a DFT study on the hydrosilylation of CO_2, catalysed by (Dippnacnac)GeH, was also undertaken by Takaki and Sagaki, which found the reaction was indeed favourable for the silane F_3SiH, much like that of ketones reported in the same publication (vide supra) [55]. The reaction proceeds through initial hydrogermylation of CO_2, a reaction reported by Roesky [34]. The second step involved a σ-metathesis of the silane Si–H bond with the Ge–O bond, via a four membered transition state, yielding a silaformate. A discussion relating to the possible addition of F_3SiH across the C=O bond of the formate moiety in (^{Dipp}nacnac)GeOC(H)O was lacking, as was the further reactivity of silyl formate.

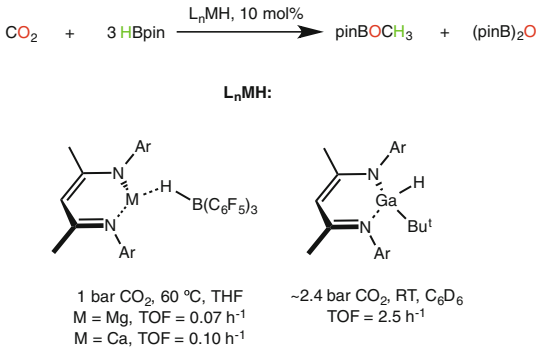

Scheme 5.15 The reduction of CO_2 with HBpin, catalysed by single-site MG hydride complexes

One can therefore not be sure if such reaction pathways were looked into, and if the published calculated reaction pathway was compared to these alternative reactivities.

5.2 Research Proposal

Given the literature precedent for oxidative addition/reductive elimination reactivity to occur at low-oxidation state and low-coordinate group 14 element species, it seems highly plausible to suggest that transition-metal mimicking catalysis could be achieved at such element centres. Further, whilst small molecule activation has been achieved by these group 14 elements, this area remains relatively unexplored in terms of applied stabilising ligands and small molecules studied. Thus, investigations into this reactivity on a stoichiometric basis using amido-alkyl and amido-alkoxy germylenes and stannylenes was to be investigated. Though redox active catalysis may be challenging, it seemed plausible that σ-metathesis would be possible at low-oxidation state low-coordinate group 14 element centres for several reason: (a) computational DFT results suggest that catalytic ketone hydrosilylation is, under the right conditions, exergonic, (b) well established group 2 catalysis occurs via σ-metathesis mechanisms, of which related reactions have been reported to occur at low-oxidation state group 14 centres, and (c) an example, all be it ill defined, of tin(II) catalysed hydrosilylation exists, which likely proceeds via a transient tin(II) hydride. So, stoichiometric studies in light of σ-metathesis was to be attempted, so as to assess the plausibility of such catalysis being performed by group 14 element(II) complexes.

5.3 Results and Discussion

5.3.1 *Stoichiometric Reactivity Studies of Amido-Alkyl and Amido-Alkoxy Germylenes and Stannylenes*

As described in Sect. 5.1.1, 2-coordinate group 14 element(II) centres can be reactive towards oxidative-addition (OA) reactions, given the generally accepted stability of the +4 oxidation state over the +2 oxidation state for these elements, aside from lead (see Chap. 1). However, where extremely bulky ligands are employed in the stabilisation of such group 14 element(II) complexes (e.g. Power's terphenyl ligands), reductive-elimination (RE) can be driven, hypothesised to be due to the steric buttressing at intermediary tetravalent group 14 species (see Sect. 5.1.1.2). We sought to explore such chemistry utilising the amido-alkyl and amido-alkoxy germylenes and stannylenes described in Chap. 4.

5.3.1.1 Reactivity of Amido-Alkyl Germylenes

We first attempted reactions of the amido-alkyl germylenes (i.e. ($^{iPr}L^{\dagger}$)GeR; R = an alkyl group), with catalytically relevant hydridic small molecules (i.e. silanes, mild boranes and alanes). Note that OA of such hydridic species has not been observed for heavier group 14 element(II) complexes. Nevertheless, generation of {($^{iPr}L^{\dagger}$)GeH}$_2$ (**1**) through either OA/RE or σ-metathesis would be of interest, and may converge with a catalytic regime. The boranes, HBcat and HBpin, showed no reaction with any of the ($^{iPr}L^{\dagger}$)GeR species, as was the case with $PhSiH_3$, Et_3SiH, $(EtO)_3SiH$, and DIBAL, at ambient or elevated temperatures (80 °C), as judged by NMR spectroscopic studies. The reaction of several ($^{iPr}L^{\dagger}$)GeR species with H_2 was also attempted, at ambient temperature and elevated temperature (80 °C), and at increased pressure (70 bar), but under no circumstance was a reaction observed.

We then turned our attention to protic substrates (Scheme 5.16), with greater literature precedent for reactions of such X–H bonds with unsaturated group 14 element complexes [16, 19, 20]. It was found that addition of a stoichiometric

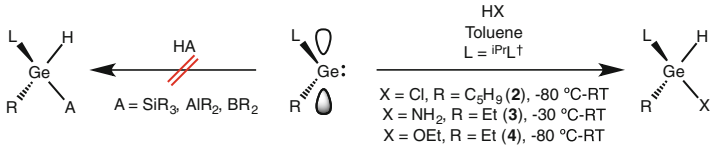

Scheme 5.16 Reactions of element–H bonds with amido-alkyl germylenes

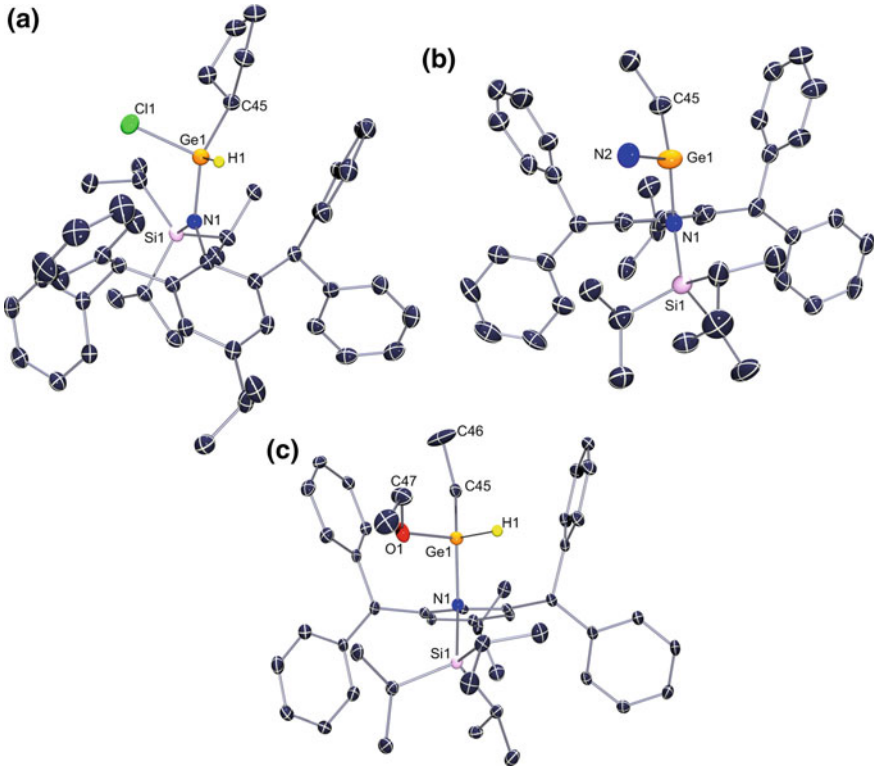

Fig. 5.3 ORTEP representations of **a** ($^{iPr}L^{\dagger}$)Ge(H)(C_5H_9)Cl (**2**), **b** ($^{iPr}L^{\dagger}$)Ge(H)(Et)NH_2 (**3**), and **c** ($^{iPr}L^{\dagger}$)Ge(H)(Et)OEt (**4**) (thermal ellipsoids at 30% probability, hydrogen atoms omitted, aside from terminal hydrides in **2** and **4**). Selected bond lengths (Å) and angles (°), **2**: Ge1–Cl1 2.189(1), Ge1–H1 1.525(6), Ge1–N1 1.864(3), Ge1–C45 1.952(4), N1–Ge1–Cl1 111.09(1), N1–Ge1–C45 122.90(2), N1–Ge1–H1 108.48(2); **4**: Ge1–O1 2.103(3), Ge1–H1 1.483(4), Ge1–N1 1.859(2), Ge1–C45 1.930(4), N1–Ge1–O1 106.65(1), N1–Ge1–C45 111.92(2), N1–Ge1–H1 108.73(1)

amount of HCl, as an Et_2O solution, to ($^{iPr}L^{\dagger}$)GeC_5H_9 resulted in oxidative addition of HCl, yielding the Ge(IV) complex ($^{iPr}L^{\dagger}$)Ge(H)(C_5H_9)Cl (Scheme 5.16, **2**). At this stage this has only be shown through X-ray crystallographic analysis, with the reaction showing the presence of multiple other species, including amounts of protonated ligand, $^{iPr}L^{\dagger}H$. The molecular structure of **2** is shown in Fig. 5.3. The Ge (IV) centre sits in a tetrahedral geometry, with the H-ligand located from difference maps and freely refined. The Ge1–H1 (1.525(6) Å), Ge–Cl1 (2.189(1) Å), Ge1–N1 (1.864(3) Å), and Ge1–C45 (1.952(4) Å) distances are all of typical lengths, giving little evidence for potential RE of any two substituents. Other structural characteristics are as would be expected.

Following this, ($^{iPr}L^{\dagger}$)GeEt was reacted with amines, anilines, and alcohols. No reaction was observed with anilines, or primary and secondary amines even after heating, suggesting perhaps that the pronounced bulk of the $^{iPr}L^{\dagger}$ ligand prevents

the approach of the substrates to the Ge(II) centre. However, ($^{iPr}L^{\dagger}$)GeEt reacted instantaneously with excess dry ammonia at ambient temperature, as assessed by a ^{1}H NMR spectroscopic analysis of a C_6D_6 solution of the crude reaction mixture. The presence of excess ammonia led to the generation of a large amount of protonated ligand (~50%), either due to over-reaction or the presence of small amounts of moisture. Accordingly, the addition of a single equivalent of gaseous ammonia to a cooled (−30 °C) solution of ($^{iPr}L^{\dagger}$)GeEt resulted in the clean formation of a single product. The ^{1}H NMR spectrum of the product suggested that the OA of an N–H bond of ammonia had occurred, forming ($^{iPr}L^{\dagger}$)Ge(H)(Et)NH_2, **3** (Scheme 5.16). The CH_2 group of the terminal Et moiety of the product appeared as two distinct multiplets (δ = 0.20 and 0.37 ppm), indicative of being bound to a chiral centre. Further, a 1H multiplet at δ = 5.52 ppm was attributed to a terminal Ge–*H* moiety. Further evidence for this was given by a 2D NMR spectroscopic analysis (COSY) which revealed that this 1H resonance coupled to the two multiplets centred around ~0.3 ppm.

Although large crystals of the product were grown, they were badly twinned, resulting in poor quality diffraction data. Structural parameters will therefore not be discussed. They did, however, reveal the connectivity to be as described above (Fig. 5.3). This was further reinforced by an accurate microanalysis of the pure crystalline solid. The reaction of ($^{iPr}L^{\dagger}$)GeEt with alcohols also readily occurred, but, similar to the reaction with ammonia, yielded considerable amounts (up to 40%) of protonated ligand if carried out uncontrolled. However, the addition of one equivalent of EtOH to ($^{iPr}L^{\dagger}$)GeEt at −80 °C (Scheme 5.16), followed by slow warming over four hours, led to the isolation of large colourless crystalline blocks of the product after recrystallisation from a minimum amount of hexane. As was the case with **3**, the ^{1}H NMR spectrum of the product revealed that the peak relating to the terminal CH_2 of the Ge–Et group was now split into two clear multiplets, which coupled to a multiplet centred at δ = 5.97 ppm (i.e. a Ge–*H*) in its COSY NMR spectrum. Further, signals assigned to the C*H*$_2$ of the Ge–OEt group were split into two clear multiplets, with each H of this CH_2 group coupling to each other, and the neighbouring CH_3 group. An X-ray crystallographic analysis of the crystalline solid confirmed the product to be ($^{iPr}L^{\dagger}$)Ge(H)(Et)OEt, **4** (Fig. 5.3), as a racemic mixture of the *R* and *S* isomers of this chiral species. As was the case with **3**, Ge1–H1 (1.483 (4) Å), Ge1–O1 (1.803(3) Å), Ge1–N1 (1.859(2) Å), and Ge1–C45 (1.930(4) Å) distances are in keeping with similar bonds in the literature, with no real evidence for potential reductive elimination from the molecule. Indeed, no change was seen in the ^{1}H NMR spectrum of **4** after extended heating in solution or the solid state. Nevertheless, the addition of ammonia and ethanol to ($^{iPr}L^{\dagger}$)GeEt are two rare examples of the facile activation of N–H and O–H bonds by a germanium(II) centre.

Finally, the addition of O_2 to ($^{iPr}L^{\dagger}$)GeC_6H_{11} was investigated, with the goal of isolating an extremely rare example of a germanone, $R_2Ge{=}O$ [76]. However, the isolated product consisted of the dimer of such a species, {($^{iPr}L^{\dagger}$)(C_6H_{11})GeO}$_2$ (**5**, Scheme 5.17), a product which has been observed previously from related reactions [77, 78]. The ^{1}H NMR spectrum of **5** shows highly broadened ligand signals

compared to those in the starting material, indicative perhaps of hindered ligand rotation, due to the dimeric nature of the product. The X-ray crystal structure of **5** (Fig. 5.4) reveals a planar central Ge_2O_2 ring, with the ligand on each germanium centre sitting *trans* on this ring, presumably so as to minimise steric repulsion between the two ligands. Both Ge1–O1 and Ge1–O1′ distances are of near identical length (1.829(1) Å and 1.819(1) Å, respectively), are in the known range of Ge–O single bonds, and are in keeping with previously reported examples of similar $(L_2GeO)_2$ species, thus rendering any potential monomer-dimer equilibrium between **5** and ($^{iPr}L^{\dagger}$)(C_6H_{11})Ge=O highly unlikely.

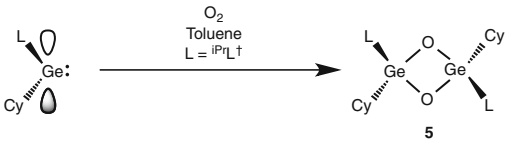

Scheme 5.17 The addition of O_2 to ($^{iPr}L^{\dagger}$)GeC_6H_{11}, forming {($^{iPr}L^{\dagger}$)$Ge(C_6H_{11})O$}$_2$ (**5**)

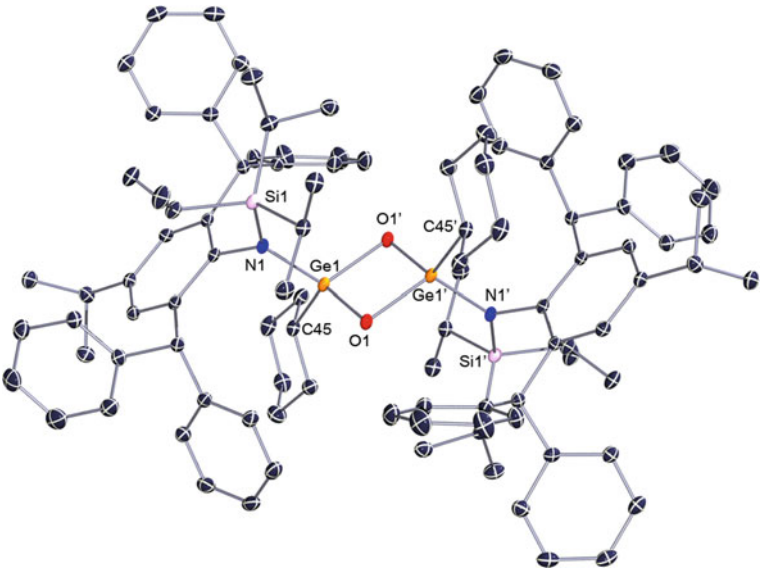

Fig. 5.4 ORTEP representations of **5** (thermal ellipsoids at 30% probability, hydrogen atoms omitted). Selected bond lengths (Å) and angles (°): Ge1–C45 2.003(2), Ge1–N1 1.883(2), Ge1–O1 1.818(1), Ge1–O1′ 1.829(1), Ge1…Ge1′ 2.6737(3), O1…O1′ 2.480(2), C45–Ge1–N1 106.24(8), O1–Ge1–N1 115.60(7), O1′–Ge1–N1 113.90(7), Ge1–O1–Ge1′ 94.29(6)

5.3.1.2 Reactivity of Amido-Alkyl Stannylenes

As with amido-alkyl germylenes, no reaction was observed between analogous stannylenes and HBpin, HBcat, $PhSiH_3$, Et_3SiH or $(EtO)_3SiH$, at ambient or elevated temperatures. However, the addition of H_2 to a solution of ($^{iPr}L^{\dagger}$)Sn$(CH_2)_2Bu^t$ at 70 bar led to the slow but quantitative conversion to protonated ligand, suggesting the stannylene is capable of H_2 activation, similar to those reported by Power [16, 19]. Whether a Sn(IV) species is formed, which then eliminates $^{iPr}L^{\dagger}H$ yielding the likely unstable Sn(II) hydride, $Bu^t(CH_2)_2SnH$, is unclear. Nevertheless, work is presently underway to achieve the related controlled activation of H_2.

The addition of protic substrates to ($^{iPr}L^{\dagger}$)SnEt generally resulted in the quantitative generation of free ligand (i.e. ammonia, anilines, primary amines, alcohols, and dry acids), even where reactions were stoichiometric and controlled (i.e. slow addition at −80 °C). The two exceptions to this were the reactions of ($^{iPr}L^{\dagger}$)SnEt with TEMPOH (TEMP = (2,2,6,6-tetramethylpiperidin-1-yl)) and Bu^tOH. Both reactions, through the elimination of EtH, generated the Sn(II) alkoxides/nitroxides, ($^{iPr}L^{\dagger}$)SnOTEMP (**6**) and ($^{iPr}L^{\dagger}$)SnOBu^t (**7**) (Scheme 5.18). Although when conducted on an NMR scale large amounts of protonated ligand were generated (typically >30%), EtH was observed as a singlet at ~0.8 ppm. Whether the mechanism occurs through RE from ($^{iPr}L^{\dagger}$)Sn(H)(Et)OR, or by a σ-metathesis is unclear. These reactions stand as examples of the stoichiometric transfer hydrogenation of ethylene by Sn(II), given that ($^{iPr}L^{\dagger}$)SnEt is initially synthesised by the addition of {($^{iPr}L^{\dagger}$)Sn(μ-H)$_2$} (**8**) to ethylene (Scheme 5.18).

The ^{1}H NMR spectrum of **6** exhibits highly broadened signals for both the $^{iPr}L^{\dagger}$ and TEMPO fragments, due to their bulk. Compound **6** crystallises as a monomer (Fig. 5.5), as with the Sn(II) alkoxides described in Chap. 4. Despite the potential radical character of TEMPO, the Sn1–O1 distance (2.039(2) Å) is in keeping with known Sn–O single bonds. The N1–Sn1–O1 angle of 96.77(7)° is indicative of a weakly stereo-active lone pair of electrons at the Sn(II) centre. Whilst **7** was not isolated as a pure compound from the reaction of ($^{iPr}L^{\dagger}$)SnEt with Bu^tOH, due to the presence of protonated ligand in the reaction mixture, it was synthesised in high yield from the addition of a toluene solution of ($^{iPr}L^{\dagger}$)SnCl to a suspension of

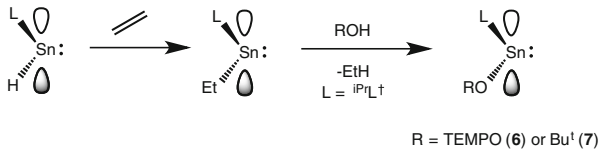

Scheme 5.18 The reaction of TEMPOH and Bu^tOH with ($^{iPr}L^{\dagger}$)SnEt

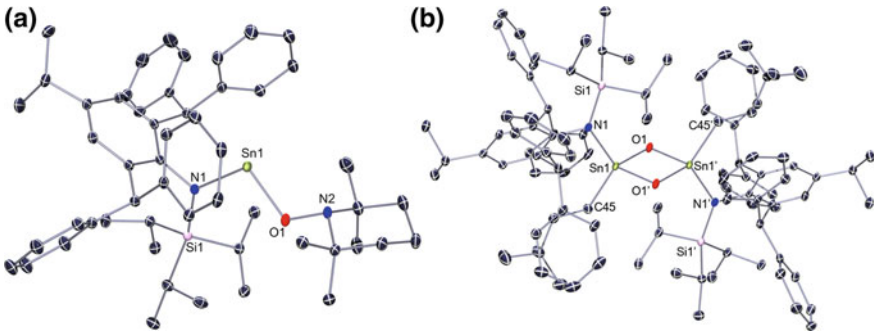

Fig. 5.5 ORTEP representations of **a** ($^{iPr}L^{\dagger}$)SnOTEMP (**6**) and **b** [($^{iPr}L^{\dagger}$)Sn{$(CH_2)_2Bu^t$}O]$_2$ (**9**) (thermal ellipsoids at 30% probability, hydrogen atoms omitted). Selected bond lengths (Å) and angles (°) for **6**: N1–Sn1 2.128(2), Sn1–O1 2.039(2), O1–N2 1.462(2), N1–Sn1–O1 96.77(7), Sn1–O1–N2 108.22(1), Si1–N1–Sn1–O1 2.47(1), N1–Sn1–O1-N2 1.72(1); **9**: Sn1–O1 2.009(3), Sn1–O1′ 2.003(2), N1–Sn1 2.065(3), Sn1–C45 2.143(6), Sn1…Sn1′ 2.9859(4), O1…O1′ 2.681 (4), N1–Sn1–C45 108.31(2), O1–Sn1–O1′ 83.83(1), Sn1–O1–Sn1′ 96.17(1)

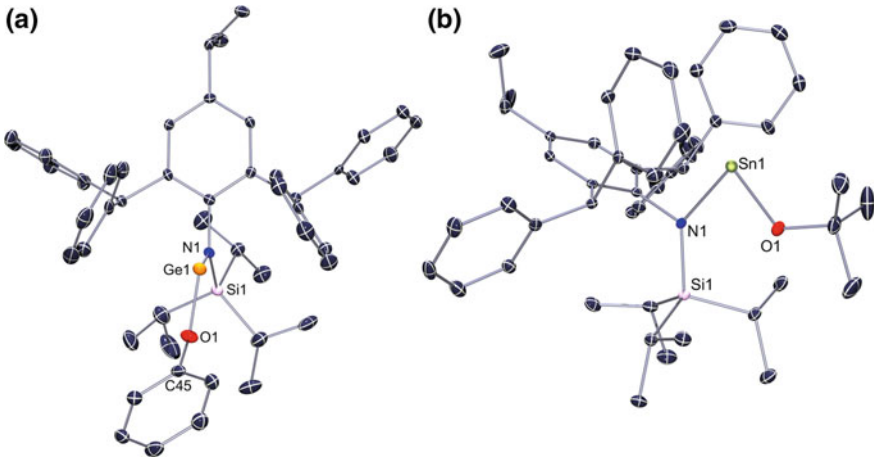

Fig. 5.6 ORTEP representations of **a** ($^{iPr}L^{\dagger}$)GeOPh (**11**) and ($^{iPr}L^{\dagger}$)SnOBu^t (**7**) (30% thermal ellipsoids, hydrogen atoms omitted). Selected bond lengths (Å) and angles (°), **11**: N1–Ge1 1.884 (2), Ge1–O1 1.831(3), O1–C45 1.365(4), N1–Ge1–O1 94.32(1), Ge1–O1–C45 120.35(2), Si1–N1–Ge1–O1 11.89(2); **7**: N1–Sn1 2.107(4), Sn1–O1 2.006(3), O1–C45 1.437(5), N1–Sn1–O1 93.83(1), Sn1–O1–C45 128.28(3), Si1–N1–Sn1–O1 11.37(3)

$KOBu^t$ in toluene, at ambient temperature. The ^1H NMR spectrum of **7** exhibits a characteristic Bu^tO singlet at ~1.02 ppm, with the $^{iPr}L^{\dagger}$ ligand signals are slightly broadened. As with other novel amido-alkoxy stannylenes discussed, **7** is monomeric in the solid state (Fig. 5.6). Structural parameters are as would be expected from previously discussed Sn(II) alkoxides.

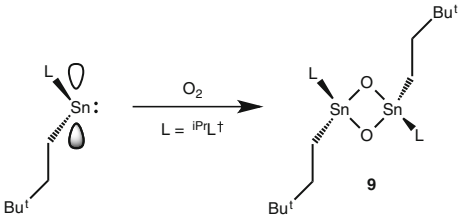

Scheme 5.19 The reaction of (^{iPr}L†)Sn(CH$_2$)$_2$Bu^t with O_2, yielding the oxo-bridged Sn(IV) dimer, **9**

Finally, the amido Sn(II) alkyl, (^{iPr}L†)Sn(CH$_2$)$_2$Bu^t, also reacts with O_2 (Scheme 5.19), in a similar fashion to the amido Ge(II) alkyl, (^{iPr}L†)GeC$_6$H$_{11}$. The structure of the product, a bis(oxo)bridged Sn(IV) dimer ([(^{iPr}L†)Sn{(CH$_2$)$_2$Bu^t}O], **9**), is shown in Fig. 5.5. It features near equal Sn1–O1 and Sn1–O1′ distances, as was the case with the Ge(IV) congener. One related four coordinate Sn(IV) dimer ({(^{Tripp}Terph)(Cl)Sn(μ-O)}$_2$) has been reported by Sheer and co-workers [79], and, as with **9**, has a non-bonding Sn…Sn distance (2.950 Å) and equal bridging Sn–O bond lengths (1.994 Å). The central Sn$_2$O$_2$ ring of **9** is planar, with the bulky ^{iPr}L† ligands of each Sn fragment sitting *trans* on the central ring, likely to minimise steric interactions. Further structural parameters can be found in Fig. 5.5.

5.3.1.3 Generation of Group 14 Element(II) Hydride Complexes from Heavier Amido-Alkoxy Tetrylenes

As the monomeric, two-coordinate Ge(II) hydrides, (^{tBuO}L*)GeH and (^{tBuO}L†)GeH, were synthesised through the metathesis of HBcat with (^{tBuO}L*)GeOBu^t and (^{tBuO}L†)GeOBu^t, respectively (see Chap. 3), it seemed likely that this reactivity would could be extended to the amido Ge(II) and Sn(II) alkoxide complexes discussed in Chap. 4. Further, as the only high yielding synthesis of Ge(II) hydride complex **1** is through the activation of H_2 by {(^{iPr}L†)Ge}$_2$, an alternative route was sought. It follows that this may be a useful route to the in situ generation of {(^{iPr}L†)Sn(μ-H)$_2$}, due to the thermal instability of this compound, and hence difficulties in its storage. The bulk synthesis of (^{iPr}L†)GeOBu^t (**10**), (^{iPr}L†)GeOPh (**11**), and (^{iP}L†)SnOPh (**12**) was first pursued, so as to investigate these species as precursors to the hydride complexes **1** and **8**.

The addition of solutions of either (^{iPr}L†)GeCl or (^{iPr}L†)SnCl in toluene to suspensions of Bu^{t}OK or PhOLi at ambient temperature led to moderate crystalline yields of **10–12**, as well as previously described **7** (Scheme 5.20). The structures of **7** and **11** are shown in Fig. 5.6, and are similar to the amido-alkoxy tetrylenes described previously. The ^{1}H NMR spectra of **7** and **10–12** are in keeping with their solid state structures.

Subsequently, **7** and **10–12** were reacted with the boranes, HBpin and HBcat (Scheme 5.20). The Ge(II) species, **10** and **11**, both slowly reacted with HBpin. The

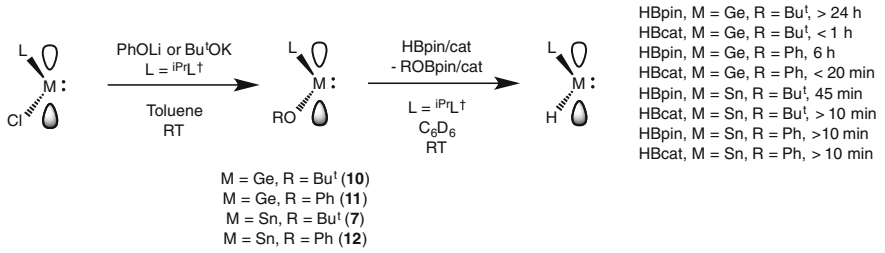

Scheme 5.20 The synthesis of amido Ge(II) and Sn(II) alkoxides, **7** and **10–12**, and their reactions with boranes, HBpin and HBcat

reaction with **10** was much slower, taking several days to reach completion. Heating the reaction mixture led to the formation of elemental germanium, with protonated ligand being the only soluble species as ascertained from the ^{1}H NMR spectrum of the solution. Whilst the reaction of **11** with HBpin proceeded much more rapidly, being complete in 6 h, large amounts of a brown partially soluble precipitate formed, likely the pinBOPh by product, making isolation of pure **1** via this route challenging. Both **10** and **11** rapidly reacted with HBcat (1 h, and 20 min, respectively), forming **1** based on the ^{1}H NMR spectrum of the reaction mixture, but again giving amounts of a partially soluble solid which was seemingly inseparable from **1**.

The reaction of HBpin with **7** proceeded over the course of 45 min at ambient temperature, with only small amounts of free ligand forming over this time (Scheme 5.20). Moreover, knowing that, for example, (^{iPr}L†)SnEt does not react with HBpin, the addition of HBpin to **7** in the presence of ethylene gives high yields of (^{iPr}L†)SnEt, after stirring for 3 h. This route can be used in the synthesis of the amido Sn(II) alkyls described in Chap. 4. As with the Ge(II) alkoxide compounds **10** and **11**, the addition of HBcat to **7** or **12**, or HBpin to **12**, yielded partially soluble solids (i.e. catBOBu^{t}, catBOPh, and pinBOPh) that could not be separated from the desired reaction products.

It was also found that all isolated Ge(II) and Sn(II) alkoxides discussed in Chap. 4 (i.e. (^{iPr}L†)GeOC(H)Pr$^{i}_{2}$, (^{iPr}L†)GeO{(CH$_2$)-*p*-MeOPh}, (^{iPr}L†)SnOC(H)Pr$^{i}_{2}$, (^{iPr}L†)SnO{(CH$_2$)-*p*-MeOPh}) reacted with HBpin to generate the relevant element(II) hydride complex, with reactions much faster for tin than for germanium (i.e. 10 min for (^{iPr}L†)SnO{(CH$_2$)-*p*-MeOPh}, 24 h for (^{iPr}L†)GeO{(CH$_2$)-*p*-MeOPh}). This suggested that the hydroboration of aldehydes and ketones catalysed by the hydride complexes, **1** and **8**, should be possible.

The reaction of silanes (i.e. PhSiH$_3$, Et$_3$SiH, (EtO)$_3$SiH) with the Ge(II) alkoxide species **10** and **11** did not proceed at ambient or higher temperatures. Whilst the Sn (II) congeners, **7** and **12**, did show signs of reaction, with a small amount of **8** being formed (indicated by its characteristic Sn–H resonance in the ^{1}H NMR spectrum) accelerated decomposition also occurred, generating protonated ligand and tin metal. These results suggested that catalytic hydrosilylation reactions would not be possible with these systems.

5.3.2 *Catalytic Reactivity Studies of Amido-Alkoxy Tetrelenes*

Having explored the reactivity of several Ge(II) and Sn(II) alkoxide complexes toward boranes, we sought to investigate their efficacy, and the related hydride complexes **1** and **8**, in the catalytic hydroboration of C=O bonds.

5.3.2.1 Catalytic Hydroboration of Aldehydes and Ketones

Given the described stoichiometric reactivity studies of **1** and **8** with aldehydes and ketones, and subsequent reactivity of the alkoxide complexes with HBpin, a hypothetical catalytic cycle for the addition of HBpin to such C=O bonds, catalysed by **1** or **8**, is outlined in Scheme 5.21.

For catalytic investigations, due to the thermal instability of **8**, the amido Sn(II) *tert*-butoxide, **7**, was utilised as a precatalyst, having confirmed that **8** is rapidly generated from **7** in situ in the presence of an excess of HBpin. Its application to the hydroboration of a number of aldehydes is summarised in Table 5.1. In the presence of 0.05 mol% **7**, benzaldehyde rapidly reacted with HBpin, with full conversion after 2.5 h (Table 5.1, Run 1). The reaction scope was expanded to *para*-substituted benzaldehydes to observe the effects of electron donation/withdrawal on reaction rate. The hydroboration of 4-bromobenzaldehyde and 4-methoxybenzaldehyde (Table 5.1, Runs 2 and 3) were both considerably slower than benzaldehyde with the same catalyst loading, taking 4.5 h and 5 h, respectively. The brominated system appears slightly more active, presumably due to electron withdrawing effects activating the carbonyl moiety, relative to deactivation due to electron donating effects of the methoxy functionality. A variety of aliphatic aldehydes were also successfully hydroborated (Table 5.1, Runs 4–6), with all examples being complete in under ten minutes at ambient temperature, all with a low catalyst loading of 0.05 mol%. These results suggest that, given the lesser

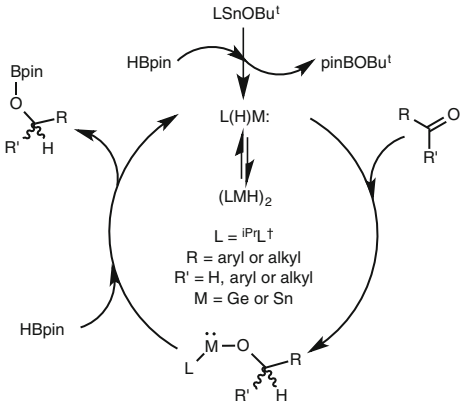

Scheme 5.21 The proposed cycle for the hydroboration of aldehydes and ketones, catalysed by **1** and **8**

Table 5.1 Hydroborations of aldehydes, RC(H)O, catalysed by **1** or **8** (see Scheme 5.1)

Run no.	Cat.[a]	Loading (mol%)	R	Time (h)[b]	Yield (%, NMR[c])	TOF (h^{-1})[d]
1	**8**	0.05	Ph	2.5	>99	800
2	**8**	0.05	PhBr-4	4.5	>99	450
3	**8**	0.05	PhOMe-4	5	>99	400
4	**8**	0.05	Et	<0.15	>99	>13,300[e]
5	**8**	0.05	Pr^i	<0.15	>99	>13,300[e]
6	**8**	0.05	Cy	<0.15	>99	>13,300[e]
7	**1**	1	Ph	1.5	>99	67
8	**1**	1	PhBr-4	4	>99	25
9	**1**	1	PhOMe-4	6	>99	17
10	**1**	0.05	Et	1	>99	2000
11	**1**	0.05	Pr^i	0.4	>99	5000
12	**1**	0.05	Cy	0.33	>99	6000

[a]Catalyst **8** generated in situ using the pre-catalyst, $^{iPr}L^{t}SnOBu^{t}$ (**7**)
[b]All reactions carried out in d_6-benzene at 20 °C using 1 equiv of HBpin
[c]Obtained by integration of RCH_2OBpin signal against tetramethylsilane internal standard
[d]Turn over frequency—average value for complete reaction
[e]TOF lower limit

activation of the aliphatic ketones, that steric bulk plays a large part in the reaction rates. Given that the likely rate-limiting step is the approach of HBpin to the intermediate alkoxide (vide infra), e.g. compounds **3** and **4**, one can speculate that the size of the alkoxide moiety could act to hinder the approach of HBpin, slowing catalytic turnover.

Utilising compound **1** as a catalyst in aldehyde hydroboration generally required higher catalyst loadings to achieve reasonable reaction times. This is consistent with the observation that the Ge(II) alkoxides reacted with HBpin far slower than their Sn(II) counterparts (vide supra). Turn over frequency (TOF) was approximately halved for the aliphatic aldehydes, cyclohexane carboxaldehyde and *iso*-butyraldehyde, and was around a sixth of the rate of the Sn(II) catalysed reaction for propionaldehyde (Table 5.1, Runs 10–12). The effects were far more pronounced for reactions involving benzaldehyde and derivatives thereof, with 4-bromobenzaldehyde and 4-methoxybenzaldehyde having TOFs of 20 fold less than those observed for the related reactions catalysed by **7** (Table 5.1, Runs 7–8). It is possible that the Ge(II) centre is both generally less reactive under the given conditions, and is also more affected by steric bulk at the alkoxide moiety, given the smaller radius of the element relative to tin. This would explain the increased loss in productivity on moving from small aliphatic aldehydes to relatively bulky aromatic substrates for the Ge(II) catalyst.

A range of aromatic and aliphatic ketones were also successfully hydroborated, further expanding the substrate scope for this system. Generally, the ketone functionalities required higher catalyst loadings in order to achieve similar reaction times. Where the fluorinated ketone, 2,2,2-trifluoro acetophenone, was reacted with

Table 5.2 Hydroborations of ketones, (R)(R′)CO, catalysed by **1** or **8**

Run no.	Cat.[a]	Loading (mol%)	R	R′	Time (h)[b]	Yield (%, NMR[c])	TOF (h^{-1})[d]
1	**8**	0.5	Ph	CF_3	<0.15	>99	1330
2	**8**	0.5	Ph	Ph	2.5	95	80
3	**8**	0.5	PhOMe-4	Me	0.25	98	800
4	**8**	0.5	PhEt-4	Me	0.25	>99	800
5	**8**	0.5	Ph	C(O)Ph[e]	0.33	96	600
6	**8**	0.5	Cy[f]		1.75	96	115
7	**8**	1	CyMe-2[g]		0.5	99	200
8	**8**	0.5	2-cyclohexene[e, h]		0.5	>99	400
9	**8**	0.5	Ad[i]		2.5	95	80
10	**8**	2	Pr^i	Pr^i	24	95	1.7
11	**1**	2.5	Ph	CF_3	0.25	>99	160
12	**1**	1.25	Ph	Ph	48	>99	1.7
13	**1**	2.5	PhOMe-4	Me	1.33	>99	30
14	**1**	2.5	PhEt-4	Me	1	>99	40
15	**1**	5	Ph	C(O)Ph[e]	0.4	94	50
16	**1**	5	Cy[f]		<0.15	>99	130
17	**1**	5	CyMe-2[g]		0.5	>99	40
18	**1**	2.5	2-cyclohexene[e, h]		1	>99	40
19	**1**	1.25	Ad[i]		4	>99	20
20	**1**	1.25	Pr^i	Pr^i	168	80	0.47

[a]Catalyst **8** generated in situ using the pre-catalyst, ($^{iPr}L^{\dagger}$)$SnOBu^t$
[b]All reactions carried out in d_6-benzene at 20 °C using 1 equiv of HBpin (unless stated otherwise)
[c]Obtained by integration of $R_2CHOBpin$ signal against tetramethylsilane internal standard
[d]Turn over frequency—average value for complete reaction
[e]2 equivs of HBpin
[f]Cyclohexanone
[g]2-Methylcyclohexanone
[h]2-Cyclohexen-1-one
[i]Adamantanone

HBpin in the presence of pre-catalyst **7** (0.5 mol%; Table 5.2, Run 1) all HBpin had been consumed in under 10 min, giving a TOF of over 1200 h^{-1}, comparable to TOFs involving aldehydes. Substituting the CF_3 group for Ph (Table 5.2, Run 2) resulted in a large reduction in catalyst activity, with the reaction being complete in 2.5 h. As before, this is most likely attributed to the increased steric encumbrance of the substrate. The hydroboration of the acetophenone derivatives, 4-methoxyacetophenone and 4-ethylacetophenone, reinforce this hypothesis given their rapid hydroboration (15 min, 0.5 mol% **7**; Table 5.2, Runs 3 and 4). Interestingly, reduction of 2-adamantanone, which is both aliphatic and highly sterically hindered, was complete in 2.5 h with 0.5 mol% catalyst loading (Table 5.2, Run 8). A similar effect was observed by Harder and co-workers,

whereby 2-adamatanone underwent Ca(II) catalysed hydrosilylation far more rapidly than seemingly more active and equally bulky ketones [43]. To observe whether the puckered fused ring system in adamantanone results in its surprisingly rapid hydroboration, 2,4-dimethyl-3-pentanone was utilised as the substrate. In this case, the reaction rate was greatly slowed, requiring an increased catalyst loading of 2 mol% and 24 h for full ketone consumption (Table 5.2, Run 10). This suggests that the free rotation of the *iso*-propyl groups of 2,4-dimethyl-3-pentanone has a notable influence on its steric bulk, and hence the rate of its hydroboration.

As was the case with aldehyde hydroborations, **1** was somewhat less effective as a catalyst than **7** in the hydroboration of ketones. Higher catalyst loadings and much longer reaction times were needed for reactions to reach completion, or at least a reasonable percentage of conversion. Benzophenone and 2,2,2-trifluoro acetophenone were converted with TOFs of 2.2 h^{-1} and 1.7 h^{-1} (Table 5.2, Runs 2 and 1), respectively, with their similar values perhaps again indicative of the increased effective steric encumberment at germanium due to its smaller covalent radius when compared to tin. As was the case with **7**, 2,4-dimethyl-3-pentanone gave by far the longest reaction times, taking 7 days to reach 80% conversion (Table 5.2, Run 20).

Preliminary investigations were carried out to determine any chemo- and diastereoselectivity of the ketone reduction catalysed by **1** and **8**. First, it was found that dihydroborations of the α-diketone, benzil, were rapid with both catalysts (using two equivalents of HBpin, Table 5.2, Runs 5 and 15) and that there was no evidence for the formation of the singly hydroborated product in either reaction. In contrast, the catalysed reactions of 2-cyclohexen-1-one with two equivalents of HBpin were complete in under 1 h, but led only to the chemoselective and quantitative reduction of the ketone functionality (Table 5.2, Runs 8 and 18), leaving the alkene fragment intact. With respect to diastereoselectivity, the hydroboration of 2-methylcyclohexanone was carried out with both catalysts. While little selectivity was observed for the tin catalyst, significant *cis*/*trans* selectivity (*ca.* 72:28) was reproducibly achieved for the Ge catalyst under several catalyst loadings. Although the origin of this selectivity is not yet clear, it is intriguing that this is the opposite of the (less pronounced) *trans*/*cis* diastereoselectivity typically observed for the hydroboration of this substrate [80]. Additionally, where enolisable aldehydes and ketones were employed, there was no observation of the enolised products for any reaction. Finally, it was found that the addition of a 20 fold excess of HBpin to 4-ethylacetophenone in the presence of 1 mol% **1** did not result in a decrease in catalyst efficiency, contrary to results reported by Hill and co-workers (see Sect. 5.1.2.1) [48], indicating that HBpin does not act as an inhibitor to the catalytic hydroboration of carbonyl species for this system. Interestingly, however, the addition of one equivalent of HBpin to $\{(^{iPr}L^{\dagger})GeD\}_2$ did result in the formation of an equilibrium mixture of $\{(^{iPr}L^{\dagger})GeD\}_2$ and **1** after 24 h. This suggests a dynamic exchange between HBpin/DBpin and $\{(^{iPr}L^{\dagger})GeD\}_2$/**1**, which must result from some adduct of these species in solution, albeit non-inhibitory.

5.3.2.2 Kinetic Study of the Hydroboration of a Ketone Catalysed by (^{IPr}L†)(H)Ge

In order to shed some light on the mechanism of the described catalytic reactions, a kinetic analysis of the hydroboration of 4-ethylacetophenone catalysed by the germanium hydride compound, **1**, was undertaken using the initial rates method as described by Weller and co-workers [81]. The order of dependence of each component of the reaction of 4-ethylacteophenone with HBpin, catalysed by **1**, was determined by the method of initial rates. Initial rate (k_{obs}) values were determined in duplicate for three different concentrations of both (^{iPr}L†)(H)Ge: and HBpin, and for four concentrations of 4-ethylacetophenone. The quoted concentrations of (^{iPr}L†)(H)Ge: assume full dissociation of **1** in solution. Each k_{obs} determination experiment was run by collecting one ^{1}H NMR spectrum per minute of reaction time, from t = 0 to t = 12 min, followed by calculation of the consumption of 4-ethylacetophenone over this time. The values of k_{obs} were calculated using approximately linear portions of each [ketone] vs. time plot, in the initial stages of each reaction run (typically within the first 7.5 min, see Fig. 5.7 for an example). The plots of the experimentally obtained k_{obs} values *vs.* the respective component concentrations indicated the order of dependence of reaction in that reaction component. It was assumed that k_{obs} was 0 at zero concentration of reaction components that had an effect on the reaction rate (i.e. HBpin and (^{iPr}L†)(H)Ge:). Results for all reactions studied are shown in Table 5.3, and are represented graphically in Fig. 5.8.

A plot of runs 3, 4 and 7–10 displayed in Table 5.3 resulted in a linear correlation between k_{obs} and [HBpin] (Fig. 5.8, *top*). The case was similar for runs 1–6, giving a linear correlation between k_{obs} and (^{iPr}L†)(H)Ge: (Fig. 5.8, *middle*). These results suggest 1st order dependence of the reaction in both **1** and HBpin. No significant change in k_{obs} was seen for runs 1, 2 and 1–13, suggesting 0th order dependence in 4-ethylacetophenone (Fig. 5.8, *bottom*). This implies that the rate-determining step of the catalytic cycle is the reaction of the alkoxide intermediate, (^{iPr}L†)GeOC(H)(Me)(*p*-Et), with HBpin, and therefore that this intermediate is the resting state in the cycle. This conclusion is consistent with the

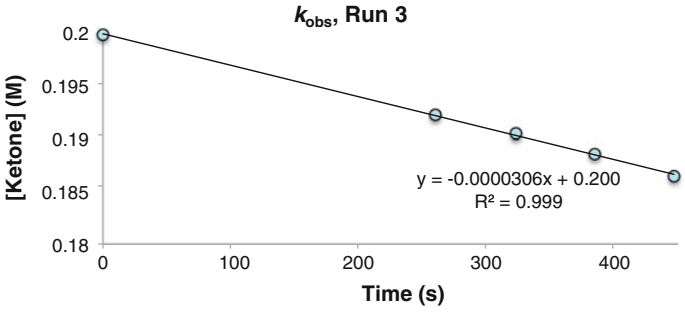

Fig. 5.7 Graphical representation of Run 3 (Table 5.3), with the gradient giving the k_{obs} value

Table 5.3 Initial rates for the hydroboration of 4-ethylacetophenone by HBpin, catalysed by (^{iPr}L†)(H)Ge: carried out under varying concentrations of reactants and catalyst

Run no.	(^{iPr}L†)(H)Ge: (mM)	[HBpin] (M)	[Ketone] (M)	k_{obs} (10^{-5} mol/Ls)
1	0.5978	0.1998	0.1880	1.522
2	0.5978	0.1998	0.1880	1.609
3	1.1957	0.1998	0.1880	3.063
4	1.1957	0.1998	0.1880	3.055
5	2.3913	0.1998	0.1880	5.714
6	2.3913	0.1998	0.1880	6.518
7	1.1957	0.0999	0.1880	1.337
8	1.1957	0.0999	0.1880	1.396
9	1.1957	0.3980	0.1880	5.625
10	1.1957	0.3980	0.1880	6.543
11	1.1957	0.1998	0.0469	2.803
12	1.1957	0.1998	0.0938	3.226
13	1.1957	0.1998	0.3740	2.453

preliminary stoichiometric reaction studies discussed in Chap. 4 and above in Sect. 5.1.3.1, in that the reaction of **1** with aldehydes and ketones is extremely rapid, whereas the reactions of the subsequent alkoxide complexes with HBpin are considerably slower. This also implies that the equilibrium between {(^{iPr}L†)GeH}$_2$ and (^{iPr}L†)(H)Ge: should have little effect on the overall reaction rate. While it cannot be certain, it seems very likely that the active species in that equilibrium is two-coordinate (^{iPr}L†)(H)Ge: which is rapidly consumed by reaction with the ketone, and is thus only present in the reaction mixture in negligible amounts, relative to the alkoxide intermediate, throughout the cycle.

5.3.2.3 Further Mechanistic Elucidation of the Hydroboration of Ketones Catalysed by (^{IPr}L†)(H)Ge Through a DFT Study

To further verify the mechanism of the catalytic reaction, computational analysis was employed. The proposed mechanism of the Ge- and Sn-catalysed hydroboration reactions initially involves attack of the O-center of the substrate at the two-coordinate metal centre, with hydrometalation subsequently proceeding via a four-membered transition state (Scheme 5.22). The monomeric, two-coordinate metal alkoxide intermediate then undergoes a σ-bond metathesis reaction with HBpin to generate the borate ester and return the catalyst, again via a four-membered cyclic transition state. This mechanism is highly reminiscent of that proposed by Hill and co-workers for {(^{Dipp}nacnac)MgH}$_2$ catalysed ketone hydroborations [25], discussed above in Sect. 5.1.2.1 (Scheme 5.10). So as to assess the feasibility of our proposal, the free energy profile of the tin hydride catalysed reaction of HBpin with the very bulky substrate, 2,4-dimethyl-3-pentanone, was calculated using DFT, with the inclusion of

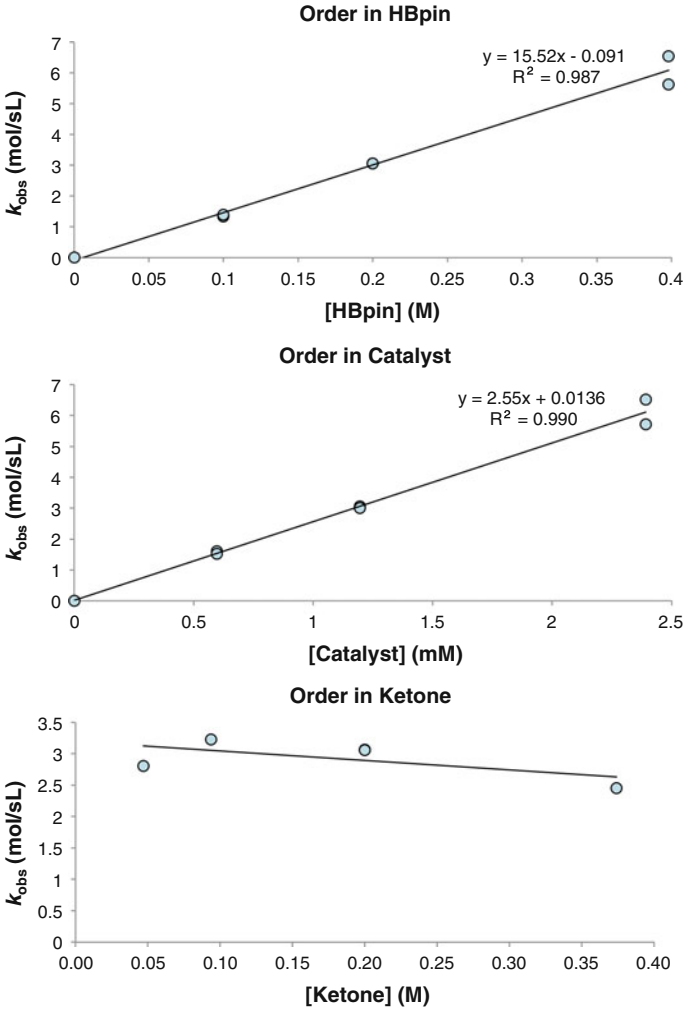

Fig. 5.8 Graphical representations of the order of the catalytic hydroboration of 4-ethylacetophenone by HBpin, catalysed by **1**, in (*top*) **1**, (*middle*) HBpin, and (*bottom*) 4-ethylacetophenone

dispersion interactions (BP86 + D(BJ)/def2-TZVPP). The calculated profile (Fig. 5.9) closely matches the proposed general mechanism and shows that both the hydrostannylation and σ-bond metathesis reactions are exergonic, by −16.7 and −3.4 kcal mol^{-1}, respectively. Furthermore, the fact that these reactions exhibit kinetic barriers of 10.5 and 16.1 kcal mol^{-1}, respectively, is fully consistent with the experimental observation that the σ-bond metathesis reaction is the rate-determining step in the catalytic cycle. Considering that these calculations were carried out on the experimentally most difficult substrate to hydroborate, it would be

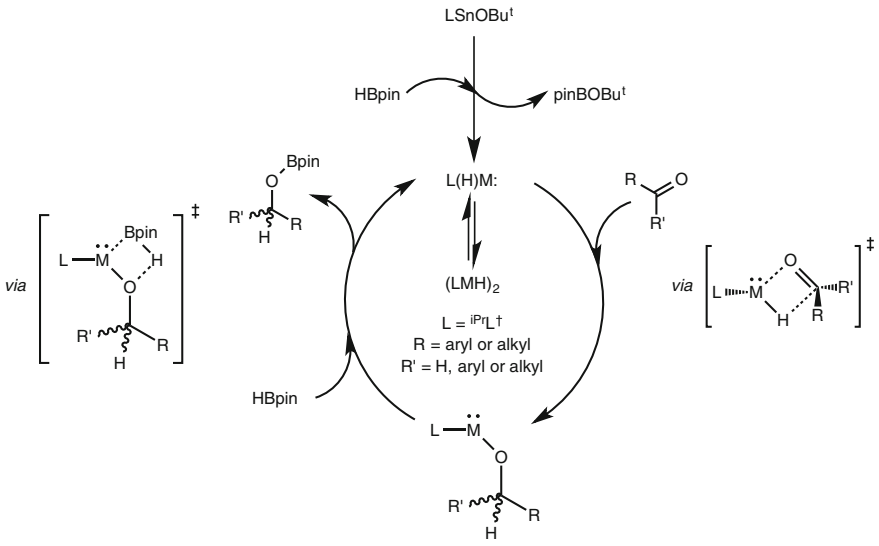

Scheme 5.22 The postulated catalytic mechanism for the hydroboration of aldehydes and ketones by HBpin in the presence of **1** or **7/8**

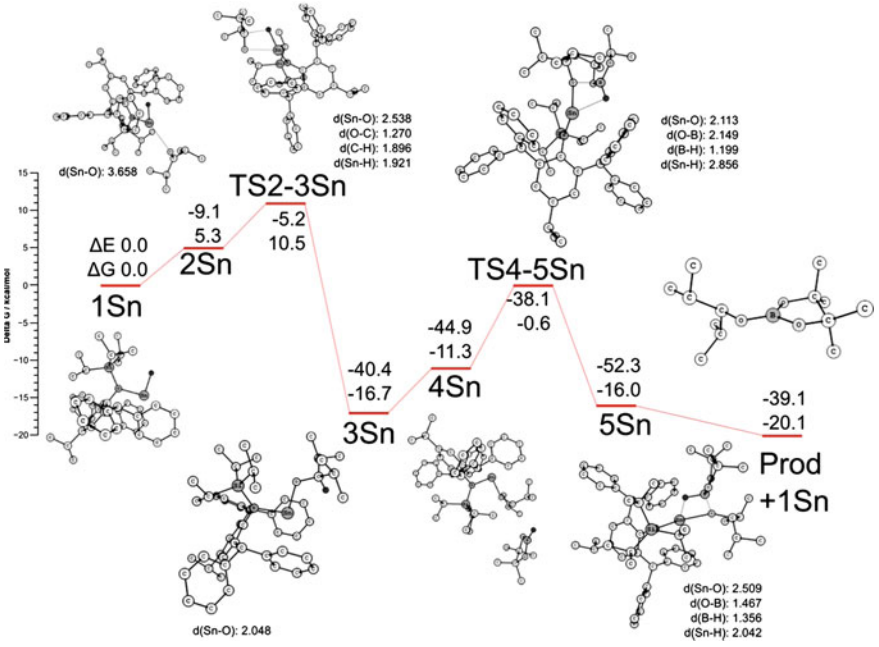

Fig. 5.9 Calculated (BP86 + D(BJ)/def2-TZVPP) free energy profile for the reaction of 2,4-dimethyl-3-pentanone with HBpin, catalysed by (^{iPr}L†)(H)Sn: Selected bond lengths (Å), and free and electronic energies (kcal mol^{-1}), are shown. Reproduced from *J. Am. Chem. Soc.*, **2014**, *136*, 3028 with permission from The American Chemical Society, Copyright 2014

expected that the kinetic barriers to the hydroboration of less bulky substrates would be significantly lower. Accordingly, the computational study clearly highlights the thermodynamic and kinetic viability of the proposed general mechanism.

5.3.2.4 Catalytic Hydroboration of Carbon Dioxide

Given both the recent developments in catalytic CO_2 hydroboration by MG element hydride complexes, and the successful hydroboration of aldehydes and ketones by **1** and **8**, we sought to study the catalytic reduction of CO_2 with these low-coordinate, low-oxidation state group 14 hydride species.

Stoichiometric Reactivity Studies of $\{(^{IPr}L^{\dagger})GeH\}_2$ with CO_2

Primarily, the stoichiometric reaction of **1** with CO_2 was carried out, to determine whether this would follow a similar reaction path to related previously reported reactions involving monomeric Ge(II) and Sn(II) hydride complexes (i.e. the generation of a Ge(II) formate species [34, 82]). The reaction of excess CO_2 with **1** in C_6D_6 proceeded rapidly, but yielded several products as ascertained through ^{1}H NMR spectroscopic analysis of the reaction mixture. There were numerous overlapping peaks relating to the Ph_2CH unit of the $^{iPr}L^{\dagger}$ ligand, in differing concentrations. Amongst the products were the presumed Ge(II) formate species, ($^{iPr}L^{\dagger}$)GeOC(H)O (Scheme 5.23, **13**), due to an observed singlet at δ = 8.05 ppm (viz. δ = 8.64 ppm for (^{Dipp}nacnac)GeOC(H)O [34]), and a species containing the OCH_2O^{2-} ligand (i.e. ($^{iPr}L^{\dagger}$)GeOCH$_2$OGe($^{iPr}L^{\dagger}$), **14**), due to a characteristic methylene resonance at δ = ∼5 ppm (viz. δ = 5.49 ppm for $(pinBO)_2CH_2$ [36] and δ = 4.48 ppm for (^{Dipp}nacnac)GeOCH$_2$OAl(H)(^{Dipp}nacnac) [33]). The presence of the Ge(II) formate species, **13**, was confirmed through its independent synthesis. That is, the addition of THF to a solid mixture of ($^{iPr}L^{\dagger}$)GeCl and OC(H)OK at ambient temperature, followed by stirring for 24 h, gave good yields of **13** (Fig. 5.10) after work-up (Scheme 5.23). This compound exhibits a characteristic 1H formate C–*H* resonance in its ^{1}H NMR spectrum at δ = 8.05 ppm, and one sharp set of ligand signals, suggesting a single ligand environment. The ^{13}C NMR spectrum similarly shows a single ligand environment, and a characteristic formate-*C* resonance at δ = 165.0 ppm (viz. δ = 164.9 ppm for (^{Dipp}nacnac)GeOC(H)O [34]). The solid state structure of **13** reveals it to be a monomer, the formate ligand binding the Ge(II) centre in an κ^2-fashion through the anionic C–O$^-$ moiety and the remaining C=O moiety. This is in contrast to (^{Dipp}nacnac)GeOC(H)O [34], in which the formate ligand is monodentate. This is likely due to the bidentate ^{Dipp}nacnac ligand, which coordinates the otherwise empty *p*-orbital at the Ge(II) centre. Due to high degrees of disorder in the formate ligand in the crystal structure of **13**, structural parameters relating to it will not be discussed here.

Having isolated **13**, the pathways leading to the formation of multiple species in the reaction between **1** and CO_2 were investigated. Whilst **13** did not show any

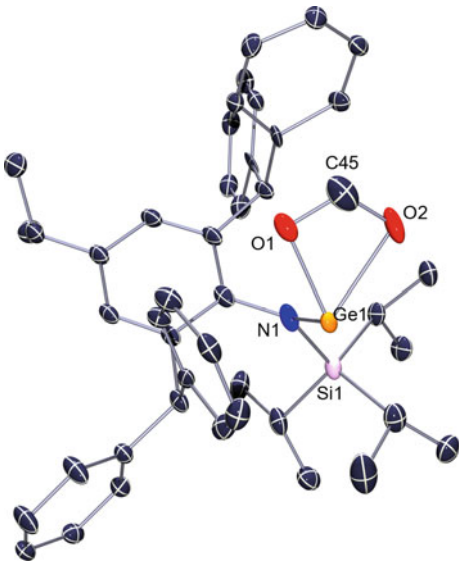

Fig. 5.10 ORTEP representation of ($^{iPr}L^{\dagger}$)GeOC(H)O (**13**) (thermal ellipsoids at 30%, hydrogens omitted). Due to disorder in the formate unit and of the Ge centre, bond lengths and angles are not given

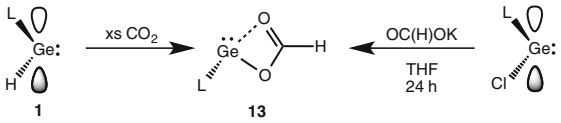

Scheme 5.23 The synthesis of ($^{iPr}L^{\dagger}$)GeOC(H)O (**13**) through addition of CO_2 to ($^{iPr}L^{\dagger}$)(H)Ge or OC(H)OK to ($^{iPr}L^{\dagger}$)(Cl)Ge

signs of reaction with excess CO_2, it did react rapidly with stoichiometric quantities of **1** at ambient temperature in C_6D_6. The ^{1}H NMR spectrum of the reaction mixture displayed a single set of ligand signals, and a new 2H singlet at $\delta = \sim 5$ ppm, attributable to a OCH_2O^{2-} ligand, with complete consumption of **1**. These observations are concordant with the formation of **14** (Scheme 5.24). It is worthy of note that, upon standing for a number of days, the ^{1}H NMR resonance at $\delta = \sim 5$ ppm greatly diminishes, with a new set of ligand peaks appearing. Also, heating **14** overnight at 60 °C gives a mixture of **14** and two new species, one matching that observed through the ambient temperature degradation of **14**, and one with a new 3H singlet resonance at $\delta = 3.49$ ppm, tentatively assigned to ($^{iPr}L^{\dagger}$)GeO*Me* (vide infra). Upon scale-up of the addition of **1**–**13**, two compounds were isolated and crystallographically characterised; **14** and a Ge(II) ether analogue, {($^{iPr}L^{\dagger}$)Ge}$_2$O (**15**) (Scheme 5.24). Moreover, **14** co-crystallised with paraformaldehyde, albeit with very high degrees of disorder in this polymeric unit. This observation suggests

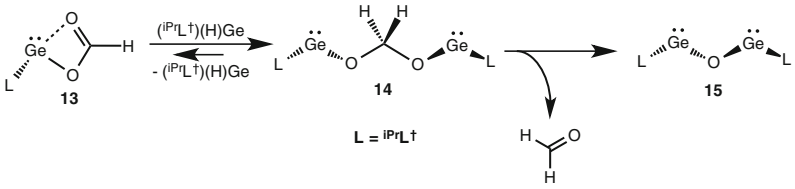

Scheme 5.24 The likely routes of formation of $\{(^{iPr}L^{\dagger})GeO\}_2CH_2$ (**14**) and $\{(^{iPr}L^{\dagger})Ge\}_2O$ (**15**) from the addition of $(^{iPr}L^{\dagger})(H)Ge$ to 13, and the subsequent spontaneous elimination of formaldehyde from **14**

that **15** is formed through the elimination of formaldehyde from **14**, as has previously been hypothesised for related intermediary species in the catalytic hydroboration of CO_2 (e.g. $pinBOCH_2OBpin$, L_2MOCH_2OBpin [36, 71]). Full ^1H NMR spectroscopic characterisation of both **14** and **15** allowed for the direct observation of this degradation pathway (note that pure **15** was subsequently synthesised through the addition of N_2O to $\{(^{iPr}L^{\dagger})Ge\}_2$).

The solid state structure of **14** confirms it to be a rare example of a metal complex containing the OCH_2O ligand (Fig. 5.11). Its formation can be compared to that of $(^{Dipp}nacnac)GeOCH_2OAl(H)(^{Dipp}nacnac)$ [33], which was synthesised in a similar manner. The Ge1–O1 (1.813 Å) and O1–C45 (1.390 Å) distances are both in accordance with reported single bonds, giving no real evidence for weakened bonding in this fragment. It is possible that the formation of *para*-formaldehyde acts as a driving force in the elimination of this unit, with the formation of multiple C–O single bonds in paraformaldehyde being thermodynamically more favourable than the relatively weak Ge–O bonds in **14**. The insolubility of paraformaldehyde in common hydrocarbon solvents likely also aids this process. The elimination of formaldehyde could also be driven by the energy gain in forming a C=O bond (799 kJ mol^{-1}) over two C–O bonds (716 kJ mol^{-1}) in **14** [83]. The N1–Ge1–O1 angle of 99.04° is indicative of a stereoactive lone pair of electrons at Ge1. Other structural parameters are summarised in Fig. 5.11. The solid state structure of **15** reveals it to be symmetrical (Fig. 5.11), similar to **14**. The two ligands sit *cis* on the central $(NGe)_2O$ chain. The N1 centres sit in a plane with the Ge1 centres, suggesting some donation of the *p*-based lone pair of electrons on N1 to the vacant *p*-orbital on Ge1. The two Si1–N1–Ge1–O1 units are twisted relative to each other, with a torsion of ~40°, which likely minimises steric interactions between the two ligands. Again, the N1–Ge1–O1 angle of 106.04° is indicative of a stereoactive lone pair of electrons at Ge1.

The mechanism for the formation of $(^{iPr}L^{\dagger})GeOCH_3$ through heating solutions of **14** likely occurs primarily through the reversibility of the addition of **1**–**13**. That is, the β-hydride elimination of **13** from **14**, which generates **1** (Scheme 5.25). As **14** also degrades to **15** and formaldehyde, then **1** can react with this formaldehyde yielding $(^{iPr}L^{\dagger})GeOMe$. Whilst there is only circumstantial evidence for this, inspection of the crystal structure of **14** reveals that the closest contact between Ge1 and a hydrogen on the bridging OCH_2O unit is relatively short (Ge1···H1′ = 2.760

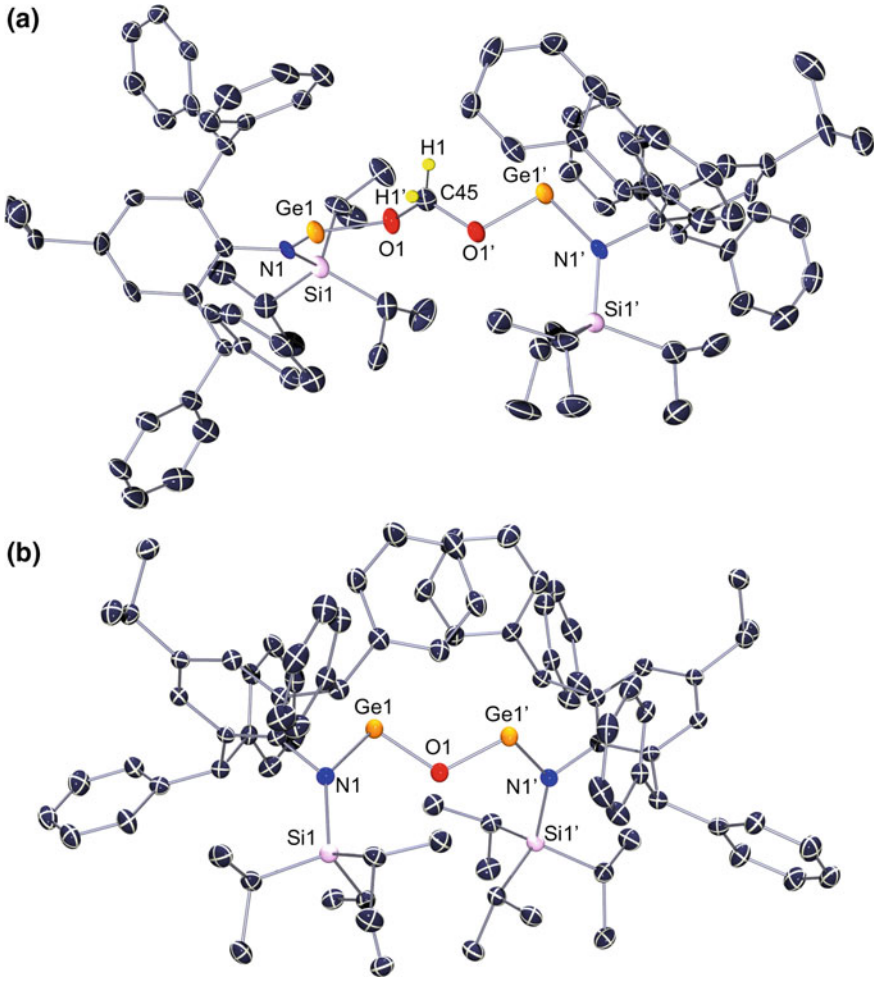

Fig. 5.11 ORTEP representation of **a** $\{(^{iPr}L^{\dagger})GeO\}_2CH_2$ (**14**) and **b** $\{(^{iPr}L^{\dagger})Ge\}_2O$ (**15**) (ellipsoids at 30% probability, hydrogen atoms omitted). Bond lengths (Å) and angles (°), **14**: N1–Ge1 1.885(9), Ge1–O1 1.810(6), O1–C45 1.391, Ge1···H1 2.737(8), N1–Ge1–O1 99.18(3), Ge1–O1–C45 113.71, O1–C45–O1′ 112.39, Ge1–O1–C45–O1′ 54.89; **15**: N1–Ge1 1.901(1), Ge1–O1 1.819, Ge1–Ge1′ 3.179(1), N1–Ge1–O1 106.04, Ge1–O1–Ge1′ 121.82. N1–Ge1–O1–Ge1′ 79.01

(8) Å), and indeed shorter than the closest of those in the Ge(II) alkyl species, $(^{iPr}L^{\dagger})GeC_6H_{11}$ and $(^{iPr}L^{\dagger})GeC_8H_{15}$ (closest Ge···H_{alkyl} = 2.8246 and 2.6198 Å, respectively), which we have shown to readily undergo β-hydride elimination of the relevant cyclic alkene (see Chap. 4, Sect. 4.3.2.1). Work is presently underway to further characterise this phenomenon.

The conclusion drawn from this study is that the reaction of **1** with CO_2 is relatively slow at atmospheric pressure. Hence, the generated Ge(II) formate

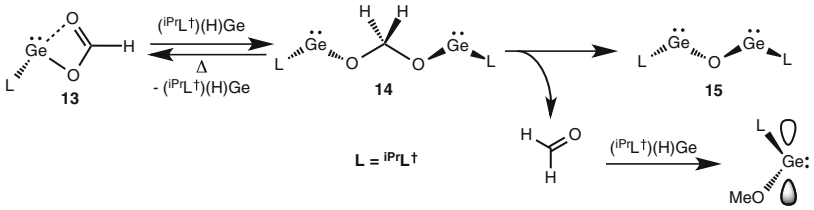

Scheme 5.25 A possible mechanism for the formation of ($^{iPr}L^{\dagger}$)GeOMe from the heating of solutions of **14**

species, **13**, is consumed through further reaction with **1** to give **14**. This slowly decomposes to **15** at ambient temperature, or undergoes β-hydride elimination at elevated temperature, reforming **1** and **13**. It is unsure whether considerable reversibility of the reaction of **1** with **13** occurs at ambient temperature. Still, these observations account for the presence of several species in the crude reaction mixture of **1** with excess CO_2.

Stoichiometric Reactivity Studies of $\{(^{iPr}L^{\dagger})Sn(\mu\text{-}H)\}_2$ with CO_2

Unlike reactions involving **1**, the reaction of **8** with one atmosphere of CO_2 at ambient temperature cleanly yields the Sn(II) congener of **13**, ($^{iPr}L^{\dagger}$)SnOC(H)O (**16**). The ^{1}H NMR spectrum of the crude reaction mixture displays a singlet resonance, integrating to 1H, at δ = 8.71 ppm, attributed to a formate C–*H* proton. Structural characterisation of the product revealed it to indeed be the Sn(II) formate complex, **16** (Fig. 5.12). As with its Ge(II) congener, **16** is monomeric in the solid state, with the formate ligand coordinating in a κ^2-fashion. Although the two Sn–O distances are very similar (Sn1–O1 2.353(2) Å, Sn1–O2 2.333(2) Å), suggesting a delocalised ligand charge, the two C–O distances in the formate ligand are quite different, with C45–O1 being considerably shorter (1.109(4) Å) than C45–O2 (1.310(4) Å). It is therefore unlikely that the charge on the formate ligand is substantially delocalised. Further structural parameters of **16** can be found in Fig. 5.12. Note that this compound can also be accessed through the addition of OC(H)OK to ($^{iPr}L^{\dagger}$)SnCl in THF, with good isolated yields. Although it is likely that **16** would undergo further reaction with **8**, this was not observed in the reaction of **8** with CO_2 described above. Hence, this reaction has not been attempted.

Reactions of Amido Germanium(II) and Tin(II) Formates with Pinacol Borane, and Related Catalytic Studies

Following the isolation of amido Ge(II) and Sn(II) formate species, (**13** and **16**, respectively) we investigated their reactivity with HBpin, in the interest of achieving the catalytic reduction of CO_2.

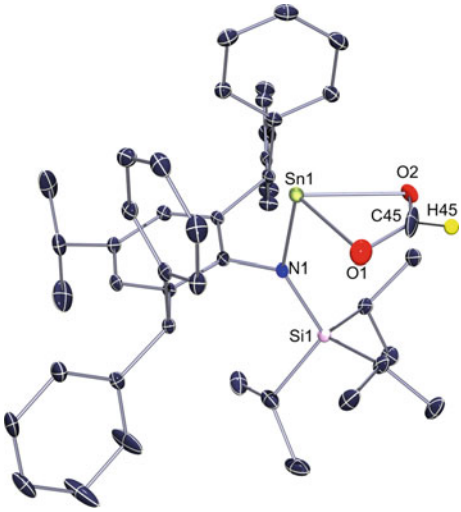

Fig. 5.12 ORTEP representation of (^{iPr}L†)SnOC(H)O (**16**) (thermal ellipsoids at 30% probability; hydrogen atoms, aside from H45, omitted). Selected bond lengths (Å) and angles (°): N1–Sn1 1.129(2), Sn1–O1 2.352(2), Sn1–O2 2.333(2), O1–C45 1.109(4), O2–C45 1.310(4), N1–Sn1–O1 100.44(8), N1–Sn1–O2 102.47(7), O1–C45–O2 125.59(4)

The addition of HBpin to C_6D_6 samples of **13** and **16** initially gave differing results: the reaction with **13** became orange, with a mixture of products in its ^{1}H NMR spectrum, with all HBpin having been consumed. The reaction of **16** with HBpin rapidly proceeded to give a single product. Over the course of four hours, however, the reaction involving **13** and HBpin converged to a single product. Both new species contained a single ligand environment, and a large singlet at $\delta = \sim 1$ ppm integrating to 12H, attributed to a pinB moiety. Crystallisation of the two products revealed them to be group 14 element(II) boronate esters, (^{iPr}L†)MOBpin (M = Ge, **17**; M = Sn, **18**). Such metal boronate esters have been suggested as intermediates in the catalytic hydroboration of CO_2 [33, 71], but as yet, none have been isolated in this context. Note that examples of TM–OBpin complexes have been structurally charactered, and marked as intermediates in TM catalysed transformations (e.g. the reduction of CO_2 to CO by B_2pin_2, catalysed by IPr.CuBpin) [84–86]. Both **17** and **18** were crystallographically characterised (Fig. 5.13), and, as with previously described alkyl and alkoxy germylenes and stannylenes stabilised by the ^{iPr}L† ligand, are monomeric in the solid state. Whilst no Ge(II)–OB or Sn(II)–OB bonds have been previously structurally characterised, examples of E(IV) congeners are known [87]. The Ge1–O1 distance in **17** (1.808 (3) Å) is in keeping with the average of the four reported Ge–OB bond lengths (1.791 Å), as is that of **18** (2.0412(2) Å) with the average of reported Sn–OB bond

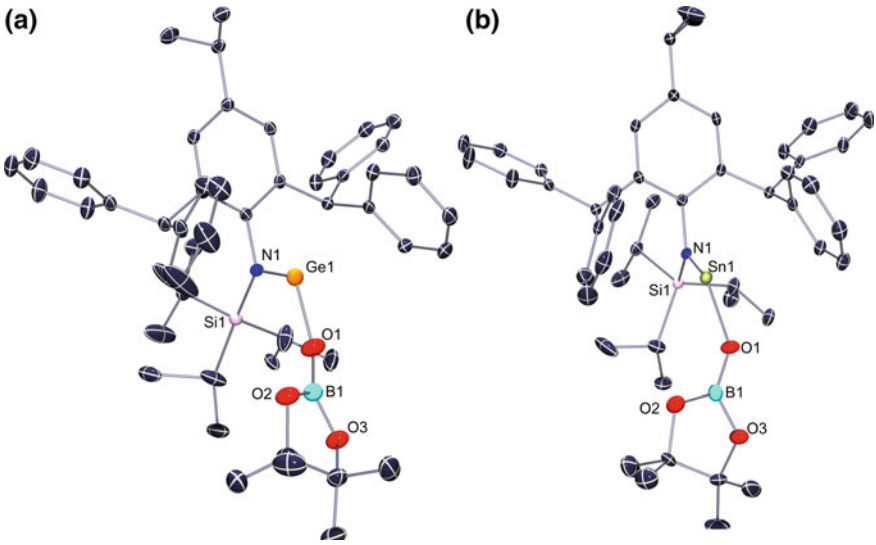

Fig. 5.13 ORTEP representations of **a** ($^{iPr}L^{\dagger}$)GeOBpin (**17**) and **b** ($^{iPr}L^{\dagger}$)SnOBpin (**18**) (thermal ellipsoids at 30%; hydrogen atoms omitted). Selected bond lengths (Å) and angles (°), **17**: N1–Ge1 1.884(3), Ge1–O1 1.808(3), O1–B1 1.344(5), O2–B1 1.374(6), O3–B1 1.362(5), N1–Ge1–O1 97.71(1), Ge1–O1–B1 132.37(3). **18**: N1–Sn1 2.108(2), Sn1–O1 2.041(2), O1–B1 1.317(4), O2–B1 1.388(5), O3–B1 1.370(5), N1–Sn1–O1 97.71(1), Sn1–O1–B1 132.37(3), N1–Sn1–O1 96.41 (8), Sn1–O1–B1 128.22 (2)

lengths (2.025 Å). O → E lone-pair overlap is likely greater in **17** due to its longer terminal O–B bond (1.344(5) Å in **17**, 1.317(4) Å in **18**), which suggests that the lone-pair donation from O1 → B1 in **17** is lessened, allowing for greater O1 → Ge1 lone-pair donation.

As previously mentioned, the initial addition of HBpin to **13** resulted in a brief colour change in the reaction mixture to bright orange. Conducting the reaction at −20 °C resulted in a bright orange solution, the colour of which did not dissipate until warming. It seems possible, then, that the addition of HBpin to **13** initially forms **1** and pinBOC(H)O, which react with each other upon warming. The resulting ($^{iPr}L^{\dagger}$)GeOCH$_2$OBpin can then eliminate formaldehyde, giving **17**. It is also possible that ($^{iPr}L^{\dagger}$)GeOCH$_2$OBpin can react with HBpin, regenerating **1** and forming (pinBO)$_2$CH$_2$. Of course, the possibility of **13** reacting directly with HBpin, forming ($^{iPr}L^{\dagger}$)GeOCH$_2$OBpin, cannot be eliminated.

The further reactivity of **17** and **18** in relation to a catalytic cycle was also investigated. No reaction was observed with CO_2. However, both compounds readily react with a further equivalent of HBpin, yielding the E(II) hydride species **1** and **8**, and (pinB)$_2$O [88]. As such, this is a possible mechanism in the CO_2 reduction catalytic cycle for the generation of (pinB)$_2$O.

Hydroboration of CO_2 Catalysed by Group 14 Element(II) Hydride Complexes

As described, the reactions of **1** and **8** with CO_2, and ensuing reactivity with HBpin, leads to a complex collection of species. Having defined some of the processes involved in their formation, we sought to investigate the hydroboration of CO_2 catalysed by **1**, and relevant precursors to **8**.

Catalytic reactions were conducted in a J Youngs Schlenk, allowing for ~2 bar pressures. The reaction vessel, with added catalyst (typically 20 mg of **1**, or **16** as a precursor to **8**), borane, and solvent (C_6D_6), was cooled to −60 °C. The Schlenk flask was purged with dry CO_2 and sealed at this temperature and pressure. Warming to ambient temperature, according to the ideal gas equation, results in an approximate pressure of 2 bar. This prevented the formation of a pressure of at least one atmosphere inside the Schlenk flask after consumption of CO_2. A simplified catalytic cycle, based on observations discussed within this chapter, can be found in Scheme 5.26. Results of catalytic CO_2 hydroboration reactions are summarised in Table 5.4. Using **1** as a catalyst, loadings of 10 mol% were needed to achieve reaction completion in 24 h, giving a TOF of 0.42 h^{-1}. A ^1H NMR spectroscopic analysis of the reaction mixture after one hour at ambient temperature revealed that two equivalents of HBpin had been consumed, with the only new pinB containing product being $(pinBO)_2CH_2$. This may suggest that the Ge(II) based system does not effect the degradation of this intermediate as efficiently as the Sn(II) system (vide infra). Indeed, at reaction completion, $(pinBO)_2CH_2$ was the major product of reaction.

As with the previously discussed carbonyl hydroboration catalysis, the Sn(II) based system was considerably more active than the corresponding Ge(II) system (Table 5.4). The hydroboration of CO_2 catalysed by **16** at 4 mol%, relative to HBpin, was complete in two hours, with 66% conversion after the first hour,

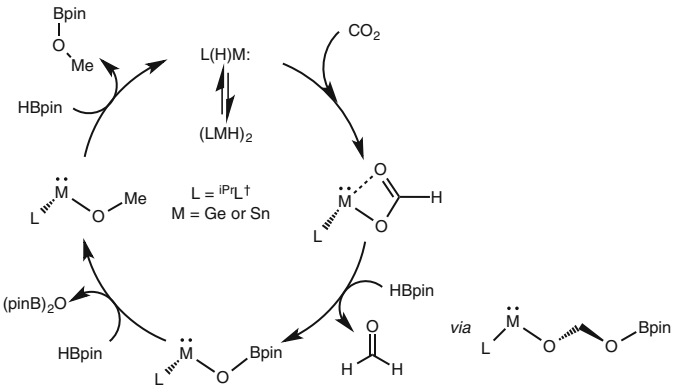

Scheme 5.26 A simplified hypothesised catalytic cycle for the reduction of CO_2 by the boranes, HBpin and HBcat, catalysed by **1** or **8**

Table 5.4 Hydroboration of CO_2 catalysed by **1** and **16**

Cat[a]	Cat. loading (mol%)	HBR_2 R_2 =	Time (h)[b]	Yield (%)[c]	% $(R_2BO)_2CH_2$[d]	% R_2BOCH_3[d]	TOF (h^{-1})
1	10	Pin	1	20	100	0	2
1	10	Pin	24	99	100	0	0.4
16	4	Pin	1	66	32	68	16.5
16	4	Pin	2	99	5	95	12.5
16	1	Pin	1	54	43	57	54
16	1	Pin	3	67	50	50	22.3
16	1	Pin	7	99[e]	0	100[e]	–[e]
16	1	Cat	0.08	99	0	100	1188

[a]Note ($^{iPr}L^{\dagger}$)SnOBu^{t} shows similar catalytic activity to 16
[b]All reactions carried out in C_6D_6 at 20 °C, under ~2 bar CO_2
[c]Determined by relative integrations in the ^{1}H and ^{11}B NMR spectra of reaction mixtures; yield based on consumption of B–H equivalents. Values given are combined yields of all products
[d]Values given as percentage of total yield
[e]Reaction under N_2 between 3 and 7 h

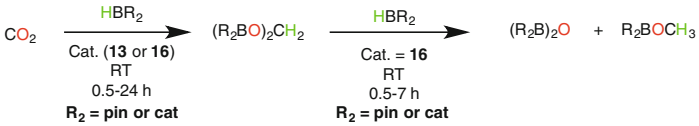

Scheme 5.27 The two-step hydroboration of CO_2, the second step only observed for the Sn(II) system

giving a TOF of 16.5 h^{-1}. Decreasing this to 1 mol% resulted in 54% conversion after one hour, and 67% at three hours, giving a TOF of 23 h^{-1} at this stage of reaction. Interestingly, at that stage, the ratio of $(pinBO)_2CH_2$ to $pinBOCH_3$ was 1:1. Leaving this reaction under an N_2 atmosphere for 4 h allowed for the conversion of all $(pinBO)_2CH_2$ to $pinBCH_3$ and $(pinB)_2O$ (Scheme 5.27). Using HBcat in the place of HBpin, with 1 mol% **16**, the reaction was complete in 5 min, giving a TOF of ~1200 h^{-1}. This value far exceeds any literature examples of CO_2 reduction with HBcat, and is in fact faster than any other reported TOF values for catalytic CO_2 reduction with any borane. In this case, the sole products from the reaction were $catBOCH_3$ and $(catB)_2O$. Note that similar TOFs were achieved using ($^{iPr}L^{\dagger}$)SnOBu^{t} as a precatalyst (viz. catalytic hydroboration of aldehydes and ketones, Sect. 5.3.2.1).

The TOFs observed for this Sn(II)-catalysed system are comparable to those seen for the Ru-catalysed CO_2 hydroboration reactions with HBpin (catalyst: $[RuH_2(H_2)_2(PCy_3)_2]$; Cy = cyclohexyl) reported by Sabo-Etienne and co-workers (TOF = 20 h^{-1}) [36], and are considerably higher than those reported for single-site MG group catalysts for the same transformation (TOF = 0.07–2.5 h^{-1}) [71, 74].

In an attempt to further increase the TOF of this reaction we employed the less bulky ^{TMS}L* ligand (^{TMS}L* = $(SiMe_3)N(Ar^*)^-$, Ar* = 2,6-$(Ph_2CH)_2$-4-MePh), using (^{TMS}L*)SnOBu^t (**19**) as the catalyst. The lessened steric bulk about the Sn(II) centre may reduce the barrier to intermediate steps involving the approach of an HBpin molecule to the Sn(II) centre of the catalyst. However, upon warming a mixture of C_6D_6 (0.5 mL), **19** (20 mg) and HBpin (105 μL) to ambient temperature, under ~2 bar pressure of CO_2, rapid deposition of elemental tin was observed. A ^{1}H NMR spectroscopic analysis of this crude reaction mixture revealed that no $pinBOCH_3$ was present, and that the only soluble species remaining were ^{iPr}L†H and HBpin. It therefore seems likely that the bulk of the Pr^i_3Si in ^{iPr}L† is of importance to the stability of transient (^{iPr}L†)Sn(μ-H)$_2$Sn(^{iPr}L†) in the catalytic cycle. In the catalytic reaction using **16**, only small amounts of protonated ligand were present in the ^{1}H NMR spectrum of the reaction mixture after one or two hours, with no observable Sn(II) hydride species (e.g. **8**). This suggests, as with other carbonyl reductions catalysed by **8**, that this species is present in the catalytic cycle for negligible amounts of time, with the rate of its consumption far greater than its production. The resting state, as determined by the ^{1}H NMR spectra of catalytic reaction mixtures, is (^{iPr}L†)SnOC(H)O, which is observed in crude catalytic mixtures. All boron containing products were verified through comparisons with the literature [36], with $(pinB)_2O$ or $(catB)_2O$ being the major by-product in all reactions. The observation of considerable amounts of $(pinBO)_2CH_2$ in reaction mixtures contrasts with other single-site MG catalysed CO_2 reductions, which exclusively yield $pinBOCH_3$ and $(pinB)_2O$ [71, 74]. The current system sees better comparisons with Ru-catalysed CO_2 reductions reported by Sabo-Etienne and co-workers [36], although even in that case only small amounts (~5%) of $(pinBO)CH_2$ were observed in the reaction after 30 min at ambient temperature.

5.4 Conclusion

The chemistry of low oxidation state complexes of the heavier group 14 elements has seen rapid growth over the past two decades. This chapter has expanded on this, in achieving stoichiometric reactions involving σ-metathesis type mechanisms, which have led to element(II) hydride generation. Related reactions using Sn(II) alkyl complexes have also led to the stoichiometric transfer hydrogenation of unactivated alkenes. Lastly, complexes of the heavier group 14 elements, germanium and tin, have been applied, for the first time, to well defined catalytic regimes; that is, the hydroboration of aldehydes, ketones, and CO_2. The rates of these reactions, particularly in tin, rival those of transition metal species capable of related transformations. These results are an important step forward for main group chemistry, and display just how synthetically versatile complexes involving these elements can be.

5.5 Experimental

5.5.1 Stoichiometric Reactions

(^{iPr}L†)Ge(Et)(H)NH$_2$ (3). A bright yellow solution of (^{iPr}L†)GeEt (200 mg, 0.28 mmol) in toluene was cooled (−25 °C), and dry NH_3 gas (8.4 mL, ∼0.35 mmol) carefully introduced above the solution with a syringe, under a slow flow of N_2. The vessel was sealed, and the reaction mixture rapidly stirred. The colour of the solution quickly dissipated. The reaction mixture was warmed to ambient temperature, stirred for 1 h, and all volatiles subsequently removed *in vacuo*. The solid residue was extracted in 10 mL of hexane, filtered, and the filtrate concentrated *in vacuo* to ∼3 mL. Storage of the solution at −30 °C for 24 h resulted in the formation of large colourless crystals of **3** (125 mg, 60%). M. p. 160–166 °C (melt); ^{1}H NMR (C_6D_6, 400 MHz, 298 K): δ = −0.04 (br d, $^3J_{HH}$ = 4.4 Hz, 2H, N*H*$_2$), 0.20 and 0.37 (m, 1H each, Ge-C*H*$_2$), 0.55 (t, $^3J_{HH}$ = 7.2 Hz, 3H, Ge-CH$_2$C*H*$_3$), 1.01 (d, $^3J_{HH}$ = 6.8 Hz, 6H, Ar†-*p*-CH(C*H*$_3$)$_2$), 1.21 and 1.25 (dd, $^3J_{HH}$ = 7.6 Hz, 9H each, SiPr$^i_3$-CH(C*H*$_3$)$_2$), 1.50 (sept, $^3J_{HH}$ = 7.6 Hz, 3H, SiPr$^i_3$-C*H*(CH$_3$)$_2$), 2.55 (sept, $^3J_{HH}$ = 6.8 Hz, 1H, Ar†-*p*-C*H*(CH$_3$)$_2$), 5.52 (m, 1H, Ge-*H*), 6.50 (s, 1H, C*H*Ph$_2$), 6.51 (s, 1H, C*H*Ph$_2$), 6.97–7.46 (m, 22H, Ar-*H*); ^{13}C{^{1}H} NMR (C_6D_6, 75.5 MHz, 298 K): δ = 8.6 (Ge-CH$_2$*C*H$_3$), 14.6 and 14.9 (Ar†-*p*-CH(*C*H$_3$)$_2$), 19.1 and 19.7 (SiPr$^i_3$-CH(*C*H$_3$)$_2$), 23.9 and 24.0 (SiPr$^i_3$-*C*H(CH$_3$)$_2$), 33.6 and 33.7 (Ar†-*p*-*C*H(CH$_3$)$_2$), 51.3 (*C*HPh$_2$), 52.8 (Ge-*C*H$_2$CH$_3$), 126.3, 126.6, 126.8, 127.6, 128.6, 128.7, 129.9, 130.0, 130.1, 130.8, 130.9, 140.8, 141.4, 142.5, 142.6, 143.1, 143.3. 144.9, 145.1, 146.3, 146.5, 146.8 (Ar-*C*); ^{29}Si{^{1}H} NMR (C_6D_6, 80 MHz, 298 K): δ = 7.6; IR, ν/cm^{-1} (ATR): 3440 and 3360 (w, NH_2), 3059 (w), 3022 (w), 2079 (m, Ge-H), 1598 (m), 1379 (m), 1364 (m), 1118 (m), 1032 (m), 909 (s), 880 (s), 853 (m), 744 (s), 725 (s); MS/EI m/z (%): 712.7 (M$^+$,1), 696.6 ((^{iPr}L†)Ge$^+$, 8), 167.2 (Ph$_2$C$^+$, 100); anal. calcd. for $C_{48}H_{63}GeNOSi$: C, 7.49%; H, 8.15%; N, 3.78%; found: C, 74.59%; H, 8.06%; N, 3.62%.

(^{iPr}L†)Ge(Et)(H)OEt (4). To a bright yellow cold solution of (^{iPr}L†)GeEt (0.25 g, 0.34 mmol) in toluene (20 mL) at −80 °C is added EtOH (20 μL, 37 mmol) using a micro pipettor. The reaction was allowed to warm to ambient temperature with stirring, over which time the reaction becomes colourless. All volatiles were subsequently removed *in vacuo* and the residue extracted in Et_2O (7 mL), and filtered. Concentration of the filtrate to 2 mL and storage at 4 °C for 2 days resulted in the formation of large colourless blocks of **4** (180 mg, 69%). M. p. 143–152 °C (melt); ^{1}H NMR (C_6D_6, 400 MHz, 298 K): δ = −0.60 and −0.14 (m, 1H each, Ge-C*H*$_2$), 0.33 (t, $^3J_{HH}$ = 7.2 Hz, 3H, Ge-CH$_2$C*H*$_3$), 1.05 (d, $^3J_{HH}$ = 6.8 Hz, 6H, Ar†-*p*-CH(C*H*$_3$)$_2$), 1.15 and 1.31 (d, $^3J_{HH}$ = 7.6 Hz, 9H each, SiPr$^i_3$-CH(C*H*$_3$)$_2$), 1.28 (t, 3H, $^3J_{HH}$ = 6.8 Hz, Ge-OCH$_2$C*H*$_3$), 1.44 (sept, $^3J_{HH}$ = 7.6 Hz, 3H, SiPr$^i_3$-C*H*(CH$_3$)$_2$), 2.60 (sept, $^3J_{HH}$ = 6.8 Hz, 1H, Ar†-*p*-C*H*(CH$_3$)$_2$), 3.67 (d of quart, $^2J_{HH}$ = 10.0 Hz, $^3J_{HH}$ = 6.8 Hz, 1H, Ge-OC*H*), 3.81 (d of quart, $^2J_{HH}$ = 10.0 Hz, $^3J_{HH}$ = 6.8 Hz, 1H, Ge-OC*H*), 5.97 (virtual d, 1H, Ge-H),

6.54 (s, 2H, C*H*Ph_2), 6.95–7.77 (m, 22H, Ar-*H*); $^{13}C\{^1H\}$ NMR (C_6D_6, 75.5 MHz, 298 K): δ = 7.7 (Ge-CH_2*C*H_3), 9.9 (Ge-O$CH_2$$CH_3$), 13.9 ($SiPr^i_3$-*C*H$(CH_3)_2$), 19.3 and 19.6 ($SiPr^i_3$-CH(*C*$H_3)_2$), 23.9 and 24.0 ($Ar^†$-*p*-CH(*C*$H_3)_2$), 33.7 (Ar-*C*H$(CH_3)_2$), 50.8 (Ge-*C*$H_2CH_3$), 51.6 (*C*H$Ph_2$), 61.9 (Ge-O*C*$H_2CH_3$), 126.2, 126.4, 126.5, 126.9, 128.0, 128.1, 128.6, 129.5, 129.7, 129.8, 129.9, 130.1, 130.8, 131.5, 142.2, 142.3, 143.6, 144.7, 145.0, 145.9, 146.2, 146.7 (Ar-*C*); $^{29}Si\{^1H\}$ NMR (C_6D_6, 80 MHz, 298 K): δ = 8.4; IR, ν/cm^{-1} (ATR): 3057 (w), 2033 (m, Ge-H), 1943 (w), 1599 (m), 1388 (m), 1365 (s, Ge-O), 1229 (s), 1158 (m), 1065 (m), 890 (m), 840 (m), 756 (s), 682 (s), 659 (s); MS/EI m/z (%): 728.6 (M^+-Pr^i, 16), 580.6 ($^{iPr}L^{†+}$-Pr^i, 41), 167.2 (Ph_2C^+, 100); anal. calcd. for $C_{48}H_{63}GeNOSi$: C, 74.80%; H, 8.24%; N, 1.82%; found: C, 74.77%; H, 8.08%; N, 1.94%.

{(^{iPr}L†)Ge(C_6H_{11})O}$_2$ (5). A bright yellow solution of ($^{iPr}L^†$)GeC_6H_{11} (0.15 g, 0.19 mmol) in Et_2O (20 mL) was cooled (−80 °C) and placed under an atmosphere of dry air by backfilling the evacuated reaction Schlenk flask from a second Schlenk flask containing air and P_2O_5. The pressure in the vessel was balanced by briefly opening to a nitrogen feed, sealed, and stirred for 10 min, over which time the solution became colourless. The reaction was subsequently concentrated *in vacuo* to 5 mL, and stored at 4 °C. Storage for 18 h yielding colourless crystalline blocks of **5** (50 mg, 33%). M.p. 182–190 °C (melt); ^1H NMR (C_6D_6, 400 MHz, 298 K): δ = 0.19 (br m, 2H, Ge-Hex^{Cy}-CH_2), 1.17 (d, $^3J_{HH}$ = 7.6 Hz, 18H, $SiPr^i_3$-CH$(CH_3)_2$), 1.20 (d, $^3J_{HH}$ = 6.8 Hz, 6H, $Ar^†$-*p*-CH(C$H_3)_2$), 1.19–1.46 (br m, 8H, Ge-Hex^{Cy}-CH_2), 1.62 (sept, $^3J_{HH}$ = 7.6 Hz, 3H, $SiPr^i_3$-C*H*$(CH_3)_2$), 1.87 (br m, 1H, Ge-C*H*), 2.80 (sept, $^3J_{HH}$ = 6.8 Hz, 1H, $Ar^†$-*p*-C*H*$(CH_3)_2$), 6.70 (s, 2H, C*H*Ph_2), 6.98–7.93 (m, 22H, Ar-*H*); $^{13}C\{^1H\}$ NMR (C_6D_6, 75.5 MHz, 298 K): δ = 16.1 ($SiPr^i_3$-*C*H$(CH_3)_2$), 21.0 (Ge-Hex^{Cy}-*C*H_2), 21.4 ($SiPr^i_3$-CH(*C*$H_3)_2$), 24.8 ($Ar^†$-*p*-CH$(CH_3)_2$), 25.6 (Ge-Hex^{Cy}-*C*H_2), 27.8 (Ge-Hex^{Cy}-*C*H_2), 28.7 (Ge-Hex^{Cy}-*C*H), 34.5 ($Ar^†$-*p*-*C*H$(CH_3)_2$), 52.0 (*C*HPh_2), 126.8, 127.3, 128.5, 129.4, 130.5, 131.3, 132.0, 142.8, 144.3, 145.8, 146.6, 148.6 (Ar-C); $^{29}Si\{^1H\}$ NMR (C_6D_6, 80 MHz, 298 K): δ = 12.9; IR, ν/cm^{-1} (ATR): 3060 (w), 1599 (w), 1381 (m), 1260 (m), 1156 (m), 1112 (m), 1074 (m), 1032 (m), 881 (s), 805 (s), 743 (s), 662 (s); MS/EI m/z (%): 623.7 ($^{iPr}L^{†+}$, 20), 167.2 (Ph_2C^+, 100); anal. calcd. for $C_{100}H_{126}Ge_2N_2O_2Si_2$: C, 75.56%; H, 7.99%; N, 1.76%; found: C, 75.47%; H, 8.13%; N, 1.86%.

(^{iPr}L†)SnO-(TEMP) (**6**). A solution of ($^{iPr}L^†$)SnEt (300 mg, 0.39 mmol) in toluene (20 mL) was cooled to −80 °C, and TEMPOH (214 mg, 0.41 mmol) was added dropwise as a solution in toluene (10 mL). The reaction mixture was allowed to warm to ambient temperature over 18 h, and all volatiles subsequently removed *in vacuo*. The residue was extracted in warm hexane (20 mL), and filtered. Concentration of the filtrate to ∼7 mL, and storage at −30 °C, yielded the product as colourless crystalline blocks of **6** (160 mg, 36%). M.p. 115–120 °C (dec.); ^1H NMR (C_6D_6, 400 MHz, 298 K): δ = 0.77 (br, 6H, TEMPO-CH_3), 0.97 (d, $^3J_{HH}$ = 6.8 Hz, 6H, $Ar^†$-*p*-CH(C$H_3)_2$), 1.12 (br, 6H, TEMPO-CH_3), 1.37 (br, 6H, TEMPO-CH_2), 1.60 (br, 18H, $SiPr^i_3$-CH(C$H_3)_2$), 2.03 (sept, $^3J_{HH}$ = 7.6 Hz, 3H, $SiPr^i_3$-C*H*$(CH_3)_2$), 2.52 (sept, $^3J_{HH}$ = 6.8 Hz, 1H, $Ar^†$-*p*-C*H*$(CH_3)_2$), 6.56 (s, 2H, C*H*Ph_2), 6.84 (m, 2H, $Ar^†$-*m*-C*H*), 6.99–7.36 (m, 20H, Ar-*H*); $^{13}C\{^1H\}$ NMR (C_6D_6, 75.5 MHz, 298 K): δ = 14.7 (br, $SiPr^i_3$-*C*H$(CH_3)_2$), 19.1 (O(TEMP)-*C*H_2),

19.7 (br, $SiPr^i_3$-CH(CH_3)$_2$), 24.2 ($Ar^†$-*p*-CH(CH_3)$_2$), 33.7 ($Ar^†$-*p*-CH(CH_3)$_2$), 36.2 (br, O(TEMP)-CH_3), 40.23 (O(TEMP)-CH_2), 51.8 (CHPh$_2$), 58.4 (O(TEMP)-NC), 126.5, 127.6, 127.4, 128.7, 128.7, 129.7, 129.9, 130.1, 131.4, 131.5, 140.8, 142.5, 144.9, 145.0, 145.6, 148.6 (Ar-*C*); ^{29}Si{^{1}H} NMR (C_6D_6, 80 MHz, 298 K): δ = 26.1; ^{119}Sn{^{1}H} NMR (C_6D_6, 149 MHz, 298 K): δ = 177.3; IR, ν/cm^{-1} (ATR): 3058 (w), 3024 (w), 1598 (m), 1296 (m), 1221 (m), 1200 (m), 1117 (m), 1032 (m), 917 (m), 878 (s), 830 (s), 754 (m); MS/EI m/z (%): 623.6 ($^{iPr}L^{†+}$, 20), 167.2 (Ph_2C^+, 100); anal. calcd. for $C_{53}H_{70}N_2OSiSn$: C, 70.89%; H, 7.86%; N, 3.12%; found: C, 71.12%; H, 7.77%; N, 2.99%.

(**^{iPr}L†)SnOBu^t** (**7**). To a solution of $^{iPr}L^†H$ (1.80 g, 2.88 mmol) in THF (70 mL) at −80 °C was added Bu^nLi (1.98 mL of a 1.6 M solution, 3.17 mmol) over 10 min. The reaction mixture was then warmed to ambient temperature over 3 h, after which time it was added slowly, via cannula, to a solution of $SnBr_2$ (0.88 g, 3.17 mmol) in THF (20 mL) at −80 °C. The resultant mixture was warmed to ambient temperature and stirred for 16 h, after which all volatiles were removed *in vacuo*. The residue was extracted into warm toluene (30 mL), and the extract filtered into a flask containing a suspension of $KOBu^t$ (323 mg, 2.88 mmol) in toluene (10 mL) at −80 °C. The resultant mixture was stirred for 2 h, then warmed to ambient temperature and stirred for a further hour. The mixture was subsequently filtered, all volatiles removed *in vacuo* from the filtrate, and the residue dissolved in the minimum amount of hexane (*ca.*10 mL). Storage of the solution at −30 °C overnight afforded pale yellow crystals of **7** (1.35 g, 56%). M.p.: 164–172 °C; ^{1}H NMR (C_6D_6, 400 MHz, 298 K), δ = 1.00 (d, $^3J_{HH}$ = 6.8 Hz, 6H, $Ar^†$-*p*-CH(CH_3)$_2$), 1.20 (s, 9H, OC(CH_3)$_3$), 1.45 (br, 18H, $SiPr^i_3$-CH(CH_3)$_2$), 2.30 (b, 3H, $SiPr^i_3$-CH(CH_3)$_2$), 2.55 (sept, $^3J_{HH}$ = 6.8 Hz, 1H, $Ar^†$-*p*-CH(CH_3)$_2$), 6.51 (s, 2H, CHPh$_2$), 6.84–7.38 (m, 22H, Ar-*H*); ^{13}C{^{1}H} NMR (C_6D_6, 75.5 MHz, 298 K), δ = 15.4 ($SiPr^i_3$-CH(CH_3)$_2$), 20.0 ($SiPr^i_3$-CH(CH_3)$_2$), 24.2 ($Ar^†$-*p*-CH(CH_3)$_2$), 33.7 ($Ar^†$-*p*-CH(CH_3)$_2$), 35.5 (OC(CH_3)$_3$), 52.1 (CHPh$_2$), 72.0 (OC(CH_3)$_3$), 126.5, 127.4, 128.7, 129.7, 130.0, 130.1, 131.4, 142.8, 144.6, 145.0, 145.4, 145.7 (Ar-*C*); ^{29}Si{^{1}H} NMR (C_6D_6, 80 MHz, 298 K), δ = 6.8; ^{119}Sn{^{1}H} NMR (C_6D_6, 149 MHz, 298 K): δ = 215; IR (ν/cm^{-1}, ATR): 3061 (w), 3026 (w), 1598 (w), 1380 (m), 1355 (m), 1227 (m), 1181 (s), 1159 (m), 945 (s), 881 (s), 832 (s), 812 (m), 760 (s), 656 (s); MS/EI *m/z* (%): 815.2 (M^+, 1), 623.2 ($^{iPr}L^{†+}$, 62), 580.1 ($^{iPr}L^{†+}$-Pr^i, 100); anal. calc. for $C_{48}H_{61}NOSiSn$: C, 70.76%; H, 7.55%; N, 1.72%; found: C, 70.76%; H, 7.69%; N, 1.70%.

[(**^{iPr}L†)Sn{(CH$_2$)$_2$Bu^t}O]$_2$** (**9**). A solution of ($^{iPr}L^†$)Sn(CH$_2$)$_2$Bu^t (0.15 g, 0.18 mmol) in toluene (20 mL) was placed under an atmosphere of dry air by backfilling the evacuated reaction Schlenk flask from a second Schlenk flask containing air and P_2O_5. The pressure in the vessel was balanced by briefly opening to a nitrogen feed, sealed, and stirred for 10 min, over which time the solution became colourless. The reaction mixture was subsequently concentrated *in vacuo* to 5 mL, and stored at 4 °C. Storage for 18 h yielded X-ray quality colourless crystalline blocks (75 mg, 49%). M.p. 147–153 °C (melt); ^{1}H NMR (C_6D_6, 400 MHz,

298 K): δ = −0.42 (br, 2H, Sn-CH_2), 0.67 (s, 9H, Sn-$CH_2CH_2C(CH_3)_3$), 0.98 (m, 2H, Sn-CH_2CH_2), 1.07 (d, $^3J_{HH}$ = 6.8 Hz, 6H, Ar†-*p*-CH(CH_3)$_2$), 1.31 (d, $^3J_{HH}$ = 7.6 Hz, 18H, SiPr$^i_3$-CH(CH_3)$_2$), 1.67 (sept, $^3J_{HH}$ = 7.6 Hz, 3H, SiPr$^i_3$-C*H*(CH_3)$_2$), 2.64 (sept, $^3J_{HH}$ = 6.8 Hz, 1H, Ar†-*p*-C*H*(CH_3)$_2$), 6.41 (s, 2H, C*H*Ph$_2$), 6.93–7.36 (m, 22H, Ar-*H*); ^{13}C{^{1}H} NMR (C_6D_6, 75.5 MHz, 298 K): δ = 15.9 (SiPr$^i_3$-*C*H(CH_3)$_2$), 20.3 (SiPr$^i_3$-CH(*C*H$_3$)$_2$), 24.4 (Ar†-*p*-CH(*C*H$_3$)$_2$), 29.3 (Sn-$CH_2CH_2C(CH_3)_3$), 32.7 (Ar†-*p*-*C*H(CH_3)$_2$), 33.7 (Sn-CH_2CH_2), 37.6 (Sn-*C*H$_2$), 51.6 (*C*HPh$_2$), 53.7 (Sn-$CH_2CH_2C(CH_3)_3$), 126.3, 127.6, 128.6, 129.7, 129.9, 130.1, 130.3, 139.7, 141.8, 145.9, 146.2, 151.0 (Ar-*C*); ^{29}Si{^{1}H} NMR (C_6D_6, 80 MHz, 298 K): δ = 5.9; IR, ν/cm^{-1} (ATR): 3060 (w), 3026 (w), 1945 (w), 1598 (w), 1380 (m), 1363 (m), 1222 (m), 1155 (m), 1116 (m), 1031 (m), 878 (s), 830 (s), 759 (s); MS/EI m/z (%): 623.4 (^{iPr}L$^{\dagger+}$, 55), 580.4 (^{iPr}L$^{\dagger+}$-Pr^i, 100); anal. calcd. for $C_{100}H_{130}N_2O_2Si_2Sn_2$: C, 72.63%; H, 7.92%; N, 1.69%; found: C, 72.49%; H, 8.10%; N, 1.79%.

(**^{iPr}L†)GeOBu^t** (**10**). To suspension of KOBu^t (92 mg, 0.82 mmol) in toluene (10 mL) was added (^{iPr}L†)GeCl (0.50 g, 0.68 mmol) as a solution in toluene (20 mL) at ambient temperature. The resulting reaction mixture was stirred at ambient temperature for 3 h, after which time all volatiles were removed *in vacuo*. The residue was extracted in warm hexane (30 mL), and the extract filtered. The filtrate was concentrated to 10 mL, and stored at −30 °C for 2 days, to yield (^{iPr}L†)GeOBu^t as large colourless blocks (350 mg, 67%). M.p.: 97–105 °C; ^{1}H NMR (C_6D_6, 400 MHz, 298 K), δ = 0.98 (d, $^3J_{HH}$ = 6.8 Hz, 6H, Ar†-*p*-CH(CH_3)$_2$), 1.09 (s, 9H, OC(CH_3)$_3$), 1.40 (br, 18H, SiPr$^i_3$-CH(CH_3)$_2$), 2.20 (b, 3H, SiPr$^i_3$-C*H*(CH_3)$_2$), 2.53 (sept, $^3J_{HH}$ = 6.8 Hz, 1H, Ar†-*p*-C*H*(CH_3)$_2$), 6.39 (s, 2H, C*H*Ph$_2$), 6.91–7.23 (m, 22H, Ar-*H*); ^{13}C{^{1}H} NMR (C_6D_6, 75.5 MHz, 298 K), δ = 15.1 (SiPr$^i_3$-*C*H(CH_3)$_2$), 20.0 (SiPr$^i_3$-CH(*C*H$_3$)$_2$), 24.1 (Ar†-*p*-CH(*C*H$_3$)$_2$), 33.5 (Ar†-*p*-*C*H(CH_3)$_2$), 34.0 (OC(*C*H$_3$)$_3$), 52.3 (*C*HPh$_2$), 73.1 (O*C*(*CH*$_3$)$_3$), 126.5, 126.6, 128.6, 128.7, 129.1, 130.1, 130.2, 131.3, 140.8, 144.8, 145.0, 145.4 (Ar-*C*); ^{29}Si{^{1}H} NMR (C_6D_6, 80 MHz, 298 K), δ = 3.1; IR (ν/cm^{-1}, ATR): 3058 (w), 1598 (m), 1312 (m), 1257 (m), 1181 (m), 1226 (w), 1074 (m), 938 (m), 881 (s), 831 (m), 760 (s), 660 (s); MS/EI *m/z* (%): 769.7 (M$^+$, 0.5), 167.2 (Ph_2C^+, 100); anal. calc. for $C_{48}H_{61}GeNOSi$: C, 75.00%; H, 8.00%; N, 1.82%; found: C, 74.92%; H, 7.95%; N, 1.91%.

(**^{iPr}L†)GeOPh** (**11**). To a solution of (^{iPr}L†)GeCl (0.50 g, 0.68 mmol) in THF (30 mL) at −80 °C was added PhOLi (75 mg, 75 mmol) as a solution in THF (10 mL). The reaction mixture was warmed to ambient temperature, and stirred for 2 h. All volatiles were subsequently removed *in vacuo* and the residue extracted in hot hexane (30 mL), concentrate to 15 mL and stored at −30 °C for 2 days, yielding colourless crystals of (^{iPr}L†)GeOPh (390 mg, 73%). M.p.: 182–189 °C; ^{1}H NMR (C_6D_6, 400 MHz, 298 K), δ = 1.00 (d, $^3J_{HH}$ = 6.8 Hz, 6H, Ar†-*p*-CH(CH_3)$_2$), 1.20 (d, $^3J_{HH}$ = 7.6 Hz, 18H, SiPr$^i_3$-CH(CH_3)$_2$), 2.03 (sept, $^3J_{HH}$ = 7.6 Hz, 3H, SiPr$^i_3$-C*H*(CH_3)$_2$), 2.52 (sept, $^3J_{HH}$ = 6.8 Hz, 1H, Ar†-*p*-C*H*(CH_3)$_2$), 6.39 (s, 2H, C*H*Ph$_2$), 6.67–7.17 (m, 27H, Ar-*H*); ^{13}C{^{1}H} NMR (C_6D_6, 75.5 MHz, 298 K), δ = 15.5 (SiPr$^i_3$-*C*H(CH_3)$_2$), 20.2 (SiPr$^i_3$-CH(*C*H$_3$)$_2$), 24.1 (Ar†-*p*-CH(*C*H$_3$)$_2$), 33.8

($Ar^{\dagger}$-*p*-*C*H(CH_3)$_2$), 52.5 (*C*HPh_2), 120.0, 121.0, 126.6, 126.7, 127.7, 128.8, 129.3, 129.7, 130.1, 131.3, 141.6, 144.6, 144.9, 145.0, 145.2, 158.5 (Ar-*C*); ^{29}Si{^{1}H} NMR (C_6D_6, 80 MHz, 298 K), δ = 9.0; IR (ν/cm^{-1}, ATR): 3060 (w), 3026 (w), 1589 (m), 1381 (w), 1241 (s), 1197 (m), 1159 (m), 1116 (m), 1031 (m), 878 (s), 838 (s), 760 (s), 735 (s), 657 (s); MS/EI *m/z* (%): 746.6 (M^+-Pr^i, 8), 696.6 ($^{iPr}L^{\dagger}Ge^+$, 59), 167.2 (Ph_2C^+, 100); anal. calc. for $C_{50}H_{57}GeNOSi$: C, 76.14%; H, 7.28%; N, 1.78%; found: C, 76.03%; H, 7.41%; N, 1.86%.

(**^{iPr}L†**)**SnOPh** (**12**). This compound was made in a similar manner to ($^{iPr}L^{\dagger}$)GeOPh, but using ($^{iPr}L^{\dagger}$)SnCl (0.5 g, 0.64 mmol) and PhOLi (70 mg, 70 mmol). The product was isolated by extraction of the crude reaction residue in toluene (10 mL), filtration of the extract, and removal of all volatiles *in vacuo*. The resulting residue was washed with hexane (5 mL), yielding ($^{iPr}L^{\dagger}$)SnOPh as a micro-crystalline off-white solid (370 mg, 69%). M.p.: 162–168 °C; ^{1}H NMR (C_6D_6, 400 MHz, 298 K), δ = 0.98 (d, $^3J_{HH}$ = 6.8 Hz, 6H, $Ar^{\dagger}$-*p*-CH(CH_3)$_2$), 1.44 (d, $^3J_{HH}$ = 7.6 Hz, 18H, $SiPr^i_3$-CH(CH_3)$_2$), 2.11 (sept, $^3J_{HH}$ = 7.6 Hz, 3H, $SiPr^i_3$-C*H*(CH_3)$_2$), 2.53 (sept, $^3J_{HH}$ = 6.8 Hz, 1H, $Ar^{\dagger}$-*p*-C*H*(CH_3)$_2$), 6.52 (s, 2H, C*H*Ph_2), 6.67–7.35 (m, 27H, Ar-*H*); ^{13}C{^{1}H} NMR (C_6D_6, 75.5 MHz, 298 K), δ = 15.8 ($SiPr^i_3$-*C*H(CH_3)$_2$), 20.2 ($SiPr^i_3$-CH(*C*H$_3$)$_2$), 24.2 ($Ar^{\dagger}$-*p*-CH(*C*H$_3$)$_2$), 33.8 ($Ar^{\dagger}$-*p*-*C*H(CH_3)$_2$), 52.3 (*C*HPh_2), 119.1, 119.8, 126.8, 127.3, 128.5, 128.6, 128.8, 130.0, 130.1, 131.6, 143.5, 144.3, 145.0, 145.8, 145.9, 161.3 (Ar-*C*); ^{29}Si{^{1}H} NMR (C_6D_6, 80 MHz, 298 K), δ = 8.0; IR (ν/cm^{-1}, ATR): 3062 (w), 3024 (w), 1587 (s), 1380 (w), 1332 (w), 1246 (s), 1198 (m), 1160 (m), 1116 (m), 1067 (m), 1030 (m), 996 (m), 879 (s), 834 (s), 752 (s); MS/EI *m/z* (%): 742.6 (($^{iPr}L^{\dagger}$)Sn^+, 2), 580.6 ($^{iPr}L^{\dagger+}$-Pr^i, 40), 167.2 (Ph_2C^+, 100).

N.B. Despite numerous attempts, an accurate elemental analysis could not be obtained for this compound.

(**^{iPr}L†**)**GeOC(H)O** (**13**). To a mixture of ($^{iPr}L^{\dagger}$)GeCl (0.50 g, 0.68 mmol) and KOC(H)O (69 mg, 0.82) was added THF (30 mL) at ambient temperature, and the reaction mixture stirred for 18 h. All volatiles were subsequently removed, and the solid residue extracted in hot hexane (20 mL) and filtered. Storage at −30 °C for 2 days resulted in the formation of colourless crystals of ($^{iPr}L^{\dagger}$)GeOC(H)O (320 mg, 64%). M.p.: 162–170 °C; ^{1}H NMR (C_6D_6, 400 MHz, 298 K), δ = 0.95 (d, $^3J_{HH}$ = 6.8 Hz, 6H, $Ar^{\dagger}$-*p*-CH(CH_3)$_2$), 1.45 (d, $^3J_{HH}$ = 7.2 Hz, 18H, $SiPr^i_3$-CH(CH_3)$_2$), 1.82 (sept, $^3J_{HH}$ = 7.2 Hz, 3H, $SiPr^i_3$-C*H*(CH_3)$_2$), 2.50 (sept, $^3J_{HH}$ = 6.8 Hz, 1H, $Ar^{\dagger}$-*p*-C*H*(CH_3)$_2$), 6.23 (s, 2H, C*H*Ph_2), 6.90–7.35 (m, 22H, Ar-*H*), 8.05 (s, 1H, GeOC(*H*)O); ^{13}C{^{1}H} NMR (C_6D_6, 75.5 MHz, 298 K), δ = 15.3 ($SiPr^i_3$-*C*H(CH_3)$_2$), 19.8 ($SiPr^i_3$-CH(*C*H$_3$)$_2$), 24.0 ($Ar^{\dagger}$-*p*-CH(*C*H$_3$)$_2$), 33.8 ($Ar^{\dagger}$-*p*-*C*H(CH_3)$_2$), 52.4 (*C*HPh_2), 126.6, 126.8, 128.8, 129.7, 130.0, 130.1, 131.1, 140.8, 141.2, 141.4, 144.5, 145.0 (Ar-*C*), 165.0 (GeO*C*(H)O); ^{29}Si{^{1}H} NMR (C_6D_6, 80 MHz, 298 K), δ = 10.6; IR (ν/cm^{-1}, ATR): 3060 (w), 3025 (w), 1663 (GeOC(H)=O), 1598 (w), 1190 (m), 1114 (m), 1075 (m), 875 (s), 737 (s), 696 (s); MS/EI *m/z* (%): 695.6 (($^{iPr}L^{\dagger}$)Ge^+, 4), 580.6 ($^{iPr}L^{\dagger+}$-Pr^i, 24), 167.2 (Ph_2C^+, 100); anal. calc. for $C_{45}H_{53}GeNO_2Si$: C, 72.98%; H, 7.21%; N, 1.89%; found: C, 72.93%; H, 7.39%; N, 2.01%.

{(^{iPr}L†)GeO}$_2$CH$_2$ (14). To a solution of (^{iPr}L†)GeOC(H)O (150 mg, 0.20 mmol) in toluene (10 mL) was added {(^{iPr}L†)GeH}$_2$ (146 mg, 0.10 mmol) as a solution in toluene (10 mL) at ambient temperature. The reaction mixture was stirred for 10 min, and all volatiles subsequently removed *in vacuo*. The residue was extracted in hexane (15 mL), the extract filtered, and the filtrate concentrated to ~7 mL. Storage of the filtrate at −30 °C for 18 h resulted in the formation of colourless blocks of {(^{iPr}L†)GeO}$_2$CH$_2$ (120 mg, 41%). M.p.: 186–194 °C; ^{1}H NMR (C_6D_6, 400 MHz, 298 K), δ = 0.98 (d, $^3J_{HH}$ = 6.8 Hz, 6H, Ar†-*p*-CH(C*H*$_3$)$_2$), 1.31 (d, $^3J_{HH}$ = 7.6 Hz, 18H, SiPr$^i_3$-CH(C*H*$_3$)$_2$), 1.83 (sept, $^3J_{HH}$ = 7.6 Hz, 3H, SiPr$^i_3$-C*H*(CH$_3$)$_2$), 2.53 (sept, $^3J_{HH}$ = 6.8 Hz, 1H, Ar†-*p*-C*H*(CH$_3$)$_2$), 4.75 (s, 2H, GeOC*H*$_2$OGe), 6.33 (s, 2H, C*H*Ph$_2$), 6.93–7.41 (m, 22H, Ar-*H*); ^{13}C{^{1}H} NMR (C_6D_6, 75.5 MHz, 298 K), δ = 14.9 (SiPr$^i_3$-*C*H(CH$_3$)$_2$), 20.0 (SiPr$^i_3$-CH(*C*H$_3$)$_2$), 24.0 (Ar†-*p*-CH(*C*H$_3$)$_2$), 33.7 (Ar†-*p*-*C*H(CH$_3$)$_2$), 52.1 (*C*HPh$_2$), 86.1 (GeO*C*H$_2$OGe), 126.5, 126.6, 127.3, 128.6, 129.0, 130.1, 130.2, 131.2, 140.8, 143.0, 145.2, 145.7 (Ar-*C*); ^{29}Si{^{1}H} NMR (C_6D_6, 80 MHz, 298 K), δ = 9.1; IR (ν/cm^{-1}, ATR): 3061 (w), 3026 (w), 1598 (w), 1380 (m), 1355 (m), 1227 (m), 1181 (s), 1159 (m), 945 (s), 881 (s), 832 (s), 812 (m), 760 (s), 656 (s); MS/EI *m/z* (%): 741.6 (M$^+$-(^{iPr}L†)Ge$^+$, 1), 580.5 (^{iPr}L$^{\dagger+}$-Pr^i, 46), 167.2 (Ph$_2$C$^+$, 100).

{(^{iPr}L†)Ge}$_2$O (15). A solution of {(^{iPr}L†)Ge}$_2$ (200 mg, 0.14 mmol) in toluene (15 mL) was stirred under an atmosphere of dry N_2O at ambient temperature for 30 min. All volatiles were subsequently removed from the reaction mixture *in vacuo*, the residue extracted in hot hexane (10 mL), and the extract filtered. Storage of the filtrate at −30 °C for 2 days led to the formation of {(^{iPr}L†)Ge}$_2$O as large colourless blocks (120 mg, 60%). M.p.: 175–183 °C; ^{1}H NMR (C_6D_6, 400 MHz, 298 K), δ = 1.02 (d, $^3J_{HH}$ = 6.8 Hz, 6H, Ar†-*p*-CH(C*H*$_3$)$_2$), 1.33 (br, 18H, SiPr$^i_3$-CH(C*H*$_3$)$_2$), 1.95 (br, 3H, SiPr$^i_3$-C*H*(CH$_3$)$_2$), 2.56 (sept, $^3J_{HH}$ = 6.8 Hz, 1H, Ar†-*p*-C*H*(CH$_3$)$_2$), 6.33 (s, 2H, C*H*Ph$_2$), 6.87–7.45 (m, 22H, Ar-*H*); ^{13}C{^{1}H} NMR (C_6D_6, 75.5 MHz, 298 K), δ = 14.9 (SiPr$^i_3$-*C*H(CH$_3$)$_2$), 19.9 (SiPr$^i_3$-CH(*C*H$_3$)$_2$), 24.1 (Ar†-*p*-CH(*C*H$_3$)$_2$), 33.8 (Ar†-*p*-*C*H(CH$_3$)$_2$), 52.8 (*C*HPh$_2$), 126.6, 127.4, 127.6, 128.6, 129.3, 130.1, 130.7, 140.8, 141.3, 144.4, 145.2, 145.5 (Ar-*C*); ^{29}Si{^{1}H} NMR (C_6D_6, 80 MHz, 298 K), δ = 9.7; IR (ν/cm^{-1}, ATR): 3062 (w), 1598 (w), 1379 (w), 1259 (m), 1116 (m), 1073 (m), 1031 (m), 881 (s), 832 (m), 804 (m), 758 (m), 660 (s); MS/EI *m/z* (%): 623.6 (^{iPr}L$^{\dagger+}$, 21), 167.2 (Ph$_2$C$^+$, 100); anal. calc. for $C_{88}H_{104}Ge_2N_2OSi_2$: C, 75.11%; H, 7.45%; N, 1.99%; found: C, 65.37%; H, 7.12%; N, 1.95%.

N.B. Despite repeated attempts, elemental analyses of this compound returned low C readings, possibly due to the formation of involatile SiC compounds, arising from the presence of Si and C in this species [89].

(^{iPr}L†)SnOC(H)O (16). This compound was made in a similar manner to (^{iPr}L†)GeOC(H)O, but using (^{iPr}L†)SnBr (0.5 g, 0.61 mmol) and KOC(H)O (61 mg, 0.73 mmol). The product by extraction of the reaction residue in toluene (20 mL), filtration of the extract, removal of all volatiles from the filtrate *in vacuo*, and washing the resulting residue with hexane (5 mL), yielding a free-flowing colourless powder (400 mg, 83%). M.p.: 162–170 °C; ^{1}H NMR (C_6D_6,

400 MHz, 298 K), δ = 0.98 (d, $^{3}J_{HH}$ = 6.8 Hz, 6H, Ar†-*p*-CH(CH_3)$_2$), 1.39 (d, $^{3}J_{HH}$ = 7.2 Hz, 18H, SiPr$^{i}_3$-CH(CH_3)$_2$), 1.84 (sept, $^{3}J_{HH}$ = 7.2 Hz, 3H, SiPr$^{i}_3$-C*H*(CH$_3$)$_2$), 2.52 (sept, $^{3}J_{HH}$ = 6.8 Hz, 1H, Ar†-*p*-C*H*(CH$_3$)$_2$), 6.54 (s, 2H, C*H*Ph$_2$), 6.86–7.36 (m, 22H, Ar-*H*), 8.71 (s, 1H, SnOC(*H*)O); ^{13}C{^{1}H} NMR (C$_6$D$_6$, 75.5 MHz, 298 K), δ = 15.6 (SiPr$^{i}_3$-*C*H(CH$_3$)$_2$), 19.6 (SiPr$^{i}_3$-CH(*C*H$_3$)$_2$), 24.1 (Ar†-*p*-CH(*C*H$_3$)$_2$), 33.8 (Ar†-*p*-*C*H(CH$_3$)$_2$), 52.2 (*C*HPh$_2$), 126.7, 127.6, 128.8, 129.8, 129.9, 130.1, 131.4, 140.8, 143.8, 144.7, 145.0, 146.0 (Ar-*C*), 173.80 (SnO*C*(H)O); ^{119}Sn{^{1}H} NMR (C$_6$D$_6$, 149 MHz, 298 K): δ = −134; IR (ν/cm^{-1}, ATR): 3060 (w), 3026 (w), 1598 (w), 1549 (SnC(H)=O), 1339 (m), 1311 (m), 1224 (m), 1197 (m), 1157 (w), 1115 (m), 1075 (w), 1031 (w), 984 (m), 919 (w), 878 (s), 836 (s), 758 (m), 721 (s); MS/EI *m/z* (%): 741.6 ((^{iPr}L†)Sn^{+}, 1), 580.1 (^{iPr}L$^{\dagger+}$-Pr^{i}, 62), 167.2 (Ph$_2$C^{+}, 100); anal. calc. for C$_{45}$H$_{53}$NO$_2$SiSn: C, 68.70%; H, 6.79%; N, 1.78%; found: C, 68.71%; H, 6.76%; N, 1.64%.

(**^{iPr}L†**)**GeOBpin** (**17**). To a solution of (^{iPr}L†)GeOC(H)O (150 mg, 0.20 mmol) was added HBpin (29 μL, 0.20 mmol), and the reaction mixture stirred at ambient temperature for 18 h. The reaction initially became intense orange, which dissipated to become colourless after 1 h. All solvents were removed from the reaction mixture, the residue extracted in hexane (10 mL), and the extract filtered. The filtrate was concentrated to 5 mL, and stored at 4 °C for 2 days, yielding large colourless blocks of (^{iPr}L†)GeOBpin (95 mg, 57%). M.p.: 152–161 °C; ^{1}H NMR (C$_6$D$_6$, 400 MHz, 298 K), δ = 0.95 (d, $^{3}J_{HH}$ = 6.8 Hz, 6H, Ar†-*p*-CH(CH_3)$_2$), 1.04 (s, 12H, Bpin-(CH_3)$_4$), 1.38 (d, $^{3}J_{HH}$ = 7.6 Hz, 18H, SiPr$^{i}_3$-CH(CH_3)$_2$), 1.96 (sept, $^{3}J_{HH}$ = 7.6 Hz, 3H, SiPr$^{i}_3$-C*H*(CH$_3$)$_2$), 2.52 (sept, $^{3}J_{HH}$ = 6.8 Hz, 1H, Ar†-*p*-C*H*(CH$_3$)$_2$), 6.34 (s, 2H, C*H*Ph$_2$), 6.96–7.39 (m, 22H, Ar-*H*); ^{13}C{^{1}H} NMR (C$_6$D$_6$, 75.5 MHz, 298 K), δ = 14.9 (SiPr$^{i}_3$-*C*H(CH$_3$)$_2$), 19.1 (SiPr$^{i}_3$-CH(*C*H$_3$)$_2$), 24.0 (pinB-*C*H$_3$), 24.7 (Ar†-*p*-CH(*C*H$_3$)$_2$), 33.7 (Ar†-*p*-*C*H(CH$_3$)$_2$), 52.8 (*C*HPh$_2$), 82.2 (pinB-*C*), 126.6, 127.6, 127.9, 128.5, 128.6, 130.1, 130.4, 130.7, 140.8, 141.6, 143.3, 145.0 (Ar-*C*); ^{29}Si{^{1}H} NMR (C$_6$D$_6$, 80 MHz, 298 K), δ = 9.2; ^{11}B{^{1}H} NMR(C$_6$D$_6$, 128 MHz, 298 K): δ = 21.8; IR (ν/cm^{-1}, ATR): 3061 (w), 3026 (w), 1686 (m), 1599 (m), 1323 (m), 1285 (m), 1199 (s), 1147 (s), 1117 (m), 1032 (m), 989 (m), 880 (s), 833 (s), 744 (m); MS/EI *m/z* (%): 796.7 (M^{+}-Pr^{i}, 2), 696.6 (^{iPr}L†Ge^{+}, 2), 167.2 (Ph$_2$C^{+}, 100); anal. calc. for C$_{47}$H$_{58}$BGeNO$_3$Si: C, 71.61%; H, 7.69%; N, 1.67%; found: C, 71.47%; H, 7.80%; N, 1.69%.

(**^{iPr}L†**)**SnOBpin** (**18**). This compound was made in a similar manner to (^{iPr}L†)GeOBpin, but using (^{iPr}L†)SnOC(H)O (150 mg, 0.19 mmol) and HBpin (28 μL, 0.19 mmol), with the reaction conducted from −40 °C to ambient temperature. The product was isolated by extraction of the crude reaction residue in hexane (15 mL), filtration of the extract, and concentration to 10 mL. Storage at −30 °C led the formation of large colourless needles (90 mg, 54%). M.p.: 152–161 °C; ^{1}H NMR (C$_6$D$_6$, 400 MHz, 298 K), δ = 0.98 (d, $^{3}J_{HH}$ = 6.8 Hz, 6H, Ar†-*p*-CH(CH_3)$_2$), 1.12 (s, 12H, Bpin-(CH_3)$_4$), 1.44 (d, $^{3}J_{HH}$ = 7.6 Hz, 18H, SiPr$^{i}_3$-CH(CH_3)$_2$), 2.09 (sept, $^{3}J_{HH}$ = 7.6 Hz, 3H, SiPr$^{i}_3$-C*H*(CH$_3$)$_2$), 2.54 (sept, $^{3}J_{HH}$ = 6.8 Hz, 1H, Ar†-*p*-C*H*(CH$_3$)$_2$), 6.50 (s, 2H, C*H*Ph$_2$), 6.84–7.37 (m, 22H, Ar-*H*); ^{13}C{^{1}H} NMR (C$_6$D$_6$, 75.5 MHz, 298 K), δ = 15.8 (SiPr$^{i}_3$-*C*H(CH$_3$)$_2$), 20.3 (SiPr$^{i}_3$-CH(*C*H$_3$)$_2$), 24.2 (Ar†-

p-CH(CH_3)$_2$), 25.1 (Bpin- (CH_3)$_4$), 33.8 (Ar†-*p*-$CH(CH_3)_2$), 52.3 ($CHPh_2$), 80.6 (Bpin-O*C*), 126.6, 127.1, 127.8, 128.8, 130.0, 130.2, 131.4, 143.1, 144.5, 144.8, 144.9, 145.0, 145.9 (Ar-*C*); $^{11}B\{^1H\}$ NMR (C_6D_6, 128 MHz, 298 K), δ = 21.7; $^{29}Si\{^1H\}$ NMR (C_6D_6, 80 MHz, 298 K), δ = 7.6; $^{11}B\{^1H\}$ NMR(C_6D_6, 128 MHz, 298 K): δ = 21.8; $^{119}Sn\{^1H\}$ NMR (C_6D_6, 149 MHz, 298 K): δ = 53.8; IR (ν/cm^{-1}, ATR): 3061 (w), 3027 (w), 1598 (m), 1387 (m), 1365 (m), 1263 (m), 1226 (m), 1116 (m), 1012 (m), 987 (m), 884 (s), 834 (s), 812 (m), 761 (m), 686 (s); MS/EI *m/z* (%): 885.4 (M^+, 0.5), 842.4 (M^+-Pr^i, 2), 580.3 ($^{iPr}L^{\dagger}$-Pr^i, 100).

N.B. Despite numerous attempts, an accurate elemental analysis could not be obtained for this compound.

5.5.2 Catalytic Reactions

5.5.2.1 Aldehyde and Ketone Hydroboration

General procedure. To a cooled (0 °C) J. Young's NMR tube was added the required amount (typically 0.5–5 mg) of catalyst or precatalyst, {($^{iPr}L^{\dagger}$)GeH}$_2$ or ($^{iPr}L^{\dagger}$)SnOBu^t, either as a crystalline solid followed by C_6D_6 (0.4 mL), or as a stock solution (2.5 mg/mL in C_6D_6). To the resultant solution was added the neat ketone or aldehyde substrate (*ca.* 0.3 mmol), and neat HBpin (using a micro-pipette). A 1:1 substrate/HBpin ratio was used in all runs, except those involving benzil and 2-cyclohexene-1-one as substrates, for which 1:2 ratios were employed. The sample volume was then made up to 0.6 mL with C_6D_6, then rapidly warmed to 20 °C and held at that temperature for the course of the reaction. The catalysed reactions were monitored by ^1H NMR spectroscopy until the reaction was either complete or conversion had slowed to a negligible rate (<5%/day). $^{13}C\{^1H\}$ and $^{11}B\{^1H\}$ NMR spectra were collected post reaction completion. For specific catalyst loadings and reaction times see Table 5.1 (aldehydes) and Table 5.2 (ketones) in the main text. No reaction initiation periods were observed for any of the catalytic runs. Control runs were carried out in the absence of catalyst between HBpin, and the aldehydes or ketones on a 0.3 mM scale (of substrate) in 0.6 mL C_6D_6. These either showed no reaction over the time taken for the analogous catalysed reaction, or substrate hydroborations were less than 5% complete (for 2,2,2-trifluoroacetophenone, benzophenone, 4-methoxybenzaldehyde, and 4-bromobenzaldehyde). All of the catalysed reactions were very clean, and, at most, only traces of by-products were spectroscopically observed. The yields of the catalysed reactions were hence determinable by a comparison of the integrations of relevant resonances for the substrate (^1H NMR), with those of the RCH_2OBpin and R_2CHOBpin resonances of the hydroborated aldehyde and ketone products, respectively. These yields were confirmed by similar comparisons between the integrals of the relevant substrate and product resonances, and the integral of the signal for the internal standard (0.1 equiv. tetramethylsilane, TMS). Isolated yields were not determined. Turn over frequencies were determined as averages over the full observed reaction courses.

Selected spectroscopic data for aldehyde hydroboration products

PhCH$_2$OBpin: product from hydroboration of benzaldehyde. NMR data are identical to those previously reported [25].

4-BrPhCH$_2$OBpin: product from hydroboration of 4-bromobenzaldehyde. ^{1}H NMR (C_6D_6, 400 MHz, 298 K), δ = 1.21 (s, 12H, Bpin-CH_3), 4.85 (s, 2H, pinBOCH_2), 7.14 (d, $^3J_{HH}$ = 8.4 Hz, 2H, Ar-*H*), 7.38 (d, $^3J_{HH}$ = 8.4 Hz, 2H, Ar-*H*); ^{13}C{^{1}H} NMR (C_6D_6, 75.5 MHz, 298 K), δ = 24.7 (Bpin-*C*H$_3$), 66.0 (O*C*H$_2$Ph), 82.9 (Bpin-*C*), 121.3, 128.7, 131.6, 138.9 (Ar-*C*); ^{11}B{^{1}H} NMR (C_6D_6, 128 MHz, 298 K), δ = 22.5.

4-MeOPhCH$_2$OBpin: product from hydroboration of 4-methoxybenzaldehyde. ^{1}H NMR (C_6D_6, 400 MHz, 298 K), δ = 1.17 (s, 12H, Bpin-CH_3), 3.53 (s, 3H, OCH_3), 4.87 (s, 2H, OCH_2), 6.80 (d, $^3J_{HH}$ = 8.4 Hz, 2H, Ar-*H*), 7.25 (d, $^3J_{HH}$ = 8.4 Hz, 2H, Ar-*H*); ^{13}C{^{1}H} NMR (C_6D_6, 75.5 MHz, 298 K), δ = 24.7 (Bpin-*C*H$_3$), 54.9 (O*C*H$_3$), 66.6 (O*C*H$_2$), 82.7 (Bpin-*C*), 114.0, 128.8, 131.8, 159.6 (Ar-*C*); ^{11}B{^{1}H} NMR (C_6D_6, 128 MHz, 298 K), δ = 22.5.

Pr^{n}OBpin: product from hydroboration of propionaldehyde. ^{1}H NMR (C_6D_6, 400 MHz, 298 K), δ = 0.96 (t, $^3J_{HH}$ = 7.6 Hz, 3H, CH$_2$CH_3), 1.22 (s, 6H, Bpin-CH_3), 1.24 (s, 6H, Bpin-CH_3), 1.62 (m, 2H, CH_2CH$_3$), 3.89 (t, $^3J_{HH}$ = 6.8 Hz, 3H, OCH_2); ^{13}C{^{1}H} NMR (C_6D_6, 75.5 MHz, 298 K), δ = 10.3 (OCH$_2$CH$_2$*C*H$_3$), 24.7 (Bpin-*C*H$_3$), 25.0 (OCH$_2$*C*H$_2$CH$_3$), 66.4 (O*C*H$_2$), 82.3 (Bpin-*C*); ^{11}B{^{1}H} NMR (C_6D_6, 128 MHz, 298 K), δ = 22.2.

Bu^{i}OBpin: product from hydroboration of isobutyraldehyde. NMR data are identical to those previously reported [25].

CyCH$_2$OBpin: product from hydroboration of cyclohexanecarboxaldehyde. ^{1}H NMR (C_6D_6, 400 MHz, 298 K), δ = 0.96–2.15 (m, 11H, Cy-*H*), 1.28 (s, 12H, Bpin-CH_3), 3.78 (d, $^3J_{HH}$ = 6.3 Hz, 2H, OCH_2); ^{13}C{^{1}H} NMR (C_6D_6, 75.5 MHz, 298 K), δ = 24.8 (Bpin-*C*H$_3$), 26.2, 26.9, 29.75 (Cy-*C*H$_2$), 39.8 (Cy-*C*H), 70.5 (O*C*H$_2$), 82.3 (Bpin-*C*); ^{11}B{^{1}H} NMR (C_6D_6, 128 MHz, 298 K), δ = 22.4.

Selected spectroscopic data for ketone hydroboration products

(CF$_3$)(Ph)CHOBpin: product from hydroboration of 2,2,2-trifluoroacetophenone. ^{1}H NMR (C_6D_6, 400 MHz, 298 K), δ = 0.96 (s, 6H, Bpin-*CH*$_3$), 1.00 (s, 6H, Bpin-*CH*$_3$), 5.58 (q, $^3J_{HF}$ = 9.2 Hz, 1H, OC*H*), 7.05 (m, 3H, Ar-*H*), 7.39 (m, 2H, Ar-*H*); ^{13}C{^{1}H} NMR (C_6D_6, 75.5 MHz, 298 K), δ = 24.4 (Bpin-*C*H$_3$), 24.5 (Bpin-*C*H$_3$), 74.9 (q, $^2J_{CF}$ = 24 Hz, O*C*HCF$_3$), 83.7 (Bpin-*C*), 124.4 (q, $^1J_{CF}$ = 281 Hz, *C*F$_3$), 129.1, 130.0, 133.9, 135.2 (Ar-*C*); ^{11}B{^{1}H} NMR (C_6D_6, 128 MHz, 298 K), δ = 22.8; ^{19}F NMR (C_6D_6, 282 MHz, 298 K), δ = −77.9.

Ph$_2$CHOBpin: product from hydroboration of benzophenone. NMR data are identical to those previously reported [25].

(4-MeOPh)(Me)CHOBpin: product from hydroboration of 4-methoxyacetophenone. ^{1}H NMR (C_6D_6, 400 MHz, 298 K), δ = 1.10 (s, 6H, Bpin-CH_3) 1.12 (s, 6H, Bpin-CH_3), 1.50 (d, $^3J_{HH}$ = 6.3 Hz, 3H, OCHCH_3), 3.45 (s, 3H, OCH_3), 5.39 (q, $^3J_{HH}$ = 6.3 Hz, 1H, OC*H*CH$_3$), 6.81 (d, $^3J_{HH}$ = 8.5 Hz, 2H, Ar-*H*), 7.32 (d, $^3J_{HH}$ = 8.5 Hz, 2H, Ar-*H*); ^{13}C{^{1}H} NMR (C_6D_6, 75.5 MHz,

298 K), δ = 24.6 (Bpin-*C*H_3), 24.7 (Bpin-*C*H_3), 25.6 (OCH*C*H_3), 54.87(O*C*H_3), 72.5 (O*C*H), 82.43 (Bpin-*C*), 113.9, 126.9, 137.3, 159.3 (Ar-*C*); $^{11}B\{^1H\}$ NMR (C_6D_6, 128 MHz, 298 K), δ = 22.4.

(**4-EtPh**)(**Me**)**CHOBpin**: product from hydroboration of 4-ethylacetophenone. ^1H NMR (C_6D_6, 400 MHz, 298 K), δ = 1.04 (s, 6H, Bpin-C*H*$_3$) 1.06 (s, 6H, Bpin-C*H*$_3$), 1.08 (t, $^3J_{HH}$ = 5.7 Hz, 3H, CH_2CH_3), 1.50 (d, $^3J_{HH}$ = 4.8 Hz, 3H, OCHC*H*$_3$), 2.44 (q, $^3J_{HH}$ = 5.7 Hz, 2H, C*H*$_2$CH$_3$), 5.44 (q, $^3J_{HH}$ = 4.8 Hz, 1H, OC*H*), 7.12 (d, $^3J_{HH}$ = 8.5 Hz, 2H, Ar-*H*), 7.35 (d, $^3J_{HH}$ = 8.5 Hz, 2H, Ar-*H*); $^{13}C\{^1H\}$ NMR (C_6D_6, 75.5 MHz, 298 K), δ = 15.9 (CH_2CH_3), 24.6 (Bpin-*C*H$_3$), 25.8 (OCH*C*H$_3$), 28.8 (*C*H$_2$CH$_3$), 72.8 (OC*H*), 82.5 (Bpin-*C*), 125.8, 128.0, 142.7, 143.1 (Ar-*C*); $^{11}B\{^1H\}$ NMR (C_6D_6, 128 MHz, 298 K), δ = 22.4.

{(**Ph**)(**pinBO**)(**H**)**C-**}$_2$: product from hydroboration of benzil. NMR data are identical to those previously reported [25].

CyOBPin: product from hydroboration of cyclohexanone. ^1H NMR (C_6D_6, 400 MHz, 298 K), δ = 1.12 (s, 12H, Bpin-C*H*$_3$), 1.19–1.93 (m, 10H, Cy-C*H*$_2$), 4.22 (m, 1H, OC*H*); $^{13}C\{^1H\}$ NMR (C_6D_6, 75.5 MHz, 298 K), δ = 24.1 (Cy-*C*H$_2$), 24.7 (Bpin-*C*H$_3$), 25.8, 34.7 (Cy-*C*H$_2$), 72.7 (O*C*H), 82.2 (Bpin-*C*); $^{11}B\{^1H\}$ NMR (C_6D_6, 128 MHz, 298 K), δ = 24.3.

2-MeCyOBPin: product from hydroboration of 2-methylcyclohexanone. NMR data are identical to those previously reported [80].

(2-cyclohexenyl)OBpin: product from hydroboration of 2-cyclohexene-1-one. NMR data are identical to those previously reported [90].

(2-adamantyl)OBpin: product from hydroboration of 2-adamantanone. ^1H NMR (C_6D_6, 400 MHz, 298 K), δ = 1.11 (s, 12H, Bpin-C*H*$_3$), 1.45–2.42 (m, 14H, adamantyl-*H*), 4.48 (m, 1H, OC*H*); $^{13}C\{^1H\}$ NMR (C_6D_6, 75.5 MHz, 298 K), δ = 24.7 (Bpin-*C*H$_3$), 27.5, 27.9, 31.5, 34.6, 36.7, 37.9 (adamantyl-*C*), 77.1 (O*C*H), 82.2 (Bpin-*C*); $^{11}B\{^1H\}$ NMR (C_6D_6, 128 MHz, 298 K), δ = 22.3.

Pr$^i_2$CHOBpin: product from hydroboration of 2,3-dimethyl-3-pentanone. ^1H NMR (C_6D_6, 400 MHz, 298 K), δ = 0.91 (d, $^3J_{HH}$ = 5.1 Hz, 6H, CH(C*H*$_3$)$_2$), 1.00 (d, $^3J_{HH}$ = 5.1 Hz, 6H, CH(C*H*$_3$)$_2$), 1.15 (s, Bpin-C*H*$_3$), 1.81 (v. oct, $^3J_{HH}$ = 5.1 Hz, $^3J_{HH}$ = 5.1 Hz, 2H, C*H*(CH$_3$)$_2$), 3.71 (t, $^3J_{HH}$ = 5.1 Hz, 1H, OC*H*); $^{13}C\{^1H\}$ NMR (C_6D_6, 75.5 MHz, 298 K), δ = 17.2 (CH(*C*H$_3$)$_2$), 19.7 (CH(*C*H$_3$)$_2$), 24.6 (Bpin-*C*H$_3$), 30.5 (*C*H(CH$_3$)$_2$), 82.1 (Bpin-*C*), 84.2 (O*C*H); $^{11}B\{^1H\}$ NMR (C_6D_6, 128 MHz, 298 K), δ = 22.4.

5.5.2.2 CO_2 Hydroboration

General Procedure. To a J Young's Schlenk Flask containing a magnetic stirrer was added 20 mg of (pre)catalyst (i.e. {($^{iPr}L^†$)GeH}$_2$, ($^{iPr}L^†$)SnOBu^t, or ($^{iPr}L^†$)SnOC(H)O) which was subsequently dissolved in C_6D_6 (0.5 mL). The Schlenk flask was cooled to −60 °C, and neat HBpin added using a micro-pipette (1 equiv., relative to catalyst mol%). The Schlenk flask was sealed, and the gas manifold of the Schlenk line purged with dry CO_2 for 10 min. The Schlenk flask was then purged with CO_2 through 3 vacuum cycles, backfilling with CO_2 in each case. The

flask was then sealed at −60 °C, and warmed, achieving ∼2 bar of CO_2 pressure. The reaction mixture was vigorously stirred for the allotted time, and subsequently transferred to a J Young's NMR tube. Both ^{1}H and ^{11}B NMR spectra of the crude reaction mixture were then collected. Where multiple NMR analyses of a reaction were taken, a greater volume of C_6D_6 was used (i.e. 1 mL). Following removal of the first ∼0.5 mL sample of reaction mixture from these reactions, the Schlenk flask was recharged with ∼2 bar CO_2, and vigorous stirring continued. The second sample was then taken after a further allotted reaction time. At reaction completion, the reaction mixtures composed $(R_2B)_2O$ and varying amounts of pinBOMe and $(pinBO)_2CH_2$ where HBpin was employed, or catBOMe where HBcat was employed, identified through comparison with reported data [35, 36].

References

1. Peng Y, Guo JD, Ellis BD, Zhu Z, Fettinger JC, Nagase S, Power PP (2009) Reaction of hydrogen or ammonia with unsaturated germanium or tin molecules under ambient conditions: oxidative addition versus arene elimination. J Am Chem Soc 131:16272
2. Rodriguez R, Gau D, Kato T, Saffon-Merceron N, De Cózar A, Cossío FP, Baceiredo A (2011) Reversible Binding of Ethylene to Silylene–Phosphine Complexes at Room Temperature. Angew Chem Int Ed 50:10414
3. Wang X, Zhu Z, Peng Y, Lei H, Fettinger JC, Power PP (2009) Room-temperature reaction of carbon monoxide with a stable diarylgermylene. J Am Chem Soc 131:6912
4. Carty AJ, Gynane MJS, Lappert MF, Miles SJ, Taylor NJ (1977) Subvalent Group 4B metal alkyls and amides. Part 6. Oxidative addition of an alkyl or aryl halide to bis[bis (trimethylsilyl)methyl]tin(II); hydrogen-1 nuclear magnetic resonance data on the tin (IV) adducts and a single-crystal X-ray study of tris[bis(trimethylsilyl)methyl]chlorotin (IV). J Chem Soc Dalton 6:2009
5. Lappert MF, Misra MC, Onyszchuk M, Rowe RS, Power PP, Slade MJ (1987) Subvalent group 14 metal compounds XI. Oxidative addition reactions of organic halides or acid anhydrides (including $CH_{4-n}Cl_n$, PhBr, $BrN(SiMe_3)_2$, But COCl, or $(CF_3CO)_2O$) to some bivalent group 14 metal amides or alkyls. J Organomet Chem 330:31
6. Spikes GH, Fettinger JC, Power PP (2005) Facile activation of dihydrogen by an unsaturated heavier main group compound. J Am Chem Soc 127:12232
7. Welch GC, San-Juan RR, Masuda JD, Stephan DW (2006) Reversible, metal-free hydrogen activation. Science 314:1124
8. Frey GD, Lavallo V, Donnadieu B, Schoeller WW, Bertrand G (2007) Facile splitting of hydrogen and ammonia by nucleophilic activation at a single carbon center. Science 316:439
9. Kubas GJ, Ryan RR, Swanson BI, Vergamini PJ, Wasserman HJ (1984) Characterization of the first examples of isolable molecular hydrogen complexes, $M(CO)_3(PR_3)_2(H_2)$ (M = molybdenum or tungsten; R = Cy or isopropyl). Evidence for a side-on bonded dihydrogen ligand. J Am Chem Soc 106:451
10. McGrady GS, Guilera G (2003) The multifarious world of transition metal hydrides. Chem Soc Rev 32:383
11. Lavallo V, Canac Y, Donnadieu B, Schoeller WW, Bertrand G (2006) CO fixation to stable acyclic and cyclic alkyl amino carbenes: stable amino ketenes with a small HOMO–LUMO gap. Angew Chem Int Ed 45:3488
12. Zhao J, Goldman AS, Hartwig JF (2005) Oxidative addition of ammonia to form a stable monomeric amido hydride complex. Science 307:1080

13. Casalnuovo AL, Calabrese JC, Milstein D (1987) Nitrogen-hydrogen activation. 1. Oxidative addition of ammonia to iridium(I). Isolation, structural characterization and reactivity of amidoiridium hydrides. Inorg Chem 26:973
14. Hudnall TW, Moerdyk JP, Bielawski CW (2010) Ammonia N–H activation by a N,N′-diamidocarbene. Chem Commun 46:4288
15. Siemeling U, Färber C, Bruhn C, Leibold M, Selent D, Baumann W, von Hopffgarten M, Goedeckec C, Frenking G (2010) N-heterocyclic carbenes which readily add ammonia, carbon monoxide and other small molecules. Chem Sci 1:697
16. Peng Y, Ellis BD, Wang X, Power PP (2008) Diarylstannylene activation of hydrogen or ammonia with arene elimination. J Am Chem Soc 130:12268
17. Hartwig JF (1998) Aromatic aminations by heterogeneous Ni^0/C catalysis. Angew Chem Int Ed 37:2046
18. Sambiagio C, Marsden SP, John-Blacker A, McGowan PC (2014) Copper catalysed Ullmann type chemistry: from mechanistic aspects to modern development. Chem Soc Rev 43:3525
19. Peng Y, Guo JD, Ellis BD, Zhu Z, Fettinger JC, Nagase S, Power PP (2009) Reaction of hydrogen or ammonia with unsaturated germanium or tin molecules under ambient conditions: oxidative addition versus arene elimination. J Am Chem Soc 131:16272
20. Brown ZD, Erickson JD, Fettinger JC, Power PP (2013) Facile, High-Yield Functionalization of Germanium and Tin by Oxidative Insertion of Tetrelenes into the E–H Bonds of Inorganic Acids (E = C, N, O, F): Arene Elimination versus Oxidative Addition and Formation of a Germanium Cation–Water Complex. Organometallics 32:617
21. Ottosson H, Steel PG (2006) Silylenes, Silenes, and Disilenes: Novel Silicon-Based Reagents for Organic Synthesis?. Chem Eur J 12:1576
22. Yao S, Xiong Y, Driess M (2011) Zwitterionic and donor-stabilized N-heterocyclic silylenes (NHSis) for metal-free activation of small molecules. Organometallics 30:1748
23. Sen SS, Khan S, Samuel PP, Roesky HW (2012) Chemistry of functionalized silylenes. Chem Sci 3:659
24. Harder S (2010) From limestone to catalysis: application of calcium compounds as homogeneous catalysts. Chem Rev 110:3852
25. Arrowsmith M, Hadlington TJ, Hill MS, Kociok-Köhn G (2012) Magnesium-catalysed hydroboration of aldehydes and ketones. Chem Commun 48:4567
26. Barrett AGM, Crimmin MR, Hill MS, Procopiou PA (2010) Heterofunctionalization catalysis with organometallic complexes of calcium, strontium and barium. Proc R Soc A 466:927
27. Leich V, Spaniol TP, Maron L, Okuda J (2014) Hydrosilylation catalysis by an earth alkaline metal silyl: synthesis, characterization, and reactivity of bis(triphenylsilyl)calcium. Chem Commun 50:2311
28. Greb L, Oña-Burgos P, Schirmer B, Grimme S, Stephan DW, Paradies J (2012) Metal-free Catalytic Olefin Hydrogenation: Low-Temperature H_2 Activation by Frustrated Lewis Pairs. Angew Chem Int Ed 51:10164
29. Stephan DW (2015) Frustrated Lewis pairs: from concept to catalysis. Acc Chem Res 48:306
30. Rivard E, Fischer RC, Wolf R, Peng Y, Merrill WA, Schley ND, Zhu Z, Pu L, Fettinger JC, Teat SJ, Nowik I, Herber RH, Takagi N, Nagase S, Power PP (2007) Isomeric Forms of Heavier Main Group Hydrides: Experimental and Theoretical Studies of the $[Sn(Ar)H]_2$ (Ar = Terphenyl) System. J Am Chem Soc 129:16197
31. Pineda LW, Jancik V, Starke K, Oswald RB, Roesky HW (2006) Stable monomeric germanium(II) and tin(II) compounds with terminal hydrides. Angew Chem 118:2664
32. Jana A, Tavčar G, Roesky HW, John M (2010) Germanium(II) hydride mediated reduction of carbon dioxide to formic acid and methanol with ammonia borane as the hydrogen source. Dalton Trans 39:9487
33. Tan G, Wang W, Bloma B, Driess M (2014) Mechanistic studies of CO_2 reduction to methanol mediated by an N-heterocyclic germylene hydride. Dalton Trans 43:6006
34. Jana A, Ghoshal D, Roesky HW, Objartel I, Schwab G, Stalke D (2009) A Germanium (II) Hydride as an Effective Reagent for Hydrogermylation Reactions. J Am Chem Soc 131:1288

35. Chakraborty C, Zhang J, Krause JA, Guan H (2010) An efficient nickel catalyst for the reduction of carbon dioxide with a borane. J Am Chem Soc 132:8872
36. Bontemps S, Vendier L, Sabo-Etienne S (2012) Borane-Mediated Carbon Dioxide Reduction at Ruthenium: Formation of C_1 and C_2 Compounds. Angew Chem Int Ed 51:1671
37. Chong CC, Hirao H, Kinjo R (2014) Catalytic transfer hydrogenation by a trivalent phosphorus compound: phosphorus-ligand cooperation pathway or P(III)/P(V) redox pathway? Angew Chem Int Ed 53:4633
38. Penafiel J, Maron L, Harder S (2014) Early main group metal catalysis: how important is the metal?. Angew Chem Int Ed 127:203
39. Blake AJ, Cunningham A, Ford A, Teat SJ, Woodward S (2000) Enantioselective reduction of prochiral ketones by catecholborane catalysed by chiral group 13 complexes. Chem Eur J 6:3586
40. Hong S, Marks TJ (2004) Organolanthanide-catalyzed hydroamination. Acc Chem Res 37:673
41. Spielmann J, Harder S (2007) Hydrocarbon-Soluble Calcium Hydride: A "Worker-Bee" in Calcium Chemistry. Chem Eur J 13:8928
42. Harder S, Brettar S (2006) Rational Design of a Well-Defined Soluble Calcium Hydride Complex. Angew Chem Int Ed 45:3474
43. Spielmann J, Harder S (2008) Reduction of Ketones with Hydrocarbon-Soluble Calcium Hydride: Stoichiometric Reactions and Catalytic Hydrosilylation. Eur. J. Inorg. Chem. 2008:1480
44. Harder S, Spielmann J (2012) Calcium-mediated hydroboration of alkenes: "Trojan horse" or "true" catalysis?. J Organometal Chem 698:7
45. Barrett AGM, Brinkmann C, Crimmin M, Hill MS, Hunt P, Procopiou PA (2009) Heavier Group 2 Metals and intermolecular hydroamination: a computational and synthetic assessment. J Am Chem Soc 131:12906
46. Crimmin MR, Arrowsmith M, Barrett AGM, Casely IJ, Hill MS, Procopiou PA (2009) Intramolecular hydroamination of aminoalkenes by calcium and magnesium complexes: a synthetic and mechanistic study. J Am Chem Soc 131:9670
47. Arrowsmith M, Hill MS, Hadlington T, Kociok-Köhn G, Weetman C (2011) Magnesium-catalyzed hydroboration of pyridines. Organometallics 30:5556
48. Arrowsmith M, Hill MS, Kociok-Köhn G (2013) Magnesium Catalysis of Imine Hydroboration. Chem Eur J 19:2776
49. Hao L, Harrod JF, Lebuis AM, Mu Y, Shu R, Samuel E, Woo HG (1998) Homogeneous catalytic hydrosilylation of pyridines. Angew Chem Int Ed 37:3126
50. Gutsulyak DV, van der Est A, Nikonov GI (2011) Facile catalytic hydrosilylation of pyridines. Angew Chem Int Ed 50:1384
51. Xie J, Zhu S, Zhou Q (2011) Transition metal-catalyzed enantioselective hydrogenation of enamines and imines. Chem Rev 111:1713
52. Willoughby CA, Buchwald SL (1994) Catalytic asymmetric hydrogenation of imines with a chiral titanocene catalyst: kinetic and mechanistic investigations. J Am Chem Soc 116:11703
53. Lindsley CW, Dimare M (1994) A boron-substituted analogue of the Shvo hydrogenation catalyst: catalytic hydroboration of aldehydes, imines, and ketones. Tetrahedron Lett 35:5141
54. Koren-Selfridge L, Londino HN, Vellucci JK, Simmons BJ, Casey CP, Clark TB (2009) A boron-substituted analogue of the Shvo hydrogenation catalyst: catalytic hydroboration of aldehydes, imines, and ketones. Organometallics 28:2085
55. Takagi N, Sakaki S (2013) Theoretical Study of Reactivity of Ge(II)-hydride Compound: Comparison with Rh(I)-Hydride Complex and Prediction of Full Catalytic Cycle by Ge(II)-hydride. J Am Chem Soc 135:8955
56. Enders D, Niemeier O, Henseler A (2007) Organocatalysis by N-heterocyclic carbenes. Chem Rev 107:5606
57. Fuerst DE, Jacobsen EN (2005) Thiourea-catalyzed enantioselective cyanosilylation of ketones. J Am Chem Soc 127:8964
58. Johnson LT, Yeh S, Hope C (2013) The social cost of carbon: implications for modernizing our electricity system. J Environ Stud Sci 3:369

59. Benson EE, Kubiak CP, Sathrum AJ, Smieja JM (2009) Electrocatalytic and homogeneous approaches to conversion of CO_2 to liquid fuels. Chem Soc Rev 38:89
60. Dubois MR, Dubois DL (2009) Development of molecular electrocatalysts for CO_2 reduction and H_2 production/oxidation. Acc Chem Res 42:1974
61. Jadhava SG, Vaidyaa PD, Bhanageb BM, Joshi JB (2014) Hydrogenation of CO_2 to methanol: Importance of metal−oxide and metal−carbide interfaces in the activation of CO_2. Chem Eng Res Des 92:2557
62. Matsuo T, Kawaguchi H (2006) From carbon dioxide to methane: Homogeneous reduction of carbon dioxide with hydrosilanes catalyzed by zirconium−borane complexes. J Am Chem Soc 128:12362
63. Mitton SJ, Turculet L (2012) Mild reduction of carbon dioxide to methane with tertiary silanes catalyzed by platinum and palladium silyl pincer complexes. Chem Eur J 18:15258
64. Laitar DS, Mueller P, Sadighi JP (2005) Efficient homogeneous catalysis in the reduction of CO_2 to CO. J Am Chem Soc 127:17196
65. Dobrovetsky R, Stephan DW (2013) Catalytic reduction of CO_2 to CO by using Zinc (II) and in situ generated carbodiphosphoranes. Angew Chem Int Ed 52:2516
66. Chakraborty S, Zhang J, Krause JA, Guan H (2010) An efficient nickel catalyst for the reduction of carbon dioxide with a borane. J Am Chem Soc 132:8872
67. Sgro MJ, Stephan DW (2012) Frustrated Lewis pair inspired carbon dioxide reduction by a ruthenium tris(aminophosphine) complex. Angew Chem Int Ed 51:11343
68. Bontemps S, Vendier L, Sabo-Etienne S (2012) Borane-Mediated Carbon Dioxide Reduction at Ruthenium: Formation of C_1 and C_2 Compounds. Angew Chem Int Ed 51:1671
69. Tijm PJA, Waller FJ, Brown DM (2001) Methanol technology developments for the new millennium. Appl Catal A Gen 221:275
70. Olah GA (2005) Beyond oil and gas: the methanol economy. Angew Chem Int Ed 44:2636
71. Anker MD, Arrowsmith M, Bellham P, Hill MS, Kociok-Köhn G, Liptrot DJ, Mahon MF, Weetman C (2014) Selective reduction of CO_2 to a methanol equivalent by $B(C_6F_5)_3$-activated alkaline earth catalysis. Chem Sci 5:2826
72. Courtemanche MA, Légaré MA, Maron L, Fontaine FG (2014) Reducing CO_2 to Methanol Using Frustrated Lewis Pairs: On the Mechanism of Phosphine–Borane-Mediated Hydroboration of CO_2. J Am Chem Soc 136:10708
73. Bontemps S, Vendier L, Sabo-Etienne S (2014) Ruthenium-catalyzed reduction of carbon dioxide to formaldehyde. J Am Chem Soc 136:4419
74. Abdalla JAB, Riddlestone IM, Tirfoin R, Aldridge S (2014) Cooperative bond activation and catalytic reduction of carbon dioxide at a group 13 metal center. Angew Chem Int Ed 127:5187
75. Courtemanche MA, Légaré MA, Maron L, Fontaine FG (2013) A highly active phosphine–borane organocatalyst for the reduction of CO_2 to methanol using hydroboranes. J Am Chem Soc 135:9326
76. Li L, Fukawa T, Matsuo T, Hashizume D, Fueno H, Tanaka K, Tamao K (2012) A stable germanone as the first isolated heavy ketone with a terminal oxygen atom. Nature Chem 4:361
77. Veith M, Becker S, Huch V (1989) Synthesis and Structure of the First Stable Germaneselone. Angew Chem Int Ed Engl 28:1237
78. Tokitoh N, Kishikawa K, Okazaki R, Sasamori T, Nakata N, Takeda N (2002) Synthesis and characterization of an extremely hindered tetraaryl-substituted digermene and its unique properties in the solid state and in solution. Polyhedron 21:563
79. Johnson BP, Almstätter S, Dielmann F, Bodensteiner M, Scheer M (2010) Synthesis and Reactivity of Low-Valent Group 14 Element Compounds. Z Anorg Allg Chem 636:1275
80. Query IP, Squier PA, Larson EM, Isley NA, Clark TBJ (2011) Alkoxide-Catalyzed Reduction of Ketones with Pinacolborane. Org Chem 76:6452
81. Sewell LJ, Huertos MA, Dickinson ME, Weller AS (2013) Dehydrocoupling of Dimethylamine Borane Catalyzed by $Rh(PCy_3)_2H_2Cl$. Inorg Chem 52:4509

82. Jana A, Roesky HW, Schulzke C, Döring A (2009) Germanium(II) hydride mediated reduction of carbon dioxide to formic acid and methanol with ammonia borane as the hydrogen source. Angew Chem Int Ed 48:1106
83. Cottrell TL (1958) The strengths of chemical bonds, 2nd edn. Butterworths, London
84. Plotzitzka J, Kleeberg C (2014) Cu^{I}-Catalyzed Conjugate Addition of Silyl Boronic Esters: Retracing Catalytic Cycles Using Isolated Copper and Boron Enolate Intermediates. Organometallics 33:6915
85. Laitar DS, Müller P, Sadighi JP (2005) Efficient Homogeneous Catalysis in the Reduction of CO_2 to CO. J Am Chem Soc 127:17196
86. Dudnik AS, Weidner VL, Motta A, Delferro M, Marks TJ (2014) Atom-efficient regioselective 1,2-dearomatization of functionalized pyridines by an earth-abundant organolanthanide catalyst. Nat Chem 6:1100
87. Murphy D, Sheehan JP, Spalding TR, Ferguson G, Lough AJ, Gallagher JF (1993) Compounds containing B–O–X bonds (X = Si, Ge, Sn, Pb). Part 4.—Crystal structures of $B(OSiPh_3)_3$, $PhB(OSiPh_3)_2$ and $PhB(OGePh_3)_2$. J Mater Chem 3:1275
88. Hawkeswood S, Stephan DW (2005) Syntheses and reactions of the bis-boryloxide $O(Bpin)_2$ (pin = $O_2C_2Me_4$). Dalton Trans 12:2182
89. Goodwin C, Smith A, Ortu F, Vitorica-Yrzebal I, Mills D (2015) Salt metathesis versus protonolysis routes for the synthesis of silylamide Hauser base (R_2NMgX; X = halogen) and amido-Grignard (R_2NMgR) complexes. Dalton Trans 45:6004
90. Oluyadi AA, Ma S, Muhoro CN (2013) Titanocene(II)-Catalyzed Hydroboration of Carbonyl Compounds. Organometallics 32:70

Chapter 6
The Use of a Bulky Boryl-Substituted Amide Ligand in Low-Oxidation State Group 14 Element Chemistry

6.1 Introduction

This chapter describes the synthesis and application of a novel boryl silyl amide ligand in low-oxidation state, low-coordinate group 14 chemistry. Background discussions relating to the chemistry involved in this final chapter have largely been covered in earlier chapter introductions. That is, the synthesis of group 14 halide complexes using monodentate ligands (Chap. 2), the synthesis and reactivity of heavier alkyne analogues (Chap. 3), and the synthesis and reactivity of heavier carbene analogues (Chaps. 4 and 5). However, as part of the original research in this chapter, the first structurally characterised example of an acyclic bis(amido) silylene has been prepared. This, therefore, warrants further discussion of the synthesis and reactivity of related acyclic silylenes, which, until very recently, were unknown as stable, isolable species.

6.1.1 Acyclic Silylenes

6.1.1.1 Synthesis of 2-Coordinate Acyclic Silylenes

The publication of early work by West and co-workers on the synthesis of $\{(Mes)_2Si\}_2$ (Mes = 2,4,6-Me_3Ph) described that, at low-temperature (−170 °C), UV irradiation of $(Mes)_2Si(TMS)_2$ (TMS = $SiMe_3$) yielded deep blue solutions, which became yellow upon warming [1]. They hypothesised that, at low-temperature, the acyclic silyene, $(Mes)_2Si$:, was formed, which dimerised upon warming (Scheme 6.1). Although such a monomeric species was never isolate by that group, they did 'trap' the intermediate through oxidative addition of the silane, Et_3SiH, to the hypothesised transient Si(II) centre. Upon warming, the Si(II) species, $(Mes)_2(H)SiSi(Et)_3$, was isolated as the sole product (Scheme 6.1). This stood as early evidence

T.J. Hadlington, *On the Catalytic Efficacy of Low-Oxidation State Group 14 Complexes*, Springer Theses, DOI 10.1007/978-3-319-51807-7_6

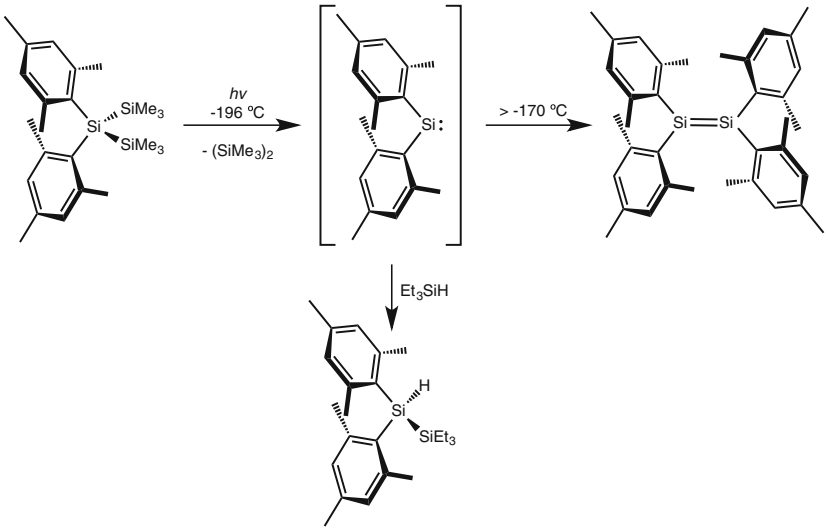

Scheme 6.1 Generation and reactivity of a transient acyclic silylene, $(Mes)_2Si$

that 2-coordinate acyclic silylenes are highly reactive species, especially given that group-14 mediated activation of Si–H bonds had not been observed prior to, and has not been observed since this example.

Further evidence for the reactivity/thermal instability of acyclic Si(II) species came from the same group some years later, in 2003 [2]. It had been noted that, despite the thermal stability and full characterisation of $\{(TMS)_2N\}_2E$: species (E = Ge, Sn, or Pb [3, 4]) as early as 1973, the Si congener was unknown. Through reduction of $\{(TMS)_2N\}_2SiBr_2$ with KC_8, the group of West was again able to transiently synthesise an acyclic silylene, $\{(TMS)_2N\}_2Si$: (Scheme 6.2), which they found to be unstable above 0 °C. In this case, the addition of alcohols (i.e. methanol and phenol) to the species below 0 °C led to the isolation of $\{(TMS)_2N\}_2Si(H)OR$ compounds (R = Me, Ph, Scheme 6.2). Using low-temperature ^{29}Si NMR analysis, the resonance relating to the 2-coordinate silicon centre in $\{(TMS)_2N\}_2Si$: was found to appear at δ = 223.9 ppm. This is shifted significantly downfield relative to previously reported cyclic bis(amido)silylenes (Fig. 6.1) [5–7]. This can be explained by the overlap of the *p*-lone-pairs of the nitrogen donor atoms with the empty *p*-orbital on the Si(II) centre. Whilst the cyclic systems allow for good overlap, in the acyclic system the free rotation of the ligand, and hence the N-donor atom, reduces this effect significantly. Therefore, the cyclic systems have a more shielded Si(II) centre relative to the acyclic congeners, resulting in a downfield shift observed for the latter. This also explains the relative instability/higher reactivity of the acyclic systems. The reduced N-lone pair donation to the Si(II) centre destabilises the empty *p*-orbital on silicon, decreasing the HOMO/LUMO gap, making the silicon centre more reactive. In the absence of adequate steric protection, such species are apparently unstable under ambient conditions.

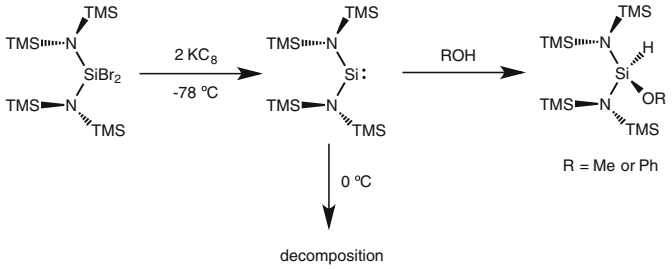

Scheme 6.2 Synthesis and reactivity of a transient acyclic silylene, $\{(TMS)_2N\}_2Si$

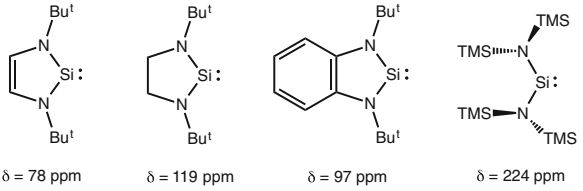

Fig. 6.1 ^{29}Si NMR shifts for some bis(amido) silylenes

Again, many years after this second transient observation of an acyclic silylene came the first examples of structurally characterised acyclic silylenes which are stable under ambient conditions, in the absence of air and moisture. These results came from the group of Power [8], and a collaborative effort from the groups of Jones and Aldridge [9, 10]. The silylene reported by Power and co-workers was stabilised by two bulky thiolate ligands, each bearing the terphenyl fragment, ^{Mes}Terph (^{Mes}Terph = 2,6-Mes_2Ph; Mes = 2,4,6-Me_3Ph). Reduction of the Si(IV) species, $(^{Mes}TerphS)_2SiBr_2$, with $\{(^{Mes}nacnac)Mg\}_2$ (^{Mes}nacnac = $[CH\{C(Me)N(Mes)\}_2]^-$) over the course of two days led to moderate isolated yields of the pale yellow acyclic silylene, $(^{Mes}TerphS)_2Si$: (Scheme 6.3). The ^{29}Si NMR spectrum of this species exhibited a single resonance at $\delta = 285$ ppm, similar to that for $\{(TMS)_2N\}_2Si$: reported by West. The S–Si–S angle in the complex (90.519(19)°) suggests the lone-pair on the Si(II) centre has a high degree of *s*-character [11], and therefore that the HOMO/LUMO gap of this silicon centre is relatively large. This perhaps explains its relatively high thermal stability (temperature of decomposition = 146 °C) in comparison to West's transient examples of acyclic silylenes, which were thermally unstable. This is understandable on two fronts: the high electronegativity of the S-donor atoms would act to stabilise the lone-pair (i.e. the HOMO) on silicon; and the donation of lone-pairs on the S-donor atoms to the Si (II) centre acts to stabilise its empty *p*-orbital (i.e. the LUMO). Indeed, a DFT analysis of the frontier orbitals of $(^{Mes}TerphS)_2Si$: revealed the HOMO/LUMO separation to be large, at 4.26 eV [8]. This perhaps explains the relatively low reactivity of the silylene (vide infra).

There have been two contributions to this field from Jones and Aldridge; one amido silyl silylene [10], and one amido boryl silylene [9]. The amido fragment in

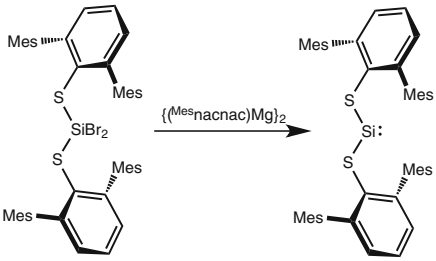

Scheme 6.3 The synthesis of $(^{Mes}TerphS)_2Si$

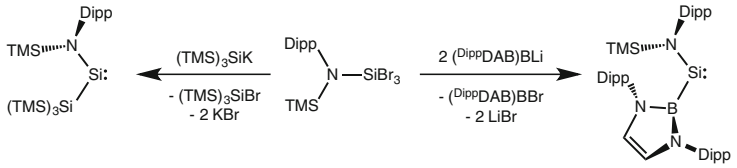

Scheme 6.4 Synthesis of the acyclic silylenes, $^{Boryl}Si:$ and $^{Silyl}Si$

each case is the widely applied (Dipp)N(TMS)$^-$ (^{Dipp}L), with both of these silylenes being synthesised from the respective amido Si(IV) tribromide, $(^{Dipp}L)SiBr_3$. In the synthesis of the amido boryl silylene, the boryl lithium reagent, (^{Dipp}DAB)BLi ($^{Dipp}DAB = [\{N(Dipp)C(H)\}_2]^{2-}$), acts as both a reducing agent and as a ligand in a salt metathesis reaction. Thus, the addition of two equivalents of (^{Dipp}DAB)BLi to $(^{Dipp}L)SiBr_3$ resulted in the formation of the deep red $(^{Dipp}L)\{(^{Dipp}DAB)B\}Si:$ ($^{Boryl}Si:$), with concomitant formation of one equivalent of (^{Dipp}DAB)BBr and two equivalents of LiBr (Scheme 6.4) [9]. The second acyclic silylene from these groups involved the bulky super-silyl group, $(TMS)_3Si$. The addition of the potassium salt of this species (i.e. $(TMS)_3SiK$) to a solution of $(^{Dipp}L)SiBr_3$ led to the formation of the purple acyclic amido silyl silylene, $(^{Dipp}L)\{(TMS)_3Si\}Si:$ ($^{Silyl}Si:$, Scheme 6.4), as two distinct rotamers [10]. As with (^{Dipp}DAB)BLi in the synthesis of $^{Boryl}Si:$, the $(TMS)_3SiK$ acts as both a reducing agent and a ligand.

The ^{29}Si NMR spectra for $^{Boryl}Si:$ and $^{Silyl}Si:$ reveal highly downfield shifts for their Si(II) centres ($^{Boryl}Si:$ $\delta = 439.7$ ppm, and $^{Silyl}Si$ $\delta = 438$ and 467 ppm, one for each rotamer), relative to $(^{Mes}TerphS)_2Si:$ ($\delta = 285$ ppm), and indeed the majority of previously reported silylenes. This is indicative of a relatively less shielded Si centre in the former species, possibly due to lessened Si(II)-*p*-orbital saturation due to the boryl and silyl ligands, respectively. To a degree, these NMR signals confirm their low-coordination environment. Both of these acyclic silylenes have much more open angles at their central Si atoms ($^{Boryl}Si:$ B–Si–N 109.7°, $^{Silyl}Si:$ Si–Si–N 116.9°) when compared with $(^{Mes}TerphS)_2Si:$ (S–Si–S 90.5°). The boryl and silyl ligands in the former, then, do not stabilise the frontier orbitals on the Si(II) centre to the same degree as the thiolate ligands in Power's silylene. This is understandable given the

strong σ-donation ability of both boryl and silyl ligands, which leads to a destabilisation of the sp^2-character lone-pair (i.e. the HOMO) on the Si(II) centres in ^{Boryl}Si: and ^{Silyl}Si:. This increases the energy of this orbital, reducing the HOMO/LUMO gap, and increasing the sp^2-hybridisation in their lone-pairs. Overall, this should lead to a more reactive silylene. DFT studies of the frontier orbitals of ^{Boryl}Si: and ^{Silyl}Si: suggested that they do indeed have narrow HOMO/LUMO separations (^{Boryl}Si: $\Delta E_{HOMO/LUMO}$ = 2.04 eV; ^{Silyl}Si: $\Delta E_{HOMO/LUMO}$ = 1.99 eV), implying that they should be highly reactive (viz. alkyl amino carbenes, $\Delta E_{HOMO/LUMO} \sim 1.9$ eV, which homolytically cleave dihydrogen and ammonia [12]).

6.1.1.2 Reactivity of Isolated 2-Coordinate Acyclic Silylenes

Power's acyclic silylene, (^{Mes}TerphS)$_2$Si:, has as yet not seen broad studies of its reactivity. However, in Power's initial publication, its reaction with MeI was reported (Scheme 6.5) [8]. The addition of an excess of MeI to the silylene led to its oxidative addition, with (^{Mes}TerphS)$_2$Si(Me)I isolated in good yield. It was mentioned that the silylene did not react with H_2, not wholly surprising given the relatively large HOMO/LUMO separation of the Si(II) centre in this species. A subsequent publication reported on the reversible formal [2 + 1] cycloaddition of ethylene to the Si(II) centre of (^{Mes}TerphS)$_2$Si:, yielding (^{Mes}TerphS)$_2$Si(η^2-C_2H_4) (Scheme 6.5) [13]. Dissolution of this latter colourless compound in hydrocarbon solvents resulted in pale yellow solutions, which contained mixtures of (^{Mes}TerphS)$_2$Si:, ethylene, and (^{Mes}TerphS)$_2$Si(μ-C_2H_4). This reaction can be compared to the previously reported reversible addition of ethylene to intra-molecularly phosphine stabilised amido aryl silylenes, (^{PN1}L)(Ph)Si: and (^{PN2}L)(Ph)Si: (Scheme 6.6) [14]. The reaction of the latter with ethylene has a $\Delta G_{300^\circ} = -0.507$ kcal mol^{-1}, and so is near thermo-neutral at ambient temperatures. The forward reaction of (^{Mes}TerphS)$_2$Si: with ethylene, on the other hand, was found to be more favoured ($\Delta G_{300^\circ} = -5.94$ kcal mol^{-1} for (^{Mes}TerphS)$_2$Si: + C_2H_4). This may be due to the donor stabilisation in (^{PN1}L)(Ph)Si(η^2-C_2H_4) and (^{PN2}L)(Ph)Si(η^2-C_2H_4), the electronic and steric saturation of which may drive their rather facile ethylene elimination reactions.

Few reactivity studies of ^{Boryl}Si: and ^{Silyl}Si: have been reported, with only the examples presented in their original publications. In stark contrast to

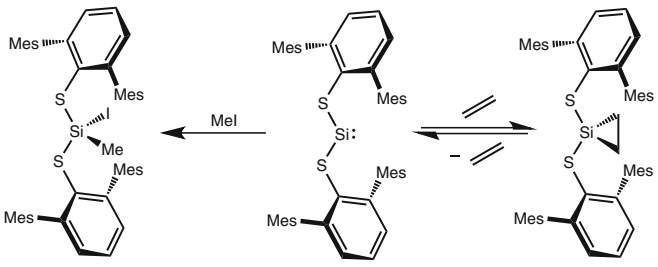

Scheme 6.5 Reactivity of (^{Mes}TerphS)$_2$Si: towards MeI and ethylene

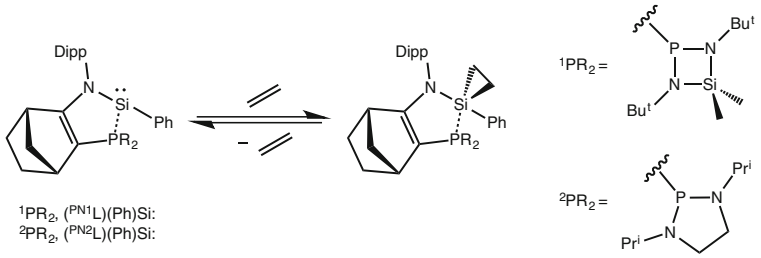

Scheme 6.6 Reactivity of donor-stabilised silylenes, (^{PN1}L)(Ph)Si: and (^{PN2}L)(Ph)Si:, towards ethylene

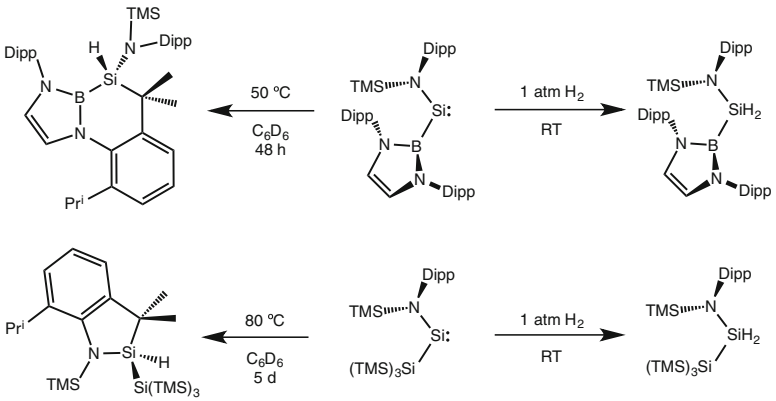

Scheme 6.7 Intramolecular CH-activation by ^{Boryl}Si: and ^{Silyl}Si:, and their reactions with H_2

(^{Mes}TerphS)$_2$Si:, both silylenes rapidly reacted with H_2 under one atmosphere of pressure and at ambient temperature, yielding the silanes, ^{Boryl}Si(H)$_2$ and ^{Silyl}Si(H)$_2$ (Scheme 6.7) [9, 10]. This observation reinforces the calculated values for the HOMO/LUMO gaps in ^{Boryl}Si:, ^{Silyl}Si:, and (^{Mes}TerphS)$_2$Si:. This was further demonstrated through the thermal instability of both ^{Boryl}Si: and ^{Silyl}Si:, which underwent ligand CH-activation reactions at elevated temperatures (^{Boryl}Si: at 50 °C, ^{Silyl}Si: at 80 °C, Scheme 6.7) [9, 10]. No such reactions were observed for the less reactive silylene, (^{Mes}TerphS)$_2$Si:.

6.2 Research Proposal

Despite broad attention over the last three decades, low-oxidation state group 14 chemistry, and in particular, related low-coordinate chemistry, has seen use of select classes of ligands. Amongst these are terphenyl ligands [15, 16], bulky silyl ligands

[17, 18], chelating β-deketiminates [19, 20], aryl silyl amides [21], and bis(silyl) amides [21]. Indeed, as described in earlier chapters, countless breakthroughs in the stabilisation and reactivity of low-oxidation state element complexes have been made using these ligands, suggesting little need for the investigation of novel ligand classes. However, we wished to employ a new ligand class in group 14 element(I) and (II) chemistry, with sterics and electronics which differ from those employed previously in this thesis. To this end, we sought to investigate potential boryl silyl amide ligands, and to use these to stabilise heavier group 14 element(I) and element (II) complexes. In doing so, we hoped to observe novel stabilisation characteristics which arise from the electronic and steric factors relating to the boryl amide ligand. This would allow comparisons to be drawn with previously utilised silyl aryl amide ligands, and in particular, those incorporating the bulky $Ar^{\dagger}$ unit ($Ar^{\dagger}$ = 4-Pr^{i}-2,6-(Ph_2CH)Ph). Ultimately, this will give useful insight into the effects of the effects of ligand bulk and electronics in this chemistry.

6.3 Results and Discussion

Our initial efforts concerning the synthesis of a novel boryl substituted amide ligand were towards the development of a bulky primary boryl amine. Given the ease of synthesis of the bulky (^{Dipp}DAB)BBr compound, we sought to utilised this, and related species, as precursors in the synthesis of novel amide ligands.

6.3.1 Synthesis of Silyl Boryl Amide Ligands

The synthesis of bis(amido) boron halide complexes is well documented, with bulky bidentate ligands (e.g. ^{Dipp}DAB) commonly used in the preparation of such species [22–24]. The steric encumbrance of the (^{Dipp}DAB)B^{-} group can be seen as comparable to that of the terphenyl ligand, ^{Dipp}Terph (2,6-$Dipp_2$Ph), and hence the boryl group seemed a good starting point for the synthesis of a boryl amide [24]. The addition of $LiNH_2$ to a THF solution of (^{Dipp}DAB)BBr led to the quantitative formation of (^{Dipp}DAB)BNH_2 (**1**, Scheme 6.8). It was also found that the addition of dry gaseous ammonia to hexane solutions of (^{Dipp}DAB)BBr led the formation of voluminous white precipitate (i.e. NH_4Br) and **1**, again, quantitatively (Scheme 6.8). The boryl amine **1** is an air-stable colourless crystalline solid, its solid state structure presented in Fig. 6.2.

The terminal B1–N1 bond in **1** is shorter than those from the bidentate DAB ligand to B1. This is in keeping with the lone-pairs of N2 and N3 being partially delocalised across the DAB unit, and also with the electron withdrawing effect of the aryl groups to which they are bound. Hence, N1 most likely has greater

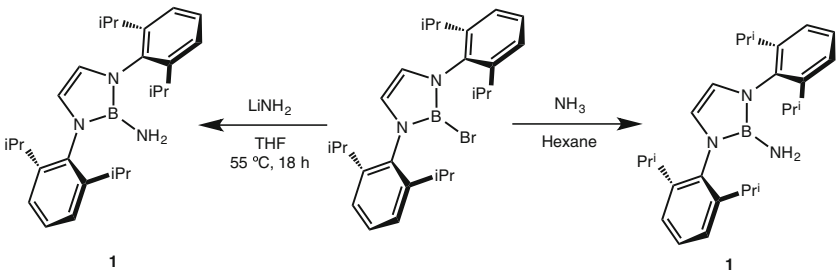

Scheme 6.8 The synthesis of (^{Dipp}DAB)BNH_2 (**1**)

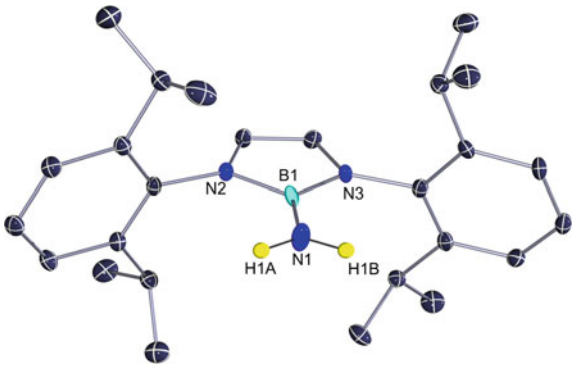

Fig. 6.2 ORTEP representation of (^{Dipp}DAB)BNH_2 (**1**) (thermal ellipsoids at 30% probability; hydrogens, aside from amine protons, omitted). Selected bond lengths (Å) and angles (°) for **1**: B1–N1 1.409(2), B1–N2 1.451(2), B1–N3 1.442(2), N1–B1–N2 125.82 (1), N1–B1–N3 128.82(1), N3–B1–N2 105.35(1)

multiple-bond character with B1. This is reinforced by the trigonal planar geometry in which both B1 and N1 centres sit (sum of angles around B1: 359.99°, N1: 360.00°; note that H1A and H1B were located from difference maps and freely refined). Other distances and angles are as one would expect.

With the amine, **1**, in hand, the synthesis of bulky secondary amine pro-ligands was targeted. Amine **1** was efficiently deprotonated by $LiBu^n$ in diethyl ether. Quenching the reaction mixture with TMSCl resulted in the pro-ligand, {(^{Dipp}DAB)B}N(H)(TMS) (^{TMS}BoNH, **2**, Scheme 6.9). Compound **2** is an oil at ambient temperature. The ^{1}H NMR spectrum of **2** reveals a relatively upfield shift for its N–*H* moiety, at $\delta = \sim 1.2$ ppm (overlapped by the Dipp-CH_3 resonances), suggesting this proton has lessened acidity than in related silyl aryl amines (e.g. $^{iPr}L^{\dagger}H$, $^{iPr}L^{\dagger} = [(Pr^i_3Si)N(Ar^{\dagger})]^-$, N–*H*, $\delta = 2.13$ ppm) discussed previously.

Pro-ligand **2** was readily deprotonated by $LiBu^n$ in ethereal solvents (Scheme 6.9), with reactions being complete in around 1 h. The same reaction in hexane reached acceptable levels of completion (i.e. ~60%) after three days at ambient temperature, yielding the solvent free lithium salt of **2** (**2.Li**, Scheme 6.9),

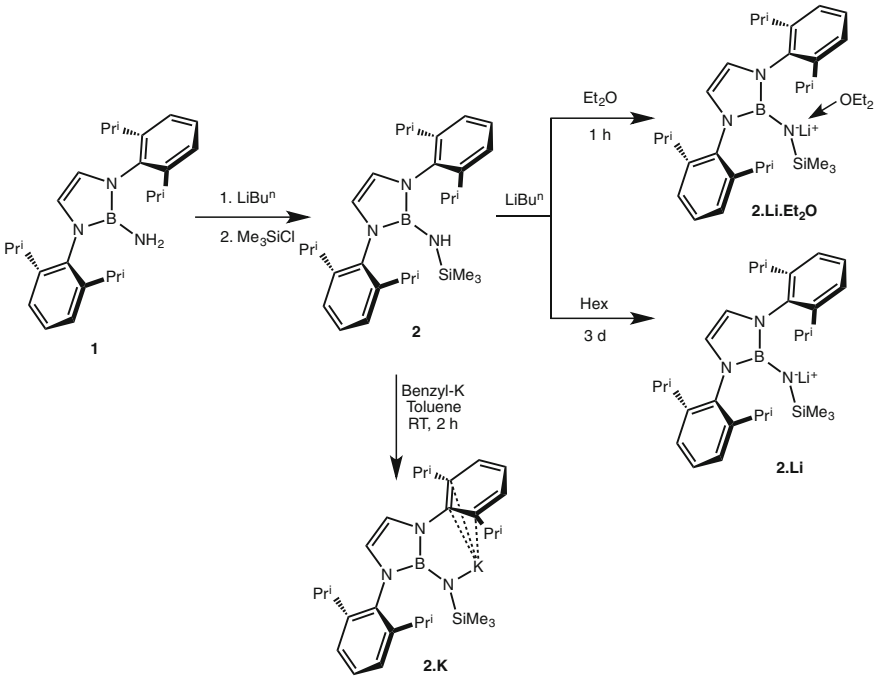

Scheme 6.9 Synthesis of the silyl boryl amine, ^{TMS}BoNH (**2**), and the generation of its alkali metal salt derivatives, **2.Li**, **2.Li.Et$_2$O**, and **2.K**

perhaps emphasising the low acidity of its N–*H* proton. The deprotonation carried out in Et_2O results in the isolation of an ether adduct of the lithium salt of **2**, ^{TMS}BoNLi.Et_2O (**2.Li.Et$_2$O**, Scheme 6.9), the ether ligand of which has a detrimental effect in certain further reactions (vide infra). The potassium salt of **2** (**2.K**, Fig. 6.3) was also generated, through reaction of **2** with benzyl potassium in toluene at ambient temperature. It is worthy of note that deprotonation of **2** with KH, in the presence of catalytic amounts of $(TMS)_2NH$, was not possible, which contrasts to previously discussed silyl aryl amines (e.g. $^{iPr}L^{\dagger}H$), which are readily deprotonated by the same KH/$(TMS)_2NH$ mixture. This is perhaps not surprising, as the boryl substituent of **2** likely enhances the σ-donor strength of the N-centre in **2**, reducing the acidity of its attached proton. The solid state structure of **2.K** reveals that the potassium centre is stabilised through η^3-interactions with one flanking Dipp group of its ligand, and through η^2-interactions with a Dipp group of a ligand in a second asymmetric unit, forming 1D polymeric chains (not shown). The N1–B1 bond in **2.K** is considerably shorter (1.379(7) Å) than those between the ^{Dipp}DAB ligand and B1 (N2–B1 1.486(5) Å, N3–B1 1.464(6) Å). The B1–N1 distance therefore likely accounts for an approximately double bond.

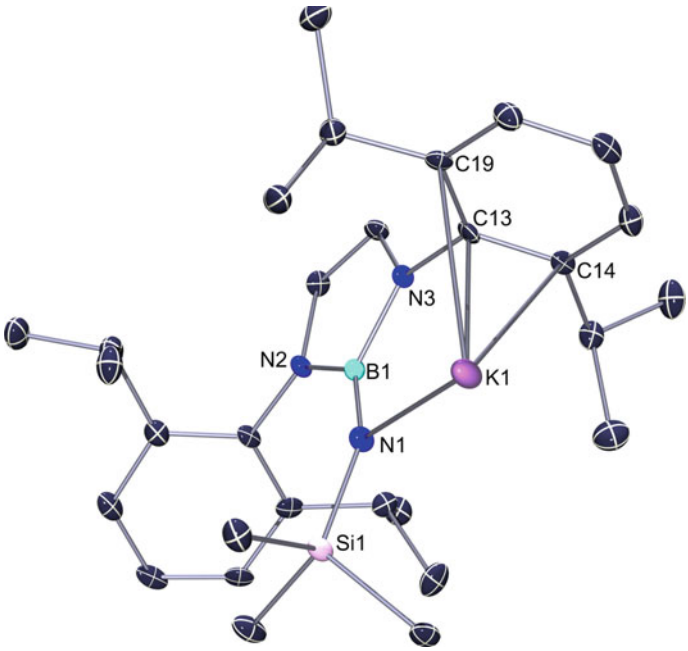

Fig. 6.3 ORTEP representation of ^{TMS}BoNK (**2.K**) (thermal ellipsoids at 30% probability; hydrogen atoms omitted). Selected distances (Å) and angles (°) for **2.K**: K1–N1 2.774(3), N1–B1 1.379(7), N2–B1 1.486(5), N3–B1 1.464(6), K1–C13 3.081(3), K1–C14 3.163(5), K1–C19 3.232 (5), B1–N1–Si1 145.01(3), 114.83(3), K1–N1–Si1 98.88(2)

6.3.2 Synthesis of Low-Oxidation State Group 14 Element Complexes Stabilised by a Silyl Boryl Amide Ligand

6.3.2.1 Synthesis and Reactivity of Group 14 Element(I) Species Stabilised by a Silyl Boryl Amide Ligand

The addition of any alkali metal salt of **2** (i.e. **2.Li**, **2.Li.Et$_2$O**, or **2.K**) to THF solutions of $GeCl_2$.dioxane led to the isolation of the amido Ge(II) chloride, (^{TMS}BoN)GeCl (**3**, Scheme 6.10), in moderate yields. The amido Sn(II) bromide derivative could be accessed through addition of the potassium salt, **2.K**, to $SnBr_2$ in THF, leading to good isolated yields of (^{TMS}BoN)SnBr (**4**, Scheme 6.10). Both **3** and **4** were structurally characterised (Fig. 6.4) and are dimeric in the solid state, with halides bridging the two metal centres in each case, albeit weakly for **3** (Ge1–Cl1′ 2.7453(3) Å). Structural parameters for the complexes are in keeping with previously described amido E(II) halides (E = Ge or Sn).

The reduction of both **3** and **4** with {(^{Mes}nacnac)Mg}$_2$ was subsequently attempted. A rapidly stirred solid mixture of **3** and {(^{Mes}nacnac)Mg}$_2$, cooled to −80 °C, rapidly became intense purple upon the addition of hexane. Warming to

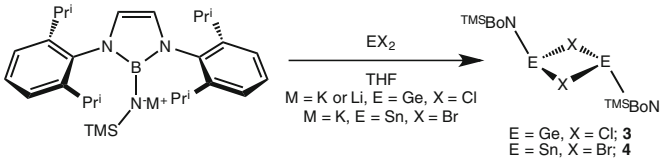

Scheme 6.10 Reactions of alkali metal salts of ^{TMS}BoN with $GeCl_2$ and $SnBr_2$, yielding **3** and **4**, respectively

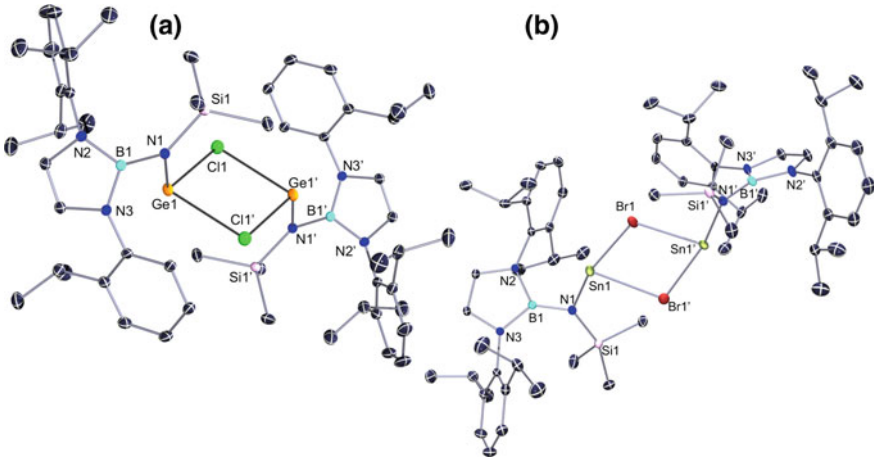

Fig. 6.4 ORTEP representation of **a** (^{TMS}BoN)GeCl (**3**) and **b** (^{TMS}BoN)SnBr (**4**) (thermal ellipsoids at 30% probability; hydrogens omitted). Selected distances (Å) and angles (°) for **3**: Ge1–Cl1 2.3576(3), Ge1–N1 1.851(1), N1–B1 1.463(2), N2–B1 1.440(2), N3–B1 1.449(2), Ge1–Cl1′ 2.7453(3), N1–Ge1-–Cl1 99.52(3), B1–N1–Ge1 109.03(7), B1–N1–Si1 120.38(8), Ge1–N1–Si1 130.58(5); **4**: Sn1–Br1 2.8046(3), Sn1–N1 2.039(3), N1–B1 1.495(4), N2–B1 1.443(4), N3–B1 1.506(4), Sn1–Br1′ 2.9286(3), N1–Sn1–Br1 102.88(3), B1–N1–Sn1 106.76(2), B1–N1–Si1 128.52(2), Sn1–N1–Si1 124.55(1)

ambient temperature, with stirring, over 2 h led to complete conversion to the amido digermyne, {(^{TMS}BoN)Ge}$_2$ (**5**, Scheme 6.11), which was subsequently isolated as deep purple/orange dichroic crystals. The ^{1}H NMR spectrum of **5** revealed it to contain one symmetrical ligand environment. The X-ray crystal structure of **5** (Fig. 6.5) revealed it to contain a long Ge–Ge single bond (2.6005 (6) Å). In keeping with this are the N1–Ge1–Ge2 and N2–Ge2–Ge1 angles of 103.09(1) and 107.05(6)°, the acuteness of which suggests high *p*-character in the Ge–Ge bond. This effect is highlighted through comparison of these angles with those in the previously discussed {(^{iPr}L†)Ge}$_2$ (N–Ge–Ge angles = 119.61(1) and 122.64(1)°), which has a shorter Ge–Ge double bond, and {(^{TMS}L*)Ge}$_2$ (N1–Ge1–Ge1′ angles = 100.09(6)°), which has a longer Ge–Ge single bond [25].

Reduction of **4** in the same manner as **3** led to a brown-red solution, the colour of which maintained if the reaction mixture was kept below −20 °C. Following work-up,

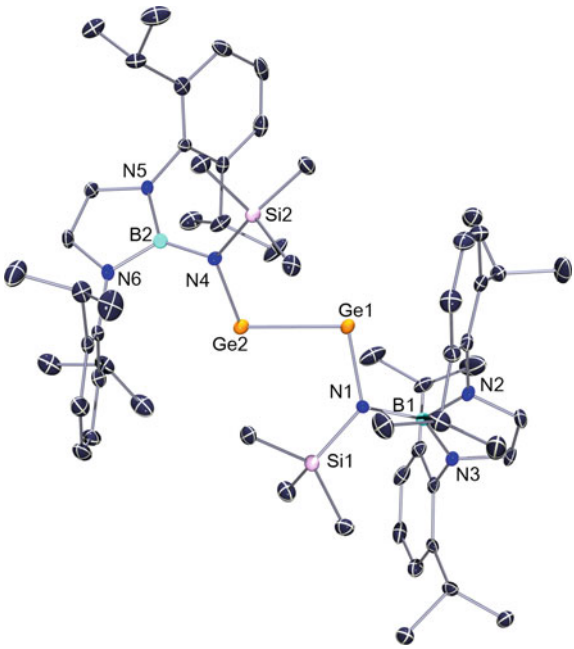

Fig. 6.5 ORTEP representation of $\{(^{TMS}BoN)Ge\}_2$ (**5**) (thermal ellipsoids at 30% probability; hydrogen atoms omitted). Selected bond lengths (Å) and angles (°) for **5**: Ge1–Ge2 2.6005(6), N1–Ge1 1.864(3), N4–Ge2 1.861(3), B1–N1 1.459(5), B2–N4 1.456(5), N1–Ge1–Ge2 103.09(1), N4–Ge2–Ge1 102.41(9), N1–Ge1–G2–N4 135.64(1)

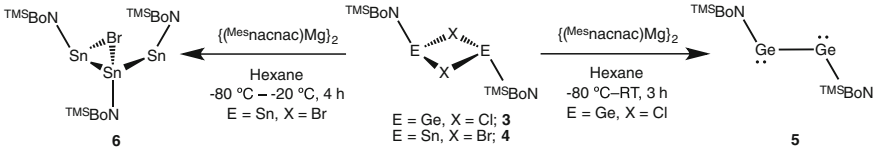

Scheme 6.11 The reduction of $(^{TMS}BoN)GeCl$ and $(^{TMS}BoN)SnBr$ with $\{(^{Mes}nacnac)Mg\}_2$, to yield $\{(^{TMS}BoN)Ge\}_2$ (**5**) and $\{(^{TMS}BoN)Sn\}_2$.$(^{TMS}BoN)SnBr$ (**6**), respectively

deep red/black crystals were isolated, but were found not to be the target distannyne (Scheme 6.11). Instead, X-ray structural analysis revealed the product to appear as a $(^{TMS}BoN)SnBr$ adduct of the target distannyne, viz. $(^{TMS}BoN)SnBr.\{(^{TMS}BoN)Sn\}_2$ (**6**, Fig 6.6). As the reaction was conducted at low-temperature in hexane, it is possible that this product resulted from the low solubility of $\{(^{Mes}nacnac)Mg\}_2$, leaving unreduced $(^{TMS}BoN)SnBr$ remaining in the reaction mixture following work-up. Attempts have not yet been made to purposely make this species, nor to make the non-coordinated distannyne in a more controlled manner. Both Sn–Sn distances in **6** are very similar (Sn1–Sn2 (3.0475(7) Å, Sn2–Sn3 3.0292(8) Å), and

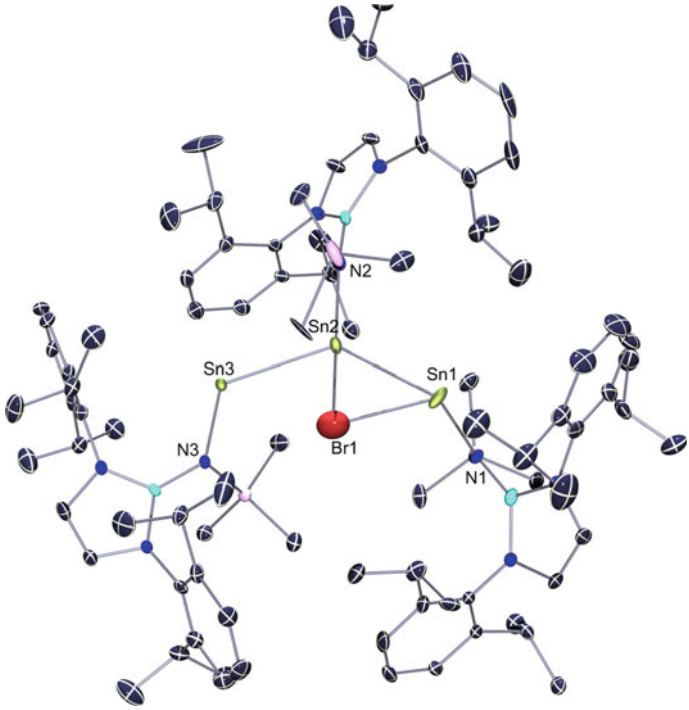

Fig. 6.6 ORTEP representation of (^{TMS}BoN)SnBr.{(^{TMS}BoN)Sn}$_2$ (**6**) (thermal ellipsoids at 30% probability; hydrogen atoms omitted). Selected bond lengths (Å) and angles (°) for **6**: S1–Sn2 3.049(1), Sn2–Sn3 3.029(1), Sn1–Br1 2.776(3), Sn2–Br1 2.772(2), N1–Sn1 2.074(7), N2–Sn2 2.166(6), N3–Sn3 2.077(6), Sn1–Sn2–Sn3 125.61(3), Sn1–Br1–Sn2 66.68(5), N1–Sn1–Sn2 116.22(2), N3–Sn3–Sn2 113.05(2), N2–Sn2–Br1 103.34(2)

are both in the range of Sn–Sn single bonds. The Br1 atom is nearly equidistant from Sn1 and Sn2, with relatively long Sn–Br bond lengths (Sn1–Br1 2.776(3) Å, Sn2–Br1 2.772(2) Å). This suggests the adducted Sn1–Br1 bond is activated to some degree.

The reactivity of the digermyne, {(^{TMS}BoN)Ge}$_2$, was briefly screened. Whilst is did activate dihydrogen, the reaction took some time to reach completion (6 h) compared with that for the previously discussed {(^{iPr}L†)Ge}$_2$, whose reaction with H_2 is complete in under half an hour. Nevertheless, like {(^{iPr}L†)Ge}$_2$, **5** gives only one product in its H_2 activation ({(^{TMS}BoN)GeH}$_2$, **7**). The Ge–*H* resonance in the ^{1}H NMR spectrum of **7** is found at δ = 5.80 ppm, somewhat upfield when compared to {(^{iPr}L†)GeH}$_2$ (Ge–*H*, δ = 8.5 ppm, very broad). Further, the sharp Ge–*H* resonance of **7** shows no sign of shifting or broadening at higher temperatures, again in contrast to that observed in {(^{iPr}L†)GeH}$_2$. This suggests that there are no dynamic isomerisation processes for dissolved **7**. Solid state characterisation of **7** (Fig. 6.7) revealed it to be a 1,2-bis(hydrido) digermene, with a double bond longer than any such interaction reported to date (Ge1–Ge1′ 2.5352(4) Å). Intriguingly,

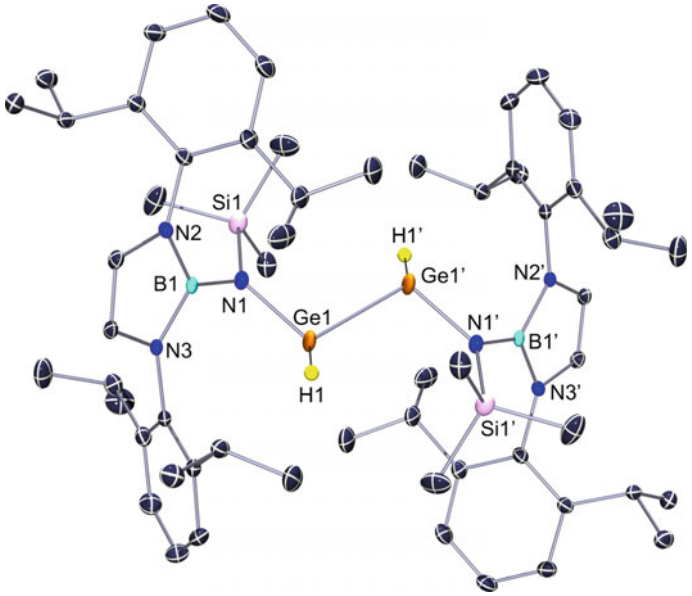

Fig. 6.7 ORTEP representation of $\{(^{TMS}BoN)GeH\}_2$ (**7**) (thermal ellipsoids at 30% probability; hydrogen atoms, aside from H1 and H1′, omitted). Selected bond lengths (Å) and angles (°) for **7**: Ge1–Ge1′ 2.5352(4), N1–Ge1 1.854(2), B1–N1 1.446(2), Ge1–H1 1.200(5), N1–Ge1–Ge1′ 107.05(6), N1–Ge1–H1 117.36(2), H1–Ge1–Ge1′ 120.16(2), N1–Ge1–Ge1′–N1′ 180.00(9)

the longest reported Ge = Ge distance (2.509 Å) belongs to the 1,2-dibromo digermene, $\{(Bbt)(Br)Ge\}_2$ (Bbt = [2,6-$\{(TMS)_2CH\}_2$-4-$\{(TMS)_3C\}Ph]^-$) [26], which was shown to undergo a mono-dimer equilibrium in solution, similar to that for $\{(^{iPr}L^{\dagger})GeH\}_2$. It is therefore surprising that **7** displays no fluxional solution-based phenomena.

Reactivity of Group 14 Element(II) Hydride Complexes Stabilised by ^{TMS}BoN

Although detailed investigations are yet to be carried out, preliminary reactivity studies revealed that **7** reacts with alkenes at ambient temperature, rapidly and quantitatively. This is despite its presumably higher coordinate nature in hydrocarbon solvents relative to *pseudo*-monomeric $\{(^{iPr}L^{\dagger})GeH\}_2$. Work is presently being carried out to ascertain the products of these reactions, and to define whether they are monomeric in the solid state (viz. germylene products of the reaction of $\{(^{iPr}L^{\dagger})GeH\}_2$ with unsaturated organic molecules).

The Sn(II) congener of **7** seemed somewhat unstable at ambient temperature. Generated through addition of HBpin (pin = pincolato) to $(^{TMS}BoN)SnOBu^t$ (**8**, Scheme 6.12, Fig. 6.8), the presumed Sn(II) hydride, $\{(^{TMS}BoN)SnH\}_2$, exists for

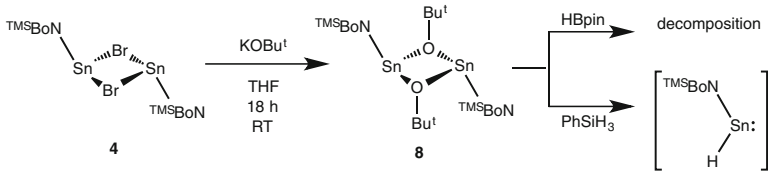

Scheme 6.12 The synthesis of (^{TMS}BoN)SnOBu^t (**8**), and its reactivity with HBpin

only a few minutes at ambient temperature. It was subsequently found the **8** reacts with $PhSiH_3$ over the course of 1 h to give a deep yellow/orange solution (Scheme 6.12). Only small amounts ($\sim$10%) of free ligand were present after this time, with a new broad singlet resonance at $\delta = \sim$14.5 ppm being attributable to a Sn–*H* moiety. This species decomposed over the course of 24 h, yielding elemental tin and ^{TMS}BoNH. Attempts to isolate this species for further analysis are presently underway. The difference in reactivity between **8** and HBpin/$PhSiH_3$ perhaps implies that the Sn–N bond in **8** can react with HBpin, leading to an unstable Sn(II) hydride complex.

As discussed in Chap. 5, catalysed hydrosilylation reactions are an efficient method for the functionalisation of organic unsaturates, but such transformations largely employ TM elements. Whilst ^{iPr}L†-stabilised group 14 element(II) species were not effective in catalysing this reaction, applying both **7** and **8** to such a catalytic regime was met with some success. In light of the reaction of **8** with $PhSiH_3$, using 5 mol% of either species **7** or **8**, the ketone $PhC(O)CF_3$ was successfully hydrosilylated by $PhSiH_3$ (Table 6.1, Scheme 6.13). The catalytic resting state, presumed to be the Ge(II) and Sn(II) alkoxide species (viz. hydroboration of C=O bonds catalysed by {(^{iPr}L†)GeH}$_2$– and {(^{iPr}L†)Sn(μ-H)}$_2$), was present in the reaction mixture involving **7** at reaction completion. However, where **8** was employed as the catalyst, gradual decomposition of the catalytic species was observed, which accelerated as the substrate (i.e. $PhC(O)CF_3$) was consumed. This led to the catalytic reaction stopping at 70% conversion, with no Sn(II) species remaining in solution. These observations are in keeping with the relative instability of the intermediary Sn(II) hydride complex, (^{TMS}BoN)(H)Sn:, or a dimer thereof. Nonetheless, this conversion was achieved at ambient temperature, whereas hydrosilylation reactions employing **7** needed to be heated at 50 °C for 16 h to effect reaction completion. This is in keeping with the previous observation of Ge (II) species being catalytically less efficient than comparable Sn(II) species. The scope of this catalytic regime is yet to be broadened, but these early results are highly promising.

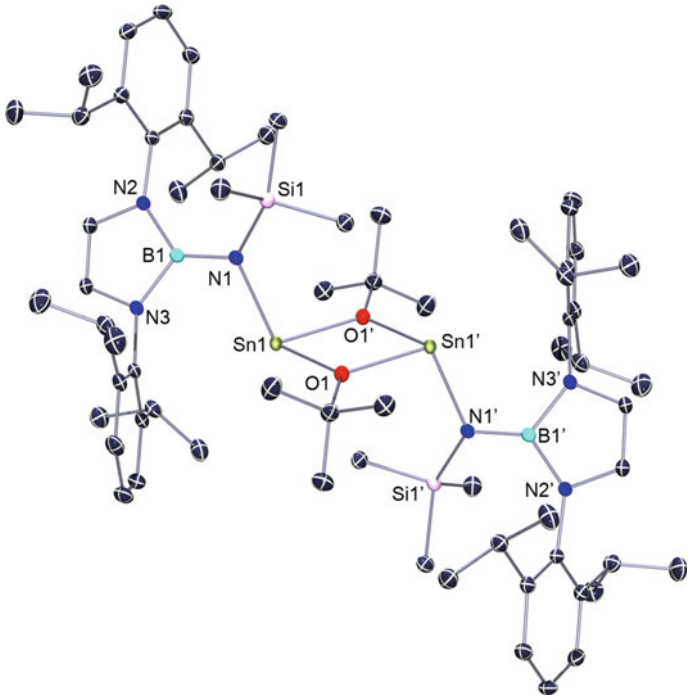

Fig. 6.8 ORTEP representation of (^{TMS}BoN)SnOBu^{t} (**8**) (thermal ellipsoids at 30% probability; hydrogen atoms omitted). Selected bond lengths (Å) and angles (°) for **8**: Sn1–O1 2.183(2), Sn1–O1′ 2.197(2), Sn1–N1 2.161(2), N1–B1 1.446(3), N2–B1 1.475(3), N3–B1 1.446(3), N1–Sn1–O1 107.57(6), N1–Sn1–O1′ 105.16(6), B1–N1–Sn1 108.18(1)

Table 6.1 Hydrosilylation of $PhC(O)CF_3$ catalysed by **7** and **8**[a]

Cat[a]	Loading (mol%)	Time (h)	Yield (%)[b]	Temp (°C)	TOF (h^{-1})
7	5	16	99	50	1.25
8	5	16	70	20	0.9

[a]All reactions were carried out in C_6D_6 with 1 equiv. of $PhSiH_3$
[b]Determined by relative integration of product versus substrate in the ^{19}F NMR spectra of reaction mixtures

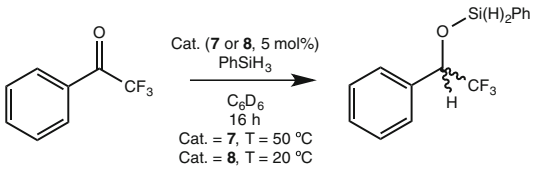

Scheme 6.13 Hydrosilylation of $PhC(O)CF_3$ catalysed by **7** and **8**

6.3.2.2 Synthesis and Reactivity of an Acyclic Bis(Amido) Silylene and Related Chemistry

As the previously discussed super-bulky amido ligands developed within our group saw limited success in silicon chemistry, we sought to apply the ^{TMS}BoN ligand system in this regard. We first attempted the synthesis of an amido Si(II) halide precursor. To this end, the alkali metal salts of **2** (i.e. **2.Li**, **2.Li.Et$_2$O**, and **2.K**) were reacted with IPr.SiCl$_2$ (IPr = :C{N(Dipp)C(H)}$_2$). In the majority of cases, only protonated **2** and free IPr were observed in reaction mixtures. However, the addition of the solvent free lithium salt, **2.Li**, to the same Si(II) precursor at −80 °C yielded small amounts of a new species, as ascertained through ^{1}H NMR spectroscopic analysis. A subsequent NMR scale reaction showed that this new species was generated almost quantitatively when **2.Li** is added to a C_6D_6 solution of IPr.SiCl$_2$ at ambient temperature, with concomitant formation of free IPr. Scale up of this reaction led to the isolation of an acyclic bis(amido) silylene, (^{TMS}BoN)$_2$Si: (**9**, Scheme 6.14). In order to remove the free IPr also present in the reaction mixture, two methods were used. Stirring the crude hexane extract of the reaction under an atmosphere of CO_2 converts free IPr to the hexane-insoluble adduct, IPr.CO_2 [27]. Similarly, addition of one equivalent of $SiBr_4$ to the crude hexane extract forms the ion separated salt $[IPrBr]^-[SiBr_3]^+$ [28], which is again insoluble in hexane. Compound **9** doesn't react with either CO_2 or $SiBr_4$, therefore filtration of both reactions, followed by recrystallisation of the concentrated filtrates, yielded pure **9** in moderate yields (Scheme 6.14). Both of these purification routes are beneficial not only in their efficiency: the formation of the CO_2 adduct, IPr.CO_2, is reversible, and the compound can be effectively converted back to free IPr by heating either the solid [27] or DCM solutions of the adduct [29]. The $[IPrBr]^-[SiBr_3]^+$, as initially reported by Fillipou, can be reduced by KC_8 to give the Si(II) dibromide adduct, IPr.SiBr$_2$,[28] which may be used in further chemistry.

The ^{1}H NMR spectrum of **9** is somewhat broadened, including the peak relating to the TMS groups of the ligand, suggesting hindered rotation of the ligands about the central Si(II)–N bonds. The ^{29}Si NMR spectrum reveals two peaks, centred at δ = −0.5 and δ = 204.6 ppm, the former relating to the TMS groups of the ligand,

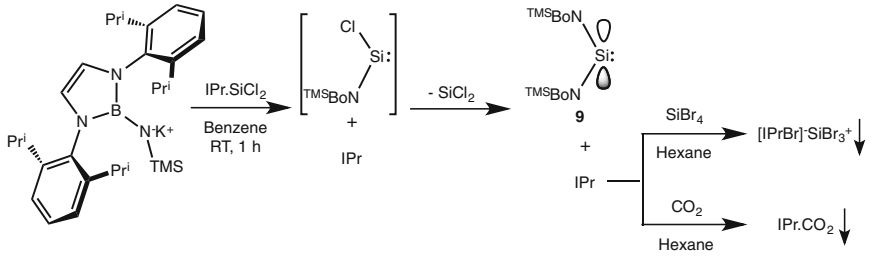

Scheme 6.14 The proposed mechanism for the formation of (^{TMS}BoN)$_2$Si: (**9**), and methods for the removal of the by-product, IPr, from its crude reaction mixtures

and the latter to the two-coordinate Si(II) centre. This Si(II) resonance is in accordance with that previously reported by West and co-workers for the transiently synthesised $\{(TMS)_2N\}_2Si$: (δ = 226 ppm), and suggests decreased overlap of lone-pairs on the ligands N-donor atoms with the Si(II) centre, relative to cyclic derivatives of bis(amido) silylenes [2]. The solid state structure of **9** (Fig. 6.9) reveals that the N-donor atoms of the two ligands do not overlap the empty *p*-orbital at the Si(II) centre, in that they are rotated significantly out of the plane of this Si(II) based *p*-orbital (Si1–N1–Si3–N4 torsion = 52.16(8)°, Si2–N4–Si3–N1 torsion = 58.97(8)°). The N1–Si3–N4 angle of 110.97(5)° suggests a degree of sp^2-character to the lone-pair on Si1 comparable to that in both ^{Boryl}Si: (B–Si–N 109.7°) and ^{Silyl}Si: (Si–Si–N 116.9°). In turn, it can be hypothesised that **9** possesses a narrow HOMO/LUMO gap.

Preliminary DFT studies on the model system, $[\{(Ar'DAB)B\}(TMS)N]_2Si$: (**9′**; Ar′DAB = $[\{N(Ar')C(H)\}_2]_{2-}$, Ar′ = 2,6-Me_2Ph) gave a HOMO/LUMO gap of 2.27 eV, which is slightly larger than those for both ^{Boryl}Si: (2.04 eV) and ^{Silyl}Si: (1.99 eV), but significantly smaller than in Power's (^{Mes}TerphS)$_2$Si: (4.26 eV). The

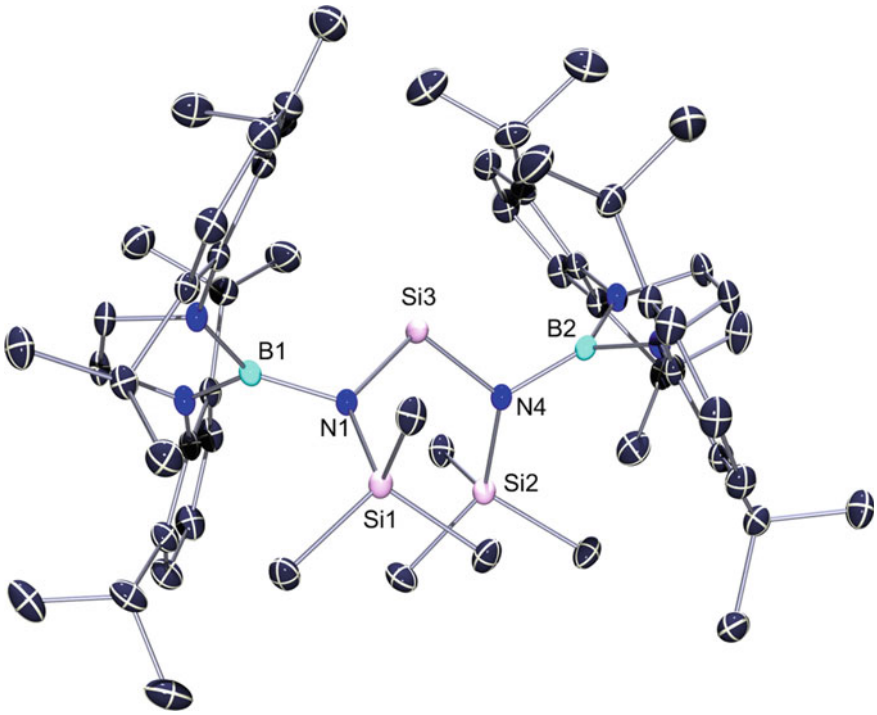

Fig. 6.9 ORTEP representation of (^{TMS}BoN)$_2$Si: (**9**) (thermal ellipsoids at 30% probability; hydrogen atoms omitted). Selected bond lengths (Å) and angles (°) for **9**: Si3–N1 1.744(1), Si3–N4 1.749(1), N1–B1 1.486(2), N4–B2 1.483(2), N1–Si3–N4 110.97(5), B1–N1–Si3 115.78(8), B2–N4–Si3 114.97(8), Si1–N1–Si3–N4 52.16(8), Si2–N4–Si3–N1 58.97(8)

vacant *p*-orbital at the Si(II) centre of **9′** accounts for the majority of its LUMO (~70%), whilst ~30% of the HOMO is localised on the Si(II) centre, as its lone pair (13% Si 3*p*, 17% Si 3*s*). Remaining contributions to the HOMO are largely in the form of the lone-pairs localised on the N-donor atoms of the ^{TMS}BoN ligands. These results suggest that the two N-donor ligands in **9** act to potentially lessen the reactivity of its Si(II) centre, given the relatively low localisation of the HOMO on this centre when compared to that in ^{Boryl}Si: (42% Si 3*p*, 23% Si 3*s*) and ^{Silyl}Si: (43% Si 3*p*, 13% Si 3*s*).

In order to observe whether its narrow HOMO/LUMO gap would lead to high reactivity in **9**, we attempted its reaction with H_2. Stirring a solution of **9** in toluene under ~3 bar H_2 for two days gave no observable reaction. Further, in contrast to ^{Boryl}Si: and ^{Silyl}Si:, **9** is thermally stable in solution for extended periods of time (80 °C, one week), with no sign of decomposition. However, **9** did react with NH_3 and O_2.

The reaction of **9** with NH_3 quantitatively formed a 1:1 mixture of protonated ligand and one new compound (Scheme 6.15). The ^{1}H NMR spectrum of the reaction mixture (Fig. 6.10) displays a singlet at δ = 4.72 ppm, which has ^{29}Si satellites ($^1J_{SiH}$ = 232 Hz). The singlet relating to the TMS group in the ligand of the new product (δ = 0.05 ppm) overlaps a broad peak, with a combined integration of 13H, relative to remaining ligand resonances. This is the approximate region where one may observe Si–N*H*$_2$ resonances [30, 31]. It therefore seems plausible that the broad overlapped peak at δ = ~0.05 ppm relates to two NH_2 groups. The proposed formulation for the new product, then, would be (^{TMS}BoN)Si(H)(NH_2)$_2$ (**10**), formed through reaction of two equivalents of NH_3 with **9**. Given the equivalent of protonated ligand in the ^{1}H NMR spectrum of the reaction mixture, the first step of the reaction is likely one of two possibilities. Either, **9** oxidatively adds ammonia, followed by reductive elimination of ^{TMS}BoNH, or one Si–N fragment of **9** undergoes σ-bond metathesis with an N–H bond of ammonia. Both routes would generate (^{TMS}BoN)(NH_2)Si:, which can then undergo oxidative addition of one further equivalent of ammonia, yielding **10**. Due to the reaction giving a mixture of ^{TMS}BoNH and **10**, it was not possible to isolate **10** as a pure compound via this route. However, the addition of ammonia to hexane solutions of (^{TMS}BoN)Si(H)Cl_2 (**11**), synthesised from the addition of **2.Li.Et$_2$O** to Si(H)Cl_3, led to a salt elimination reaction, giving good crystalline yields of **10** (Scheme 6.15).

Compounds **10** and **11** are colourless solids, and each have characteristic Si–H resonances in their ^{1}H NMR spectra. The ^{1}H NMR spectrum of **10**, synthesised from **11**, is in keeping with that observed for the NMR scale reaction of **9** with NH_3. Both **10** and **11** exhibit typical Si–H stretching bands in their IR spectra (~2200 ν/cm^{-1}), whilst **10** has two broad stretching frequencies relating to the NH_2 moieties (~3200 and ~3400 ν/cm^{-1}). The solid state structures have N1–Si1 distances (**10**: 1.755 Å, **11**: 1.710 Å) of similar length to the N1–Si3 (1.749 Å) and N4–Si3 (1.744 Å) bonds in **9**, further suggesting poor N lone-pair donation to the empty *p*-orbital of Si3 in **9**. Other metrical data for **10** and **11** can be found in Fig. 6.11.

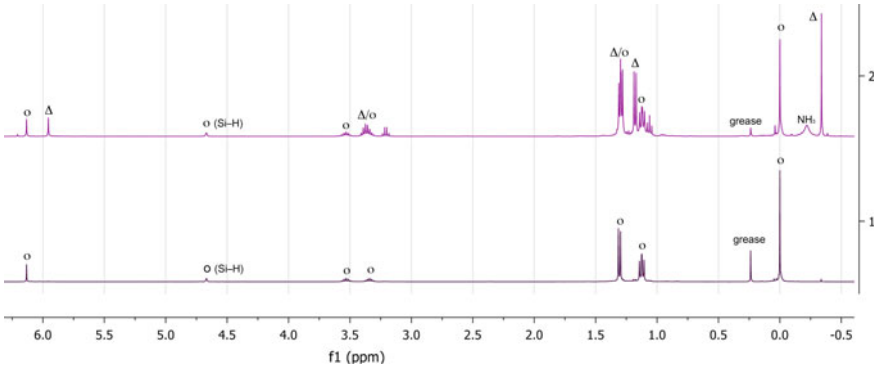

Fig. 6.10 Stack plot of the crude reaction mixture of **9** with excess NH_3, yielding a 1:1 mixture of **10** and ^{TMS}BoNH (*above*), and pure **10** synthesised through the addition of NH_3 to (^{TMS}BoN)Si(H)Cl_2 (*below*), in the range of −0.5–6.5 ppm; Δ = ^{TMS}BoNH, o = (^{TMS}BoN)Si(H)$(NH_2)_2$. Reproduced from *Chem. Commun.*, **2016**, *52*, 1717 with permission from The Royal Soceity of Chemistry

Scheme 6.15 The reactivity of **9** with ammonia, with the proposed mechanism for the formation of the Si(IV) product, (^{TMS}BoN)Si(H)$(NH_2)_2$ (**10**); and an alternative route to **10** through the synthesis of (^{TMS}BoN)Si(H)Cl_2 (**11**), and its subsequent reaction with NH_3

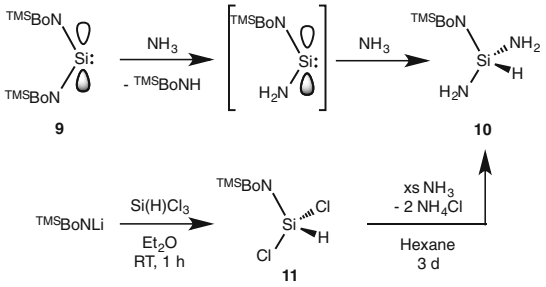

The reaction of **9** with O_2 was initially conducted on an NMR scale, with the yellow solution of **9** in C_6D_6 becoming colourless rapidly after being shaken under an atmosphere of dry O_2. The ^{1}H NMR spectrum of the reaction mixture was extremely complex, and suggested unsymmetrical ligand environments, based on the splitting of resonances attributable to the C–*H* moieties of the DAB backbone. X-ray structural analysis of the product ((^{TMS}BoN)(κ^2-^{TMS}BoN′O)SiOH, **12**), recrystallised from Et_2O, revealed the reaction to have involved the addition of a single equivalent of O_2 to the Si(II) centre of **9**, resulting in a tetra-valent silicon species (Scheme 6.16a, Fig. 6.12). One oxygen bound to the central Si(IV) centre has CH-activated an Pr^i group of a flanking ligand, forming a C–O bond. The hydrogen atom from this transformation can be found on the remaining O atom bound to the silicon centre. The ^{1}H NMR spectrum of redissolved crystalline **12** is in keeping with that observed from the NMR scale reaction of **9** with O_2. The complexity of this NMR spectrum arises from the activation of only one ligand. Not only is this activated ligand now unsymmetrical, but as the central Si(IV) atom is a chiral centre, so the second ligand is also in an unsymmetrical environment. This is

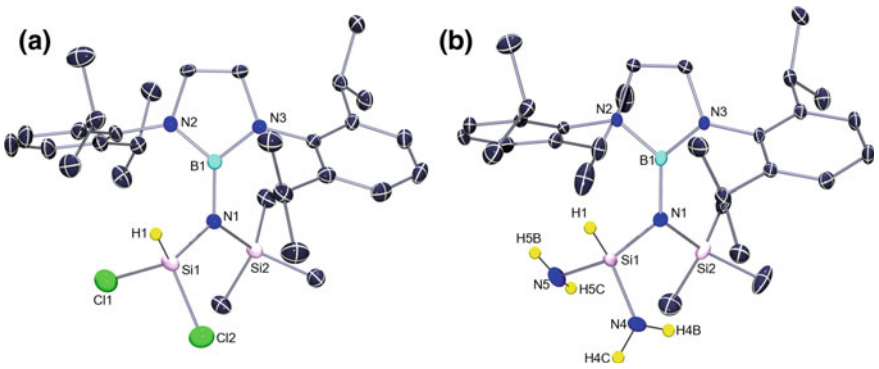

Fig. 6.11 ORTEP representation of (**a**) (^{TMS}BoN)$_2$Si(H)Cl$_2$ (**11**) and (**b**) (^{TMS}BoN)$_2$Si(H)(NH$_2$)$_2$ (**10**) (thermal ellipsoids at 30% probability; hydrogen atoms, aside from N–H and Si–H moieties, omitted). Selected bond lengths (Å) and angles (°) for **10**: Si1–N1 1.755(3), Si1–N4 1.707(4), Si1–N5 1.711(4), B1–N1 1.469(4), Si1–H1 1.332(3), N4–Si1–H1 105.59(1), H1–Si1–N5 112.89(1), N4–Si1–N5 105.07(2); **11**: Si1–N1 1.710(3), Si1–Cl1 1.964(2), Si1–Cl2 2.054(2), B1–N1 1.463 (5), Si1–H1 1.388(4), Cl1–Si1–H1 107.00(2), H1–Si1–Cl2 111.16(2), Cl1–Si1–Cl2 105.51(9)

further shown by the ^{29}Si NMR spectrum of **12**, which has one peak for each Si centre. We postulate that **12** is formed first through the formation of a dioxasilirane, through formal [2 + 1] addition of an O_2 molecule to the Si(II) centre of **9**. Indeed, an analogous reaction is known for a silylene stabilised by both a modified β-diketiminate ligand and a carbene, (^{Dipp}nacnac′)Si.NHC (Scheme 6.16b). The

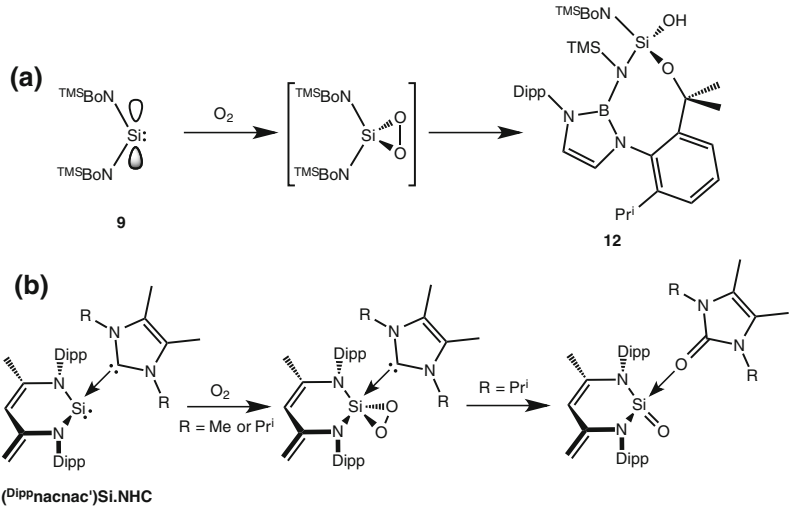

Scheme 6.16 **a** The reaction of **9** with O_2, yielding (^{TMS}BoN)(κ^2-^{TMS}BoN′O)SiOH (**12**), and the proposed mechanism for its formation, and **b** the reported generation of an NHC-stabilised dioxasilirane, and its oxygen abstraction, yielding a urea-stabilised N-heterocyclic silanone

addition of O_2 to **9** in the manner described would lead to a strained O–O single bond, and potentially forming a diradical. This would then give good grounds for a CH-activation reaction occurring. Attempts to isolate a siloxirane intermediate were unsuccessful, with a variable temperature ^{1}H NMR experiment revealing that the CH-activation product is already generated at −50 °C. Attempts to oxidise the Si(II) centre using other oxidants (e.g. N_2O, Me_3NO) were unsuccessful, with no reaction observed in all cases.

Following the isolation of the silylene, **9**, we sought comparison with the heavier group 14 element congeners. It was not possible to synthesise the germanium analogue, either by addition of a further equivalent of any alkali metal salts of **2** to the amido Ge(II) chloride, **3**, or by direct addition of two equivalents of an alkali metal salt of **2** to Ge(II) dichloride. However, the addition of two equivalents of **2.K** to either $SnBr_2$ or $PbBr_2$, in THF, led to the isolation of (^{TMS}BoN)$_2$Sn: (**13**) and (^{TMS}BoN)$_2$Pb: (**14**) in good yields (Scheme 6.17). Both compounds are deep orange/red crystalline solids, which display a single set of ligand peaks in their ^{1}H NMR spectra. As with **9**, the majority of these peaks are broadened, likely due to the bulk of the ^{TMS}BoN ligand. The solid state structure of **13** (Fig. 6.13a) reveals it to be monomeric, with a N1–Sn1–N4 angle of 106.21°, which is in accordance with previously reported acyclic bis (amido) stannylenes, and expectedly more acute than the related angle for **9**. Interestingly, the N4–B2 distance (1.409 Å) is somewhat shorter than the same bond in the second ligand (N1–B1 1.475 Å). The bond distance between this second ligand and the Sn(II) centre (N1–Sn1 2.142 Å) is subsequently shorter than

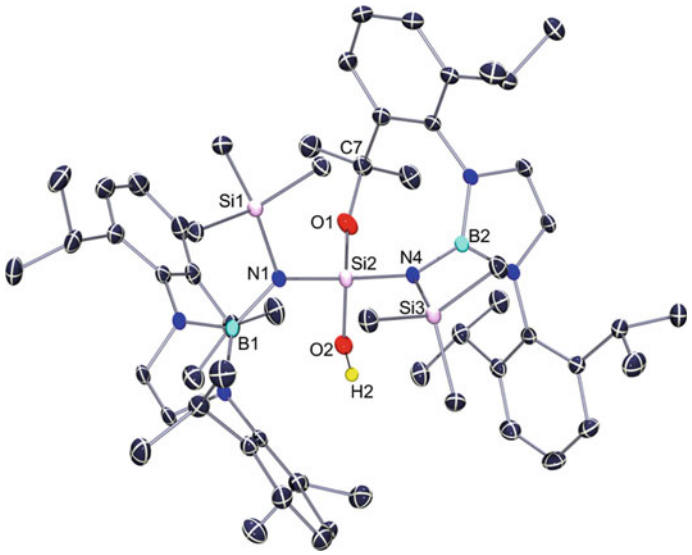

Fig. 6.12 ORTEP representation of (^{TMS}BoN)(κ^2-^{TMS}BoN′O)SiOH (**12**) (thermal ellipsoids at 30% probability; hydrogen atoms, aside from H2, omitted). Selected bond lengths (Å) and angles (°): Si2–N1 1.729(1), Si2–N4 1.730(1), Si2–O1 1.620(1), Si2–O2 1.638(1), O1–C7 1.431(2), N1–B1 1.484(2), N4–1.467(2), N1–Si2–N4 117.92(6), O1–Si2–O2 106.50(6), Si2–O1–C7 156.29(1)

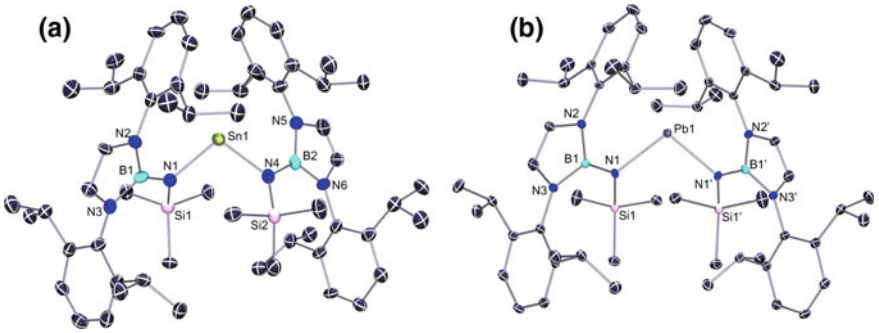

Fig. 6.13 ORTEP representation of **a** (^{TMS}BoN)$_2$Sn: (**13**) and **b** (^{TMS}BoN)$_2$Pb: (**14**) (thermal ellipsoids at 30% probability; hydrogen atoms omitted). Selected bond lengths (Å) and angles (°) for **13**: Sn1–N1 2.142(5), Sn1–N4 2.173(5), N1–B1 1.475(7), N4–B2 1.409(7), N1–Sn1–N4 106.21(2), Si1–N1–Sn1–N4 57.71(3), Si2–N4–Sn1–N1 58.77(3); **14**: Pb1–N1 2.282(1), N1–B1 1.431(5), N1–Pb1–N1′ 105.73(1), Si1–N1–Pb1–N1′ 57.22(1)

Scheme 6.17 The synthesis of (^{TMS}BoN)$_2$Sn: (**13**) and (^{TMS}BoN)$_2$Pb: (**14**)

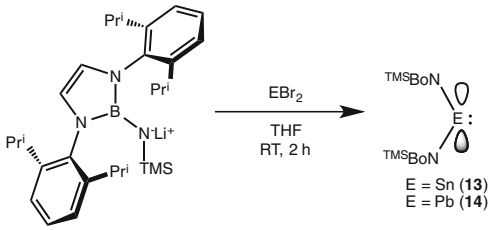

for N4–Sn1 (2.173 Å), suggesting a greater degree of donation of the N1 lone-pair to Sn1 than that for N4 to Sn1. The plumbylene, **14**, represents a relatively rare example of an acyclic bis(amido) plumbylene (Fig. 6.13b). Its Pb–N distances (Pb1–N1 2.282 Å) are longer than other reported examples, suggesting poor overlap of lone-pairs on these N centres with the Pb(II) centre. This is reinforced by the slightly shorter N1–B1 distance (1.431 Å) when compared with N2–B1 (1.462 Å) and N3–B1 (1.466 Å) distances. The N1–Pb1–N1′ angle (105.73°) is quite similar to that of the Sn(II) congener, **13**.

Preliminary reactivity studies imply that **13** and **14** are not highly reactive. This is perhaps highlighted by their stability under an atmosphere of pure oxygen for two days. This is in stark contrast to **9**, which reacts readily with O_2 at temperatures as low as −50 °C. Further reactivity studies are presently under way.

6.4 Conclusion

This relatively short study has shed light on the effects of exchanging the bulky tetraphenyl aniline unit (e.g. $Ar^{\dagger}NH_2$) in previously described ligands (e.g. $^{iPr}L^{\dagger}$), with the $\{(^{Dipp}DAB)B\}NH_2$ moiety. The novel amine, $\{(^{Dipp}DAB)B\}NH_2$, has been used in the synthesis of the silyl-boryl amine proligand, $^{TMS}BoNH$, which has been employed in low-oxidation state, low-coordinate group 14 chemistry. Stark contrasts in the bonding of both an amido digermyne and 1,2-hydrido amido digermene stabilised by ^{TMS}BoN were found, when compared to related $^{iPr}L^{\dagger}$ systems. Further, ^{TMS}BoN stabilised Ge(II) and Sn(II) hydrides were found to be active in ketone hydrosilylation, which was not the case for the analogous $^{iPr}L^{\dagger}$-substituted complexes. Finally, acyclic bis(amido) tetrelenes, $(^{TMS}BoN)_2E$: (E = Si, Sn, and Pb) have been synthesised, with $(^{TMS}BoN)_2Si$: being the first fully characterised example of this class of Si(II) compound. Whilst this Si(II) centred complex readily reacted with both NH_3 and O_2, both $(^{TMS}BoN)_2Sn$: and $(^{TMS}BoN)_2Pb$: did not, and are in fact stable under O_2 for days. These results, taken as a whole, further display the importance of ligand design in affecting the chemistry achievable at these low-coordinate group 14 element centres. This is perhaps most true for realising catalysis with low-oxidation state group 14 elements, where a fine balance of the energy of the frontier orbitals is of the upmost importance. Whilst this area is in its infancy, developments discussed here, and earlier in this thesis, display the potential that lies therein.

6.5 Experimental

$(^{Dipp}DAB)BNH_2$ (1).

Route (a): To a mixture of $(^{Dipp}DAB)BBr$ (20 g, 43.0 mmol) and $LiNH_2$ (1.2 g, 51.6 mmol) was added THF (100 mL) at ambient temperature. The reaction mixture was then heated at 55 °C for 18 h, after which time all volatiles were removed in vacuo. The solid residue was extracted in hot hexane (100 mL), and the resulting suspension filtered through a Celite pad in air. The filtrate was stored at −30 °C for 16 h to yield a large crop of **1** as a colourless crystalline solid (12 g, 70%). Evaporation of the mother liquor to dryness under a flow of N_2 gas, followed by washing the residue with cold hexane (10 mL), yielded a further 2.5 g of solid product, that was essentially pure by ^1H NMR spectroscopic analysis. Combined yield 14.5 g (84%).

Route (b): A solution of $(^{Dipp}DAB)BBr$ (10 g, 21.5 mmol) was rapidly stirred under a flow of dry NH_3, with immediate formation of copious white precipitate (i.e. NH_4Br). After 20 min the reaction vessel was sealed, and stirred for a further 4 h. The reaction was subsequently warmed to ~60 °C and filtered. Removal of all volatiles from the filtrate in vacuo led to the isolation of essentially pure **1** (6.5 g, 75%). M.p. 76–80 °C; ^1H NMR (C_6D_6, 400 MHz, 298 K), δ = 1.19 (br s, 2H,

B–NH_2), 1.25 (d, $^3J_{HH}$ = 7.6 Hz, 12H, Dipp-CH(CH_3)$_2$), 1.27 (d, $^3J_{HH}$ = 7.6 Hz, 12H, Dipp-CH(CH_3)$_2$), 3.37 (sept, $^3J_{HH}$ = 7.6 Hz, 4H, Dipp-CH(CH$_3$)$_2$), 5.94 (s, 2H, {N(Dipp)C(H)}$_2$), 7.17–7.21 (m, 6H, Ar-*H*); ^{13}C{^{1}H} NMR (C_6D_6, 75.5 MHz, 298 K), δ = 24.3 (Dipp-CH(*C*H$_3$)$_2$), 24.4 (Dipp-CH(*C*H$_3$)$_2$), 28.6 (Dipp-*C*H(CH$_3$)$_2$), 116.9 ({N(Dipp)*C*(H)}), 123.9, 127.6, 138.7, 147.6 (Ar-*C*); ^{11}B{^{1}H} NMR (C_6D_6, 128 MHz, 298 K), δ = 22.9; IR, ν/cm^{-1} (ATR): 3410 (m, NH_2), 3064 (w), 2959 (s), 1592 (m), 1360 (m), 1276 (m), 1177 (m), 1118 (s), 1056 (m), 934 (w), 804 (s), 732 (m); MS/EI m/z (%): 404.2 (MH^+, 100); acc. mass calcd. for $C_{26}H_{39}BN_3$ (MH^+): 404.3237; found: 404.3240.

^{TMS}BoNH (2). To a solution of (^{Dipp}DAB)BNH_2 (10 g, 24.9 mmol) in Et_2O (100 mL) at −80 °C was added LiBu^n (16.3 mL, 1.6 M in hexane, 26.1 mmol) over the course of 5 min. The reaction mixture was subsequently removed from the cold bath and stirred for 1 h. Over this time some precipitate forms, presumably (^{Dipp}DAB)BN(H)Li. The reaction mixture was subsequently quenched with TMSCl (3.32 mL, 26.1 mmol) at 0°C, and stirred for 1 h. The reaction mixture was filtered, and all volatiles removed *in vacuo* from the filtrate to yield ^{TMS}BoNH as an essentially pure oil, which is used directly for further chemistry. M.p.: Oil at ambient temperature; ^{1}H NMR (C_6D_6, 400 MHz, 298 K), δ = -0.29 (s, 9H, N–*TMS*), 1.23 (d, $^3J_{HH}$ = 7.6 Hz, 12H, Dipp-CH(CH_3)$_2$), 1.34 (d, $^3J_{HH}$ = 7.6 Hz, 12H, Dipp-CH(CH_3)$_2$), 3.42 (sept, $^3J_{HH}$ = 7.6 Hz, 4H, Dipp-CH(CH$_3$)$_2$), 6.01 (s, 2H, {N(Dipp)C(H)}$_2$), 7.15–7.31 (m, 6H, Ar-*H*); ^{13}C{^{1}H} NMR (C_6D_6, 75.5 MHz, 298 K), δ = 1.8 (N–*TMS*), 23.8 (Dipp-CH(*C*H$_3$)$_2$), 25.2 (Dipp-CH(*C*H$_3$)$_2$), 28.6 (Dipp-*C*H(CH$_3$)$_2$), 117.8 ({N(Dipp)*C*(H)}), 124.0, 139.4, 147.4 (Ar-*C*); ^{11}B{^{1}H} NMR (C_6D_6, 128 MHz, 298 K), δ = 23.1; ^{29}Si NMR (C_6D_6, 80 MHz, 298 K), δ = 2.8; IR, ν/cm^{-1} (ATR): 3354 (br w, NH), 3067 (w), 3028 (w), 1584 (w), 1567 (w), 1249 (m), 1112 (w), 1070 (m), 980 (w), 900 (m), 878 (s), 834 (s), 803 (s), 696 (m); MS/EI m/z (%): 475.5 (MH^+, 100).

^{TMS}BoNLi (2.Li). To a solution of ^{TMS}BoNH (5 g, 10.5 mmol) in hexane (50 mL) was added LiBu^n (6.9 ml, 1.6 M in hexane, 11.0 mmol) at ambient temperature, and the reaction mixture stirred for 3 days, over which time some white precipitate had formed. The reaction mixture was subsequently concentrated to ∼25 mL, and stored at −30 °C overnight to afford a white powder, which was isolated by filtration, and dried in vacuo (3 g, 59%). ^{1}H NMR (C_6D_6, 400 MHz, 298 K), δ = −0.36 (s, 9H, N–*TMS*), 1.25 (d, $^3J_{HH}$ = 7.0 Hz, 12H, Dipp-CH(CH_3)$_2$), 1.35 (d, $^3J_{HH}$ = 7.0 Hz, 12H, Dipp-CH(CH_3)$_2$), 3.72 (sept, $^3J_{HH}$ = 7.0 Hz, 4H, Dipp-CH(CH$_3$)$_2$), 6.04 (s, 2H, {N(Dipp)C(H)}$_2$), 7.16–7.19 (m, 6H, Ar-*H*).

^{TMS}BoNLi.Et$_2$O (2.Li.Et$_2$O). To a solution of ^{TMS}BoNH (5 g, 10.5 mmol) in Et_2O (50 mL) was added LiBu^n (6.9 ml, 1.6 M in hexane, 11.0 mmol) at −40 °C, then the reaction mixture warmed to ambient temperature, and stirred for 2 h. Volatiles were subsequently removed in vacuo, and the micro-crystalline powder washed with cold hexane (10 mL) to afford the product (4.6 g, 79%). ^{1}H NMR (C_6D_6, 400 MHz, 298 K), δ = −0.06 (s, 9H, N–*TMS*), 0.64 (t, $^3J_{HH}$ = 7.8 Hz, 6H, Li–O(CH$_2$CH_3)$_2$) 1.29 (d, $^3J_{HH}$ = 7.6 Hz, 12H, Dipp-CH(CH_3)$_2$), 1.39 (d, $^3J_{HH}$ = 7.6 Hz, 12H, Dipp-CH(CH_3)$_2$), 2.74 (q, $^3J_{HH}$ = 7.8 Hz, 4H, Li–O

($CH_2CH_3)_2$), 3.83 (sept, $^3J_{HH}$ = 7.6 Hz, 4H, Dipp-C*H*$(CH_3)_2$), 6.14 (s, 2H, {N(Dipp)C(*H*)}$_2$), 7.16–7.18 (m, 6H, Ar-*H*).

^{TMS}BoNK (2.K). To a suspension of benzyl potassium (1.5 g, 11.6 mmol) in toluene (10 mL), at −40 °C, was added a solution of ^{TMS}BoNH (5 g, 10.5 mmol) in toluene (40 mL). The reaction mixture was warmed to ambient temperature and stirred for 2 h, whereupon the majority of the suspended benzyl potassium has been consumed. The reaction mixture was allowed to settle, filtered, and all volatiles removed from the filtrate in vacuo. The resulting residue was washed with hexane (2 × 10 mL), and the pale brown solid dried in vacuo, giving ^{TMS}BoNK as a free-flowing powder (4.7 g, 87%). ^{1}H NMR (C_6D_6, 400 MHz, 298 K), δ = −0.23 (s, 9H, N–*TMS*), 1.30 (d, $^3J_{HH}$ = 7.0 Hz, 12H, Dipp-CH(C*H*$_3)_2$), 1.38 (d, $^3J_{HH}$ = 7.0 Hz, 12H, Dipp-CH(C*H*$_3)_2$), 3.83 (sept, $^3J_{HH}$ = 7.0 Hz, 4H, Dipp-C*H*$(CH_3)_2$), 6.12 (s, 2H, {N(Dipp)C(*H*)}$_2$), 7.08-7.13 (m, 6H, Ar-*H*).

(^{TMS}BoN)GeCl (3). A solution ^{TMS}BoNLi.Et_2O (2 g, 3.6 mmol) in THF (30 mL) was added to a solution of $GeCl_2$.dioxane (0.92 g, 3.97 mmol) in THF (5 mL) at −80 °C. The reaction mixture was allowed to warm to ambient temperature over the course of 4 h, and all volatiles subsequently removed in vacuo. The oily residue was extracted in hexane (20 mL), filtered, and the filtrate concentrated in vacuo to ∼7 mL. Storage at −30 °C for 18 h resulted in the formation of large colourless blocks of (^{TMS}BoN)GeCl (1.2 g, 57%). M.p.: 104–110 °C (melt); ^{1}H NMR (C_6D_6, 400 MHz, 298 K), δ = 0.16 (s, 9H, N–*TMS*), 1.11 (d, $^3J_{HH}$ = 7.0 Hz, 12H, Dipp-CH(C*H*$_3)_2$), 1.28 (d, $^3J_{HH}$ = 7.0 Hz, 12H, Dipp-CH(C*H*$_3)_2$), 3.29 (sept, $^3J_{HH}$ = 7.0 Hz, 4H, Dipp-C*H*$(CH_3)_2$), 6.18 (s, 2H, {N(Dipp)C(*H*)}$_2$), 7.07–7.18 (m, 6H, Ar-*H*), ^{13}C{^{1}H} NMR (C_6D_6, 75.5 MHz, 298 K), δ = 4.0 (N–*TMS*), 22.9 (Dipp-CH(*C*H$_3)_2$), 26.5 (Dipp-CH(*C*H$_3)_2$), 29.3 (Dipp-*C*H$(CH_3)_2$), 119.6 ({N(Dipp)*C*(H)}), 124.0, 124.4, 137.9, 145.5 (Ar-*C*); ^{11}B{^{1}H} NMR (C_6D_6, 128 MHz, 298 K), δ = 24.4; ^{29}Si NMR (C_6D_6, 80 MHz, 298 K), δ = 0.2; IR, ν/cm^{-1} (ATR): 3066 (w), 1570 (w), 1301 (m), 1245 (s), 1116 (m), 1075 (m), 959 (m), 902 (s), 799 (s), 781 (m), 679 (s); MS/EI m/z (%): 580.5 (M^+-2H, 1), 403.4 (^{Dipp}DAB-BNH_2^+, 100); anal. calcd. for $C_{29}H_{45}BClGeN_3Si$: C, 57.78%; H, 7.78%; N, 7.21%; found: C, 59.78%; H, 7.84%; N, 7.16%.

(^{TMS}BoN)SnBr (4). A solution of ^{TMS}BoNK (1.5 g, 2.9 mmol) in THF (25 mL) was added dropwise to a solution of $SnBr_2$ (0.86 g, 3.1 mmol) in THF (10 mL) at −80 °C. The reaction mixture was allowed to warm to ambient temperature over 2 h, and all volatiles were subsequently removed in vacuo. Extraction of the resulting residue in warm hexane (25 mL), followed by filtration and removal of volatiles from the filtrate in vacuo led to the isolation of essentially pure (^{TMS}BoN)SnBr as a free-flowing pale yellow powder (1.5 g, 77%). X-ray quality crystals were grown by storage of a saturated hexane solution of (^{TMS}BoN)SnBr at 4 °C for 2 days. M.p.: 126–132 °C (melt); ^{1}H NMR (C_6D_6, 400 MHz, 298 K), δ = 0.09 (s, 9H, N–*TMS*), 1.13 (d, $^3J_{HH}$ = 7.0 Hz, 12H, Dipp-CH(C*H*$_3)_2$), 1.41 (d, $^3J_{HH}$ = 7.0 Hz, 12H, Dipp-CH(C*H*$_3)_2$), 3.52 (sept, $^3J_{HH}$ = 7.0 Hz, 4H, Dipp-C*H*$(CH_3)_2$), 6.12 (s, 2H, {N(Dipp)C(*H*)}$_2$), 7.10–7.20 (m, 6H, Ar-*H*), ^{13}C{^{1}H} NMR (C_6D_6, 75.5 MHz, 298 K), δ = 5.2 (N–*TMS*), 23.2 (Dipp-CH(*C*H$_3)_2$), 26.5 (Dipp-CH(*C*H$_3)_2$), 29.1 (Dipp-*C*H$(CH_3)_2$), 119.2 ({N(Dipp)*C*(H)}), 124.0, 124.4,

139.7, 147.1 (Ar-*C*); $^{11}B\{^{1}H\}$ NMR (C_6D_6, 128 MHz, 298 K), δ = 24.7; ^{29}Si NMR (C_6D_6, 80 MHz, 298 K), δ = 0.7; $^{119}Sn\{^{1}H\}$ NMR (C_6D_6, 149 MHz, 298 K), δ = 105.4; IR, ν/cm^{-1} (ATR): 3064 (w), 1629 (w), 1584 (w), 1376 (s), 1326 (s), 1270 (m), 1239 (s), 1041 (s), 971 (m), 874 (s), 823 (s), 799 (s), 668 (s); MS/EI m/z (%): 475.5 (^{TMS}BoNH$^+$, 100).

{(^{TMS}BoN)Ge}$_2$ (5). To a rapidly stirred solid mixture of (^{TMS}BoN)GeCl (1.0 g, 1.81 mmol) and {(^{Mes}nacnac)Mg}$_2$ (645 mg, 0.91 mmol), cooled to −80 °C, was added hexane (30 mL), the reaction mixture warmed to ambient temperature, and stirred for 2 h. All volatiles were subsequently removed *in vacuo* in order to force precipitation of {(^{Mes}nacnac)MgCl}$_2$. The bright purple residue was extracted in hexane (20 mL), filtered, and the filtrate concentrated in vacuo to ∼5 mL. Storage at 4 °C for 18 h resulted in the formation of deep purple/orange dichroic crystals of {(^{TMS}BoN)Ge}$_2$ (520 mg, 53%). M.p.: 142–152 °C (decomp.); ^{1}H NMR (C_6D_6, 400 MHz, 298 K), δ = −0.25 (s, 18H, N–*TMS*), 1.15 (d, $^{3}J_{HH}$ = 7.0 Hz, 24H, Dipp-CH(C*H*$_3$)$_2$), 1.23 (d, $^{3}J_{HH}$ = 7.0 Hz, 24H, Dipp-CH(C*H*$_3$)$_2$), 3.43 (sept, $^{3}J_{HH}$ = 7.0 Hz, 8H, Dipp-C*H*(CH$_3$)$_2$), 6.20 (s, 4H, {N(Dipp)C(*H*)}$_2$), 7.06-7.16 (m, 12H, Ar-*H*), $^{13}C\{^{1}H\}$ NMR (C_6D_6, 75.5 MHz, 298 K), δ = 1.7 (N–*TMS*), 23.8 (Dipp-CH(*C*H$_3$)$_2$), 25.2 (Dipp-CH(*C*H$_3$)$_2$), 29.2 (br., Dipp-*C*H(CH$_3$)$_2$), 118.6 ({N(Dipp)*C*(H)}), 124.0, 124.4, 139.4, 146.6 (Ar-*C*); $^{11}B\{^{1}H\}$ NMR (C_6D_6, 128 MHz, 298 K), δ = 23.2; ^{29}Si NMR (C_6D_6, 80 MHz, 298 K), δ = 2.0; IR, ν/cm^{-1} (ATR): 3065 (w), 1931 (w), 1381 (s), 1246 (s), 1115 (m), 1075 (m), 1021 (w), 971 (w), 935 (w), 899 (m), 859 (s), 778 (s), 682 (s); MS/EI m/z (%): 1023.0 (M$^+$-SiMe$_3$, 1), 948.9 (M$^+$-(SiMe$_3$)$_2$, 8), 547.4 (^{TMS}BoN)Ge$^+$, 9), 475.5 (^{TMS}BoNH$^+$, 100); anal. calcd. for $C_{58}H_{90}B_2Ge_2N_6Si_2$: C, 63.65%; H, 8.29%; N, 7.68%; found: C, 63.45%; H, 8.31%; N, 7.64%.

{(^{TMS}BoN)Sn}2.(^{TMS}BoN)SnBr (6). This species was synthesised in the same manner as {(^{TMS}BoN)Ge}$_2$, with work-up conducted below −20 °C, using (^{TMS}BoN)SnBr (0.25 g, 0.39 mmol), and {(^{Mes}nacnac)Mg}$_2$ (274 mg, 0.19 mmol). X-ray quality crystals were grown from a concentrated hexane solution at −30 °C, in low yield.

N.B. Due to both the low yield of this product, and its thermal instability, no further data has been acquired for **6**.

{(^{TMS}BoN)GeH}$_2$ (7). A solution of {(^{TMS}BoN)Ge}$_2$ (200 mg, 0.18 mmol) in toluene was stirred under an atmosphere of H_2 for 16 h, over which time its purple colour faded, leaving a bright orange solution. Volatiles were removed in vacuo, and the residue extracted in hexane (10 mL). Filtration and concentration of the extract in vacuo to ∼3 mL, and storage at 4 °C, led to the formation of orange/purple dichroic crystals of **7** (95 mg, 48%). M.p.: 125–133 °C (melt); ^{1}H NMR (C_6D_6, 400 MHz, 298 K), δ = −0.09 (s, 18H, N–*TMS*), 1.17 (d, $^{3}J_{HH}$ = 7.0 Hz, 24H, Dipp-CH(C*H*$_3$)$_2$), 1.32 (d, $^{3}J_{HH}$ = 7.0 Hz, 24H, Dipp-CH(C*H*$_3$)$_2$), 3.43 (sept, $^{3}J_{HH}$ = 7.0 Hz, 8H, Dipp-C*H*(CH$_3$)$_2$), 5.80 (s, 1H, Ge–*H*), 6.20 (s, 4H, {N(Dipp)C(*H*)}$_2$), 7.10-7.17 (m, 12H, Ar-*H*), $^{13}C\{^{1}H\}$ NMR (C_6D_6, 75.5 MHz, 298 K), δ = 4.2 (N–*TMS*), 23.1 (Dipp-CH(*C*H$_3$)$_2$), 26.4 (Dipp-CH(*C*H$_3$)$_2$), 29.0 (br., Dipp-*C*H(CH$_3$)$_2$), 118.8 ({N(Dipp)*C*(H)}), 124.0, 124.4, 139.4, 146.3 (Ar-*C*); $^{11}B\{^{1}H\}$ NMR (C_6D_6, 128 MHz, 298 K), δ = 23.2; ^{29}Si NMR

(C_6D_6, 80 MHz, 298 K), δ = 3.1; IR, ν/cm^{-1} (ATR): 3064 (w), 2041 and 1955 (m, Ge–H), 1576 (m), 1326 (s), 1247 (s), 1117 (m), 1073 (m), 980 (w), 900 (m), 868 (s), 800 (s), 699 (s), 674 (s); MS/EI m/z (%): 948.8 (M^+-$(H)_2$-$(SiMe_3)_2$, 1), 475.5 ($^{TMS}BoNH^+$, 100); anal. calcd. for $C_{58}H_{92}B_2Ge_2N_6Si_2$: C, 63.53%; H, 8.46%; N, 7.66%; found: C, 63.48%; H, 8.28%; N, 7.54%.

(^{TMS}BoN)SnOBu^t (8). A solution of (^{TMS}BoN)SnBr (1.0 g, 1.49 mmol) in toluene (20 mL) was added to a suspension of KOBu^t (192 mg, 1.30 mmol) in toluene (15 mL) at ambient temperature, and the reaction mixture stirred for 16 h. All volatiles were subsequently removed in vacuo, the residue extracted in hexane (10 mL), and filtered. Removal of volatiles from the filtrate in vacuo led the isolation of (^{TMS}BoN)SnOBu^t as a colourless powder (600 mg, 61%). X-ray quality crystals were grown by storage of a concentrated hexane solution of (^{TMS}BoN)SnOBu^t at −30 °C for 4 days. M.p.: 104–110 °C (melt); ^{1}H NMR (C_6D_6, 400 MHz, 298 K), δ = 0.12 (s, 9H, N–*TMS*), 1.18 (s, 9H, Sn–O*Bu^t*), 1.19 (d, $^3J_{HH}$ = 7.0 Hz, 12H, Dipp-CH(C*H*$_3$)$_2$), 1.40 (d, $^3J_{HH}$ = 7.0 Hz, 12H, Dipp-CH(C*H*$_3$)$_2$), 3.55 (sept, $^3J_{HH}$ = 7.0 Hz, 4H, Dipp-C*H*(CH$_3$)$_2$), 6.14 (s, 2H, {N(Dipp)C(*H*)}$_2$), 7.14–7.19 (m, 6H, Ar-*H*), ^{13}C{^{1}H} NMR (C_6D_6, 75.5 MHz, 298 K), δ = 5.1 (N–*TMS*), 23.3 (Dipp-CH(*C*H$_3$)$_2$), 26.2 (Dipp-CH(*C*H$_3$)$_2$), 28.9 (Dipp-*C*H(CH$_3$)$_2$), 35.8 (Sn–OC(*C*H$_3$)$_3$), 72.8 (Sn–O*C*(CH$_3$)$_3$), 118.8 ({N(Dipp)*C*(H)}), 124.5, 139.9, 147.5 (Ar-*C*); ^{11}B{^{1}H} NMR (C_6D_6, 128 MHz, 298 K), δ = 24.5; ^{29}Si NMR (C_6D_6, 80 MHz, 298 K), δ = −1.4; IR, ν/cm^{-1} (ATR): 3064 (w), 1599 (w), 1367 (s), 1294 (s), 1238 (s), 1173 (s), 1117 (s), 1063 (m), 970 (m), 932 (w), 887 (s), 868 (s), 825 (s), 798 (m), 699 (m), 669 (s); MS/EI m/z (%): 667.5 (M^+, 0.5), 475.5 ($^{TMS}BoNH^+$, 100).

(^{TMS}BoN)$_2$Si: (9). To a rapidly stirred solution of IPr.$SiCl_2$ (1.0 g, 2.06 mmol) in benzene (10 mL) was rapidly added a solution of ^{TMS}BoNLi (1.0 g, 2.08 mmol) in benzene (10 mL) at ambient temperature. All volatiles were subsequently removed from the pale yellow solution in vacuo, and the residue extracted in warm hexane, and filtered. The resulting solution was either stirred under and atmosphere of CO_2, or a solution of $SiBr_4$ (1.04 mL, 2 M in hexane, 2.08 mmol) was added, and the resultant solution rapidly stirred for 2 h, whereupon a copious white precipitate formed in both cases. The reaction was again filtered, and all volatiles removed from the filtrate in vacuo. The residue was redissolved in Et_2O (5 mL), the solution concentrated to ∼2 mL, and stored at −30 °C for 18 h, after which time large pale yellow crystals of **9** had formed (520 mg, 51%). M.p.: 152–160 °C (melt); ^{1}H NMR (C_6D_6, 400 MHz, 298 K), δ = −0.12 (s, 18H, N–*TMS*), 1.14 (br, 24H, Dipp-CH(C*H*$_3$)$_2$), 1.28 (br, 24H, Dipp-CH(C*H*$_3$)$_2$), 3.47 (br, d, $^3J_{HH}$ = 7.0 Hz, 8H, Dipp-C*H*(CH$_3$)$_2$), 6.02 (s, 4H, {N(Dipp)C(*H*)}$_2$), 7.05–7.25 (br m, 12H, Ar-*H*); ^{13}C{^{1}H} NMR (C_6D_6, 75.5 MHz, 298 K), δ = 6.7 (N–*TMS*), 23.5 (br, Dipp-CH(*C*H$_3$)$_2$), 26.9 (br, Dipp-CH(*C*H$_3$)$_2$), 28.5 (br, Dipp-*C*H(CH$_3$)$_2$), 29.6 (br, Dipp-*C*H(CH$_3$)$_2$), 120.8 ({N(Dipp)*C*(H)}), 124.2, 124.6, 141.1, 146.4 (Ar-*C*); ^{11}B{^{1}H} NMR (C_6D_6, 128 MHz, 298 K), δ = 23.7; ^{29}Si NMR (C_6D_6, 80 MHz, 298 K), δ = 3.1 (N–*TMS*), 204.6 (N–*Si*–N); IR, ν/cm^{-1} (ATR): 3064 (w), 1584 (w), 1377 (s), 1323 (m), 1297 (m), 1266 (s), 1245 (s), 1118 (m), 1067 (m), 955 (m), 931 (m), 868 (s), 803 (s), 696 (s); MS/EI m/z (%): 977.1 (M^+, 2), 475.5 ($^{TMS}BoNH^+$,

100); anal. calcd. for $C_{58}H_{90}B_2N_6Si_3$: C, 71.28%; H, 9.28%; N, 8.60%; found: C, 71.15%; H, 9.17%; N, 8.50%.

(^{TMS}BoN)Si(H)(NH_2)$_2$ (10). Route (a): A solution of (^{TMS}BoN)$_2$Si: (150 mg, 0.15 mmol) in toluene (5 mL) was stirred under an atmosphere of NH_3 for 20 min, and all volatiles subsequently removed in vacuo. The residue was extracted in hexane (5 mL), the extract filtered, and all volatiles removed from the filtrate in vacuo, giving an oily residue, the ^{1}H NMR spectrum of which shows the presence of one new product, and ^{TMS}BoNH, in a 1:1 ratio.

Route (b): A solution of (^{TMS}BoN)Si(H)Cl$_2$ (300 mg, 0.54 mmol) in hexane (15 mL) was stirred under an atmosphere of NH_3 for 3 days, after which time a large amount of white precipitate had formed. The suspension was filtered, the solid washed with hexane (10 mL), and the extracts combined. Concentration of the combined filtrates in vacuo—to ~5 mL and storage at 4 °C for 4 days led to the formation of large colourless plates of (^{TMS}BoN)Si(H)(NH_2)$_2$ (180 mg, 63%). M. p.: 64–70 °C (melt); ^{1}H NMR (C_6D_6, 400 MHz, 298 K), δ = −0.05 (s, 9H, N–*TMS*), −0.5 (overlapping br s, 4H, Si–(NH_2)$_2$), 1.16 (d, $^3J_{HH}$ = 7.0 Hz, 6H, Dipp-CH(C*H*$_3$)$_2$), 1.19 (d, $^3J_{HH}$ = 7.0 Hz, 6H, Dipp-CH(C*H*$_3$)$_2$), 1.36 (d, $^3J_{HH}$ = 7.0 Hz, 12H, Dipp-CH(C*H*$_3$)$_2$), 3.39 (sept, $^3J_{HH}$ = 7.0 Hz, 2H, Dipp-C*H*(CH$_3$)$_2$), 3.58 (sept, $^3J_{HH}$ = 7.0 Hz, 2H, Dipp-C*H*(CH$_3$)$_2$), 4.72 (s, 1H, Si–*H*, $^1J_{SiH}$ = 232 Hz), 6.18 (s, 2H, {N(Dipp)C(*H*)}$_2$), 7.14–7.20 (m, 6H, Ar-*H*), ^{13}C{^{1}H} NMR (C_6D_6, 75.5 MHz, 298 K), δ = 3.3 (N–*TMS*), 22.8 (Dipp-CH(*C*H$_3$)$_2$), 23.2 (Dipp-CH(*C*H$_3$)$_2$), 26.3 (Dipp-CH(*C*H$_3$)$_2$), 26.5 (Dipp-CH(*C*H$_3$)$_2$), 28.4 (Dipp-*C*H(CH$_3$)$_2$), 28.9 (Dipp-*C*H(CH$_3$)$_2$), 118.8 ({N(Dipp)*C*(H)}), 123.8, 124.0, 127.5, 139.6, 146.3, 147.4 (Ar-*C*); ^{11}B{^{1}H} NMR (C_6D_6, 128 MHz, 298 K), δ = 23.9; ^{29}Si NMR (C_6D_6, 80 MHz, 298 K), δ = −35.7 (d, $^1J_{SiH}$ = 232 Hz. N–*Si*(H)(NH_2)$_2$), 2.4 (N–*TMS*); IR, ν/cm^{-1} (ATR): 3473 and 3396 (m, NH_2), 3064 (w), 2167 (m, SiH), 1540 (m), 1380 (s), 1295 (m), 1247 (s), 1180 (w), 1119 (m) 1076 (m), 982 (s), 910 (s), 835 (s), 803 (s), 691 (s); MS/EI m/z (%): 435.6 (M^+, 46); anal. calcd. for $C_{29}H_{50}BN_5Si_2$: C, 65.02%; H, 9.41%; N, 13.07%; found: C, 64.84%; H, 9.27%; N, 12.89%.

(^{TMS}BoN)Si(H)Cl$_2$ (11). To a solution of Si(H)Cl$_3$ (0.21 mL, 2.18 mmol) in Et$_2$O (10 mL) was added a solution of ^{TMS}BoNLi.Et$_2$O (1.0 g, 1.81 mmol) in Et$_2$O at 0 °C, dropwise over 5 min. The reaction mixture was warmed to ambient temperature and stirred for 1 h, whereupon volatiles were removed in vacuo. The residue was extracted in hexane (10 mL), the extract filtered, and volatiles removed from the filtrate in vacuo to afford a micro crystalline powder, which was essentially pure **11** (820 mg, 79%). X-ray quality crystals were grown from a concentrated hexane solution of (^{TMS}BoN)Si(H)Cl$_2$ at −30 °C for 18 h. M.p.: 71–79 °C (melt); ^{1}H NMR (C_6D_6, 400 MHz, 298 K), δ = −0.09 (s, 9H, N–*TMS*), 1.11 (d, $^3J_{HH}$ = 7.0 Hz, 12H, Dipp-CH(C*H*$_3$)$_2$), 1.33 (br, $^3J_{HH}$ = 7.0 Hz, 12H, Dipp-CH(C*H*$_3$)$_2$), 3.15 (br sept, $^3J_{HH}$ = 7.0 Hz, 2H, Dipp-C*H*(CH$_3$)$_2$), 3.43 (br sept, $^3J_{HH}$ = 7.0 Hz, 2H, Dipp-C*H*(CH$_3$)$_2$), 5.65 (s, 1H, Si–*H*), 6.10 (s, 2H, {N(Dipp)C(*H*)}$_2$), 7.12–7.23 (m, 6H, Ar-*H*), ^{13}C{^{1}H} NMR (C_6D_6, 75.5 MHz, 298 K), δ = 2.5 (N–*TMS*), 23.6 and 23.0 (Dipp-CH(*C*H$_3$)$_2$), 26.4 and 26.5 (Dipp-CH(*C*H$_3$)$_2$), 28.4 and 29.3 (Dipp-*C*H(CH$_3$)$_2$), 119.5 ({N(Dipp)*C*(H)}), 124.1, 124.4,

138.4, 146.1, 146.7 (Ar-*C*); $^{11}B\{^1H\}$ NMR (C_6D_6, 128 MHz, 298 K), δ = 23.0; ^{29}Si NMR (C_6D_6, 80 MHz, 298 K), δ = −21.5 (d, $^1J_{SiH}$ = 232 Hz. N–*Si*(H)Cl-$_2$), 9.2 (N–*TMS*); IR, ν/cm^{-1} (ATR): 3065 (w), 2260 (m, SiH), 1512 (w), 1326 (s), 1290 (m), 1252 (s), 1168 (m), 1119 (s), 1081 (m), 979 (s), 955 (s), 891 (s), 830 (s), 758 (s), 698 (s), 657 (s); MS/EI m/z (%): 573.5 (M^+, 50%); anal. calcd. for $C_{29}H_{46}BCl_2N_3Si_2$: C, 60.62%; H, 8.07%; N, 7.31%; found: C, 60.63%; H, 8.16%; N, 7.16%.

(^{TMS}BoN)(κ^2-^{TMS}BoN'O)SiOH (12). A solution of (^{TMS}BoN)$_2$Si: (150 mg, 0.15 mmol) in toluene (5 mL) was stirred under an atmosphere of O_2 for 20 min, and all volatiles subsequently removed in vacuo. The residue was extracted in hexane (5 mL), the extract filtered, and all volatiles removed from the filtrate in vacuo. The residue was redissolved in Et_2O (5 mL), concentrated to ∼1 mL, and stored at ambient temperature for 3 days, whereupon colourless crystals of (^{TMS}BoN)(κ^2-^{TMS}BoN′O)SiOH had grown (60 mg, 39%). M.p.: 166–175 °C (melt); ^1H NMR (C_6D_6, 400 MHz, 298 K), δ = −0.09 (s, 18H, N–*TMS*), 1.17 (d, $^3J_{HH}$ = 7.0 Hz, 24H, Dipp-CH(C*H*$_3$)$_2$), 1.32 (d, $^3J_{HH}$ = 7.0 Hz, 24H, Dipp-CH(C*H*$_3$)$_2$), 3.43 (sept, $^3J_{HH}$ = 7.0 Hz, 8H, Dipp-C*H*(CH$_3$)$_2$), 5.80 (s, 1H, Ge–*H*), 6.20 (s, 4H, {N(Dipp)C(*H*)}$_2$), 7.10–7.17 (m, 12H, Ar-*H*), $^{13}C\{^1H\}$ NMR (C_6D_6, 75.5 MHz, 298 K), δ = 4.2 (N–*TMS*), 23.1 (Dipp-CH(*C*H$_3$)$_2$), 26.4 (Dipp-CH(*C*H$_3$)$_2$), 29.0 (br., Dipp-*C*H(CH$_3$)$_2$), 118.8 ({N(Dipp)*C*(H)}), 124.0, 124.4, 139.4, 146.3 (Ar-*C*); $^{11}B\{^1H\}$ NMR (C_6D_6, 128 MHz, 298 K), δ = 23.2; ^{29}Si NMR (C_6D_6, 80 MHz, 298 K), δ = 3.1; IR, ν/cm^{-1} (ATR): ∼3200 (v br, SiO–H), 3061 (w), 1624 (m), 1588 (w), 1382 (m), 1326 (m), 1258 (s), 1072 (s), 1043 (s), 967 (m), 922 (m), 871 (s), 838 (s), 796 (s), 695 (m); MS/EI m/z (%): 1009.1 (M^+, 0.5), 475.6 (^{TMS}BoNH$^+$, 10).

N.B. Despite repeated attempts, an accurate elemental analysis could not be obtained for this compound.

(^{TMS}BoN)$_2$Sn: (13). A solution of ^{TMS}BoNK (1.5 g, 2.9 mmol) in THF (25 mL) was added dropwise to a solution of $SnBr_2$ (0.40 g, 1.45 mmol) in THF (10 mL) at −80 °C. The reaction mixture was allowed to warm to ambient temperature over 2 h, giving a deep red/orange solution. All volatiles were subsequently removed in vacuo. Extraction of the resulting solid in warm hexane (25 mL), filtration of the extract, and removal of volatiles from the filtrate in vacuo led to the isolation of essentially pure (^{TMS}BoN)SnBr as a free-flowing pale orange powder (1.22 g, 79%). X-ray quality crystals were grown from a concentrated hexane solution of (^{TMS}BoN)$_2$Sn: stored at 4 °C for 2 days. M.p.: 104–110 °C (melt); ^1H NMR (C_6D_6, 400 MHz, 298 K), δ = 0.11 (s, 18H, N–*TMS*), 1.16 (d, $^3J_{HH}$ = 7.0 Hz, 24H, Dipp-CH(C*H*$_3$)$_2$), 1.29 (br d, $^3J_{HH}$ = 7.0 Hz, 24H, Dipp-CH(C*H*$_3$)$_2$), 3.43 (br sept, $^3J_{HH}$ = 7.0 Hz, 8H, Dipp-C*H*(CH$_3$)$_2$), 5.94 (s, 4H, {N(Dipp)C(*H*)}$_2$), 7.06–7.18 (m, 12H, Ar-*H*), $^{13}C\{^1H\}$ NMR (C_6D_6, 75.5 MHz, 298 K), δ = 5.6 (N–*TMS*), 23.4 (br, Dipp-CH(*C*H$_3$)$_2$), 26.4 (br, Dipp-CH(*C*H$_3$)$_2$), 28.6 (br, Dipp-*C*H(CH$_3$)$_2$), 119.8 (br, {N(Dipp)*C*(H)}), 124.0, 124.4, 141.7, 146.8 (Ar-*C*); $^{11}B\{^1H\}$ NMR (C_6D_6, 128 MHz, 298 K), δ = 23.2; ^{29}Si NMR (C_6D_6, 80 MHz, 298 K), δ = 4.2; IR, ν/cm^{-1} (ATR): 3063 (w), 1583 (w), 1305 (s), 1241 (s), 1178 (m), 1116 (s), 1065 (s), 971 (m), 934 (w), 890 (s), 862 (s), 799 (s), 696 (m), 661 (s); MS/EI m/z (%): 593.4

(M^+-^{TMS}BoN, 0.5), 475.5 (^{TMS}BoNH$^+$, 100); anal. calcd. for $C_{58}H_{90}B_2N_6Si_2Sn$: C, 65.23%; H, 8.50%; N, 7.87%; found: C, 61.60%; H, 8.66%; N, 7.63%.

N.B. Despite repeated attempts, elemental analyses of this compound repeatedly returned low C readings, possibly due to the formation of involatile SiC compounds, arising from the presence of Si and C in this species [32].

(^{TMS}BoN)$_2$Pb: (14). This compound was made in an analogous fashion to (^{TMS}BoN)$_2$Sn:, using ^{TMS}BoNK (0.3 g, 0.59 mmol) and $PbBr_2$ (108 mg, 0.30 mmol). The crude reaction residue, following removal of volatiles, was extracted in warm hexane (20 mL) and the extract filtered. Storage of the filtrate at 4 °C for 16 h led to the formation of large dichroic red/orange blocks of (^{TMS}BoN)$_2$Pb: (130 mg, 38%). M.p.: 104–110 °C (melt); ^{1}H NMR (C_6D_6, 400 MHz, 298 K), δ = 0.05 (s, 18H, N–*TMS*), 1.17 (d, $^3J_{HH}$ = 7.0 Hz, 24H, Dipp-CH(C*H*$_3$)$_2$), 1.31 (br d, $^3J_{HH}$ = 7.0 Hz, 24H, Dipp-CH(C*H*$_3$)$_2$), 3.39 (br, 4H, Dipp-C*H*(CH$_3$)$_2$), 3.68 (br, 4H, Dipp-C*H*(CH$_3$)$_2$ 5.94 (s, 4H, {N(Dipp)C(*H*)}$_2$), 7.06–7.18 (m, 12H, Ar-*H*), ^{13}C{^{1}H} NMR (C_6D_6, 75.5 MHz, 298 K), δ = 4.8 (N–*TMS*), 22.7 (br, Dipp-CH(*C*H$_3$)$_2$), 24.4 (br, Dipp-CH(*C*H$_3$)$_2$), 25.6 (br, Dipp-CH(*C*H$_3$)$_2$), 27.6 (br, Dipp-CH(*C*H$_3$)$_2$), 28.0 (br, Dipp-*C*H(CH$_3$)$_2$), 28.9 (br, Dipp-*C*H(CH$_3$)$_2$), 119.5 (br, {N(Dipp)*C*(H)}), 124.1, 124.6 (br), 141.8, 147.1 (br) (Ar-*C*); ^{11}B{^{1}H} NMR (C_6D_6, 128 MHz, 298 K), δ = 23.3; ^{29}Si NMR (C_6D_6, 80 MHz, 298 K), δ = −6.9; IR, ν/cm^{-1} (ATR): 3063 (w), 1583 (w), 1305 (s), 1241 (s), 1178 (m), 1116 (s), 1065 (s), 971 (m), 934 (w), 890 (s), 862 (s), 799 (s), 696 (m), 661 (s); MS/EI m/z (%): 681.6 (M^+-^{TMS}BoN, 5), 475.5 (^{TMS}BoNH, 100); anal. calcd. for $C_{58}H_{90}B_2N_6Si_2Pb$: C, 60.24%; H, 7.85%; N, 7.27%; found: C, 60.18%; H, 7.73%; N, 7.38%.

References

1. West R, Fink MJ, Michl J (1981) Tetramesityldisilene, a stable compound containing a silicon-silicon double bond. Science 214:1343
2. Lee GH, West R, Müller T (2003) Bis[bis(trimethylsilyl)amino]silylene, an unstable divalent silicon compound. J Am Chem Soc 125:8114
3. Harris DH, Lappert MF (1974) Monomeric, volatile bivalent amides of group IVB elements, M(NR$^1_2$)$_2$ and M(NR^{1}R^2)$_2$(M = Ge, Sn, or Pb; R^1 = Me$_3$Si, R^2 = Me$_3$C). JCS Chem Commun 21:895
4. Gynane MJS, Harris DH, Lappert MF, Power PP, Rividre P, Rividre-Baudet M (1977) Subvalent Group 4B metal alkyls and amides. Part 5. The synthesis and physical properties of thermally stable amides of germanium(II), tin(II), and lead(II). JCS Dalton 7:2004
5. Denk MJ, Lennon R, Hayashi R, West R, Belyakov LV, Verne HP, Haaland A, Wagner M, Metzler N (1994) Synthesis and structure of a stable silylene. J Am Chem Soc 116:2691
6. Gehrhus B, Lappert MF, Heinicke J, Boesec R, Blaser DJ (1995) Synthesis, structures and reactions of new thermally stable silylenes. Chem Soc Chem Commun 1931
7. Haaf M, Schmiedl A, Schmedake TA, Powell DR, Millevolte AJ, Denk M, West R (1998) Synthesis and reactivity of a stable silylene. J Am Chem Soc 120:12714
8. Rekken BD, Brown TM, Fettinger JC, Tuononen HM, Power PP (2012) Isolation of a stable, acyclic, two-coordinate silylene. J Am Chem Soc 134:6504

9. Protchenko AV, Birjkumar KH, Dange D, Schwarz AD, Vidovic D, Jones C, Kaltsoyannis N, Mountford P, Aldridge S (2012) A stable two-coordinate acyclic silylene. J Am Chem Soc 134:6500
10. Protchenko AV, Schwarz AD, Blake MP, Jones C, Kaltsoyannis N, Mountford P, Aldridge S (2013) A generic one-pot route to acyclic two-coordinate silylenes from silicon(IV) precursors: Synthesis and Structural Characterization of a Silylsilylene. Angew Chem Int Ed 52:568
11. Mizuhata Y, Sasamori T, Tokitoh N (2009) Stable heavier carbene analogues. Chem Rev 109:3479
12. Frey GD, Lavallo V, Donnadieu B, Schoeller WW, Bertrand G (2007) Facile splitting of hydrogen and ammonia by nucleophilic activation at a single carbon center. Science 316:439
13. Lips F, Fettinger JC, Mansikkamäki A, Tuononen HM, Power PP (2014) Reversible complexation of ethylene by a silylene under ambient conditions. J Am Chem Soc 136:634
14. Rodriguez R, Gau D, Kato T, Saffon-Merceron N, de Cózar A, Cossío FP, Baceiredo A (2011) Reversible binding of ethylene to silylene–phosphine complexes at room temperature. Angew Chem Int Ed 50:10414
15. Power PP (2003) Silicon, germanium, tin and lead analogues of acetylenes. Chem Commun 17:2091
16. Ghadwal RS, Roesky HW, Pröpper K, Dittrich B, Klein S, Frenking G (2011) A dimer of silaisonitrile with two-coordinate silicon atoms. Angew Chem Int Ed 50:5374
17. Sekiguchi A, Kinjo R, Ichinohe M (2004) A stable compound containing a silicon-silicon triple bond. Science 305:1755
18. Inoue S, Eisenhut C (2013) A dihydrodisilene transition metal complex from an N-heterocyclic carbene-stabilized silylene monohydride. J Am Chem Soc 135:18315
19. Driess M, Yao S, Brym M, van Wüllen C, Lentz D (2006) A new type of N-heterocyclic silylene with ambivalent reactivity. J Am Chem Soc 128:9628
20. Woodul WD, Carter W, Müller R, Richards AF, Stasch A, Kaupp M, Murphy DM, Driess M, Jones C (2011) A neutral, monomeric germanium(I) radical. J Am Chem Soc 133:10074
21. Lappert MF, Protchenko AV, Power PP, Seeber AL (2008) Metal amide chemistry. Wiley, New Jersey
22. Weber L, Dobber E, Stammle HG, Neumann B, Boese R, Bläser D (1997) Reaction of 1,3-Dialkyl-4,5-dimethylimidazol-2-ylidenes with 2-Bromo-2,3-dihydro-1H-1,3,2-diazaboroles (Alkyl=^{i}Pr and ^{t}Bu). Chem Ber 130:705
23. Weber L, Kahlert J, Böhling L, Brockhinke A, Stammler HG, Neumann B, Harder RA, Lowb PJ, Fox MA (2013) Electrochemical and spectroelectrochemical studies of C-benzodiazaborolyl-ortho-carboranes. Dalton Trans 42:2266
24. Segawa Y, Suzuki Y, Yamashita M, Nozaki K (2008) Chemistry of boryllithium: Synthesis, structure, and reactivity. J Am Chem Soc 130:16069
25. Li J, Schenk C, Goedecke C, Frenking G, Jones C (2011) A digermyne with a Ge–Ge single bond that activates dihydrogen in the solid state. J Am Chem Soc 133:18622
26. Sasamori T, Sugiyama Y, Takeda N, Tokitoh N (2005) Structure and properties of an overcrowded 1,2-Dibromodigermene. Organometallics 24:3309
27. Duong HA, Tekavec TA, Arif AM, Louie J (2004) Reversible carboxylation of N-heterocyclic carbenes. Chem Commun 1:112
28. Filippou AC, Chernov O, Schnakenburg G (2009) Lewis base stabilized dichlorosilylene. Angew Chem Int Ed 48:5687
29. Zhou H, Zhang WZ, Liu CH, Qu JP, Lu XB (2008) CO_2 adducts of N-heterocyclic carbenes: Thermal stability and catalytic activity toward the coupling of CO_2 with epoxides. J Org Chem 73:8039
30. Wraage K, Schmidt HG, Noltemeyer M, Roesky HW (1999) Preparation and structural investigations of $(dippNSiMe_3Si)_2(Cp^*Ti)_2(NH)_6$ (dipp = 2,6-$^{i}Pr_2C_6H_3$), $[dippNSiMe_3Si(NH_2)NH]_3$ and $[dippNSiMe_3Ge(NH_2)NH]_3$. Eur J Inorg Chem 5:863

31. Reiche C, Kliem S, Klingebiel U, Noltemeyer M, Voit C, Herbst-Irmer R, Schmatz S (2003) Aminosilanolates as precursors of four- and eight-membered (SiNSiO)-rings. J Organomet Chem 667:24
32. Goodwin C, Smith A, Ortu F, Vitorica-Yrzebal I, Mills D (2015) Salt metathesis versus protonolysis routes for the synthesis of silylamide Hauser base (R_2NMgX; X = halogen) and amido-Grignard (R_2NMgR) complexes. Dalton Trans 45:6004

Appendix A
General Synthetic Considerations

All manipulations were carried out using standard Schlenk and glove box techniques under an atmosphere of high purity dinitrogen. Diethyl ether and pentane were distilled over Na/K alloy (25:75), while THF, hexane and toluene were distilled over molten potassium. Dichloromethane was distilled over CaH_2. ^{1}H, $^{13}C\{^{1}H\}$, ^{19}F, $^{29}Si\{^{1}H\}$, $^{119}Sn\{^{1}H\}$ and $^{11}B\{^{1}H\}$ NMR spectra were recorded on either Bruker AvanceIII 400 or Varian Inova 500 spectrometers and were referenced to the resonances of the solvent used, external $CFCl_3$, external $SiMe_4$, external $SnMe_4$ or external $BF_3(OEt_2)$. NMR solvents (d6-benzene, d8-toluene) were stirred over a potassium mirror for 24 h, and distilled into a J Young's ampoule containing activated 4 Å mol sieves. Mass spectra were obtained from the EPSRC National Mass Spectrometric Service at Swansea University, or run using an Agilent Technologies 5975D inert MSD with a solid state probe. IR spectra were recorded for solid samples using an Agilent Cary 630 attenuated total reflectance (ATR) spectrometer. Melting points were determined in sealed glass capillaries under dinitrogen, and are uncorrected. Micro analyses were carried out by London Metropolitan University. Liquid aldehyde and ketone substrates were dried over activated molecular sieves or flame-dried $MgSO_4$. BBr_3 was stored over elemental Hg, as to remove trace Br_2. All other reagents were used as received.

T.J. Hadlington, *On the Catalytic Efficacy of Low-Oxidation State Group 14 Complexes*, Springer Theses, DOI 10.1007/978-3-319-51807-7

Appendix B
Crystallographic Data

X-ray diffraction studies were performed on a Bruker X8 APEX CCD using a graphite monochromator with Mo Kα radiation (λ = 0.71073 Å), an Oxford Gemini Ultra diffractometer using a graphite monochromator with Mo Kα radiation (λ = 0.71073 Å) or Cu Kα radiation (1.54180 Å), or the MX1 and MX2 beamlines of the Australian Synchrotron. The software package Blu-Ice [1] was used for synchrotron data acquisition, while the program XDS [2] was employed for synchrotron data reduction. All structures were solved by direct methods and refined on F2 by full matrix least squares (SHELX97 [3]) using all unique data.

References

1. McPhillips TM, McPhillips S, Chiu HJ, Cohen AE, Deacon AM, Ellis PJ, Garman E, Gonzalez A, Sauter NK, Phizackerley RP, Soltis SM, Kuhn P (2002) *Blu-Ice* and the Distributed Control System: software for data acquisition and instrument control at macromolecular crystallography beamlines. Synchrotron Rad 9:401
2. Kabsch WJ (1993) Automatic processing of rotation diffraction data from crystals of initially unknown symmetry and cell constants. Appl Cryst 26:795
3. Sheldrick GM (1997) SHELX-97, University of Göttingen

T.J. Hadlington, *On the Catalytic Efficacy of Low-Oxidation State Group 14 Complexes*, Springer Theses, DOI 10.1007/978-3-319-51807-7

Appendix C
Computational Studies

Computational studies were carried out in collaboration with Prof. Gernot Frenking, Marburg University. Details of specific methods used in DFT studies can be found in the experimental part of the relevant journal article.

T.J. Hadlington, *On the Catalytic Efficacy of Low-Oxidation State Group 14 Complexes*, Springer Theses, DOI 10.1007/978-3-319-51807-7